

The background of the cover features a stylized brain composed of various colored regions (yellow, orange, green, blue, purple, red) interconnected by a network of white lines and dots, resembling a neural network or graph. The top half of the cover has a solid blue background, while the bottom half is white.

CLOSING THE LOOP ON NEUROMODULATION FOR NEUROLOGICAL DISEASES

EDITED BY: Doris D. Wang, John D. Rolston, Coralie de Hemptinne and
Jens Volkmann

PUBLISHED IN: Frontiers in Neuroscience



frontiers

Frontiers eBook Copyright Statement

The copyright in the text of individual articles in this eBook is the property of their respective authors or their respective institutions or funders. The copyright in graphics and images within each article may be subject to copyright of other parties. In both cases this is subject to a license granted to Frontiers.

The compilation of articles constituting this eBook is the property of Frontiers.

Each article within this eBook, and the eBook itself, are published under the most recent version of the Creative Commons CC-BY licence.

The version current at the date of publication of this eBook is CC-BY 4.0. If the CC-BY licence is updated, the licence granted by Frontiers is automatically updated to the new version.

When exercising any right under the CC-BY licence, Frontiers must be attributed as the original publisher of the article or eBook, as applicable.

Authors have the responsibility of ensuring that any graphics or other materials which are the property of others may be included in the CC-BY licence, but this should be checked before relying on the CC-BY licence to reproduce those materials. Any copyright notices relating to those materials must be complied with.

Copyright and source acknowledgement notices may not be removed and must be displayed in any copy, derivative work or partial copy which includes the elements in question.

All copyright, and all rights therein, are protected by national and international copyright laws. The above represents a summary only. For further information please read Frontiers' Conditions for Website Use and Copyright Statement, and the applicable CC-BY licence.

ISSN 1664-8714

ISBN 978-2-88976-245-3

DOI 10.3389/978-2-88976-245-3

About Frontiers

Frontiers is more than just an open-access publisher of scholarly articles: it is a pioneering approach to the world of academia, radically improving the way scholarly research is managed. The grand vision of Frontiers is a world where all people have an equal opportunity to seek, share and generate knowledge. Frontiers provides immediate and permanent online open access to all its publications, but this alone is not enough to realize our grand goals.

Frontiers Journal Series

The Frontiers Journal Series is a multi-tier and interdisciplinary set of open-access, online journals, promising a paradigm shift from the current review, selection and dissemination processes in academic publishing. All Frontiers journals are driven by researchers for researchers; therefore, they constitute a service to the scholarly community. At the same time, the Frontiers Journal Series operates on a revolutionary invention, the tiered publishing system, initially addressing specific communities of scholars, and gradually climbing up to broader public understanding, thus serving the interests of the lay society, too.

Dedication to Quality

Each Frontiers article is a landmark of the highest quality, thanks to genuinely collaborative interactions between authors and review editors, who include some of the world's best academicians. Research must be certified by peers before entering a stream of knowledge that may eventually reach the public - and shape society; therefore, Frontiers only applies the most rigorous and unbiased reviews.

Frontiers revolutionizes research publishing by freely delivering the most outstanding research, evaluated with no bias from both the academic and social point of view. By applying the most advanced information technologies, Frontiers is catapulting scholarly publishing into a new generation.

What are Frontiers Research Topics?

Frontiers Research Topics are very popular trademarks of the Frontiers Journals Series: they are collections of at least ten articles, all centered on a particular subject. With their unique mix of varied contributions from Original Research to Review Articles, Frontiers Research Topics unify the most influential researchers, the latest key findings and historical advances in a hot research area! Find out more on how to host your own Frontiers Research Topic or contribute to one as an author by contacting the Frontiers Editorial Office: frontiersin.org/about/contact

CLOSING THE LOOP ON NEUROMODULATION FOR NEUROLOGICAL DISEASES

Topic Editors:

Doris D. Wang, University of California, San Francisco, United States

John D. Rolston, The University of Utah, United States

Coralie de Hemptinne, University of Florida, United States

Jens Volkmann, University Hospital Würzburg, Germany

Citation: Wang, D. D., Rolston, J. D., de Hemptinne, C., Volkmann, J., eds. (2022).

Closing the Loop on Neuromodulation for Neurological Diseases.

Lausanne: Frontiers Media SA. doi: 10.3389/978-2-88976-245-3

Table of Contents

- 05 *Using EEG Alpha States to Understand Learning During Alpha Neurofeedback Training for Chronic Pain***
Kajal Patel, James Henshaw, Heather Sutherland, Jason R. Taylor, Alexander J. Casson, Karen Lopez-Diaz, Christopher A. Brown, Anthony K. P. Jones, Manoj Sivan and Nelson J. Trujillo-Barreto
- 17 *The Evoked Compound Action Potential as a Predictor for Perception in Chronic Pain Patients: Tools for Automatic Spinal Cord Stimulator Programming and Control***
Julie G. Pilitsis, Krishnan V. Chakravarthy, Andrew J. Will, Karen C. Trutnau, Kristin N. Hageman, David A. Dinsmoor and Leonid M. Litvak
- 28 *Chronic Sensing of Subthalamic Local Field Potentials: Comparison of First and Second Generation Implantable Bidirectional Systems Within a Single Subject***
Daniel D. Cummins, Ryan B. Kochanski, Roee Gilron, Nicole C. Swann, Simon Little, Lauren H. Hammer and Philip A. Starr
- 35 *Adaptive Parameter Modulation of Deep Brain Stimulation Based on Improved Supervisory Algorithm***
Yulin Zhu, Jiang Wang, Huiyan Li, Chen Liu and Warren M. Grill
- 48 *Case Report: Embedding “Digital Chronotherapy” Into Medical Devices—A Canine Validation for Controlling Status Epilepticus Through Multi-Scale Rhythmic Brain Stimulation***
Mayela Zamora, Sebastian Meller, Filip Kajin, James J. Sermon, Robert Toth, Moaad Benjaber, Derk-Jan Dijk, Rafal Bogacz, Gregory A. Worrell, Antonio Valentin, Benoit Duchet, Holger A. Volk and Timothy Denison
- 58 *Patient, Caregiver, and Decliner Perspectives on Whether to Enroll in Adaptive Deep Brain Stimulation Research***
Simon Outram, Katrina A. Muñoz, Kristin Kostick-Quenet, Clarissa E. Sanchez, Lavina Kalwani, Richa Lavingia, Laura Torgerson, Demetrio Sierra-Mercado, Jill O. Robinson, Stacey Pereira, Barbara A. Koenig, Philip A. Starr, Aysegul Gunduz, Kelly D. Foote, Michael S. Okun, Wayne K. Goodman, Amy L. McGuire, Peter Zuk and Gabriel Lázaro-Muñoz
- 68 *Sleep-Aware Adaptive Deep Brain Stimulation Control: Chronic Use at Home With Dual Independent Linear Discriminate Detectors***
Ro’ee Gilron, Simon Little, Robert Wilt, Randy Perrone, Juan Anso and Philip A. Starr
- 78 *Prefrontal Physiomarkers of Anxiety and Depression in Parkinson’s Disease***
Coralie de Hemptinne, Witney Chen, Caroline A. Racine, Andreea L. Seritan, Andrew M. Miller, Maria S. Yaroshinsky, Sarah S. Wang, Roee Gilron, Simon Little, Ian Bledsoe, Marta San Luciano, Maya Katz, Edward F. Chang, Heather E. Dawes, Jill L. Ostrem and Philip A. Starr

- 88** *Differential Effects of Pathological Beta Burst Dynamics Between Parkinson's Disease Phenotypes Across Different Movements*
Raumin S. Neuville, Matthew N. Petrucci, Kevin B. Wilkins, Ross W. Anderson, Shannon L. Hoffman, Jordan E. Parker, Anca Velisar and Helen M. Bronte-Stewart
- 98** *Controlling Clinical States Governed by Different Temporal Dynamics With Closed-Loop Deep Brain Stimulation: A Principled Framework*
Gerd Tinkhauser and Eduardo Martin Moraud
- 109** *Dopaminergic Modulation of Spectral and Spatial Characteristics of Parkinsonian Subthalamic Nucleus Beta Bursts*
Matthias Sure, Jan Vesper, Alfons Schnitzler and Esther Florin
- 118** *A New Implantable Closed-Loop Clinical Neural Interface: First Application in Parkinson's Disease*
Mattia Arlotti, Matteo Colombo, Andrea Bonfanti, Tomasz Mandat, Michele Maria Lanotte, Elena Pirola, Linda Borellini, Paolo Rampini, Roberto Eleopra, Sara Rinaldo, Luigi Romito, Marcus L. F. Janssen, Alberto Priori and Sara Marceglia
- 130** *Closing the Loop With Cortical Sensing: The Development of Adaptive Deep Brain Stimulation for Essential Tremor Using the Activa PC+S*
Tomasz M. Frączek, Benjamin I. Ferleger, Timothy E. Brown, Margaret C. Thompson, Andrew J. Haddock, Brady C. Houston, Jeffrey G. Ojemann, Andrew L. Ko, Jeffrey A. Herron and Howard J. Chizeck
- 144** *Practical Closed-Loop Strategies for Deep Brain Stimulation: Lessons From Chronic Pain*
Jordan Prosky, Jackson Cagle, Kristin K. Sellers, Ro'ee Gilron, Cora de Hemptinne, Ashlyn Schmitgen, Philip A. Starr, Edward F. Chang and Prasad Shirvalkar
- 153** *Synchronized Intracranial Electrical Activity and Gait Recording in Parkinson's Disease Patients With Freezing of Gait*
De-Feng Liu, Bao-Tian Zhao, Guan-Yu Zhu, Yu-Ye Liu, Yu-Tong Bai, Huan-Guang Liu, Yin Jiang, Xin Zhang, Lin-Shi, Hua Zhang, An-Chao Yang and Jian-Guo Zhang



Using EEG Alpha States to Understand Learning During Alpha Neurofeedback Training for Chronic Pain

Kajal Patel^{1,2*}, James Henshaw², Heather Sutherland², Jason R. Taylor², Alexander J. Casson³, Karen Lopez-Diaz², Christopher A. Brown⁴, Anthony K. P. Jones², Manoj Sivan^{2,5} and Nelson J. Trujillo-Barreto²

¹ School of Medicine, University of Manchester, Manchester, United Kingdom, ² Division of Neuroscience and Experimental Psychology, University of Manchester, Manchester, United Kingdom, ³ Department of Electrical and Electronic Engineering, University of Manchester, Manchester, United Kingdom, ⁴ Department of Psychological Sciences, University of Liverpool, Liverpool, United Kingdom, ⁵ Academic Department of Rehabilitation Medicine, University of Leeds, Leeds, United Kingdom

OPEN ACCESS

Edited by:

John D. Rolston,
The University of Utah, United States

Reviewed by:

Aleksandra Dagmara
Kawala-Stemiuk,
Opole University of Technology,
Poland
Tomohisa Asai,
Advanced Telecommunications
Research Institute International (ATRI),
Japan

*Correspondence:

Kajal Patel
kj.patel1020@gmail.com

Specialty section:

This article was submitted to
Neural Technology,
a section of the journal
Frontiers in Neuroscience

Received: 23 October 2020

Accepted: 22 December 2020

Published: 22 February 2021

Citation:

Patel K, Henshaw J,
Sutherland H, Taylor JR, Casson AJ,
Lopez-Diaz K, Brown CA, Jones AKP,
Sivan M and Trujillo-Barreto NJ (2021)
Using EEG Alpha States
to Understand Learning During Alpha
Neurofeedback Training for Chronic
Pain. *Front. Neurosci.* 14:620666.
doi: 10.3389/fnins.2020.620666

Objective: Alpha-neurofeedback (α -NFB) is a novel therapy which trains individuals to volitionally increase their alpha power to improve pain. Learning during NFB is commonly measured using static parameters such as mean alpha power. Considering the biphasic nature of alpha rhythm (high and low alpha), dynamic parameters describing the time spent by individuals in high alpha state and the pattern of transitioning between states might be more useful. Here, we quantify the changes during α -NFB for chronic pain in terms of dynamic changes in alpha states.

Methods: Four chronic pain and four healthy participants received five NFB sessions designed to increase frontal alpha power. Changes in pain resilience were measured using visual analogue scale (VAS) during repeated cold-pressor tests (CPT). Changes in alpha state static and dynamic parameters such as fractional occupancy (time in high alpha state), dwell time (length of high alpha state) and transition probability (probability of moving from low to high alpha state) were analyzed using Friedman's Test and correlated with changes in pain scores using Pearson's correlation.

Results: There was no significant change in mean frontal alpha power during NFB. There was a trend of an increase in fractional occupancy, mean dwell duration and transition probability of high alpha state over the five sessions in chronic pain patients only. Significant correlations were observed between change in pain scores and fractional occupancy ($r = -0.45$, $p = 0.03$), mean dwell time ($r = -0.48$, $p = 0.04$) and transition probability from a low to high state ($r = -0.47$, $p = 0.03$) in chronic pain patients but not in healthy participants.

Conclusion: There is a differential effect between patients and healthy participants in terms of correlation between change in pain scores and alpha state parameters. Parameters providing a more precise description of the alpha power dynamics than the mean may help understand the therapeutic effect of neurofeedback on chronic pain.

Keywords: alpha states, alpha rhythm, neurofeedback, EEG biofeedback, chronic pain

INTRODUCTION

Neurofeedback (NFB) is a neuromodulatory therapy which trains patients to develop volitional control over their brain activity (Patel et al., 2020). Neurofeedback systems provide patients with a real-time representation of their electroencephalogram (EEG) signals (Alkoby et al., 2018). This facilitates recognition and practice of mental strategies that allow them to achieve brain states associated with therapeutic benefit (Bagdasaryan and Le Van Quyen, 2013). NFB has been implemented in a variety of conditions ranging from anxiety, depression to chronic pain with promising results being reported by several studies (Schoenberg and David, 2014; Melo et al., 2019).

One of the areas where neurofeedback has been increasingly explored is chronic pain. Alpha power has been known to be lower in chronic pain patients compared to healthy individuals in a number of chronic pain conditions (Chang et al., 2001; Boord et al., 2008; Saithong et al., 2012; Jensen et al., 2013b; Lim et al., 2016; Nickel et al., 2017). Hence, several studies have attempted to increase the alpha power in these patient groups using neurofeedback with the aim of alleviating pain either by targeting alpha rhythm in isolation (Elbogen et al., 2019; Mayaud et al., 2019) or in combination with other rhythms like beta and theta rhythms (Jensen et al., 2013a; Hassan et al., 2015; Al-Taleb et al., 2019; Vučković et al., 2019). Whilst most of these studies report a significant reduction in pain in these individuals following neurofeedback, very few of these studies have been able to show a direct correlation between the reduction in pain and the change in neurophysiological signal as highlighted by a recent systematic review (Patel et al., 2020). All of the neurofeedback studies conducted in the past decade have used mean alpha power to measure changes in neurophysiological signals (Jensen et al., 2013a; Hassan et al., 2015; Al-Taleb et al., 2019; Elbogen et al., 2019; Mayaud et al., 2019; Vučković et al., 2019). This raises the question of whether the indices commonly used to gauge the success of learning truly reflect the neurophysiological changes underlying pain relief following neurofeedback.

The choice of learning index has indeed been a highly debated topic in the field of neurofeedback. Two widely used indices include mean alpha power and percentage time above a pre-determined alpha power threshold (Travis et al., 1974; Hardt and Kamiya, 1976; Lansky et al., 1979; Dempster and Vernon, 2009). Whilst some researchers believe that mean alpha power is the most sensitive index of the two (Hardt and Kamiya, 1976; Dempster and Vernon, 2009), others have argued that dynamic indices might be more informative. For instance, early work found that durations of periods of high alpha power obeyed a non-trivial asymmetrically shifted exponential distribution (Bohdaneck et al., 1978). A recent study (Ossaditchi et al., 2017) looked at changes following neurofeedback in terms of alpha spindles and reported that there was an increase only in frequency of alpha spindles with no change in the amplitude of these spindles. Whilst there are not many studies in the field of neurofeedback and chronic pain that have taken this approach of analyzing dynamic nature of alpha rhythm, the idea of bi-modal alpha amplitude states is being increasingly explored in other fields as discussed below.

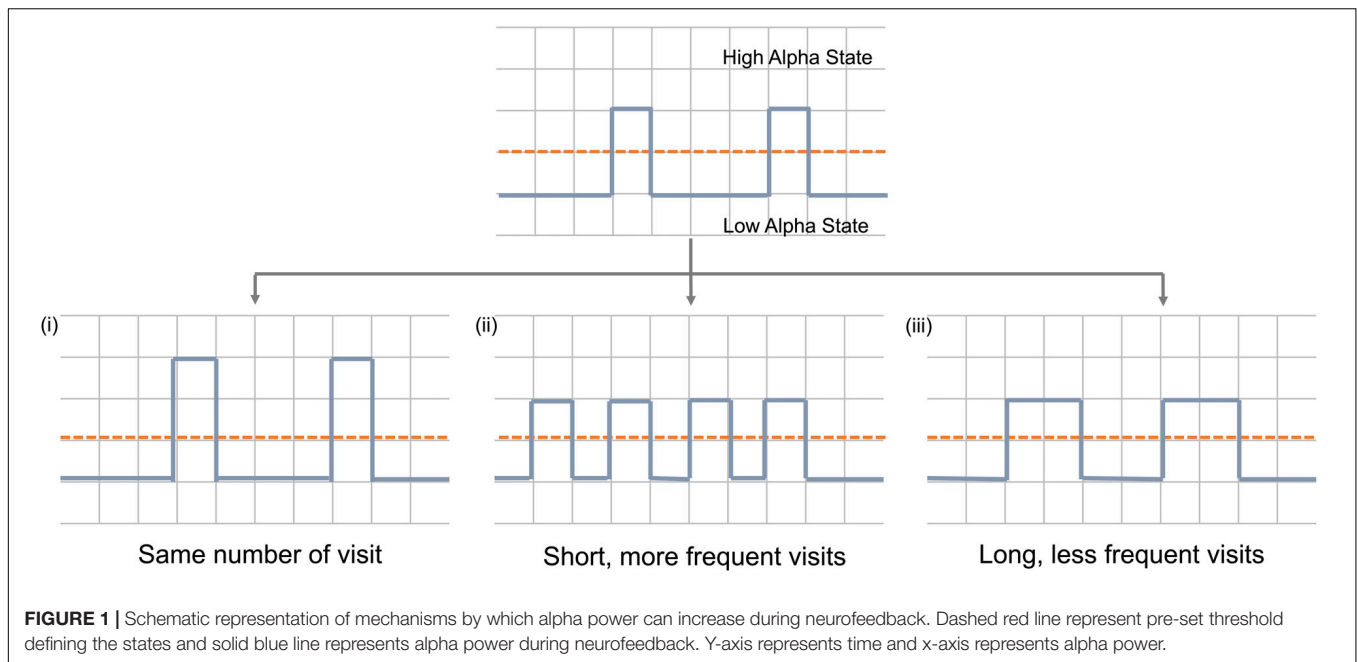
It has been shown that the alpha rhythm has bi-stable dynamics, whereby the alpha power erratically jumps between high and low amplitude modes or states (Freyer et al., 2009; Roberts et al., 2015). Changes in such bi-stable dynamics following any form of intervention can be captured in a number of ways. For instance, one can measure the amount of total time that an individual stays in the high (low) alpha state, also referred to as fractional occupancy, or the chance of transitioning from one state to the other, also known as transition probabilities (Khanna et al., 2014; Quinn et al., 2018; Kottaram et al., 2019). To explore this further, some studies have also mapped out the distribution of high alpha state durations (Quinn et al., 2018). Such measures have been shown to correlate with motor and cognitive function in Parkinson's disease (Chu et al., 2020) and schizophrenia (Khanna et al., 2015) and furthermore, cognitive manipulation of these states can be achieved through interventions (Seitzman et al., 2017). However, no studies have used these dynamic parameters of alpha rhythm to measure neurophysiological changes in chronic pain."

It is not clear how well the currently used indices capture such complex dynamic expression of the alpha rhythm. Understanding the temporal changes in these states might give us more insight into neuronal mechanisms which underlie pain processing as higher alpha rhythm has been associated with increased resilience to pain (Jensen et al., 2013b; Lim et al., 2016; Villafaina et al., 2019). Furthermore, distribution of times that the neuronal networks dwell in each state and the pattern of transition between the states might be key to understanding how these systems process painful stimuli as well as provide insight into the mechanism by which NFB alters neuronal signaling and pain processing.

Brain activity can be assumed to occupy one of the two alpha states over time. An increase in average alpha power can be achieved in one of three ways (or a combination of them) (**Figure 1**): (i). Firstly, due to an increase in the power of the high alpha state with the number of visits remaining constant; (ii) due to more frequent visits to the high alpha state and (iii) due to longer time spent in each visit to that high state.

Whilst there are many ways in which brain activity may be modulated, it is unclear which of these parameters are more sensitive to the effect of NFB training or whether a combination of them will describe individual differences better (specificity). It might be the case that it is possible to voluntarily control alpha activity only through one of these mechanisms. The sensitivity and/or specificity of these parameters may vary between chronic pain patients and healthy participants. More importantly, it is not known how changes in any one of these parameters correlate with changes in behavioral outcomes. Therefore, in order to be able to sensitively measure meaningful NFB learning, a greater understanding of the temporal dynamics of alpha power changes, their susceptibility to voluntary control and their correlation to behavioral outcomes is required.

This study attempted to understand the changes in temporal dynamics of EEG which occur during alpha NFB using a bimodal alpha states model. Brain alpha states analysis was conducted on electroencephalogram (EEG) data during five α -NFB sessions in chronic pain patients as well as healthy participants to gain an



insight into differences in the way brain activity changes in these two groups during the intervention.

MATERIALS AND METHODS

Study Design

This was an exploratory study conducted in the Human Pain Research Group laboratory at Salford Royal Hospital, United Kingdom, with the aim of testing the proof-of-concept of an alpha NFB system in training individuals to modulate their alpha activity in order to increase their resilience to pain. This study was sponsored by the University of Manchester and approved by the National NHS Research Ethics Committee (REC reference 18/NS/0102, IRAS ID 244779). Written informed consent was obtained from the participants according to the Declaration of Helsinki. This study was a registered clinical trial NCT04097522.

Participant Recruitment

Participant recruitment has been summarized in **Figure 2**. Ten participants (6 females, 4 males) were recruited for the study. Chronic pain conditions studied included fibromyalgia, chronic headache and lower back pain. EEG data from eight participants, four healthy participants and four chronic pain patients, who completed all five neurofeedback sessions was included in the final analysis. The patient group was heterogeneous including a range of chronic pain conditions in order to make the results widely applicable to chronic pain in general. Adults above the age of 18 years who were able to give informed consent were eligible. Exclusion criteria included concomitant psychotherapy, previous brain injury, stroke or surgery, and any brain or spinal cord implants.

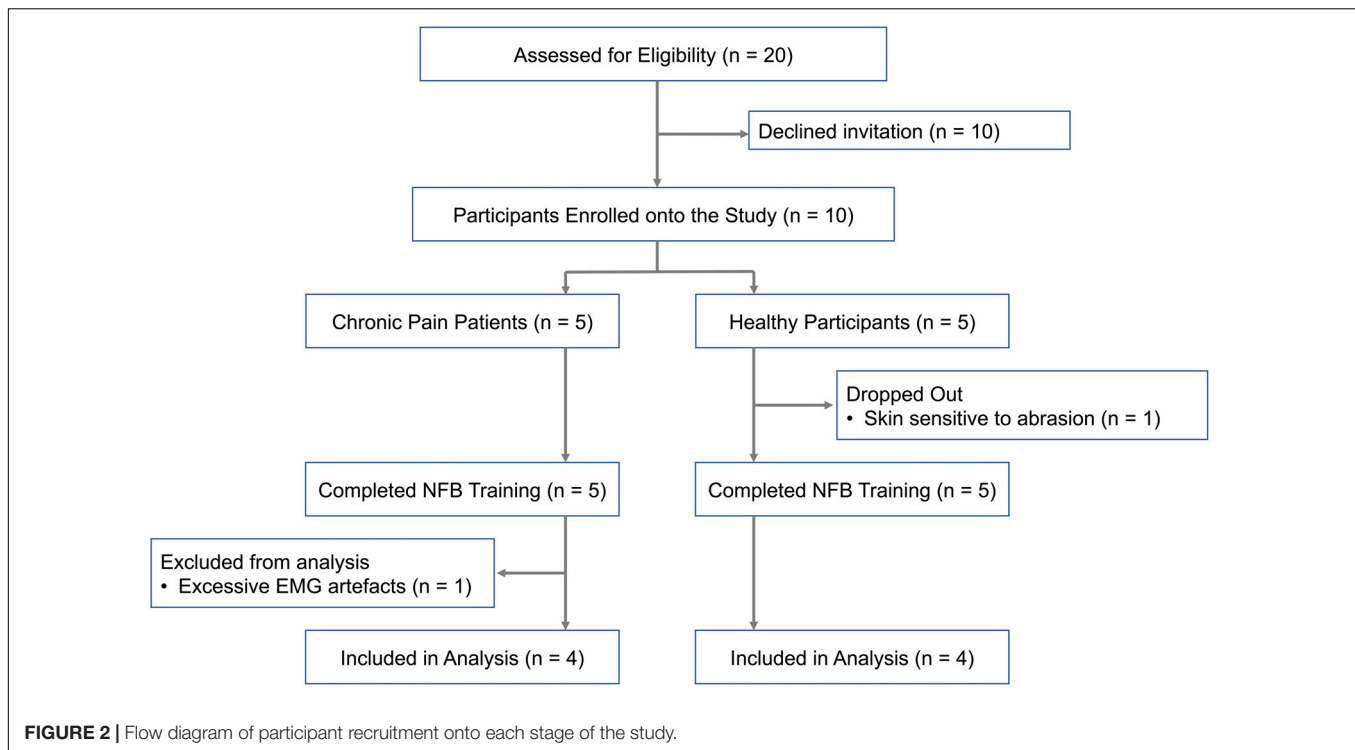
General Procedure

NFB training consisted of five sessions spread across approximately 3 weeks. The experimental protocol and conditions were same for both the groups. At the beginning and end of each session, resting state alpha power was recorded with eyes-open for 2 min. Pain resilience was also assessed at the start and end of each session before measuring resting-state alpha activity by inducing experimental pain using Cold-Pressor Test (CPT) at 10°C cold water for 3 min. The participants were asked to give a pain rating on the scale of 0 (no pain) to 10 (worst pain) using the Visual Analogue Scale (VAS) every 30 s. An average pain rating was obtained by calculating the mean of the six VAS pain ratings provided over the course of the 3 min CPT block. Change in pain scores was calculated for each session by comparing pain rating in each session with pain ratings before any NFB.

Neurofeedback System

EEG was acquired using a 64-channel Standard BrainCap-MR with multitrodes by Brain Products (Herrsching, Germany) (actiCHamp Plus (64 channels) [Apparatus], 2019). The NFB system used a sampling frequency of 1,000 Hz and channel impedances were kept below 20 kΩ. All electrodes were referenced to channel Fz with AFz used as the ground electrode. Neurofeedback was delivered using an in-house developed MATLAB script. A 10-s sliding window was used for filtering the EEG data at the frequency band of interest which was 8–13 Hz. Power calculation and feedback were then provided on the last 2-s period of data from this 10-s sliding window.

Each session consisted of two NFB training blocks of 5 min each with a 1 min break between the blocks. Participants were provided with continuous visual feedback in the form of a dial ranging from 0 to 10, where an increase in mean alpha power



recorded from frontal channels AF3 and AF4 caused the arrow on the dial to move toward 10 and vice versa. The participants were instructed to keep their needle on or close to 10 for the duration of training. The 0 and 10 corresponded to 2nd and 98th percentile of their alpha power during resting-state respectively. Feedback was provided for alpha frequency (8–13 Hz) from frontal electrodes AF3 and AF4.

Off-Line Analysis

All the EEG pre-processing and analysis was performed using EEGLab (Delorme and Makeig, 2004) and fieldtrip (Oostenveld et al., 2011) toolboxes through a script written in MATLAB 2019a 9.6 software (Mathworks Inc., United States) (Natick MTMI, MATLAB, 2018). The raw signal data from AF3 and AF4 were down sampled to 250 Hz and segmented into 1 s non-overlapping epochs. The EEG acquired was first cleaned by visual inspection to remove epochs with high amplitude technical artifacts. No more than 10% of the total epochs were discarded during process. Independent Component Analysis (ICA) was then used to remove components associated with eye blinks, eye movements and muscle movement using SASICA plugin. On average 3–5 components were removed. Frequency analysis was performed using Fourier Transformation to obtain the average alpha power in the frequency range 8–13 Hz for each 1 s epoch of data gathered during resting state and NFB block.

EEG Brain Alpha States Parameters

The dynamics of alpha power fluctuations were first characterized using a symbolic dynamic method. Each 1s epoch was labeled as “1,” if the mean power was higher than a certain pre-defined

threshold (high alpha state) or “0” if the power was lower than the threshold. The threshold was computed individually for each participant and defined as a percentage of the maximum alpha power during the resting-state eyes-open EEG from the first session. To assess the sensitivity of the analysis to threshold choice, three different threshold values were analyzed, 30, 50, and 70%. The maximum alpha power was defined as $1.5 \times$ interquartile range for each individual. This was done in order to prevent random high-amplitude fluctuations in alpha power from being used to set a threshold.

After symbolization, the following alpha state parameters were calculated based on the state sequences obtained:

- **Fractional Occupancy:** Defined as the fraction of all epochs occupied by high alpha state.
- **Dwell Time (duration) Distribution:** Defined as the frequency of dwell times of each state during neurofeedback. Dwell time of the high (low) state is computed as the counts of contiguous epochs where the alpha power was successively in the high (low) state before transitioning to the low (high) state in each state visit. The distribution was then plotted as a violin chart and described in terms of mean, median, mode, variance and tail weights for each plot.
- **Transition Probability:** Defined as the likelihood (probability) of transitioning from one state to another. This was estimated by assuming an observable Markov Process to explain the state sequences. This was achieved by using the `hesitate()` function on MATLAB [which is based on a Hidden Markov Model (Quinn et al., 2018)], and

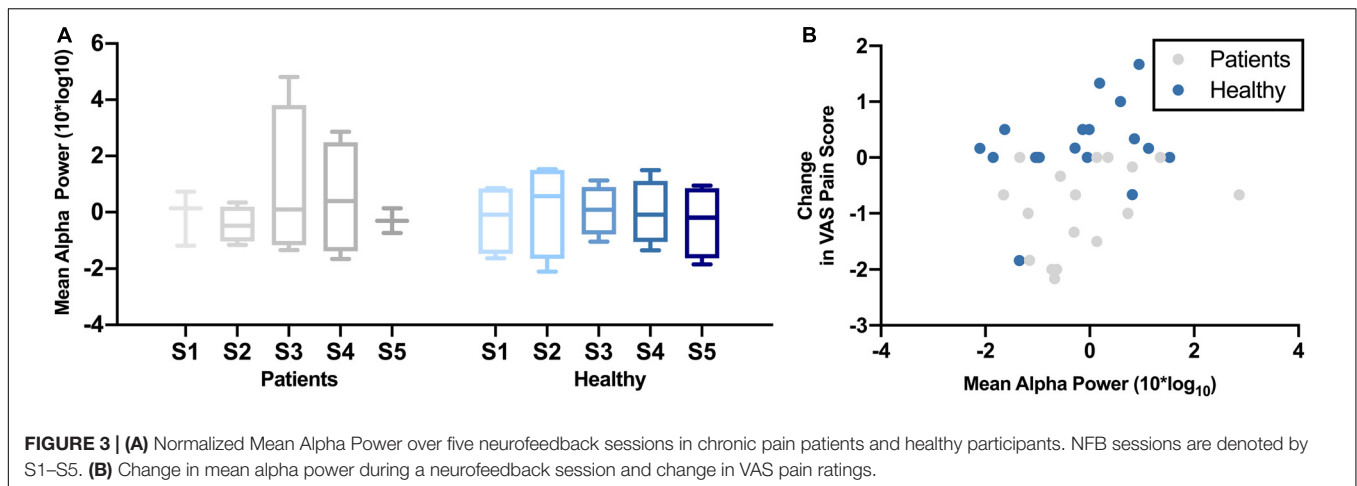


FIGURE 3 | (A) Normalized Mean Alpha Power over five neurofeedback sessions in chronic pain patients and healthy participants. NFB sessions are denoted by S1–S5. **(B)** Change in mean alpha power during a neurofeedback session and change in VAS pain ratings.

forcing the states' emission probability to be the identity matrix.

Analysis based on these dynamic parameters was contrasted with more traditional (static) evaluation based on the normalized and log-transformed mean alpha power in each NFB session. Each parameter from a single neurofeedback session was then correlated with change in pain scores reported by the participant in that particular session.

Statistical Analysis

Statistical analysis was performed using IBM SPSS Statistics version 25 (IBM Corp, 2017). Each alpha state parameter was analyzed using a Friedman Test in order to analyze changes in repeated recordings of alpha power parameters over the five neurofeedback sessions. Correlation between these parameters and behavioral outcomes were tested using Pearson's correlation. Use of parametric tests was possible due to availability of more datapoints and a normal distribution of these points. Generally, statistical significance was accepted with a *p*-value of less than 0.05 for all the tests.

RESULTS

Changes in Mean Alpha Power

Figure 3A shows the change in mean alpha power over the five NFB sessions in chronic pain patients and healthy participants. There was no significant change in mean frontal alpha power over the five NFB sessions in patients [$\chi^2(4) = 0.80$, $p = 0.94$] or healthy participants [$\chi^2(4) = 1.40$, $p = 0.84$]. The correlation between mean alpha power and change in pain scores during cold-pressor test in that session were as follows: chronic pain patients $r = 0.32$, $p = 0.21$; Healthy participants $r = 0.44$, $p = 0.05$ (Figure 3B).

EEG Alpha State Temporal Characteristics

Figure 4 shows the changes in different alpha state parameters over five NFB sessions in chronic pain patients and healthy

participants. Descriptive statistics of these parameters are provided in Table 1.

Fractional Occupancy

There was no significant change in fractional occupancy over the five NFB sessions in patients [$\chi^2(4) = 1.97$, $p = 0.74$] or healthy [$\chi^2(4) = 4.40$, $p = 0.36$] participants. However, a gradual increase in mean fractional occupancy was seen in chronic pain patients with each subsequent session until the fourth session where there was a drop compared to the third session, nevertheless, the fractional occupancy in the fourth and fifth session remained higher than the first session (Figure 4A).

Dwell Time Distribution

Dwell times followed a heavy tail distribution whereby most visits to the high alpha state were of short duration (Figure 4C). The frequency of visits decreased as the dwell duration increase. There was no significant change in mean dwell time over the five NFB sessions in patients [$\chi^2(4) = 2.13$, $p = 0.71$] or healthy participants [$\chi^2(4) = 3.00$, $p = 0.56$]. Although, the results were not statistically significant, there were some important trends in data over sessions. Over the course of the NFB training, there was an increase in the heaviness of the tail in chronic pain patients as shown by the increasing thickness of tails in Figure 4C until session five. There were more visits with longer dwell times over the course of the neurofeedback training. There was also a slight increase in the length of the tail until session five. In contrast, the distribution of dwell times in healthy participants did not show consistent change over the five sessions.

Transition Probability

Figure 4E shows a heat-map demonstrating the probabilities of transitioning from low to high alpha state and vice versa as well as the probabilities of remaining in a low or high state during each NFB session. Statistical analysis performed on transition probability from low to high alpha state showed that there was no significant change in probability of transitioning from low to high alpha state over the five NFB sessions in patients [$\chi^2(4) = 2.57$, $p = 0.63$] or healthy participants [$\chi^2(4) = 6.20$, $p = 0.18$].

TABLE 1 | Descriptive statistics of EEG alpha state parameters over five NFB sessions in chronic pain patients and healthy participants.

	Chronic pain patients					Healthy participants				
	S1	S2	S3	S4	S5	S1	S2	S3	S4	S5
Mean amplitude										
Mean (SD)	-0.10 (0.98)	-0.44 (0.64)	0.92 (2.75)	0.50 (2.01)	-3.0 (0.43)	-0.24 (1.27)	0.14 (1.71)	0.07 (0.89)	-0.01 (1.17)	-0.32 (1.32)
Fractional occupancy										
Mean (SD)	0.62 (0.35)	0.66 (0.37)	0.82 (0.23)	0.69 (0.45)	0.69 (0.29)	0.68 (0.20)	0.77 (0.25)	0.70 (0.17)	0.72 (0.17)	0.62 (0.16)
Dwell times										
Mean	4.13	6.45	9.09	6.82	5.99	3.86	6.09	4.98	4.07	3.27
Median	2.00	2.00	4.00	2.00	2.00	2.00	3.00	2.00	2.00	2.00
Mode	2.00	1.00	2.00	2.00	1.00	1.00	2.00	1.00	1.00	1.00
Variance	133%	168%	129%	145%	174%	133%	115%	137%	122%	121%
Tail wgt.	1.96	2.55	1.84	3.96	2.04	1.98	2.21	2.21	2.18	2.54
Transition probability										
Low > Low	0.63	0.72	0.43	0.81	0.70	0.47	0.45	0.43	0.38	0.34
Low > High	0.37	0.28	0.57	0.19	0.30	0.53	0.55	0.57	0.62	0.66
High > High	0.78	0.84	0.88	0.91	0.71	0.75	0.84	0.75	0.76	0.69
High > Low	0.22	0.16	0.12	0.09	0.29	0.25	0.16	0.25	0.24	0.31

Threshold for transition to high alpha state was set at 30% of maximum alpha power. The NFB sessions are denoted by S1–S5.

However, there were some overall trends which emerged when considering all of the transition probabilities. During the first session, compared to chronic pain patients, healthy participants had a slightly higher probability of transitioning from low to high alpha state, lower probability of moving from high to low alpha state, were more likely to remain in high alpha state and less likely to remain in the low alpha state. Over the course of training, in the chronic pain group, there was no trend in the probability of transitioning from low to high alpha state. There was a decrease in the probability of transitioning from high to low state. There was an increase in the probability of patients remaining in high alpha state which increased with each session until the last session.

In the healthy participant group, there was a trend of a small increase in the probability of transitioning from low to high alpha state over the five sessions but no steady change in the probability of transitioning from high to low state. **Figure 5** shows a schematic representation of changes in the probability of transitioning from low to high alpha state over five neurofeedback sessions in chronic pain patients.

Correlation With Reduction in VAS Pain Ratings

Figures 4B,D,F show the correlation of each of the EEG alpha state parameter with reduction in VAS pain scores. None of the parameters were significantly correlated with change in pain scores in healthy participants including: Fractional Occupancy ($r = 0.19$, $p = 0.20$), Mean Dwell Duration ($r = -0.22$, $p = 0.34$), Transition Probability from low to high alpha state ($r = 0.03$, $p = 0.46$). In the chronic pain group, there was a significant negative correlation between change in pain scores and Fractional Occupancy ($r = -0.45$, $p = 0.03$), Mean Dwell Times ($r = -0.48$, $p = 0.04$) as well as Transition Probability from low to high alpha state ($r = -0.47$, $p = 0.03$).

Sensitivity to Thresholds

Sensitivity of Parameters to Threshold

Figure 6 shows how changes in different alpha state parameters differ for different thresholds.

Fractional occupancy of chronic pain participants during the first session was similar to healthy participants for each threshold (**Figures 6A–C**). Although statistically non-significant, for all thresholds, chronic pain participants then showed a trend of an increase in fractional occupancy over the first three sessions, with a drop in the last two sessions. Nevertheless, the fractional occupancy in the last two sessions remained above that observed in the first session. Furthermore, the slope of change in fractional occupancy was steeper at higher thresholds (**Figure 6C**) compared to lower thresholds (**Figure 6A**). There was no consistent change in fractional occupancy in healthy participants over sessions.

Dwell time distribution of chronic pain patients was also similar to healthy participants across all thresholds during the first session (**Figures 6D–F**). However, across all thresholds, this distribution did not change much over sessions for healthy participants. However, the heaviness and the length of the tail increased over sessions in chronic pain patients. The increase in heaviness and length of tail was more prominent at higher thresholds. However, these changes in mean amplitude over sessions was not statistically significant.

The transition probability matrices of chronic pain patients were similar to healthy participants at the beginning of training across all thresholds. Overall, across all thresholds, there was a general trend of an increase in the probability of transitioning from low to high alpha state and decrease in probability of transitioning from high alpha to low alpha state over sessions in both chronic pain patients and healthy participants across all thresholds except for the last session. However, the change in probability was greater for lower thresholds compared to high

CHANGES IN ALPHA POWER PARAMETERS DURING NEUROFEEDBACK TRAINING SESSIONS

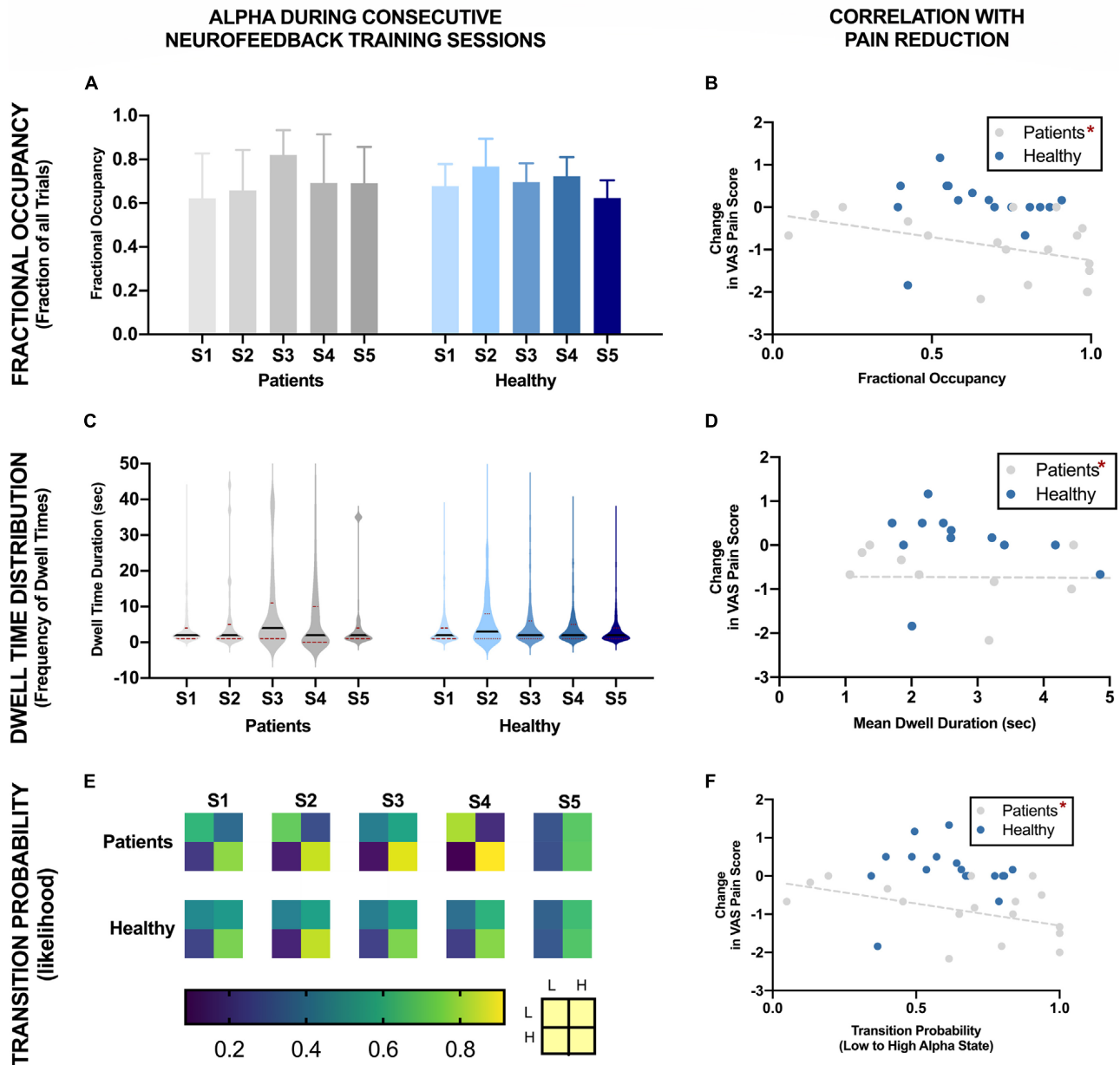


FIGURE 4 | EEG Brain alpha states characteristics over five NFB sessions in chronic pain patients and healthy participants and their correlation with reduction in VAS pain ratings. The NFB sessions are denoted by S1–S5. Error bars show standard error. L refers to low alpha state and H refers to high alpha state. *Statistically significance of $p < 0.05$.

thresholds and greater for chronic pain patients compared to healthy participants.

Sensitivity of Correlation to Threshold

Figure 7 shows the correlation of different parameters at different threshold with reduction in VAS pain scores. Change in pain scores was significantly correlated with fractional occupancy, mean dwell time and transition probability when

the threshold was set at 30% of maximum alpha power as discussed above. These correlations were significant only in the chronic pain patients and not in the healthy participants. These correlations were not significant when the thresholds of 50% and 70% of maximum resting-state alpha power were used. Interestingly, there was a cluster of datapoints with fractional occupancy and transition probability much higher than the rest of the chronic pain

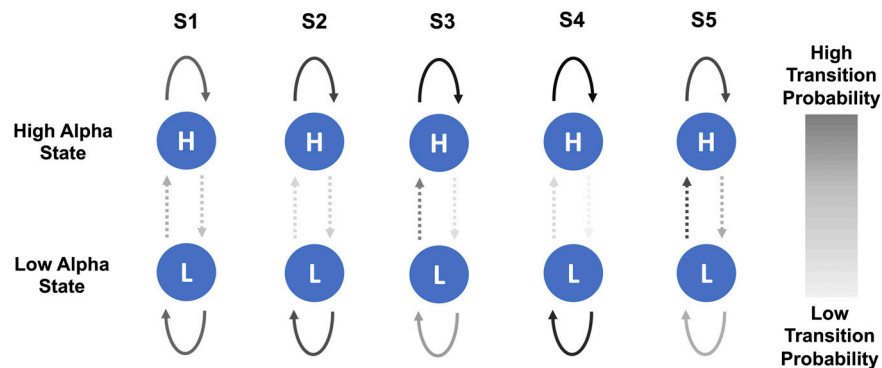


FIGURE 5 | Schematic representation of changes in probability of transitioning from low to high alpha state and vice versa over the course of five NFB sessions in chronic pain patients. The NFB sessions are denoted by S1–S5.

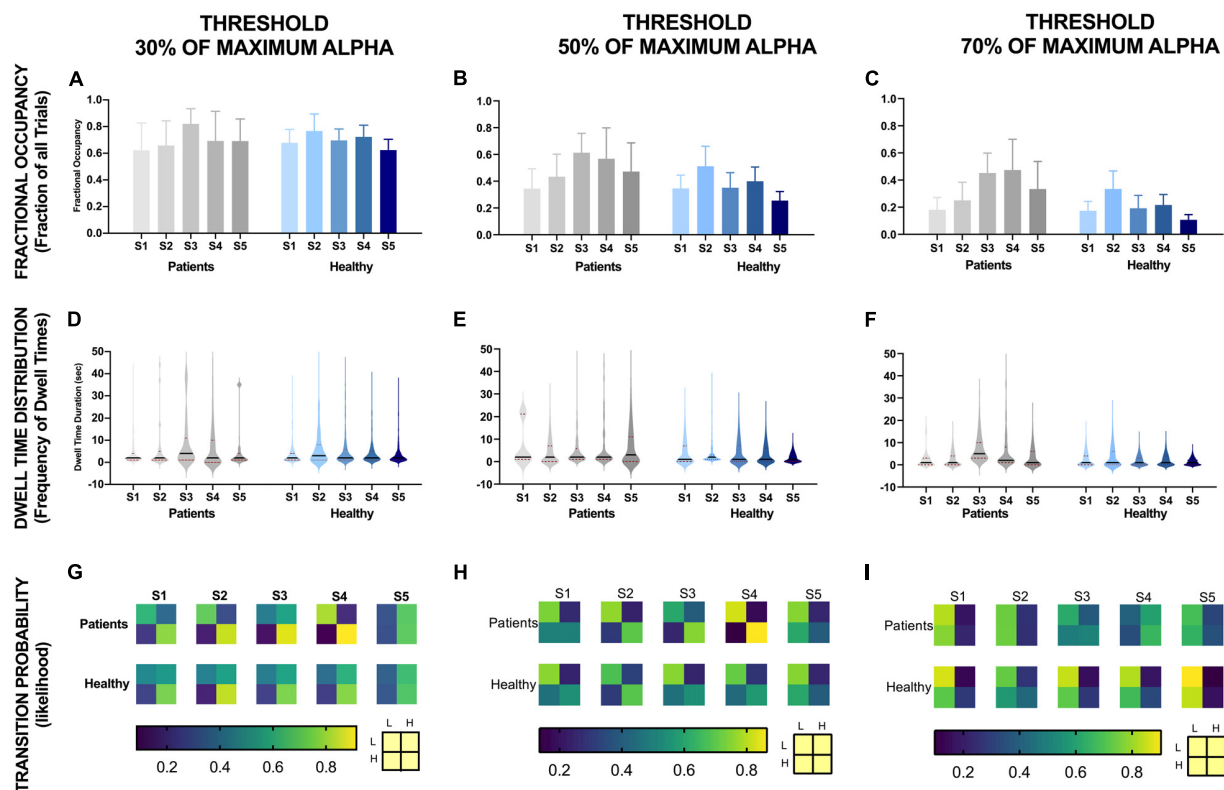


FIGURE 6 | EEG alpha state parameters over five NFB sessions in chronic pain patients and healthy participants for different thresholds. NFB sessions are denoted by S1–S5.

patient group, which could potentially affect the results of the statistical tests.

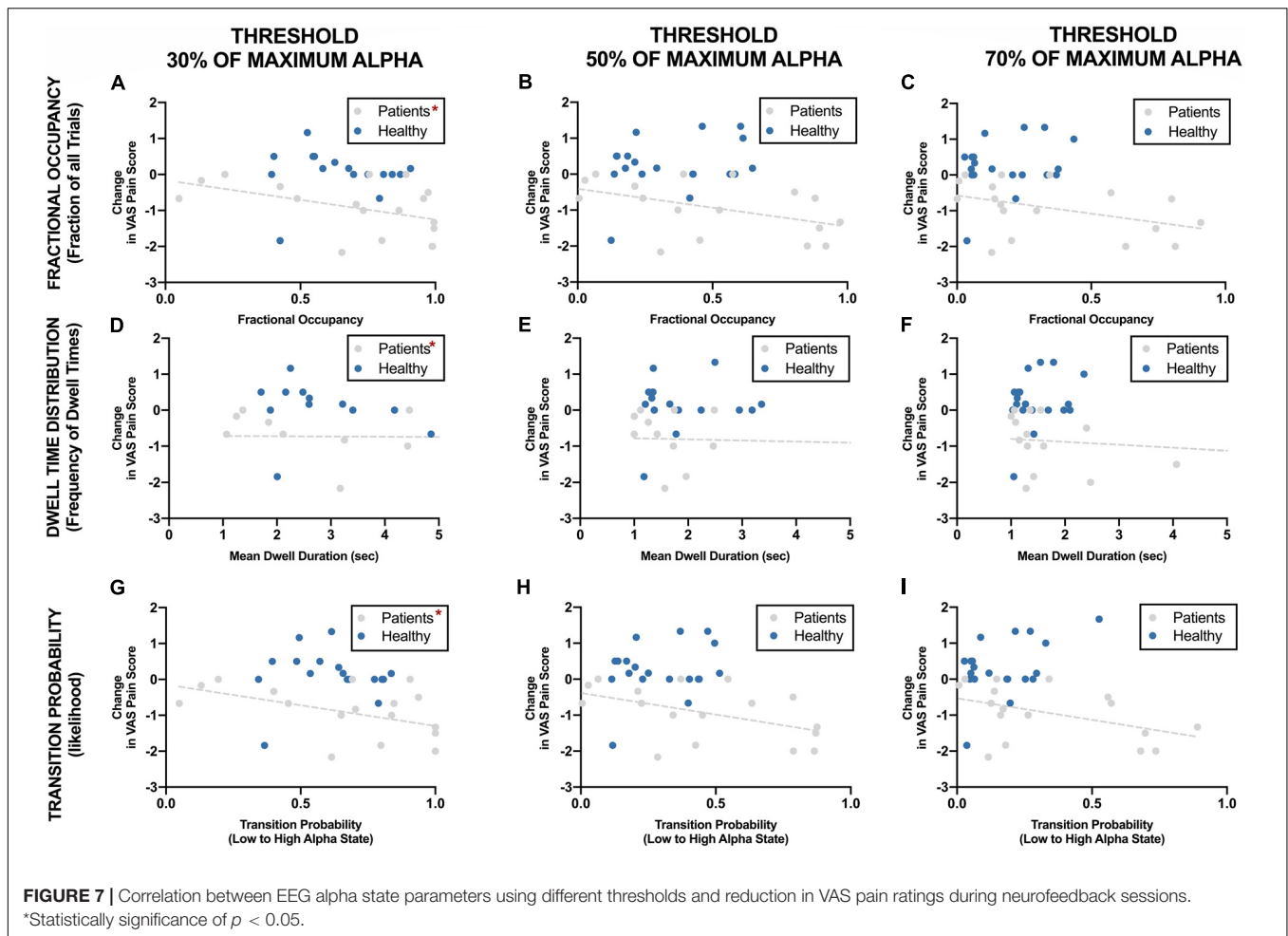
Baseline EEG Alpha Parameters

Supplementary Figure 1 shows EEG Alpha state parameters at baseline before any neurofeedback was delivered in the two groups. There was no statistically significant difference in the mean alpha power, fractional occupancy, dwell time distribution or transition probability between healthy participants and

chronic pain patients at rest. Although chronic pain patients had a longer and heavier tail for dwell time distribution, the difference in the mean dwell time was not significant between the groups.

DISCUSSION

In this study, we found that over five alpha neurofeedback sessions, there was no increase in mean alpha power in patients, however, there was a trend of increase in other



alpha state parameters such as fractional occupancy, dwell time distribution and transition probability. Our results suggest that with neurofeedback training, participants were more likely to make transitions from a low alpha state to a high alpha state and once in the high alpha state, they were more likely to remain in that state before reverting back to low alpha state. Such trends were consistent only in chronic pain patients and not in healthy participants. This is the first study to our knowledge to have compared mean alpha power and alpha state parameters following NFB for pain. We propose an EEG alpha states-based approach to analyzing learning following neurofeedback and provide interesting insight into changes in neurophysiological signals that occur with neurofeedback learning as well as link this to possible mechanisms that may underlie the therapeutic benefit of this neuromodulatory technique.

Negative correlation of alpha state parameters with changes in VAS pain rating during cold-pressor tests was statistically significant for fractional occupancy, mean dwell time and transition probability, meaning that we saw that the greater the fractional occupancy, the longer the high alpha state visit and the higher the transition probability from low to high state, the greater the reduction in pain. Furthermore, these correlations were sensitive to the threshold used to differentiate

low and high alpha state, such that significant correlations were present between alpha state parameter and behavioral outcome only when threshold for high alpha state was set as above 30% of maximum alpha power during eyes-open resting-state and not for the higher thresholds. There was a marginally significant positive trend between change in pain ratings and mean alpha power, however, the direction of this trend was opposite to expected.

Being able to measure any therapeutic change sensitively and displaying this as feedback to the patients is important in order to reinforce mental strategies which lead to an increase in alpha. Failure to detect such small changes may prevent patients from recognizing practices which lead to these changes as the required positive or negative feedback would not be provided. Our results have a number of implications in terms of designing future neurofeedback studies. Firstly, it has implications in terms of EEG data analysis that should be performed in neurofeedback studies, whereby we encourage other researchers to not only report changes in mean alpha amplitude but also to report changes in parameters of alpha states dynamics. This will enable us to assess whether a patient is actually responding to neurofeedback therapy and also allow us to further our understanding of how the brain responds to such therapy. Secondly, such dynamic

alpha states parameters can also be used to fine-tune the way neurofeedback is delivered. Feedback signals shown to the patients can be based on such alpha dynamic features rather than a cruder measure such as mean amplitude. Considering that these parameters are more reflective of the bistable dynamics of alpha rhythm, providing feedback based on them may lead to a more physiologically meaningful (causal) change in alpha power and encourage control strategies which actually translate to pain reduction.

These results suggest that perhaps changes in fractional occupancy, mean dwell times and transition probability may have different implications in terms of the functioning of the underlying neuronal network than changes in mean amplitude alone, and it might be the case it is changes in these dynamic parameters which might be responsible for the increased resilience to pain. For instance, it has been suggested that longer dwell times might reflect an increased stability of the network giving rise to the respective alpha state (Khanna et al., 2015). Increased transition probability means an increased chance of sequential activation of the state (Khanna et al., 2015). Pain relief may be mediated through increased transitioning of individuals' alpha from low to high alpha state as it may reflect the receptiveness of the brain for the incoming stimulus (Michel and Koenig, 2018). Another reason why such patterns of sequential activation might influence pain might be that the sequence in which these alpha states are present may have a meaning in itself and influence how the incoming stimulus is being processed (Buzsáki and Watson, 2012; Khanna et al., 2015; Michel and Koenig, 2018). This has been suggested before based on the neuronal workspace model where alpha states have been interpreted as "atoms of thoughts" (Ros et al., 2014; Villafaina et al., 2019), each representing specific mental processes making up a conscious mind. Hence, the sequence of mental processes or transition properties from one state to another can be thought to carry a meaning in itself (Ros et al., 2014; Villafaina et al., 2019).

Another interesting observation was regarding the presence of changes in alpha state parameters in the chronic pain patients with little consistent change in healthy volunteers. One possible explanation for this might be that chronic pain patients have more scope for improvement in these parameters since their alpha state parameters were lower, although not significantly, than healthy participants during the first session. However, another explanation for this might be that perhaps neurons are more susceptible to plasticity by external factors in chronic pain patients than healthy individuals. This idea of chronic pain patients having lower alpha than healthy participants and lower alpha being correlated with greater pain has been reported widely in the literature (Jensen et al., 2013b; Lim et al., 2016; Villafaina et al., 2019).

This discrepancy in the EEG changes between chronic pain patients and healthy participants may also be due to a motivational effect. We did not assess the motivation of our participants at the beginning of the training, hence the impact of any such factor on the performance of the individual cannot be determined in our study. Nevertheless, our results show that chronic pain patients are as capable, if not more capable,

than healthy participants at learning to control their alpha activity. One would have anticipated that since the neuronal networks have already been rewired in chronic pain patients to attend to pain signals (Katz and Rothenberg, 2005; Reddan and Wager, 2019), it might be more difficult for chronic pain patients to change their brain activity following prolonged exposure to pain. Our results suggest that brains of chronic pain patients might be more plastic than we think. If this is the case, then such neuromodulatory therapy may have substantial potential for systematic development for personalized therapy in the future.

The initial rationale for alpha states modeling in this paper was simply to have a description of the dynamics of alpha power fluctuations between the low and high alpha states. Since the participants were required to follow the feedback provided to them, an extrinsic threshold, used to define these two "empirical" states, was derived based on an *ad hoc* criterion of what alpha power would be considered "good" or "high" enough for the neurofeedback to have an effect. There are no suggestions in the literature in terms of what this threshold should be, hence, we analyzed our data for a range of thresholds.

Ideally however, this threshold can be determined based on a characterization of the bistable dynamics of the endogenous alpha fluctuations of each subject, rather than based on an external criterion. The bistable nature of the alpha rhythm means that whilst in the low alpha state, the amplitude of the alpha fluctuates around a low "mean" value for some time and then spontaneously switches to the high alpha state, where it starts fluctuating around a high "mean" alpha value (Freyer et al., 2009, 2011; Roberts et al., 2015). This gives a bimodal distribution of the alpha amplitudes when viewed in double logarithmic coordinates, which can be best described by the sum of two exponential distributions (one for each alpha mode) (Freyer et al., 2009; Roberts et al., 2015). Hence the "meeting point" of the two distributions, (which is not the same as the midpoint of the low and high mean values), would be a more physiologically meaningful threshold for defining the two intrinsic alpha states. Moreover, changes in such an "intrinsic" threshold evaluated pre and post neurofeedback intervention, might correlate with a pain effect, which might in itself be a potential marker of pain modulation. Hence, although the extrinsic threshold used in our study might be sub-optimal, these preliminary findings provide useful insights into the underlying mechanisms of neurofeedback which warrant further in-depth analysis.

The limiting factors of our study were the small sample size and the small number of sessions. This means the results should be interpreted with caution. This could perhaps explain why we did not see a significant increase in the different EEG parameters. It might be the case that with provision of further NFB sessions, we would have seen significant increase. However, this preliminary study has enabled us to identify learning indices which can still detect learning in these initial sessions when the other commonly used parameters do not show noticeable change. In fact, the alpha states dynamic approach presented here might be a better way to model alpha rhythm as it exploits the bistable nature of alpha rhythm better.

On a methodical note, we used a sliding window to calculate the alpha power. This approach introduces a smoothing effect that can “smear out” the finer dynamics of the alpha rhythm. Since the alpha rhythm shows some scale invariance (Van De Ville et al., 2010), this short window averaging will still preserve some of the dynamical features of the alpha rhythm, which we believe support results reported here. To improve on this, we propose that future analysis can then focus on characterizing the dynamics of the instantaneous alpha power fluctuations. Such an approach has the potential to uncover new and possibly more sensitive effects of α -NFB for the treatment of chronic pain.

CONCLUSION

In conclusion, we have observed changes in dynamic alpha state parameters that are not reflected in mean alpha power during alpha neurofeedback for pain. Our study found that changes in alpha state parameters might potentially be more sensitive predictors of learning than currently used measures. Over the course of five alpha neurofeedback sessions in this study, whilst there was no change in mean alpha power, there was a trend of increase in fractional occupancy, dwell time duration, and transition probability of high alpha state. Furthermore, fractional occupancy, mean dwell times and transitional probability was correlated with change in pain scores, such that in sessions where an individual spends more time in the high alpha state, had longer high alpha state visits or had higher probability of transitioning from low to high alpha state were likely to report greater reduction in pain. We hope that our results will encourage others to measure learning using similar approach. Reporting such temporal dynamics alongside changes in mean alpha power will not only enable us to measure success more sensitively but may also provide insight into the mechanisms of neurofeedback training.

REFERENCES

- actiCHamp Plus (64 channels) [Apparatus] (2019). *Gilching*. Gilching: Brain Products GmbH.
- Alkoby, O., Abu-Rmileh, A., Shriki, O., and Todder, D. (2018). Can we predict who will respond to neurofeedback? A review of the inefficacy problem and existing predictors for successful EEG neurofeedback learning. *Neuroscience* 378, 155–164. doi: 10.1016/j.neuroscience.2016.12.050
- Al-Taleb, M. K. H., Purcell, M., Fraser, M., Petric-Gray, N., and Vuckovic, A. (2019). Home used, patient self-managed, brain-computer interface for the management of central neuropathic pain post spinal cord injury: usability study. *J. Neuroeng. Rehabil.* 16:128.
- Bagdasaryan, J., and Le Van Quyen, M. (2013). Experiencing your brain: neurofeedback as a new bridge between neuroscience and phenomenology. *Front. Hum. Neurosci.* 7:680. doi: 10.3389/fnhum.2013.00680
- Bohdanek, Z., Lfinsk, P., Indra, M., and Radii-Weiss, T. (1978). EEG alpha and non-alpha intervals alternation. *Biol. Cybern.* 30, 109–113. doi: 10.1007/bf00337324
- Boord, P., Siddall, P. J., Tran, Y., Herbert, D., Middleton, J., and Craig, A. (2008). Electroencephalographic slowing and reduced reactivity in neuropathic pain following spinal cord injury. *Spinal Cord* 46, 118–123. doi: 10.1038/sj.sc.3102077

DATA AVAILABILITY STATEMENT

The raw data supporting the conclusions of this article will be made available by the authors, without undue reservation, to any qualified researcher.

ETHICS STATEMENT

The studies involving human participants were reviewed and approved by the National NHS Research Ethics Committee. The patients/participants provided their written informed consent to participate in this study.

AUTHOR CONTRIBUTIONS

KP, JH, HS, JT, AC, KL-D, CB, AJ, MS, and NT-B designed the study. KP, JH, and HS conducted the study, including patient recruitment, data collection, and data analysis. KP prepared the manuscript draft with important intellectual input from JH, HS, JT, AC, KL-D, CB, AJ, MS, and NT-B during interpretation of the data and refining of the manuscript. All authors approved the final manuscript.

FUNDING

This work was supported by the Dunhill Trust.

SUPPLEMENTARY MATERIAL

The Supplementary Material for this article can be found online at: <https://www.frontiersin.org/articles/10.3389/fnins.2020.620666/full#supplementary-material>

- Buzsáki, G., and Watson, B. O. (2012). Brain rhythms and neural syntax: implications for efficient coding of cognitive content and neuropsychiatric disease. *Dialogues Clin. Neurosci.* 14, 345–367. doi: 10.31887/dcms.2012.14.4/gbuzsaki
- Chang, P. F., Arendt-Nielsen, L., Graven-Nielsen, T., Svensson, P., and Chen, A. C. N. (2001). Different EEG topographic effects of painful and non-painful intramuscular stimulation in man. *Exp. Brain Res.* 141, 195–203. doi: 10.1007/s002210100864
- Chu, C., Wang, X., Cai, L., Zhang, L., Wang, J., Liu, C., et al. (2020). Spatiotemporal EEG microstate analysis in drug-free patients with Parkinson's disease. *Neuroimage Clin.* 25:102132. doi: 10.1016/j.nicl.2019.102132
- Delorme, A., and Makeig, S. (2004). EEGLAB: an open source toolbox for analysis of single-trial EEG dynamics. *J. Neurosci. Methods* 134, 9–21. doi: 10.1016/j.jneumeth.2003.10.009
- Dempster, T., and Vernon, D. (2009). Identifying indices of learning for alpha neurofeedback training. *Appl. Psychophysiol. Biofeedback* 34, 309–318. doi: 10.1007/s10484-009-9112-3
- Elbogen, E. B., Alsobrooks, A., Battles, S., Molloy, K., Dennis, P. A., Beckham, J. C., et al. (2019). Mobile neurofeedback for pain management in veterans with TBI and PTSD. *Pain Med.* doi: 10.1093/pm/pnz269 [Epub ahead of print].
- Freyer, F., Aquino, K., Robinson, P. A., Ritter, P., and Breakspear, M. (2009). Bistability and non-Gaussian fluctuations in spontaneous cortical activity. *J. Neurosci.* 29, 8512–8524. doi: 10.1523/jneurosci.0754-09.2009

- Freyer, F., Roberts, J. A., Becker, R., Robinson, P. A., Ritter, P., and Breakspear, M. (2011). Biophysical mechanisms of multistability in resting-state cortical rhythms. *J. Neurosci.* 31, 6353–6361. doi: 10.1523/jneurosci.6693-10.2011
- Hardt, J. V., and Kamiya, J. (1976). Conflicting results in EEG alpha feedback studies - Why amplitude integration should replace percent time. *Biofeedback Self Regul.* 1, 63–75. doi: 10.1007/bf00998691
- Hassan, M. A., Fraser, M., Conway, B. A., Allan, D. B., and Vuckovic, A. (2015). The mechanism of neurofeedback training for treatment of central neuropathic pain in paraplegia: a pilot study. *BMC Neurol.* 15:200. doi: 10.1186/s12883-015-0445-7
- IBM Corp (2017). *IBM SPSS Statistics for Windows, Version 25.0*. Armonk, NY: IBM Corp.
- Jensen, M. P., Sherlin, L. H., Askew, R. L., Fregni, F., Witkop, G., Gianas, A., et al. (2013a). Effects of non-pharmacological pain treatments on brain states. *Clin. Neurophysiol.* 124, 2016–2024. doi: 10.1016/j.clinph.2013.04.009
- Jensen, M. P., Sherlin, L., Gertz, K., Braden, A., Kupper, A., Gianas, A., et al. (2013b). Brain EEG activity correlates of chronic pain in persons with spinal cord injury: clinical implications. *Spinal Cord* 51, 55–58. doi: 10.1038/sc.2012.84
- Katz, W. A., and Rothenberg, R. (2005). The nature of pain: pathophysiology. *J. Clin. Rheumatol.* 11(2 Suppl.), S11–S15.
- Khanna, A., Pascual-Leone, A., and Farzan, F. (2014). Reliability of resting-state microstate features in electroencephalography. *PLoS One* 9:e114163. doi: 10.1371/journal.pone.0114163
- Khanna, A., Pascual-Leone, A., Michel, C. M., and Farzan, F. (2015). Microstates in resting-state EEG: current status and future directions. *Neurosci. Biobehav. Rev.* 49, 105–113. doi: 10.1016/j.neubiorev.2014.12.010
- Kottaram, A., Johnston, L. A., Cocchi, L., Ganella, E. P., Everall, I., Pantelis, C., et al. (2019). Brain network dynamics in schizophrenia: reduced dynamism of the default mode network. *Hum. Brain Mapp.* 40, 2212–2228. doi: 10.1002/hbm.24519
- Lansky, P., Bohdanecky, Z., Indra, M., and Radil-Weiss, T. (1979). Alpha detection. *Biofeedback Self Regul.* 4, 127–131.
- Lim, M., Kim, J. S., Kim, D. J., and Chung, C. K. (2016). Increased low-and high-frequency oscillatory activity in the prefrontal cortex of fibromyalgia patients. *Front. Hum. Neurosci.* 10:111. doi: 10.3389/fnhum.2016.00111
- Mayaud, L., Wu, H., Barthélemy, Q., Favenne, P., Delpierre, Y., Congedo, M., et al. (2019). Alpha-phase synchrony EEG training for multi-resistant chronic low back pain patients: an open-label pilot study. *Eur. Spine J.* 28, 2487–2501. doi: 10.1007/s00586-019-06051-9
- Melo, D. L. M., Carvalho, L. B. C., Prado, L. B. F., and Prado, G. F. (2019). Biofeedback therapies for chronic insomnia: a systematic review. *Appl. Psychophysiol. Biofeedback* 44, 259–269. doi: 10.1007/s10484-019-09442-2
- Michel, C. M., and Koenig, T. (2018). EEG microstates as a tool for studying the temporal dynamics of whole-brain neuronal networks: a review. *Neuroimage* 180(Pt B), 577–593. doi: 10.1016/j.neuroimage.2017.11.062
- Natick MTMI. MATLAB (2018). *Matlab Version 9.6 (R2019a)*. Natick, MA: MathWorks.
- Nickel, M. M., May, E. S., Tiemann, L., Schmidt, P., Postorino, M., Ta Dinh, S., et al. (2017). Brain oscillations differentially encode noxious stimulus intensity and pain intensity. *Neuroimage* 148, 141–147. doi: 10.1016/j.neuroimage.2017.01.011
- Oostenveld, R., Fries, P., Maris, E., and Schoffelen, J. M. (2011). FieldTrip: Open source software for advanced analysis of MEG, EEG, and invasive electrophysiological data. *Comput. Intell. Neurosci.* 2011:156869.
- Ossadtchi, A., Shamaeva, T., Okorokova, E., Moiseeva, V., and Lebedev, M. A. (2017). Neurofeedback learning modifies the incidence rate of alpha spindles, but not their duration and amplitude. *Sci. Rep.* 7:3772.
- Patel, K., Sutherland, H., Henshaw, J., Taylor, J. R., Brown, C. A., Casson, A. J., et al. (2020). Effects of neurofeedback in the management of chronic pain: a systematic review and meta-analysis of clinical trials. *Eur. J. Pain* 24, 1440–1457. doi: 10.1002/ejp.1612
- Quinn, A. J., Vidaurre, D., Abeysuriya, R., Becker, R., Nobre, A. C., and Woolrich, M. W. (2018). Task-evoked dynamic network analysis through Hidden Markov Modeling. *Front. Neurosci.* 12:603. doi: 10.3389/fnins.2018.00603
- Reddan, M. C., and Wager, T. D. (2019). Brain systems at the intersection of chronic pain and self-regulation. *Neurosci. Lett.* 702, 24–33. doi: 10.1016/j.neulet.2018.11.047
- Roberts, J. A., Boonstra, T. W., and Breakspear, M. (2015). The heavy tail of the human brain. *Curr. Opin. Neurobiol.* 31, 164–172. doi: 10.1016/j.conb.2014.10.014
- Ros, T., Baars, B. J., Lanius, R. A., and Vuilleumier, P. (2014). Tuning pathological brain oscillations with neurofeedback: a systems neuroscience framework. *Front. Hum. Neurosci.* 8:1008. doi: 10.3389/fnhum.2014.01008
- Saithong, N., Poolpoem, W., Panavaranan, P., Saetang, J., and Wongsawat, Y. (2012). “EEG-based acute pain control system,” in *Proceedings of the Information and Communications Technology Computer Aided Surgery*, Vol. 3, eds T. Dohi and H. Liao (New York, NY: Springer), 101–112. doi: 10.1007/978-4-431-54094-6_12
- Schoenberg, P. L. A., and David, A. S. (2014). Biofeedback for psychiatric disorders: a systematic review. *Appl. Psychophysiol. Biofeedback* 39, 109–135. doi: 10.1007/s10484-014-9246-9
- Seitzman, B. A., Abell, M., Bartley, S. C., Erickson, M. A., Bolbecker, A. R., and Hetrick, W. P. (2017). Cognitive manipulation of brain electric microstates. *Neuroimage* 146, 533–543. doi: 10.1016/j.neuroimage.2016.10.002
- Travis, T. A., Kondo, C. Y., and Knott, J. R. (1974). Parameters of eyes-closed alpha enhancement. *Psychophysiology* 11, 674–681. doi: 10.1111/j.1469-8986.1974.tb01136.x
- Van De Ville, D., Britz, J., and Michel, C. M. (2010). EEG microstate sequences in healthy humans at rest reveal scale-free dynamics. *Proc. Natl. Acad. Sci. U.S.A.* 107, 18179–18184. doi: 10.1073/pnas.1007841107
- Villafaina, S., Collado-Mateo, D., Fuentes-García, J. P., Cano-Plasencia, R., and Gusi, N. (2019). Impact of fibromyalgia on alpha-2 EEG power spectrum in the resting condition: a descriptive correlational study. *Biomed Res. Int.* 2019:7851047.
- Vuëkovia, A., Altaieb, M. K. H., Fraser, M., McGeady, C., and Purcell, M. (2019). EEG correlates of self-managed neurofeedback treatment of central neuropathic pain in chronic spinal cord injury. *Front. Neurosci.* 13:762. doi: 10.3389/fnins.2019.00762

Conflict of Interest: The authors declare that the research was conducted in the absence of any commercial or financial relationships that could be construed as a potential conflict of interest.

Copyright © 2021 Patel, Henshaw, Sutherland, Taylor, Casson, Lopez-Diaz, Brown, Jones, Sivan and Trujillo-Barreto. This is an open-access article distributed under the terms of the Creative Commons Attribution License (CC BY). The use, distribution or reproduction in other forums is permitted, provided the original author(s) and the copyright owner(s) are credited and that the original publication in this journal is cited, in accordance with accepted academic practice. No use, distribution or reproduction is permitted which does not comply with these terms.



The Evoked Compound Action Potential as a Predictor for Perception in Chronic Pain Patients: Tools for Automatic Spinal Cord Stimulator Programming and Control

Julie G. Pilitsis¹, Krishnan V. Chakravarthy², Andrew J. Will³, Karen C. Trutnau³, Kristin N. Hageman⁴, David A. Dinsmoor^{4*} and Leonid M. Litvak⁴

¹ Department of Neurosurgery, Albany Medical Center, Albany, NY, United States, ² Department of Anesthesiology, University of California, San Diego, La Jolla, CA, United States, ³ Twin Cities Pain Clinic, Edina, MN, United States, ⁴ Medtronic PLC, Minneapolis, MN, United States

OPEN ACCESS

Edited by:

Doris D. Wang,
University of California,
San Francisco, United States

Reviewed by:

Ignacio Delgado Martinez,
Hospital del Mar Medical Research
Institute (IMIM), Spain
Lawrence Poree,
University of California,
San Francisco, United States

*Correspondence:

David A. Dinsmoor
david.a.dinsmoor@medtronic.com

Specialty section:

This article was submitted to
Neural Technology,
a section of the journal
Frontiers in Neuroscience

Received: 28 February 2021

Accepted: 21 June 2021

Published: 12 July 2021

Citation:

Pilitsis JG, Chakravarthy KV,
Will AJ, Trutnau KC, Hageman KN,
Dinsmoor DA and Litvak LM (2021)
The Evoked Compound Action
Potential as a Predictor for Perception
in Chronic Pain Patients: Tools
for Automatic Spinal Cord Stimulator
Programming and Control.
Front. Neurosci. 15:673998.
doi: 10.3389/fnins.2021.673998

Objectives: Spinal cord stimulation (SCS) is a drug free treatment for chronic pain. Recent technological advances have enabled sensing of the evoked compound action potential (ECAP), a biopotential that represents neural activity elicited from SCS. The amplitudes of many SCS paradigms – both sub- and supra-threshold – are programmed relative to the patient's perception of SCS. The objective of this study, then, is to elucidate relationships between the ECAP and perception thresholds across posture and SCS pulse width. These relationships may be used for the automatic control and perceptually referenced programming of SCS systems.

Methods: ECAPs were acquired from 14 subjects across a range of postures and pulse widths with swept amplitude stimulation. Perception (PT) and discomfort (DT) thresholds were recorded. A stimulation artifact reduction scheme was employed, and growth curves were constructed from the sweeps. An estimate of the ECAP threshold (ET), was calculated from the growth curves using a novel approach. Relationships between ET, PT, and DT were assessed.

Results: ETs were estimated from 112 separate growth curves. For the postures and pulse widths assessed, the ET tightly correlated with both PT ($r = 0.93$; $p < 0.0001$) and DT ($r = 0.93$; $p < 0.0001$). The median accuracy of ET as a predictor for PT across both posture and pulse width was 0.5 dB. Intra-subject, ECAP amplitudes at DT varied up to threefold across posture.

Conclusion: We provide evidence that the ET varies across both different positions and varying pulse widths and suggest that this variance may be the result of postural dependence of the recording electrode-tissue spacing. ET-informed SCS holds promise as a tool for SCS parameter configuration and may offer more accuracy over alternative approaches for neural and perceptual control in closed loop SCS systems.

Keywords: evoked potential, closed-loop (CL), neuromodulation, perception, spinal cord stimulation, pain

INTRODUCTION

Spinal cord stimulation (SCS) – the precise, targeted delivery of electrical energy to the spinal cord for drug-free chronic pain control – has been an important tool for neurosurgeons, anesthesiologists, and pain management specialists since first clinical use in 1967 (Shealy et al., 1967). For many years, the gate control theory served as the putative mechanism of action for the analgesic effects of SCS (Melzack and Wall, 1965). Later work has employed bioinformatics and proteomics to elucidate the susceptibilities of the biochemical and molecular pathways of pain to SCS (Vallejo et al., 2016; Cedeño et al., 2020; Tilley et al., 2021).

Despite advances in understanding the mechanistic effects of SCS on nociceptive pathways, clinicians are still tasked with the practical realities of programming their patients' SCS systems to achieve the desired clinical result (Sheldon et al., 2020). This process is typically an iterative endeavor between the patient and their provider. Electrodes on the stimulation leads are selected in relation to anatomical structures or loci of sensation, and stimulation amplitudes are generally set relative to perception of stimulation (Benyamin et al., 2014; Rigoard et al., 2015). The well-known postural dependencies on perception threshold must also be considered during programming (Olin et al., 1998). These dependencies apply whether or not perceptible SCS is the therapeutic intent; for instance, a given set of stimulation parameters may be sub-perception for one posture but not another. Historically, patients have been tasked with manually adjusting their stimulation parameters to account for postural shifts that result in over- or under-stimulation (Abejon et al., 2014). This burden has been eased in some instances with closed-loop SCS systems that automatically adapt stimulation parameters in response to postural shifts (Schultz et al., 2012; Kumar et al., 2018).

More recently, spinal evoked compound action potentials (ECAPs) have been studied as a direct measure of spinal cord activation that may be used to control closed-loop SCS systems (Russo et al., 2018). The spinal ECAP is described as a triphasic bipotential, the amplitude of which represents the extent of synchronous activation in the dorsal column axons in response to SCS (Parker et al., 2012). The morphology of the ECAP is influenced by the SCS pulse width employed (Chakravarthy et al., 2020). As the ECAP consists of the superposition of multiple fiber types firing together, changes in pulse width shifts the overall composition of the individual fiber types contributing to the ECAP (Anaya et al., 2020).

While recent work has considered interdependencies between SCS frequency, ECAP amplitude ($ECAP_{amp}$), and paresthesia intensity (Gmel et al., 2021), the relationship between the ECAP and perception thresholds across posture and pulse width – a critical parameter for SCS programming – have yet to be studied. In this feasibility study, therefore, we report on a novel ECAP-based estimate of neural threshold that can accurately track the perception of SCS by blending a unique set of psycho- and biophysical findings into an analytical framework. Further, we hypothesize that the availability of these measures may be used

for automated SCS parameter configuration and control, both in- and out-of-clinic.

MATERIALS AND METHODS

In this feasibility study, spinal ECAPs and perception thresholds were collected from clinical research subjects undergoing commercial SCS trials. The ECAP recordings were then processed to reduce residual stimulation artifact and estimate $ECAP_{amp}$. Next, the $ECAP_{amp}$ were plotted as a function of stimulation current on growth curves; key neurophysiologic attributes were calculated by fitting these plots to a unique closed-form expression of the growth curve. Finally, a novel measure of neural activation was calculated from the growth curves and related to the subjects' perception of the SCS. These relationships were assessed across the SCS pulse width and the subjects' postures. A more detailed treatment of these steps is provided below.

Leads, Stimulating, and Recording System

A custom research system capable of both delivering balanced, biphasic stimulation and recording the ECAP elicited from the stimulation was utilized in this study. The system was configured to interface with commercially available, 8-electrode, 60 cm long percutaneous SCS leads (Model 977D260, Medtronic plc). Briefly, the system consists of an isolated, clinical-grade stimulator (Digitimer DS5) and amplifier (Digitimer D440). The ECAPs and associated stimulation artifact are digitized and stored off-line for further processing (Biopac MP160). Both the performance – pre-clinical and clinical – and design of the research system are detailed more fully elsewhere (Chakravarthy et al., 2020).

Clinical Data Acquisition

This study was a non-significant risk feasibility trial assessing the effects of stimulation parameters, electrode choice, activity, and processing methods on ECAP estimation. All human clinical work for this single-site, multi-surgeon, US based study was approved by Western Institutional Review Board (WIRB study #1188981) and was conducted in accordance with the Declaration of Helsinki. Written informed consent from each subject was obtained.

Included in this analysis are fourteen ambulatory subjects already undergoing a commercial trial to assess the suitability of SCS as an aid in the management of chronic, intractable pain of the trunk and/or limbs, including unilateral or bilateral pain. Subjects received no specific treatment as a result of their participation in this study and consequently there was no control group. The sample size used here ($N = 14$) was consistent with, or exceeded that, used by others ($N = 16$ and $N = 5$) when assessing the spinal ECAP and perception thresholds (Parker et al., 2012; Gmel et al., 2021). Each subject had two partially overlapping, staggered leads placed near T9 and spanning about three vertebral levels; the exact lead placement was at the clinical discretion of the implanting physician and was selected to optimize paresthesia coverage. While others have reported placing leads linearly when recording spinal ECAPs

(Parker et al., 2012), a partially overlapping, staggered midline placement is most consistent with contemporary lead placement practice (Kapural et al., 2015). At the end of the commercial trial and just prior to lead removal, the subject's leads were connected to the research system. Spinal ECAPs were acquired from each subject across a selection of postures (seated, supine, right and/or left lateral recumbency, standing) and stimulation pulse widths (60, 90, and 120 μ s) at a common frequency of 50 Hz. The stimulation frequency was fixed to avoid introducing frequency variability as a confounder on the perception and ECAP measures acquired in this study (Gmel et al., 2021). Given the ability of the subject to comfortably adopt certain postures, not all postures and pulse width combinations were tested with each subject.

The stimulation itself was delivered on a single lead in a tripolar (guarded cathode) configuration (Sankarasubramanian et al., 2011) at either end of the lead with bipolar recording electrodes assigned to the opposite end. The stimulation tripole location (cephalad or caudal) was selected per subject preference; in some instances, both configurations were used. For each stimulation recording, stimulation was gradually ramped up from 0 mA slowly over about a minute in 0.1 mA increments until the subject reported a perception of stimulation (the perception threshold, or PT). The stimulation was then ramped up further until the subject reported discomfort (the discomfort threshold, or DT). Here, DT was defined as the point at which the subject would not want to experience the stimulation for more than a half-minute. These ramped deliveries of SCS with associated biopotential recording are referred to as “growth curve sweeps” herein. Recording sessions were kept under 2 h to limit subject fatigue. All measurements and data analyses were performed identically between subjects; no specific randomization or investigator blinding was otherwise employed. Following data

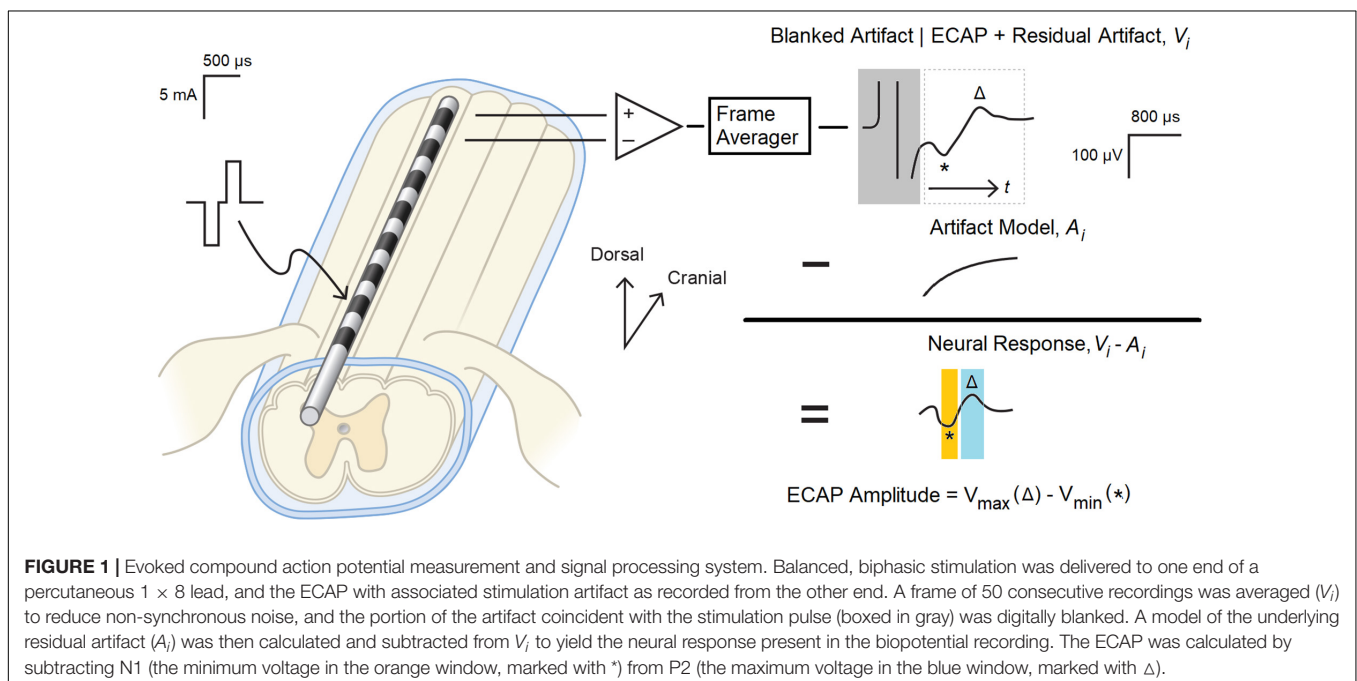
collection, the subjects' leads were disconnected from the research system.

Artifact Reduction and ECAP Estimation Methods

Artifact reduction is an important consideration for ECAP estimation, as waveforms recorded from the spinal cord may be partially corrupted by stimulation artifact (Parker et al., 2012; Chakravarthy et al., 2020). The application of an appropriate artifact reduction scheme is particularly important when assessing small amplitude ECAPs close to the perceptual threshold. Artifact reduction helps limit misclassification of non-physiologic biopotentials as “true” neural signal by the ECAP estimator. Prior to subsequent analysis, therefore, the acquired biopotentials were first averaged to reduce non-synchronous noise and then processed to reduce stimulation artifact as shown in **Figure 1**. All signal processing in this manuscript was performed with MATLAB (MathWorks, Natick, MA, United States).

First, consecutive frames of 50 evoked responses from each growth curve sweep were averaged (a window of 1 s, given the 20 ms period between the 50 Hz stimulation pulses) to produce a voltage waveform $V_i(t)$, with “ t ” representing time elapsed since the end of the stimulus plus 200 μ s. The “ i ” in the above expression is the frame index. The 200 μ s delay was chosen to blank out the artifact that manifests coincident with the delivery of the stimulation pulse (**Figure 1**, upper right).

After averaging, an artifact modeling method was utilized to minimize the artifact while recovering the neural response. The estimate of artifact $A(t)$ was obtained by optimally fitting equation $A(t) = c_1 \exp\left(\frac{t}{\tau}\right) + c_2 t + c_3$ to the data $V_i(t)$ by determining parameters c_1, c_2, c_3, τ . After the artifact model was



determined, the $ECAP_{amp}$ was then subsequently estimated as a difference (in μV) between the P2 and N1 features of the ECAP appearing in the denoised waveform $V_i - A_i$ (Figure 1, middle right). N1 was defined as the minimum amplitude of the filtered waveform in the temporal window from 0.3 to 0.6 ms, while P2 was defined as the maximum amplitude in the temporal window from 0.7 to 1.1 ms (Figure 1, lower right). These temporal windows were set given the anticipated latencies and morphological characteristics of the ECAP (Parker et al., 2012).

The Growth Curve and an Associated Closed-Form Expression

The growth curve or growth function may be defined as the relationship between the stimulation current and the estimate of neural activation as quantified with an ECAP; the threshold is defined as the intercept of the linear portion of the curve with the x -axis (Adenis et al., 2018). A substantially linear response is seen above threshold for growth curves acquired in the spine (Parker et al., 2012) with ideally no neural response apparent below threshold. A hypothetical example of such a growth curve is shown in Figure 2, Curve A. Here, the $ECAP_{amp}$ is plotted as a function of the stimulation current (I_{stim}). Below threshold (picked arbitrarily at 4 mA), no ECAP is observed. Above threshold, the $ECAP_{amp}$ grows linearly at 15 $\mu V/mA$. The entire growth curve may be described completely with just two parameters: the x -axis intercept (I_{thr}), and the slope (S_{resp}) of the suprathreshold component that represents the extent of neural activation.

Two important differences exist between the ideal growth curve described above and those observed clinically, however.

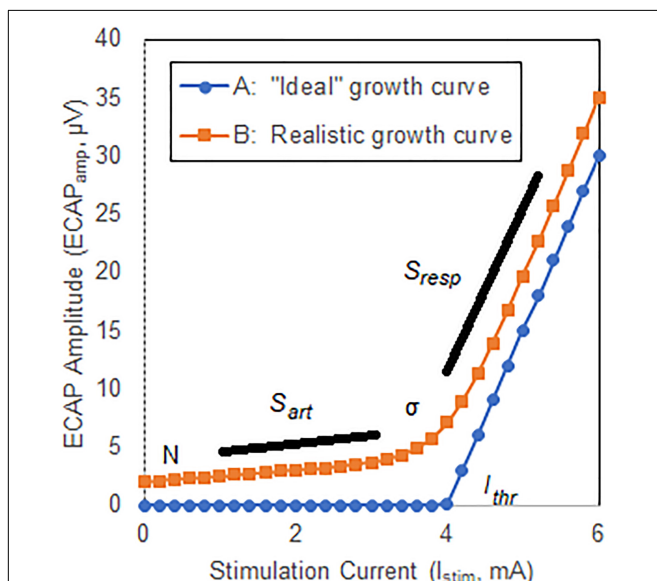


FIGURE 2 | Illustrative ECAP growth curves. Curve A shows an “ideal” case where no neural activation is present up to a threshold I_{thr} , at which point the neural response grows linearly with a slope S_{resp} . Curve B shows a more representative model that includes curvature, σ , near neural threshold, and misclassification of stimulation artifact as neural response.

First, there is a substantial curvilinear component near threshold; neural activation does not instantaneously transition from zero to linear growth once a threshold is crossed. Second, a non-physiologic component of the ECAP estimate that grows linearly with increasing stimulation current – generally attributable to misclassification of stimulation artifact as ECAP – may manifest below threshold. The extent of this latter effect depends on the degree by which the signal chain rejects artifact and preserves neural response. Both these effects are shown in another hypothetical example in Figure 2, Curve B. First, a smooth transition from no neural activation to the linear response modeled with S_{resp} is introduced by means of parameter σ (described below) which is set in this example at 0.3 mA. Second, the growth curve consists of the “pure” neural activation of Figure 2, Curve A but also includes contribution from stimulation artifact misclassified as ECAP. Here, the artifact grows linearly with a slope (S_{art}) of 0.5 $\mu V/mA$. An offset N of 2 μV is also included.

For analysis purposes, then, a five-parameter equation is introduced that captures the contribution of both stimulation artifact and the underlying neural signal with associated curvature near threshold to the overall growth curve. Such an equation is shown here:

$$ECAP_{amp}(I_{stim}) = R(I_{stim}, I_{thr}, \sigma) \cdot S_{resp} + I_{stim} \cdot S_{art} + N$$

As described above, S_{resp} models the rate of growth of the response in the linear region, while S_{art} relates to rate of growth of the artifact with current. N captures the contribution of residual noise. The neural growth curve component $R(I, I_{thr}, \sigma)$ is modeled as follows:

$$R(I_{stim}, I_{thr}, \sigma) = \left(\sigma \ln \left(\exp \left(-\frac{I_{stim} - I_{thr}}{\sigma} \right) + 1 \right) + (I_{stim} - I_{thr}) \right)$$

The shape of $R(I, I_{thr}, \sigma)$ relates to the cumulative distribution of fiber thresholds in the dorsal columns, while I_{thr} and σ characterize the spreading of current between the stimulating electrodes and the dorsal column fibers. The utility of these equations lies with the potential to gain insight into the underlying neural electrophysiology and associated phenomena by analysis of the constituent components driving the morphology of the growth curve.

Perception and the ECAP Threshold – A Novel Growth Curve Derived Measure of Neural Threshold

The ECAP threshold (ET) – a novel measure defined here for relating the ECAP to PT in the subsequent analysis – may be calculated from the expressions developed in Section “The Growth Curve and an Associated Closed-Form Expression” as:

$$ET = I_{thr} - G \sigma,$$

with G equal to 1.5.

The basis for this equation relates to selecting a point in the neural growth curve $R(I, I_{thr}, \sigma)$ where (1) only a few fibers are excited [i.e., $R(ET, I_{thr}, \sigma)$ is

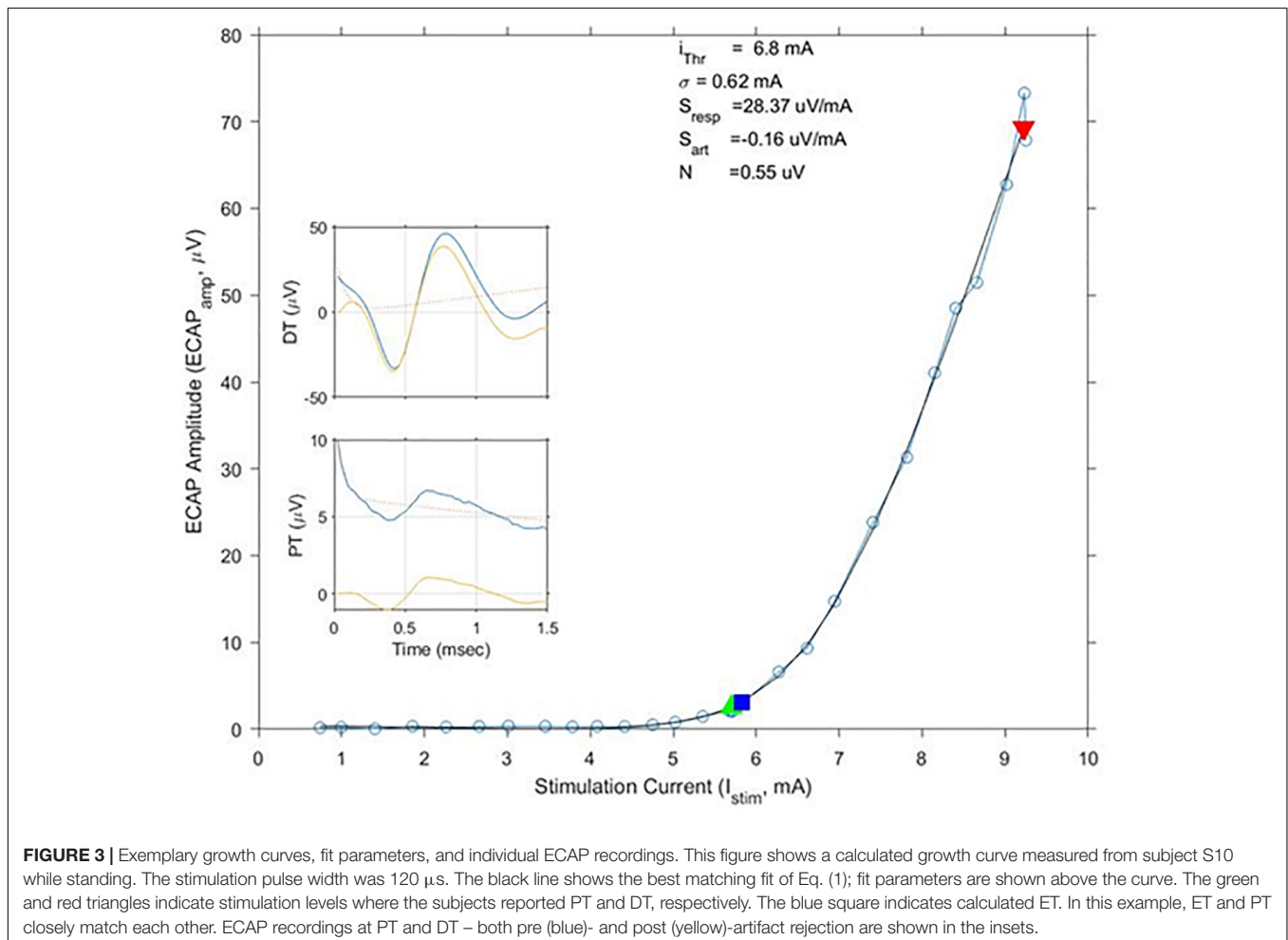
close to zero], and (2) the distribution of nerve fibers $R'(ET, I_{thr}, \sigma) = \frac{1}{\left(\exp\left(-\frac{ET - I_{thr}}{\sigma}\right) + 1\right)} = 1/(\exp(-G) + 1)$ is independent of I_{thr} and σ . Regarding the first point, the perceptual threshold corresponds to excitation of only a few sensory fibers in many neural systems (Delgutte, 1990; Lobarinas et al., 2013; Tinsley et al., 2016). The second point is motivated by the observation that the current from the electrodes travels between the stimulation electrodes and fibers in the dorsal columns through, and is shunted by, the CSF (Anaya et al., 2020). The CSF thickness is dependent on anatomy of the patient as well as patient's posture. Conceptually, the thicker the CSF, the smaller the proportion of current that is coupled into the dorsal columns. Thus, one may reasonably assume parameters I_{thr} and σ are dependent on patient posture and anatomy. By selecting ET where $R'(ET, I_{thr}, \sigma)$ becomes independent of these parameters, a point on the growth curve may be selected where underlying excitation of the dorsal columns is constant. While the above considerations are satisfied for any $G \gg 1$, the optimal value for G (set to 1.5 in this analysis) was selected by sweeping this parameter and finding the value that maximizes the match between the ET and the psychophysical data.

Similar consideration is also relevant to the electrodes allocated for sensing. While emphasis in the literature is generally on spacing variation between the stimulating electrodes and the cord (Parker et al., 2012), variation between the sensing electrodes and the cord must be considered too. The above approach serves conceptually to desensitize the sensing electrodes as well to the anticipated posture and anatomical variation.

In this paper, growth curves from the clinically acquired sweeps – following denoising and artifact reduction – were fit to Eq. (1) by optimally adjusting parameters I_{thr} , σ , S_{art} , S_{resp} and N . ETs were then calculated from these growth curves using Eq. (3) with $G = 1.5$. The relationships between ET, PT, and DT across posture and pulse width were plotted.

RESULTS

The average age of the 14 subjects was 55.9 ± 12.3 years old with 7 females and 7 males. A total of 113 growth curves were obtained from the subjects, and ECAP responses could be estimated in 112 cases. The fit of the growth curves to Eq. (1) was extremely strong ($r = 0.997$; $p < 0.0001$). Two examples of the fit along with the extracted parameters are shown in **Figure 3**. **Figure 4**



shows the relationship between ET, PT, and DT across all postures and pulse widths tested. **Figure 5** shows a subset of the data in **Figure 4** for a single test condition (90 μ s stimulation pulse width while seated). The variability of each individual subject's PT and ET is shown in **Figure 6**. Finally, **Figure 7** shows an example of the extent of variation in $ECAP_{amp}$ seen at a single condition (DT) across posture.

Relating ET, PT, and DT for the Group

As evidenced in **Figure 4**, strong correlations were exhibited between both ET and PT ($r = 0.93$; $p < 0.0001$, $N = 112$), and ET and DT ($r = 0.93$; $p < 0.0001$, $N = 108$). Fewer data sets are included with the ET and DT comparison since DT was not obtainable in some configurations. A subset of the data from **Figure 4** was plotted separately in **Figure 5**; namely, those data sets where stimulation was delivered with a single pulse width (90 μ s) while seated. This was done to assess whether other trends manifested when posture and pulse width were controlled. These results again exhibit ET as highly predictive of both PT ($r = 0.98$; $p < 0.0001$) and DT ($r = 0.96$; $p < 0.0001$).

Recognizing that changes in both posture and pulse width result in changes to perception threshold (Cameron and Alo, 1998; Abejon et al., 2014), **Figure 6**

examines the utility of ET to track changes in PT within individual subjects. Since subjects may differ widely in their average PT (**Figure 5**), the data for each individual subject was normalized by dividing PTs obtained for a given posture/pulse width combination by the average PT obtained across all combinations. The same operation was performed on ET. Thus, **Figure 6** shows the intra-subject relationships between PT and ET in decibels across posture and pulse width. Subject 7 was not included in **Figure 6**, as only two conditions were tested in this subject.

Intra-Subject ET, PT, and DT Relationships

Consistent with prior literature, large changes in PT were frequently observed across the postures assessed. Among the subjects, the largest relative change was seen in subject S02; a postural change from prone to supine position resulted in a change of approximately 12 dB. The supine position was not measured in every subject due to time constraints and subject comfort. In circumstances where it was assessed, however, it was typically associated with the lowest PT. As reported previously, PTs generally increased with decreasing pulse widths, with lowest PTs associated with 120 μ s and highest PTs with 60 μ s.

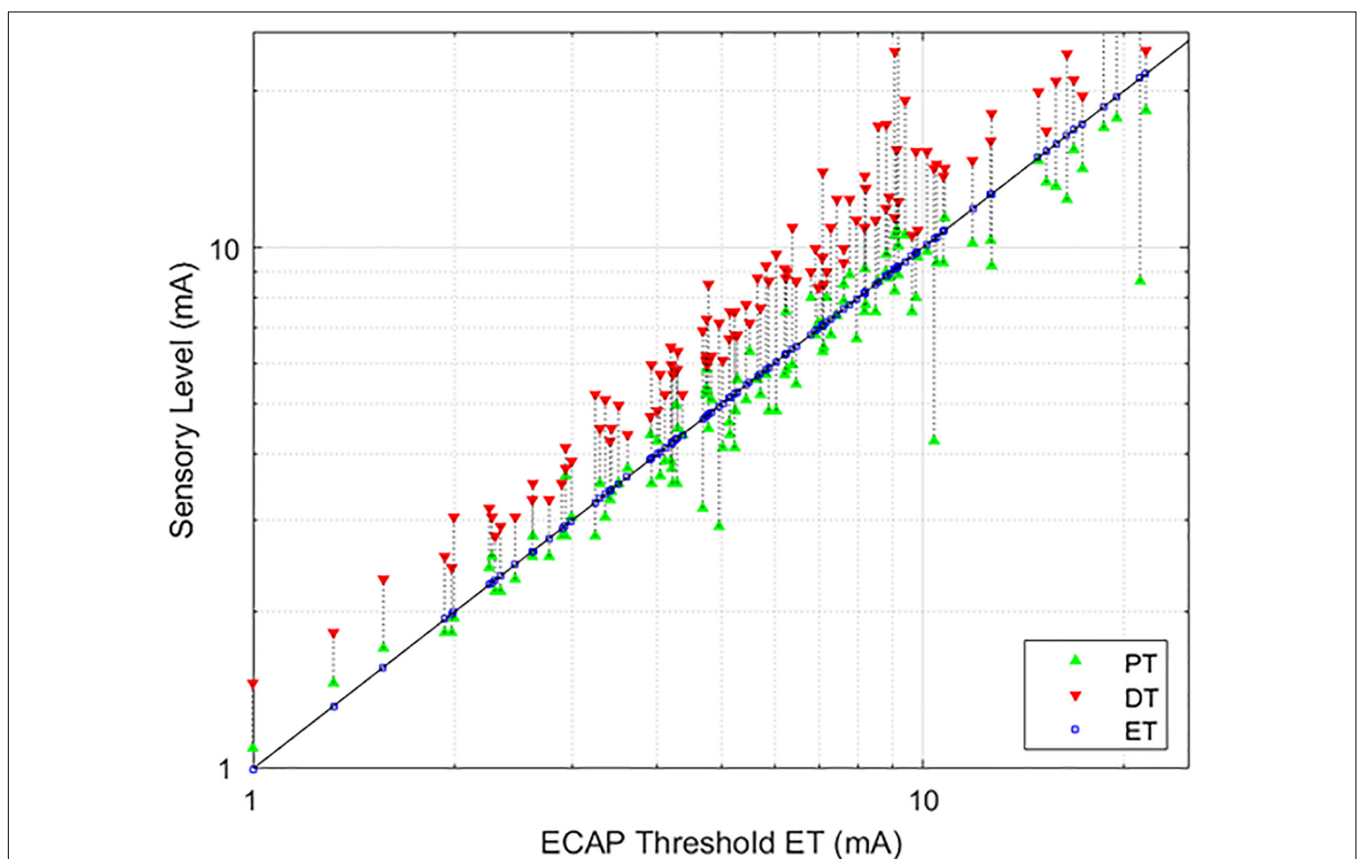


FIGURE 4 | Relationships between PT and DT as a function of ET. The stimulation currents resulting in PT (green, upwards triangle) and DT (red, downwards triangle) are plotted with respect to ET; ET is also marked with a blue square for ease of reference. A green triangle without a corresponding red triangle indicates cases where DT could not be measured. In these circumstances, the required current was in excess of the maximum stimulation setting (25 mA) of the research system.

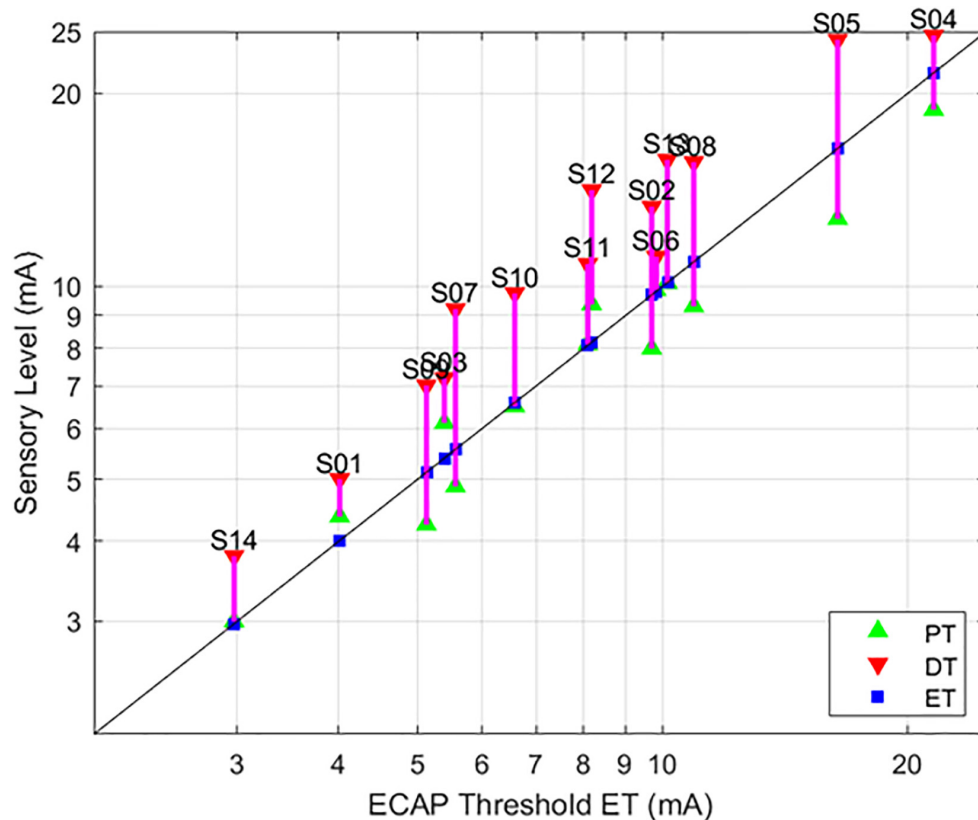


FIGURE 5 | Relationships between PT and DT as a function of ET, with 90 μ s stimulation while seated. This figure – incorporating a subset of data from **Figure 4** – serves to illustrate the tight correlation between ET and the sensory measures employed here when posture and stimulation pulse width are controlled. The sensory measures were averaged if the subject was tested in the same condition multiple times.

Changes in ET closely correlated to changes in PT within subjects, with an overall correlation between relative ET and PT of 0.91 ($p < 0.001$). Except for subject S05, this correlation was significant for all subjects with r levels between 0.75 and 0.99. In addition, the correlation was higher than 0.95 for 9 of 13 subjects. When treating ET as a predictor of DT across various conditions, the ET predicted change in DT within 0.5 dB (median, 95% confidence interval 0.4–0.6 dB obtained by bootstrapping). The accuracy in predicting changes to PT due to posture was 0.5 dB (0.3–0.6 dB) and 0.5 dB (0.4–0.6 dB) for 90 and 120 μ s pulse widths, respectively. In addition, even when PTs changed substantially when subjects were asked to return to a particular posture from a different one (an example of which is included in **Figure 7**), ET was able to closely track the changes in PT.

DISCUSSION

ET and PT Across Posture and Pulse Width

Others have previously reported that posture affects the ECAP (Parker et al., 2012). However, this is the first report describing the use of the neural threshold estimate, ET, to relate the ECAP

to two clinically relevant findings about perception with posture and stimulation pulse width. First, the ET may be used to both accurately track changes in PT across patients, as well as predict changes in intra-subject PT variation with postural shift. In addition, we report the novel observation that PT and ET can vary across the same nominal posture by as much as 5 dB in some subjects. Second, the ET tracks perceptual changes associated with different pulse widths. The second finding is particularly important as various pulse widths may differentially excite particular fiber populations or volumes of neural activation in the dorsal columns (Holsheimer et al., 2011); the ability to optimize pulse width setting based on ECAPs may offer an additional programming option for patients who seek best pain relief.

This variability reported above appears subject dependent, with subjects S04 and S14 exhibiting large changes in PT and ET for the same nominal posture. Conversely, subjects S03 and S10 were very consistent across posture. It is possible that the leads were still somewhat mobile since the subjects were studied at the end of their commercial SCS trial or that anatomical factors such as spinal canal width or CSF thickness played a role. Further, the postural variability reported may or may not be representative of variability observed after permanent implantation and several months of use. Postural dependencies on stimulation perception

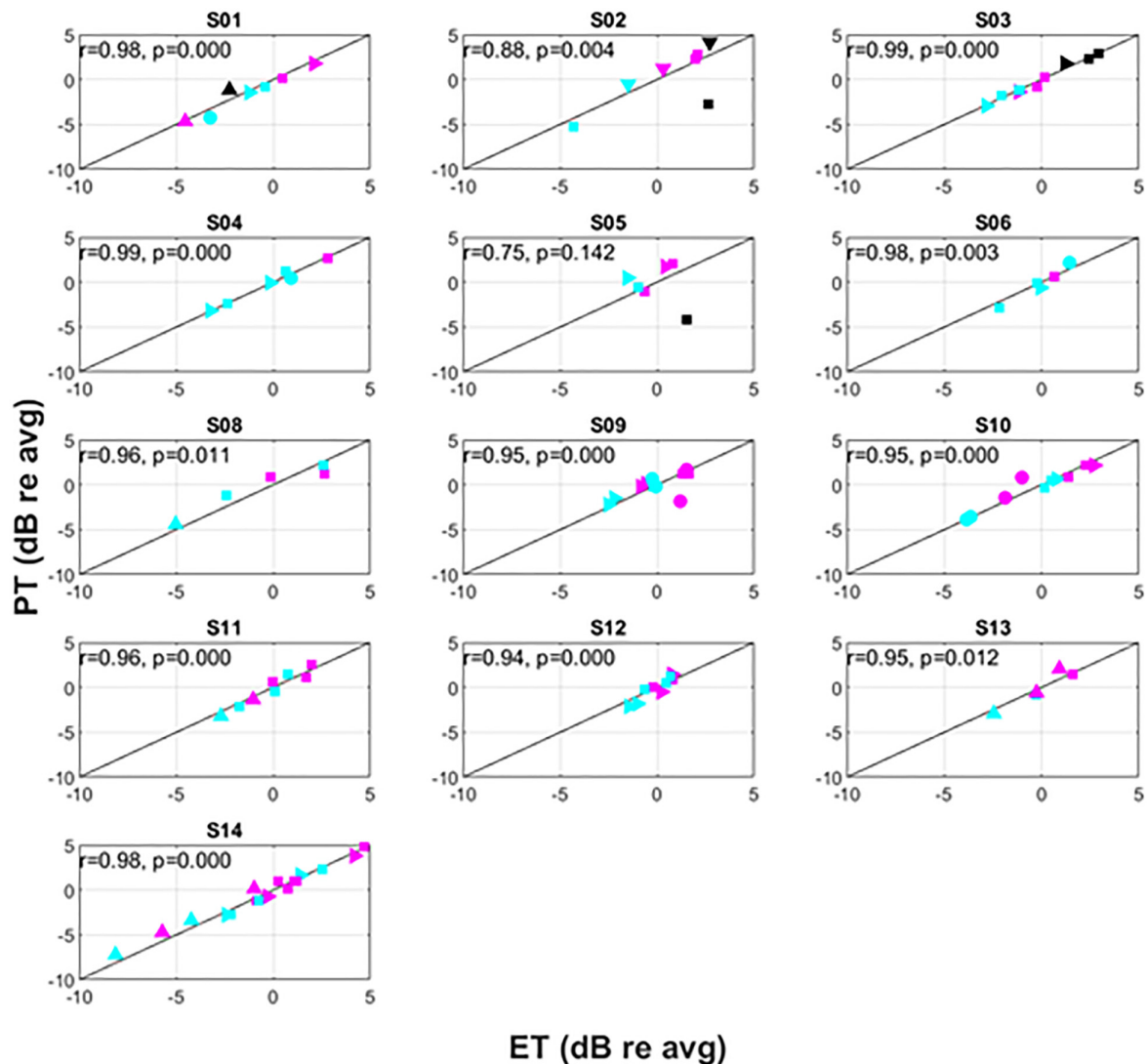


FIGURE 6 | Intra-subject variation of PT versus ET. The symbols correspond to different postures as follows: supine (Δ), prone (▽), right lateral recumbency (▷), sitting (◻), standing (○). The colors correspond to pulse widths as follows: 60 μs (black), 90 μs (magenta), 120 μs (cyan).

are observed even in long-term (e.g., 4 year) SCS users, however (Cameron and Alo, 1998).

Clinical Considerations for ET and Closed-Loop SCS

The measurement of ET involves capturing the ECAP growth curve. Accurate assessment of ET hinges on an ECAP estimation scheme – particularly near the “knee” of the growth curve, where σ is calculated – that is robust against misclassification of artifact as true neural signal. In 112 out of 113 cases, the growth curve could be measured at levels below those that were uncomfortable, suggesting the practicality of measuring ECAP growth curves either in-clinic or out-of-clinic with an implanted device. Even in the present study where stimulation was increased slowly to allow the subject

to report PT and DT, the median sweep time was 46 s; the measurement can be further optimized for clinical use by utilization of adaptive procedures to rapidly estimate ET (Nehmé et al., 2014).

Previous reports of spinal ECAP sensing with associated closed-loop control focused on the utility of $ECAP_{amp}$ as a feedback control variable for SCS (Russo et al., 2018). This report proposes the alternative measure of ET as a basis for both SCS control and perception-referenced parameter configuration. The application of the ET here – versus simply $ECAP_{amp}$ – is potentially advantageous, owing to the desensitization of the system to the growth curve variability with perception presented in this manuscript. For closed-loop SCS systems with real-time stimulation control, system operation near the perceptual threshold approximates the performance of ET as a feedback control variable without the burden of assessing ET via repeated

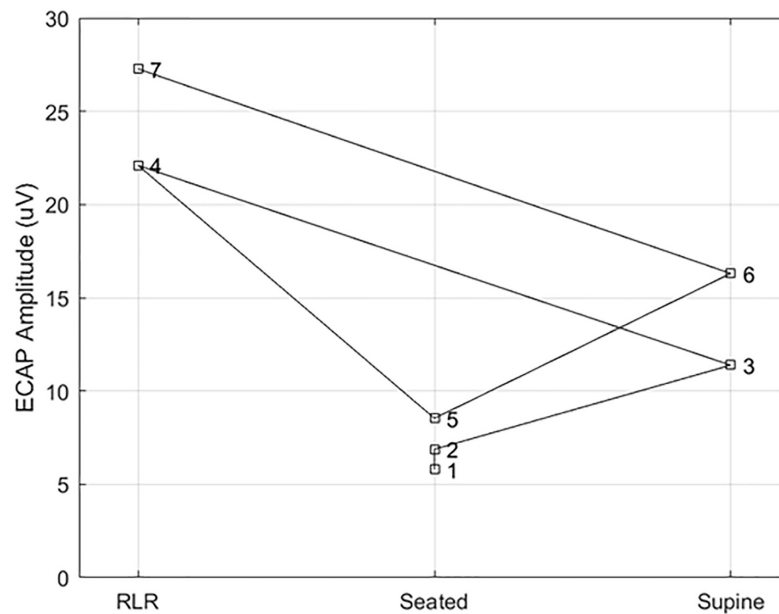


FIGURE 7 | Example ECAP variability at a fixed point of perception across posture. Here, the ECAP amplitude at a fixed point of perception – in this case, the discomfort threshold – was assessed in subject S14 multiple times across three different postures (right lateral recumbency, seated, and supine). A stimulation pulse width of 90 μ s was used in all cases, with the number by each marker indicating the measurement order. The ECAP measurements taken at DT for a given posture are within 5 μ V of each other; however, the ECAP measurement corresponding to DT varies widely from posture to posture.

acquisition of the growth curve. Again, however, this benefit is only realized if the system is not susceptible to misclassification of artifact as neural activation. Yet another option may be to use a posture sensor that automatically selects different $ECAP_{amp}$ as the feedback control variable for a closed-loop SCS system.

To better illustrate the comparative benefit of ET-informed SCS configuration and control, consider **Figure 7**. This example shows the $ECAP_{amp}$ at DT for subject S14 in the right lateral recumbency (RLR), seated, and supine positions. The ECAP measurements taken at DT for a given posture are within 5 μ V of each other; however, the ECAP measurement corresponding to DT differed by almost a factor of 3 between the RLR and seated positions. Thus, if the stimulation amplitude was configured to produce an ECAP of 15 μ V, such stimulation would be comfortable (sub-DT) in the RLR position but uncomfortable (supra-DT) in the seated position. These findings suggest that caution is warranted when using closed-loop SCS that relies on stability of the $ECAP_{amp}$, particularly across postures. On the other hand, ET tightly tracks ($r = 0.98$; $p < 0.0001$) the almost 4 DB of variation seen for repeated PT measurement in the same posture (**Figure 6** bottom panel). If the therapeutic intent is an even perception of stimulation, the ET may offer potential as a feedback control variable for a closed-loop system.

A complete treatment of the biophysical phenomena driving ECAP variability with postural change is not provided here. As discussed in Section “Perception and the ECAP Threshold – A Novel Growth Curve Derived Measure of Neural Threshold,” though, the recording electrodes are expected to change their relative position to the spinal cord much like the stimulating electrodes do across posture and motion. Accordingly, the

$ECAP_{amp}$ variability seen with postural change may not be attributable solely to variable stimulation current coupling to the neural tissue. This theoretical argument agrees with our observation that the constant $ECAP_{amp}$ associated with comfortable stimulation in one posture may still result in uncomfortable perception in other postures.

Limitations

Several limitations exist with this single-site feasibility study. First, lead position differed among subjects and the anatomical features relevant to perception – such as CSF thickness and spinal canal width – were not controlled between subjects. As this study occurred at the end of a commercial SCS trial, there was not an opportunity for post-trial imaging beyond x-ray. In future work, we will obtain post-procedure CT/MRI to better assess these co-variables. Second, a limited of set pulse widths were studied. This analysis relied on small amplitude ECAP detection at the edge of perception. Even with the robust stimulation artifact reduction scheme employed here, shorter pulse widths were utilized to limit opportunity for artifact misclassification by the $ECAP_{amp}$ estimator (Chakravarthy et al., 2020). Third, all testing was performed in-clinic under controlled experimental settings; different assessments of perception may be offered by the subjects if they were at home and engaged in everyday activities. Finally, the same parameter sets were not tested in each subject; this was primarily driven by time and comfort limitations of the subjects. Despite the limitations listed above, the analysis of the 112 growth curves acquired from the 14 subjects provides valuable insight for further research into the interdependencies between ECAP measures, posture, and stimulation configuration.

CONCLUSION

Evoked compound action potentials hold promise as an important electrophysiologic biosignal to optimize the programming and control of SCS systems. While further clinical study is needed to assess the potential benefit of ET-informed neural threshold estimation versus other ECAP derived measures – such as *ECAP_{amp}* alone – this work demonstrates that the ET is feasible to measure and tracks perception across posture and stimulation pulse width. Collectively, these observations are of importance to clinical practice with ECAP-informed SCS systems and supports automatic SCS configuration and dose control that moves beyond the present reliance on manually acquired perception thresholds.

DATA AVAILABILITY STATEMENT

The datasets presented in this article are not readily available because the datasets are the property of Medtronic plc. Requests to access the datasets should be directed to DD.

REFERENCES

- Abejon, D., Rueda, P., Parodi, E., and Del Saz, J. (2014). Effects of movement and postural positions in spinal cord stimulation in the new rechargeable systems. *Pain Physician* 17, 345–352.
- Adenis, V., Gourévitch, B., Mamelle, E., Recugnat, M., Stahl, P., Gnansia, D., et al. (2018). ECAP growth function to increasing pulse amplitude or pulse duration demonstrates large inter-animal variability that is reflected in auditory cortex of the guinea pig. *PLoS One* 13:e0201771. doi: 10.1371/journal.pone.0201771
- Anaya, C. J., Zander, H. J., Graham, R. D., Sankarasubramanian, V., and Lempka, S. F. (2020). Evoked potentials recorded from the spinal cord during neurostimulation for pain: a computational modeling study. *Neuromodulation* 23, 64–73. doi: 10.1111/ner.12965
- Benyamin, R., Grider, J. S., Vallejo, R., Tilley, D. M., and Kaye, A. D. (2014). “Spinal cord stimulation: principles and applications,” in *Principles of Neurophysiological Assessment, Mapping, and Monitoring*, eds A. D. Kaye and S. F. Davis (New York, NY: Springer), 245–258. doi: 10.1007/978-1-4614-8942-9_21
- Cameron, T., and Alo, K. M. (1998). Effects of posture on stimulation parameters in spinal cord stimulation. *Neuromodulation* 1, 177–183. doi: 10.1111/j.1525-1403.1998.tb00014.x
- Cedeño, D. L., Smith, W. J., Kelley, C. A., and Vallejo, R. (2020). Spinal cord stimulation using differential target multiplexed programming modulates neural cell-specific transcriptomes in an animal model of neuropathic pain. *Mol. Pain* 16:1744806920964360. doi: 10.1177/1744806920964360
- Chakravarthy, K., Bink, H., and Dinsmoor, D. (2020). Sensing evoked compound action potentials from the spinal cord: novel preclinical and clinical considerations for the pain management researcher and clinician. *J. Pain Res.* 13, 3269–3279. doi: 10.2147/JPR.S289098
- Delgutte, B. (1990). Physiological mechanisms of psychophysical masking: observations from auditory-nerve fibers. *J. Acoust. Soc. Am.* 87, 791–809. doi: 10.1121/1.398891
- Gmel, G. E., Escapa, R., Parker, J., Mugan, D., Al-Kaisy, A., and Palmisani, S. (2021). The effect of spinal cord stimulation frequency on the neural response and perceived sensation in patients with chronic pain. *Front. Neurosci.* 15:625835. doi: 10.3389/fnins.2021.625835
- Holsheimer, J., Buitenweg, J. R., Das, J., De Sutter, P., Manola, L., and Nuttin, B. (2011). The effect of pulse width and contact configuration on paresthesia

ETHICS STATEMENT

The studies involving human participants were reviewed and approved by Western Institutional Review Board. The patients/participants provided their written informed consent to participate in this study.

AUTHOR CONTRIBUTIONS

JP, KC, KH, DD, and LL took part in the conception, design, analysis, and interpretation of the data. KT, AW, DD, and KH were involved in data collection. All authors have approved the submission of this manuscript.

FUNDING

The authors declare that this study received funding from Medtronic plc. The funder had the following involvement with the study: providing the research system and technical personnel, as well as financial support to Twin Cities Pain Clinic to run the study.

- coverage in spinal cord stimulation. *Neurosurgery* 68, 1452–1461. doi: 10.1227/NEU.0b013e31820b4f47
- Kapural, L., Yu, C., Doust, M. W., Gliner, B. E., Vallejo, R., Sitzman, B. T., et al. (2015). Novel 10-KHz high-frequency therapy (HF10 Therapy) is superior to traditional low-frequency spinal cord stimulation for the treatment of chronic back and leg pain: the SENZA-RCT randomized controlled trial. *Anesthesiology* 123, 851–860. doi: 10.1097/ALN.0000000000000774
- Kumar, V., Prusik, J., Lin, Y., Hwang, R., Feustel, P., and Pilitsis, J. G. (2018). Efficacy of alternating conventional stimulation and high frequency stimulation in improving spinal cord stimulation outcomes: a pilot study. *Neuromodulation* 21, 466–471. doi: 10.1111/ner.12755
- Lobarinas, E., Salvi, R., and Ding, D. (2013). Insensitivity of the audiogram to carboplatin induced inner hair cell loss in chinchillas. *Hear. Res.* 302, 113–120. doi: 10.1016/j.heares.2013.03.012
- Melzack, R., and Wall, P. D. (1965). Pain mechanisms: a new theory. *Science* 150, 971–979. doi: 10.1126/science.150.3699.971
- Nehmé, A., El Zir, E., Moukarzel, N., Haidar, H., Vanpoucke, F., and Arnold, L. (2014). Measures of the electrically evoked compound action potential threshold and slope in HiRes 90KTM users. *Cochlear Implants Int.* 15, 53–60. doi: 10.1179/1754762813Y.0000000039
- Olin, J. C., Kidd, D. H., and North, R. B. (1998). Postural changes in spinal cord stimulation perceptual thresholds. *Neuromodulation* 1, 171–175. doi: 10.1111/j.1525-1403.1998.tb00013.x
- Parker, J. L., Karantonis, D. M., Single, P. S., Obradovic, M., and Cousins, M. J. (2012). Compound action potentials recorded in the human spinal cord during neurostimulation for pain relief. *Pain* 153, 593–601. doi: 10.1016/j.pain.2011.11.023
- Rigoard, P., Jacques, L., Delmotte, A., Poon, K., Munson, R., Monlezun, O., et al. (2015). An algorithmic programming approach for back pain symptoms in failed back surgery syndrome using spinal cord stimulation with a multicolumn surgically implanted epidural lead: a multicenter international prospective study. *Pain Pract.* 15, 195–207. doi: 10.1111/papr.12172
- Russo, M., Cousins, M. J., Brooker, C., Taylor, N., Boesel, T., Sullivan, R., et al. (2018). Effective relief of pain and associated symptoms with closed-loop spinal cord stimulation system: preliminary results of the avalon study. *Neuromodulation* 21, 38–47. doi: 10.1111/ner.12684
- Sankarasubramanian, V., Buitenweg, J. R., Holsheimer, J., and Veltink, P. (2011). Triple leads programmed to perform as longitudinal guarded cathodes in spinal

- cCord stimulation: a modeling study. *Neuromodulation* 14, 401–410; discussion 411. doi: 10.1111/j.1525-1403.2011.00383.x
- Schultz, D., Schultz, D. M., Webster, L., Kosek, P., Dar, U., Tan, Y., et al. (2012). Randomized trial sensor-driven position-adaptive spinal cord stimulation for chronic pain. *Pain Physician* 15, 1–12.
- Shealy, C. N., Mortimer, J. T., and Reswick, J. B. (1967). Electrical inhibition of pain by stimulation of the dorsal columns: preliminary clinical report. *Anesth. Analg.* 46, 489–491.
- Sheldon, B., Staudt, M. D., Williams, L., Harland, T. A., and Pilitsis, J. G. (2020). Spinal cord stimulation programming: a crash course. *Neurosurg. Rev.* 44, 709–720. doi: 10.1007/s10143-020-01299-y
- Tilley, D. M., Lietz, C. B., Cedeno, D. L., Kelley, C. A., Li, L., and Vallejo, R. (2021). Proteomic modulation in the dorsal spinal cord following spinal cord stimulation therapy in an in vivo neuropathic pain model. *Neuromodulation?* 24, 22–32. doi: 10.1111/ner.13103
- Tinsley, J. N., Molodtsov, M. I., Prevedel, R., Wartmann, D., Espigulé-Pons, J., Lauwers, M., et al. (2016). Direct detection of a single photon by humans. *Nat. Commun.* 7:12172. doi: 10.1038/ncomms12172
- Vallejo, R., Tilley, D. M., Cedeño, D. L., Kelley, C. A., DeMaegd, M., and Benyamin, R. (2016). Genomics of the effect of spinal cord stimulation on an animal model of neuropathic pain. *Neuromodulation?* 19, 576–586. doi: 10.1111/ner.12465
- Conflict of Interest:** JP, KC, KT, and AW are consultants for Medtronic plc. KH, DD, and LL are employees of Medtronic plc.

Copyright © 2021 Pilitsis, Chakravarthy, Will, Trutnau, Hageman, Dinsmoor and Litvak. This is an open-access article distributed under the terms of the Creative Commons Attribution License (CC BY). The use, distribution or reproduction in other forums is permitted, provided the original author(s) and the copyright owner(s) are credited and that the original publication in this journal is cited, in accordance with accepted academic practice. No use, distribution or reproduction is permitted which does not comply with these terms.



Chronic Sensing of Subthalamic Local Field Potentials: Comparison of First and Second Generation Implantable Bidirectional Systems Within a Single Subject

Daniel D. Cummins^{1†}, Ryan B. Kochanski^{2†}, Roei Gilron², Nicole C. Swann³, Simon Little⁴, Lauren H. Hammer^{4*} and Philip A. Starr^{2†}

OPEN ACCESS

Edited by:

John D. Rolston,
The University of Utah, United States

Reviewed by:

Ilknur Telkes,
Albany Medical College, United States
Konrad Ciecierski,
Research and Academic Computer
Network, Poland

*Correspondence:

Daniel D. Cummins
daniel.cummins@ucsf.edu

[†]These authors have contributed
equally to this work and share first
authorship

[‡]These authors have contributed
equally to this work and share senior
authorship

Specialty section:

This article was submitted to
Neural Technology,
a section of the journal
Frontiers in Neuroscience

Received: 15 June 2021

Accepted: 16 July 2021

Published: 10 August 2021

Citation:

Cummins DD, Kochanski RB,
Gilron R, Swann NC, Little S,
Hammer LH and Starr PA (2021)
Chronic Sensing of Subthalamic Local
Field Potentials: Comparison of First
and Second Generation Implantable
Bidirectional Systems Within a Single
Subject. *Front. Neurosci.* 15:725797.
doi: 10.3389/fnins.2021.725797

¹ School of Medicine, University of California, San Francisco, San Francisco, CA, United States, ² Department of Neurological Surgery, University of California, San Francisco, San Francisco, CA, United States, ³ Department of Human Physiology, University of Oregon, Eugene, OR, United States, ⁴ Department of Neurology, University of California, San Francisco, San Francisco, CA, United States

Background: Many adaptive deep brain stimulation (DBS) paradigms rely upon the ability to sense neural signatures of specific clinical signs or symptoms in order to modulate therapeutic stimulation. In first-generation bidirectional neurostimulators, the ability to sense neural signals during active stimulation was often limited by artifact. Newer devices, with improved design specifications for sensing, have recently been developed and are now clinically available.

Objective: To compare the sensing capabilities of the first-generation Medtronic PC + S and second-generation Percept PC neurostimulators within a single patient.

Methods: A 42-year-old man with Parkinson's disease was initially implanted with left STN DBS leads connected to a PC + S implantable pulse generator. Four years later, the PC + S was replaced with the Percept PC. Local field potential (LFP) signals were recorded, both with stimulation OFF and ON, at multiple timepoints with each device and compared. Offline processing of time series data included artifact removal using digital filtering and template subtraction, before subsequent spectral analysis. With Percept PC, embedded processing of spectral power within a narrow frequency band was also utilized.

Results: In the absence of stimulation, both devices demonstrated a peak in the beta range (approximately 20 Hz), which was stable throughout the 4-year period. Similar to previous reports, recordings with the PC + S during active stimulation demonstrated significant stimulation artifact, limiting the ability to recover meaningful LFP signal. In contrast, the Percept PC, using the same electrodes and stimulation settings, produced time series data during stimulation with spectral analysis revealing a peak in the beta-band. Online analysis by the Percept demonstrated a reduction in beta-band activity with increasing stimulation amplitude.

Conclusion: This report highlights recent advances in implantable neurostimulator technology for DBS, demonstrating improvements in sensing capabilities during active stimulation between first- and second-generation devices. The ability to reliably sense during stimulation is an important step toward both the clinical implementation of adaptive algorithms and the further investigation into the neurophysiology underlying movement disorders.

Keywords: deep brain stimulation, subthalamic nucleus, bidirectional neural interface, local field potential, beta oscillations

INTRODUCTION

Recent advancements in implantable neurostimulators have included the capability of sensing local field potentials (LFPs), offering new avenues for the understanding and treatment of movement disorders, psychiatric disease, epilepsy, and chronic pain. These bidirectional systems have potential for use in adaptive (feedback-controlled) modes of stimulation. For example, beta-band (13–30 Hz) activity within the subthalamic nucleus (STN) has been used as a control variable for adaptive DBS (aDBS) in preliminary in-clinic studies (Little et al., 2013, 2016; Velisar et al., 2019), as has theta (4–7 Hz) oscillations from the globus pallidus in cervical dystonia (Piña-Fuentes et al., 2019). Chronic use of adaptive stimulation paradigms depends on accurate sensing of neural signals during therapeutic stimulation.

Early experience with chronic sensing with a bidirectional DBS device was provided by an investigational first-generation device, Activa PC + S (Medtronic), released in 2012. This was the first fully implantable DBS device with brain sensing capabilities that was designed for continuous stimulation. In contrast, prior studies had been limited to either intraoperative recordings with microelectrodes (Holdefer et al., 2010) or postoperative studies with externalized leads (Little et al., 2013). One significant technical challenge in the early PC + S device was stimulation-induced artifact, which limited the ability to extract subcortical LFP signals during stimulation (Abosch et al., 2012; Neumann et al., 2017; Swann et al., 2018). Methods developed to remove artifacts from such signals were limited by introduction of additional low-frequency, non-stationary oscillation artifact (Dastin-van Rijn et al., 2020). While one study reported successful implementation of aDBS paradigms utilizing STN LFP recordings with stimulation ON, this required use of “distributed mode” adaptive algorithms implemented on an external computer, rather than embedded within the device (Velisar et al., 2019). These constraints challenged the clinical implementation of aDBS using this system.

The successor to the Medtronic Activa PC + S, the Medtronic Percept PC, is the first FDA-approved implantable neurostimulator for movement disorders that is capable of both stimulation and sensing of subcortical LFPs. It has multiple changes in design specifications compared to the Activa PC + S, aimed to decrease artifact and allow for more reliable sensing during active stimulation (Goyal et al., 2021). The device can stream in-clinic time series data with stimulation, visualize real-time spectral power within a 5 Hz bandwidth of interest, chronically store up to 60 days of spectral power within a 5 Hz

bandwidth of interest (one data point stored every 10 min), and store power spectra in response to patient-triggering of the device through their patient programmer. To directly compare the sensing capabilities of these two devices, we report our experience of a single PD patient treated with STN DBS who received the Percept PC neurostimulator following previous longstanding stimulation and sensing with the PC + S.

METHODS

Ethics Approval and Informed Consent

The work described was approved by the University of California, San Francisco institutional review board and informed consent was obtained from the patient prior to all data collection.

Patient

A 42-year-old man with a 4-year history of Parkinson’s disease, underwent awake, microelectrode-guided bilateral STN DBS lead (Medtronic Model 3389) placement in 2016. Lead placement in the STN was as followed: contacts 1 and 2 in the dorsal (motor) territory of the STN; contact 0 in ventral STN; and contact 3 in the white matter dorsal to STN. The left STN lead was connected to Activa PC + S through an investigational protocol (Swann et al., 2018), while the right STN lead was connected to a non-sensing Medtronic Activa SC. Pre-implantation Movement Disorder Society-Unified Parkinson Disease Rating Scale (MDS-UPDRS) III OFF-medication score was 21, characterized by predominantly right-sided motor symptoms of rigidity, resting tremor, and shuffling gait. Pre-implantation MDS-UPDRS III improved to a score of 9 (57% improvement) with levodopa challenge. Therapeutic DBS settings were: monopolar stimulation at contact 1 (second most ventral contact) with amplitude of 2.9 V (therapy current of 1.3 mA), pulse width of 60 μ s, and a stimulation frequency of 131.3 Hz. In the ON-stimulation, OFF-medication state, the patient’s MDS-UPDRS III had improved to a score of 4 at three 4 months and 3 at 6 months following the start of DBS therapy. He was also noted to have reduced his daily levodopa dose by 70% by 3 months postoperatively. In September 2020, the PC + S implantable pulse generator (at end of service for approximately 2 months) was replaced by the Medtronic Percept PC (Model B35200). Therapeutic stimulation parameters were kept nearly identical to the prior PC + S settings, utilizing a 130 Hz stimulation rate and the PC + S equivalent therapy current (PC + S is a constant-voltage device) as the

amplitude for the constant-current Percept device. The right STN remained connected to a functional non-sensing Activa SC through all recordings, and thus data from right STN was not collected. For recordings from the PC + S, right-hemisphere and left-hemisphere STN stimulation were either ON or OFF at the same time. For recordings from Percept PC, right STN stimulation was ON for all recordings (both with left-hemisphere stimulation ON and OFF).

In-Clinic Data Sampling and Processing

PC + S Data

LFP signals from the left STN were recorded by the PC + S using the two contacts adjacent to the stimulation cathode (contacts 0 and 2) at postoperative months 3, 7, and 11 following implantation. At least two 60-s recordings of data were recorded at each follow-up session while the subject was at rest, in the OFF-medication state. Signals were sampled at 800 Hz with both stimulation OFF and ON. Signals were subsequently low-pass filtered using an offline third-order low-pass Butterworth filter with a 100 Hz cutoff prior to further analysis. Power spectra were calculated using the Welch method, with a hamming window of 1 s and 50% overlap. Spectrograms were also produced with a hamming window of 1 s and 50% overlap.

Percept PC Data

Time series LFPs from the left STN were also recorded by the Percept PC using the same bipolar montage (contacts 0 and 2) on postoperative days 0 and 9 following the implantable pulse generator (IPG) replacement. The first recording with Percept PC was performed 2 h after emergence from general anesthesia. Eighteen total minutes of times series data in 25–90 s intervals were recorded while the subject was at rest, in the OFF-medication state. Signals were sampled at 250 Hz with both stimulation OFF and ON at a stimulation amplitude matching the previous PC + S settings. A stereotyped non-physiologic artifact occurring approximately every 5.8 s was removed from the signal by averaging aligned epochs encompassing the artifact to produce an artifact template, which was then subtracted from the raw

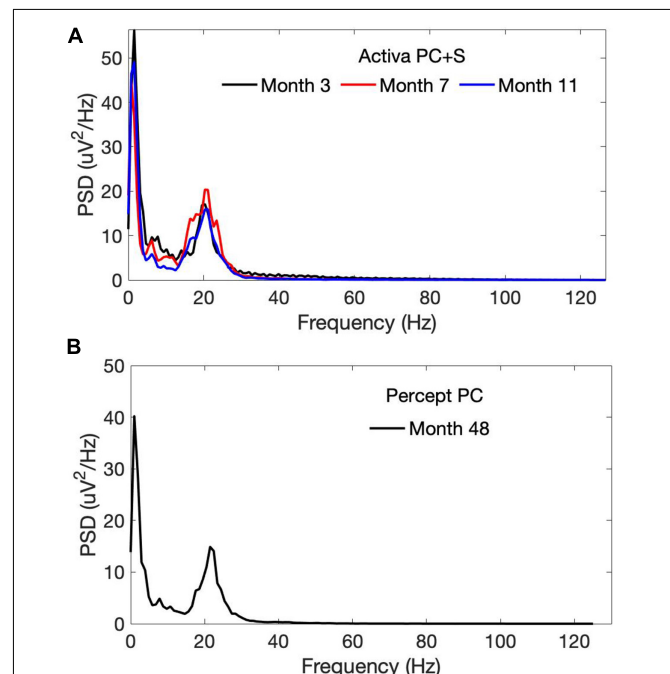
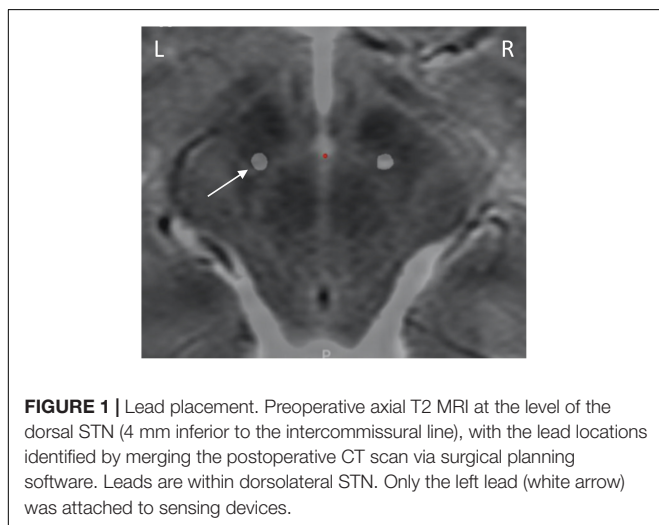
signal. Signals were processed using identical methods as those utilized for PC + S data.

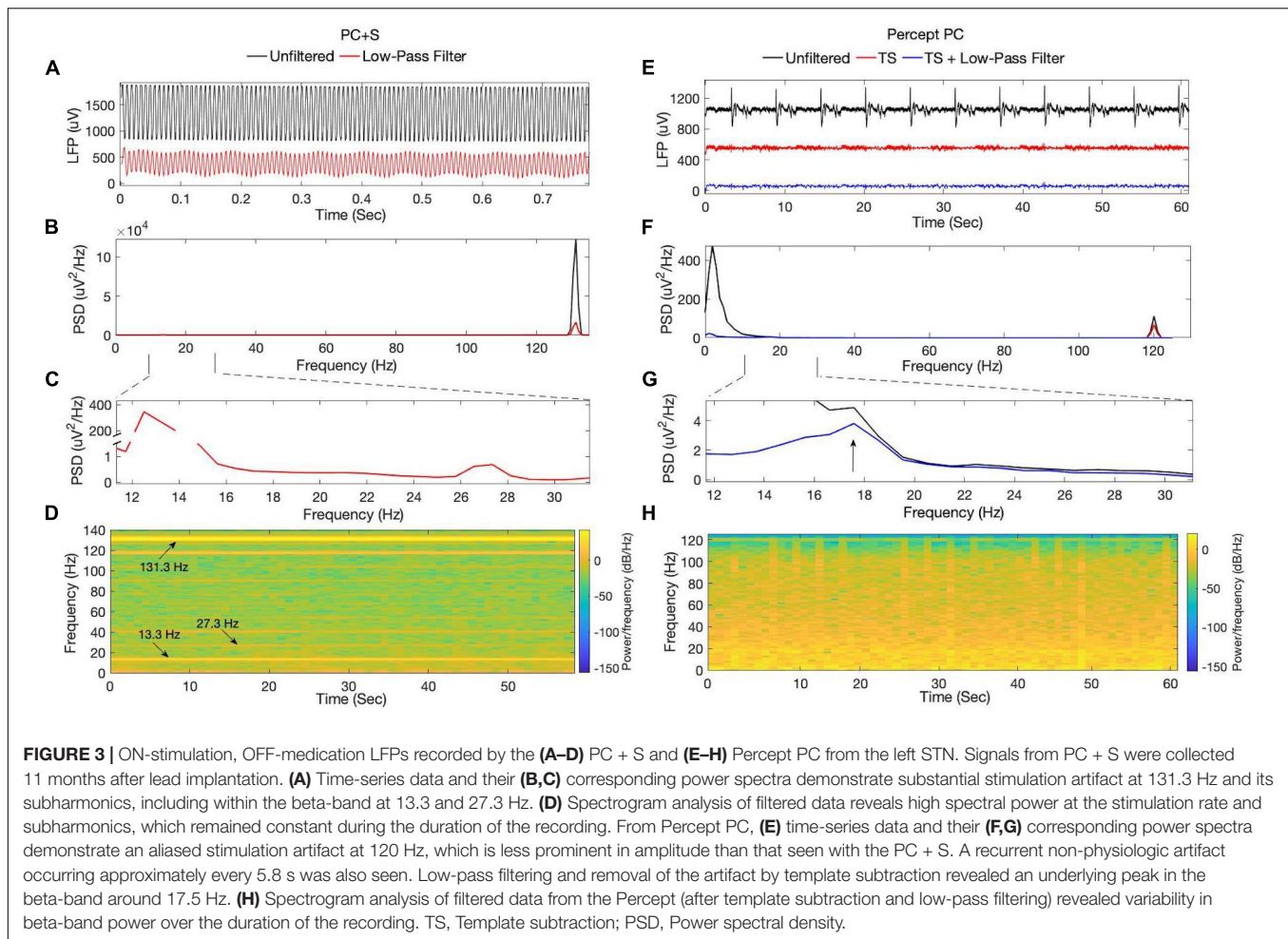
Data obtained from the Percept PC also included the power spectrum (below 96.68 Hz) of a 20-s data sample during the OFF-stimulation condition, calculated within the device and visualized on the Clinician Programmer tablet in clinic. The frequency of peak beta-band activity was noted. The Percept was then set to calculate the integrated power over a 5 Hz frequency band centered over the beta peak of interest, using consecutive non-overlapping 3-s windows of the LFP signals. This narrowband beta power was streamed to the clinician programmer along with concurrent stimulation amplitude during a clinic visit, and subsequently downloaded for analysis.

RESULTS

A postoperative computed tomography (CT) scan performed at 7 months following the original implantation was merged with preoperative magnetic resonance imaging (MRI) via StealthStation S8 planning software (Medtronic, Minneapolis, MN), which confirmed lead location within the dorsolateral STN (**Figure 1**).

OFF-stimulation, OFF-medication recordings using the PC + S demonstrated a beta-band peak at approximately 20 Hz, which persisted across longitudinal timepoints 3–11 months after initial lead implantation (**Figure 2A**). This beta peak was





also seen 4 years after initial implantation with OFF-stimulation recordings from the Percept PC (Figure 2B).

ON-stimulation recordings using the PC + S demonstrated stimulation artifact (Figures 3A–D), with substantial spectral power at the stimulation rate and multiple subharmonics (including within the beta band at 13.3 and 27.3 Hz). Use of different digital filters or steeper roll-off did not improve removal of stimulation artifact. Subharmonic frequency bands demonstrated spectral power with little variability throughout a 60 s recording at constant stimulation amplitude. No other peaks in spectral power were appreciated within the beta-band. ON-stimulation recordings using the Percept PC demonstrated less stimulation artifact (Figures 3E–H). Additionally, a non-physiologic artifact occurring approximately every 5.8 s was present (only when stimulation was switched ON, even if stimulation amplitude was 0 mA). In contrast to the PC + S, noise removal using the above-described template subtraction method and low-pass filtering revealed an underlying spectral peak in the beta-band (diminished in amplitude by therapeutic DBS, described further below).

The beta-band power calculated on-board and streamed from the Percept PC device was summed across the 5 Hz band centered at 19.53 Hz. An attenuation in beta-band activity with

increasing stimulation amplitude was seen on both recording days (Figure 4). This attenuation corresponded with a qualitative reduction in right-sided bradykinesia and rigidity.

DISCUSSION

This report highlights recent technological advances in implantable neurostimulator technology for DBS, demonstrating improved sensing capability during therapeutic stimulation, comparing second-generation with first generation devices. We evaluated the Medtronic Activa PC + S and the newer Percept PC within a single patient, with use of matched therapeutic stimulation settings and same sensing montage, providing a controlled comparison of the sensing capabilities of the two devices. The ON-stimulation recordings in our patient exemplified previously described limitations of the PC + S (Swann et al., 2018). While OFF-stimulation recordings produced LFP signals with a peak in the beta-range (Figure 2), recovery of neural signals once stimulation was turned ON at a therapeutic amplitude was limited by artifact (Figures 3A–D). Stimulation artifact produced spectral peaks at the stimulation rate and subharmonics throughout recordings from PC + S

data following filtering (**Figure 3D**). Though within the beta range, the 13.3 and 27.3 Hz content was considered artifactual (in agreement with Medtronic engineers), given the concurrent presence of other subharmonics and the lack of variability expected for dynamic physiologic bursts of beta activity (Tinkhauser et al., 2017; Lofredi et al., 2019). Subharmonic artifact could not be filtered without potentially removing underlying neural signals given the overlap in spectral content of the subharmonics and STN LFP spectral bands of interest. Conversely, the spectrogram from Percept PC in **Figure 3H** demonstrated substantially smaller stimulation artifact without subharmonics. Apart from those related to stimulation, other artifacts described in the literature include a 200 Hz artifact from internal firmware processing, a 32 Hz artifact from the device's internal clock, and electrocardiogram (ECG) artifact (Blumenfeld et al., 2017; Swann et al., 2018). These artifacts were not seen in this case.

The Percept PC is the first commercially available DBS device for movement disorders that incorporates a brain sensing capability (Neumann et al., 2017; Goyal et al., 2021; Jimenez-Shahed, 2021; Koeglsperger et al., 2021; Feldmann et al., 2021). In contrast to the PC + S, ON-stimulation LFP recordings from our patient using the Percept PC contained less stimulation artifact, which could be easily removed using simple digital filters (**Figures 3C–E**). This improvement in the sensing capabilities of

the Percept PC can be attributed to multiple changes in technical specifications compared to the PC + S (Goyal et al., 2021), that were based on experience with first-generation neurostimulators. The Percept PC employs a front-end blanking switch, which limits the temporal overlap between stimulation and sensing (sense blanking duration can be set by the clinician/researcher between 0 and 2.5 ms). Implementation of a fully differential amplifier also improves common mode noise rejection. Finally, signals are initially sampled at 100 kHz, low-pass filtered on-board the device, and subsequently down-sampled to 250 Hz for spectral analysis and output, which minimizes the risk of harmonics of the stimulation rate being aliased into frequency bands of interest.

Other sources of noise previously reported with the PC + S, arising from interactions between sampling clocks and stimulation rates, were not seen with the Percept PC (Goyal et al., 2021). ECG has remained a persistent source of artifact in many recordings from Percept PC (affecting 65.2% of left subclavicular Percept PC implants in one report, Neumann et al., 2021), though this was not seen in our patient. LFPs collected from the Percept in this patient did, however, demonstrate a repetitive artifact (**Figure 3C**) not previously described with either device. The stereotyped morphology of the artifact allowed for removal using template subtraction. It is unclear what the source of this artifact is, and has to date been unique to this

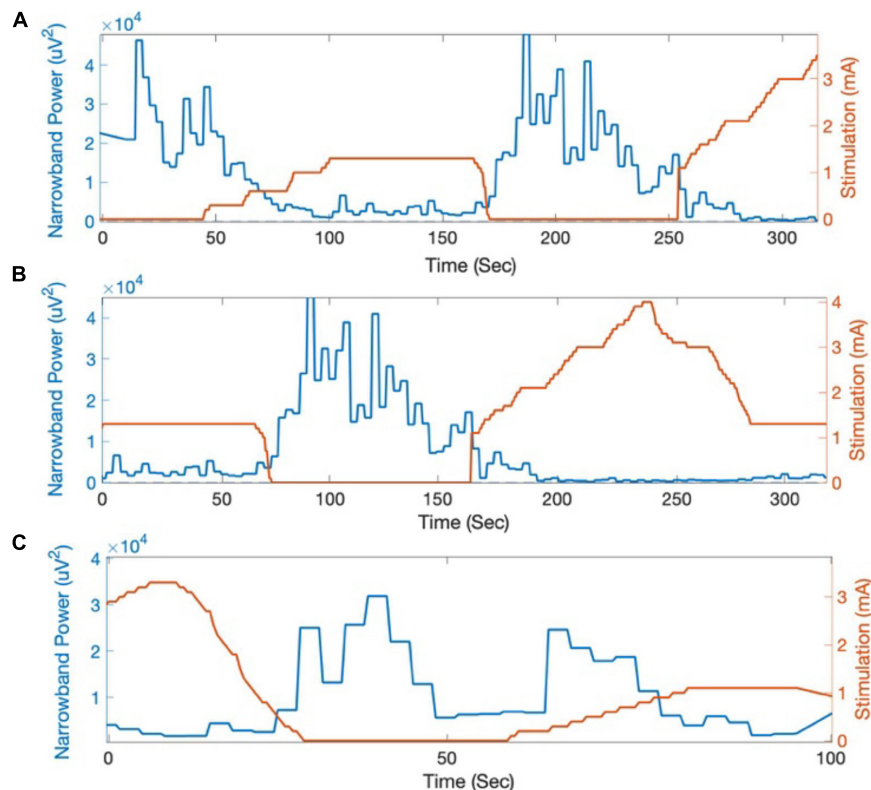


FIGURE 4 | Beta-band power (centered at 19.53 Hz) calculated on-board by the Percept PC in response to changes in stimulation amplitude. Across multiple trials at **(A,B)** day 0 and **(C)** day 9 following Percept PC implantation, beta-band activity (LFP power integrated across a 5 Hz band and averaged in 3-s intervals) reliably decreased in response to increased stimulation amplitude.

patient among those implanted with the Percept PC at our institution and in the available literature (Goyal et al., 2021; Neumann et al., 2021). This artifact was apparent both from data at postoperative day 0 (in the post-anesthesia care unit) and postoperative day 9 (in the movement disorders clinic), excluding an environmental source. The only other wearable or implantable stimulating device at the time of recordings was the patient's right-hemisphere Activa SC DBS device. STN stimulation has been documented to introduce stimulation artifact in microelectrode recordings at the contralateral STN (Novak et al., 2009). However, it is not clear if or how the right-sided stimulation by the Activa SC may cause the recurrent polyphasic artifact every 5.8 s seen with Percept PC.

LFP beta-band power has been suggested as a marker for therapeutic efficacy of DBS in Parkinson's disease (Ray et al., 2008; Neumann et al., 2017). The improved sensing during stimulation capability of Percept PC allowed for a demonstration of the reduction in LFP beta-band power as a result of active stimulation (Figure 4). Of note, this patient provides one of the first demonstrations outside of the operative setting of a reliable and durable beta-band peak persisting over 4 years of active stimulation (Figure 2; Abosch et al., 2012; Giannicola et al., 2012; Neumann et al., 2017).

As a commercial device that can be implanted without physician-sponsored regulatory approvals, the Percept PC facilitates investigations into the neurophysiology underlying movement disorders, as it is accessible to a wide number of patients and academic centers. Since it is a primary cell device and long term sensing and streaming of time series data would deplete the battery prematurely, it is less powerful as a research tool than Medtronic's second generation investigational sensing device, Summit RC + S (Stanslaski et al., 2018). Percept PC implements a single sampling rate at 250 Hz, which limits its use in exploring higher-frequency oscillations of potential significance (López-Azcárate et al., 2010; Özkurt et al., 2011). In contrast, the PC + S permitted sampling frequencies up to 800 Hz and the RC + S up to 1,000 Hz. The Percept PC also uses a passive recharge similar to that implemented in the Activa PC + S, which is associated with greater susceptibility to ECG and motion artifact than the RC + S, which offers an active recharge mode. Finally, remote, high resolution, time-domain sampling of continuous data, can

be performed with the RC + S (Gilron et al., 2021), but is not possible with the Percept PC.

Nevertheless, as a commercially available sensing device, Percept PC is an important step toward the clinical implementation of adaptive algorithms. Although its sensing capability is a standard feature of Percept PC and is commercially available now, the use of the device for adaptive DBS is not yet enabled. A multi-center clinical trial of adaptive DBS, ADAPT-PD, is currently underway using this device (Jimenez-Shahed, 2021).

DATA AVAILABILITY STATEMENT

The raw data supporting the conclusions of this article will be made available by the authors, without undue reservation.

ETHICS STATEMENT

The studies involving human participants were reviewed and approved by University of California, San Francisco (IRB number: 10-02130). The patients/participants provided their written informed consent to participate in this study.

AUTHOR CONTRIBUTIONS

SL, LH, and PS conceived the study. DC, RK, RG, and NS collected the data. DC, LH, and SL developed the data analysis plan. DC, LH, and PS drafted the manuscript and figures. All authors contributed to the article and approved the submitted version.

FUNDING

This work and manuscript was funded by the National Institutes of Health (NIH) grant UH3NS100544. This NIH grant funds research on patients with Parkinson's Disease implanted with the Medtronic PC + S and RC + S devices.

REFERENCES

- Abosch, A., Lanctin, D., Onaran, I., Eberly, L., Spaniol, M., and Ince, N. F. (2012). Long-term recordings of local field potentials from implanted deep brain stimulation electrodes. *Neurosurgery* 71, 804–814. doi: 10.1227/NEU.0b013e3182676b91
- Blumenfeld, Z., Koop, M. M., Prieto, T. E., Shreve, L. A., Velisar, A., Quinn, E. J., et al. (2017). Sixty-hertz stimulation improves bradykinesia and amplifies subthalamic low-frequency oscillations. *Mov. Disord.* 32, 80–88. doi: 10.1002/mds.26837
- Dastin-van Rijn, E. M., Provenza, N. R., Calvert, J. S., Gilron, R., Allawala, A. B., Darie, R., et al. (2020). Uncovering biomarkers during therapeutic neuromodulation with PARRM: period-based artifact reconstruction and removal method. *Neuroscience* 2021:100010. doi: 10.1101/2020.10.02.322743
- Feldmann, L. K., Neumann, W.-J., Krause, P., Lofredi, R., Schneider, G.-H., and Kühn, A. A. (2021). Subthalamic beta band suppression reflects effective neuromodulation in chronic recordings. *Eur. J. Neurol.* 28, 2372–2377. doi: 10.1111/ene.14801
- Giannicola, G., Rosa, M., Servello, D., Menghetti, C., Carrabba, G., Pacchetti, C., et al. (2012). Subthalamic local field potentials after seven-year deep brain stimulation in Parkinson's disease. *Exp. Neurol.* 237, 312–317. doi: 10.1016/j.expneurol.2012.06.012
- Gilron, R., Little, S., Perrone, R., Wilt, R., de Hemptinne, C., Yaroshinsky, M. S., et al. (2021). Long-term wireless streaming of neural recordings for circuit discovery and adaptive stimulation in individuals with Parkinson's disease. *Nat. Biotechnol.* 1–8. doi: 10.1038/s41587-021-00897-5 [Epub ahead of print].
- Goyal, A., Goetz, S., Stanslaski, S., Oh, Y., Rusheen, A. E., Klassen, B., et al. (2021). The development of an implantable deep brain stimulation device with simultaneous chronic electrophysiological recording and stimulation in humans. *Biosens. Bioelectron.* 176:112888. doi: 10.1016/j.bios.2020.112888
- Holdefer, R. N., Cohen, B. A., and Greene, K. A. (2010). Intraoperative local field recording for deep brain stimulation in Parkinson's disease

- and essential tremor. *Move. Disord.* 25, 2067–2075. doi: 10.1002/mds.23232
- Jimenez-Shahed, J. (2021). Device profile of the percept PC deep brain stimulation system for the treatment of Parkinson's disease and related disorders. *Exp. Rev. Med. Devices* 18, 319–332. doi: 10.1080/17434440.2021.1909471
- Koeglsperger, T., Mehrkens, J. H., and Bötzel, K. (2021). Bilateral double beta peaks in a PD patient with STN electrodes. *Acta Neurochir.* 163, 205–209. doi: 10.1007/s00701-020-04493-5
- Little, S., Beudel, M., Zrinzo, L., Foltynie, T., Limousin, P., Hariz, M., et al. (2016). Bilateral adaptive deep brain stimulation is effective in Parkinson's disease. *J. Neurol. Neurosurg. Psychiatry* 87, 717–721. doi: 10.1136/jnnp-2015-310972
- Little, S., Pogossyan, A., Neal, S., Zavala, B., Zrinzo, L., Hariz, M., et al. (2013). Adaptive deep brain stimulation in advanced Parkinson disease. *Ann. Neurol.* 74, 449–457. doi: 10.1002/ana.23951
- Lofredi, R., Tan, H., Neumann, W.-J., Yeh, C.-H., Schneider, G.-H., Kühn, A. A., et al. (2019). Beta bursts during continuous movements accompany the velocity decrement in Parkinson's disease patients. *Neurobiol. Dis.* 127, 462–471. doi: 10.1016/j.nbd.2019.03.013
- López-Azcárate, J., Tainta, M., Rodríguez-Oroz, M. C., Valencia, M., González, R., Guridi, J., et al. (2010). Coupling between beta and high-frequency activity in the human subthalamic nucleus may be a pathophysiological mechanism in Parkinson's disease. *J. Neurosci.* 30, 6667–6677. doi: 10.1523/JNEUROSCI.5459-09.2010
- Neumann, W.-J., Sorkhabi, M. M., Benjaber, M., Feldmann, L. K., Saryyeva, A., Krauss, J. K., et al. (2021). The sensitivity of ECG contamination to surgical implantation site in adaptive closed-loop neurostimulation systems. *BioRxiv* [Preprint]. doi: 10.1101/2021.01.15.426827
- Neumann, W.-J., Staub-Bartelt, F., Horn, A., Schanda, J., Schneider, G.-H., Brown, P., et al. (2017). Long term correlation of subthalamic beta band activity with motor impairment in patients with Parkinson's disease. *Clin. Neurophysiol.* 128, 2286–2291. doi: 10.1016/j.clinph.2017.08.028
- Novak, P., Klemp, J. A., Ridings, L. W., Lyons, K. E., Pahwa, R., and Nazzaro, J. M. (2009). Effect of deep brain stimulation of the subthalamic nucleus upon the contralateral subthalamic nucleus in Parkinson disease. *Neurosci. Lett.* 463, 12–16. doi: 10.1016/j.neulet.2009.07.040
- Özkurt, T. E., Butz, M., Homburger, M., Elben, S., Vesper, J., Wojtecki, L., et al. (2011). High frequency oscillations in the subthalamic nucleus: A neurophysiological marker of the motor state in Parkinson's disease. *Exp. Neurol.* 229, 324–331. doi: 10.1016/j.expneurol.2011.02.015
- Piña-Fuentes, D., van Zijl, J. C., van Dijk, J. M. C., Little, S., Tinkhauser, G., Oterdoom, D. L. M., et al. (2019). The characteristics of pallidal low-frequency and beta bursts could help implementing adaptive brain stimulation in the parkinsonian and dystonic internal globus pallidus. *Neurobiol. Dis.* 121, 47–57. doi: 10.1016/j.nbd.2018.09.014
- Ray, N. J., Jenkinson, N., Wang, S., Holland, P., Brittain, J. S., Joint, C., et al. (2008). Local field potential beta activity in the subthalamic nucleus of patients with Parkinson's disease is associated with improvements in bradykinesia after dopamine and deep brain stimulation. *Exp. Neurol.* 213, 108–113. doi: 10.1016/j.expneurol.2008.05.008
- Stanslaski, S., Herron, J., Chouinard, T., Bourget, D., Isaacson, B., Kremen, V., et al. (2018). A chronically implantable neural coprocessor for investigating the treatment of neurological disorders. *IEEE Trans. Biomed. Circ. Syst.* 12, 1230–1245. doi: 10.1109/TBCAS.2018.2880148
- Swann, N. C., de Hemptinne, C., Miocinovic, S., Qasim, S., Ostrem, J. L., Galifianakis, N. B., et al. (2018). Chronic multisite brain recordings from a totally implantable bidirectional neural interface: experience in 5 patients with Parkinson's disease. *J. Neurosurg.* 128, 605–616. doi: 10.3171/2016.11.JNS161162
- Tinkhauser, G., Pogossyan, A., Tan, H., Herz, D. M., Kühn, A. A., and Brown, P. (2017). Beta burst dynamics in Parkinson's disease OFF and ON dopaminergic medication. *Brain* 140, 2968–2981. doi: 10.1093/brain/awx252
- Velisar, A., Syrkin-Nikolau, J., Blumenfeld, Z., Trager, M. H., Afzal, M. F., Prabhakar, V., et al. (2019). Dual threshold neural closed loop deep brain stimulation in Parkinson disease patients. *Brain Stimul.* 12, 868–876. doi: 10.1016/j.brs.2019.02.020

Conflict of Interest: The authors declare that the research was conducted in the absence of any commercial or financial relationships that could be construed as a potential conflict of interest.

Publisher's Note: All claims expressed in this article are solely those of the authors and do not necessarily represent those of their affiliated organizations, or those of the publisher, the editors and the reviewers. Any product that may be evaluated in this article, or claim that may be made by its manufacturer, is not guaranteed or endorsed by the publisher.

Copyright © 2021 Cummins, Kochanski, Gilron, Swann, Little, Hammer and Starr. This is an open-access article distributed under the terms of the Creative Commons Attribution License (CC BY). The use, distribution or reproduction in other forums is permitted, provided the original author(s) and the copyright owner(s) are credited and that the original publication in this journal is cited, in accordance with accepted academic practice. No use, distribution or reproduction is permitted which does not comply with these terms.



Adaptive Parameter Modulation of Deep Brain Stimulation Based on Improved Supervisory Algorithm

Yulin Zhu^{1,2}, Jiang Wang², Huiyan Li³, Chen Liu² and Warren M. Grill^{1*}

¹ Department of Biomedical Engineering, Duke University, Durham, NC, United States, ² School of Electrical and Information Engineering, Tianjin University, Tianjin, China, ³ School of Automation and Electrical Engineering, Tianjin University of Technology and Education, Tianjin, China

OPEN ACCESS

Edited by:

John D. Rolston,
The University of Utah, United States

Reviewed by:

Ryoma Morigaki,
Tokushima University, Japan
Fei Su,
Shandong Agricultural University,
China

*Correspondence:

Warren M. Grill
warren.grill@duke.edu
orcid.org/0000-0001-5240-6588

Specialty section:

This article was submitted to
Neural Technology,
a section of the journal
Frontiers in Neuroscience

Received: 31 July 2021

Accepted: 20 August 2021

Published: 16 September 2021

Citation:

Zhu Y, Wang J, Li H, Liu C and
Grill WM (2021) Adaptive Parameter
Modulation of Deep Brain Stimulation
Based on Improved Supervisory
Algorithm.
Front. Neurosci. 15:750806.
doi: 10.3389/fnins.2021.750806

Clinically deployed deep brain stimulation (DBS) for the treatment of Parkinson's disease operates in an open loop with fixed stimulation parameters, and this may result in high energy consumption and suboptimal therapy. The objective of this manuscript is to establish, through simulation in a computational model, a closed-loop control system that can automatically adjust the stimulation parameters to recover normal activity in model neurons. Exaggerated beta band activity is recognized as a hallmark of Parkinson's disease and beta band activity in model neurons of the globus pallidus internus (GPi) was used as the feedback signal to control DBS of the GPi. Traditional proportional controller and proportional-integral controller were not effective in eliminating the error between the target level of beta power and the beta power under Parkinsonian conditions. To overcome the difficulties in tuning the controller parameters and improve tracking performance in the case of changes in the plant, a supervisory control algorithm was implemented by introducing a Radial Basis Function (RBF) network to build the inverse model of the plant. Simulation results show the successful tracking of target beta power in the presence of changes in Parkinsonian state as well as during dynamic changes in the target level of beta power. Our computational study suggests the feasibility of the RBF network-driven supervisory control algorithm for real-time modulation of DBS parameters for the treatment of Parkinson's disease.

Keywords: Parkinson's disease, feedback signal, beta power, RBF neural network, supervisory control algorithm

INTRODUCTION

Parkinson's disease (PD) is a progressive neurodegenerative disorder resulting from death of dopaminergic neurons in the substantia nigra (Titcombe et al., 2001; Novikova et al., 2006; Bras et al., 2008; Jankovic, 2008; de Paor and Lowery, 2009). Deep brain stimulation (DBS), that delivers high-frequency electrical pulses via an implanted pulse generator to focal targets in the basal ganglia (BG) including the subthalamic nucleus (STN), the globus pallidus internus (GPi), or the ventrolateral thalamus (Vim), is a widely used therapy for treating PD when drug therapy such as the administration of levodopa no longer provides adequate control of symptoms (Haeri et al., 2005; Kiss et al., 2007; Vidailhet et al., 2007; Mehta and Sethi, 2009; Follett et al., 2010; Santaniello et al., 2011). Present open-loop DBS delivers invariant stimulation with parameters selected manually based solely on previous empirical evidence. Pre-programmed stimulation is applied regardless of

changes in the patient's clinical symptoms or underlying physiological activity, and open-loop DBS is limited in terms of efficacy, side effects and efficiency (Modolo et al., 2012; Popovych and Tass, 2012; Priori et al., 2012).

Optimization of stimulation parameters according to the individual and time-varying needs of patients is necessary to improve the treatment of PD (Androulidakis et al., 2008; Steiner et al., 2017). Several studies suggested that closed-loop DBS is an effective approach to improve therapeutic efficacy while limiting side effects and prolonging battery life (Doshi et al., 2003; Rosin et al., 2011; Little et al., 2013; Wu et al., 2015). Inspired by successful clinical use of closed-loop stimulation based on ECoG recordings in the treatment of epilepsy, this approach was initially adopted for DBS parameter modulation where the stimulation signal was switched on when beta oscillatory power exceeded a pre-set threshold in a primate model of PD (Little et al., 2013) and was subsequently extended to a dual threshold algorithm (Velisar et al., 2019). The design of closed-loop DBS, which uses a feedback signal and real-time adjustment of stimulation parameters, is considered the next frontier in the field of neuromodulation (Pizzolato and Mandat, 2012; Broccard et al., 2014; Hebb et al., 2014; Arlotti et al., 2016a; Swann et al., 2018).

A range of challenges are associated with closed-loop DBS including detectable control signals that are stable and robust in the long term (Little and Brown, 2012; Hoang et al., 2017; Steiner et al., 2017), understanding the relationship between patient states and brain control signals (Buzsáki et al., 2012), closed-loop control algorithms for automatic adjustment of stimulation parameters (Pirini et al., 2009; Guo and Rubin, 2011; Gorzelic et al., 2013), and comparisons of open-loop versus closed-loop DBS and clarification of their underlying mechanisms (Parastarfeizabadi and Kouzani, 2017). Therefore, the objective of this manuscript is to develop a computational model-based closed-loop scheme to adjust automatically the stimulation parameters for suppressing abnormal oscillatory activity in the BG. Local field potential (LFP) signals directly recorded from the DBS electrode appear to be a promising source of feedback signals (Mazzoni et al., 2015), and beta-band oscillations in the LFP are related to bradykinesia and rigidity in persons with PD (Beudel et al., 2017; Rosa et al., 2017; Deffains and Bergman, 2019; Lofredi et al., 2019; Montgomery, 2020). Here, a biophysically-based computational network model serves as the plant for the design of closed-loop control systems, from which LFP signals are obtained to simulate clinically detectable and recordable signals.

The highly nonlinear dynamics of the cortex-basal ganglia-thalamus network make the selection of controller parameters a substantial challenge (Kumaravelu et al., 2016). For traditional proportional-integral-derivative (PID) control, it is difficult to select appropriate controller gains, and the dependence on the precise mathematical model of the plant means that control accuracy cannot be guaranteed (Su et al., 2019). Neural network control has several potential advantages in this application. First, the capacity of neural network controllers to represent arbitrary functions avoids the complex mathematical analysis required for traditional adaptive control theory. In addition to modeling the complex and non-linear plant, neural networks can also act as the controller and continuously adjust the internal connection

weights according to learning rules to minimize a given performance index. Thus, a supervisory control method based on radial basis function (RBF) neural networks was developed in this manuscript. In section "Materials and Methods," we introduce the feedback signal selected for closing the loop of DBS and detail the design of the closed-loop control system. The control effects of a traditional controller and the intelligent supervisory controller are analyzed and compared in section "Results," and the results are discussed in section "Discussion." The proposed algorithm adaptively produced effective stimulation signals in response to changes in the state (plant) and the reference (target) signal.

MATERIALS AND METHODS

Cortical-Basal Ganglia-Thalamus Network Model

A biophysically-based model of the cortex-basal ganglia-thalamus network (Kumaravelu et al., 2016), modified from the original Rubin-Terman model (Rubin and Terman, 2004), was adopted as a platform to develop and evaluate the controllers. The model included representations of neurons in cortex (CTX), striatum (STR) [sum of direct striatum (dSTR) and indirect striatum (idSTR)], STN, globus pallidus (GP) (sum of externa part GPe and interna part GPi) and thalamus (TH), and all the nuclei were interconnected through either excitatory or inhibitory synaptic connections to form a network. Each nucleus contained 10 single-compartment model neurons (Figure 1).

The neurons of the STN, GP, TH, and STR were modeled using Hodgkin-Huxley (HH) type equations:

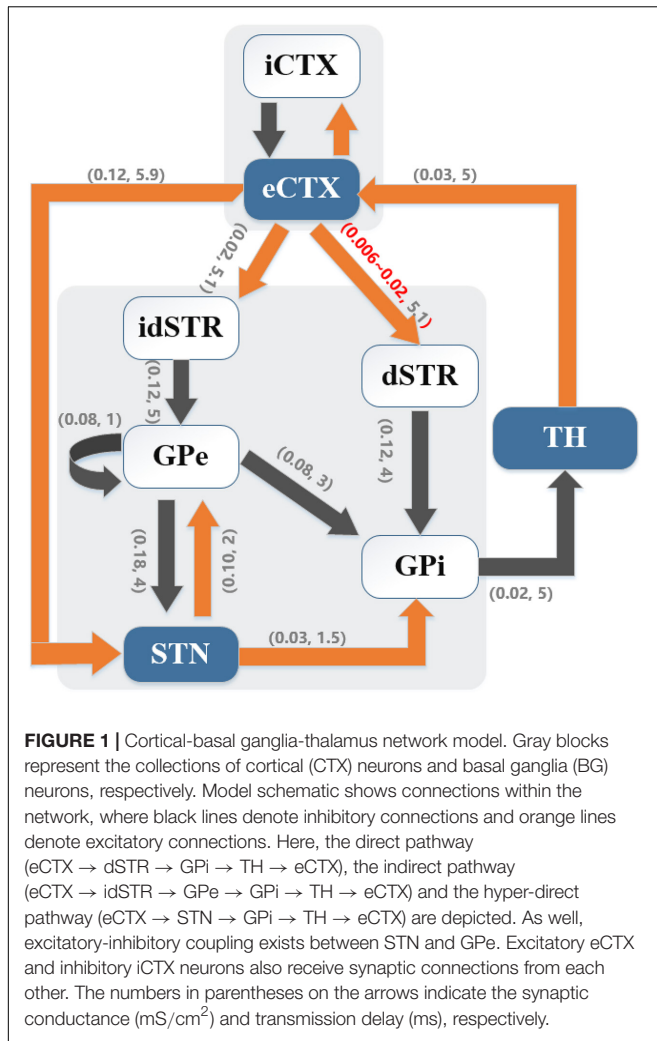
$$\begin{aligned} C \frac{dv_{STN}}{dt} &= -I_{Na} - I_K - I_l - I_T - I_{CaK} - I_a - I_L - I_{syn} \\ C \frac{dv_{GP}}{dt} &= -I_{Na} - I_K - I_l - I_T - I_{Ca} - I_{ahp} - I_{syn} + I_{app_GP}, \\ C \frac{dv_{TH}}{dt} &= -I_{Na} - I_K - I_l - I_T - I_{syn} + I_{app_TH} \\ C \frac{dv_{STR}}{dt} &= -I_l - I_K - I_{Na} - I_m - I_{syn} \end{aligned} \quad (1)$$

where C represented the membrane capacitance and was set to $1 \mu\text{F}/\text{cm}^2$ for all cell models, v_i ($i \in \{\text{STN, GP, TH, STR}\}$) represented the transmembrane potential of the corresponding model neuron and was expressed in mV. I_{Na} , I_K , and I_l were the sodium current, potassium current and non-specific leak current, I_L , I_T , and I_{Ca} were, respectively, the L-type, T-type, and high-threshold calcium current, and I_a , I_m , I_{CaK} , and I_{AHP} were, respectively, A-type, outward M-type potassium, calcium-dependent and after-threshold potassium current. Parameters and equations of the ionic currents are provided in Table 1. Therein, a , b , c , $d1$, $d2$, h , m , n , p , q , and r were activation or inactivation variables, and the gating kinetics took the form

$$\frac{dX}{dt} = \frac{\lambda_X(X_\infty - X)}{\tau_X}, \quad (2)$$

where X represented one of a , b , c , $d1$, $d2$, h , m , n , p , q , or r . Steady-state gating variables were calculated using

$$X_\infty = \frac{1}{1 + \exp(-(v + w_X)/\sigma_X)}, \quad (3)$$



where w_X and σ_X were the half voltage and slope, respectively. Gating kinetics for STR took the form

$$\frac{dX}{dt} = \alpha_X(1 - X) - \beta_X \times X. \quad (4)$$

I_{syn} represented the sum of synaptic currents, with each projection from presynaptic neuron α to postsynaptic neuron β ($\alpha, \beta \in \{CTX, STR, STN, GP, TH\}$) given by $I_{\alpha \rightarrow \beta} = g_{\alpha, \beta} \times (v_\beta - E_{syn}) \times S$, where $g_{\alpha, \beta}$ described the maximal synaptic conductance, and E_{syn} represented the reversal potential (uniformly set as -85 mV). An alpha synapse S was used to model the synaptic dynamics

$$S = \frac{t - t_d}{\tau} \times e^{-\frac{t-t_d}{\tau}}, \quad (5)$$

where t_d was the synaptic transmission delay, and τ represented the time constant of 5 ms. Further, bias currents I_{app_i} ($i \in \{GPe, GPi, TH\}$) represented other synaptic inputs that were not described explicitly in this model.

The dynamics of the CTX neurons were described based on the model developed by Izhikevich (2003)

$$\begin{aligned} \frac{dv_{CTX}}{dt} &= 0.04 \times v_{CTX}^2 + 5 \times v_{CTX} + 140 - u_{CTX} - I_{interCTX} - I_{TH \rightarrow CTX} \\ \frac{du_{CTX}}{dt} &= a \times (0.2 \times v_{CTX} - u_{CTX}) \end{aligned} \quad (6)$$

where v_{CTX} represented the transmembrane potential and u_{CTX} was the recovery variable. The time scale of the recovery variable u_{CTX} was chosen as $a = 0.02$ and $a = 0.1$, respectively, for excitatory-CTX (eCTX) and inhibitory-CTX (iCTX) neurons. If the transmembrane potential of CTX neuron exceeded 30 mV, then v_{CTX} was set to a resting potential equal to -65 mV and u_{CTX} was set to $u_{CTX} + d$ (for eCTX, $d = 8$; for iCTX, $d = 2$). $I_{interCTX}$ represented the reciprocal synaptic current from iCTX neurons to eCTX neurons or that from eCTX neurons to iCTX neurons, and $I_{TH \rightarrow CTX}$ was the synaptic input from TH.

The Parkinsonian state was simulated by the adjustment of model parameters implemented using a parkinsonism variable, pd , where $pd = 0$ and $pd = 1$ were defined as the healthy state and full Parkinsonian state, respectively. The M-type potassium current in striatal neurons was reduced $g_m = 2.6 - 0.9 \times pd$, cortico-striatal coupling strength was decreased $g_{CTX, STR} = 0.07 - 0.044 \times pd$ and coupling strength between GPe neurons was increased $g_{GPe, GPe} = 0.0125 + 0.0375 \times pd$. To quantify the difference between the healthy and Parkinsonian states, changes of firing rates and firing patterns of model neurons were analyzed. It was considered that one neuron produced a spike or action potential once its transmembrane potential was greater than the threshold $V_{thre} = -20$ mV, with the time of crossing the threshold defined as the firing time. The average firing rates were calculated based upon the firing time during the entire simulation period. In addition, spike synchrony that characterizes the dynamic patterns in each population of model neurons was measured. Defining $v^j(t)$ as the membrane potential time course of the j th neuron from a population of n neurons, then we could average over the population $V(t) = \frac{1}{n} \sum_{i=1}^n v^i(t)$. The variance of membrane potential $v^j(t)$ and the variance of the averaged membrane potential $V(t)$ were expressed as $\sigma_{v_i}^2 = \langle [v_i(t)]^2 \rangle_t - \langle v_i(t) \rangle_t^2$ and $\sigma_V^2 = \langle [V(t)]^2 \rangle_t - \langle V(t) \rangle_t^2$, respectively ($\langle \cdots \rangle_t = \frac{1}{T} \int_0^T \cdots dt$ referred to the average value of the variables within the time of T), and the level of synchrony was calculated according to the following equation,

$$\chi = \frac{\sigma_V^2}{\frac{1}{n} \sum_{i=1}^n \sigma_{v_i}^2}, \quad (7)$$

where χ was normalized between 0 and 1, with $\chi = 0$ indicating neurons within one population fire out of sync and $\chi = 1$ indicating neurons within that population discharge synchronously.

Control Problem Description

Parkinson's disease is characterized by diverse changes in neuronal activity, and single neuron action potentials,

TABLE 1 | Equations and parameters for subthalamic nucleus (STN), globus pallidus (GP), TH, and striatum (STR) model neurons.

STN	
Ionic currents	$I_{Na} = 49m^3h(v - 60)$, $I_K = 57n^4(v + 90)$, $I_l = 0.35(v + 60)$, $I_T = 5p^2q(v - 165)$ $I_{CaK} = r^2(v + 90)$, $I_a = 5a^2b(v + 90)$, $I_L = 15c^2d_1d_2(v - 165)$
Gating kinetics	$\lambda_m = 1$, $w_m = 40$, $\sigma_m = 8$, $\tau_m = 0.2 + 3 / (1 + \exp((v + 53)/0.7))$ $\lambda_h = 1$, $w_h = 45.5$, $\sigma_h = -6.4$, $\tau_h = 24.5 / (\exp((v + 50)/15) + \exp((v + 50)/16))$ $\lambda_n = 1$, $w_n = 41$, $\sigma_n = 14$, $\tau_n = 11 / (\exp(-(v + 40)/14) + \exp(-(v + 40)/50))$ $\lambda_p = 1$, $w_p = 56$, $\sigma_p = 6.7$, $\tau_p = 5 + 0.33 / (\exp((v + 27)/10) + \exp(-(v + 102)/15))$ $\lambda_q = 1$, $w_q = 85$, $\sigma_q = -5.8$, $\tau_q = 400 / (\exp((v + 50)/15) + \exp(-(v + 50)/16))$ $\lambda_r = 1$, $w_r = -0.17$, $\sigma_r = 0.08$, $\tau_r = 2$ $\lambda_a = 1$, $w_a = 45$, $\sigma_a = 14.7$, $\tau_a = 1 + 1 / (1 + \exp((v + 40)/0.5))$ $\lambda_b = 1$, $w_b = 90$, $\sigma_b = -7.5$, $\tau_b = 200 / (\exp((v + 60)/30) + \exp(-(v + 40)/10))$ $\lambda_c = 1$, $w_c = 30.6$, $\sigma_c = 5$, $\tau_c = 45 + 10 / (\exp((v + 27)/20) + \exp(-(v + 50)/15))$ $\lambda_{d1} = 1$, $w_{d1} = 60$, $\sigma_{d1} = -7.5$, $\tau_{d1} = 400 + 500 / (\exp((v + 40)/15) + \exp(-(v + 20)/20))$ $\lambda_{d2} = 1$, $w_{d2} = -0.1$, $\sigma_{d2} = -0.02$, $\tau_{d2} = 130$
GP	
Ionic currents	$I_{Na} = 120m_\infty^3h(v - 55)$, $I_K = 30n^4(v + 80)$, $I_l = 0.1(v + 65)$, $I_T = 0.5a_\infty^3rv$, $I_{Ca} = 0.15s_\infty^2(v - 120)$, $I_{AHP} = 10 \times (v + 80) \times CA / (CA + 10)$
Gating kinetics	$w_m = 37$, $\sigma_m = 10$ $\lambda_h = 0.05$, $w_h = 58$, $\sigma_h = -12$, $\tau_h = 0.05 + 0.27 / (1 + \exp((v + 40)/12))$ $\lambda_n = 0.1$, $w_n = 50$, $\sigma_n = 14$, $\tau_n = 0.05 + 0.27 / (1 + \exp((v + 40)/12))$ $\lambda_r = 1$, $w_r = 70$, $\sigma_r = -2$, $\tau_r = 15$ $w_a = 57$, $\sigma_a = 2$ $w_s = 35$, $\sigma_s = 2$ $dCA/dt = 10^{-4} \times (-I_{Ca} - I_l - 15 \times CA)$
TH	
Ionic currents	$I_{Na} = 3m^3h(v - 50)$, $I_K = 5(0.75 \times (1 - h))^4(v + 75)$, $I_l = 0.05(v + 70)$, $I_T = 5p_\infty^2rv$
Gating kinetics	$w_m = 37$, $\sigma_m = 7$ $\lambda_h = 1$, $w_h = 41$, $\sigma_h = -4$, $\tau_h = 1 / (0.128 \times \exp(-(v + 46)/18) + 4 / (1 + \exp(-(v + 23)/5)))$ $w_p = 60$, $\sigma_p = 6.2$ $\lambda_r = 1$, $w_r = 84$, $\sigma_r = -4$, $\tau_r = 0.15 \times (28 + \exp(-(v + 25)/10.5))$
STR	
Ionic currents	$I_{Na} = 100m^3h(v - 50)$, $I_K = 80n^4(v + 100)$, $I_l = 0.1(v + 67)$ $I_m = g_m p(v + 100)$
Gating kinetics	$\alpha_m = 0.32 \times (54 + v) / (1 - \exp(-(v + 54)/4))$, $\beta_m = 0.28 \times (27 + v) / (-1 + \exp((v + 27)/5))$ $\alpha_h = 0.128 \times \exp(-(v + 50)/18)$, $\beta_h = 4 / (1 + \exp(-(v + 27)/5))$ $\alpha_n = 0.032 \times (52 + v) / (1 - \exp(-(v + 52)/5))$, $\beta_n = 0.5 \exp(-(v + 57)/40)$ $\alpha_p = 3.209 \times 10^{-4} \times (30 + v) / 1 - \exp(-(v + 30)/9)$ $\beta_p = -3.209 \times 10^{-4} \times (30 + v) / (1 - \exp(-(v + 30)/9))$

electrocorticograms, LFPs, and electroencephalograms have been considered as feedback control signals for closed-loop DBS (Hoang et al., 2017). The LFP generated by model GPi neurons was adopted as the feedback signal for closed loop control. A simple average of transmembrane potentials was adopted to calculate the LFP of the modeled population due to its ability to capture subthreshold activity and thereby reflect oscillatory phenomena (Pettersen et al., 2012; Mazzoni et al., 2015). Expression of the GPi LFP was given as

$$\text{LFP}(t) = \frac{1}{n} \sum_{i=1}^n v_{\text{GPi}_i}. \quad (8)$$

Here, $n = 10$ represented the total number of GPi neurons and v_{GPi_i} corresponded to the transmembrane potential of the i th GPi neuron. The power within particular frequency bands

of the LFP signal was determined from power spectra using the Chronux neural signal analysis package [length of moving window 1 s, step size 0.1 s and tapers in the form of [3 5] (3 is the time-bandwidth product and 5 is the number of tapers to be used)], and the beta band power was defined as the total power over 13–30 Hz.

Our goal was to design an adaptive closed-loop controller to adjust automatically the stimulation signals delivered to the model neurons of the GPi based on the beta LFP activity calculated from the model GPi neurons as the feedback control signal. We defined the stimulation signal as I_{sti} and delivered it directly to each GPi neuron, and the resulting transmembrane potential was expressed as

$$C \frac{dv_{\text{GPi}}}{dt} = -I_l - I_K - I_{Na} - I_T - I_{Ca} - I_{ahp} - I_{\text{STN} \rightarrow \text{GPi}} - I_{\text{GPe} \rightarrow \text{GPi}} - I_{\text{dSTR} \rightarrow \text{GPi}} + I_{\text{app_GPi}} + I_{\text{sti}}. \quad (9)$$

I_{sti} was constructed by using the controller output $u(t)$ to construct a variable frequency pulse train stimulation signal [amplitude of $300 \mu\text{A}/\text{cm}^2$, pulse duration of 0.3 ms and period of $1,000/u(t)$ ms (frequency of $u(t)$)]. After the end of each stimulation period, we recalculated the beta power of the LFP signal and repeated the above steps to update continuously the optimal controller output. The transmembrane potentials of model neurons in that other nuclei were unaffected by direct electrical stimulation but their activity was influenced during stimulation via either excitatory or inhibitory synaptic connections.

The classical error-based PID control law has the form

$$u_{pid}(t) = k_p e(t) + k_i \int e(t) dt + k_d \frac{de(t)}{dt}, \quad (10)$$

where $e(t) = y_d(t) - y(t)$ ($y_d(t)$ and $y(t)$ represented the beta power in LFP signals of the GPi from healthy control and controlled Parkinsonian states, respectively). The performance of the PID controller depends greatly on selecting the appropriate gains, and this can be a time-consuming manual process. As the LFP was a highly dynamic variable subject to large changes, differential action might amplify noise interference. Therefore, the differential term was omitted, and both proportional (P) and proportional-integral (PI) controllers were designed to minimize the error between the desired and measured beta band power in the LFP.

A stable self-tuning controller was designed using a dynamic RBF network. **Figure 2** is a block diagram of the RBF supervisory control system and a schematic diagram of the RBF network. The neural network-based controller acted as a feedforward controller, by building an inverse model of the controlled plant. The input layer, hidden layer and output layer determined the structure of the RBF neural network. $x = [x_1, x_2, \dots, x_i, \dots, x_n]^T$ (n was the number of input layer nodes) represented the network input vector and $h = [h_1, h_2, \dots, h_j, \dots, h_m]^T$ (m was the number of hidden layer nodes) represented the hidden layer output. Each hidden layer node had a central value c_j , the Euclidean distance of which to network input x_i was described as $\|x_i - c_j\|$. As well, each hidden layer node was an arithmetic element with activation function given by

$$h_j = \exp\left(-\frac{\|x - c_j\|^2}{2b_j^2}\right). \quad (11)$$

The center vector $c = [c_1, c_2, \dots, c_m]$ and the width vector $b = [b_1, b_2, \dots, b_m]^T$ determined the influence of the Gaussian function, where the width of the Gaussian basis function directly influenced the mapping capability to network input, while the center value correlated with its sensitivity to network input.

If we set the weight vector as $w = [w_1, w_2, \dots, w_m]^T$, then the network output can be obtained as

$$u_{rbf}(t) = h_1 w_1 + \dots + h_j w_j + \dots + h_m w_m. \quad (12)$$

The structure of the RBF network was selected as $1 - n_m - 1$, that is, containing 1 input layer node, n_m hidden layer nodes and 1 output layer node. The number of hidden layer nodes was

set to 11, network weights were initially set to random values between 0 and 1, and parameters of Gaussian function were set as $c = [-2, -1, 0, 1, 2]^T$, $b = [5, 5, 5, 5, 5]^T$. The weights of the RBF controller were continuously adjusted on-line to make the feedback error $e(t)$ approach zero, which equated to $u_p(t)$ approaching zero. Consequently, the RBF controller gradually occupied the leading position and even replaced the function of the P/PI controller. The RBF network error index was designed in the form of $E(t) = \frac{1}{2}(u_p(t) - u(t))^2$, to lead $u_p(t)$ ($e(t)$) to converge to 0. Considering that the total controller output was the sum of the traditional P/PI controller and the adaptive RBF controller $u(t) = u_{rbf}(t) + u_p(t)$, the error index can be written as

$$E(t) = \frac{1}{2} (u_{rbf}(t) - u(t))^2 \quad (13)$$

According to the gradient descent method, the network weights were adjusted as follows

$$\Delta w_j(t) = -\eta \frac{\partial E(t)}{\partial w_j(t)} = -\eta (u_{rbf}(t) - u(t)) h_j(t), \quad (14)$$

$$w(t) = w(t-1) + \Delta w(t) + \alpha(w(t-1) + w(t-2)). \quad (15)$$

Further, applying the gradient descent method to the adjustment of c and b will optimize effective learning by the RBF network, thus we had

$$\Delta b_j(t) = -\eta \frac{\partial E}{\partial b_j} = -\eta (u_{rbf}(t) - u(t)) w_j h_j \frac{\|x - c_j\|}{b_j^3}, \quad (16)$$

$$b(t) = b(t-1) + \Delta b(t) + \alpha(b(t-1) + b(t-2)), \quad (17)$$

$$\Delta c_j(t) = -\eta \frac{\partial E}{\partial c_j} = -\eta (u_{rbf}(t) - u(t)) w_j h_j \frac{x - c_j}{b_j^2}, \quad (18)$$

$$c(t) = c(t-1) + \Delta c + \alpha(c(t-1) - c(t-2)). \quad (19)$$

where $\eta \in (0, 1)$ represented the learning rate $\eta = 0.30$ and $\alpha \in (0, 1)$ represented the momentum factor $\alpha = 0.05$.

A quantitative index of the control effect was defined as the root mean square error between the controlled output and the reference signal,

$$\text{RMSE} = \sqrt{\frac{1}{N} \sum_{i=1}^N (y_i - y_d)^2} \quad (20)$$

where N represented the sampling point of the feedback signal.

RESULTS

The biophysically-based cortical-Basal-thalamus network model was used to test the effectiveness of closed-loop DBS. Performance of the RBF network-based supervisory algorithm

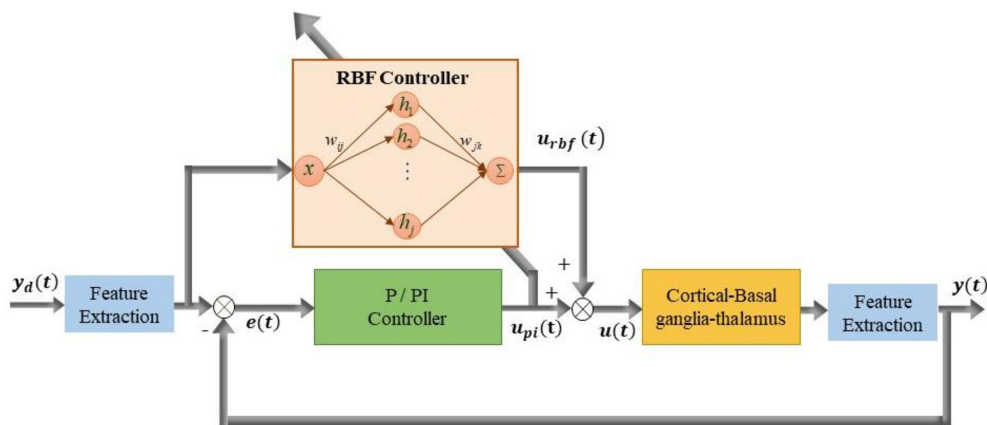


FIGURE 2 | Block diagram of improved supervisory algorithm under the guidance of radial basis function (RBF) network. Stimulation signal $u(t)$ is applied to GPi model neurons and the simulated beta power $y(t)$ is obtained from LFP of the GPi. The stimulation signal $u(t)$ is determined by the joint action of the P controller output $u_{pi}(t)$ and RBF network controller output $u_{rbf}(t)$.

was evaluated by considering changes in the state of the plant intended to represent dynamics including cycling of medication and progress of the disease, as well as dynamic changes in the reference (target) signal.

Firing Rates and Firing Patterns of Model BG Neurons

The transmembrane potentials of model GPe, GPi, and STN neurons in the cortical-Basal-thalamus network model are displayed in **Figure 3**. The Parkinsonian condition resulted in changes in both the rate and pattern of model neuron activity. As a result of excitation via the indirect pathway and hyper-direct pathway together with inhibition via the direct pathway, firing rates in the Parkinsonian condition increased in STN and GPi model neurons and decreased in GPe model neurons (**Figure 4A**), consistent with previous experimental studies (Kita and Kita, 2011). Moreover, increased spike synchrony was observed across all nuclei in the Parkinsonian state compared to the healthy state (**Figure 4B**). These indexes were analyzed using one-way analysis of variance (ANOVA), which revealed a significant difference in firing rate (STN: $F = 901$ and $p < 0.001$, GPe: $F = 48$ and $p < 0.001$, and GPi: $F = 184$ and $p < 0.001$) and synchrony index (STN: $F = 239$ and $p < 0.001$, GPe: $F = 1554$ and $p < 0.001$, and GPi: $F = 62$ and $p < 0.001$) between healthy state and Parkinsonian state. The model thus exhibited features of the pathophysiological neural activity occurring in PD and was a suitable testbed to develop and analyze closed-loop control strategies.

The GPi, which is clinically accessible for both recording of LFPs and delivery of DBS, was selected as the source of the feedback signal for closed loop DBS (**Figures 5A,B**). Compared to the healthy state, where the LFP exhibited little power in the beta band, the LFP in the Parkinsonian condition exhibited oscillatory activity, generating a significant peak in the power spectrum (**Figure 5C**). The LFP signals were filtered within the beta band to extract differences between healthy and Parkinsonian states, and the filtered GPi LFP activity in the healthy state (**Figure 5D**)

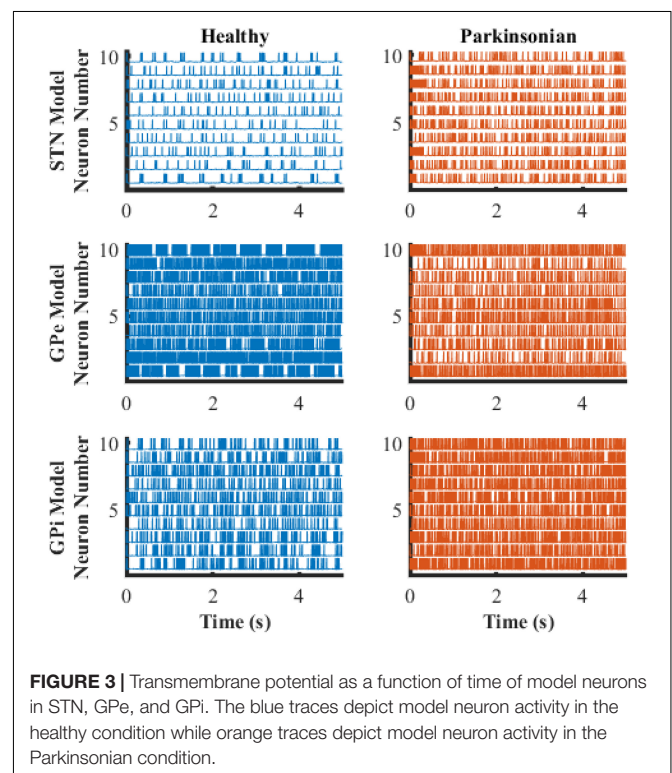


FIGURE 3 | Transmembrane potential as a function of time of model neurons in STN, GPe, and GPi. The blue traces depict model neuron activity in the healthy condition while orange traces depict model neuron activity in the Parkinsonian condition.

served as a reference to guide the modulation of Parkinsonian neural activity by DBS, thus constituting a closed-loop system to suppress exaggerated beta oscillatory activity (**Figure 5E**).

Limitation of Traditional P and PI Controllers

We first quantified the relationship between the stimulation frequency and the beta power (**Figure 6**), where $f = 0$ is equivalent to the Parkinsonian state without DBS. Low frequency stimulation actually increased beta power, and the beta power was

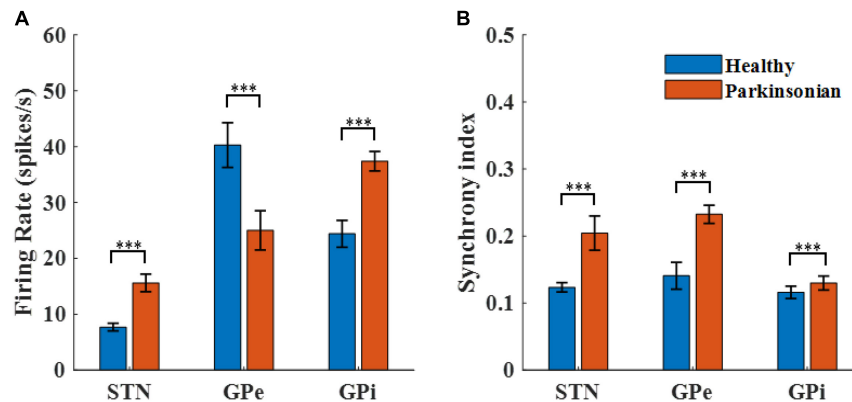


FIGURE 4 | Characterization of model neuron activity in healthy and Parkinsonian conditions. **(A)** Firing rates (mean \pm standard error) for model STN, GPe, and GPi neurons in healthy (blue) and Parkinsonian (orange) conditions. Values are averaged across three runs for each nucleus. **(B)** Spike synchrony (mean \pm standard error) for model STN, GPe, and GPi neurons under healthy (blue) and Parkinsonian (orange) conditions. All model neurons exhibit increases in spike synchrony in the Parkinsonian state as compared to the healthy state. (***) represented a significant difference, $p < 0.001$.

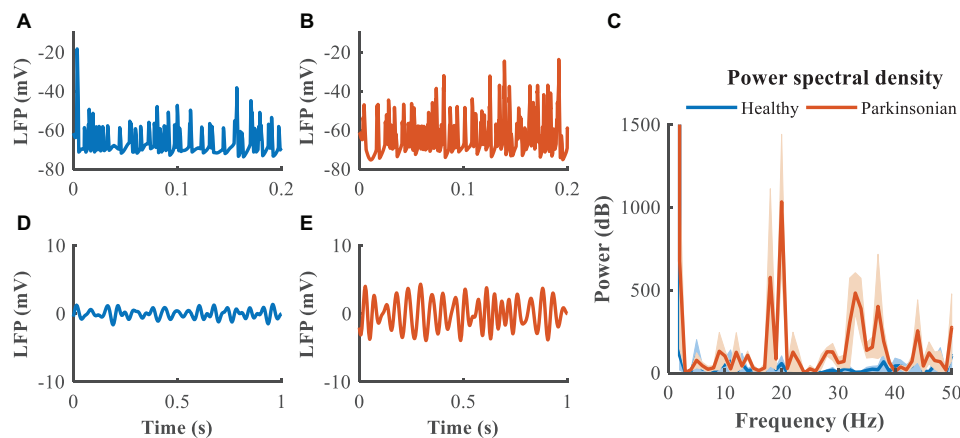


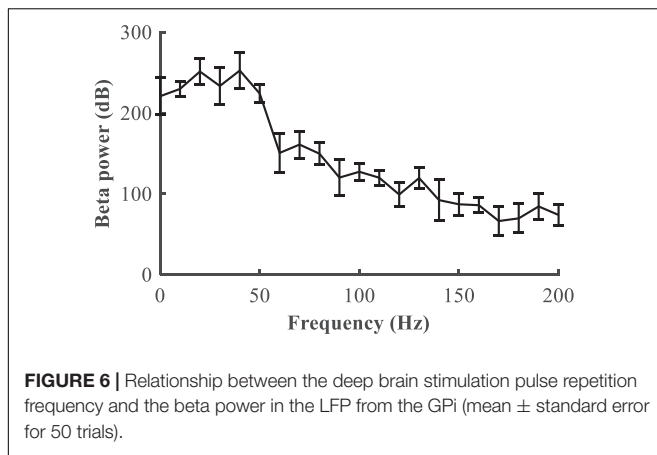
FIGURE 5 | Local field potential (LFP) activity from model neurons in the GPi. In panels **(A,B)**, blue trace depicts the LFP in the healthy state while the orange trace depicts the LFP in the Parkinsonian state. Panel **(C)** illustrates the power spectral density of the GPi LFP across 10 trials to quantify the corresponding oscillatory activity, where shaded error region represents standard errors. Panels **(D,E)** depict the band-pass filtered (13–30 Hz) LFP activity in the GPi.

progressively reduced as the stimulation frequency was increased higher than 50 Hz. A beta power of 120 dB was calculated from the healthy state and set as the desired state, and the range of stimulation frequencies was between 5 and 200 Hz. The modulation of DBS was reformulated as a train of monophasic pulses with an initial stimulation frequency of 5 Hz, and the updated stimulation frequency was generated based upon the error between the actual and target beta power in the LFP from the GPi model neurons.

The performance of the P controller and PI controller in regulating the beta band LFP in the GPi with GPi DBS were compared (**Figures 7, 8**), where the blue dotted lines represented the healthy state and the orange traces represented the controlled PD state. Small k_p appeared to make no difference to the suppression of beta band activity, while large k_p caused strong oscillations between effective and ineffective suppression of beta band activity

(**Figure 7**). The performance following addition of the integral controller with different combinations of k_p and k_i was assessed (**Figure 8**). The control of beta power in the GPi LFP was strongly dependent on the selection of k_p and k_i , where effective values ($k_p = 0.5$, $k_i = 0.5$) promoted the suppression of high beta power while ineffective values ($k_p = 0.1$, $k_i = 0.01$) did not contribute to improvement of the PD state. The search of proportional and integral gains through trial-and-error produced fluctuations in performance and created uncertainty about the effectiveness of closed-loop DBS, especially in the face of changes in the properties of the plant.

A substantial improvement in control performance was achieved by the supervisory algorithm, where suppression of the exaggerated beta power present in the Parkinsonian condition was achieved within 1 s (**Figure 9A**). The weights of the RBF network were adjusted in real-time, in response to the



update of the beta power of the GPI (**Figure 9B**). As the beta power was gradually suppressed, the RBF network took over the leading role that the P/PI controller played in the initial control stage (**Figure 9C**). Ultimately, the DBS pulse repetition frequency was calculated as shown in **Figure 9D**, and the DBS signal is depicted in **Figure 9E**. Changes in beta power between the healthy state, open-loop 130 Hz DBS, P controller, PI controller and adaptive DBS were compared by calculating the root mean square error between the controlled output signal and the reference signal during the last 4 s of simulation. The averaged RMSE were 18.64, 112.41, 39.38, and 23.89, respectively. In cases of open-loop 130 Hz DBS, P control ($k_p=0.1$), PI control ($k_p=0.5, k_i=0.5$) and combined P and RBF control, indicating that the improved supervisory algorithm drive the beta power to the target setting with a higher accuracy.

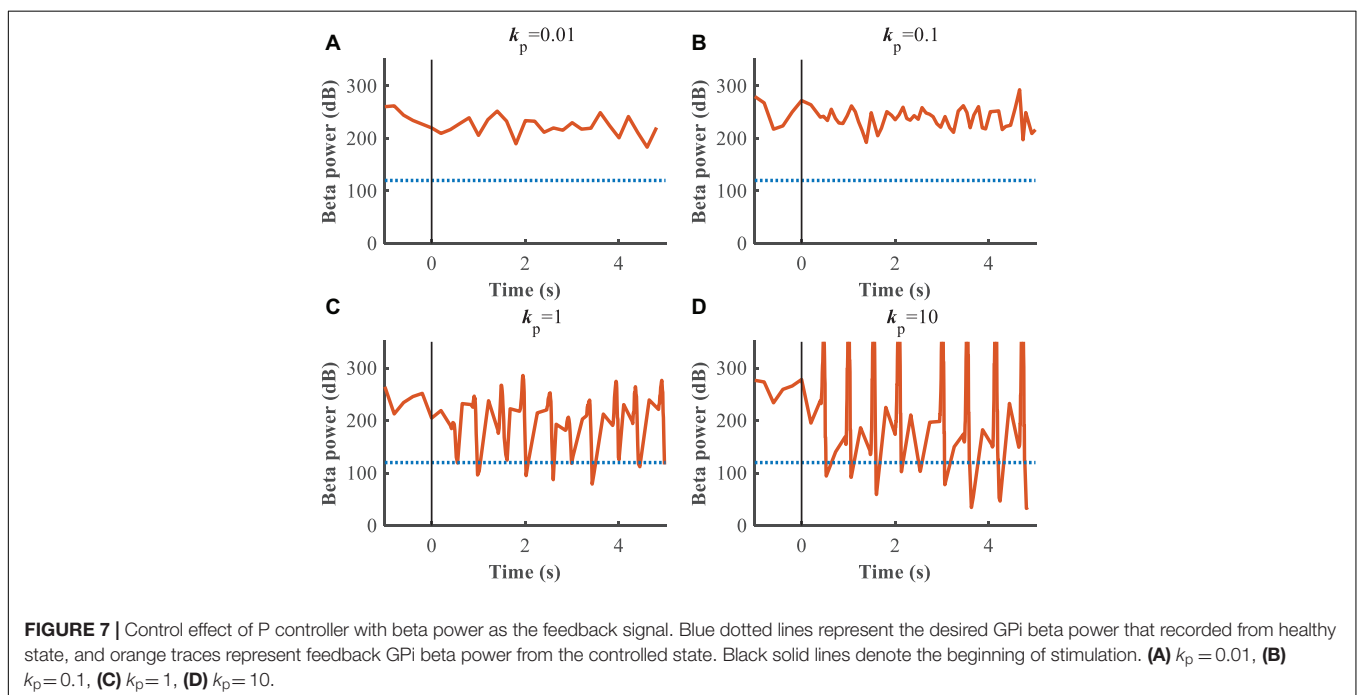
Evaluation of Robustness of the Supervisory Algorithm

The closed-loop RBF network-based supervisory control algorithm achieved effective tracking of the target beta power, but several challenges required further consideration. First, Parkinson's disease is a chronic and progressive disease in which the patient's condition gradually worsens over time, and individual variation should be considered in model-based evaluations. Second, the reference waveform was the LFP signal from the healthy network model. Although this signal carries abundant information, it does not represent the variety of different disease states, for example during cycling of medication, and this potentially limits the generalizability of the control system.

To evaluate further the performance of the proposed closed-loop algorithm in the face of changes in the Parkinsonian state (**Figure 10**), the parkinsonism variable pd was randomly generated from 0 to 1. Controlled beta power gradually converged to the desired healthy signal after 1 s, demonstrating the adaptive capability of the RBF network across disease states. In addition, beta power exhibits dynamic changes, especially prior to and during movement, and thus tracking of time-varying beta power may be required to promote desired movement behavior. In the face of a time varying reference beta power signal switching at 1 Hz (**Figure 11**), the controlled beta power still followed the dynamic reference signal, albeit with substantial overshoot.

DISCUSSION

This manuscript proposed an improved supervisory control algorithm for adaptively adjusting the stimulation signal to



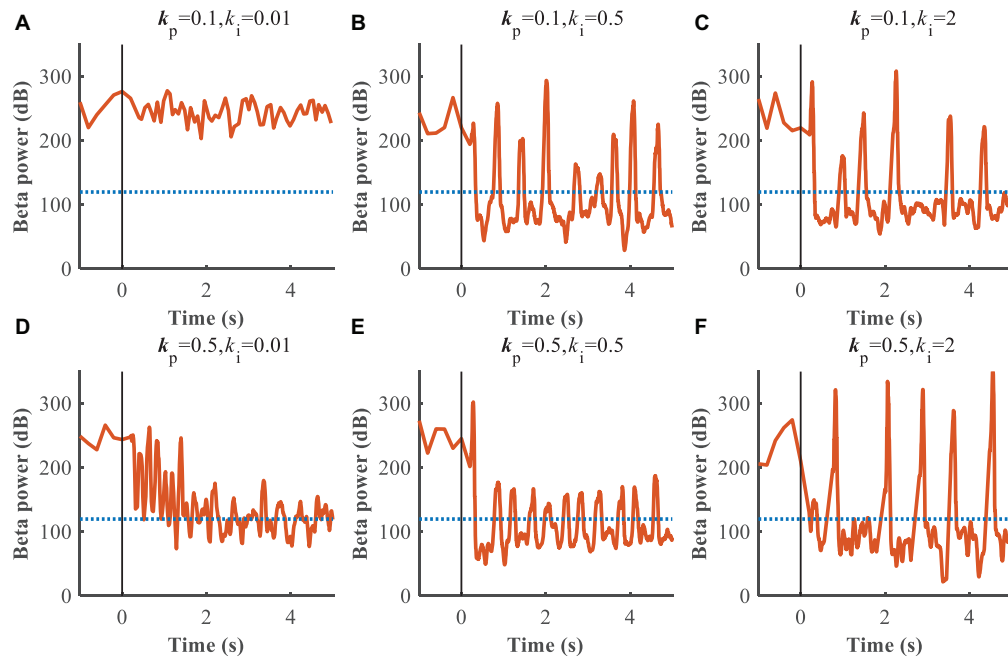


FIGURE 8 | Control effect of PI controller with beta power as the feedback signal. Blue dotted lines represent the desired GPI beta power that recorded from healthy state, and orange traces represent feedback GPI beta power from the controlled state. Black solid lines denote the beginning of stimulation. **(A)** $k_p=0.1, k_i=0.01$, **(B)** $k_p=0.1, k_i=0.5$, **(C)** $k_p=0.1, k_i=2$, **(D)** $k_p=0.5, k_i=0.01$, **(E)** $k_p=0.5, k_i=0.5$, **(F)** $k_p=0.5, k_i=2$.

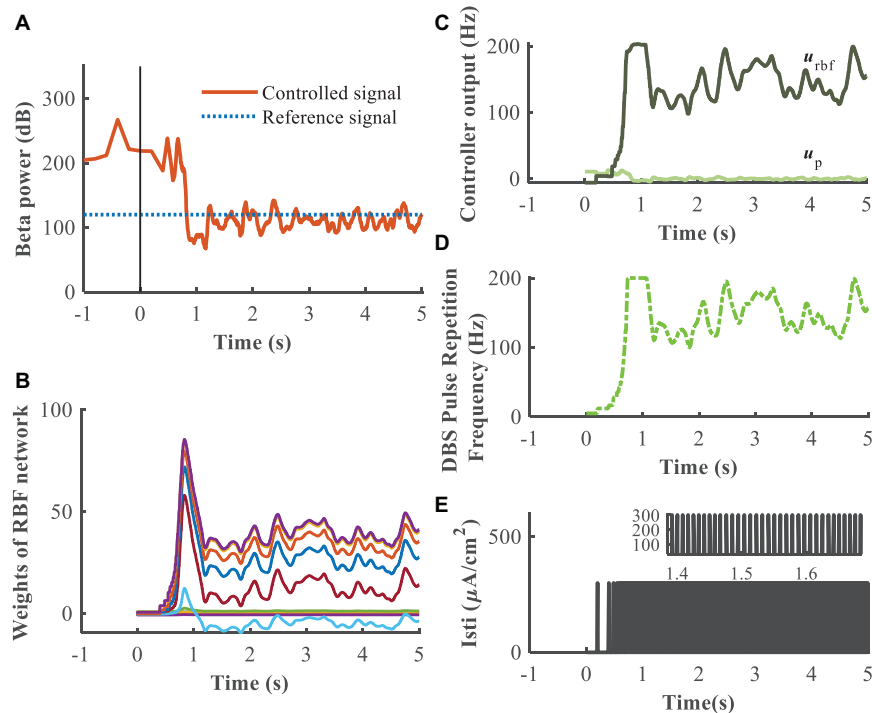


FIGURE 9 | Feedback control using the RBF controller with beta power as the control signal ($k_p=0.1$). Panel **(A)** depicts the dynamic process of the controller reducing beta power in the GPI, panel **(B)** shows the evolution of real-time updated weights of the RBF network, **(C)** plots the trend of P controller and RBF controller, respectively, **(D)** generates the DBS pulse repetition frequency. Panel **(E)** is the stimulation signal, a series of 0.3 ms duration 300 $\mu\text{A}/\text{cm}^2$ amplitude pulses with the instantaneous frequency determined by the controller.

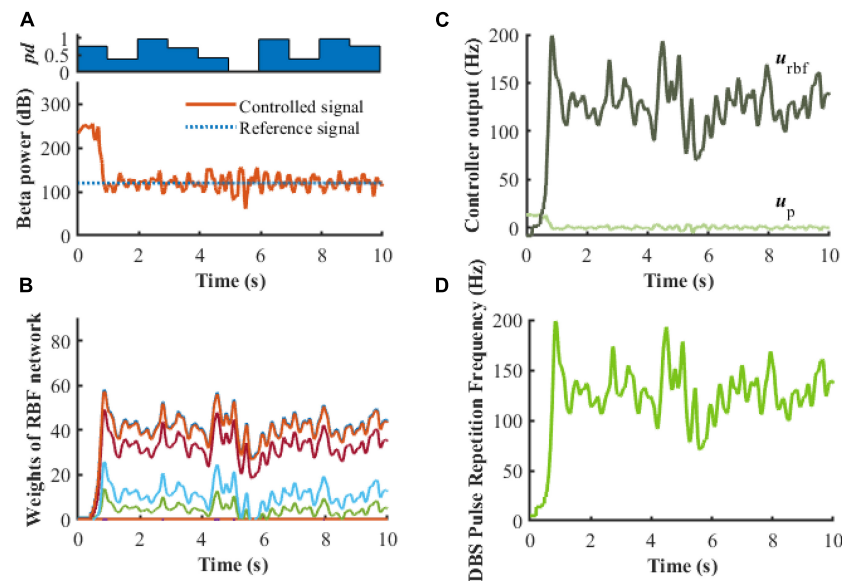


FIGURE 10 | Robustness analysis of the RBF controller in the presence of dynamic changes in the Parkinsonian state ($k_p = 0.1$). **(A)** Dynamic change of Parkinsonian state is characterized by the parameter, pd . The RBF-controller modulated beta power during dynamic changes is depicted in the bottom panel. Panel **(B)** shows the evolution of real-time updated weights of the RBF network, **(C)** plots the trend of P controller and RBF controller, and **(D)** generates the DBS pulse repetition frequency. Here, the stimulation amplitude is set to $300 \mu\text{A}/\text{cm}^2$ and the pulse duration is set to 0.3 ms.

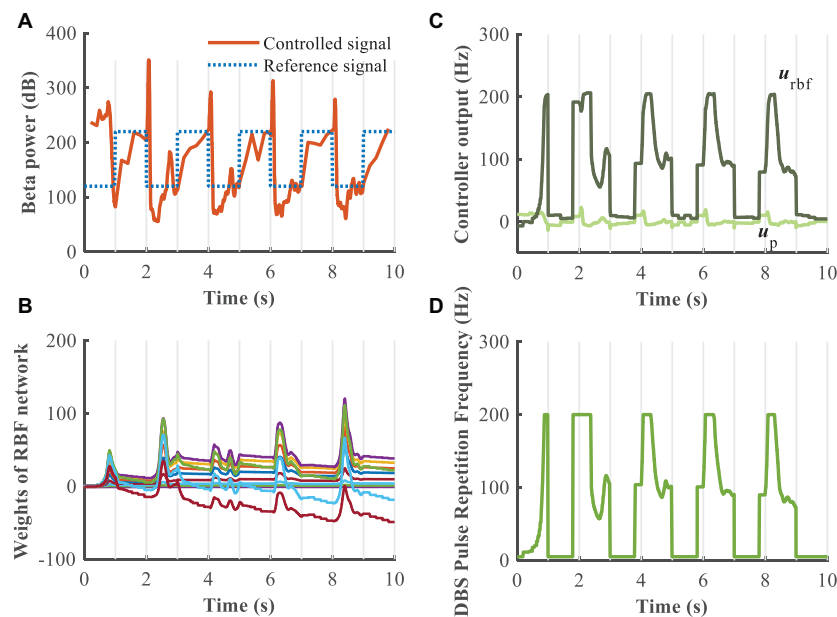


FIGURE 11 | Robustness analysis of the RBF controller during dynamic changes in the reference beta power ($k_p = 0.1$). **(A)** Dynamic change of the reference beta power is characterized by the blue dotted line. The RBF-controller modulated beta power is depicted in the bottom panel. Panel **(B)** shows the evolution of real-time updated weights of the RBF network, **(C)** plots the trend of P controller and RBF controller, and **(D)** generates the DBS pulse repetition frequency. Here, the stimulation amplitude is set to $300 \mu\text{A}/\text{cm}^2$ and the pulse duration is set to 0.3 ms.

improve DBS control of the Parkinsonian state. Myriad control algorithms have been applied to the design of closed-loop DBS system, for example, on-off control, dual-threshold control, delayed feedback control, PID control, fuzzy control, and model

predictive control (Little et al., 2013; Liu et al., 2015, 2016; Popovych et al., 2017; Su et al., 2019; Velisar et al., 2019). For on-off control and dual-threshold control, a stimulus was triggered by the control signal exceeding or falling below

a threshold. Energy consumption was reduced as compared to traditional open-loop stimulation, but selection of optimal stimulation parameters during the DBS-on stage still needed to be addressed. The design of delayed feedback controller or PID controller depended strongly on the selection of controller gains and delay time constant, and the performance was dependent on the plant. Thus, such controllers may exhibit limited adaptability for individual variations due to, for example, changes in medication status or active versus inactive state. More advanced control algorithms, for example fuzzy control and model predictive control, have been developed for modulation of DBS parameters. However, the robustness of the control algorithm was improved at the cost of using a non-standard signal—the unmodulated controller output was applied directly to the stimulated targets, and this may be difficult to implement with an implanted pulse generator. In addition, Gao et al. (2020) proposed a deep reinforcement learning-based approach to construct an adaptive DBS framework. The reinforcement signal provided by the environment was an evaluation of the quality of the action that the agent produced. It should be noted that the external environment yielded evaluations (reward or punishment) rather than correct answers to the output of the learning system, and the performance of the learning system was improved by reinforcing the actions that were rewarded. Neural networks have the capacity to approximate arbitrary complex nonlinear systems, and an RBF network was adopted in this manuscript for selecting the appropriate pulse repetition frequency of DBS. The proposed RBF-based algorithm constituted supervised learning that provided a corresponding target output for each input. Through the feedback structure, the stability and robustness can be guaranteed, and the precision and adaptability were improved.

A biophysically feasible cortex-basal ganglia-thalamus computational network model that represents the Parkinsonian state in 6-OHDA lesioned rats was used as the plant and to calculate LFP signals and the effects of DBS. DBS of the STN or the GPi are currently the most common and effective surgical targets for the treatment of PD, but there does not appear to be one superior target. Several studies compared the efficacy of stimulating STN versus GPi and that both STN-DBS and GPi-DBS are equally effective in improving motor dysfunction (Honey et al., 2017; Zhang et al., 2021). STN-DBS contributes to more significant medication reduction and is favorable to decrease energy consumption due to the smaller stimulating region, but STN-DBS appears to increase the incidence of psychiatric complication. If medication reduction is not a major concern, GPi-DBS has the advantage of direct dyskinesia suppression. LFP signals from the GPi, which can be directly obtained through DBS leads in clinical application (Stanslaski et al., 2012; Arlotti et al., 2016b; Parastarfeizabadi and Kouzani, 2019) and carry abundant potential information from synchronous neural activity were extracted and processed as the feedback signal for closing the loop (Little and Brown, 2012; Priori et al., 2012; Hebb et al., 2014; Arlotti et al., 2016a; Sinclair

et al., 2018). The design of the closed-loop control system followed a traditional strategy. For such a highly nonlinear and complex plant, the selection of optimal proportional gains was challenging, and simulation results illustrated that the P controller did not achieve effective tracking of the reference signal. The RBF neural network exhibits both self-learning and self-adaptation and was the foundation for constructing an intelligent control system. The improved supervisory control algorithm with the RBF network controller showed satisfactory tracking performance and was able to regulate the beta oscillatory power across dynamic changes in the plant and the reference signal.

The proposed algorithm has several potential advantages for clinical implementation. First, although the closed-loop control algorithm was designed based on a biophysical model of the cortex-basal ganglia-thalamus network, precise parameters (e.g., synaptic conductance, reversal potentials) and network structure (e.g., synaptic connectivity) were not necessary since the RBF network builds an inverse representation based on input output information. Second, DBS stimulation signals were delivered through and LFP recordings were obtained from same implanted electrode, thereby avoiding the requirement of additional external sensors. A limitation of this simulation study is the setting of the desired tracking signal, and the variable dynamics of the cortical-Basal-thalamus network were not fully considered. Further exploration combined with the selection of biological markers that relate to specific symptoms and states remains an important challenge. Further, understanding the relationship between stimulation parameter changes and changes in specific patient symptoms, including the time course of such changes, is crucial to improving clinical treatment. For example, data-driven input-output model identification might be a promising solution for quantifying responsiveness to specific stimulation signals.

DATA AVAILABILITY STATEMENT

The original contributions presented in the study are included in the article/supplementary material, further inquiries can be directed to the corresponding author.

AUTHOR CONTRIBUTIONS

YZ was responsible for manuscript development, concept, and study design, and wrote the manuscript. WG conceived the project, and supervised the study design and manuscript development. JW collaborated in manuscript development and concept. HL and CL collaborated in methodology design and implementation. All authors read and approved the final manuscript.

FUNDING

This work was supported in part by grant R37 NS040894 from the US National Institutes of Health.

REFERENCES

- Androulidakis, A. G., Brücke, C., Kempf, F., Kupsch, A., Aziz, T., Ashkan, K., et al. (2008). Amplitude modulation of oscillatory activity in the subthalamic nucleus during movement. *Eur. J. Neurosci.* 27, 1277–1284. doi: 10.1111/j.1460-9568.2008.06085.x
- Arlotti, M., Rosa, M., Marceglia, S., Barbieri, S., and Priori, A. (2016a). The adaptive deep brain stimulation challenge. *Parkinsonism Relat. Disord.* 28, 12–17. doi: 10.1016/j.parkreldis.2016.03.020
- Arlotti, M., Rossi, L., Rosa, M., Marceglia, S., and Priori, A. (2016b). An external portable device for adaptive deep brain stimulation (aDBS) clinical research in advanced Parkinson's Disease. *Med. Eng. Phys.* 38, 498–505. doi: 10.1016/j.medengphys.2016.02.007
- Beudel, M., Oswal, A., Jha, A., Foltynie, T., Zrinzo, L., Hariz, M., et al. (2017). Oscillatory beta power correlates with Akinesia-rigidity in the Parkinsonian subthalamic nucleus. *Mov. Disord.* 32, 174–175. doi: 10.1002/mds.26860
- Bras, J., Singleton, A., Cookson, M. R., and Hardy, J. (2008). Emerging pathways in genetic Parkinson's disease: potential role of ceramide metabolism in Lewy body disease. *FEBS J.* 275, 5767–5773. doi: 10.1111/j.1742-4658.2008.06709.x
- Broccard, F., Mullen, T., Chi, Y., Peterson, D., Iversen, J., Arnold, M., et al. (2014). Closed-loop brain-machine-body interfaces for noninvasive rehabilitation of movement disorders. *Ann. Biomed. Eng.* 42, 1573–1593. doi: 10.1007/s10439-014-1032-6
- Buzsáki, G., Anastassiou, C. A., and Koch, C. (2012). The origin of extracellular fields and currents—EEG, ECoG, LFP and spikes. *Nat. Rev. Neurosci.* 13, 407–420. doi: 10.1038/nrn3241
- de Paor, A. M., and Lowery, M. M. (2009). Analysis of the mechanism of action of deep brain stimulation using the concepts of dither injection and the equivalent nonlinearity. *IEEE Trans. Biomed. Eng.* 56, 2717–2720. doi: 10.1109/TBME.2009.2019962
- Deffains, M., and Bergman, H. (2019). Parkinsonism-related β oscillations in the primate basal ganglia networks—recent advances and clinical implications. *Parkinsonism Relat. Disord.* 59, 2–8. doi: 10.1016/j.parkreldis.2018.12.015
- Doshi, P. K., Chhaya, N. A., and Bhatt, M. A. (2003). Bilateral subthalamic nucleus stimulation for Parkinson's disease. *Neurol. India* 51, 43–48.
- Follett, K. A., Weaver, F. M., Stern, M., Hur, K., Harris, C. L., Luo, P., et al. (2010). Pallidal versus subthalamic deep-brain stimulation for Parkinson's Disease. *N. Engl. J. Med.* 362, 2077–2091. doi: 10.1056/NEJMoa0907083
- Gao, Q., Naumann, M., Jovanov, I., Lesi, V., Kamaravelu, K., Grill, W. M., et al. (2020). “Model-based design of closed loop deep brain stimulation controller using reinforcement learning,” in *Proceedings of the 2020 ACM/IEEE 11th International Conference on Cyber-Physical Systems (ICCPs)*, (Sydney, NSW: IEEE), 108–118. doi: 10.1109/ICCPs48487.2020.00018
- Gozelic, P., Schiff, S., and Sinha, A. (2013). Model-based rational feedback controller design for closed-loop deep brain stimulation of Parkinson's disease. *J. Neural Eng.* 10:026016. doi: 10.1088/1741-2560/10/2/026016
- Guo, Y., and Rubin, J. E. (2011). Multi-site stimulation of subthalamic nucleus diminishes thalamocortical relay errors in a biophysical network model. *Neural Netw.* 24, 602–616. doi: 10.1016/j.neunet.2011.03.010
- Haeri, M., Sarbaz, Y., and Gharibzadeh, S. (2005). Modeling the Parkinson's tremor and its treatments. *J. Theor. Biol.* 236, 311–322. doi: 10.1016/j.jtbi.2005.03.014
- Hebb, A., Zhang, J., Mahoor, M., Tsiokos, C., Matlack, C., Chizeck, H., et al. (2014). Creating the Feedback Loop. *Neurosurg. Clin. North Am.* 25, 187–204. doi: 10.1016/j.nec.2013.08.006
- Hoang, K., Cassar, I., Grill, W., and Turner, D. (2017). Biomarkers and stimulation algorithms for adaptive brain stimulation. *Front. Neurosci.* 11:564. doi: 10.3389/fnins.2017.00564
- Honey, C. R., Hamani, C., Kalia, S. K., Sankar, T., Picillo, M., Munhoz, R. P., et al. (2017). Deep brain stimulation target selection for Parkinson's disease. *Can. J. Neurol. Sci.* 44, 3–8. doi: 10.1017/cjn.2016.22
- Izhikevich, E. M. (2003). Simple model of spiking neurons. *IEEE Trans. Neural Netw.* 14, 1569–1572. doi: 10.1109/TNN.2003.820440
- Jankovic, J. (2008). Parkinson's disease: clinical features and diagnosis. *J. Neurol. Neurosurg. Psychiatry* 79, 368–376. doi: 10.1136/jnnp.2007.131045
- Kiss, Z. H. T., Doig-Beyaert, K., Eliasziw, M., Tsui, J., Haffenden, A., Suchowersky, O., et al. (2007). The Canadian multicentre study of deep brain stimulation for cervical dystonia. *Brain* 130, 2879–2886. doi: 10.1093/brain/awm229
- Kita, H., and Kita, T. (2011). Cortical stimulation evokes abnormal responses in the dopamine-depleted rat basal ganglia. *J. Neurosci.* 31, 10311–10322. doi: 10.1523/JNEUROSCI.0915-11.2011
- Kumaravelu, K., Brocker, D. T., and Grill, W. M. (2016). A biophysical model of the cortex-basal ganglia-thalamus network in the 6-OHDA lesioned rat model of Parkinson's disease. *J. Comput. Neurosci.* 40, 207–229. doi: 10.1007/s10827-016-0593-9
- Little, S., and Brown, P. (2012). What brain signals are suitable for feedback control of deep brain stimulation in Parkinson's disease? *Ann. N. Y. Acad. Sci.* 1265, 9–24. doi: 10.1111/j.1749-6632.2012.06650.x
- Little, S., Pogosyan, A., Neal, S., Zavala, B., Zrinzo, L., Hariz, M., et al. (2013). Adaptive deep brain stimulation in advanced Parkinson disease. *Ann. Neurol.* 74, 449–457. doi: 10.1002/ana.23951
- Liu, C., Wang, J., deng, B., Wei, X., Yu, H.-T., and Li, H.-Y. (2015). Variable universe fuzzy closed-loop control of tremor predominant Parkinsonian state based on parameter estimation. *Neurocomputing* 151, 1507–1518. doi: 10.1016/j.neucom.2014.10.028
- Liu, C., Wang, J., Li, H., Lu, M., deng, B., Yu, H., et al. (2016). Closed-loop modulation of the pathological disorders of the basal Ganglia Network. *IEEE Trans. Neural Netw. Learn. Syst.* 28, 371–382. doi: 10.1109/TNNLS.2015.2508599
- Lofredi, R., Tan, H., Neumann, W.-J., Yeh, C. H., Schneider, G.-H., Kühn, A., et al. (2019). Beta bursts during continuous movements accompany the velocity decrement in Parkinson's disease patients. *Neurobiol. Dis.* 127, 462–471. doi: 10.1016/j.nbd.2019.03.013
- Mazzoni, A., Lindén, H., Cuntz, H., Lansner, A., Panzeri, S., and Einevoll, G. (2015). Computing the Local Field Potential (LFP) from Integrate-And-Fire Network Models. *PLoS Comput. Biol.* 11:e1004584. doi: 10.1371/journal.pcbi.1004584
- Mehta, S. H., and Sethi, K. D. (2009). Bilateral deep brain stimulation versus best medical therapy for patients with advanced Parkinson's disease. *Curr. Neurol. Neurosci. Rep.* 9, 266–267. doi: 10.1007/s11910-009-0039-0
- Modolo, J., Beuter, A., Thomas, A. W., and Legros, A. (2012). Using “Smart Stimulators” to treat Parkinson's disease: re-engineering neurostimulation devices. *Front. Comput. Neurosci.* 6:69. doi: 10.3389/fncom.2012.00069
- Montgomery, E. (2020). Debugging adaptive deep brain stimulation for Parkinson's disease. *Mov. Disord.* 35, 1891–1891. doi: 10.1002/mds.28235
- Novikova, L., Garriss, B. L., Garriss, D. R., and Lau, Y.-S. (2006). Early signs of neuronal apoptosis in the substantia nigra pars compacta of the progressive neurodegenerative mouse 1-methyl-4-phenyl-1,2,3,6-tetrahydropyridine/probenecid model of Parkinson's disease. *Neuroscience* 140, 67–76. doi: 10.1016/j.neuroscience.2006.02.007
- Parastarfeizabadi, M., and Kouzani, A. (2017). Advances in closed-loop deep brain stimulation devices. *J. Neuroeng. Rehabil.* 14:79. doi: 10.1186/s12984-017-0295-1
- Parastarfeizabadi, M., and Kouzani, A. (2019). A miniature dual-biomarker-based sensing and conditioning device for closed-loop DBS. *IEEE J. Transl. Eng. Health Med.* 7:2000308. doi: 10.1109/JTEHM.2019.2937776
- Pettersen, K., Linden, H., Dale, A., and Einevoll, G. (2012). “Extracellular spikes and CSD,” in *Handbook of Neural Activity Measurement*, eds R. Brette and A. Destexhe (Cambridge: Cambridge University Press), 92–135. doi: 10.1017/CBO9780511979958.004
- Pirini, M., Rocchi, L., Sensi, M., and Chiari, L. (2009). A computational modelling approach to investigate different targets in deep brain stimulation for Parkinson's disease. *J. Comput. Neurosci.* 26, 91–107. doi: 10.1007/s10827-008-0100-z
- Pizzolatto, G., and Mandat, T. (2012). Deep brain stimulation for movement disorders. *Front. Integr. Neurosci.* 6:2. doi: 10.3389/fnint.2012.00002
- Popovich, O. V., Lysyansky, B., and Tass, P. A. (2017). Closed-loop deep brain stimulation by pulsatile delayed feedback with increased gap between pulse phases. *Sci. Rep.* 7:1033. doi: 10.1038/s41598-017-01067-x
- Popovich, O. V., and Tass, P. A. (2012). Desynchronizing electrical and sensory coordinated reset neuromodulation. *Front. Hum. Neurosci.* 6:58. doi: 10.3389/fnhum.2012.00058
- Priori, A., Foffani, G., Rossi, L., and Marceglia, S. (2012). Adaptive deep brain stimulation (aDBS) controlled by local field potential oscillations. *Exp. Neurol.* 245, 77–86. doi: 10.1016/j.expneurol.2012.09.013
- Rosa, M., Arlotti, M., Marceglia, S., Cogiamanian, F., Ardolino, G., Di Fonzo, A., et al. (2017). Adaptive deep brain stimulation controls levodopa-induced side

- effects in Parkinsonian patients: DBS controls levodopa-induced side effects. *Mov. Disord.* 32, 628–629. doi: 10.1002/mds.26953
- Rosin, B., Slovik, M., Mitelman, R., Rivlin-Etzion, M., Haber, S. N., Israel, Z., et al. (2011). Closed-loop deep brain stimulation is superior in ameliorating Parkinsonism. *Neuron* 72, 370–384. doi: 10.1016/j.neuron.2011.08.023
- Rubin, J. E., and Terman, D. (2004). High frequency stimulation of the subthalamic nucleus eliminates pathological thalamic rhythmicity in a computational model. *J. Comput. Neurosci.* 16, 211–235. doi: 10.1023/B:JCNS.0000025686.47117.67
- Santaniello, S., Fiengo, G., Glielmo, L., and Grill, W. M. (2011). Closed-loop control of deep brain stimulation: a simulation study. *IEEE Trans. Neural Syst. Rehabil. Eng.* 19, 15–24. doi: 10.1109/TNSRE.2010.2081377
- Sinclair, N. C., Mcdermott, H. J., Bulluss, K. J., Fallon, J. B., Perera, T., Xu, S. S., et al. (2018). Subthalamic nucleus deep brain stimulation evokes resonant neural activity. *Ann. Neurol.* 83, 1027–1031. doi: 10.1002/ana.25234
- Stanslaski, S., Afshar, P., Cong, P., Giftakis, J., Stypulkowski, P., Carlson, D., et al. (2012). Design and validation of a fully implantable, chronic, closed-loop neuromodulation device with concurrent sensing and stimulation. *IEEE Trans. Neural Syst. Rehabil. Eng.* 20, 410–421. doi: 10.1109/tnsre.2012.2183617
- Steiner, L. A., Neumann, W.-J., Staub-Bartelt, F., Herz, D. M., Tan, H., Pogossyan, A., et al. (2017). Subthalamic beta dynamics mirror Parkinsonian bradykinesia months after neurostimulator implantation. *Mov. Disord.* 32, 1183–1190. doi: 10.1002/mds.27068
- Su, F., Kumaravelu, K., Wang, J., and Grill, W. M. (2019). Model-based evaluation of closed-loop deep brain stimulation controller to adapt to dynamic changes in reference signal. *Front. Neurosci.* 13:956. doi: 10.3389/fnins.2019.00956
- Swann, N. C., de Hemptinne, C., Thompson, M. C., Miocinovic, S., Miller, A. M., Gilron, R., et al. (2018). Adaptive deep brain stimulation for Parkinson's disease using motor cortex sensing. *J. Neural Eng.* 15:046006. doi: 10.1088/1741-2552/aabc9b
- Titcombe, M. S., Glass, L., Guehl, D., and Beuter, A. (2001). Dynamics of Parkinsonian tremor during deep brain stimulation. *Chaos* 11, 766–773. doi: 10.1063/1.1408257
- Velisar, A., Syrkin-Nikolau, J., Blumenfeld, Z., Trager, M. H., Afzal, M. F., Prabhakar, V., et al. (2019). Dual threshold neural closed loop deep brain stimulation in Parkinson disease patients. *Brain Stimul.* 12, 868–876. doi: 10.1016/j.brs.2019.02.020
- Vidailhet, M., Vercueil, L., Houeto, J.-L., Krstkowiak, P., Lagrange, C., Yelnik, J., et al. (2007). Bilateral, pallidal, deep-brain stimulation in primary generalised dystonia: a prospective 3 year follow-up study. *Lancet Neurol.* 6, 223–229. doi: 10.1016/S1474-4422(07)70035-2
- Wu, H., Ghekiere, H., Beeckmans, D., Tambuyzer, T., van Kuyck, K., Aerts, J.-M., et al. (2015). Conceptualization and validation of an open-source closed-loop deep brain stimulation system in rat. *Sci. Rep.* 5:9921. doi: 10.1038/srep09921
- Zhang, J., Li, J., Chen, F., Liu, X., Jiang, C., Hu, X., et al. (2021). STN versus GPi deep brain stimulation for dyskinesia improvement in advanced Parkinson's disease: a meta-analysis of randomized controlled trials. *Clin. Neurol. Neurosurg.* 201:106450. doi: 10.1016/j.clineuro.2020.106450

Conflict of Interest: The authors declare that the research was conducted in the absence of any commercial or financial relationships that could be construed as a potential conflict of interest.

Publisher's Note: All claims expressed in this article are solely those of the authors and do not necessarily represent those of their affiliated organizations, or those of the publisher, the editors and the reviewers. Any product that may be evaluated in this article, or claim that may be made by its manufacturer, is not guaranteed or endorsed by the publisher.

Copyright © 2021 Zhu, Wang, Li, Liu and Grill. This is an open-access article distributed under the terms of the Creative Commons Attribution License (CC BY). The use, distribution or reproduction in other forums is permitted, provided the original author(s) and the copyright owner(s) are credited and that the original publication in this journal is cited, in accordance with accepted academic practice. No use, distribution or reproduction is permitted which does not comply with these terms.



Case Report: Embedding “Digital Chronotherapy” Into Medical Devices—A Canine Validation for Controlling Status Epilepticus Through Multi-Scale Rhythmic Brain Stimulation

OPEN ACCESS

Edited by:

Coralie de Hemptinne,
University of Florida, United States

Reviewed by:

Aleksandra Dagmara Kawala-Sterniuk,
Opole University of
Technology, Poland
Aritra Kundu,
University of Texas at Austin,
United States

*Correspondence:

Mayela Zamora
mayela.zamora@eng.ox.ac.uk
Sebastian Meller
sebastian.meller@tiho-hannover.de

† These authors have contributed
equally to this work and share first
authorship

‡ These authors share
senior authorship

Specialty section:

This article was submitted to
Neural Technology,
a section of the journal
Frontiers in Neuroscience

Received: 30 June 2021

Accepted: 24 August 2021

Published: 24 September 2021

Citation:

Zamora M, Meller S, Kajin F,
Sermon JJ, Toth R, Benjaber M,
Dijk D-J, Bogacz R, Worrell GA,
Valentin A, Duchet B, Volk HA and
Denison T (2021) Case Report:
Embedding “Digital Chronotherapy”
Into Medical Devices—A Canine
Validation for Controlling Status
Epilepticus Through Multi-Scale
Rhythmic Brain Stimulation.
Front. Neurosci. 15:734265.
doi: 10.3389/fnins.2021.734265

Mayela Zamora^{1†}, **Sebastian Meller**^{2†}, **Filip Kajin**², **James J. Sermon**^{1,3}, **Robert Toth**³,
Moaad Benjaber^{1,3}, **Derk-Jan Dijk**^{4,5}, **Rafal Bogacz**³, **Gregory A. Worrell**⁶,
Antonio Valentin⁷, **Benoit Duchet**³, **Holger A. Volk**^{2‡} and **Timothy Denison**^{1,3‡}

¹ Institute of Biomedical Engineering, Department of Engineering Science, University of Oxford, Oxford, United Kingdom,

² Department of Small Animal Medicine and Surgery, University of Veterinary Medicine Hannover, Hanover, Germany, ³ MRC
Brain Network Dynamics Unit, Nuffield Department of Clinical Neurosciences, University of Oxford, Oxford, United Kingdom,

⁴ Surrey Sleep Research Centre, University of Surrey, Guildford, United Kingdom, ⁵ UK Dementia Research Institute, Care
Research and Technology Centre, Imperial College London and The University of Surrey, Guildford, United Kingdom,

⁶ Department of Neurology, Mayo Clinic, Rochester, MN, United States, ⁷ Department of Clinical Neurophysiology, King's
College Hospital NHS Trust, London, United Kingdom

Circadian and other physiological rhythms play a key role in both normal homeostasis and disease processes. Such is the case of circadian and infradian seizure patterns observed in epilepsy. However, these rhythms are not fully exploited in the design of active implantable medical devices. In this paper we explore a new implantable stimulator that implements chronotherapy as a feedforward input to supplement both open-loop and closed-loop methods. This integrated algorithm allows for stimulation to be adjusted to the ultradian, circadian and infradian patterns observed in patients through slowly-varying temporal adjustments of stimulation and algorithm sub-components, while also enabling adaption of stimulation based on immediate physiological needs such as a breakthrough seizure or change of posture. Embedded physiological sensors in the stimulator can be used to refine the baseline stimulation circadian pattern as a “digital zeitgeber,” i.e., a source of stimulus that entrains or synchronizes the subject’s natural rhythms. This algorithmic approach is tested on a canine with severe drug-resistant idiopathic generalized epilepsy exhibiting a characteristic diurnal pattern correlated with sleep-wake cycles. Prior to implantation, the canine’s cluster seizures evolved to status epilepticus (SE) and required emergency pharmacological intervention. The cranially-mounted system was fully-implanted bilaterally into the centromedian nucleus of the thalamus. Using combinations of time-based modulation, thalamocortical rhythm-specific tuning of frequency parameters as well as fast-adaptive modes based on activity, the canine experienced no further SE events post-implant as of the time of writing (7 months). Importantly, no significant cluster seizures have been observed either, allowing the reduction of rescue medication. The use of digitally-enabled chronotherapy as a

feedforward signal to augment adaptive neurostimulators could prove a useful algorithmic method in conditions where sensitivity to temporal patterns are characteristics of the disease state, providing a novel mechanism for tailoring a more patient-specific therapy approach.

Keywords: deep brain stimulation, centromedian thalamus, circadian, entrainment, epilepsy, chronotherapy, status epilepticus, Arnold tongues

INTRODUCTION

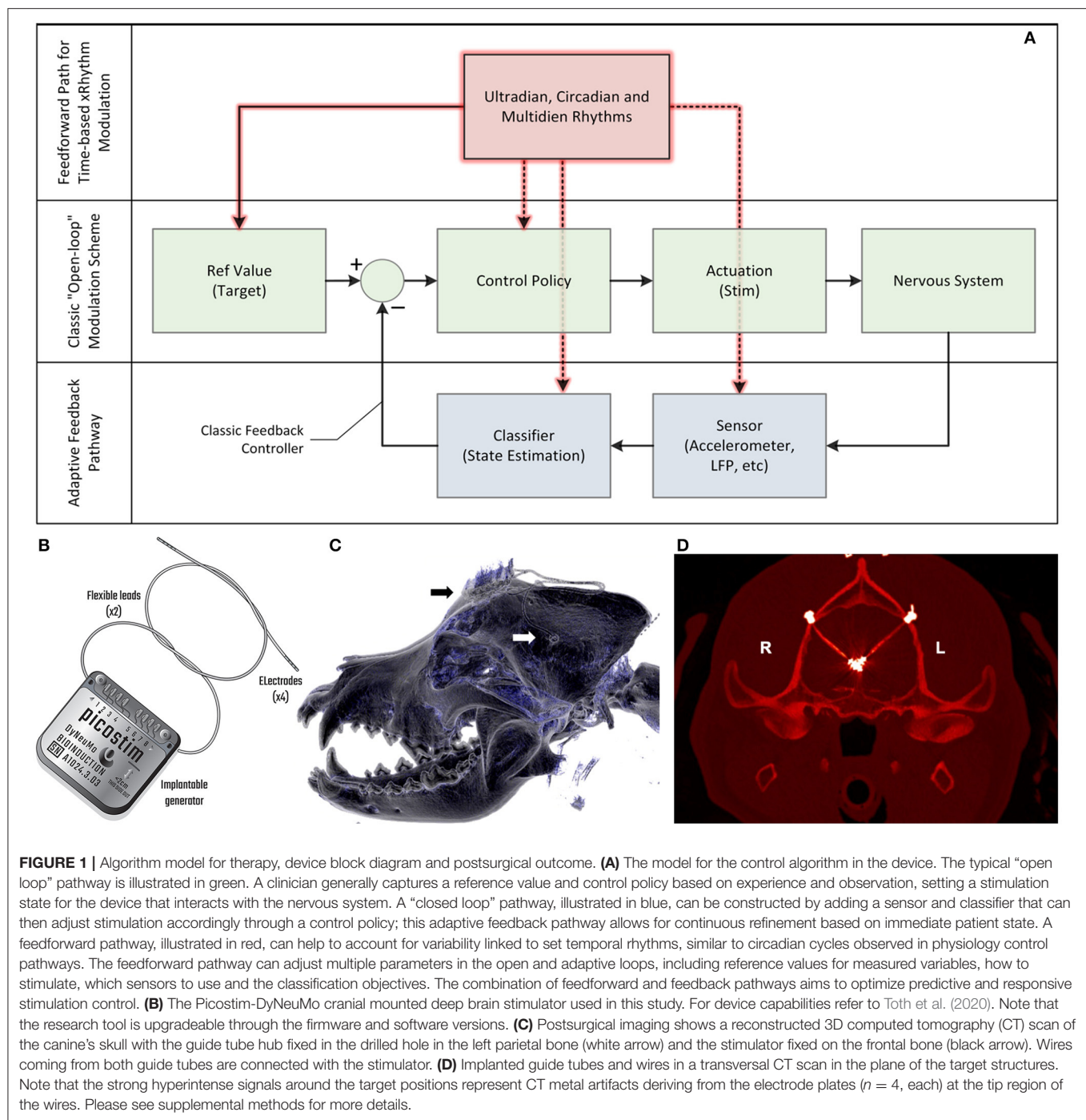
Physiological rhythms play a role in both normal homeostasis and disease processes, yet the design of active implantable medical devices often does not fully exploit them, especially in brain stimulators. For example, in the treatment of epilepsy with deep brain stimulation (DBS), the default stimulation approach is to apply high-frequency (HF) stimulation in an attempt to suppress seizure propagation (Fisher et al., 2010)—a method adapted from the successful treatment of Parkinson's disease (PD). While beneficial in many cases, occasionally resulting in periods with seizure freedom (Velasco et al., 2007; Valentin et al., 2013), an exploration of alternative strategies, or a combination of strategies (Schulze-Bonhage, 2019) could give new insights for epilepsy treatment. Similar opportunities exist in other disease states such as movement disorders and neuropsychiatry. One approach is to exploit the precise digital time control of implantable systems to interact with the rhythmic processes in the brain.

Normal and pathological rhythms arise at multiple timescales. At one temporal extreme, 24 h (circadian) and multiday (infradian) seizure patterns are observed in epilepsy (Baud et al., 2018; Gregg et al., 2020; Leguia et al., 2021). Despite these temporal fluctuations, current FDA-approved DBS and responsive neurostimulation (RNS) devices for control of seizures run a fixed algorithm regardless of the time. Vagal nerve stimulators do enable two settings for implementing diurnal control, which show promise for managing side-effects and correlating therapy with symptoms (Fisher et al., 2021). Similarly, disrupted sleep-wake cycles are a common co-morbidity of PD, depression and epilepsy, but current DBS devices default to fixed, tonic stimulation parameters that are configured based on an assessment of efficacy during a daytime follow-up (Malhotra, 2018). At the faster end of the spectrum, thalamocortical oscillations are signatures of both healthy and diseased brain states that fluctuate in intensity on the order of tens to hundreds of milliseconds (Oswal et al., 2013). While these oscillations are used for adaptive algorithms, the stimulation paradigm is still largely reliant on gating HF stimulation for suppressing these lower frequency oscillations (Little et al., 2013; Priori et al., 2013; Swann et al., 2018). Stimulation at lower frequencies, utilizing oscillation frequencies recorded during natural behavior, however may provide additional benefits over HF stimulation due to the entrainment properties of the target neural population. DBS parameters could in principle be tuned to act as a “digital chronotherapy” that modulates endogenous rhythmicity in brain activity over multiple timescales.

In this case study, we apply a new implantable stimulator in the centromedian nucleus of the thalamus (CMN) that implements multi-scale, rhythm-entrained stimulation as an experimental medicine treatment for SE. For human generalized seizures, the CMN is involved early or late in the seizure and when involved, appears to lead the cortex (Martín-López et al., 2017). Probably for this reason, this nucleus appears to be particularly useful for the treatment of super refractory SE in human patients (Valentín et al., 2012; Sa et al., 2019; Stavropoulos et al., 2021). SE is a serious ictal condition that is considered an emergent situation and can be fatal if these self-sustaining seizures cannot be interrupted. The stimulator's control algorithm applies feedforward input to supplement both open-loop and adaptive methods (**Figure 1A**). This integrated algorithm allows for electrical stimulation paradigms to be adjusted in response to slowly varying (e.g., diurnal/circadian) patterns through temporally-based adjustments of stimulation and algorithm sub-components, while also enabling adaptive stimulation based on immediate physiological needs such as a breakthrough seizure in epilepsy. The use of embedded field-potential sensing enabled subject-specific characterization of thalamocortical network activity. The field-potentials guided the application of targeted stimulation entrainment as an attempt to reinforce “beneficial” rhythms and avoid pathological ones. In aggregate, the physiological sensors and embedded timing control can serve to optimize the baseline stimulation circadian pattern as a digital zeitgeber, complementing or reinforcing existing zeitgebers.

CASE OVERVIEW

A 4-year-old, mixed-breed (Newfoundland/Saint Bernard), neutered male dog weighing 60 kg was presented with severe drug-resistant idiopathic epilepsy, at the Tier II confidence level of diagnostic certainty (De Risio et al., 2015). The carer's seizure diaries were used for comparative analysis of seizure type prevalence and frequency, seizure-free episodes and semiology of cluster seizures before and after surgery. The dog, treated as a veterinary patient, did not adequately respond to an array of antiseizure medication; treatment consisted of phenobarbital, potassium bromide, imepitoin, topiramate and gabapentin in various combinations (see **Figure 4** for details). Multiple dosages of diazepam or levetiracetam as pulse therapy were used following any given seizure to prevent cluster seizures (Packer et al., 2015). The dog's diet was enriched with 6% medium-chain



triglycerides (MCT) with the goal to improve seizure control (Berk et al., 2020).

None of the epilepsy management options provided an adequate response and seizure severity increased to frequent SE. As no further medical treatment was available under the German Medicinal Products Act, the carer elected and gave informed consent for attempting DBS for epilepsy management. The Picostim-DyNeuMo research system (Bioinduction, Bristol, UK)

was implanted with bilateral electrodes targeting the CMN, with the implantable pulse generator placed subcutaneously on the frontal cranium (**Figure 1**); refer to the supplemental methods for details. The Picostim-DyNeuMo can record intracranial signals and be remotely accessed for monitoring and therapy refinement; embedded circadian schedulers and sensors allow for adaptation of stimulation based on temporal patterns and inertial signals as well (Toth et al., 2020).

METHODS

Initially after implantation, HF stimulation was used for stimulation consistent with prior reports of CMN stimulation (130 Hz/90 μ s). However, in the first post-implant cluster seizures, increasing HF amplitudes led to intolerable side-effects without seizure cessation (head-pulling and other involuntary motion) and the cluster sequence proceeded unabated. This motivated the use of an analytical approach for low frequency entrainment.

Theoretical Mechanism for Parameter Selection: Arnold Tongue Analysis for Estimation of Entrainment

Our aim was to select stimulation frequencies which would reinforce neurotypical physiological behavior and avoid pathological rhythms. Prominent mesoscopic neural rhythms can be entrained through periodic electrical stimulation with specific amplitude and frequency predicted by Arnold tongues analysis. Entrainment may be subharmonic, characterized by a winding number $p:q$, with p and q integers, where p is the average number of oscillations achieved by the rhythm for a given q periodic pulses of the driving stimulation. Arnold tongues (Arnold, 1983; Pikovsky et al., 2002) can be observed in the stimulation frequency/amplitude space as patterns of constant winding number, typically elongated and triangular in shape. The $p:q$ Arnold tongue represents the range of stimulation frequencies and amplitudes compatible with $p:q$ entrainment. Arnold tongues have previously been reported in computational models of brain circuits, in particular in the context of circadian rhythms (Bordyugov et al., 2015; Skeldon et al., 2017) and transcranial stimulation (Trevisan et al., 2006; Ali et al., 2013; Herrmann et al., 2016).

The concept of Arnold tongues can be illustrated using the simplest model describing the influence of periodic stimulation on an oscillator. This model is the sine circle map (Glass and Mackey, 1979; Perez and Glass, 1982; Glass, 2001), where a phase oscillator with constant natural frequency is forced by periodic stimulation of controlled frequency and amplitude. A stimulation pulse will advance or delay a neuron's phase depending on where the neuron is in its firing cycle and on the neuron's type (Stiefel et al., 2008). Similarly, stimulation in the sine circle map advances or delays the phase of the oscillator, such that the change is proportional to the sine of the oscillator's phase at the time of stimulation. Varying stimulation frequency and amplitude reveals a family of Arnold tongues as shown in **Figure 2** for a natural frequency of 13 Hz. Highlighted in **Figure 2A** are the 1:1 and 2:1 tongues, which encompass stimulation parameters resulting in the oscillator frequency being entrained at exactly the stimulation frequency and at twice the stimulation frequency, respectively. Since the 1:1 tongue is the largest, 1:1 entrainment is the easiest to achieve in practice. For a fixed stimulation frequency, a broader range of natural frequencies can follow 1:1 entrainment, which will therefore be most robust to perturbations acting to change the rhythm's natural frequency.

Therapeutic Strategy—Basal Stimulation Frequency and Fast Adaptation

With remote telemetry, we were able to assess the spectral content of thalamocortical signals from our dataset based on prior characterization studies; representative power spectral density (PSD) plots are included in **Figure 2B**. Applying the entrainment hypothesis, we remotely tuned the stimulation frequency to the canine's dominant rhythm during restful, alert activity (13 Hz/350 μ s/1.3 mA bilateral), while trying to avoid a sub-harmonic rhythm which might align with the 2 Hz oscillation that correlated with seizure onset and initiation. Similar low frequency rhythms have also been suggested to induce absence seizures in human subjects (Velasco et al., 1997). The final entrainment model that guided therapy is summarized in the Arnold Tongue plot of **Figure 2C**. The adoption of this setting coincided with the end of the immediate cluster seizure event and it has been used thereafter as the default stimulation pattern. As an emergency fall-back for breakthrough seizures, a HF mode with elevated amplitude (130 Hz/90 μ s/1.5 mA bilateral) was implemented which could be triggered by the carer through tap activation, using the built-in accelerometer (**Figure 1B**). Note that the levels for the emergency HF stimulation would not be tolerated during normal activities of daily living, e.g., it can induce reversible head-pulling, but were acceptable for an emergent state.

Therapeutic Strategy—Diurnal Rhythms and Slow Adaptation

Since physiological rhythms can vary throughout the day (Gregg et al., 2020; Leguia et al., 2021), the stimulation might benefit from temporal adjustments regardless of immediate physiological state. In case of our canine stimulation could lead to hypervigilance, so the therapy was adjusted to vary over time, supplemented by adaptive transitions based on activity/inactivity.

The temporal pattern to stimulation adjustment was introduced so as to align maximum stimulation intensity with times of peak seizure activity, as recorded in the seizure diary kept by the carer. The historic seizure activity up to the date of implantation is presented in a rose plot, inset in the right panel of **Figure 3**. The timing of seizures motivated a circadian adaptive pattern for stimulation; note that seizures were generally linked to sleep states according to the carer.

The aim was to account for immediate variation in activity, while accounting for daytime naps, since the highest probability of seizures correlated with the sleep state. The final adaptive algorithm, merging chronotherapy and sensor-based inputs, consisted of three layers of control with increasing stimulation intensity: (1) a circadian basal rate while the dog is awake and active; (2) a protective sleep mode with elevated entrainment stimulation; and (3) a high-amplitude, HF stimulation pattern to try and abort a breakthrough seizure through existing DBS methods. The embedded algorithm is illustrated by the circles enclosing the rose diagram in **Figure 3**. The inner ring of stimulation is the default state at 13 Hz when the dog is active; the *night-time* activity uses elevated stimulation 0.7 mA for

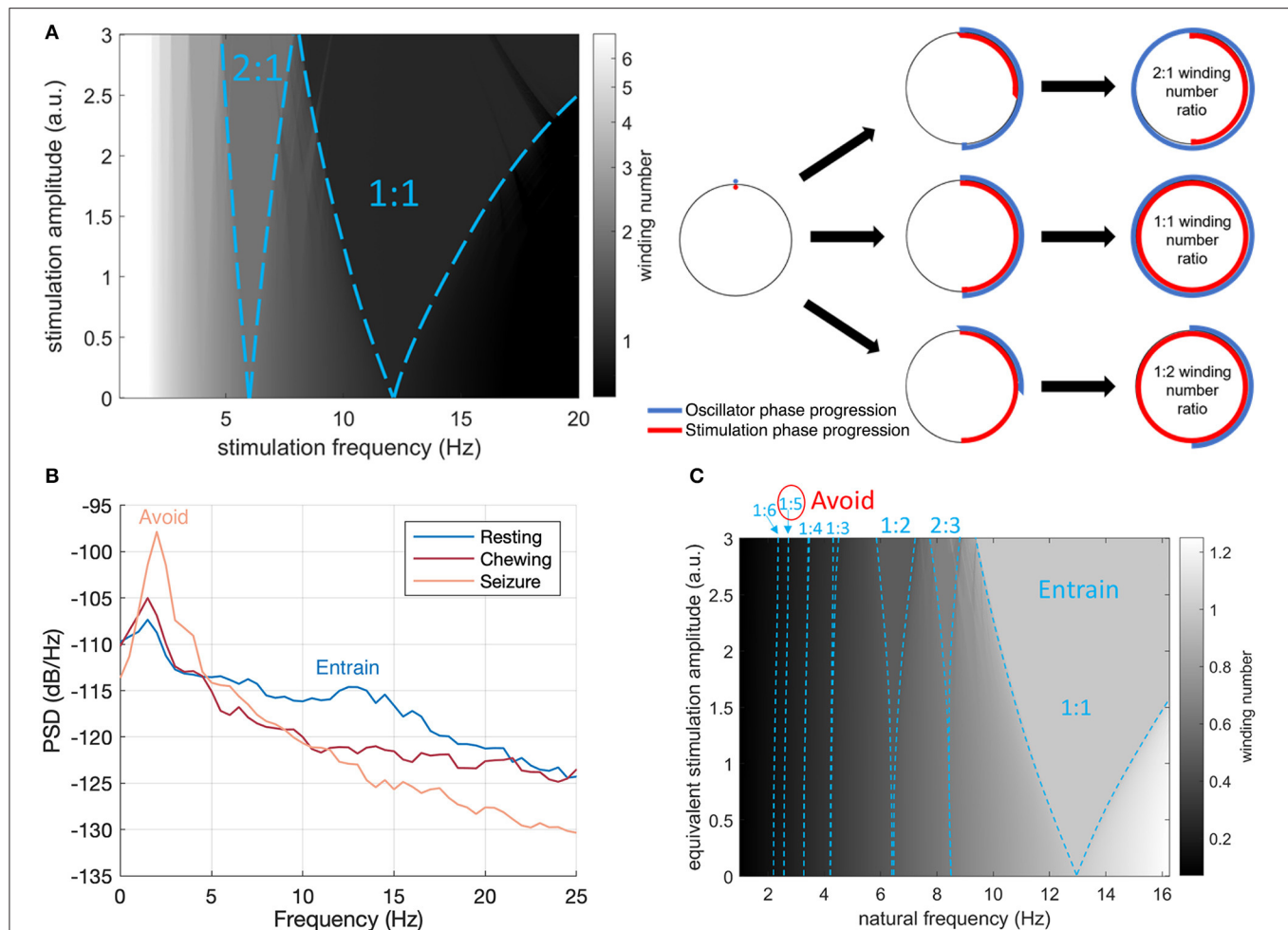
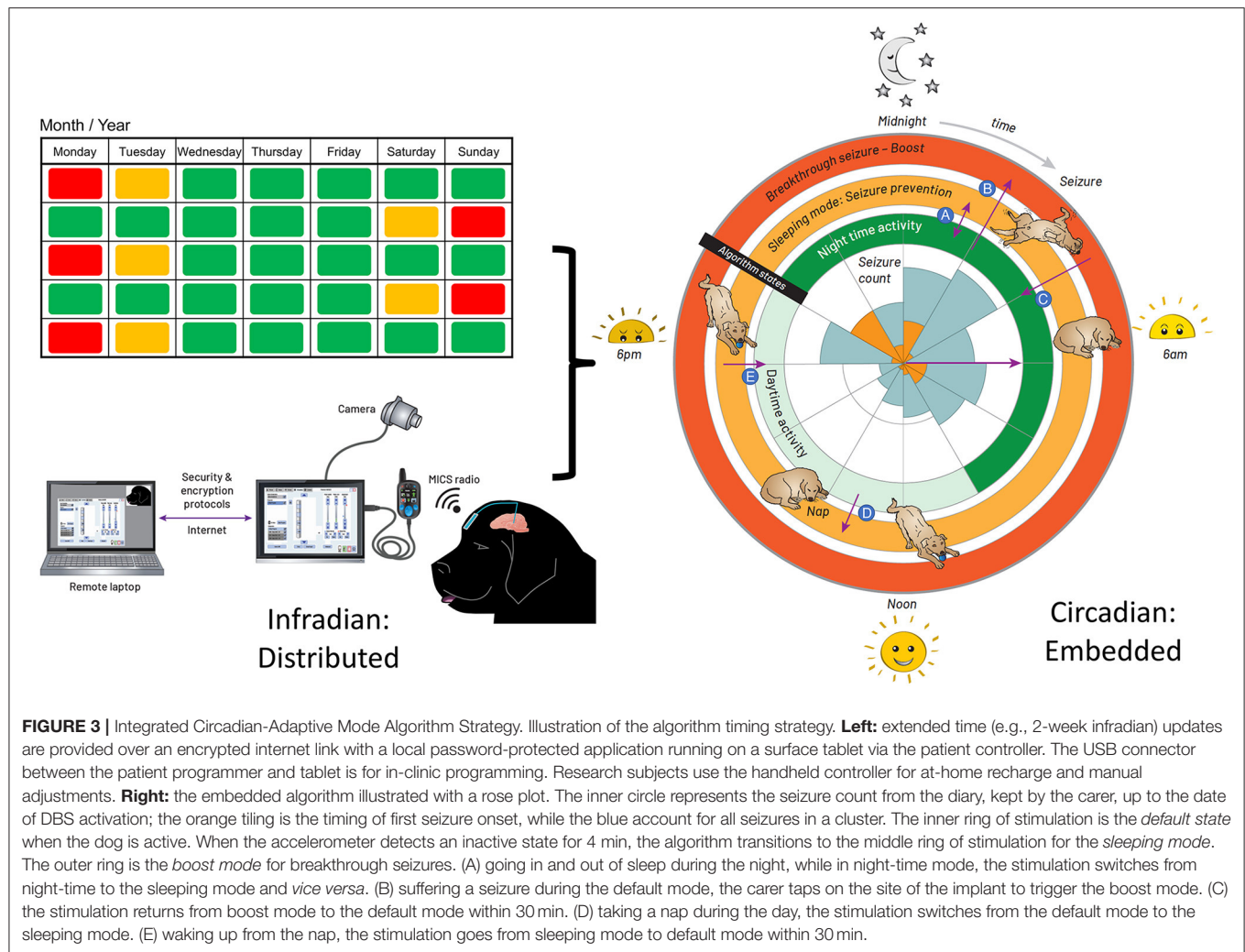


FIGURE 2 | Arnold Tongues and Stimulation Frequency Strategy. (A) Winding number and Arnold tongues in the sine circle map as a function of stimulation (driver) frequency and amplitude for an oscillator with a natural frequency of 13 Hz. Arnold tongues correspond to areas of constant winding number. The 1:1 tongue (winding number of 1) and the 2:1 tongue (winding number of 2) are highlighted with blue dashed lines. For stimulation parameters falling within the p:q tongue, the rhythm will be entrained at p/q times the stimulation frequency. The sine circle map was simulated as $\theta_{i+1} = \theta_i + 2\pi \left(\frac{f_d}{f_s} \right) + I \sin \theta_i$, where θ_i is the oscillator phase right after stimulation pulse i , f_0 is the natural frequency of the oscillator, f_s is the stimulation frequency and I is the stimulation amplitude. The winding number was calculated after $N = 50$ stimulation pulses as the average of $\frac{\theta_N - \theta_0}{2\pi N}$ over 20 trials with random initial phases θ_0 uniformly distributed between 0 and 2π . (B) Intracranial field potentials from the implanted signals (left hemisphere, contacts 0–3) remotely accessed through wireless telemetry. Representative signals were gathered during different activities of daily living to characterize frequency content. The stimulation therapy strategy aims to entrain the healthy rhythm around 13 Hz, while avoiding the peak at 2 Hz observed during seizure. (C) Illustration of the final stimulation strategy. The winding number in the sine circle map is shown here for a fixed stimulation frequency (13 Hz) as a function of natural frequency (e.g., inherent thalamocortical rhythm) and stimulation amplitude. Selected Arnold tongues are highlighted in blue. Stimulation at 13 Hz can reliably entrain the desired 12 Hz thalamocortical oscillation (large 1:1 tongue) while avoiding induction of pathological tongues in the region of 2–3 Hz. The 1:5 and 1:6 tongues obtained from 13 Hz stimulation are indeed so narrow that they will not lead to any entrainment in practice. To account for the fact that neural oscillations at lower frequencies typically have higher power ($1/f$ power law) and would therefore require more energy to entrain, the vertical axis represents equivalent stimulation amplitude (stimulation amplitude multiplied by f_0/f_{\max} , where f_0 is the natural frequency and f_{\max} the maximum frequency shown). This is conservative as the 1:5 and 1:6 tongues disappear at higher stimulation amplitudes.

additional protection, while the *daytime* stimulation is lowered to 0.5 mA to avoid any side-effects of stimulation and conserve energy during low seizure probability intervals. When the accelerometer detects an inactive state for 4 mins, the algorithm transitions to the middle ring of stimulation for the *sleeping mode*, which elevates stimulation amplitude to 1.3 mA at 13 Hz to provide greater entrainment during the increased risk of seizures during sleep. Finally, the outer ring, or *boost mode*, is designed for breakthrough seizures, activated by the carer with a single tap on

the device programmed with a detection threshold of 7 g in the z-axis (orthogonal from the device plane). In this mode, a burst of 130 Hz, 1.5 mA bipolar stimulation is provided to interrupt a sustained seizure.

We remotely synchronized the device for the longer infradian rhythms (Baud et al., 2018). Remote telemetric access allowed us to characterize physiology and reprogram the system in the home environment, as well as check battery levels and tissue-electrode interface impedances. On the left side of **Figure 3**, extended time



(e.g., 2-week infradian) updates are provided over an encrypted internet link with a local password-protected application running on a surface tablet. The patient controller is used to wirelessly update the embedded stimulation parameters.

RESULTS

Prevention of Status Epilepticus

The data is summarized in **Figure 4** based on seizure diary and care plan summary. **Figure 4A** shows the seizure number and medication dosage per month since epilepsy onset, while **Figure 4B** shows the same data on a daily basis from 7 months before until 7 months after implantation and stimulation onset.

Status epilepticus: 3 months before implantation, the seizure severity increased dramatically. Seizures regularly escalated into SE, with three occurring prior to surgery, requiring the use of rescue intervention. After implantation and the use of described stimulation patterns, no SE occurred.

Rescue medications: After implantation of the device, levetiracetam administration as pulse therapy, with major

side-effects, was initially continued after seizure occurrence in order to further interrupt cluster seizure evolution or SE (repetitive administration every 8 h with successive dose reduction over several days). It was possible to successfully break the cluster seizure emergence or evolution in seven seizure occurrence periods (total of nine seizures) via stimulation only without administering levetiracetam as additional rescue medication in these periods (**Figure 4B**). Phenobarbital as chronic treatment was continued over the whole observation time after implantation with a dose reduction from 13.3 to 12.5 mg/kg/day in November 2020. The carer also stopped MCT supplementation and the other antiseizure medications.

Breakthrough seizure intervention: In terms of proactively interrupting ongoing seizures by the carer, the *boost* (HF burst) emergency mode disrupted 14 seizures, while eight seizures continued after interruption attempt. Another eight seizures were not interrupted because they were noticed too late or the *boost mode* was deactivated at those time points. The success rate of the active interruption attempts was thus approximately 64%.

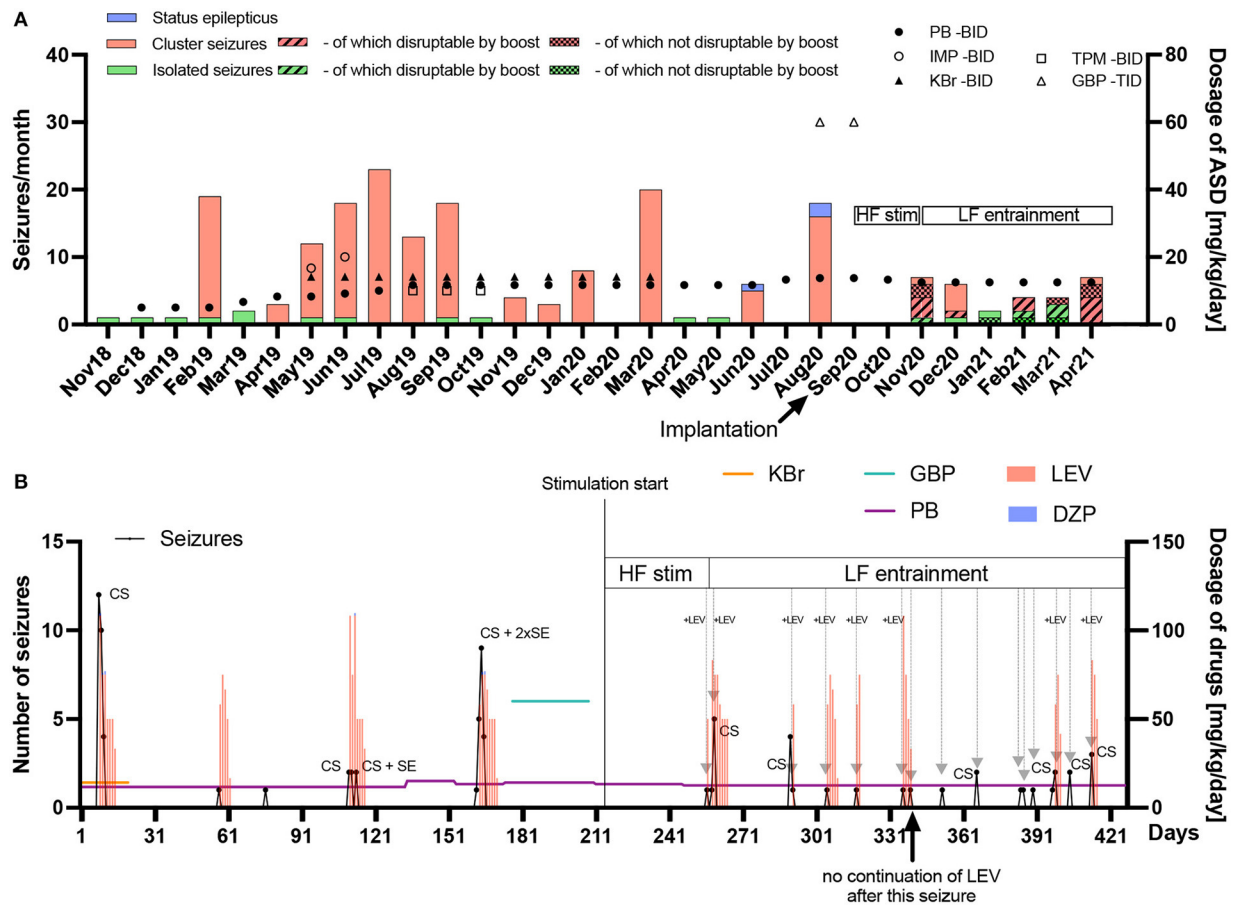


FIGURE 4 | Frequency and chronic/acute pharmacological treatment of seizures until seven months after implantation. **(A)** The seizure frequency (left y-axis) and average daily antiseizure drug (ASD) dosage in mg/kg/day (right y-axis) of phenobarbital (PB), imepitoin (IMP), potassium bromide (KBr), topiramate (TPM) and gabapentin (GBP) twice (BID) or thrice (TID) daily are shown for every month since epilepsy onset in November 2018. When stimulation was started, no further status epilepticus (SE) occurred. After implantation, high frequency (HF) stimulation was applied after seizures occurred in order to prevent SE or further cluster seizure evolution. Since HF did not bring the desired result in the first cluster seizure (November 2020), the frequency was subsequently changed to low frequency (LF) entrainment adapted to the canine's local field potentials. PB was chronically administered as monotherapy (reduction from 13.3 to 12.5 mg/kg/day in November 2020), while other chronic medical and dietary therapy with medium-chain triglycerides was stopped after surgery. With the HF bursting *boost mode* for the interruption of ongoing seizures four seizures out of six attempts in November 2020 were interrupted. One seizure was noticed too late. In December 2020, one seizure was interrupted while five further ones occurred without interruption attempt. In January 2021, one attempt of seizure interruption was without success, while another seizure was noticed too late. In February 2021, two out of three attempts of seizure interruption were successful. In March 2021, three seizures were interrupted while two continued after attempt. In April 2021, four seizures were interrupted, two continued and one was noticed too late. The overall success rate of interruption attempts was 64%. Electrical stimulation has the potential of reducing acute and chronic pharmacological interventions. **(B)** The seizure number (left y-axis) in black dots and lines and average daily ASD dosage in mg/kg/day (right y-axis) for chronic (horizontal colored lines) and emergency treatment (vertical bars) with levetiracetam (LEV) or diazepam (DZP) are shown on a day-to-day basis since begin of March 2020 until end of April 2021 (seven months pre and post implantation). Gray arrows represent successful avoidance of further seizure occurrence/evolution after a single seizure or in cluster seizures (CS) via stimulation with (+LEV) or without LEV intervention. It turned out that initially, only the combination of acute LEV treatment and LF-entrainment prevented or interrupted cluster seizure evolution. Since February 2021, however, LEV was not administered after seizure occurrence due to severe side-effects, with LF-entrainment alone achieving cluster cessation, except in two CS events which consisted of rapid successive but few seizures in April 2021. Eight seizure evolution interruptions were conducted together with LEV and seven without LEV after stimulation onset, with only seven interruptions with LEV during LF-entrainment. DBS has the potential of reducing acute pharmacological interventions.

Significant Trends for Reduction of Cluster Seizures

General trends: The mean number of seizures during a seizure occurrence period, i.e., periods of isolated seizures (IS) or coherent cluster seizures (CS), as well as the mean duration of these periods (IS = 0 h; CS > 0 h) as a measurement for

severity were assessed before and after start of low frequency (LF) entrainment (including preoperative seizures). Since all SE were part of a CS event, they were included for these measurements. The overall number of seizures within a seizure occurrence period since epilepsy onset was 4.67 ± 5.99 [mean \pm SD, range 1–26] with seizures occurring over a time period of 16.21 ± 21.35 h

[mean \pm SD, range 0–74.5] per seizure occurrence period. Before the start of LF entrainment (including preoperative seizures), the number of seizures during an ictal period was 5.84 ± 6.73 [mean \pm SD, range 1–26] vs. 1.77 ± 1.24 [mean \pm SD, range 1–5] after LF entrainment started [$p < 0.05$]. The time between the first and last seizure during a seizure occurrence period was 20.57 ± 23.42 h [mean \pm SD, range 0–74.5] vs. 5.48 ± 8.95 h [mean \pm SD, range 0–24] before and after start of LF entrainment (including preoperative seizures), respectively [$p < 0.05$].

The graph in **Figure 4A** shows that the seizure number decreased in general without showing increased episode frequency, while the graph in **Figure 4B** shows that seizure episodes got more frequent, but less severe than before stimulation.

DISCUSSION

Physiology generally merges feedforward (e.g., circadian) and feedback (e.g., homeostatic) control mechanisms. Implantable bioelectronic systems, while capable of precision timing and adaptive control, have not yet fully adopted a similar integrated control scheme. One reason is the complexity of additional control variables that might burden the clinician while configuring the system; ultimately an additional benefit must be demonstrated to justify the added complexity. However, many systems might yield immediate benefit by simply synchronizing stimulation modification to other diurnal variables such as medication timing. For example, fixed tonic stimulation of neural targets that couple into the reticular activating network have shown impact on sleep architecture (Voges et al., 2015). The fact that many areas of neuromodulation—epilepsy, PD, chronic pain and depression—have sleep co-morbidities also motivates an exploration of aligning stimulation with diurnal cycles to both enhance therapy and avoid side-effects (Sladky et al., 2021).

Alignment of rhythms at multiple scales requires a consideration of entrainment properties. We used the model of Arnold tongues from dynamic systems theory for selecting objectively the stimulation frequency. Arnold tongues can be useful for considering how stimulation might lead to non-linear effects which might not be intuitively predicted and have surprising side-effects. For example, PD patients can have half-harmonic locking of gamma rhythms (e.g., 65 Hz peak) in response to 130 Hz stimulation frequency (Swann et al., 2016). This non-linear mapping of brain stimulation to network oscillations might result inadvertently in reinforcing undesirable side-effects such as dyskinesia (Swann et al., 2016). Critically, these observations support the hypothesis that the conditions for Arnold tongues and subharmonic entrainment of the cortex are present with DBS of the basal ganglia. There is evidence that the alpha rhythm might also play a role in epilepsy (Abela et al., 2019); our strategy of attempting to entrain at a slightly higher frequency might also provide potential benefits, which warrants further investigation. For longer temporal scales such as circadian rhythms, the impact of stimulation as a “digital zeitgeber” might also result in additional phase shifts between existing zeitgebers (e.g., daylight or eating) and the endogenous

circadian rhythm. Such phase shifts could either help restore sleep patterns, or create undesirable side effects, depending on the entrainment characteristics. Validating and applying these non-linear models of entrainment with additional clinical research might help to optimize the timing of stimulation at multiple temporal scales of physiology.

Finally, risk mitigations for novel adaptive stimulation methods must be considered. In the Picostim-DyNeuMo system, these mitigations include constraining the stimulation space to a predefined set of parameters screened by clinicians. In addition, we define a fallback program that a patient or carer can revert to in the case of issues arising with the adaptive mode. This action resets the system to open-loop stimulation, which is the default for most existing neuromodulation approach. An overview of the risk strategy method can be found in Gunduz et al. (2019).

CASE LIMITATIONS

This case report has several limitations. The study is of a single canine, which limits the statistical conclusions, but primarily serves as pilot validation of the implant technology. Although our results are consistent with recent human case studies (Valentín et al., 2012; Sa et al., 2019; Stavropoulos et al., 2021) where the benefit of CMN thalamic stimulation at LF relative to HF was observed providing further support for the clinical value of thalamic LF stimulation, additional tests are needed. We adapted the stimulation based on physiological measurements and chose a higher frequency stimulation for entrainment. In addition, the application of experimental medicine prevented us from applying a self-control such as terminating treatment and assessing the impact on seizures. During the course of stimulation exploration, however, we were able to confirm that stimulation at 2 Hz in the CMN increased the probability of seizures (induction < 24 h after setting) consistent with previous observations (Velasco et al., 1997). The case is ongoing and the reported results are limited to the first 7 months of follow-up. Prior studies of epilepsy have shown changing efficacy over many years, although arguably for the better on average (Nair et al., 2020). In addition, we are relying on manual seizure diary which can be unreliable (Ukai et al., 2021); the strongest evidence we have are the SE events, which are severe enough to not be missed by the carer. Finally, the Picostim-DyNeuMo is limited by law to investigational device applications at this time.

SUMMARY

The synchronization of brain stimulation to endogenous rhythms is an emerging concept for therapy optimization. The use of digitally-enabled chronotherapy as a feedforward signal to augment adaptive neurostimulators could prove to be a useful algorithmic method where sensitivity to temporal rhythms are characteristics of the disease state, tailoring a more patient-specific therapy approach. Computational models predicting Arnold tongues can also guide the design of patient-specific stimulation parameters, which has often been a heuristic process.

In this proof-of-concept study, using a novel chronotherapy-enabled device in a canine with severe drug-resistant idiopathic epilepsy, these methods had favorable outcomes in terms of improving seizure semiology, reducing coherent cluster seizures and controlling (or avoiding) SE. The carer reports a reduced fear of seizures and improved personal quality of life based on the reduction of seizure severity with the stimulation. The adaptability of this approach allows for individualized therapies that are supported by emerging adaptive devices with both physiological sensing and chronotherapy capability. In addition, this report of DBS in canine epilepsy further highlights the possibility of using veterinary medicine as a vehicle to test new device and treatment paradigms (Potschka et al., 2013).

DATA AVAILABILITY STATEMENT

The raw data supporting the conclusions of this article will be made available by the authors, without undue reservation.

AUTHOR CONTRIBUTIONS

TD and HV: conceptualization. TD, HV, and D-JD: design of the study. SM, HV, and FK: surgery and veterinary care. TD, D-JD, GW, and AV: algorithm definition. MZ and MB: algorithm implementation. SM, MZ, RT, RB, BD, and JS: data analysis. TD,

SM, FK, RT, MZ, BD, and JS: figures. TD, MZ, SM, and HV: writing original draft. All authors writing, reviewing and editing.

FUNDING

MZ and JS were supported by the Medical Research Council grant MC_UU_00003/3, RB and BD by grants MC_UU_12024/5 and MC_UU_00003/1. TD was funded by the Royal Academy of Engineering.

ACKNOWLEDGMENTS

The authors would like to thank the directors and staff of Bioinduction for their invaluable help in the development and support of the Picostim-DyNeuMo research system. We also thank Theresia Henne and Anke Nagel for their support in the presurgical planning. Special thanks go to the patient's family for the dedication and care. We also extend our appreciation to Karen Wendt for her help translating during the follow up remote sessions with the carer.

SUPPLEMENTARY MATERIAL

The Supplementary Material for this article can be found online at: <https://www.frontiersin.org/articles/10.3389/fnins.2021.734265/full#supplementary-material>

REFERENCES

- Abela, E., Pawley, A. D., Tangwiriyasakul, C., Yaakub, S. N., Chowdhury, F. A., Elwes, R. D. C., et al. (2019). Slower alpha rhythm associates with poorer seizure control in epilepsy. *Ann. Clin. Transl. Neurol.* 6, 333–343. doi: 10.1002/acn3.710
- Ali, M. M., Sellers, K. K., and Frohlich, F. (2013). Transcranial alternating current stimulation modulates large-scale cortical network activity by network resonance. *J. Neurosci.* 33, 11262–11275. doi: 10.1523/JNEUROSCI.5867-12.2013
- Arnol'd, V. I. (1983). Remarks on the perturbation theory for problems of Mathieu type. *Russian Mathematic. Surv.* 38:215. doi: 10.1070/RM1983v038n04ABEH004210
- Baud, M. O., Kleen, J. K., Mirro, E. A., Andrechak, J. C., King-Stephens, D., Chang, E. F., et al. (2018). Multi-day rhythms modulate seizure risk in epilepsy. *Nat. Commun.* 9:88. doi: 10.1038/s41467-017-02577-y
- Berk, B. A., Law, T. H., Packer, R. M. A., Wessmann, A., Bathen-Nöthen, A., Jokinen, T. S., et al. (2020). A multicenter randomized controlled trial of medium-chain triglyceride dietary supplementation on epilepsy in dogs. *J. Veter. Intern. Med.* 34, 1248–1259. doi: 10.1111/jvim.15756
- Bordyugov, G., Abraham, U., Granada, A., Rose, P., Imkeller, K., Kramer, A., et al. (2015). Tuning the phase of circadian entrainment. *J. R. Soc. Interface* 12:20150282. doi: 10.1098/rsif.2015.0282
- De Rasio, L., Bhatti, S., Muñana, K., Penderis, J., Stein, V., Tipold, A., et al. (2015). International veterinary epilepsy task force consensus proposal: diagnostic approach to epilepsy in dogs. *BMC Vet. Res.* 11:148. doi: 10.1186/s12917-015-0462-1
- Fisher, B., DesMarteau, J. A., Koontz, E. H., Wilks, S. J., and Melamed, S. E. (2021). Responsive vagus nerve stimulation for drug resistant epilepsy: a review of new features and practical guidance for advanced practice providers. *Front. Neurol.* 11:610379. doi: 10.3389/fneur.2020.610379
- Fisher, R., Salanova, V., Witt, T., Worth, R., Henry, T., Gross, R., et al. (2010). Electrical stimulation of the anterior nucleus of thalamus for treatment of refractory epilepsy. *Epilepsia* 51, 899–908. doi: 10.1111/j.1528-1167.2010.02536.x
- Glass, L. (2001). Synchronization and rhythmic processes in physiology. *Nature* 410, 277–284. doi: 10.1038/35065745
- Glass, L., and Mackey, M. C. (1979). A simple model for phase locking of biological oscillators. *J. Math. Biol.* 7, 339–352. doi: 10.1007/BF00275153
- Gregg, N. M., Nasser, M., Kremen, V., Patterson, E. E., Sturges, B. K., Denison, T. J., et al. (2020). Circadian and multiday seizure periodicities, and seizure clusters in canine epilepsy. *Brain Commun.* 2:fcaa008. doi: 10.1093/braincomms/fcaa008
- Gunduz, A., Opri, E., Gilron, R., Kremen, V., Worrell, G., Starr, P., et al. (2019). Adding wisdom to “smart” bioelectronic systems: a design framework for physiologic control including practical examples. *Bioelectron. Med.* 2, 29–41. doi: 10.2217/bem-2019-0008
- Herrmann, C. S., Murray, M. M., Ionta, S., Hutt, A., and Lefebvre, J. (2016). Shaping intrinsic neural oscillations with periodic stimulation. *J. Neurosci.* 36, 5328–5337. doi: 10.1523/JNEUROSCI.0236-16.2016
- Leguia, M. G., Andrzejak, R. G., Rummel, C., Fan, J. M., Mirro, E. A., Tchong, T. K., et al. (2021). Seizure cycles in focal epilepsy. *JAMA Neurol.* 78, 454–463. doi: 10.1001/jamaneurol.2020.5370
- Malhotra, R. K. (2018). Neurodegenerative disorders and sleep. *Sleep Med. Clin.* 13, 63–70. doi: 10.1016/j.jsmc.2017.09.006
- Martín-López, D., Jiménez-Jiménez, D., Cabañés-Martínez, L., Selway, R. P., and Valentin, A. (2017). The role of thalamus versus cortex in epilepsy: evidence from human ictal centromedian recordings in patients assessed for deep brain stimulation. *Int. J. Neural Syst.* 27:1750010. doi: 10.1142/S0129065717500101
- Nair, D. R., Laxer, K. D., Weber, P. B., Murro, A. M., Park, Y. D., Barkley, G. L., et al. (2020). Nine-year prospective efficacy and safety of brain-responsive neurostimulation for focal epilepsy. *Neurology* 95, e1244–e1256. doi: 10.1212/WNL.00000000000010154

- Oswal, A., Brown, P., and Litvak, V. (2013). Synchronized neural oscillations and the pathophysiology of Parkinson's disease. *Curr. Opin. Neurol.* 26, 662–670. doi: 10.1097/WCO.0000000000000034
- Packer, R. M. A., Nye, G., Porter, S. E., and Volk, H. A. (2015). Assessment into the usage of levetiracetam in a canine epilepsy clinic. *BMC Vet. Res.* 11:25. doi: 10.1186/s12917-015-0340-x
- Perez, R., and Glass, L. (1982). Bistability, period doubling bifurcations and chaos in a periodically forced oscillator. *Phys. Lett. A* 90, 441–443. doi: 10.1016/0375-9601(82)90391-7
- Pikovsky, A., Rosenblum, M., and Kurths, J. (2002). Synchronization: a universal concept in nonlinear science. *Am. J. Phys.* 70, 655–655. doi: 10.1119/1.1475332
- Potschka, H., Fischer, A., von Ruden, E. L., Hulsmeyer, V., and Baumgartner, W. (2013). Canine epilepsy as a translational model? *Epilepsia* 54, 571–579. doi: 10.1111/epi.12138
- Priori, A., Foffani, G., Rossi, L., and Marceglia, S. (2013). Adaptive deep brain stimulation (aDBS) controlled by local field potential oscillations. *Exp. Neurol.* 245, 77–86. doi: 10.1016/j.expneurol.2012.09.013
- Sa, M., Singh, R., Pujar, S., D'Arco, F., Desai, N., Eltze, C., et al. (2019). Centromedian thalamic nuclei deep brain stimulation and Anakinra treatment for FIRES—Two different outcomes. *Eur. J. Paediatr. Neurol.* 23, 749–754. doi: 10.1016/j.ejpn.2019.08.001
- Schulze-Bonhage, A. (2019). Long-term outcome in neurostimulation of epilepsy. *Epilepsy Behav.* 91, 25–29. doi: 10.1016/j.yebeh.2018.06.011
- Skeldon, A. C., Phillips, A. J., and Dijk, D. J. (2017). The effects of self-selected light-dark cycles and social constraints on human sleep and circadian timing: a modeling approach. *Sci. Rep.* 7:45158. doi: 10.1038/srep45158
- Sladky, V., Nejedly, P., Mivalt, F., Brinkmann, B. H., Kim, I., Louis, S., et al. (2021). Distributed brain co-processor for neurophysiologic tracking and adaptive stimulation: application to drug resistant epilepsy. *bioRxiv* 8:434476. doi: 10.1101/2021.03.08.434476
- Stavropoulos, I., Selway, R., Hasegawa, H., Hughes, E., Rittey, C., Jiménez-Jiménez, D., et al. (2021). Low frequency centromedian thalamic nuclei deep brain stimulation for the treatment of super refractory status epilepticus: a case report and a review of the literature. *Brain Stimul.* 14, 226–229. doi: 10.1016/j.brs.2020.12.013
- Stiefel, K. M., Gutkin, B. S., and Sejnowski, T. J. (2008). Cholinergic neuromodulation changes phase response curve shape and type in cortical pyramidal neurons. *PLoS ONE* 3:e3947. doi: 10.1371/journal.pone.0003947
- Swann, N. C., de Hemptinne, C., Miocinovic, S., Qasim, S., Wang, S. S., Ziman, N., et al. (2016). Gamma oscillations in the hyperkinetic state detected with chronic human brain recordings in parkinson's disease. *J. Neurosci.* 36, 6445–6458. doi: 10.1523/JNEUROSCI.1128-16.2016
- Swann, N. C., de Hemptinne, C., Thompson, M. C., Miocinovic, S., Miller, A. M., Gilron, R., et al. (2018). Adaptive deep brain stimulation for Parkinson's disease using motor cortex sensing. *J. Neural Eng.* 15:046006. doi: 10.1088/1741-2552/aabc9b
- Toth, R., Zamora, M., Ottaway, J., Gillbe, T., Martin, S., Benjaber, M., et al. (2020). "DyNeuMo Mk-2: an investigational circadian-locked neuromodulator with responsive stimulation for applied chronobiology," in *Proceedings of the 2020 IEEE International Conference on Systems, Man, and Cybernetics (SMC)*, Toronto, ON, 3433–3440.
- Trevisan, M. A., Mindlin, G. B., and Goller, F. (2006). Nonlinear model predicts diverse respiratory patterns of birdsong. *Phys. Rev. Lett.* 96:058103. doi: 10.1103/PhysRevLett.96.058103
- Ukai, M., Parmentier, T., Cortez, M. A., Fischer, A., Gaitero, L., Lohi, H., et al. (2021). Seizure frequency discrepancy between subjective and objective ictal electroencephalography data in dogs. *J. Vet. Intern. Med.* 16:158. doi: 10.1111/jvim.16158
- Valentín, A., Navarrete, G. E., Chelvarajah, R., Torres, R., Navas, M., Vico, L., et al. (2013). Adaptive deep brain stimulation in advanced Parkinson disease. *Ann. Neurol.* 74, 449–457. doi: 10.1002/ana.23951
- Valentín, A., Navarrete, G. E., C., R., T., et al. (2013). Deep brain stimulation of the centromedian thalamic nucleus for the treatment of generalized and frontal epilepsies. *Epilepsia* 54, 1823–1833. doi: 10.1111/epi.12352
- Valentín, A., Nguyen, H. Q., Skupenova, A. M., Agirre-Arrizubieta, Z., Jewell, S., Mullatti, N., et al. (2012). Centromedian thalamic nuclei deep brain stimulation in refractory status epilepticus. *Brain Stimul.* 5, 594–598. doi: 10.1016/j.brs.2011.10.002
- Velasco, F., Velasco, A. L., Velasco, M., Jiménez, F., Carrillo-Ruiz, J. D., and Castro, G. (2007). "Deep brain stimulation for treatment of the epilepsies: the centromedian thalamic target," in *Operative Neuromodulation* (Vienna: Springer), 337–342.
- Velasco, M., Velasco, F., Velasco, A. L., Brito, F., Jimenez, F., Marquez, I., et al. (1997). Electrocortical and behavioral responses produced by acute electrical stimulation of the human centromedian thalamic nucleus. *Electroencephalogr. Clin. Neurophysiol.* 102, 461–471. doi: 10.1016/S0013-4694(96)95203-0
- Voges, B. R., Schmitt, F. C., Hamel, W., House, P. M., Kluge, C., Moll, C. K., et al. (2015). Deep brain stimulation of anterior nucleus thalami disrupts sleep in epilepsy patients. *Epilepsia* 56, e99–e103. doi: 10.1111/epi.13045

Conflict of Interest: TD has business relationships with Bioinduction for research tool design and deployment. GW has a financial interest in Cadence Neuroscience Inc.

The remaining authors declare that the research was conducted in the absence of any commercial or financial relationships that could be construed as a potential conflict of interest.

Publisher's Note: All claims expressed in this article are solely those of the authors and do not necessarily represent those of their affiliated organizations, or those of the publisher, the editors and the reviewers. Any product that may be evaluated in this article, or claim that may be made by its manufacturer, is not guaranteed or endorsed by the publisher.

Copyright © 2021 Zamora, Meller, Kajin, Sermon, Toth, Benjaber, Dijk, Bogacz, Worrell, Valentín, Duchet, Volk and Denison. This is an open-access article distributed under the terms of the Creative Commons Attribution License (CC BY). The use, distribution or reproduction in other forums is permitted, provided the original author(s) and the copyright owner(s) are credited and that the original publication in this journal is cited, in accordance with accepted academic practice. No use, distribution or reproduction is permitted which does not comply with these terms.



Patient, Caregiver, and Decliner Perspectives on Whether to Enroll in Adaptive Deep Brain Stimulation Research

Simon Outram^{1*}, Katrina A. Muñoz², Kristin Kostick-Quenet², Clarissa E. Sanchez², Lavina Kalwani², Richa Lavingia³, Laura Torgerson², Demetrio Sierra-Mercado^{2,4}, Jill O. Robinson², Stacey Pereira², Barbara A. Koenig¹, Philip A. Starr⁵, Aysegul Gunduz^{6,7}, Kelly D. Foote⁶, Michael S. Okun⁶, Wayne K. Goodman⁸, Amy L. McGuire², Peter Zuk² and Gabriel Lázaro-Muñoz²

OPEN ACCESS

Edited by:

Doris D. Wang,
University of California,
San Francisco, United States

Reviewed by:

Ignacio Delgado Martinez,
Hospital del Mar Medical Research
Institute (IMIM), Spain
Brent Winslow,
Design Interactive, United States

*Correspondence:

Simon Outram
simon.outram@ucsf.edu

Specialty section:

This article was submitted to
Neural Technology,
a section of the journal
Frontiers in Neuroscience

Received: 30 June 2021

Accepted: 16 August 2021

Published: 07 October 2021

Citation:

Outram S, Muñoz KA, Kostick-Quenet K, Sanchez CE, Kalwani L, Lavingia R, Torgerson L, Sierra-Mercado D, Robinson JO, Pereira S, Koenig BA, Starr PA, Gunduz A, Foote KD, Okun MS, Goodman WK, McGuire AL, Zuk P and Lázaro-Muñoz G (2021) Patient, Caregiver, and Decliner Perspectives on Whether to Enroll in Adaptive Deep Brain Stimulation Research. *Front. Neurosci.* 15:734182. doi: 10.3389/fnins.2021.734182

¹ Program in Bioethics, University of California, San Francisco, San Francisco, CA, United States, ² Center for Medical Ethics and Health Policy, Baylor College of Medicine, Houston, TX, United States, ³ Baylor College of Medicine, Houston, TX, United States, ⁴ Department of Anatomy and Neurobiology, School of Medicine, University of Puerto Rico, San Juan, Puerto Rico, ⁵ Department of Neurosurgery, University of California, San Francisco, San Francisco, CA, United States, ⁶ Fixel Institute for Neurological Diseases, Program for Movement Disorders and Neurorestoration, Department of Neurology, University of Florida, Gainesville, FL, United States, ⁷ Department of Biomedical Engineering, University of Florida, Gainesville, FL, United States, ⁸ Department of Psychiatry and Behavioral Sciences, Baylor College of Medicine, Houston, TX, United States

This research study provides patient and caregiver perspectives as to whether or not to undergo adaptive deep brain stimulation (aDBS) research. A total of 51 interviews were conducted in a multi-site study including patients undergoing aDBS and their respective caregivers along with persons declining aDBS. Reasons highlighted for undergoing aDBS included hopes for symptom alleviation, declining quality of life, desirability of being in research, and altruism. The primary reasons for not undergoing aDBS issues were practical rather than specific to aDBS technology, although some persons highlighted a desire to not be the first to trial the new technology. These themes are discussed in the context of “push” factors wherein any form of surgical intervention is preferable to none and “pull” factors wherein opportunities to contribute to science combine with hopes and/or expectations for the alleviation of symptoms. We highlight the significance of study design in decision making. aDBS is an innovative technology and not a completely new technology. Many participants expressed value in being part of research as an important consideration. We suggest that there are important implications when comparing patient perspectives vs. theoretical perspectives on the choice for or against aDBS. Additionally, it will be important how we communicate with patients especially in reference to the complexity of study design. Ultimately, this study reveals that there are benefits and potential risks when choosing a research study that involves implantation of a medical device.

Keywords: aDBS, altruism, decision-making, interviews, quality of life, research, study design, symptoms

INTRODUCTION

Deep brain stimulation (DBS) is a well-established neurosurgical procedure whereby electrodes are surgically implanted into the brain to address common motor symptoms associated with movement disorders. For just over two decades, DBS has had remarkable success in the alleviation of select symptoms relating to Parkinson's disease (PD) and has become an important therapy for motor symptoms and movement disorders (Hariz, 2017; Hartmann et al., 2019; Artusi et al., 2020). Given the relative success of DBS, there has been considerable interest in whether DBS might be used for treating other brain disorders including Alzheimer's disease, obsessive compulsive disorder (OCD), and Tourette syndrome. A body of literature has emerged exploring both the likely efficacy and the ethical implications of a broader application of DBS, especially focusing upon the medical and ethical implications of addressing psychological symptomologies as opposed to motor symptoms (Widge et al., 2016a,b; Siegel et al., 2017; Aldehri et al., 2018; Lawrence et al., 2018; Víaña and Gilbert, 2019; Vicheva et al., 2020; Xu et al., 2020; Bonomo and Vetrano, 2021; Smith et al., 2021).

In addition to potentially broadening the scope of DBS usage, an innovative form of DBS is being trialed—known as adaptive deep brain stimulation (aDBS) or closed loop DBS—wherein a sensor electrode is employed to track fluctuations in brain activity possibly associated with clinical symptoms and the system is programmed to deploy or to adjust the level of stimulation (Habets et al., 2018; Swann et al., 2018; Little and Brown, 2020). In part, the development of aDBS was in response to some of the side effects of conventional DBS, including dysarthria, imbalance, hypomania, and dyskinesia as there was an inability to reduce these side effects by adjusting stimulation in real time (Widge et al., 2016b; Habets et al., 2018). By addressing this limitation, aDBS theoretically would be able to provide a more personalized or tailored program of stimulation, thus reducing the likelihood of over- or under-stimulation. Moreover, since this strategy does not employ continuous stimulation, aDBS technology has the potential to increase battery life, decreasing surgeries, and thus reducing morbidities associated with battery replacement surgeries. aDBS does, however, raise philosophical questions about the capacity of the device to stimulate or not stimulate without human input. As Klein et al. (2016) have penned, aDBS is a distinctly novel form of neuromodulation by which “one has effectively constructed a device that autonomously determines what the patient may or may not feel.” This has raised concerns about the impact of aDBS on personal autonomy given that that the algorithm self-directs the stimulation (Goering et al., 2017; Lázaro-Muñoz et al., 2017; Kostick and Lázaro-Muñoz, 2021).

These philosophical concerns may or may not play a role in the decision-making process of prospective DBS surgery patients. Individuals considering aDBS must decide (i) whether they feel brain surgery of any type is their best option, (ii) whether they feel that experimental aDBS is preferable to standard—non-adaptive—DBS (if available for their condition), and (iii) whether they want to be part of a research study (given that aDBS is only offered as part of research rather than as standard clinical practice). The following manuscript provides empirical data on

how patients and caregivers reach a decision on accepting or declining aDBS surgery for the alleviation of the symptoms of dystonia, OCD, essential tremor, PD, and Tourette syndrome.

METHODS AND ANALYSIS

This study was embedded into aDBS clinical trials at Baylor College of Medicine, UCSF, and the University of Florida. Clinical trial.gov numbers are as follows: Baylor College of Medicine—NCT03457675, NCT04281134; UCSF—NCT03131817, NCT01934296, and NCT03582891; University of Florida—NCT02649166, NCT02056873. Semi-structured interviews were conducted with trial patients and their caregivers using a similar set of questions, both prior to surgery and approximately 6 months post-surgery. Individuals who decided not to participate in the aDBS trial were interviewed at one time point post-decline. Interviews were conducted in person or *via* Zoom/phone and lasted an average of 30–35 min for patients and caregivers and 20–25 min for decliners. The interviews were audio recorded and transcribed verbatim, with consent. All transcripts were de-identified prior to analysis. This study was approved by the Baylor College of Medicine Institutional Review Board.

Each interview cohort (patients, patient caregivers, and study decliners) was asked about the decision to participate or not to participate in a trial which would implant aDBS: Why did you decide to enroll in the study? (patients); what do you think about the patient's decision to enroll in the study (patient caregivers); why did you decide not to enroll in the study? (study decliners). To identify patient responses to these questions, two members of the research team independently coded each interview transcript using MAXQDA 2018 qualitative data analysis software (Kuckartz). In line with established principles of qualitative research, we conducted interviews until reaching theme saturation, understood as a point at which interviewees were no longer raising novel themes relative to previous interviewees (Saunders et al., 2018). These text segments were then progressively abstracted (SO) utilizing thematic content analysis to identify a set of themes and sub-themes, which were corroborated (KM). The frequencies were not intended to suggest any level of statistical significance but were treated as descriptive data detailing how often a particular theme emerged organically and/or in response to interview questions.

RESULTS

Response rate were as follows: Response rates: 21 out of 23 patients = 91.3%, 20 out of 20 caregivers, and 10 out of 14 decliners = 71.4%. Of the 21 patients who agreed to interview, all but one had a respective caregiver who was also interviewed. One patient did not feel there was anyone who counted as being in a caregiver role for them. Demographic variables are provided to indicate the characteristics of the population interviewed (see **Tables 1–3**). Although data was reviewed to see if there were

TABLE 1 | Patient demographics[†].

Variable	Group					
	OCD <i>n</i> = 5	Essential tremor <i>n</i> = 3	Tourette syndrome <i>n</i> = 4*	Parkinson's <i>n</i> = 8	Dystonia <i>n</i> = 1	Total <i>n</i> = 21*
Age						
Mean	35.6	71.3	32.5	54.6	57	50.1
Min-max	31–40	71–72	24–41	28–71	–	24–72
How do you describe your gender?						
Male	2 (40%)	2 (66.7%)	1 (50%)	6 (75%)	–	11 (57.9%)
Female	3 (60%)	1 (33.3%)	1 (50%)	2 (25%)	1 (100%)	8 (42.1%)
Are you of Hispanic, Latino, or Spanish origin?						
Yes	1 (20%)	–	–	3 (37.5%)	–	4 (21.1%)
No	3 (60%)	3 (100%)	2 (100%)	5 (62.5%)	1 (100%)	14 (73.7%)
No response	1 (20%)	–	–	–	–	1 (5.3%)
Race						
Asian	–	–	–	1 (12.5%)	–	1 (5.3%)
White	4 (80%)	3 (100%)	2 (100%)	6 (75%)	1 (100%)	15 (78.9%)
Other	1 (20%)	–	–	1 (12.5%)	–	3 (15.8%)
Total household income (before taxes) from all sources in the last year						
\$0 to \$49,999	2 (40%)	1 (33.3%)	1 (50%)	2 (25%)	–	6 (31.6%)
\$50,000 to \$99,999	2 (40%)	–	–	1 (12.5%)	–	3 (15.8%)
\$100,000 to \$149,999	1 (20%)	1 (33.3%)	1 (50%)	2 (25%)	–	5 (26.3%)
\$150,000 or more	–	1 (33.3%)	–	3 (37.5%)	1 (100%)	5 (26.3%)
Source of health insurance**						
Employer	–	–	–	1 (12.5%)	–	1 (5.3%)
Parents or partner	3 (60%)	–	1 (50%)	1 (12.5%)	1 (100%)	6 (31.6%)
Medicaid or other state insurance	2 (40%)	–	–	3 (37.5%)	–	5 (26.3%)
Medicare	–	3 (100%)	1 (50%)	2 (25%)	–	6 (31.6%)
Private health insurance	–	–	–	1 (12.5%)	–	1 (5.3%)
Other	–	–	1 (50%)	–	–	1 (5.3%)

[†]All patients with essential tremor, Tourette syndrome, Parkinson's disease, and dystonia had additional implanted hardware and no patients with OCD had additional hardware. The additional hardware was placement of cortical strips in addition to the DBS leads.

*Two patients receiving aDBS for Tourette syndrome did not complete the demographics survey. All "Total" percentages are therefore calculated with *n* = 19 as a denominator and within-disorder percentages for Tourette syndrome calculated with *n* = 2 as a denominator.

**Sums to greater than 100% because patients were able to select multiple options.

any immediately evident differences in population characteristics between patients and decliners, the small size of the population precluded further detailed statistical analysis.

It may be of note that most decliners (7) were high-income (>\$100,000), while just under half of patients were. Figures were too small to draw any conclusions from this difference. It should also be noted that income figures are difficult to compare due to major differences between states in respect to cost of living and average income. Nearly all patients received health care through either parents/partner (6), Medicaid (7), or Medicare (6). Only one patient received health care through their employer. By contrast, only half (5) of decliners received health care through their employer, only 1 through parent/partner, only 1 through Medicare, and 0 through Medicaid. Again, figures are too small to draw conclusions about these differences.

A condensed summary providing frequency of themes for undergoing aDBS is provided in **Table 4**, below.

Patients' and Caregivers' Reasons for Trial Participation

Hopes for Symptom Alleviation Through aDBS

Hopes for symptom alleviation from aDBS surgery played a significant role in the decision-making process. In total, 27 out of 41 interviewees (66%) expressed hope for some form of benefit from aDBS. A greater percentage of patients shared that they were hopeful that the surgery would alleviate their symptoms (17/21, 81%) than caregivers (10/20, 50%). As **Table 5** indicates, interviewees tended to see aDBS as a good option *given the circumstances*; they recognized that although it may not work, they felt there was nothing to lose at this point in their disease progression. However, even some patients who self-identified as reasonably healthy decided to enroll in an aDBS trial, hoping that it would prevent their symptoms from getting worse (see final quote in **Table 5**).

TABLE 2 | Caregiver demographics.

Variable	Group				
	OCD <i>n</i> = 5	Essential Tremor <i>n</i> = 3	Tourette Syndrome <i>n</i> = 4*	Parkinson's Disease <i>n</i> = 8	Total <i>n</i> = 20*
Age					
Mean	52	69	48.3	57.8	56.5
Min-max	30–70	65–73	23–68	31–72	23–73
How do you describe your gender?					
Female	3 (60%)	2 (66.7%)	3 (100%)	6 (75%)	14 (73.7%)
Male	2 (40%)	1 (33.3%)	–	2 (25%)	5 (26.3%)
Are you of Hispanic, Latino, or Spanish origin? (<i>n</i> = 18)**					
Yes	1 (20%)	–	–	1 (14.3%)	2 (11.1%)
No	4 (80%)	3 (100%)	3 (100%)	6 (85.7%)	16 (88.9%)
How do you describe your race?***					
American Indian or Alaska Native	1 (20%)	–	–	1 (12.5%)	2 (10.5%)
White	4 (80%)	3 (100%)	3 (100%)	7 (87.5%)	17 (89.5%)
Other	1 (20%)	–	–	1 (12.5%)	2 (10.5%)
What is your relationship to the patient?					
Spouse	2 (40%)	3 (100%)	1 (33.3%)	8 (100%)	14 (73.7%)
Mother	3 (60%)	–	2 (66.7%)	–	5 (26.3%)

*One caregiver of a patient receiving aDBS for Tourette syndrome did not complete the demographics survey. All "Total" percentages are therefore calculated with *n* = 19 as a denominator and within-disorder percentages for Tourette syndrome calculated with *n* = 3 as a denominator.

**One caregiver of a patient receiving aDBS for Parkinson's disease completed other survey questions but did not respond to this question.

***Sums to greater than 100% as respondents were asked to select all that apply.

Quality of Life

Relatedly, about half of the interviewees (20/41, 49%) reported a decline in quality of life as a reason for trial participation, with 14/21 (67%) patients and 6/20 (30%) caregivers raising quality of life issues as a rationale for choosing to have aDBS surgery (see **Table 6**, below).

The Desirability of Being in Research

A number of patients 11/41 (27%; including nine patients and two caregivers) referred to being in a research trial—rather than specific benefits of aDBS—as being an important consideration in choosing to enter the respective study. These considerations were largely centered upon the benefits of being closely monitored as a research patient and a generalizable technological enthusiasm. Finally, receiving treatment free of charge due to being in research was specifically raised by two patients (see **Table 7**, below).

Altruism and Helping Oneself

Altruism was another of the more frequently occurring rationales for electing to participate in an aDBS trial, with 12/41 (29%) of interviewees referring to one or more forms of altruistic rationale. As summarized in **Table 8**, the expression of altruism varied significantly, from hoping to contribute to science, to helping others with the same condition, to potentially helping future patients or family members. Often, the distinction between each was blurred or different expressions of altruism were referred to by the same interviewee. It is notable that altruism was expressed far more often by patients (11/21) than caregivers (1/20), suggesting patients might see themselves as directly giving

or contributing more often than caregivers. It is possible that patients felt more justified in deciding to undergo brain surgery on themselves for altruistic reasons, while caregivers primarily thought about benefits and risks to the patient rather than the general population (see **Table 8**, below).

It is important to note that for several interviewees, altruism was not an exclusive motivation but instead was combined with the hope that the technology would improve their own lives, as illustrated in the following quotes:

From a selfish standpoint I want to try it, but also from a standpoint of helping me, helping the research, I felt that it would be good to participate. [Patient]

If I can add on a little bit that could possibly help down the road for myself or other people, great. That to me is worth it. [Patient]

At first, I really liked the idea that it could help further OCD research, just that of course, first and foremost, I will be really thankful to have a chance at feeling better. [Patient]

Recommendations From Others

Although perhaps relatively non-controversial, an important consideration among interviewees was the advice of others that undertaking to have aDBS would be a good choice. This particularly related to advice from a patient's primary care provider. A total of nine interviewees (22%) including seven patients and two caregivers indicated that this was important in their decision making. **Table 9** provides illustrative excerpts from interviews on this subject.

TABLE 3 | Decliner demographics.

Variable	Group		
	OCD (n = 2)	Parkinson's (n = 8)	Total (n = 10)
Age (n = 9)*			
Mean	39	54.6	52.9
Min-max	–	38–68	38–68
How do you describe your gender?			
Female	1 (50%)	4 (50%)	5 (50%)
Male	1 (50%)	4 (50%)	5 (50%)
Are you of Hispanic, Latino, or Spanish origin?			
No	2 (100%)	8 (100%)	10 (100%)
Yes	–	–	–
How do you describe your race?			
Asian	–	1 (12.5%)	1 (10%)
White	2 (100%)	7 (87.5%)	9 (90%)
Total household income (before taxes) from all sources in the last year (n = 9)**			
\$0 to \$49,999	1 (50%)	–	1 (11.1%)
\$50,000 to \$99,999	–	1 (14%)	1 (11.1%)
\$100,000 to \$149,999	–	3 (43%)	3 (33.3%)
\$150,000 or more	1 (50%)	3 (43%)	4 (44.4%)
Source of health insurance			
Employer	1 (50%)	4 (50%)	5 (50%)
Parents or partner	–	1 (12.5%)	1 (10%)
Healthcare marketplace	–	1 (12.5%)	1 (10%)
Medicare	–	1 (12.5%)	1 (10%)
Private health insurance	1 (50%)	–	1 (10%)
Other	–	1 (12.5%)	1 (10%)

*One decliner of aDBS for OCD completed other survey questions but did not respond to this question.

**One decliner of aDBS for Parkinson's disease completed other survey questions but did not respond to this question.

TABLE 4 | Relative frequency of themes for undergoing aDBS.

Theme	Frequency (including patients and caregivers)
Hopes for symptom alleviation	27
Declining or low quality of life	20
Altruistic motivations	12
Perceived benefits of being in research	11
Recommendations from others and trust in surgical team	9
Relatively low risk of aDBS	6
Benefits of new technology	5

Study Decliners' Reasons for Not Enrolling in an aDBS Trial

Study decliners provided a range of rationales for why they chose to decline aDBS (Table 10). The primary rationale for declining was practical, with 7 out of 10 (70%) highlighting that they declined aDBS because the study was located inconveniently, involved too much time in follow-up, or was not scheduled in manner that was convenient to them. Other factors were more specific and include not being

able to have an MRI (20% of decliners), people seeing the wires (20% of decliners), and concerns over health insurance (20%).

Balancing the Risks and Benefits of aDBS Surgery as Novel Technology

The status of aDBS as a novel form of technology was a key consideration for both patients and individuals declining aDBS. Patients tended to view the novelty of the technology as a positive, or opportunity to offer a more personalized and improved treatment system (newer = better), while study decliners saw it more negatively, as simply too experimental and risky (hesitancy to be among the first). It may be interesting to highlight that of total number of patients and caregivers interviewed, only 5 out of 41 (12%) referred specifically to the new technology as reason for choosing to have aDBS. A far greater percentage, 5 out of 10 decliners (50%) referred to concerns over new technology as one of the reasons for not undertaking to have aDBS (see Table 11, below).

Another theme that emerged was how for several participants aDBS was considered a relatively low additional risk in comparison to DBS. Six interviewees (five study participants and

TABLE 5 | Hope for improvement of symptoms.

It's a good opportunity that she may not have otherwise had the chance to get, and I'll take 75% odds of improvement any day of the week. [Caregiver]

I figured after about 13 years of dealing with this, anything's worth trying at this point. [Patient]

So when we talked about it, when he was first offered the opportunity, we kind of were like, "Well, the worst that will happen is that it doesn't work. And then you're in no worse position than you are now." [Caregiver]

There's no guarantee. This may not work. It may not make her feel better, but it may. [Caregiver]

I will be really thankful to have a chance at feeling better, have a chance at being able to confront my OCD better and decrease some of those OCD symptoms. If that's what happens, that obviously would be amazing. [Patient]

I still drive motorcycles and cars and we eat out. But if I didn't do anything, it would change because I would feel really bad if she had to feed me. I wouldn't like that. [Patient]

TABLE 6 | Quality of life.

And the one thing I really want to get, my goal is to get my tics under control enough to where I can drive to and from work and pick up full term hours again. [Patient]

[W]e feel like it's developed into what it's developed into, which I think has put us in a lot more severe category of OCD and what she's dealing with, which is, luckily, like I said, we stumbled across this because it seems like a potential solution to be able to help her gain some of that control back in her life and develop the skills and techniques to be able to move forward after this. [Caregiver]

I know she sits there day in, day out and maybe thinks about it all the time, but her life has passed her by. She rarely leaves the house and when she does it's extremely difficult. [Caregiver]

It's worse now than it's ever been, especially in the past three, four years that I've known him. The past three years that I've lived with him. I know at this point, daily life has become a huge struggle for him, just on the basis of how severe his Tourette's has become. [Caregiver]

[A]fter knowing her and going through treatment and trying different medications, and those types of things, finding this was what we felt as a last option to really be able to hopefully get her some long-term long lasting relief. [Caregiver]

This seems like a good time because I am trying to get lots done and I could have a, I'm trying to get lots done in my life, like I'm not retired or anything. So the intention was to get it early while the surgery is low risk on me as a person, and there's a good potential for increased quality of life for many years. [Patient]

I feel like I have several medicines but none of them works. [Caregiver]

I am sort of a different case because I am so young. So I kind of see it as I have an opportunity to do something that could benefit me more for a longer period of time. [Patient]

TABLE 7 | Benefits of being in research.

I talked to a couple people about it, and they said that you got a lot more access to the research team and you get a lot better care and you're monitored much closer. [Patient]

First of all, I think he'll get more attention. Yeah, he'll be looked after better because he's got a lot of people following this and checking up on us and checking on him. [Caregiver]

I think it's wonderful. I think joining the study is probably going to give her better care in the long run than she would have had if she didn't join the study. There'd be more follow-up appointments, more tweaking of the monitors and this kind of stuff. [Caregiver]

Well, it just sounded intriguing to me. It just sounded as if it was one step further, one step better than just the old normal kind of DBS. [Patient]

I should be part of the newest, latest, and greatest that they have available. And so that's kind of one reason. [Patient]

I just completely given up, on getting better. Cause I'm never, unless I win Power ball, or something or somebody wants to just generously pay for my surgery, it would never happen. So, I was excited when I came upon this study. [Patient]

TABLE 8 | Expressions of altruism.

We wish he could participate in more studies, but it's hard to get involved – so it was nice that there was one that might help the science, and that he qualified for. [Caregiver]

[I]f this can help others or science, I figure I'm going to have the deep brain DBS surgery. [Patient]

I can't imagine how many other people are suffering in this way or in severe ways too, and how debilitating it is. If there's anything that I can do on that other end to help while I'm still doing the surgery that I want to do to help myself, if I can add on a little bit that could possibly help down the road for myself or other people, great. That to me is worth it. [Patient]

I talked to her [patient's daughter] just a few minutes ago about it and she asked me everything that went on today and I told her and she knows that someday she may have to go through this same thing. [Patient]

two caregivers) referred to their decision being influenced by this perception of relatively minimal extra risk of having aDBS, as compared to conventional DBS (see **Table 12**). It was notable that of the six interviewees referring to this issue, all but one were from the PD cohort.

DISCUSSION

Of those issues considered important in decision-making by persons who enrolled in aDBS, hopes for alleviation of symptoms and declining quality of life often arose together as reasons

TABLE 9 | Recommendations from others.

I had been seeing Dr. [anonymous] for almost 9 years, and last year around [month] he mentioned the DBS study and he thought that I would be a good candidate, so I decided to participate. [Patient]

My sister knew a guy that had it. And she said that her friend said it was one of the best things he's ever done in his life and I started looking into it and I started reading about it. Then I looked up the, the, I looked up the, I found a rating of places that have it done, and I thought this is the top one in [location anonymous]. [Patient]

He [patient's doctor] said, "You know," he said, "I'm out of options as far as medication." He's like, "We did them all." He said, "We just can't give you more strength of what you've got going." He says, "I recommend you go see them about getting the surgery." We did. [Patient]

TABLE 10 | Specific reasons not to have aDBS.

Practical issues

Well, it's mainly logistics because I live in [STATE 1] and it'd be hard to keep up with it from [STATE 2] and all that. And that was a big reason for it.

[I]f I had to wait until May or June and then maybe it didn't work I would kind of kick myself in the butt, like, "Why didn't you just do the old one, [NAME], and have higher chance of success, you know?"

Not being able to have an MRI in the future

[T]here are two other reasons I think that almost took precedent. One was the effect that I may not be able to get another MRI for the rest of my life, and that actually troubles me because I have some other issues that may require a surgery and therefore the consideration of an MRI. One is the stenosis of the cervical spine.

Cosmetic/Noticeable wires

Maybe vanity, you know? Just people thinking, talking, "Well, why does [Respondent Name] have two wires sticking out of his head?" Just that. You know? Again, I go back to the fact that, okay, if I was severe, I really wouldn't care what people say.

Impact on health insurance ($n = 2/10$ decliners)

[P]otentially losing any insurance in the future because of a complication from a research device. You know I just – I wouldn't know where that's gonna go until it's – maybe some mandates in place to say you know, insurance your gonna pay for this.

TABLE 11 | Evaluation of aDBS's novelty.

Positive evaluation

[T]here is the potential to have it be a lot more specialized to the individual.

[T]hey can fine tune it a lot better than you can with just the old style.

Negative evaluation

My 21 year old daughter said to me, you can be the fifth person, you can be the sixth person, you can be the tenth person, but you will not be one of the first people.

This was like, "Well, you know, it's starting as a study, and we haven't put it many people," and I was just not ready to go there yet.

I didn't really have any main concerns, other than the fact that it was new.

TABLE 12 | Additional risk of aDBS over conventional DBS.

It's not the kind of trial where you have some people on a placebo and some people on the drug, so some people benefit. So, the way that I look at it is like it seems that I can pretty much just benefit. I mean, I consider the risks to be relatively low. [Patient]

I could always go to the tried and true so I could kind of have the option that they already have, which is the standard, I guess. [Patient]

I think I would have done deep brain stimulation even if it wasn't in the adaptive. I think the adapter was an added bonus for me. [Patient]

to have aDBS surgery. Another of the more frequently cited rationales for having aDBS was that being in research would provide access to a team of experts that might not otherwise be made available in standard clinical practice. Altruism also featured as an important rationale and was often combined with a hope that surgery might benefit the patient. Finally, personal recommendations from physicians or friends featured reasons to undergo aDBS surgery. Persons declining aDBS cited inconvenience, time commitments, and concerns about health insurance coverage as reasons not to undertake aDBS surgery. Finally, it was notable how relative risk featured in these deliberations in respect to the technology on offer. For some, the offer of a novel, experimental technology was considered a positive attribute and thus inclined them toward choosing aDBS. For others, the experimental nature of the technology concerned them and was a reason (among others) not to have aDBS. For a third group, the additional risk of being part of

trial was counterbalanced by the knowledge that the adaptive element of aDBS, if ineffective, could be de-activated, allowing them to revert to standard DBS technology; as such, they saw the additional risk of aDBS over DBS as minimal compared to the overall risk of brain surgery itself. Notably absent from the decision making process was either an explicit enthusiasm or concern regarding the automaticity of the adaptive system. This is interesting both because automaticity (i.e., automatic change in stimulation using aDBS) has been raised in respect to potential concerns about aDBS (as seen above—Goering et al., 2017; Lázaro-Muñoz et al., 2017; Kostick and Lázaro-Muñoz, 2021) and that trust in automaticity has been seen as important factor in public enthusiasm (or otherwise) for other forms of automated technology such as automated cars (Jian et al., 2000; Hoff and Bashir, 2015; Schaefer et al., 2016). In part, this may be an artifact of the study question design wherein the purpose was to find the primary reason or reasons for entry into the study

or non-enrollment. One could speculate that the enthusiasm or distrust of automaticity might still be part of the decision making process, but it did not appear high on agenda when considering the decision to have aDBS or decline aDBS. In a study being conducted at present, the research team is exploring interviewees' understandings of the specific features of aDBS including automatic stimulation.

This study provides much needed empirical data on reasons for and against electing to surgically implant a neural device that is both innovative and potential ethically complex due to software algorithm-based control of an individual's brain stimulation treatment in real time. It highlights the depth and breadth of considerations made in choosing whether to enter or decline aDBS research trials, and brings to the fore those elements of the decision that are important to persons themselves making this decision. These empirical decision-making factors include "push" factors wherein any form of surgical intervention is preferable to none and "pull" factors wherein opportunities to contribute to science combine with hopes and/or expectations for the alleviation of symptoms. Interviewee responses highlight that, regardless of whether they decided to participate in an aDBS trial or now, this was a decision made after considerable deliberation and often in consultation with others; as seen in respect to the number of people considering recommendations from others. No single issue determined whether someone elected to have aDBS or chose to decline. This depth of consideration reflects similar findings by Lawrence et al. (2018), who write in the context of conventional DBS that "participants seemed very aware of the risks, and very aware of their own difficulties processing information, and there was no indication that participants would make quick decisions to undergo DBS."

Our findings suggest that those who chose to undergo aDBS often did so through either by reason of wanting to help others or a combination of altruism and a desire to help oneself. As similar complex interplay is found in a study by Locock and Smith (2011) in their own study of who takes part in such trials, whereby they conclude "While altruistic motivations were undoubtedly present in our participants' decisions, potential personal benefit emerged as the prime motivator in this group of respondents. Where altruistic reasons were expressed, they tended to be in combination with personal reasons, or to be founded more on notions of 'social exchange,' than any purely selfless motivation." In an additional complexity, altruism was expressed through a broad spectrum of rationales for having aDBS ranging from helping to forward scientific and human progress to a much closer identification of the community of persons suffering from the same or similar symptoms and even to personal identification of other persons who may benefit as a result of the individual joining the research. McCann et al. (2010) suggest that the term "conditional altruism" can be helpful when characterizing the decision to enter randomized control trials and "trial participation seemed to be something of a 'win: win' situation—one in which they [trial participants] could both help others and benefit (or at least not be harmed) personally." The incorporation of scientific objectives as part of the individuals' altruistic thinking may well have enabled the sort of win/win expectation, or at the very least one win out of a potential two.

The data also highlight the degree to which participants do not conceptualize their participation in terms of a clear boundary between research and clinical objectives. Rather than constituting a therapeutic misconception (see Appelbaum et al., 1987; McConville, 2017 for discussion of this term), we suggest that this blurred line of distinction reflects study designs wherein aDBS is an extension of existing technology that can be switched off if it proves to be ineffective or associated with undesirable side effects. Persons considering whether to have aDBS surgery as part of research weighed the advantages and disadvantages and chose accordingly; they did not deny the possibility of disadvantages in entering into the research process, but factored this into their decision-making. It is argued that interviewees were aware of the research vs. clinical distinction but, when choosing to undertake aDBS surgery, explicitly combined the scientific objective of creating generalizable knowledge with at least a hope that aDBS would alleviate their symptoms. In doing so, they blended the scientific objective—which some incorporated as their own motivation—with what might be referred to as qualified expectation of clinical benefit.

It is important to highlight—as some participants articulated—that if participant enrolls in the trial and gets aDBS, there still an option to turn off the adaptive component and treat them with conventional DBS. Mergenthaler et al. (2021) have referred to "opportunity studies" vs. "experimental trials." In the former, there is likely to be only "a marginal increase in risk over the risk associated with the clinical intervention itself," while in the case of experimental trials, investigators test devices as "stand-alone procedures" and subjects are "unlikely to receive neurosurgery if not for enrollment in research." These offer very different contexts for choice and perceptions of risk. These considerations influence not only decision making about entering into a trial but also post-trial concerns about continued access to experimental technology or removal of such technology (the subject of a forthcoming manuscript by the team). In some cases, interviewees appear to express a clear understanding that they were entering into what Mergenthaler refers to as an "opportunity" study but it remains unclear as to the degree to which others fully understood this complex research/clinical relationship and the possibility of switching from aDBS to DBS.

One of the more notable expectations of aDBS was that rather than specifically alleviating symptoms, some saw aDBS surgery as an opportunity to maintain their existing quality of life by preventing decline, sometimes specifically identifying having a number of high-quality years still available to them if aDBS is successful (Schuepbach et al., 2019 for recent discussion of early stage intervention and quality of life). While these were patients with diagnosed disease who have symptoms and diagnosed condition, to a limited extent their comments raise a number of questions regarding the timing of surgical intervention. It is important to note that we do not have a clear understanding of whether DBS or aDBS can reverse symptoms for all conditions or slow the progression of the disease.

Finally, arguably, the most provocative and significant finding is that some people perceive the experimental aspect of their participation as positive (where they are first in line to receive a promising new treatment), while others perceive it as negative

(that they are first in line to be “guinea pigs” for a treatment with potentially negative down-the-road consequences). As such, our findings suggest a strong need to re-address the theoretical perception of research as being largely one of additional risk, over and above clinical practice (see Lantos, 2014). As our interviews suggest, a considerable number of persons were drawn toward having aDBS because they felt that being part of research would be advantageous to them. In doing so, they often merged technological enthusiasm, wanting the best and newest technology, and an expectation of greater care and attention. These expectations are well worth considering in respect to broader literature on patient perspectives on entering into research (McCann et al., 2010, 2013; Locock and Smith, 2011; Jenkins et al., 2013; Hughes-Morley et al., 2015).

LIMITATIONS

These in-depth interviews were intended to identify the range of responses that were offered by interviewees when discussing their choice to enter or decline aDBS trial participation. This approach is limited in the sense that it cannot provide generalizable results as it is restricted to these specific responses. Though we reached theme saturation in all three interviewee cohorts—participants, caregivers, and decliners—substantially more people interviewed were patients and respective caregivers, which biases our analysis to this perspective in respect to the depth of analysis.

CONCLUSION

Our study highlights the requirement to improve our understanding of the considerations made in choosing whether to undergo aDBS surgery as part of research. Looking in detail at this choice making process is strongly suggestive of the need to reflect upon some of the more theoretically based concerns about aDBS raised and compare these to rationales expressed by patients, caregivers, and decliners about their choice to enter or decline aDBS. In addition, the study highlights the need for further research into how prospective study enrollees come to understand complex study protocols wherein an innovative technology is overlaid with an established clinical procedure. By improving our empirical knowledge of choice-making within this context, we should be able to improve our communication

strategies, thus minimizing the likelihood of unwarranted expectations and misunderstandings of what is an inherently complex study protocol. Finally, in the light of our findings that many participants viewed research as positive, the study highlights that we need to pay close attention to what patients believe are the benefits of being in research. In doing so, we can be better placed to make sure that such expectations are met.

DATA AVAILABILITY STATEMENT

The datasets presented in this article are not readily available as raw data will not be shared outside of the research team. Upon request, sections of the data may be provided for specific requests after the permissions of participants are requested and received.

ETHICS STATEMENT

The studies involving human participants were reviewed and approved by the Baylor College of Medicine Institutional Review Board. Written informed consent for participation was not required for this study in accordance with the national legislation and the institutional requirements.

AUTHOR CONTRIBUTIONS

SO wrote the first draft. GL-M, PZ, AM, WG, BK, LT, SP, JR, and KK-Q contributed to conception and design. KM, KK-Q, CS, LK, RL, LT, DS-M, JR, BK, PS, AG, KF, MO, WG, AM, PZ, and GL-M contributed to recruitment and implementation. SO, KK-Q, KM, CS, LK, RL, LT, and PZ analyzed the data. PZ, KK-Q, AM, SP, and GL-M wrote sections of the manuscript. All authors contributed to manuscript revision and read and approved the submitted version of the manuscript.

FUNDING

This research for this article was funded by the BRAIN Initiative-National Institutes of Health (NIH), parent grant R01MH114854 and supplemental grant R01MH114854-01S1 (GL-M, AM, and WG).

REFERENCES

- Aldehri, M., Temel, Y., Alnaami, I., Jahanshahi, A., and Heschem, S. (2018). Deep brain stimulation for Alzheimer's Disease: an update. *Surg. Neurol. Int.* 9:58.
- Appelbaum, P. S., Roth, L. H., Lidz, C. W., Benson, P., and Winslade, W. (1987). False hopes and best data: consent to research and the therapeutic misconception. *Hastings Cent. Rep.* 17, 20–24. doi: 10.2307/3562038
- Artusi, C. A., Dwivedi, A., Romagnolo, A., Bortolani, S., Marsili, L., Imbalzano, G., et al. (2020). Differential response to pallidal deep brain stimulation among monogenic dystonias: systematic review and meta-analysis. *J. Neurol. Neurosurg. Psychiatry* 91, 426–433. doi: 10.1136/jnnp-2019-322169
- Bonomo, G., and Vetrano, I. G. (2021). A systematic review of deep brain stimulation targets for obsessive-compulsive disorder. *Neurosurgery* 88, E456–E457.
- Goering, S., Klein, E., Dougherty, D. D., and Widge, A. S. (2017). Staying in the loop: relational agency and identity in next-generation DBS for psychiatry. *AJOB Neurosci.* 8, 59–70. doi: 10.1080/21507740.2017.1320320
- Habets, J. G., Heijmans, M., Kuijff, M. L., Janssen, M. L., Temel, Y., and Kubben, P. L. (2018). An update on adaptive deep brain stimulation in Parkinson's disease. *Mov. Disord.* 33, 1834–1843.
- Hariz, M. (2017). My 25 stimulating years with DBS in Parkinson's disease. *J. Parkinsons Dis.* 7, S33–S41.

- Hartmann, C. J., Fliegen, S., Groiss, S. J., Wojtecki, L., and Schnitzler, A. (2019). An update on best practice of deep brain stimulation in Parkinson's disease. *Ther. Adv. Neurol. Disord.* 12:1756286419838096.
- Hoff, K. A., and Bashir, M. (2015). Trust in automation: integrating empirical evidence on factors that influence trust. *Hum. Factors* 57, 407–434. doi: 10.1177/0018720814547570
- Hughes-Morley, A., Young, B., Waheed, W., Small, N., and Bower, P. (2015). Factors affecting recruitment into depression trials: systematic review, meta-synthesis and conceptual framework. *J. Affect. Disord.* 172, 274–290. doi: 10.1016/j.jad.2014.10.005
- Jenkins, V., Farewell, V., Farewell, D., Darmanin, J., Wagstaff, J., Langridge, C., et al. (2013). Drivers and barriers to patient participation in RCTs. *Br. J. Cancer* 108, 1402–1407. doi: 10.1038/bjc.2013.113
- Jian, J. Y., Bisantz, A. M., and Drury, C. G. (2000). Foundations for an empirically determined scale of trust in automated systems. *Int. J. Cogn. Ergon.* 4, 53–71. doi: 10.1207/s15327566ijce0401_04
- Klein, E., Goering, S., Gagne, J., Shea, C. V., Franklin, R., Zorowitz, S., et al. (2016). Brain-computer interface-based control of closed-loop brain stimulation: attitudes and ethical considerations. *Brain Comput. Interfaces* 3, 140–148. doi: 10.1080/2326263x.2016.1207497
- Kostick, K. M., and Lázaro-Muñoz, G. (2021). Neural safeguards against global impacts of memory modification on identity: ethical and practical considerations. *AJOB Neurosci.* 12, 45–48. doi: 10.1080/21507740.2020.1866111
- Lantos, J. D. (2014). Lessons from the controversy over the SUPPORT study. *Arch. Dis. Child. Fetal Neonatal Ed.* 99:F4.
- Lawrence, R. E., Kaufmann, C. R., DeSilva, R. B., and Appelbaum, P. S. (2018). Patients' beliefs about deep brain stimulation for treatment-resistant depression. *AJOB Neurosci.* 9, 210–218. doi: 10.1080/21507740.2018.1553897
- Lázaro-Muñoz, G., McGuire, A. L., and Goodman, W. K. (2017). Should we be concerned about preserving agency and personal identity in patients with Adaptive Deep Brain Stimulation systems? *AJOB Neurosci.* 8, 73–75. doi: 10.1080/21507740.2017.1320337
- Little, S., and Brown, P. (2020). Debugging adaptive deep brain stimulation for Parkinson's Disease. *Mov. Disord.* 35, 555–561. doi: 10.1002/mds.27996
- Locock, L., and Smith, L. (2011). Personal benefit, or benefiting others? Deciding whether to take part in clinical trials. *Clin. Trials* 8, 85–93. doi: 10.1177/1740774510392257
- McCann, S. K., Campbell, M. K., and Entwistle, V. A. (2010). Reasons for participating in randomised controlled trials: conditional altruism and considerations for self. *Trials* 11:31.
- McCann, S., Campbell, M., and Entwistle, V. (2013). Recruitment to clinical trials: a meta-ethnographic synthesis of studies of reasons for participation. *J. Health Serv. Res. Policy* 18, 233–241. doi: 10.1177/1355819613483126
- McConville, P. (2017). Presuming patient autonomy in the face of therapeutic misconception. *Bioethics* 31, 711–715. doi: 10.1111/bioe.12384
- Mergenthaler, J. V., Chiong, W., Dohan, D., Feler, J., Lechner, C. R., Starr, P. A., et al. (2021). A qualitative analysis of ethical perspectives on recruitment and consent for human intracranial electrophysiology studies. *AJOB Neurosci.* 12, 57–67. doi: 10.1080/21507740.2020.1866098
- Saunders, B., Sim, J., Kingstone, T., Baker, S., Waterfield, J., Bartlam, B., et al. (2018). Saturation in qualitative research: exploring its conceptualization and operationalization. *Qual. Quant.* 52, 1893–1907. doi: 10.1007/s11135-017-0574-8
- Schaefer, K. E., Chen, J. Y., Szalma, J. L., and Hancock, P. A. (2016). A meta-analysis of factors influencing the development of trust in automation: implications for understanding autonomy in future systems. *Hum. Factors* 58, 377–400. doi: 10.1177/0018720816634228
- Schuepbach, W. M., Tonder, L., Schnitzler, A., Krack, P., Rau, J., Hartmann, A., et al. (2019). Quality of life predicts outcome of deep brain stimulation in early Parkinson disease. *Neurology* 92, e1109–e1120.
- Siegel, A. M., Barrett, M. S., and Bhati, M. T. (2017). Deep brain stimulation for Alzheimer's disease: ethical challenges for clinical research. *J. Alzheimers Dis.* 56, 429–439. doi: 10.3233/jad-160356
- Smith, A. H., Choi, K. S., Waters, A. C., Aloysi, A., Mayberg, H. S., Kopell, B. H., et al. (2021). Replicable effects of deep brain stimulation for obsessive-compulsive disorder. *Brain Stimul.* 14, 1–3. doi: 10.1016/j.brs.2020.10.016
- Swann, N. C., de Hemptinne, C., Thompson, M. C., Miocinovic, S., Miller, A. M., Ostrem, J. L., et al. (2018). Adaptive deep brain stimulation for Parkinson's disease using motor cortex sensing. *J. Neural Eng.* 15:046006. doi: 10.1088/1741-2552/aabc9b
- Viaña, J. N. M., and Gilbert, F. (2019). Deep brain stimulation for people with Alzheimer's disease: anticipating potential effects on the tripartite self. *Dementia* 18, 2836–2855. doi: 10.1177/1471301218761147
- Vicheva, P., Butler, M., and Shotbolt, P. (2020). Deep brain stimulation for obsessive-compulsive disorder: a systematic review of randomised controlled trials. *Neurosci. Biobehav. Rev.* 109, 129–138. doi: 10.1016/j.neubiorev.2020.01.007
- Widge, A. S., Deckersbach, T., Eskandar, E. N., and Dougherty, D. D. (2016a). Deep brain stimulation for treatment-resistant psychiatric illnesses: what has gone wrong and what should we do next? *Biol. Psychiatry* 79, e9–e10.
- Widge, A. S., Licon, E., Zorowitz, S., Corse, A., Arulpragasam, A. R., Camprodon, J. A., et al. (2016b). Predictors of hypomania during ventral capsule/ventral striatum deep brain stimulation. *J. Neuropsychiatry Clin. Neurosci.* 28, 38–44. doi: 10.1176/appi.neuropsych.15040089
- Xu, W., Zhang, C., Deeb, W., Patel, B., Wu, Y., Voon, V., et al. (2020). Deep brain stimulation for Tourette's syndrome. *Transl. Neurodegener.* 9:4.

Conflict of Interest: The authors declare that the research was conducted in the absence of any commercial or financial relationships that could be construed as a potential conflict of interest.

The handling editor declared a shared affiliation with three of the authors, SO, BK, and PS, at the time of review.

Publisher's Note: All claims expressed in this article are solely those of the authors and do not necessarily represent those of their affiliated organizations, or those of the publisher, the editors and the reviewers. Any product that may be evaluated in this article, or claim that may be made by its manufacturer, is not guaranteed or endorsed by the publisher.

Copyright © 2021 Outram, Muñoz, Kostick-Quenet, Sanchez, Kalwani, Lavingia, Torgerson, Sierra-Mercado, Robinson, Pereira, Koenig, Starr, Gunduz, Foote, Okun, Goodman, McGuire, Zuk and Lázaro-Muñoz. This is an open-access article distributed under the terms of the Creative Commons Attribution License (CC BY). The use, distribution or reproduction in other forums is permitted, provided the original author(s) and the copyright owner(s) are credited and that the original publication in this journal is cited, in accordance with accepted academic practice. No use, distribution or reproduction is permitted which does not comply with these terms.



Sleep-Aware Adaptive Deep Brain Stimulation Control: Chronic Use at Home With Dual Independent Linear Discriminate Detectors

Ro'ee Gilron^{1*}, Simon Little², Robert Wilt¹, Randy Perrone¹, Juan Anso¹ and Philip A. Starr¹

¹ Department of Neurological Surgery, University of California San Francisco, San Francisco, CA, United States,

² Department of Neurology, University of California San Francisco, San Francisco, CA, United States

OPEN ACCESS

Edited by:

Jens Volkmann,
Universitätsklinikum Würzburg,
Germany

Reviewed by:

Pavel Bobrov,
Institute of Higher Nervous Activity
and Neurophysiology (RAS), Russia
Alfons Schnitzler,
Heinrich Heine University Düsseldorf,
Germany

*Correspondence:

Ro'ee Gilron
roeegilron@gmail.com

Specialty section:

This article was submitted to
Neural Technology,
a section of the journal
Frontiers in Neuroscience

Received: 29 June 2021

Accepted: 13 September 2021

Published: 18 October 2021

Citation:

Gilron R, Little S, Wilt R,
Perrone R, Anso J and Starr PA
(2021) Sleep-Aware Adaptive Deep
Brain Stimulation Control: Chronic
Use at Home With Dual Independent
Linear Discriminate Detectors.
Front. Neurosci. 15:732499.
doi: 10.3389/fnins.2021.732499

Adaptive deep brain stimulation (aDBS) is a promising new technology with increasing use in experimental trials to treat a diverse array of indications such as movement disorders (Parkinson's disease, essential tremor), psychiatric disorders (depression, OCD), chronic pain and epilepsy. In many aDBS trials, a neural biomarker of interest is compared with a predefined threshold and stimulation amplitude is adjusted accordingly. Across indications and implant locations, potential biomarkers are greatly influenced by sleep. Successful chronic embedded adaptive detectors must incorporate a strategy to account for sleep, to avoid unwanted or unexpected algorithm behavior. Here, we show a dual algorithm design with two independent detectors, one used to track sleep state (wake/sleep) and the other used to track parkinsonian motor state (medication-induced fluctuations). Across six hemispheres (four patients) and 47 days, our detector successfully transitioned to sleep mode while patients were sleeping, and resumed motor state tracking when patients were awake. Designing "sleep aware" aDBS algorithms may prove crucial for deployment of clinically effective fully embedded aDBS algorithms.

Keywords: DBS (deep brain stimulation), Parkinson's disease, adaptive DBS, human neuroscience, sleep


INTRODUCTION

Commercially available sensing enabled deep brain stimulation (DBS) devices are now being used to treat epilepsy [Neuropace RNS, (Nair and Morrell, 2019)], movement disorders and obsessive-compulsive disorder (Medtronic Percept), (Feldmann et al., 2021; Frank et al., 2021; Jimenez-Shahed, 2021; Thenaisie et al., 2021). These devices typically record field potentials either cortically or subcortically and are designed to deliver personalized stimulation in response to sensed brain activity (Gunduz et al., 2019; Bronte-Stewart et al., 2020). For most indications, a neural biomarker of interest is typically selected and analysis is performed on predefined power bands in the frequency domain, computed from the sensed field potential recordings (Gunduz et al., 2019; Yin et al., 2021). Biomarkers are then compared to a predefined threshold and stimulation current is adjusted between stimulation amplitude limits. These adaptive algorithms are now routinely tested not only in clinical settings but at home (Gilron et al., 2021).

As studies transition from brief in clinic testing to chronic testing at home, it is important to consider that sleep has a profound influence on most biomarkers of interest. Sleep is typically disturbed in neurological conditions and could be modulated for therapeutic

Sleep & PD detector classification state table

Conceptual example



		PD state biomarker lower threshold	PD state biomarker upper threshold
Sleep state threshold	PD biomarker: Low Sleep biomarker: Low Mode: awake Target Current: 1.5mA	PD biomarker: Med Sleep biomarker: Low Mode: awake Target Current: HOLD	PD biomarker: High Sleep biomarker: Low Mode: awake Target Current: 3mA
	PD biomarker: Low Sleep biomarker: High Mode: asleep Target Current: 2mA	PD biomarker: Med Sleep biomarker: High Mode: asleep Target Current: 2mA	PD biomarker: High Sleep biomarker: High Mode: asleep Target Current: 2mA

FIGURE 1 | Independent classification of sleep and PD motor state. The Summit RC + S can configure two independent linear detectors. These detectors operate using a “state table.” The control signal for the PD biomarker (which operates along the columns) has two thresholds, whereas the control signal for the sleep state has one threshold. Each quadrant in the state table can be defined with a unique target current in order to functionally separate sleep from wake “modes” in the adaptive DBS algorithm. In the conceptual example above, when the sleep control signal is above threshold target current ramps to 2 mA regardless of the PD state biomarker position with respect to PD state thresholds.

purposes (Chen et al., 2019). However, to date, the “mental model” for adaptive DBS algorithms have not yet incorporated a special “mode” to detect sleep (Little and Brown, 2020). Sleep aware algorithms are important since control signals can cause unexpected or unwanted algorithm behavior in response to sleep related changes in brain physiology (Urrestarazu et al., 2009; Zahed et al., 2021).

Here, we show a general purpose strategy to **Figure 1** detect and respond to sleep using a dedicated “sleep detector” working in conjunction with an independent detector of specific motor signs in Parkinson’s disease (PD). The incorporation of sleep aware behavior into adaptive DBS (aDBS) algorithms may prove crucial to long term use of adaptive DBS protocols (Toth et al., 2020).

MATERIALS AND METHODS

Participants and Device

Details of surgery, DBS implant, lead locations and device characteristics are extensively described in a prior publication (Gilron et al., 2021). Briefly, four individuals with PD referred for DBS were implanted bilaterally with cylindrical DBS leads in the subthalamic nucleus (STN) (Medtronic model 3389) and paddle-type quadripolar leads in the subdural space over MC (motor cortex, Medtronic model 0913025). The cortical and subcortical leads from each side were connected to an investigational sensing RC + S implantable pulse generator (IPG) allowing independent control of each hemisphere (**Figure 2**).

The Summit RC + S device is a rechargeable IPG that is capable of streaming data to a host computer from up to four field potential bipolar recordings (Stanslaski et al., 2018). Spectral power is computed within the device from (up to eight) predefined power bands. Power bands can be summed and input into two independent linear detectors that execute stimulation commands according to a state table (**Figure 1**). Data were imported from the RC + S raw format using a newly released package for RC + S analysis (Sellers et al., 2021).

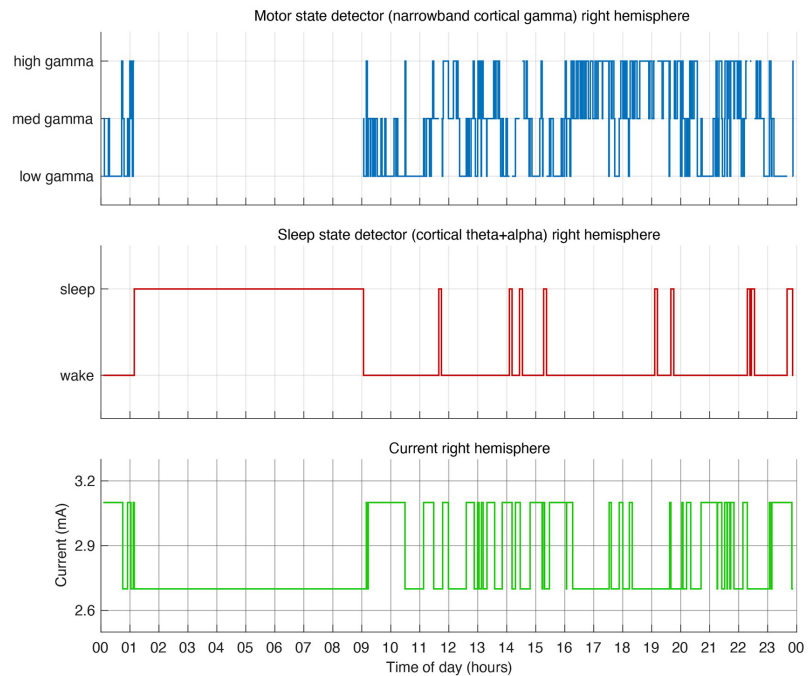
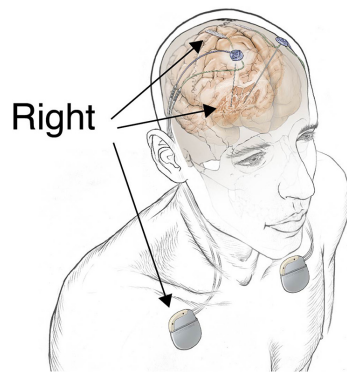
Deep Brain Stimulation Mental Model

One of the main challenges deploying adaptive algorithms chronically in the home environment is that sleep has a profound effect on cortical and subcortical field potentials. For instance, many algorithms for adaptive DBS in PD rely on responding to subcortical beta (12–30 Hz) as a control signal delivering less stimulation when subcortical beta is low. However, this may lead to inadequate stimulation for many patients since subcortical beta is also depressed during sleep (**Figure 3**), and some rely on stimulation to improve sleep (for example, to roll over in bed). Therefore there is a need to create a “sleep” aware algorithm that may switch modes when sleep is detected. To do so, we developed such an algorithm using the embedded “state table” in the RC + S IPG.

The “state table” (**Figure 1**) adaptive controller in the RC + S IPG was used to create two independent embedded adaptive detectors. The first linear detector tracked Parkinsonian motor state and the second tracked sleep state. The mental model for the first linear detector relied on following medication

Independent dual motor & sleep state detector

A



B

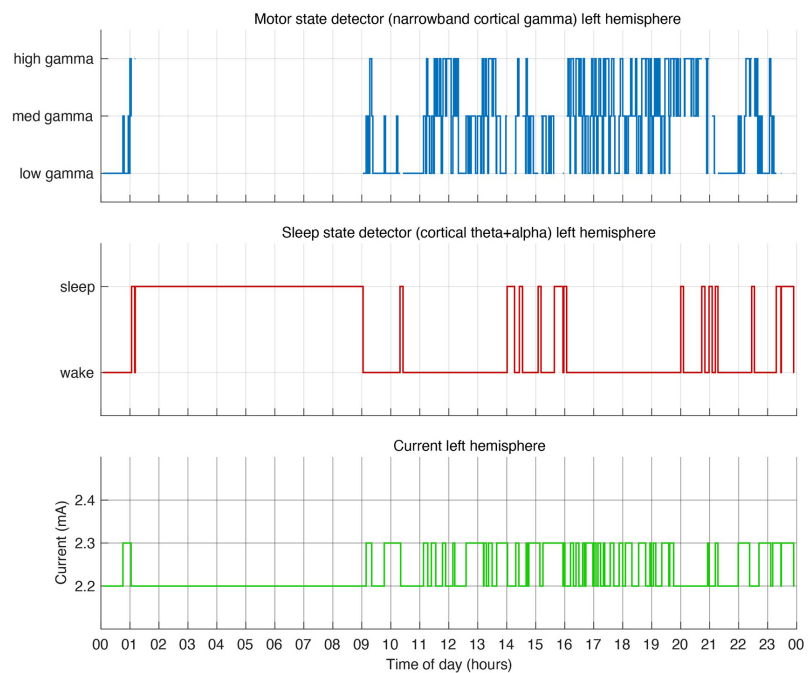
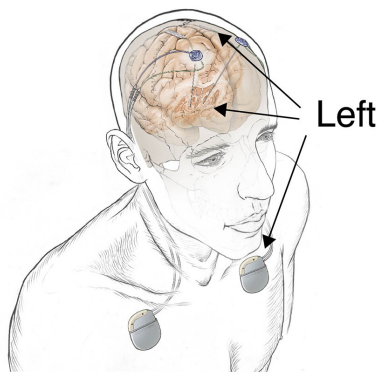
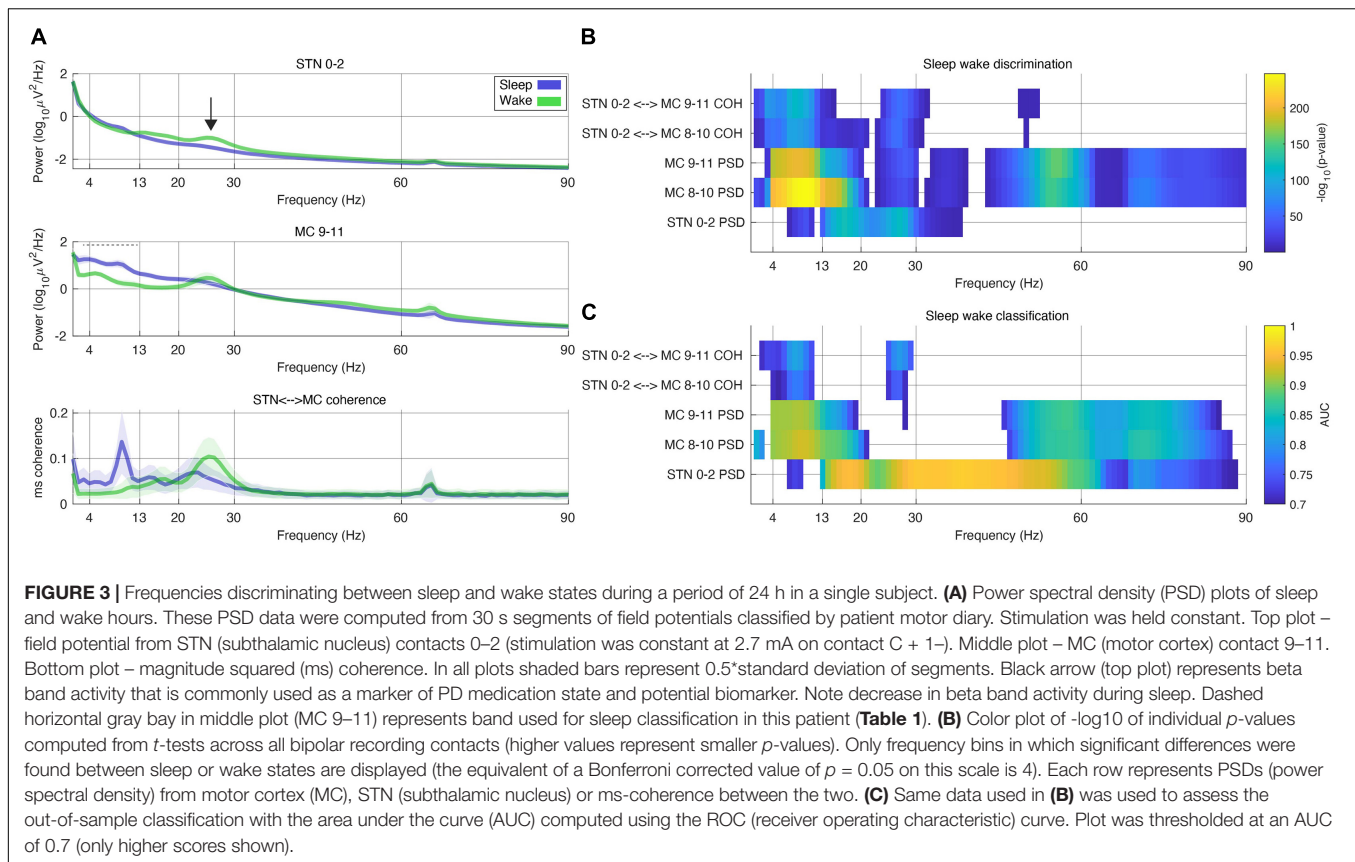


FIGURE 2 | Dual independent PD and sleep state detectors. Detector operates in embedded fashion in each hemisphere independently. **(A)** Schematic drawing of lead locations indicating right hemisphere cortical sensing paddle; right STN stimulation lead and implanted pulse generator (IPG). Detector activity depicted in top 3 plots. **(B)** Schematic of the left hemisphere mirrors the right, bottom 3 plots show detector activity. **(A,B)** During hours in which the patient is awake the detector control signal (blue line) tracks parkinsonian motor signs using a narrowband gamma cortical signal (thought to indicate a pro-dyskinetic state). In this case stimulation cycles between 2.6 mA (if high levels of gamma detected) and 3.2 mA (low levels of gamma) in the right hemisphere (2.2–2.4 mA on the left). If sleep is detected (red line) by cortical alpha + theta control signal, stimulation is held at 2.6 mA (right) or 2.2 mA (left). Current is shown in green line. Time of day (24 h clock) is on x-axis.



state as measured by biomarkers of Parkinsonian “off” states (indicating low mobility) and “on” states (indicating potential for dyskinesia). During off periods patients received additional stimulation and in on states they received less stimulation in order to avoid stimulation induced dyskinesia (Gilron et al., 2021). The second linear detector relies on tracking sleep state as measured by a sleep biomarker. When sleep was detected, constant stimulation was delivered according to the state table, regardless of the position of the first linear detector (equivalent to clinically optimized open loop stimulation). **Figure 1** contains a sample state table.

Of note, RC + S has two independent programmable linear detectors. Each detector has two thresholds, which result in 9 possible unique states. Each state can be programmed with a specific target amplitude for each program (and specific rate for each state across programs). Here we are only using 6 of the possible 9 states, but future studies may use all 9 states (for example, for detection of multiple motor signs, or specific sleep stages). States are numbered (0–8) starting top left and ending bottom right.

Detector Settings

Biomarkers for Parkinsonian “on” and “off” states and sleep states (wake/sleep) were selected empirically per patient (Gilron et al., 2021). First, frequency bands in which oscillations (local maxima in the field potential power spectral density) were present

in either STN or cortical field potentials, were pre-selected and configured using the embedded power detectors. Next, each patient streamed “training” data during their activities of daily living across several “wake/sleep” cycles and Parkinsonian “on/off” cycles. Patient state was assessed using a motor diary, wearables and patient self report. Biomarkers that best separated Parkinsonian state and sleep state were empirically selected. Detector thresholds were initially set at 25 and 75% percentiles of the range of training data for embedded power detector for Parkinsonian state and 50% percentile for sleep state detector and empirically adjusted over several days until satisfactory performance was achieved. **Table 1** contains the complete parameter set used to program the detector in one patient during a single 24 h period.

Rapid eye movement (REM) periods could cause the sleep detector to mistakenly identify a “wake” state. In order to counter “wake” classification in these instances we used long termination rates such that the biomarker of interest must be below the threshold for a certain amount of time before it transitions out of the sleep state. Most of the algorithm adjustments in patient 1 (throughout the testing period) involved gradually shortening the termination value at the expense of some misclassification during putative REM sleep. The detector was initially designed for increased sensitivity at the cost of decreased specificity. The sensitivity vs. specificity tradeoff may be an important design consideration for future detectors.

TABLE 1 | Example of dual detector parameter set from a single patient and hemisphere.

Setting	Value	Notes
Stimulation rate	130.2 Hz	Stimulation rate
Stimulation pulse	60 μ s	Stim pulse width
Stimulation contact	+1-case	Monopolar stimulation
Shared parameters for both detectors		
Time domain sampling rate	500 Hz	Sampling rate for time domain data
LPF1	450 Hz	Embedded low pass filter before amplification
LPF2	1,700 Hz	Embedded low pass filter after amplification
FFT interval	500 ms	Interval in which FFT is computed
FFT size	1,024	Number of points for onboard FFT computation
Ramp up rate	0.03 mA/sec	Rate at which stimulation changes from lower to higher amplitudes
Ramp down rate	0.12 mA/sec	Rate at which stimulation changes from higher to lower amplitudes
Motor detector		
Sense channel	+ 9–8	MC (motor cortex)
Linear detector power band input	64.45 – 66.41 Hz	Predefined power band for embedded on board power computation
Update rate	60	Number of FFT intervals averaged in non-moving average, represents 30 s of data. Defines algorithm rate (e.g., algorithm state is determined every 30 s). This is referred to as "detector count" below.
Onset	0	Number of detector counts must be above threshold to change to state. A value of 0 means that as soon as the threshold is crossed stimulation ramps to the target state.
Termination	4	Number of detector counts must be below threshold to change to state. Detector value must be below threshold for 2 consecutive minutes (update rate \times 4; =4 min in this case) before it transitions to state.
State change blank	30	In units of FFT interval. On state change power values are not computed into linear detector for 15 s (FFT interval \times 30).
Target current state 0	3.1 mA	Target stim to ramp to when stimulation is below lower threshold (for the first linear detector- "LD0")
Target current state 1	HOLD	Target stim to ramp to when stimulation between upper and lower thresholds (for the first linear detector – "LD0")
Target current state 2	2.7 mA	Target stim to ramp to when stimulation is above lower threshold (for the first linear detector – "LD0")
Sleep Detector:		
Sense channel	+9–8	MC (motor cortex)
Linear detector power band input	3.42 – 12.21 Hz	Predefined power band for embedded on board power computation
Update rate	60	Number of FFT intervals averaged in non-moving average, represents 30 s of data. Defines algorithm rate (e.g., algorithm state is determined every 30 s)
Onset	0	Number of detector counts must be above threshold to change to state (in "update rate" units).
Termination	10	Number of detector counts must be below threshold to change to state. Detector value must be below threshold for 5 consecutive minutes (update rate \times 10; = 10 min in this case) before it transitions to state.
State change blank	30	In units of FFT interval. On state change power values are not computed into linear detector for 15 s (FFT interval \times 30).
Target current state 3	2.7 mA	Target stim to ramp to when stimulation is below lower threshold (for the second linear detector – "LD1")
Target current state 4	2.7 mA	Target stim to ramp to when stimulation between upper and lower thresholds (for the second linear detector – "LD1")
Target current state 5	2.7 mA	Target stim to ramp to when stimulation is above lower threshold (for the second linear detector – "LD1")

Data Collection for Testing Period

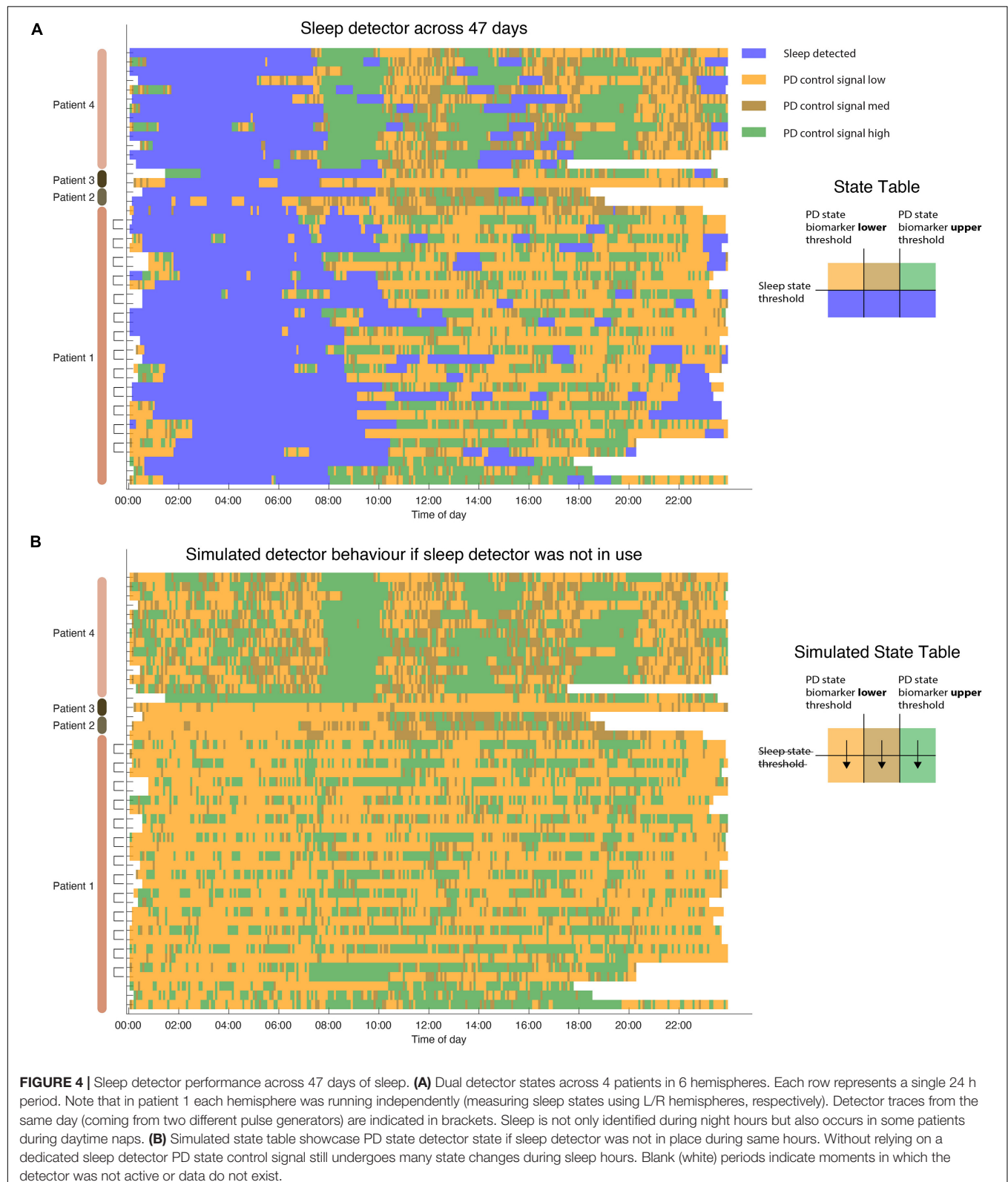
Though the RC + S device is capable of streaming a rich array of information including time domain field potentials and adaptive state, it can also be programmed to only store a log of the adaptive DBS state (according to the state table). This log is stored in a FIFO (first in first out) buffer which can be downloaded

on demand. Patients collected DBS state data during long term tests of embedded adaptive detectors in which the embedded detector was deployed for up to a week at a time. During this time patients used custom software¹ to download these logs from

¹<https://github.com/openmind-consortium/App-SCBS-PatientFacingApp>

the device on a daily basis. This had the advantage of allowing the patient full mobility without the need to be near a computer for wireless streaming. In addition, it avoided losing data due to

dropped packets (Sellers et al., 2021). Data were tested over the course of 47 days (24 h) across four patients and six hemispheres. Patient one used sleep classifiers for 17 days but frequently



ran a classifier concurrently in both hemispheres, generating 30 data sets (Figures 2, 4), patient 2 ran a classifier for 2 days in one hemisphere, patient 3 ran a classifier for 2 days, 1 day for each hemisphere, and patient 4 ran a classifier for 13 days in one hemisphere.

Evaluation of Sleep Detector Performance

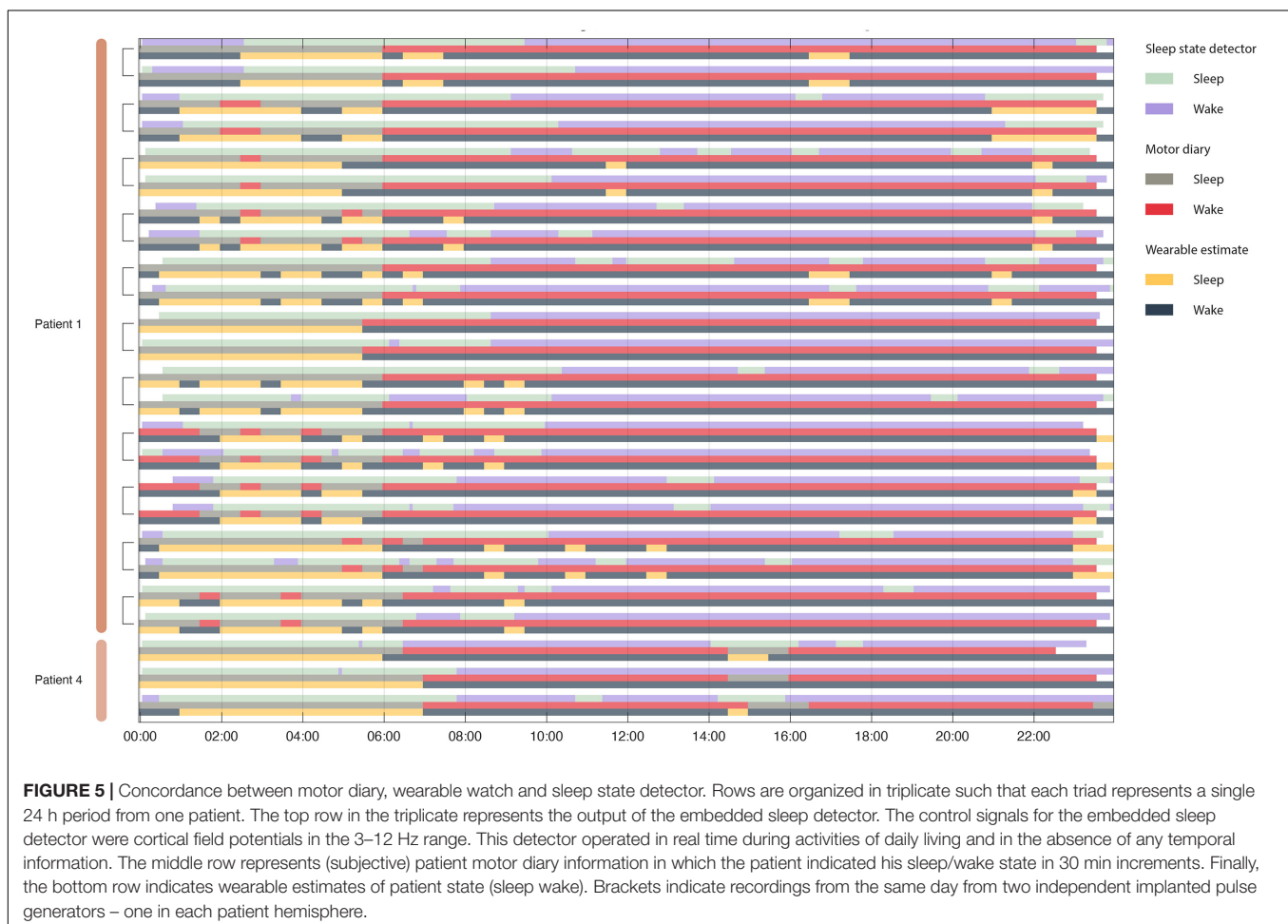
The performance of the sleep detector was checked empirically in each patient before it was deployed. Using patient motor diaries, wearables and the RC + S onboard accelerometer, patient sleep state was verified and a concordance between sleep state and the objective (actigraphy based) and subjective (motor diary) measures was computed.

In 27/47 nights of sleep we collected motor diaries and wearable actigraphy data. In filling out motor diaries patients estimated their sleep state in 30 min increments. Concurrently a wearable watch (PKG, Global Kinetics) was worn by patients during testing (Joshi et al., 2019). The PKG produced a report that estimated a median bradykinesia value every 30 min. A value above “80” in the bradykinesia metric from the PKG watch was interpreted as “asleep” (Gilron et al., 2021).

To test the statistical performance of the classifier we computed a non-parametric p -value for each 24 h period using the following procedure: We compared the concordance between the output of the sleep detector and the “true” patient state as indicated by either the motor diary or the PKG watch. To test the statistical significance of this concordance (accuracy) value we created a non-parametric null distribution of classification (a random choice between sleep/wake classification at each point in time repeated 10,000 times for each 24 h period). The concordance result of the embedded adaptive state classification was then compared to the null distribution of concordances to derive a p -value. All p -values were corrected for multiple comparisons using the Bonferroni method. In addition the sensitivity and specificity of the sleep classification was computed for each 24 h period.

Effect of Sleep State on Power and Coherence Metrics

In order to assess the effect of sleep on biomarker power and coherence metrics we had one patient stream neural data (in addition to classifier state) during a 24 h period when the sleep detector was active, but stimulation was held constant in the clinically optimized current settings (2.7 mA,



C + 1—, 60 μ s, 130.2 Hz). Sleep states were defined by the classifier and PSD (power spectral density) and coherence metrics were computed from bipolar recordings in STN and MC (motor cortex) using 30 s segments of continuous data [as described in Gilron et al. (2021)].

To assess the response of other frequencies on the discrimination of sleep state (wake/asleep, as defined by patient motor diaries) frequencies were swept in 1 Hz increments using PSD and coherence metrics with a 2 Hz sliding window. The data from each frequency bin was subjected to a two sided *t*-test and computed for each frequency, contact pair and measure (coherence/psd). *P*-values were corrected for multiple comparisons using the Bonferroni method.

Since our embedded detector used cortical alpha and theta bands as the sleep detector, we wanted to evaluate the capacity of subcortical and coherence based metrics to classify sleep state as well. Using the cortically based detector labels as ground truth, we calculated the mean AUC using a 5-fold stratified cross validated linear discriminant model across all frequency bands. This allowed us to assess the potential performance of the detector using subcortical sensing that is more readily available in commercial devices as well as using coherence based metrics.

RESULTS

Sleep state was reliably captured by a cortical biomarker as verified using patient motor diaries and self report. Each IPG (implanted pulse generator) controlled stimulation to one hemisphere with an embedded detector for sleep and an additional detector tracking PD state (Figure 2). The mean concordance between sleep measurements across both hemispheres (in cases in which dual detectors were deployed) was 88% (range 77–98%) across thirteen 24-h periods.

In one subject the embedded detector was run over a period of 24 h while streaming neural data to a research computer [as described in Gilron et al. (2021)]. This was done in order to examine other frequency bands and brain recording locations that might also dissociate sleep from wake states. In particular there is interest in subcortical classification of sleep states, as cortical sensing is not currently offered outside of IDE (investigational device exemption) studies. Subcortical alpha, beta and low gamma all significantly dissociated sleep from wake states (Figure 3). Cortical theta, alpha, beta and broadband gamma discriminate sleep states as well. Finally coherence between subcortical and cortical structures was able to dissociate sleep states in the theta, alpha and beta bands.

In addition to investigating other frequencies that can distinguish sleep from wake states we also assessed the out of sample classification of sleep states across the same 24 h period. Using 5-fold cross validation we found that STN alpha, beta and gamma all discriminate sleep states with peak AUC scores of 0.7 (using the cortical theta-alpha detector as “ground truth”).

Algorithm performance was tested using embedded mode during which patients are not tethered to a computer and the adaptive algorithm operates in embedded mode in real-time. Across 47 days (4 unique patients, 6 hemispheres) algorithm captured sleep state (Figure 4A). Algorithm performance was

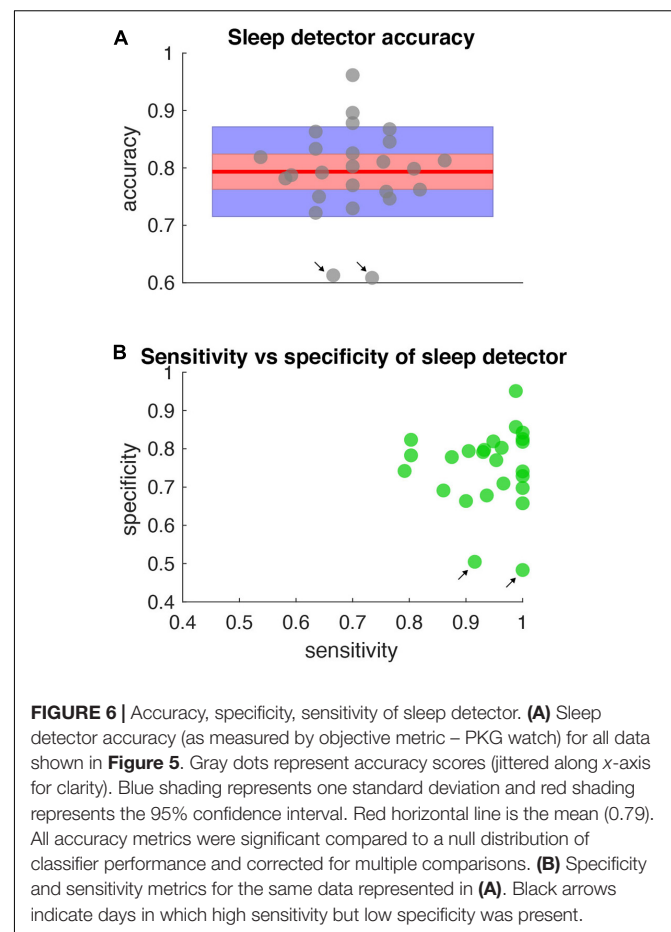
stable across months (maximum span between recording was 4 months). To assess whether a dedicated detector for sleep was needed we simulated algorithm performance without the use of a sleep detector. Indeed, all patients displayed large variation in the control signal during periods of sleep (Figure 4B) which could result in unwanted behavior depending on the aDBS (adaptive DBS) algorithm used to control PD motor states during waking hours. In some cases this would result in lower stimulation levels during sleep which could produce adverse effects on sleep in PD patients (Zahed et al., 2021).

To validate the performance of the sleep detector objective and subjective metrics of sleep state were collected. Patients filled out motor diaries (subjective) and wore a wearable watch (objective), both of which produced estimates patient sleep state that could be used to assess classifier performance (Figure 5).

All sleep night detections were significantly above chance (the null distribution had concordances between 38 and 60% with a mean at 50%) for both motor diary and wearable “ground truth” metrics (Figure 6).

DISCUSSION

This study showcases a method to incorporate sleep sensing into adaptive DBS algorithms. In Summit RC + S we deployed two



embedded linear detectors that operate independently. Tracking sleep states using embedded detectors is stable and repeatable, shown here across 47 days of embedded detector performance in four patients (**Figure 4**). During these days the algorithm successfully transitioned to a predefined “sleep mode” when patients were asleep, delivering targeted constant stimulation, whereas during waking hours a PD state tracking mode was entered in which the adaptive algorithm tracked PD related motor state changes (Gilron et al., 2021).

The sleep detector algorithm achieved high concordance with external measurements of sleep as measured by both objective (motor diary) and subjective (watch) metrics. The high concordance is notable since the detector classified sleep solely based on field potential information in real time, during activities of daily living without access to actigraphy or temporal based information (**Figure 5**). The sleep detector achieved high degrees of sensitivity and specificity but future sleep algorithms may explore sensitivity and specificity trade offs depending on the application (**Figure 6**).

Sleep has dramatic effects on cortical and subcortical field potentials (Gilron et al., 2021; Zahed et al., 2021). This includes broadband reductions in gamma frequency as well as increases in alpha frequencies and reductions in canonical parkinsonian oscillatory activity in beta frequency. Since beta frequencies are a common target for adaptive DBS studies in PD, addressing sleep induced reductions may be critical for future algorithm development.

Though our sleep study used cortical alpha and theta band activity to classify sleep state we show that other bands, notably subcortical bands achieve high classification rates (larger than AUC of 0.9 – **Figure 3C**). This high degree of sensitivity and specificity from a variety of power bands, target brain locations and coherent network activity suggest that a variety of control algorithms might be employed to incorporate sleep into adaptive DBS algorithms.

Using a separate independent detector for sleep allows adaptive DBS algorithms to finetune their response to diurnal fluctuations in control signals that may operate on different time scales than sleep changes. For example, targeting beta bursts has long been proposed as a mechanism to target pathological beta burst oscillations in PD (Little and Brown, 2012, 2020; Tinkhauser et al., 2017; Velisar et al., 2019; Bronte-Stewart et al., 2020; Petrucci et al., 2020), but these bursts operate on the timescale of 200–800 milliseconds whereas sleep related field potential changes take place on timescales of minutes to hours. The use of independent detectors allows each detector to operate using disparate timescales most appropriate for capturing desired state.

Sleep was frequently detected during the day, corresponding to daytime naps (**Figure 5**). This highlights a benefit of using physiological measures of sleep state rather than simpler chronologically scheduled implant schedules (Toth et al., 2020). Other potential methods for sleep classification are actigraphy based (to determine position and activity level) or simple patient control (patient switching to a sleep “mode”). Appropriately targeting and incorporating sleep into aDBS algorithms has benefits for risk mitigation, as it does not rely on the patient to remember to switch device state or actigraphy methods

which may produce false negatives (such as lying in bed while awake).

Sleep aware aDBS may also aid in algorithm development as it allows testing putative algorithm performance (**Figure 4B**). Prior to implementing adaptive detectors it is useful to test algorithm performance by examining state changes without stimulation amplitude changes. By incorporating a dual detector strategy that incorporates sleep control signals as well as dedicated detectors tracking patient state one can separate sleep effects from other effects on the control signal. This can allow *a priori* testing to help avoid unwanted or unexpected algorithm performance during sleep. This could prove particularly useful for adaptive algorithms for which operation during sleep is important.

Future studies may attempt to more selectively target sleep by deploying personalized therapy depending on patient sleep state (for example, REM sleep versus deep sleep). Sleep itself is often disturbed in patients with DBS due to their underlying neurological conditions, and this represents a major non-motor contributor to quality of life. Adaptive strategies that improve sleep quality may work in tandem with daytime strategies to address non-motor as well as motor dysfunction in PD.

DATA AVAILABILITY STATEMENT

The raw data supporting the conclusions of this article will be made available by the authors, without undue reservation.

ETHICS STATEMENT

The studies involving human participants were reviewed and approved by the University of California, San Francisco, Institutional Review Board (IRB) under a physician-sponsored investigational device exemption (IDE) from the FDA (protocol G180097). The patients/participants provided their written informed consent to participate in this study.

AUTHOR CONTRIBUTIONS

RG and PS conceived the study and experiments. SL provided clinical supervision. RP wrote the software interface for Summit RC + S. RG and RW collected the data. RG and SL provided key analytic tools. RG drafted the manuscript and figures. All authors contributed to manuscript revision, read, and approved the submitted version.

FUNDING

This work was funded by NIH grant UH3NS100544 and U24NS113637.

ACKNOWLEDGMENTS

We would like to thank Timothy Denison and Fawad Jamshed from Oxford for support in developing a quality management system to aid deploying adaptive DBS in the home environment.

REFERENCES

- Bronte-Stewart, H. M., Petrucci, M. N., O'Day, J. J., Afzal, M. F., Parker, J. E., Kehnemouyi, Y. M., et al. (2020). Perspective: evolution of Control Variables and Policies for Closed-Loop Deep Brain Stimulation for Parkinson's Disease Using Bidirectional Deep-Brain-Computer Interfaces. *Front. Hum. Neurosci.* 14:353. doi: 10.3389/fnhum.2020.00353
- Chen, Y., Gong, C., Hao, H., Guo, Y., Xu, S., Zhang, Y., et al. (2019). Automatic Sleep Stage Classification Based on Subthalamic Local Field Potentials. *IEEE Trans. Neural. Syst. Rehabil. Eng.* 27, 118–128. doi: 10.1109/TNSRE.2018.2890272
- Feldmann, L. K., Neumann, W.-J., Krause, P., Lofredi, R., Schneider, G.-H., and Kühn, A. A. (2021). Subthalamic beta band suppression reflects effective neuromodulation in chronic recordings. *Eur. J. Neurol.* 28, 2372–2377. doi: 10.1111/ene.14801
- Frank, A. C., Scangos, K. W., Larson, P. S., Norbu, T., Lee, A. T., and Lee, A. M. (2021). Identification of a personalized intracranial biomarker of depression and response to DBS therapy. *Brain Stimul.* 14, 1002–1004. doi: 10.1016/j.brs.2021.06.009
- Gilron, R., Little, S., Perrone, R., Wilt, R., de Hemptinne, C., Yaroshinsky, M. S., et al. (2021). Long-term wireless streaming of neural recordings for circuit discovery and adaptive stimulation in individuals with Parkinson's disease. *Nat. Biotechnol.* 39, 1078–1085. doi: 10.1038/s41587-021-00897-5
- Gunduz, A., Opri, E., Gilron, R., and Kremen, V. (2019). Adding wisdom to “smart” bioelectronic systems: a design framework for physiologic control including practical examples. *Bioelectron. Med.* 2, 29–41. doi: 10.2217/bem-2019-0008
- Jimenez-Shahed, J. (2021). Device profile of the percept PC deep brain stimulation system for the treatment of Parkinson's disease and related disorders. *Expert Rev. Med. Devices* 18, 319–332. doi: 10.1080/17434440.2021.1909471
- Joshi, R., Bronstein, J. M., Keener, A., Alcazar, J., Yang, D. D., Joshi, M., et al. (2019). PKG Movement Recording System Use Shows Promise in Routine Clinical Care of Patients With Parkinson's Disease. *Front. Neurol.* 10:1027. doi: 10.3389/fneur.2019.01027
- Little, S., and Brown, P. (2012). What brain signals are suitable for feedback control of deep brain stimulation in Parkinson's disease?. *Ann. N. Y. Acad. Sci.* 1265, 9–24. doi: 10.1111/j.1749-6632.2012.06650.x
- Little, S., and Brown, P. (2020). Debugging Adaptive Deep Brain Stimulation for Parkinson's Disease. *Mov. Disord.* 35, 555–561. doi: 10.1002/mds.27996
- Nair, D., and Morrell, M. (2019). Nine-year Prospective Safety and Effectiveness Outcomes from the Long-Term Treatment Trial of the RNS® System (S36.005). *Neurology* 92 (Suppl. 15):NairS36.005.
- Petrucci, M. N., Anderson, R. W., O'Day, J. J., Kehnemouyi, Y. M., Herron, J. A., and Bronte-Stewart, H. M. (2020). “A closed-loop deep brain stimulation approach for mitigating burst durations in people with Parkinson's disease,” in *42nd Annual International Conference of the IEEE Engineering in Medicine & Biology Society (EMBC)*. (Montreal: IEEE Engineering in Medicine and Biology Society), 3617–3620. doi: 10.1109/EMBC44109.2020.9176196
- Sellers, K. K., Gilron, R., Anso, J., Louie, K. H., Shirvalkar, P. R., Chang, E. F., et al. (2021). Analysis-rcs-data: open-source toolbox for the ingestion, time-alignment, and visualization of sense and stimulation data from the Medtronic Summit RC+S system. *bioRxiv* [Preprint]. doi: 10.1101/2021.06.07.447439
- Stanslaski, S., Herron, J., Chouinard, T., Bourget, D., Isaacson, B., Kremen, V., et al. (2018). A Chronically Implantable Neural Coprocessor for Investigating the Treatment of Neurological Disorders. *IEEE Trans. Biomed. Circuits Syst.* 12, 1230–1245. doi: 10.1109/TBCAS.2018.2880148
- Thenaisie, Y., Palmisano, C., Canessa, A., Keulen, B. J., Capetian, P., Castro Jimenez, M., et al. (2021). Towards adaptive deep brain stimulation: clinical and technical notes on a novel commercial device for chronic brain sensing. *medRxiv* [Preprint]. doi: 10.1101/2021.03.10.21251638
- Tinkhauser, G., Pogossyan, A., Little, S., Beudel, M., Herz, D. M., Tan, H., et al. (2017). The modulatory effect of adaptive deep brain stimulation on beta bursts in Parkinson's disease. *Brain* 140, 1053–1067. doi: 10.1093/brain/awx010
- Toth, R., Zamora, M., Ottaway, J., Gillbe, T., Martin, S., Benjaber, M., et al. (2020). DyNeuMo Mk-2: an Investigational Circadian-Locked Neuromodulator with Responsive Stimulation for Applied Chronobiology. *Conf. Proc. IEEE Int. Conf. Syst. Man Cybern.* 2020, 3433–3440. doi: 10.1109/SMC42975.2020.9283187
- Urrestarazu, E., Iriarte, J., Alegre, M., Clavero, P., Rodríguez-Oroz, M. C., Guridi, J., et al. (2009). Beta activity in the subthalamic nucleus during sleep in patients with Parkinson's disease. *Mov. Disord.* 24, 254–260. doi: 10.1002/mds.22351
- Velisar, A., Syrkin-Nikolau, J., Blumenfeld, Z., Trager, M. H., Afzal, M. F., Prabhakar, V., et al. (2019). Dual Threshold Neural Closed Loop Deep Brain Stimulation in Parkinson disease Patients. *Brain Stimul.* 12, 868–876. doi: 10.1016/j.brs.2019.02.020
- Yin, Z., Zhu, G., Zhao, B., Bai, Y., Jiang, Y., Neumann, W.-J., et al. (2021). Local field potentials in Parkinson's disease: a frequency-based review. *Neurobiol. Dis.* 155:105372. doi: 10.1016/j.nbd.2021.105372
- Zahed, H., Zuzuarregui, J. R. P., Gilron, R., Denison, T., Starr, P. A., and Little, S. (2021). The Neurophysiology of Sleep in Parkinson's Disease. *Mov. Disord.* 36, 1526–1542. doi: 10.1002/mds.28562

Conflict of Interest: Devices were provided at no charge by Medtronic. PS is inventor on US patent 9,295,838 “Methods and systems for treating neurological movement disorders”; the patent covers cortical detection of physiological biomarkers in movement disorders, which is also discussed in this manuscript.

The remaining authors declare that the research was conducted in the absence of any commercial or financial relationships that could be construed as a potential conflict of interest.

Publisher's Note: All claims expressed in this article are solely those of the authors and do not necessarily represent those of their affiliated organizations, or those of the publisher, the editors and the reviewers. Any product that may be evaluated in this article, or claim that may be made by its manufacturer, is not guaranteed or endorsed by the publisher.

Copyright © 2021 Gilron, Little, Wilt, Perrone, Anso and Starr. This is an open-access article distributed under the terms of the Creative Commons Attribution License (CC BY). The use, distribution or reproduction in other forums is permitted, provided the original author(s) and the copyright owner(s) are credited and that the original publication in this journal is cited, in accordance with accepted academic practice. No use, distribution or reproduction is permitted which does not comply with these terms.



Prefrontal Physiomarkers of Anxiety and Depression in Parkinson's Disease

Coralie de Hemptinne¹, Witney Chen¹, Caroline A. Racine¹, Andreea L. Seritan², Andrew M. Miller¹, Maria S. Yaroshinsky¹, Sarah S. Wang³, Roe Gilron¹, Simon Little³, Ian Bledsoe³, Marta San Luciano³, Maya Katz³, Edward F. Chang¹, Heather E. Dawes¹, Jill L. Ostrem³ and Philip A. Starr^{1*}

¹ Department of Neurological Surgery, University of California, San Francisco, San Francisco, CA, United States,

² Department of Psychiatry, University of California, San Francisco, San Francisco, CA, United States, ³ Department of Neurology, University of California, San Francisco, San Francisco, CA, United States

OPEN ACCESS

Edited by:

Waldemar Karwowski,
University of Central Florida,
United States

Reviewed by:

J. Luis Lujan,
Mayo Clinic College of Medicine
and Science, United States
Brent Winslow,
Design Interactive, United States

*Correspondence:

Philip A. Starr
Philip.starr@ucsf.edu

Specialty section:

This article was submitted to
Neural Technology,
a section of the journal
Frontiers in Neuroscience

Received: 27 July 2021

Accepted: 17 September 2021

Published: 21 October 2021

Citation:

de Hemptinne C, Chen W, Racine CA, Seritan AL, Miller AM, Yaroshinsky MS, Wang SS, Gilron R, Little S, Bledsoe I, San Luciano M, Katz M, Chang EF, Dawes HE, Ostrem JL and Starr PA (2021) Prefrontal Physiomarkers of Anxiety and Depression in Parkinson's Disease. *Front. Neurosci.* 15:748165. doi: 10.3389/fnins.2021.748165

Objective: Anxiety and depression are prominent non-motor symptoms of Parkinson's disease (PD), but their pathophysiology remains unclear. We sought to understand their neurophysiological correlates from chronic invasive recordings of the prefrontal cortex (PFC).

Methods: We studied four patients undergoing deep brain stimulation (DBS) for their motor signs, who had comorbid mild to moderate anxiety and/or depressive symptoms. In addition to their basal ganglia leads, we placed a permanent prefrontal subdural 4-contact lead. These electrodes were attached to an investigational pulse generator with the capability to sense and store field potential signals, as well as deliver therapeutic neurostimulation. At regular intervals over 3–5 months, participants paired brief invasive neural recordings with self-ratings of symptoms related to depression and anxiety.

Results: Mean age was 61 ± 7 years, mean disease duration was 11 ± 8 years and a mean Unified Parkinson's Disease Rating Scale, with part III (UPDRS-III) off medication score of 37 ± 13 . Mean Beck Depression Inventory (BDI) score was 14 ± 5 and Beck Anxiety Index was 16.5 ± 5 . Prefrontal cortex spectral power in the beta band correlated with patient self-ratings of symptoms of depression and anxiety, with r -values between 0.31 and 0.48. Mood scores showed negative correlation with beta spectral power in lateral locations, and positive correlation with beta spectral power in a mesial recording location, consistent with the dichotomous organization of reward networks in PFC.

Interpretation: These findings suggest a physiological basis for anxiety and depression in PD, which may be useful in the development of neurostimulation paradigms for these non-motor disease features.

Keywords: Parkinson's disease, electrocorticography, mood, electrophysiology, prefrontal cortex

INTRODUCTION

Anxiety and depression are prominent non-motor symptoms of Parkinson's disease (PD) that are clinically debilitating (Seppi et al., 2019) and may predate the onset of motor signs (Postuma et al., 2015). Functional imaging studies in patients with PD and comorbid anxiety (Dan et al., 2017; Wang et al., 2017) and depression (Luo et al., 2014; Dan et al., 2017; Wang et al., 2018, 2020; Lin et al., 2020) point to involvement of prefrontal cortical areas, but the associated circuit mechanisms are poorly understood. Much progress has been made in understanding circuit mechanisms related to *motor* signs of PD utilizing invasive intracranial recording at both cortical (Panov et al., 2017) and subcortical (Brittain and Brown, 2014) sites in the motor network. This technique offers much higher spatiotemporal resolution and a more favorable signal-to-noise ratio than most non-invasive methods, and has led to the identification of potential electrophysiological markers for both the severity of motor signs and for the effectiveness of therapeutic intervention (Brittain and Brown, 2014).

Invasive studies in non-parkinsonian disorders have begun to elucidate networks and frequency bands important to mood fluctuations (Kirkby et al., 2018; Sani et al., 2018) and clinical depression (Lipsman et al., 2014; Clark et al., 2016; Merkl et al., 2016; Veerakumar et al., 2019; Scangos et al., 2020). Most invasive human physiological studies have been done perioperatively, using externalized brain leads either during a surgical intervention or for a few days after implantation, in a hospital setting. This method precludes the study of dynamically evolving longitudinal symptoms. Neurostimulation devices that incorporate brain sensing with therapeutic neurostimulation, also called "bidirectional interfaces," offer many advantages over short term perioperative recordings (Starr, 2018). Advantages include wireless data streaming in real time or from internal device storage, the opportunity to record in fully naturalistic environments, and the possibility of repeated measures of neural activity paired with external monitors, or with patient self-rating of symptoms, over many cycles of symptom exacerbation and remission. A limitation of invasive recording is the sparse spatial coverage, and the inherent risks of inserting a second lead in the context of a clinically indicated surgery. However, despite the minimal risk and wide spatial sampling of non-invasive methods such as scalp electroencephalography and functional magnetic resonance imaging, these non-invasive methods are not suited to performing repeated measures in a patient's home environment.

To understand prefrontal physiological correlates of anxiety and depression in PD, we studied four patients with PD who met standard clinical criteria for basal ganglia deep brain stimulation (DBS) for their motor signs (Fang and Tolleson, 2017), and who also had comorbid anxiety and/or depressive symptoms. In addition to their standard therapeutic basal ganglia leads, we implanted a permanent quadripolar subdural lead over areas of the right prefrontal cortex (PFC) previously implicated in the pathophysiology of anxiety (Dan et al., 2017; Wang et al., 2017) or depression (Luo et al., 2014; Dan et al., 2017; Wang et al., 2018, 2020; Lin et al., 2020) by non-invasive studies in PD. Daily brain recordings were paired with self-ratings of anxiety and

depression. We show that prefrontal oscillatory activity in the beta band, an already well described biomarker of parkinsonian akinesia and rigidity from recordings in the motor system (Brittain and Brown, 2014), predicts anxiety and depressive symptoms in PD. We interpret our results in the framework of a contemporary model of mood regulation, in which an imbalance in reciprocal mesial and lateral prefrontal networks can lead to depression (Rolls, 2016; Loonen and Ivanova, 2017).

MATERIALS AND METHODS

This protocol was approved by the Institutional Review Board of the University of California, San Francisco (UCSF), under a physician-sponsored investigational device exemption. Informed consent was obtained under the Declaration of the Principles of Helsinki. The study was registered on ClinicalTrials.gov (NCT03131817)¹.

Subjects

Subjects were recruited from the Movement Disorders and Neuromodulation Center at UCSF. Participants had a diagnosis of idiopathic PD and had been offered implantation of a deep brain stimulator system for relief of motor signs. Participants underwent preoperative evaluation by a movement disorders neurologist, a psychiatrist and a neuropsychologist. Motor impairment was assessed using the Unified Parkinson's Disease Rating Scale, with part III (UPDRS-III) done in the off- and on-medication states (**Table 1**). Neuropsychological and psychiatric evaluations were conducted using the Montreal Cognitive Assessment, the Beck Anxiety Inventory (BAI), the Beck Depression Inventory (BDI) and the Structured Clinical Interview for DSM-5. Inclusion criteria required mild to moderate depression (BDI > 13) and/or anxiety symptoms (BAI > 7). Patients were excluded for active suicidal ideation on the Columbia Suicidality Severity Rating Scale or significant cognitive impairment (Montreal Cognitive Assessment score <20).

Surgery

Subjects were implanted unilaterally or bilaterally with quadripolar DBS leads placed in either the subthalamic nucleus (STN; Medtronic Model 3389) or Globus Pallidus (GP; Medtronic Model 3387), according to clinical considerations (**Table 1**). Placement of the DBS lead was confirmed using microelectrode recordings in the awake state (Starr, 2002). In addition to the standard therapeutic DBS electrode(s) used to treat motor signs, patients were implanted with a flexible 4-contact electrocorticography (ECoG) lead (Medtronic 5387A) in the subdural space over the right PFC (**Figure 1A**). ECoG contacts were 4 mm in diameter and spaced 10 mm apart. The ECoG strips targeted the dorsolateral prefrontal cortex (DLPFC), the orbitofrontal cortex (OFC) or the frontopolar cortex (FPC), in order to evaluate a wide area of PFC in the course of this exploratory study. The cortical lead was placed through the

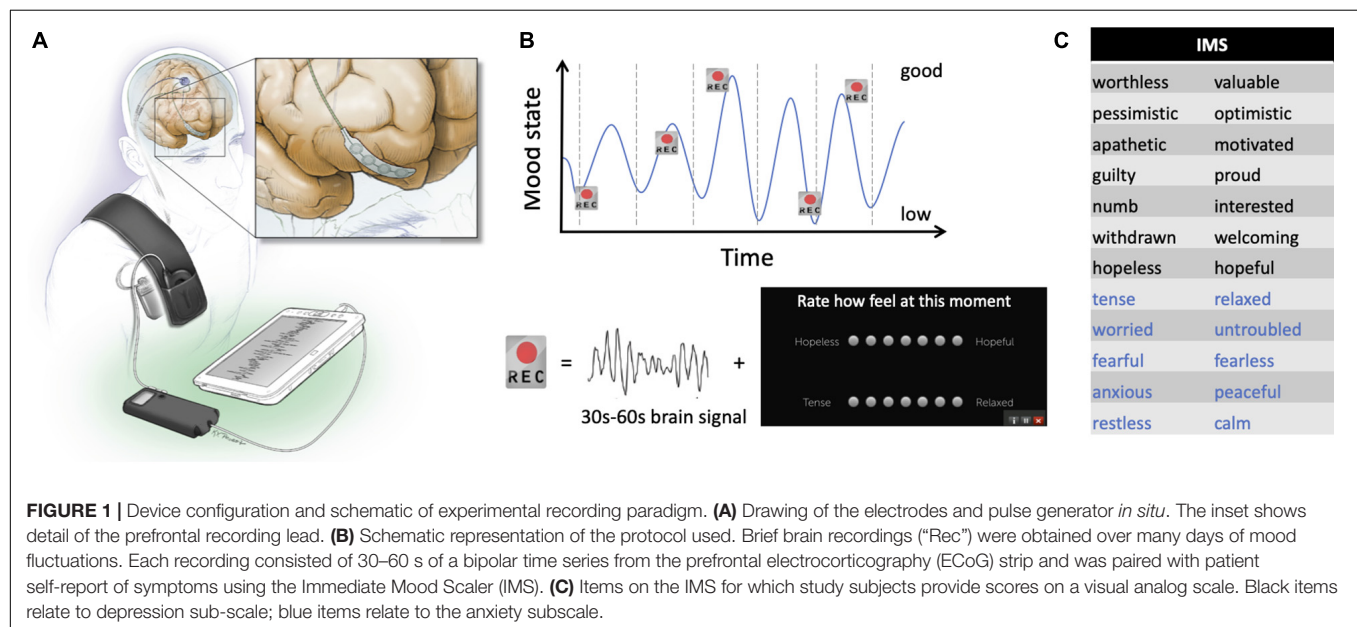
¹clinicaltrials.gov/ct2/show/NCT03131817

TABLE 1 | Patient demographics and details of recording.

	Study subject	PD1	PD3	PD4	PD5	Mean and STD
Demographics	Gender	F	M	F	F	
	Age (years)	53	55	67	70	61 ± 7
	Disease duration (years)	25	5	6	9	11.25 ± 8
	Preoperative UPDRS-III (off/on)	39/19	16/15	41/15	50/25	Off: 36.5 ± 14.5 On: 18.5 ± 4.7
	Preoperative depression and anxiety severity (BDI/BAI)	10/16	17/16	9/10	21/24	BDI: 14 ± 5 BAI: 16.5 ± 5
	Preoperative cognitive state (MoCA)	26	29	27	29	27.75 ± 1.5
Details of recording	DBS lead side/target	R and L/STN	R/GP	R/STN	R/GP	
	Cortical region side/target	R/FPC	R/DLPFC	R/OFC	R/OFC	
	Coordinates of recording contact* (contact #: x,y,z)	C8: 18.6 74.6 6.0 C9: 26.9 70.6 1.6	C10: 26.6 80.3 2.4 C11: 33.9 76.6 6.7	C8: 13.4 45.4 15.7 C10: 31.1 13.8 6.9	C8: 18.2 42.6 11.2 C9: 28.3 42.6 9.7	
	#Recordings paired with IMS scores	88	49	46	40	55.75 ± 21.8
	#Total days of recording	51	45	31	30	39.25 ± 10.4
	#Months over which recordings were done	5	5	3	5	4.5 ± 1
	IMS total score (mean ± std)	18.7 ± 3.8	−4.6 ± 6.4	26.4 ± 6.3	6.6 ± 7.6	

F, Female; M, Male; UPDRS, Unified Parkinson's Disease Rating Scale; off, 12 h off PD medication; on, on regular PD medication; BDI, Beck Depression Inventory; BAI, Beck Anxiety Inventory; MoCA, Montreal Cognitive Assessment; STN, Subthalamic Nucleus; GPi, Globus Pallidus interna; R, Right; L, Left; FPC, Frontopolar cortex; DLPFC, dorsolateral prefrontal cortex; OFC, orbitofrontal cortex; IMS, Immediate mood scaler, for assessing momentary mood state.

*Contact coordinates are relative to the midcommissural point.



original DBS burr hole in two patients. In two others, a second small burr hole was placed above the right orbit to access the OFC, which could not be accessed through the convexity burr hole due to the stiffness of the ECoG paddle. An intraoperative cone-beam CT merged to the preoperative MRI was used to confirm correct placement of the ECoG strip (Panov et al., 2017).

The cortical strip and ipsilateral DBS electrode were connected to lead extenders (model 37087, Medtronic), tunneled down the

neck and attached to a Medtronic Activa PC+S pulse generator placed in a pocket over the pectoralis muscle under general anesthesia (Figure 1A). This investigational bidirectional device allows both delivery of therapeutic stimulation and chronic recording of field potentials (Stanslaski et al., 2018). For patients implanted with bilateral DBS electrodes, the left STN electrode was attached to a separate Activa SC pulse generator to deliver therapeutic stimulation.

Electrode Locations and Tractography

To localize ECoG electrodes in individual patients, the preoperative T1 MRI was used to reconstruct cortical surface models in FreeSurfer (Dale et al., 1999; Fischl et al., 2002). A CT scan taken 2–3 months after surgery was used to determine the location of each cortical electrode. We projected ECoG contacts onto the cortical surface mesh with the *imgpipe* toolbox (Hamilton et al., 2017) using a surface vector projection method (Kubaneck and Schalk, 2015). Once we identified cortical locations for each ECoG electrode on individualized cortical reconstructions, we projected all patients' recording electrodes onto the Desikan-Killiany atlas brain (Desikan et al., 2006).

For tractography, we obtained High Angular Resolution Diffusion Imaging (HARDI) on a 3 Tesla MR scanner (General Electric, Inc.), using a spin-echo echo-planar imaging (SE EPI) pulse sequence (TE = 71 ms, TR = 7765 ms, flip angle $\alpha = 90^\circ$), FOV 28 cm \times 28 cm, at least 70 axial slices, 2 mm³ isotropic voxels, *b*-value = 2000 s mm⁻² in 55 non-collinear gradient directions and a signal to noise ratio >60. In PD1, *b*-value was 1,000 s mm⁻² in 32 non-collinear gradient directions. A single non-diffusion-weighted *b*0 image was also obtained. The diffusion-weighted tractography was explored using a deterministic tractography software package (Brainlab Elements, Feldkirchen, Germany). Preoperative MRI, postoperative CT and HARDI scans were automatically merged and corrected for distortion. The ECoG contacts used for recordings were manually segmented on the CT scan. The regions of interest (ROIs) were then created by adding 2 mm to each contact and using these as seed regions for fiber tracking analyses, using an FA threshold of 0.17 and a minimum length of 8 cm.

Experimental Design

Patients underwent chronic brain recording and monitoring of their symptoms during typical daily activities at home, over 3–5 months. Cortical recordings (30 or 60 s durations) were initially self-triggered, but patients subsequently found it easier to have the device automatically trigger neural recordings 2–3 times per day on a time schedule that was individualized to capture times of the day when low or high moods were typically experienced. **Figure 1B** shows a schematic representation of the paradigm used in this study. The recording montage was selected based on signal quality. Signals were sampled at 422 Hz, with a 0.5 Hz high pass filter, and a gain of 2,000. Signals were stored on the pulse generator and downloaded non-invasively by radiotelemetry during in-clinic research visits. Subjects were instructed to self-report their anxiety and depressive symptoms using the Immediate Mood Scaler (IMS, Posit Science) within a 30-min window of the time of the neural recordings. Assessments done without paired brain signal and outside that window were excluded from analysis, resulting in a variable number of recordings across patients (**Table 1**). The IMS is a validated tablet-based tool that assesses momentary mood symptoms (Nahum et al., 2017), correlates well with standardized self-report measures of depression (PHQ-9) and anxiety (GAD-7), and further captures symptom fluctuations in-the-moment. Subjects rated their current emotional state using 12 pairs of

words thought to represent extremes of depressive (item 1–7, **Figure 1C**, black words) and anxiety (items 8–12, **Figure 1C**, blue words) related dimensions. The score range was –3 to 3 for each pair, with higher scores indicating more positive mood. Subjects were also instructed to assess the severity of their motor signs (rigidity, bradykinesia, tremor), their pain level, and the presence of suicidal thoughts using the same application (also on a score range of –3 to 3). We are not aware of a validated tool for self-assessment of motor signs at home. Changes in their basal ganglia DBS stimulation parameters, and changes in medications were occasionally required for clinical care and were tracked.

Signal Processing and Statistics

Analyses were performed in Matlab. The first 2 s of each brain recording was discarded because of transient direct current offsets generated by the devices' high-pass filter. For each brain recording, the power spectral density (PSD) was calculated using the Welch periodogram method (Matlab function *pwelch*) using a Hamming window, fast Fourier transform of 422 points and 50% overlap (frequency resolution of 1 Hz). The PSD was then log transformed and averaged over multiple frequency bands: 2–5 Hz delta, 5–8 Hz theta, 8–13 Hz alpha, 13–30 Hz beta, 13–20 Hz low beta, 20–30 Hz high beta, 30–45 Hz low gamma. For each patient, each frequency band was correlated with the total IMS score, or IMS subscores, using Spearman correlations because of discontinuous variables. A false-discovery rate (FDR) correction for multiple comparisons was used and a corrected *p*-value of 0.05 was considered statistically significant.

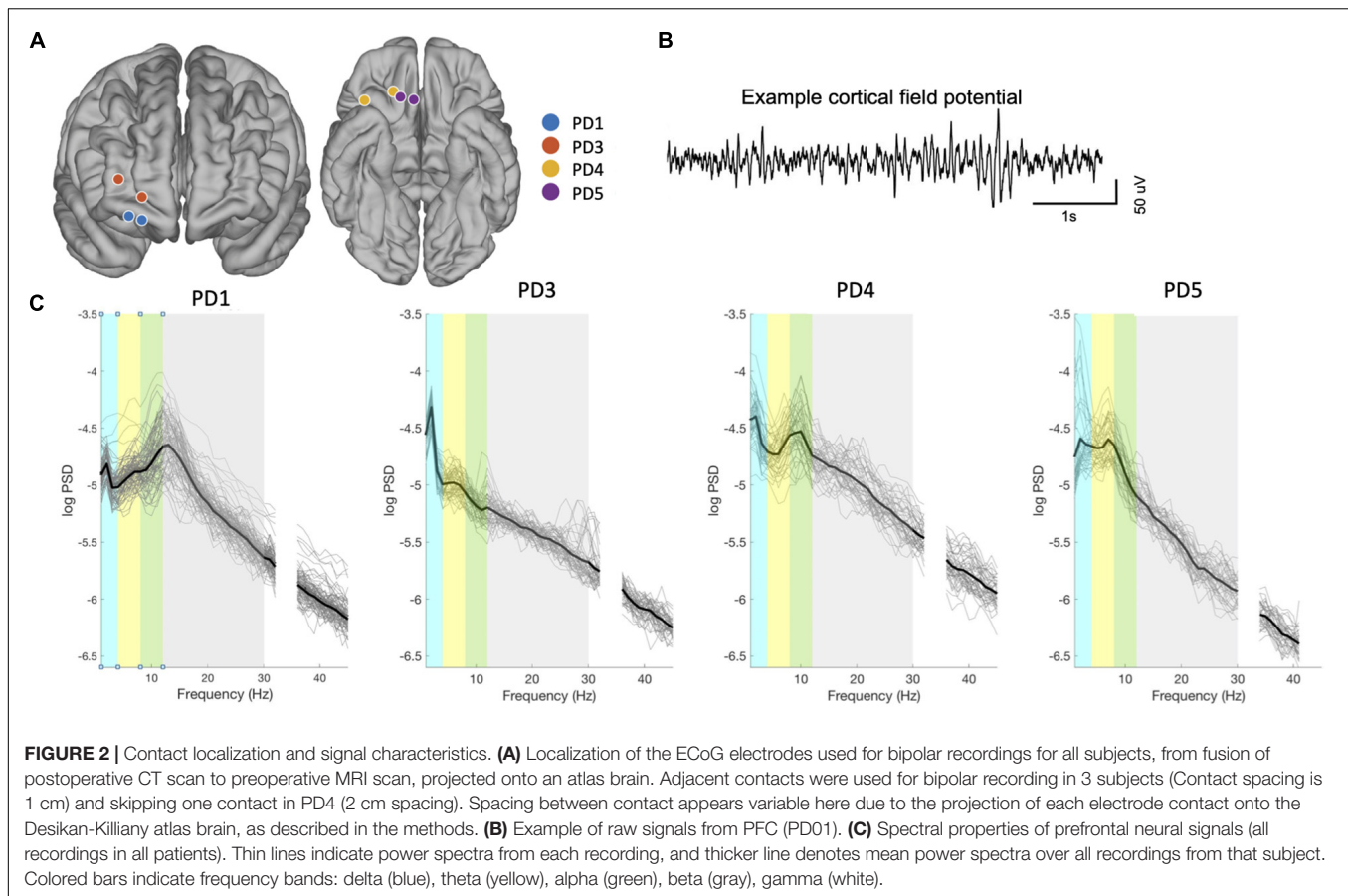
RESULTS

Subjects

Four subjects with PD (3 females, 1 male) were studied. A fifth patient was implanted but did not provide regular symptom assessments and was thus excluded from further analyses. The mean age of study participants was 61 ± 7 years, mean disease duration was 11 ± 8 years and a mean UPDRS-III off medication score of 37 ± 13 . Subjects had mild to moderate depression and anxiety (mean BDI score of 14 ± 5 and a mean BAI score of 16.5 ± 5). Patient demographics provided in **Table 1**.

Recording Locations and Signals

Chronic recordings through the prefrontal ECoG paddle were obtained while delivering therapeutic stimulation through the DBS lead (**Figure 1A**). In each subject, 40–89 recordings paired with symptom assessments were collected over a 3 to 5-month period beginning at least 10 days postoperatively (**Table 1**). The mean time between the brain recording and the mood assessment was 9 ± 10 min. Locations of the recording contacts used for each patient are represented on a template brain in **Figure 2A**, with coordinates in **Table 1**. An example ECoG time series is shown in **Figure 2B**. In all subjects, recordings were characterized by a spectral peak in theta, alpha, or beta frequencies as shown on **Figure 2C**, consistent with prefrontal ECoG time series in patients without PD (Helfrich and Knight, 2019).



Self-Reported Mood States Are Correlated With Prefrontal Beta Band Activity

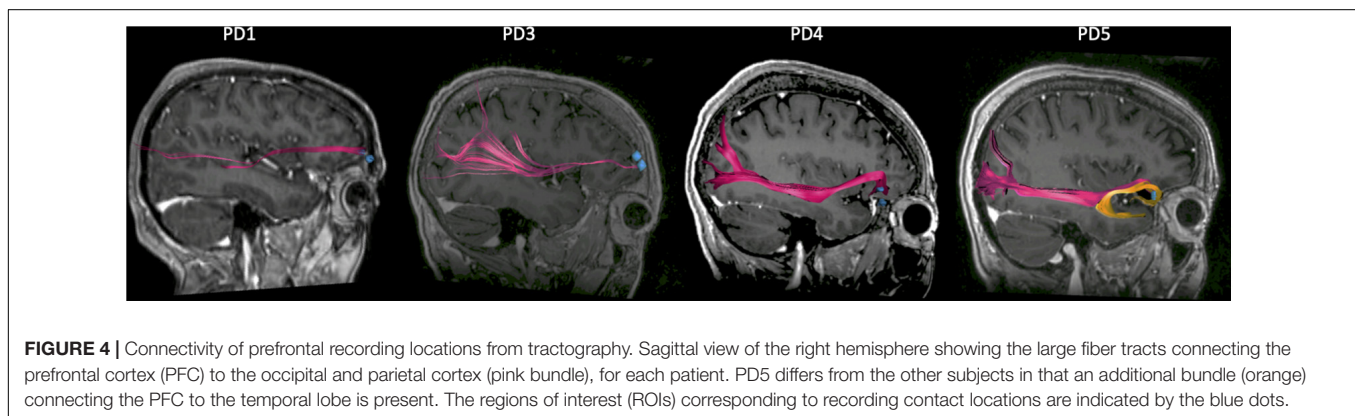
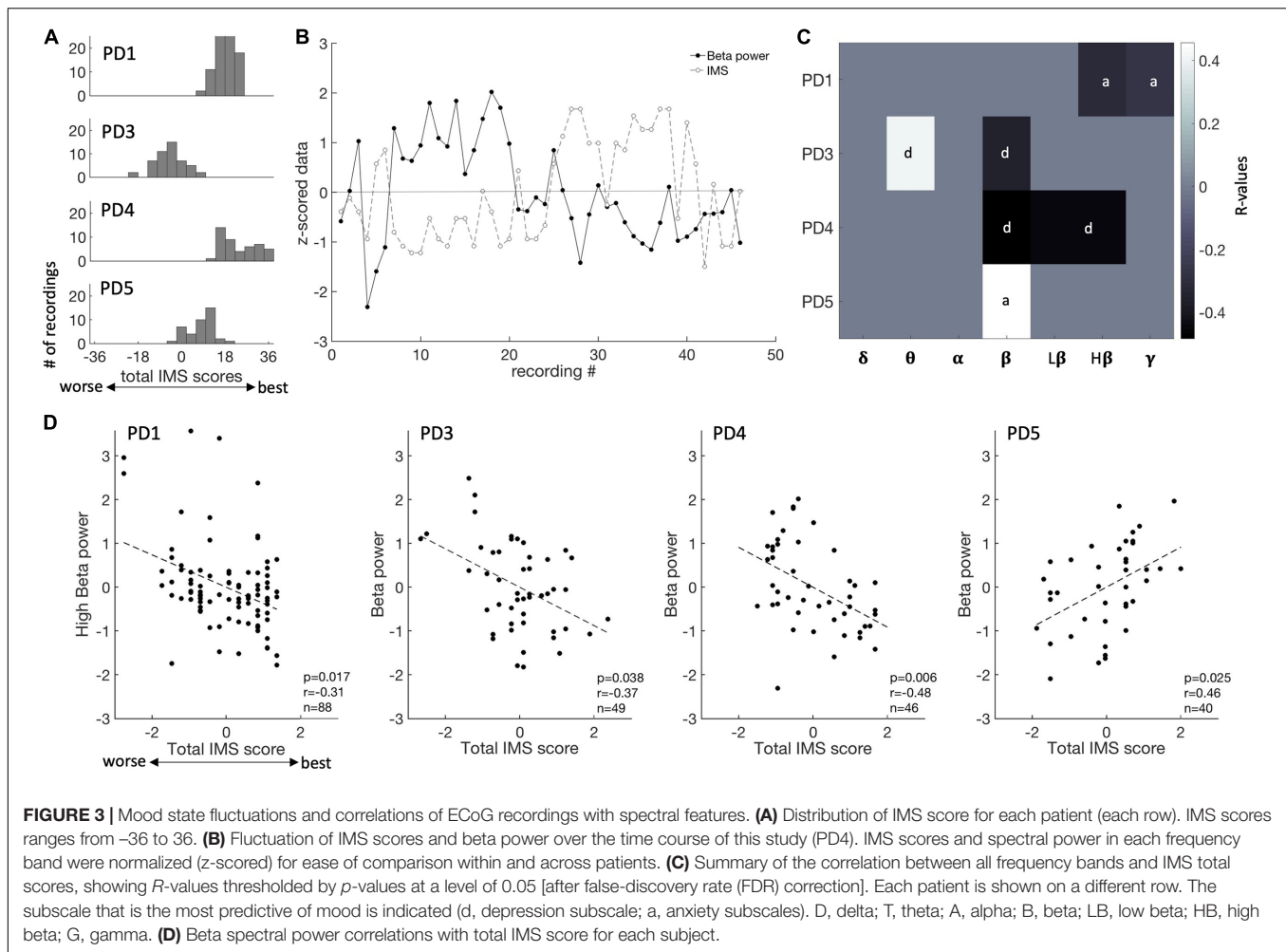
Patients' symptoms were chronically assessed using the IMS, a tablet-based application that assesses momentary fluctuations of both anxiety and depressive symptoms with a total score ranging from -36 (worse) to 36 (best). These assessments, referred to here as "mood states," fluctuated within ranges that were specific to each patient (**Figure 3A** and **Table 1**). We correlated spectral power in predefined frequency bands against total IMS scores and IMS subscores. An example of fluctuations in mood state as well as spectral power in the beta range is shown on **Figure 3B** (PD4). Across all four subjects, we found that beta power was a consistent predictor of mood states as shown in **Figure 3C** ($p < 0.05$, FDR corrected). In three subjects (PD1, 3 and 4), beta power was negatively correlated with total IMS scores (lower spectral power was associated with higher scores, corresponding to less anxiety and/or depression), while a positive correlation was found in PD5 (**Figure 3D**). One subject (PD3) also had a positive correlation between theta power and the IMS total score and another subject (PD1) had a negative correlation with gamma power ($p < 0.05$, FDR corrected, **Figure 3C**). In two subjects (PD3 and PD4) the correlation of beta activity with total IMS was driven mainly by depression subscores, while in the other two subjects (PD1 and PD5), IMS correlations were driven mainly by anxiety subscores.

Recording Location May Explain Inverse Beta Correlation for PD5

Since PD5 showed an opposite correlation between beta activity and IMS scores compared to other subjects, we sought to explain this based on contact location and connectivity to other brain regions. The recording montage for PD5 was the most mesial of all four subjects but did overlap with that of PD4 (**Figure 2A**). We thus used tractography to map the largest fiber tracts originating from the tissue immediately underneath the recording contacts in each subject. A seed object was made around each electrode contact in the bipolar recording montage. In all four subjects, the seed was the origin of fibers traveling in the inferior fronto-occipital fasciculus (IFOF), a pathway connecting widespread areas of PFC to the occipital and parietal cortex (Burks et al., 2018; pink bundle on **Figure 4**). The recording contacts in PD5, however, were uniquely associated with the uncinate fasciculus connecting mesial PFC to the temporal lobe (Hau et al., 2017; orange bundle on **Figure 4**), suggesting that recordings in this patient may have probed a different functional network compared to the other more laterally placed recording locations.

Potential Confounding Variables

Given that symptoms were assessed at different times of the day, we studied the effect of time on symptoms assessment and found that the IMS scores were not correlated with the time at which



they were done ($p > 0.05$, FDR corrected). In addition, since beta power is a marker of motor states in the basal ganglia nuclei, we also showed that cortical beta power did not covary with severity of motor signs ($p > 0.05$, FDR corrected). Thus, correlations between mood scores and cortical beta power were unlikely to have been confounded by these factors. While some changes to stimulation parameters and medications were made during the recording period to address clinical needs of the patient (Table 2),

we did not observe consistent changes in self-ratings nor spectral power corresponding to the timing of those changes.

DISCUSSION

We utilized chronic wireless invasive brain recording to elucidate the physiological basis for depression and anxiety

TABLE 2 | Initial deep brain stimulator settings, medications, and their changes during the study.

Study subject	PD1	PD3	PD4	PD5
Initial DBS settings	C + 2-, 2.3 mV, 60 ms, 140 Hz	C + 2-, 2.5 V, 90 ms, 140 Hz	1 + 2-, 1.5 V 90 ms, 140 Hz	1-2 + , 3.2 V, 70 ms, 140 Hz
Changes in DBS settings during the study	Added additional contact: C + 1- 2-, and increased amplitude to 3.0 V at 88 days*	Increased amplitude to 3 V at 120 days*	Increased amplitude to 1.9 V at 30 days*	Changed stimulation contacts to 0 + 1 at 68 days*
Initial PD medications –levodopa equivalents	850	1,000	1,415	992
Change in PD levodopa equivalents	reduced to 650 at 38 days*	None	None	Increased to 1,192 at 68 days*
Initial psychiatric medication	Citalopram 20 mg	Lorazepam 1 mg	Duloxetine 20 mg Lexapro 20 mg Artane 2.5 mg	Duloxetine 90 mg QD
Change in psychiatric medication during the study	None	None	Lexapro decreased to 10 mg at 57 days*	Took mirtazapine 3.75 mg for 2 weeks starting at 113 days

C, case of pulse generator (monopolar stimulation mode), V, Volts, ms, microseconds, Hz, Hertz; DBS, deep brain stimulation, PD, Parkinson's disease.

*Refers to the number of days since the start of brain recording.

in PD. We enrolled patients who met clinical criteria for basal ganglia DBS for motor signs of PD, who also had mild-to-moderate comorbid anxiety or depressive disorders. Over several months, prefrontal ECoG recordings were paired with patients' self-reported mood scores. We show that variation in specific frequency bands, especially the beta band, explained part of the variance in mood scores. In recordings from DLPFC, FPC and lateral OFC, increased beta band activity correlated with worsening depression or anxiety symptom severity, while the opposite was true in the subject with the most mesially located contact pair in OFC. This is consistent with the anatomic localization of reciprocal reward and non-reward networks in the PFC (Rolls, 2016; Xia et al., 2017).

Invasive Recording to Evaluate Non-motor Manifestations of Parkinson's Disease

In movement disorders, specific *motor* signs have been related to alterations in oscillatory synchronization within and between structures of the basal ganglia-thalamocortical motor circuit. For example, beta band (13–30 Hz) oscillatory activity is exaggerated in the rigid-akinetic form of PD (Brittain and Brown, 2014), while gamma band (60–90 Hz) oscillations are elevated in levodopa-induced or stimulation-induced dyskinesia (Swann et al., 2016). The physiological signatures of non-motor symptoms, however, are much less understood. Invasive recording studies of the PFC (Chen et al., 2019) and STN (Kuhn et al., 2005; Buot et al., 2013; Huebl et al., 2014; Peron et al., 2017) have explored emotional functions of these brain regions, but only within task paradigms and during brief in-hospital sessions. EEG evaluation of PD patients with and without depressive symptoms showed differences in spectral power in alpha and low beta frequencies, but these were not localized to a particular brain region. This study is the first to evaluate cortical signatures of mood state in PD using invasive recording.

The method of chronic wireless recording from an implanted sensing-enabled interface was critical for tracking neural correlates of mood fluctuations over long periods during normal daily life. A disadvantage of this method, compared to perioperative ECoG with externalized leads (Panov et al., 2017; Sani et al., 2018), is lower channel count that precludes wide spatial coverage. To address this, we explored different prefrontal areas in each subject, and for statistical evaluation utilized a within-subjects repeated measures approach with over 40 samples per subject, rather than pooling data across subjects. Because the study took place over months, data were collected while clinically indicated therapeutic basal ganglia neurostimulation was also ongoing, which precluded acquiring simultaneous basal ganglia recordings (Swann et al., 2018). Recently introduced second generation sensing-enabled interfaces are engineered to allow depth recordings during stimulation (Giron et al., 2021). We cannot exclude a possible effect of changes in medications or stimulation on cortical physiology, but changes were tracked and were infrequent. Only the right hemisphere was explored, based on safety consideration for an invasive investigational study, as well as evidence of greater mood-elevating effects of acute prefrontal stimulation on the right side, in non-parkinsonian disorders (Rao et al., 2018).

Opposite Beta Correlations May Reflect Reciprocal Roles of Two Reward-Related Networks

Our findings suggest that beta band activity may index the severity of non-motor symptoms in networks linked to the PFC. There are thought to be two reciprocally related corticostriatal reward processing networks involving the PFC (Rolls, 2016; Xia et al., 2017). A “non-reward” (missed reward) network, whose cortical localization maps to lateral OFC, DLPFC, and dorsal cingulate cortex, is activated when an action does not lead to positive reward. A positive reward network, involving mesial PFC and pregenual cingulate cortex,

is active when action *does* lead to a reward. The mesial reward network also has major connections to the temporal lobe (Loonen and Ivanova, 2016a,b). Consistent with this framework, and with the possibility that depressed mood may reflect dysfunctional reward networks, non-invasive studies indicate that functional connectivity (resting state MRI fluctuations) in these reciprocal cortical areas have opposite correlations with severity of depression (in non-parkinsonian mood disorders) (Cheng et al., 2016). Our results from this initial invasive recording study in PD support this dichotomous circuit model, showing elevated beta in states of depressed mood or anxiety in the lateral OFC and DLPFC, and the inverse in mesial OFC. Of note, while the two subjects with OFC recording leads had overlapping recording montages, DTI-based tractography showed differing connectivity of these montages. Only those from PD5 (the only subject to have increased beta activity during epochs of *better* mood), showed temporal lobe connectivity consistent with involvement in the mesial positive reward network.

Beta Activity and the Maintenance of Attractor States

In the normal function of *motor* networks, beta band oscillatory activity is thought to favor “maintenance of the *status quo*,” that is, elevated while holding specific postures, and desynchronizing for fluid movements to occur (Engel and Fries, 2010). By analogy, in PFC, we hypothesize that beta oscillations could function to maintain specific affective states, depending on the region of the PFC involved. This hypothesis dovetails with the recently proposed “non-reward attractor” theory of depression, postulating that depression can be triggered by abnormally prolonged activation of the lateral prefrontal network sensitive to missed or absent reward (Rolls, 2016). Beta band activity thus might serve to maintain “attractor states”: increased beta in lateral OFC and DLPFC could contribute to maintenance of a “depressive” attractor state, while increased beta in mesial OFC would promote a “rewarding” or mood-elevating attractor state. Given the strong influence of dopamine depletion and dopaminergic medications on mood and anxiety (Seppi et al., 2019), it is possible that our findings are specific to patients with PD and would not generalize to mood disorders in non-parkinsonian states. However, in patients with major depressive disorder undergoing placement of DBS leads in the subgenual cingulate (part of the mesial reward network), severity of depression across subjects inversely correlated with the amplitude of beta band oscillations (Clark et al., 2016), as in subject PD5 in this study, suggesting a role for beta activity in maintenance of reward networks across multiple diagnoses.

Implications for Treatment of Non-motor Signs of Parkinson's Disease

Depression, anxiety, and behavioral changes in PD may be difficult to treat and may become a primary source of disability in mid-stage PD after motor signs are adequately treated medically or by surgical intervention (Schupbach et al., 2006). Our work

provides a framework for therapeutic neuromodulation of beta activity in non-motor networks in PD. Non-invasive methods of neuromodulation of DLPFC show promise for mood disorders in PD (Rektorova and Anderkova, 2017). Subcortical intervention, where fibers converge on smaller targets, may be more efficient for modulating mood networks. Theta burst stimulation of ventral STN, for example, has been used to modulate theta band activity in DLPFC (Bentley et al., 2020). STN stimulation paradigms that reduce lateral prefrontal beta activity merit investigation and could be facilitated by the enhanced spatial resolution offered by recently introduced “directional” DBS leads (Aman et al., 2020).

DATA AVAILABILITY STATEMENT

The raw data supporting the conclusions of this article will be made available by the authors, without undue reservation.

ETHICS STATEMENT

The studies involving human participants were reviewed and approved by the Institutional Review Board of the University of California, San Francisco. The patients/participants provided their written informed consent to participate in this study.

AUTHOR CONTRIBUTIONS

CH, EC, HD, and PS: conception and design of the study. CH, WC, CR, AS, AM, MY, SW, RG, SL, IB, MS, MK, JO, and PS: acquisition of data. CH, WC, RG, and SL: analysis of data. CH, WC, and PS: drafting a significant portion of the manuscript or figures. All authors contributed to the article and approved the submitted version.

FUNDING

This research was funded by the Michael J. Fox Foundation and the Defense Advanced Research Projects Agency (DARPA) under Cooperative Agreement Number W911NF-14-2-0043, issued by the Army Research Office contracting office in support of DARPA's SUBNETS program. The views, opinions and/or findings expressed are those of the author(s) and should not be interpreted as representing the official views or policies of the Department of Defense or the US Government.

ACKNOWLEDGMENTS

We are grateful to the study participants. We thank Sheila Rajagopalan and Joncarmen Mergenthaler for their contribution, Katherine Scangos and Andrew Lee for proofreading the manuscript, and Ken Probst for providing medical art for **Figure 1A**.

REFERENCES

- Aman, J. E., Johnson, L. A., Sanabria, D. E., Wang, J., Patriat, R., Hill, M., et al. (2020). Directional deep brain stimulation leads reveal spatially distinct oscillatory activity in the globus pallidus internus of Parkinson's disease patients. *Neurobiol. Dis.* 139:104819. doi: 10.1016/j.nbd.2020.104819
- Bentley, J. N., Irwin, Z. T., Black, S. D., Roach, M. L., Vaden, R. J., Gonzalez, C. L., et al. (2020). Subcortical intermittent theta-burst stimulation (iTBS) increases theta-power in dorsolateral prefrontal cortex (DLPFC). *Front. Neurosci.* 14:41. doi: 10.3389/fnins.2020.00041
- Brittain, J. S., and Brown, P. (2014). Oscillations and the basal ganglia: motor control and beyond. *Neuroimage* 85(Pt 2), 637–647. doi: 10.1016/j.neuroimage.2013.05.084
- Buot, A., Welter, M. L., Karachi, C., Pochon, J. B., Bardinet, E., Yelnik, J., et al. (2013). Processing of emotional information in the human subthalamic nucleus. *J. Neurol. Neurosurg. Psychiatry* 84, 1331–1338. doi: 10.1136/jnnp-2011-302158
- Burks, J. D., Conner, A. K., Bonney, P. A., Glenn, C. A., Baker, C. M., Boettcher, L. B., et al. (2018). Anatomy and white matter connections of the orbitofrontal gyrus. *J. Neurosurg.* 128, 1865–1872. doi: 10.3171/2017.3.jns.162070
- Chen, W., de Hemptinne, C., Leibbrand, M., Miller, A. M., Larson, P. S., and Starr, P. A. (2019). Altered prefrontal theta and gamma activity during an emotional face processing task in Parkinson disease. *J. Cogn. Neurosci.* 31, 1768–1776. doi: 10.1162/jocn_a_01450
- Cheng, W., Rolls, E. T., Qiu, J., Liu, W., Tang, Y., Huang, C. C., et al. (2016). Medial reward and lateral non-reward orbitofrontal cortex circuits change in opposite directions in depression. *Brain* 139(Pt 12), 3296–3309. doi: 10.1093/brain/aww255
- Clark, D. L., Brown, E. C., Ramasubbu, R., and Kiss, Z. H. T. (2016). Intrinsic local beta oscillations in the subgenual cingulate relate to depressive symptoms in treatment-resistant depression. *Biol. Psychiatry* 80, e93–e94.
- Dale, A. M., Fischl, B., and Sereno, M. I. (1999). Cortical surface-based analysis. I. Segmentation and surface reconstruction. *Neuroimage* 9, 179–194.
- Dan, R., Ruzicka, F., Bezdicek, O., Ruzicka, E., Roth, J., Vymazal, J., et al. (2017). Separate neural representations of depression, anxiety and apathy in Parkinson's disease. *Sci. Rep.* 7:12164.
- Desikan, R. S., Segonne, F., Fischl, B., Quinn, B. T., Dickerson, B. C., Blacker, D., et al. (2006). An automated labeling system for subdividing the human cerebral cortex on MRI scans into gyral based regions of interest. *Neuroimage* 31, 968–980. doi: 10.1016/j.neuroimage.2006.01.021
- Engel, A. K., and Fries, P. (2010). Beta-band oscillations—signalling the status quo? *Curr. Opin. Neurobiol.* 20, 156–165. doi: 10.1016/j.conb.2010.02.015
- Fang, J. Y., and Tolleson, C. (2017). The role of deep brain stimulation in Parkinson's disease: an overview and update on new developments. *Neuropsychiatr. Dis. Treat.* 13, 723–732. doi: 10.2147/ndt.s113998
- Fischl, B., Salat, D. H., Busa, E., Albert, M., Dieterich, M., Haselgrove, C., et al. (2002). Whole brain segmentation: automated labeling of neuroanatomical structures in the human brain. *Neuron* 33, 341–355.
- Gilron, R., Little, S., Perrone, R., Wilt, R., deHemptinne, C., Yaroshinsky, M. S., et al. (2021). Long-term wireless streaming of neural recordings for circuit discovery and adaptive stimulation in individuals with Parkinson's disease. *Nat. Biotechnol.* 39, 1078–1085. doi: 10.1038/s41587-021-00897-5
- Hamilton, L. S., Chang, D. L., Lee, M. B., and Chang, E. F. (2017). Semi-automated anatomical labeling and Inter-subject warping of high-density intracranial recording electrodes in electrocorticography. *Front. Neuroinform.* 11:62. doi: 10.3389/fninf.2017.00062
- Hau, J., Sarubbo, S., Houde, J. C., Corsini, F., Girard, G., Deledalle, C., et al. (2017). Revisiting the human uncinate fasciculus, its subcomponents and asymmetries with stem-based tractography and microdissection validation. *Brain Struct. Funct.* 222, 1645–1662. doi: 10.1007/s00429-016-1298-6
- Helfrich, R. F., and Knight, R. T. (2019). Cognitive neurophysiology of the prefrontal cortex. *Handb. Clin. Neurol.* 163, 35–59. doi: 10.1016/b978-0-12-804281-6.00003-3
- Huebl, J., Spitzer, B., Brucke, C., Schonecker, T., Kupsch, A., Alesch, F., et al. (2014). Oscillatory subthalamic nucleus activity is modulated by dopamine during emotional processing in Parkinson's disease. *Cortex* 60, 69–81. doi: 10.1016/j.cortex.2014.02.019
- Kirkby, L. A., Luongo, F. J., Lee, M. B., Nahum, M., Van Vleet, T. M., Rao, V. R., et al. (2018). An amygdala-hippocampus subnetwork that encodes variation in human mood. *Cell* 175, 1688–1700.e14.
- Kubaneck, J., and Schalk, G. (2015). NeuralAct: a tool to visualize electrocortical (ECoG) activity on a three-dimensional model of the cortex. *Neuroinformatics* 13, 167–174. doi: 10.1007/s12021-014-9252-3
- Kuhn, A. A., Hariz, M. I., Silberstein, P., Tisch, S., Kupsch, A., Schneider, G. H., et al. (2005). Activation of the subthalamic region during emotional processing in Parkinson disease. *Neurology* 65, 707–713. doi: 10.1212/01.wnl.0000174438.78399.bc
- Lin, H., Cai, X., Zhang, D., Liu, J., Na, P., and Li, W. (2020). Functional connectivity markers of depression in advanced Parkinson's disease. *Neuroimage Clin.* 25:102130. doi: 10.1016/j.nicl.2019.102130
- Lipsman, N., Kaping, D., Westendorff, S., Sankar, T., Lozano, A. M., and Womelsdorf, T. (2014). Beta coherence within human ventromedial prefrontal cortex precedes affective value choices. *Neuroimage* 85(Pt 2), 769–778. doi: 10.1016/j.neuroimage.2013.05.104
- Loonen, A. J., and Ivanova, S. A. (2016a). Circuits regulating pleasure and happiness: the evolution of the amygdalar-hippocampal-habenular connectivity in vertebrates. *Front. Neurosci.* 10:539. doi: 10.3389/fnins.2016.00539
- Loonen, A. J., and Ivanova, S. A. (2016b). Circuits regulating pleasure and happiness-mechanisms of depression. *Front. Hum. Neurosci.* 10:571. doi: 10.3389/fnhum.2016.00571
- Loonen, A. J. M., and Ivanova, S. A. (2017). Commentary on “A non-reward attractor theory of depression”: a proposal to include the habenula connection. *Neurosci. Biobehav. Rev.* 83, 736–741. doi: 10.1016/j.neubiorev.2017.02.007
- Luo, C., Chen, Q., Song, W., Chen, K., Guo, X., Yang, J., et al. (2014). Resting-state fMRI study on drug-naïve patients with Parkinson's disease and with depression. *J. Neurol. Neurosurg. Psychiatry* 85, 675–683. doi: 10.1136/jnnp-2013-306237
- Merkel, A., Neumann, W. J., Huebl, J., Aust, S., Horn, A., Krauss, J. K., et al. (2016). Modulation of beta-band activity in the subgenual anterior cingulate cortex during emotional empathy in treatment-resistant depression. *Cereb. Cortex* 26, 2626–2638. doi: 10.1093/cercor/bhv100
- Nahum, M., Van Vleet, T. M., Sohal, V. S., Mirzabekov, J. J., Rao, V. R., Wallace, D. L., et al. (2017). Immediate mood scaler: tracking symptoms of depression and anxiety using a novel mobile mood scale. *JMIR Mhealth Uhealth* 5:e44. doi: 10.2196/mhealth.6544
- Panov, F., Levin, E., de Hemptinne, C., Swann, N. C., Qasim, S., Miocinovic, S., et al. (2017). Intraoperative electrocorticography for physiological research in movement disorders: principles and experience in 200 cases. *J. Neurosurg.* 126, 122–131. doi: 10.3171/2015.11.jns.151341
- Peron, J., Renaud, O., Haegelen, C., Tamarit, L., Milesi, V., Houvenaghel, J. F., et al. (2017). Vocal emotion decoding in the subthalamic nucleus: an intracranial ERP study in Parkinson's disease. *Brain Lang.* 168, 1–11. doi: 10.1016/j.bandl.2016.12.003
- Postuma, R. B., Berg, D., Stern, M., Poewe, W., Olanow, C. W., Oertel, W., et al. (2015). MDS clinical diagnostic criteria for Parkinson's disease. *Mov. Disord.* 30, 1591–1601. doi: 10.1002/mds.26424
- Rao, V., Sellers, K., Wallace, D., Lee, M., Bijanzadeh, M., Sani, O., et al. (2018). Direct electrical stimulation of lateral orbitofrontal cortex acutely improves mood in individuals with symptoms of depression. *Curr. Biol.* 28, 3893–3902.e4.
- Rektorova, I., and Anderkova, L. (2017). Noninvasive brain stimulation and implications for nonmotor symptoms in Parkinson's disease. *Int. Rev. Neurobiol.* 134, 1091–1110. doi: 10.1016/bs.irn.2017.05.009
- Rolls, E. T. (2016). A non-reward attractor theory of depression. *Neurosci. Biobehav. Rev.* 68, 47–58. doi: 10.1016/j.neubiorev.2016.05.007
- Sani, O. G., Yang, Y., Lee, M. B., Dawes, H. E., Chang, E. F., and Shanechi, M. M. (2018). Mood variations decoded from multi-site intracranial human brain activity. *Nat. Biotechnol.* 36, 954–961. doi: 10.1038/nbt.4200
- Scangos, K. W., Ahmad, H. S., Shafi, A., Sellers, K. K., Dawes, H. E., Krystal, A., et al. (2020). Pilot study of an intracranial electroencephalography biomarker of depressive symptoms in epilepsy. *J. Neuropsychiatry Clin. Neurosci.* 32, 185–190. doi: 10.1176/appi.neuropsych.19030081
- Schupbach, M., Gargiulo, M., Welter, M. L., Mallet, L., Behar, C., Houeto, J. L., et al. (2006). Neurosurgery in Parkinson disease: a distressed mind in a repaired body? *Neurology* 66, 1811–1816. doi: 10.1212/01.wnl.0000234880.51322.16

- Seppi, K., Ray Chaudhuri, K., Coelho, M., Fox, S. H., Katzenschlager, R., Perez Lloret, S., et al. (2019). Update on treatments for nonmotor symptoms of Parkinson's disease—an evidence-based medicine review. *Mov. Disord.* 34, 180–198. doi: 10.1002/mds.27602
- Stanslaski, S., Herron, J., Chouinard, T., Bourget, D., Isaacson, B., Kremen, V., et al. (2018). A chronically implantable neural coprocessor for investigating the treatment of neurological disorders. *IEEE Trans. Biomed. Circuits Syst.* 12, 1230–1245. doi: 10.1109/tbcas.2018.2880148
- Starr, P. A. (2002). Placement of deep brain stimulators into the subthalamic nucleus or Globus pallidus internus: technical approach. *Stereotact. Funct. Neurosurg.* 79, 118–145. doi: 10.1159/000070828
- Starr, P. A. (2018). Totally implantable bidirectional neural prostheses: a flexible platform for innovation in neuromodulation. *Front. Neurosci.* 12:619. doi: 10.3389/fnins.2018.00619
- Swann, N. C., de Hemptinne, C., Miocinovic, S., Qasim, S., Ostrem, J. L., Galifianakis, N. B., et al. (2018). Chronic multisite brain recordings from a totally implantable bidirectional neural interface: experience in 5 patients with Parkinson's disease. *J. Neurosurg.* 128, 605–616. doi: 10.3171/2016.11.jns161162
- Swann, N. C., de Hemptinne, C., Miocinovic, S., Qasim, S., Wang, S. S., Ziman, N., et al. (2016). Gamma oscillations in the hyperkinetic state detected with chronic human brain recordings in Parkinson's disease. *J. Neurosci.* 36, 6445–6458. doi: 10.1523/jneurosci.1128-16.2016
- Veerakumar, A., Tiruvadi, V., Howell, B., Waters, A. C., Crowell, A. L., Voytek, B., et al. (2019). Field potential 1/f activity in the subcallosal cingulate region as a candidate signal for monitoring deep brain stimulation for treatment-resistant depression. *J. Neurophysiol.* 122, 1023–1035. doi: 10.1152/jn.00875.2018
- Wang, H., Chen, H., Wu, J., Tao, L., Pang, Y., Gu, M., et al. (2018). Altered resting-state voxel-level whole-brain functional connectivity in depressed Parkinson's disease. *Parkinsonism Relat. Disord.* 50, 74–80. doi: 10.1016/j.parkreldis.2018.02.019
- Wang, M., Liao, H., Shen, Q., Cai, S., Zhang, H., Xiang, Y., et al. (2020). Changed resting-state brain signal in Parkinson's patients with mild depression. *Front. Neurol.* 11:28. doi: 10.3389/fneur.2020.00028
- Wang, X., Zhang, J., Yuan, Y., Li, T., Zhang, L., Ding, J., et al. (2017). Cerebral metabolic change in Parkinson's disease patients with anxiety: a FDG-PET study. *Neurosci. Lett.* 653, 202–207. doi: 10.1016/j.neulet.2017.05.062
- Xia, X., Fan, L., Cheng, C., Eickhoff, S. B., Chen, J., Li, H., et al. (2017). Multimodal connectivity-based parcellation reveals a shell-core dichotomy of the human nucleus accumbens. *Hum. Brain Mapp.* 38, 3878–3898. doi: 10.1002/hbm.23636

Conflict of Interest: PS receives research support from Medtronic Inc., (investigational implantable devices utilized here were provided at no charge). PS and JO receive funding for fellowship training from Medtronic Inc.

The remaining authors declare that the research was conducted in the absence of any commercial or financial relationships that could be construed as a potential conflict of interest.

Publisher's Note: All claims expressed in this article are solely those of the authors and do not necessarily represent those of their affiliated organizations, or those of the publisher, the editors and the reviewers. Any product that may be evaluated in this article, or claim that may be made by its manufacturer, is not guaranteed or endorsed by the publisher.

Copyright © 2021 de Hemptinne, Chen, Racine, Seritan, Miller, Yaroshinsky, Wang, Gilron, Little, Bledsoe, San Luciano, Katz, Chang, Dawes, Ostrem and Starr. This is an open-access article distributed under the terms of the Creative Commons Attribution License (CC BY). The use, distribution or reproduction in other forums is permitted, provided the original author(s) and the copyright owner(s) are credited and that the original publication in this journal is cited, in accordance with accepted academic practice. No use, distribution or reproduction is permitted which does not comply with these terms.



Differential Effects of Pathological Beta Burst Dynamics Between Parkinson's Disease Phenotypes Across Different Movements

Raumin S. Neuville^{1,2†}, Matthew N. Petrucci^{1†}, Kevin B. Wilkins¹, Ross W. Anderson¹, Shannon L. Hoffman¹, Jordan E. Parker^{1,3}, Anca Velisar^{1,4} and Helen M. Bronte-Stewart^{1,5*}

¹ Department of Neurology and Neurological Sciences, Stanford University School of Medicine, Stanford, CA, United States,

² School of Medicine, University of California, Irvine, Irvine, CA, United States, ³ Department of Psychology, University of California, Los Angeles, Los Angeles, CA, United States, ⁴ Smith-Kettlewell Eye Research Institute, San Francisco, CA, United States, ⁵ Department of Neurosurgery, Stanford University School of Medicine, Stanford, CA, United States

OPEN ACCESS

Edited by:

Coralie de Hemptinne,
University of Florida, United States

Reviewed by:

J. Luis Lujan,
Mayo Clinic College of Medicine
and Science, United States
Madeleine Lowery,
University College Dublin, Ireland

*Correspondence:

Helen M. Bronte-Stewart
hbs@stanford.edu

[†]These authors have contributed
equally to this work

Specialty section:

This article was submitted to
Neural Technology,
a section of the journal
Frontiers in Neuroscience

Received: 30 June 2021

Accepted: 19 October 2021

Published: 11 November 2021

Citation:

Neuville RS, Petrucci MN,
Wilkins KB, Anderson RW,
Hoffman SL, Parker JE, Velisar A and
Bronte-Stewart HM (2021) Differential
Effects of Pathological Beta Burst
Dynamics Between Parkinson's
Disease Phenotypes Across Different
Movements.
Front. Neurosci. 15:733203.
doi: 10.3389/fnins.2021.733203

Background: Resting state beta band (13–30 Hz) oscillations represent pathological neural activity in Parkinson's disease (PD). It is unknown how the peak frequency or dynamics of beta oscillations may change among fine, limb, and axial movements and different disease phenotypes. This will be critical for the development of personalized closed loop deep brain stimulation (DBS) algorithms during different activity states.

Methods: Subthalamic (STN) and local field potentials (LFPs) were recorded from a sensing neurostimulator (Activa[®] PC + S, Medtronic PLC.) in fourteen PD participants (six tremor-dominant and eight akinetic-rigid) off medication/off STN DBS during 30 s of repetitive alternating finger tapping, wrist-flexion extension, stepping in place, and free walking. Beta power peaks and beta burst dynamics were identified by custom algorithms and were compared among movement tasks and between tremor-dominant and akinetic-rigid groups.

Results: Beta power peaks were evident during fine, limb, and axial movements in 98% of movement trials; the peak frequencies were similar during each type of movement. Burst power and duration were significantly larger in the high beta band, but not in the low beta band, in the akinetic-rigid group compared to the tremor-dominant group.

Conclusion: The conservation of beta peak frequency during different activity states supports the feasibility of patient-specific closed loop DBS algorithms driven by the dynamics of the same beta band during different activities. Akinetic-rigid participants had greater power and longer burst durations in the high beta band than tremor-dominant participants during movement, which may relate to the difference in underlying pathophysiology between phenotypes.

Keywords: beta oscillations, Parkinson's disease (PD), local field potentials (LFP), subthalamic nucleus (STN), deep brain stimulation (DBS), beta bursts, akinetic rigid, tremor dominant

INTRODUCTION

Exaggerated resting state beta band (13–30 Hz) oscillations and synchrony are pathophysiological markers of hypokinetic aspects of Parkinson's disease (PD). When averaged over time, these oscillations appear as elevated portions of the local field potential (LFP) power spectral density (PSD) above the broadband 1/f spectrum (He, 2014; Shreve et al., 2017). Beta band power is attenuated on dopaminergic medication and during subthalamic (STN) deep brain stimulation (DBS); the degree of attenuation has been correlated to the degree of improvement in bradykinesia and rigidity, whereas averaged resting state beta band power is less robustly correlated with PD motor signs (Brown et al., 2001; Cassidy et al., 2002; Levy et al., 2002; Williams et al., 2002; Priori et al., 2004; Kühn et al., 2006, 2008, 2009; Weinberger et al., 2006; Ray et al., 2008; Bronte-Stewart et al., 2009; Eusebio et al., 2011; Whitmer et al., 2012; Quinn et al., 2015; Kehnemouyi et al., 2021).

Recently, it has been shown that physiological resting state beta oscillations are represented by short duration fluctuations in power (beta bursts) in the striatum and cortex of healthy non-human primates (Feingold et al., 2015). These authors suggested that the precise temporal dynamics of beta bursts may be more reliable markers of PD than averaging beta activity over periods of time. Burst dynamics in PD have been studied during rest (Tinkhauser et al., 2017; Anderson et al., 2020), but less is known about real time beta burst dynamics during movement and whether beta burst dynamics differ during fine motor or limb movements and/or during gait and freezing of gait (FOG) (Anidi et al., 2018; Lofredi et al., 2019; Kehnemouyi et al., 2021). The duration of beta bursts is a relevant neural control variable for closed loop DBS systems, which can precisely target (shorten) the duration of beta bursts, but it is not known how this variable may change among movements which may necessitate a different response from a closed-loop algorithm (Petrucchi et al., 2020a).

In addition to differences among tasks, it is unclear how beta burst dynamics may differ between sub bands of beta or between Parkinson's disease phenotypes. Previous studies that have evaluated phenotype differences primarily focused on high (20–35 Hz) and low (10–20 Hz) beta band power in the operating room or perioperative state (i.e., the week after implantation). Differences in high beta band power were demonstrated between tremor-dominant (TD) and akinetic-rigid (AR) phenotypes at rest, but not during movement in an elbow-flexion task in the operating room (Godinho et al., 2021). Furthermore, within band differences between rest and movement were observed for each phenotype (low beta for tremor-dominant and high beta for akinetic-rigid). Differences in resting state high beta power have also been reported in the immediate post-operative period between people with and without FOG, as assessed off medication in the pre-operative period (Toledo et al., 2014). To date, no study has compared burst durations within sub bands of beta, between disease phenotypes, and during different movements using a chronically implanted device. In this study, we investigated whether beta band peak frequencies were conserved or were different during fine, limb, and/or axial movements in people with PD, and whether there were differences in beta band and

sub band power and burst dynamics between the akinetic-rigid and tremor-dominant phenotypes.

MATERIALS AND METHODS

Human Participants

Fourteen participants (10 male) with clinically established PD underwent bilateral implantation of DBS leads (model 3389, Medtronic PLC., Minneapolis, MN, United States) in the sensorimotor region of the subthalamic nucleus (STN) using a standard functional frameless stereotactic technique and microelectrode recording (MER) (Brontë-Stewart et al., 2010; Quinn et al., 2015). Long-acting dopaminergic medication was withdrawn over 24 h (72 h for extended-release dopamine agonists) and short-acting medication was withdrawn for over 12 h before surgery and before each study visit. One participant took an extra short-acting carbidopa/levodopa tablet 5 h before the experiments and was included as their resting state LFP spectra were similar 6.25 and 8.5 h later, suggesting resolution of an attenuating effect of medication on beta power (Trager et al., 2016). The preoperative selection criteria and assessment of participants have been previously described (Taylor Tavares et al., 2005; Bronte-Stewart et al., 2009; de Solages et al., 2010). The dorsal and ventral borders of each STN were determined using MER, and the base of electrode 0 of the Medtronic 3389 lead was placed at the MER defined ventral border of the STN (Marceglia et al., 2006; de Solages et al., 2010, 2011). The DBS leads were located in the STN (**Figure 1A**). All participants signed a written consent and the study was approved by the Food and Drug Administration, Investigational Device Exemption and the Stanford School of Medicine Institutional Review Board. Each participant was classified as TD or AR phenotype based on previously described criteria (Quinn et al., 2015; Trager et al., 2016; Shreve et al., 2017) and the more and less affected sides were determined by unilateral Unified Parkinson's Disease Rating Scale (UPDRS) part III sub-scores.

Experimental Protocol

All experiments were performed within 2 months after DBS lead placement in the off medication/off DBS state. Recordings were collected in the Stanford Human Motor Control and Neuromodulation Laboratory. Experiments started with a resting state recording, during which each participant sat still for 30 s. Participants completed four different movement tasks (**Figure 2**): (1) quantitative digitography (QDG) on an engineered keyboard (Bronte-Stewart et al., 2000; Taylor Tavares et al., 2005; Trager et al., 2015) (2) instrumented repetitive wrist-flexion extension (WFE) (Koop et al., 2006, 2008; Louie et al., 2009), (3) stepping in place (SIP) on dual force plates (Nantel et al., 2011), and (4) free walking (FW). During the QDG task, participants were seated with their elbow flexed at approximately 90° and the wrist was supported by a pad alongside a customized engineered keyboard. Visual and auditory feedback was minimized, as the participants had their eyes closed and wore headphones that played white noise to limit auditory feedback from the key tapping. With the

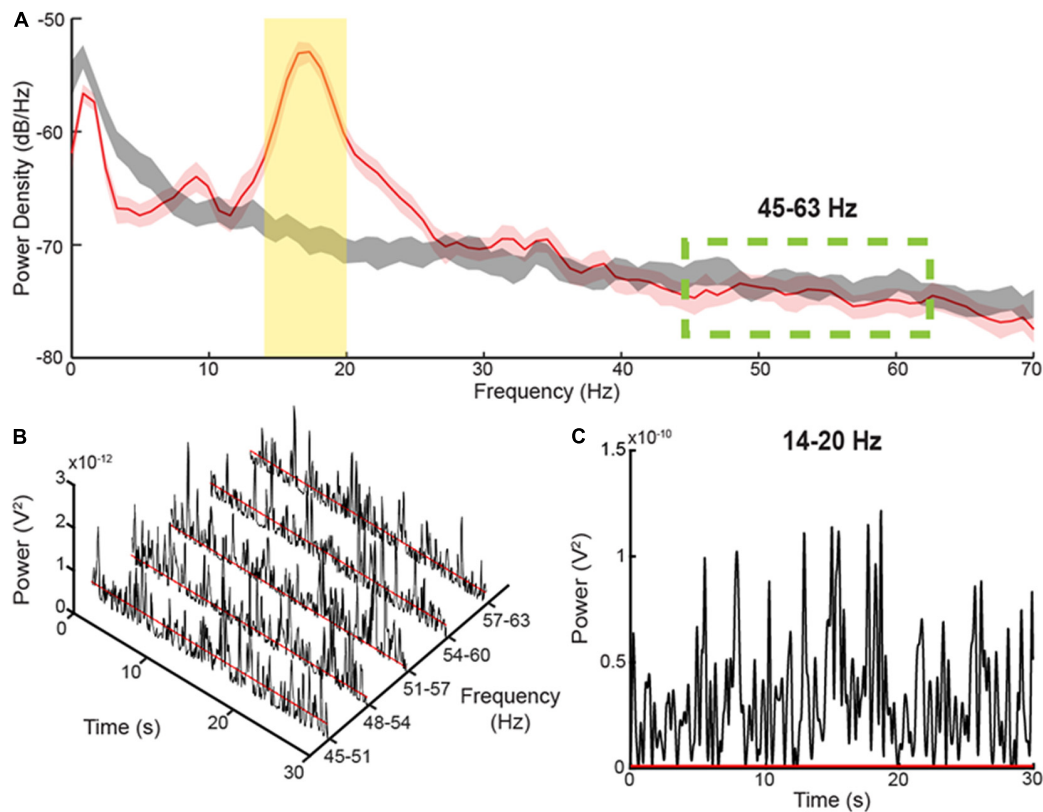


FIGURE 1 | Method for determining burst durations **(A)** PSD diagrams of 30 s during a Parkinsonian resting state (red) versus pink noise (gray), which can be considered simulated 1/f baseline activity in the brain. The yellow, shaded area represents the 6 Hz band centered on the peak of the PSD. The green-dashed lines display the area where there is no elevation of the resting state PSD above the pink noise simulated 1/f activity. **(B)** Consecutive, 6 Hz envelopes of the filtered and squared resting state LFP during the resting state within the non-pathological, high frequency range. The red lines signify the median power of the troughs from each envelope. **(C)** The envelope of a 6 Hz band within the elevated area of the PSD diagram. The threshold for determining burst durations, represented by the red line, was calculated by multiplying the average median trough powers within the high frequency range by a factor of four.

index and middle fingers placed on individual keys, participants were instructed to tap each key in an alternating pattern as fast and regularly as possible for 30 s. For the instrumented rWFE task, participants were seated with their elbow flexed at approximately 90° and the hand in the mid-pronated-supinated position before they were asked to flex and extend their wrists as fast as possible for 30 s. During the SIP task, participants were instructed to perform alternating stepping on dual force plates for 100 s. For the FW task, all participants walked for approximately 1 min within a lab space that consisted of circular and straight paths (two participants only walked within the straight path) with interspersed 90–180° turns. All movements were self-paced.

Data Acquisition and Analysis

Local field potentials (LFPs) from the STN were recorded from the electrode pair of the DBS lead that had the greatest resting state beta band peak power and the least artifact (electrode pairs 0–2 or 1–3 of the Medtronic 3389 lead; **Supplementary Table 1**). The pre-amplified LFP was high-pass filtered at 2.5 Hz and low-pass filtered at 100 Hz. LFP data was sampled at a rate of 422 Hz (10-bit resolution). The gains used for the

experiments were set at 2,000, and since these experiments were off stimulation, we set the center frequency of the Activa® PC + S neurostimulator to the lowest frequency setting of 2.5 Hz (Blumenfeld et al., 2017). The uncompressed LFP data were extracted via telemetry using the Activa® PC + S tablet programmer and then transferred to a computer for offline analysis in MATLAB (version 9.5, The MathWorks Inc., Natick, MA, United States). LFP data used for analysis was from the first 30 s of movement or from the maximum length of continuous movement without cueing. The power spectra were estimated using Welch's method, which used a 1-s Hanning window with 50% overlap (Welch, 1967). The peak frequency in the beta band was detected using a peak detection algorithm (de Solages et al., 2010). The peak detection algorithm runs through each point in the PSD under 40 Hz and labels a peak when both the central and lower frequency, adjacent bin are greater than the mean of the 3rd to 5th bins in the direction of lower frequency and the central and higher frequency, adjacent bin are greater than the mean of the 3rd to 6th bins in the direction of higher frequency. The chosen peak was then verified by visual inspection. If more than one peak was detected, the peak with the greatest power was chosen. In two movement episodes,



FIGURE 2 | The (A) quantitative digitography (QDG), (B) instrumented repetitive wrist-flexion extension (WFE), (C) stepping in place (SIP), and (D) forward walking (FW) tasks.

the algorithm failed to detect a peak, which was evident on visual inspection.

Local Field Potential Burst Dynamics Determination

The method for determining the burst dynamics was adopted from Anderson et al. (2020; **Figure 1**), which uses a baseline threshold calculated from a portion of the PD LFP spectrum that corresponds to the power and burst dynamics of a simulated, physiological 1/f spectrum. The baseline method captures a broader range of beta burst durations than high power burst detection methods. The LFP within the band of interest was first filtered using a 6-Hz bandwidth, zero-phase 8th order Butterworth filter, and then squared. An envelope was formed by interpolating between the consecutive peaks of the filtered, squared signal, **Figure 1C**. The threshold for characterizing individual bursts is calculated by averaging the median trough amplitudes from 5 consecutive overlapping 6 Hz bands in the 45–63 Hz PD gamma spectrum and multiplying the median trough power by a factor of four, **Figures 1B,C**. The 5 overlapping bands used to define the threshold were set to the following frequencies: 45–51 Hz, 48–54 Hz, 51–57 Hz, 54–60 Hz, and 57–63 Hz. In contrast to the elevated, beta frequency band of the PD spectrum, the higher frequency band (45–63 Hz) is not elevated above

the physiological LFP activity or 1/f signal, and contains burst dynamics resembled that of physiological neural activity (He, 2014; Anderson et al., 2020). Burst duration was calculated as the time between consecutive crossings of the envelope across the baseline threshold. The average power of each burst was also calculated (mean burst power) by averaging the power envelope between consecutive crossings across the baseline threshold.

Statistics

The primary outcome variables were peak frequency during movement, power, mean burst power, and mean burst duration. Power, mean burst power, and mean burst duration were calculated separately for low beta (14–20 Hz) and high beta (22–28 Hz) frequency bands. We used 6 Hz bands to allow for equal comparison of burst durations between bands (Anderson et al., 2020). Normalization of all power values was completed through division by the average power of the squared signal in the 45–63 Hz frequency band during the resting state; this high frequency band overlaps with the physiological 1/f curve and is clear of elevated, Parkinsonian beta activity (Anidi et al., 2018). Independent *t*-tests were used to compare age, disease duration, and pre-operative UPDRS scores between the TD and AR phenotypes. One-way repeated measures ANOVAs compared peak frequencies in the PSDs and variation in power and burst

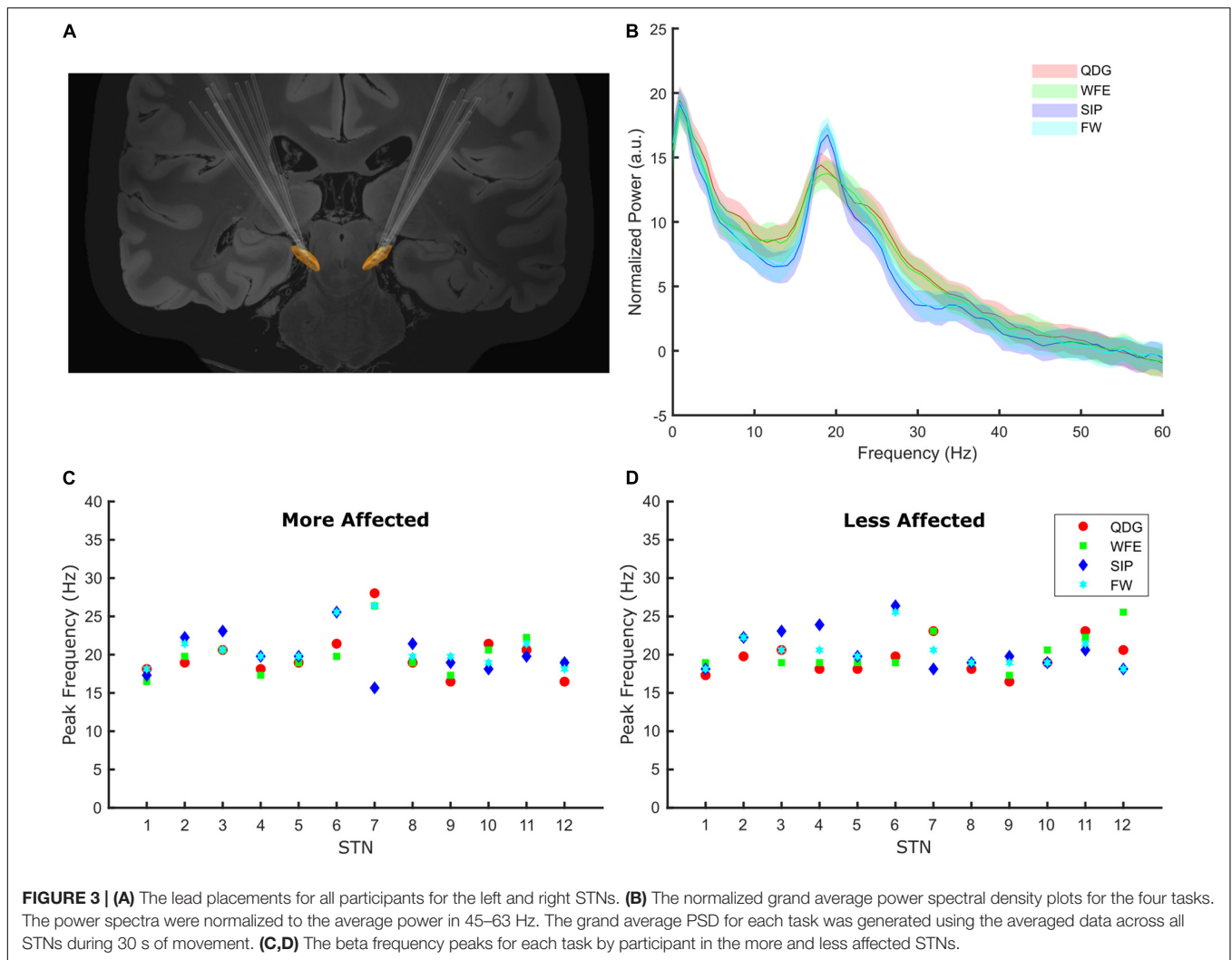


FIGURE 3 | (A) The lead placements for all participants for the left and right STNs. **(B)** The normalized grand average power spectral density plots for the four tasks. The power spectra were normalized to the average power in 45–63 Hz. The grand average PSD for each task was generated using the averaged data across all STNs during 30 s of movement. **(C,D)** The beta frequency peaks for each task by participant in the more and less affected STNs.

metrics among the different movement tasks in high and low beta with each STN treated individually and PD phenotype as a between-subjects factor. Analyses were corrected for multiple comparisons using Bonferroni correction. In the presence of a violation of Mauchly's test of sphericity, the Greenhouse–Geisser correction was applied. There was one trial per movement task for each participant.

RESULTS

Of the 14 participants, six were classified as TD and eight were classified as AR. The age of the group (mean \pm SD) was 57.0 ± 10.2 years (TD 60.4 ± 10.8 years; AR 54.4 ± 9.5 years), and the disease duration from symptom onset was 7.7 ± 3.7 years (TD 8.7 ± 4.3 years; AR 7.0 ± 3.2 years). UPDRS III scores (mean \pm SD) in the pre-operative off- and on-medication state were 39.2 ± 14.8 (TD 44.7 ± 12.3 ; AR 37.6 ± 16.1) and 23.2 ± 14.1 (TD 19.2 ± 7.7 ; AR 25.4 ± 16.5), respectively. There were no significant differences in age, disease duration, or pre-operative UPDRS scores between participants classified as TD

and AR ($p > 0.05$). The DBS leads were well placed within the STN, **Figure 3A**.

Peak Frequency Was Conserved Across Different Movements

Among the cohort of 24 STNs (8 TD and 16 AR) for whom peaks could be detected, peaks of elevated beta power were detected in 98% (94/96) of all movement episodes during the different tasks across all STNs, demonstrating that exaggerated beta band oscillations and synchrony were present during fine motor, limb and axial movements. In two TD participants, no peak was detected in either hemisphere, so they were excluded from this analysis. Beta peaks across the four movement tasks is depicted in the grand average PSDs in **Figure 3B**. The peak frequency did not differ across the movement tasks [$F(1.62,35.53) = 0.58$, $p = 0.53$, partial $\eta^2 = 0.026$] or between phenotypes [$F(1,22) = 0.39$, $p = 0.54$, partial $\eta^2 = 0.017$], and there was no interaction between task and phenotype [$F(1.62,35.53) = 2.93$, $p = 0.076$, partial $\eta^2 = 0.12$] on peak frequency. Peak frequency across

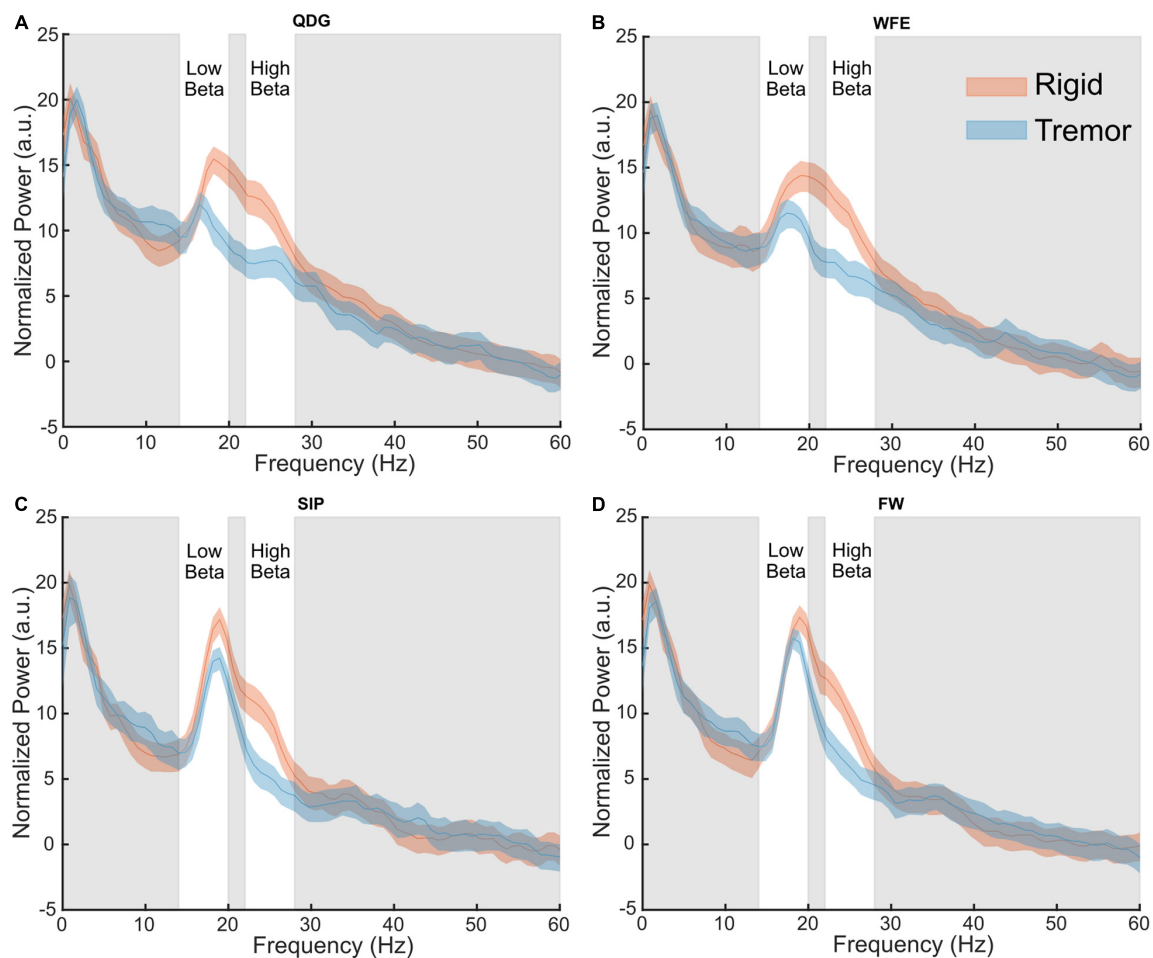


FIGURE 4 | Grand average normalized power spectral density plots for each phenotype in the (A) QDG, (B) WFE, (C) SIP, and (D) FW tasks. There were significant differences ($p < 0.05$) between phenotypes in the high beta band.

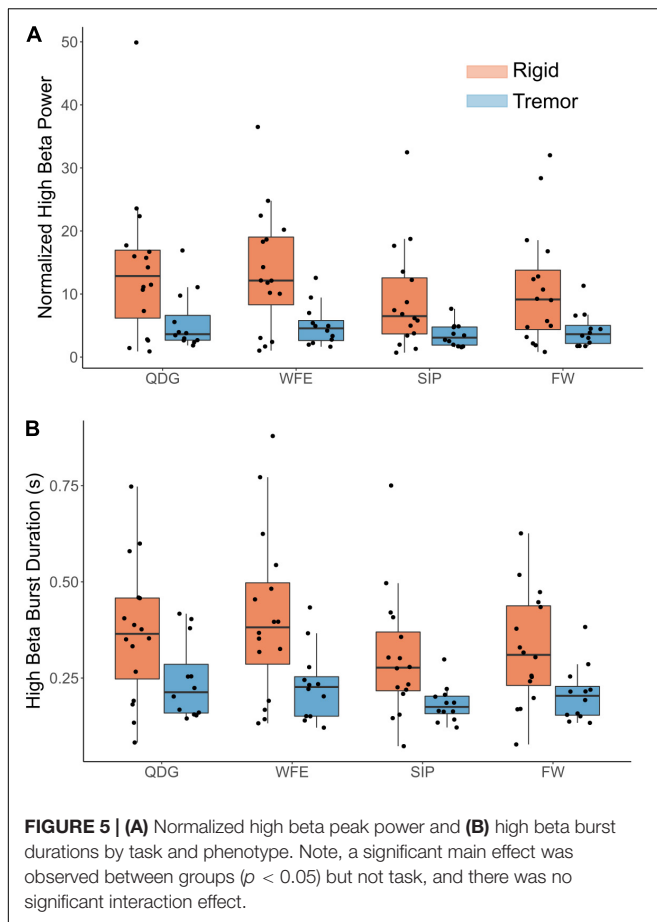
movements was similar in the more (Figure 3C) and less affected (Figure 3D) STNs.

Differences in Power Between Tremor-Dominant and Akinetic-Rigid Groups in the High Beta Band

Normalized power was analyzed across movement tasks and between the TD and AR groups in high and low beta for the full cohort of 28 STNs (Figure 4). In high beta, there was a significant effect of phenotype [$F(1,26) = 8.84$, $p = 0.006$, partial $\eta^2 = 0.25$], but not of task [$F(1.33,34.62) = 2.93$, $p = 0.085$, partial $\eta^2 = 0.10$] (Figure 4). Normalized high beta power was greater for the AR group compared to the TD group across all movements (Figure 5A). In low beta, there were no differences in normalized power between phenotypes [$F(1,26) = 1.27$, $p = 0.270$, partial $\eta^2 = 0.047$] or across tasks [$F(1.39,36.18) = 0.88$, $p = 0.39$, partial $\eta^2 = 0.033$]. There was also no interaction between task and PD phenotype for normalized power in either low beta [$F(1.39,36.18) = 0.088$, $p = 0.85$, partial $\eta^2 = 0.003$] or high beta [$F(1.33,34.62) = 0.59$, $p = 0.49$, partial $\eta^2 = 0.022$].

Differences Between the Akinetic-Rigid and Tremor-Dominant Groups and Across Tasks in the High Beta Band

Mean burst duration was analyzed across movement tasks and between the TD and AR groups in high and low beta for 27 STNs (11 TD and 16 AR) (Figure 5B). Burst data for one STN of a TD patient was excluded because burst duration in low beta during the FW task was identified as a statistical outlier (greater than 3 SD from the mean). In high beta, there was both a significant effect of phenotype [$F(1,25) = 8.92$, $p = 0.006$, partial $\eta^2 = 0.26$] and of task [$F(1.75,43.67) = 4.48$, $p = 0.021$, partial $\eta^2 = 0.15$]. High beta mean burst duration was greater for the AR phenotype compared to the TD phenotype across all movements (Figure 5B). Pairwise comparisons between movement tasks did not reveal significant differences between specific tasks with the Bonferroni correction ($p > 0.05$). In low beta, there were no differences in mean burst duration between phenotypes [$F(1,25) = 2.34$, $p = 0.14$, partial $\eta^2 = 0.085$] or across tasks [$F(1.36,33.87) = 0.18$, $p = 0.75$, partial $\eta^2 = 0.007$]. There was no interaction between task and PD phenotype for mean burst



duration for either low beta [$F(1.36,33.87) = 0.44$, $p = 0.57$, partial $\eta^2 = 0.017$] or high beta [$F(1.75,43.67) = 0.43$, $p = 0.63$, partial $\eta^2 = 0.017$].

Differences in Mean Burst Power Between Parkinson's Disease Phenotypes, but Not Across Tasks, in High Beta

Mean burst power was analyzed across movement tasks and between PD phenotypes in high and low beta (**Figure 5A**). In high beta, there was a significant effect of phenotype [$F(1,25) = 9.06$, $p = 0.006$, partial $\eta^2 = 0.266$], but no effect of task [$F(1.34,33.50) = 0.41$, $p = 0.59$, partial $\eta^2 = 0.016$]. High beta mean burst power was greater for the AR phenotype compared to the TD phenotype across all movements. In low beta, there were no differences in mean burst power between phenotypes [$F(1,25) = 3.12$, $p = 0.090$, partial $\eta^2 = 0.11$] or across tasks [$F(1.30,32.52) = 0.24$, $p = 0.69$, partial $\eta^2 = 0.010$]. There was no interaction between task and PD phenotype for mean burst power in both low [$F(1.30,32.52) = 0.084$, $p = 0.84$, partial $\eta^2 = 0.003$] and high [$F(1.34,33.50) = 0.040$, $p = 0.90$, partial $\eta^2 = 0.002$] beta.

DISCUSSION

The results of this study demonstrate that pathological beta oscillations and synchrony are present during ongoing movement and that the frequencies of the beta band peak were similar among fine, limb and axial movements. However, people with PD classified as akinetic-rigid showed greater high beta power and high beta burst duration and burst power across all tasks compared to those classified as tremor-dominant. This difference may point to an important difference in pathophysiology between phenotypes.

The Clinical Significance of the Conservation of Beta Band Peak Frequency Across Movements

Several studies have demonstrated that beta power decreased before, at the onset of, and during movement in human participants with PD and in non-human primates (Kühn et al., 2004; Litvak et al., 2011; Joundi et al., 2013; Johnson et al., 2016; Blumenfeld et al., 2017; Syrkin-Nikolau et al., 2017; Anidi et al., 2018; Fischer et al., 2018; Hell et al., 2018; Lofredi et al., 2019). This has led to a frequent generalization in the literature that beta power “goes away” during movement. The results of this study demonstrate that beta peaks were still evident during movement, and that the peak frequencies were conserved among fine motor and limb movements and during gait. This may alleviate concerns regarding the implementation of closed loop DBS in freely moving people. Up to now, closed loop DBS classifier algorithms have used estimates of resting state beta band power as the control variable (Little et al., 2013, 2016a,b; Rosa et al., 2015, 2017; Piña-Fuentes et al., 2017, 2019; Afzal et al., 2019; Velisar et al., 2019; Petrucci et al., 2020b). Such algorithms require knowledge of the peak frequency of the band of interest and until now it was not known whether the same beta band could be used to drive closed loop DBS when the person is working at their computer, eating, dressing, or when walking. Although others have seen that there was a slight shift in peak frequency between different motor states (Canessa et al., 2020), we observed no significant difference across four different tasks. The conservation of the choice of the band of interest (determined by the peak frequency) among fine, limb, and axial movements suggests that the same classifier algorithms will be appropriate across movement states. Additionally, even if small differences are observed in peak frequencies, most current methods for tracking beta band look across a bandwidth of $6 \pm \text{Hz}$ and therefore are robust against shifts in peak frequencies that still fall within these bandwidths (Afzal et al., 2019; Velisar et al., 2019; Petrucci et al., 2020a).

Differences in Pathophysiology Between Motor Phenotypes

Our results demonstrate that the AR group shows greater high beta power and burst metrics across tasks compared to the TD group. This is the first study to show neural oscillatory differences in the STN between PD phenotypes across different movement states. High beta oscillations in the STN have been posited to relate to STN-cortical connections in PD, whereas

low beta oscillations relate to intrinsic pathophysiology within the basal ganglia (Oswal et al., 2020). Specifically, coupling in high beta between the STN and supplementary motor area (SMA) correlates with fiber density between those two regions. Furthermore, improvement in rigidity with DBS has been shown to be related to connectivity to the SMA (Akram et al., 2017). The differences observed in our study between AR and TD may reflect differences in these STN-cortical interactions. This is further supported by the previous work demonstrating greater high beta power in freezers compared to non-freezers (Toledo et al., 2014) and tremor-dominant vs. akinetic-rigid (Godinho et al., 2021) at rest. Together, these results point to a pathological low beta oscillation that is consistent across phenotypes and then a potentially separate high beta oscillation that may be more specific to akinetic-rigid symptoms regardless of task. These differences could be utilized to improve patient-specific closed-loop algorithms due to recent advances in technology (SummitTM RC + S, Medtronic PLC.) that can track multiple bands simultaneously.

LIMITATIONS

Due to the limited number of investigative devices (Activa[®] PC + S, Medtronic PLC., Minneapolis, MN, United States) allocated to centers, the sample size was small but comparable to previous studies (Quinn et al., 2015; Blumenfeld et al., 2017; Syrkin-Nikolau et al., 2017; Anidi et al., 2018). Additionally, the tremor-dominant cohort displayed a mix of presence versus absence of tremor across the tasks and therefore it is difficult to say with certainty that the observed differences in high beta are a phenological difference between phenotypes or that the action of the tremor itself is specific to high beta. We did confirm in at least 2 participants that there was not an appreciable difference in high beta during the tremor and non-tremor periods when tremor arose in the middle of the trial (see **Supplementary Figures 1–8**). A larger cohort of tremor-dominant participants is needed to confirm these findings.

CONCLUSION

The results of this study demonstrated that exaggerated beta power was evident during fine motor, limb and axial movements and that the peaks of the frequency band of elevated power were similar during such different movements. Furthermore, there were significant differences in beta power and burst durations between the akinetic-rigid and tremor-dominant phenotypes in the high beta, but not low beta. These findings are critical for future closed loop DBS systems, which will require an input that is both indicative of the disease state as well as robust through the patient's activities of daily living.

DATA AVAILABILITY STATEMENT

The raw data supporting the conclusions of this article will be made available by the authors, without undue reservation.

ETHICS STATEMENT

The studies involving human participants were reviewed and approved by the Stanford School of Medicine Institutional Review Board. The patients/participants provided their written informed consent to participate in this study.

AUTHOR CONTRIBUTIONS

RN: conceptualization, methodology, software, validation, formal analysis, investigation, data curation, writing – original draft and review and editing, visualization, supervision, and project administration. MP: conceptualization, methodology, validation, formal analysis, writing – review and editing, and supervision. KW: formal analysis, writing – review and editing, and visualization. RA: methodology, software, validation, formal analysis, investigation, writing – original draft and review and editing, visualization, and supervision. SH: formal analysis, writing – review and editing, and visualization. JP: methodology and validation. AV: software and investigation. HB-S: conceptualization, methodology, writing – original draft and review and editing, supervision, and funding acquisition. All authors contributed to the article and approved the submitted version.

FUNDING

This work was supported by the NINDS Grant 5 R21 NS096398-02 and UH3 NS107709, Parkinson's Foundation PF-FBS-1899 (to RA), Parkinson's Foundation PF-FBS-2024 (to KW), The Michael J. Fox Foundation (9605), Robert and Ruth Halperin Foundation, the Sanchez Family Foundation, John A. Blume Foundation, and Helen M. Cahill Award for Research in Parkinson's Disease and Medtronic PLC., provided devices but no financial support.

ACKNOWLEDGMENTS

We would like to thank Johanna O'Day, Muhammad Furqan Afzal, Thomas Prieto, and the rest of the members of the Human Motor Control and Neuromodulation Laboratory, and most importantly, the participants who dedicated their time to this study.

SUPPLEMENTARY MATERIAL

The Supplementary Material for this article can be found online at: <https://www.frontiersin.org/articles/10.3389/fnins.2021.733203/full#supplementary-material>

REFERENCES

- Afzal, M. F., Velisar, A., Anidi, C., Neuville, R., Prabhakar, V., and Bronte-Stewart, H. (2019). Proceedings #61: subthalamic neural closed-loop deep brain stimulation for bradykinesia in Parkinson's disease. *Brain Stimul.* 12, e152–4. doi: 10.1016/j.brs.2019.03.019
- Akram, H., Sotiropoulos, S. N., Jbabdi, S., Georgiev, D., Mählke, P., Hyam, J., et al. (2017). Subthalamic deep brain stimulation sweet spots and hyperdirect cortical connectivity in Parkinson's disease. *Neuroimage* 158, 332–345. doi: 10.1016/j.neuroimage.2017.07.012
- Anderson, R., Kehnemouy, Y., Neuville, R., Wilkins, K., Anidi, C., Petrucci, M., et al. (2020). A novel method for calculating beta band burst durations in Parkinson's disease using a physiological baseline. *J. Neurosci. Methods* 343:108811. doi: 10.1016/j.jneumeth.2020.108811
- Anidi, C., O'Day, J. J., Anderson, R. W., Afzal, M. F., Syrkin-Nikolau, J., Velisar, A., et al. (2018). Neuromodulation targets pathological not physiological beta bursts during gait in Parkinson's disease. *Neurobiol. Dis.* 120, 107–117. doi: 10.1016/j.nbd.2018.09.004
- Blumenfeld, Z., Koop, M. M., Prieto, T. E., Shreve, L. A., Velisar, A., Quinn, E. J., et al. (2017). Sixty-hertz stimulation improves bradykinesia and amplifies subthalamic low-frequency oscillations. *Mov. Disord.* 32, 80–88. doi: 10.1002/mds.26837
- Bronte-Stewart, H., Barberini, C., Koop, M. M., Hill, B. C., Henderson, J. M., and Wingeier, B. (2009). The STN beta-band profile in Parkinson's disease is stationary and shows prolonged attenuation after deep brain stimulation. *Exp. Neurol.* 215, 20–28. doi: 10.1016/j.expneurol.2008.09.008
- Brontë-Stewart, H., Louie, S., Batya, S., and Henderson, J. M. (2010). Clinical motor outcome of bilateral subthalamic nucleus deep-brain stimulation for Parkinson's disease using image-guided frameless stereotaxy. *Neurosurgery* 67, 1088–1093. doi: 10.1227/NEU.0b013e3181ecc887
- Bronte-Stewart, H. M., Ding, L., Alexander, C., Zhou, Y., and Moore, G. P. (2000). Quantitative digitography (QDG): a sensitive measure of digital motor control in idiopathic Parkinson's disease. *Mov. Disord.* 15, 36–47. doi: 10.1002/1531-8257(200001)15:1<36::aid-mds1008>3.0.co;2-m
- Brown, P., Marsden, J., Defebvre, L., Cassim, F., Mazzone, P., Oliviero, A., et al. (2001). Intermuscular coherence in Parkinson's disease: relationship to bradykinesia. *NeuroReport* 12, 2577–2581. doi: 10.1097/00001756-200108080-00057
- Canessa, A., Palmisano, C., Isaias, I. U., and Mazzoni, A. (2020). Gait-related frequency modulation of beta oscillatory activity in the subthalamic nucleus of parkinsonian patients. *Brain Stimul.* 13, 1743–1752. doi: 10.1016/j.brs.2020.09.006
- Cassidy, M., Mazzone, P., Oliviero, A., Insola, A., Tonalì, P., Lazzaro, V. D., et al. (2002). Movement-related changes in synchronization in the human basal ganglia. *Brain* 125, 1235–1246. doi: 10.1093/brain/awf135
- de Solages, C., Hill, B. C., Koop, M. M., Henderson, J. M., and Bronte-Stewart, H. (2010). Bilateral symmetry and coherence of subthalamic nuclei beta band activity in Parkinson's disease. *Exp. Neurol.* 221, 260–266. doi: 10.1016/j.expneurol.2009.11.012
- de Solages, C., Hill, B. C., Yu, H., Henderson, J. M., and Bronte-Stewart, H. (2011). Maximal subthalamic beta hypersynchrony of the local field potential in Parkinson's disease is located in the central region of the nucleus. *J. Neurol. Neurosurg. Psychiatry* 82, 1387–1389. doi: 10.1136/jnnp.2010.223107
- Eusebio, A., Thevathasan, W., Gaynor, L. D., Pogossyan, A., Bye, E., Foltynie, T., et al. (2011). Deep brain stimulation can suppress pathological synchronisation in parkinsonian patients. *J. Neurol. Neurosurg. Psychiatry* 82, 569–573. doi: 10.1136/jnnp.2010.217489
- Feingold, J., Gibson, D. J., DePasquale, B., and Graybiel, A. M. (2015). Bursts of beta oscillation differentiate postperformance activity in the striatum and motor cortex of monkeys performing movement tasks. *Proc. Natl. Acad. Sci. U. S. A.* 112, 13687–13692. doi: 10.1073/pnas.1517629112
- Fischer, P., Chen, C. C., Chang, Y.-J., Yeh, C.-H., Pogossyan, A., Herz, D. M., et al. (2018). Alternating modulation of subthalamic nucleus beta oscillations during stepping. *J. Neurosci.* 38, 5111–5121. doi: 10.1523/JNEUROSCI.3596-17.2018
- Godinho, F., Fim Neto, A., Bianqueti, B. L., de Luccas, J. B., Varjão, E., Terzian Filho, P. R., et al. (2021). Spectral characteristics of subthalamic nucleus local field potentials in Parkinson's disease: phenotype and movement matter. *Eur. J. Neurosci.* 53, 2804–2818. doi: 10.1111/ejn.15103
- He, B. J. (2014). Scale-free brain activity: past, present, and future. *Trends Cogn. Sci.* 18, 480–487. doi: 10.1016/j.tics.2014.04.003
- Hell, F., Plate, A., Mehrkens, J. H., and Bötzel, K. (2018). Subthalamic oscillatory activity and connectivity during gait in Parkinson's disease. *Neuroimage Clin.* 19, 396–405. doi: 10.1016/j.nicl.2018.05.001
- Johnson, L. A., Nebeck, S. D., Muralidharan, A., Johnson, M. D., Baker, K. B., and Vitek, J. L. (2016). Closed-loop deep brain stimulation effects on Parkinsonian motor symptoms in a non-human primate - is beta enough? *Brain Stimul.* 9, 892–896. doi: 10.1016/j.brs.2016.06.051
- Joundi, R. A., Brittain, J.-S., Green, A. L., Aziz, T. Z., Brown, P., and Jenkinson, N. (2013). Persistent suppression of subthalamic beta-band activity during rhythmic finger tapping in Parkinson's disease. *Clin. Neurophysiol.* 124, 565–573. doi: 10.1016/j.clinph.2012.07.029
- Kehnemouy, Y. M., Wilkins, K. B., Anidi, C. M., Anderson, R. W., Afzal, M. F., and Bronte-Stewart, H. M. (2021). Modulation of beta bursts in subthalamic sensorimotor circuits predicts improvement in bradykinesia. *Brain* 144, 473–486. doi: 10.1093/brain/awaa394
- Koop, M. M., Andrzejewski, A., Hill, B. C., Heit, G., and Bronte-Stewart, H. M. (2006). Improvement in a quantitative measure of bradykinesia after microelectrode recording in patients with Parkinson's disease during deep brain stimulation surgery. *Mov. Disord.* 21, 673–678. doi: 10.1002/mds.20796
- Koop, M. M., Shvitz, N., and Brontë-Stewart, H. (2008). Quantitative measures of fine motor, limb, and postural bradykinesia in very early stage, untreated Parkinson's disease. *Mov. Disord.* 23, 1262–1268. doi: 10.1002/mds.22077
- Kühn, A. A., Kempf, F., Brücke, C., Doyle, L. G., Martinez-Torres, I., Pogossyan, A., et al. (2008). High-Frequency Stimulation of the Subthalamic Nucleus Suppresses Oscillatory β Activity in Patients with Parkinson's Disease in Parallel with Improvement in Motor Performance. *J. Neurosci.* 28, 6165–6173. doi: 10.1523/JNEUROSCI.0282-08.2008
- Kühn, A. A., Kupsch, A., Schneider, G.-H., and Brown, P. (2006). Reduction in subthalamic 8–35 Hz oscillatory activity correlates with clinical improvement in Parkinson's disease. *Eur. J. Neurosci.* 23, 1956–1960. doi: 10.1111/j.1460-9568.2006.04717.x
- Kühn, A. A., Tsui, A., Aziz, T., Ray, N., Brücke, C., Kupsch, A., et al. (2009). Pathological synchronisation in the subthalamic nucleus of patients with Parkinson's disease relates to both bradykinesia and rigidity. *Exp. Neurol.* 215, 380–387. doi: 10.1016/j.expneurol.2008.11.008
- Kühn, A. A., Williams, D., Kupsch, A., Limousin, P., Hariz, M., Schneider, G.-H., et al. (2004). Event-related beta desynchronization in human subthalamic nucleus correlates with motor performance. *Brain* 127, 735–746. doi: 10.1093/brain/awh106
- Levy, R., Ashby, P., Hutchison, W. D., Lang, A. E., Lozano, A. M., and Dostrovsky, J. O. (2002). Dependence of subthalamic nucleus oscillations on movement and dopamine in Parkinson's disease. *Brain* 125, 1196–1209. doi: 10.1093/brain/awf128
- Little, S., Beudel, M., Zrinzo, L., Foltynie, T., Limousin, P., Hariz, M., et al. (2016a). Bilateral adaptive deep brain stimulation is effective in Parkinson's disease. *J. Neurol. Neurosurg. Psychiatry* 87, 717–721. doi: 10.1136/jnnp-2015-310972
- Little, S., Tripoliti, E., Beudel, M., Pogossyan, A., Cagnan, H., Herz, D., et al. (2016b). Adaptive deep brain stimulation for Parkinson's disease demonstrates reduced speech side effects compared to conventional stimulation in the acute setting. *J. Neurol. Neurosurg. Psychiatry* 87, 1388–1389. doi: 10.1136/jnnp-2016-313518
- Little, S., Pogossyan, A., Neal, S., Zavala, B., Zrinzo, L., Hariz, M., et al. (2013). Adaptive deep brain stimulation in advanced Parkinson disease. *Ann. Neurol.* 74, 449–457. doi: 10.1002/ana.23951
- Litvak, V., Jha, A., Eusebio, A., Oostenveld, R., Foltynie, T., Limousin, P., et al. (2011). Resting oscillatory cortico-subthalamic connectivity in patients with Parkinson's disease. *Brain* 134, 359–374. doi: 10.1093/brain/awq332
- Lofredi, R., Tan, H., Neumann, W.-J., Yeh, C.-H., Schneider, G.-H., Kühn, A. A., et al. (2019). Beta bursts during continuous movements accompany the velocity decrement in Parkinson's disease patients. *Neurobiol. Dis.* 127, 462–471. doi: 10.1016/j.nbd.2019.03.013
- Louie, S., Koop, M. M., Frenklach, A., and Bronte-Stewart, H. (2009). Quantitative lateralized measures of bradykinesia at different stages of Parkinson's disease: the role of the less affected side. *Mov. Disord.* 24, 1991–1997. doi: 10.1002/mds.22741

- Marceglia, S., Foffani, G., Bianchi, A. M., Baselli, G., Tamma, F., Egidi, M., et al. (2006). Dopamine-dependent non-linear correlation between subthalamic rhythms in Parkinson's disease. *J. Physiol. (Lond.)* 571, 579–591. doi: 10.1113/jphysiol.2005.100271
- Nantel, J., de Solages, C., and Bronte-Stewart, H. (2011). Repetitive stepping in place identifies and measures freezing episodes in subjects with Parkinson's disease. *Gait Posture* 34, 329–333. doi: 10.1016/j.gaitpost.2011.05.020
- Oswal, A., Yeh, C.-H., Neumann, W.-J., Gratwicke, J., Akram, H., Horn, A., et al. (2020). Neural signatures of pathological hyperdirect pathway activity in Parkinson's disease. *bioRxiv* [Preprint]. doi: 10.1101/2020.06.11.146886
- Petrucchi, M. N., Anderson, R. W., O'Day, J. J., Kehnemouyi, Y. M., Herron, J. A., and Bronte-Stewart, H. M. (2020a). A Closed-loop Deep Brain Stimulation Approach for Mitigating Burst Durations in People with Parkinson's Disease. *Annu. Int. Conf. IEEE Eng. Med. Biol. Soc.* 2020, 3617–3620. doi: 10.1109/EMBC44109.2020.9176196
- Petrucchi, M. N., Neuville, R. S., Afzal, M. F., Velisar, A., Anidi, C. M., Anderson, R. W., et al. (2020b). Neural closed-loop deep brain stimulation for freezing of gait. *Brain Stimul.* 13, 1320–1322. doi: 10.1016/j.brs.2020.06.018
- Piña-Fuentes, D., Beudel, M., Little, S., Brown, P., Oterdoom, D. L. M., and van Dijk, J. M. C. (2019). Adaptive deep brain stimulation as advanced Parkinson's disease treatment (ADAPT study): protocol for a pseudo-randomised clinical study. *BMJ Open* 9:e029652. doi: 10.1136/bmjopen-2019-029652
- Piña-Fuentes, D., Little, S., Oterdoom, M., Neal, S., Pogossyan, A., Tijssen, M. A. J., et al. (2017). Adaptive DBS in a Parkinson's patient with chronically implanted DBS: a proof of principle. *Mov. Disord.* 32, 1253–1254. doi: 10.1002/mds.26959
- Priori, A., Foffani, G., Pesenti, A., Tamma, F., Bianchi, A. M., Pellegrini, M., et al. (2004). Rhythm-specific pharmacological modulation of subthalamic activity in Parkinson's disease. *Exp. Neurol.* 189, 369–379. doi: 10.1016/j.expneurol.2004.06.001
- Quinn, E. J., Blumenfeld, Z., Velisar, A., Koop, M. M., Shreve, L. A., Trager, M. H., et al. (2015). Beta oscillations in freely moving Parkinson's subjects are attenuated during deep brain stimulation. *Mov. Disord.* 30, 1750–1758. doi: 10.1002/mds.26376
- Ray, N. J., Jenkinson, N., Wang, S., Holland, P., Brittain, J. S., Joint, C., et al. (2008). Local field potential beta activity in the subthalamic nucleus of patients with Parkinson's disease is associated with improvements in bradykinesia after dopamine and deep brain stimulation. *Exp. Neurol.* 213, 108–113. doi: 10.1016/j.expneurol.2008.05.008
- Rosa, M., Arlotti, M., Ardolino, G., Cogiamanian, F., Marceglia, S., Fonzo, A. D., et al. (2015). Adaptive deep brain stimulation in a freely moving parkinsonian patient. *Mov. Disord.* 30, 1003–1005. doi: 10.1002/mds.26241
- Rosa, M., Arlotti, M., Marceglia, S., Cogiamanian, F., Ardolino, G., Fonzo, A. D., et al. (2017). Adaptive deep brain stimulation controls levodopa-induced side effects in Parkinsonian patients. *Mov. Disord.* 32, 628–629. doi: 10.1002/mds.26953
- Shreve, L. A., Velisar, A., Malekmohammadi, M., Koop, M. M., Trager, M., Quinn, E. J., et al. (2017). Subthalamic oscillations and phase amplitude coupling are greater in the more affected hemisphere in Parkinson's disease. *Clin. Neurophysiol.* 128, 128–137. doi: 10.1016/j.clinph.2016.10.095
- Syrkin-Nikolau, J., Koop, M. M., Prieto, T., Anidi, C., Afzal, M. F., Velisar, A., et al. (2017). Subthalamic neural entropy is a feature of freezing of gait in freely moving people with Parkinson's disease. *Neurobiol. Dis.* 108, 288–297. doi: 10.1016/j.nbd.2017.09.002
- Taylor Tavares, A. L., Jefferis, G. S. X. E., Koop, M., Hill, B. C., Hastie, T., Heit, G., et al. (2005). Quantitative measurements of alternating finger tapping in Parkinson's disease correlate with UPDRS motor disability and reveal the improvement in fine motor control from medication and deep brain stimulation. *Mov. Disord.* 20, 1286–1298. doi: 10.1002/mds.20556
- Tinkhauser, G., Pogossyan, A., Little, S., Beudel, M., Herz, D. M., Tan, H., et al. (2017). The modulatory effect of adaptive deep brain stimulation on beta bursts in Parkinson's disease. *Brain* 140, 1053–1067. doi: 10.1093/brain/awx010
- Toledo, J. B., López-Azcárate, J., García-García, D., Guridi, J., Valencia, M., Artieda, J., et al. (2014). High beta activity in the subthalamic nucleus and freezing of gait in Parkinson's disease. *Neurobiol. Dis.* 64, 60–65. doi: 10.1016/j.nbd.2013.12.005
- Trager, M. H., Koop, M. M., Velisar, A., Blumenfeld, Z., Nikolau, J. S., Quinn, E. J., et al. (2016). Subthalamic beta oscillations are attenuated after withdrawal of chronic high frequency neurostimulation in Parkinson's disease. *Neurobiol. Dis.* 96, 22–30. doi: 10.1016/j.nbd.2016.08.003
- Trager, M. H., Velisar, A., Koop, M. M., Shreve, L., Quinn, E., and Bronte-Stewart, H. (2015). Arrhythmokinesis is evident during unimanual not bimanual finger tapping in Parkinson's disease. *J. Clin. Mov. Disord.* 2:8. doi: 10.1186/s40734-015-0019-2
- Velisar, A., Syrkin-Nikolau, J., Blumenfeld, Z., Trager, M. H., Afzal, M. F., Prabhakar, V., et al. (2019). Dual threshold neural closed loop deep brain stimulation in Parkinson disease patients. *Brain Stimul.* 12, 868–876. doi: 10.1016/j.brs.2019.02.020
- Weinberger, M., Mahant, N., Hutchison, W. D., Lozano, A. M., Moro, E., Hodaie, M., et al. (2006). Beta oscillatory activity in the subthalamic nucleus and its relation to dopaminergic response in Parkinson's disease. *J. Neurophysiol.* 96, 3248–3256. doi: 10.1152/jn.00697.2006
- Welch, P. (1967). The use of fast Fourier transform for the estimation of power spectra: a method based on time averaging over short, modified periodograms. *IEEE Trans. Audio Electroacoustics* 15, 70–73. doi: 10.1109/TAU.1967.1161901
- Whitmer, D., de Solages, C., Hill, B., Yu, H., Henderson, J. M., and Bronte-Stewart, H. (2012). High frequency deep brain stimulation attenuates subthalamic and cortical rhythms in Parkinson's disease. *Front. Hum. Neurosci.* 6:155. doi: 10.3389/fnhum.2012.00155
- Williams, D., Tijssen, M., van Bruggen, G., Bosch, A., Insola, A., Lazzaro, V. D., et al. (2002). Dopamine-dependent changes in the functional connectivity between basal ganglia and cerebral cortex in humans. *Brain* 125, 1558–1569. doi: 10.1093/brain/awf156

Conflict of Interest: HB-S is a member of the Medtronic PLC., Clinical Advisory Board.

The remaining authors declare that the research was conducted in the absence of any commercial or financial relationships that could be construed as a potential conflict of interest.

Publisher's Note: All claims expressed in this article are solely those of the authors and do not necessarily represent those of their affiliated organizations, or those of the publisher, the editors and the reviewers. Any product that may be evaluated in this article, or claim that may be made by its manufacturer, is not guaranteed or endorsed by the publisher.

Copyright © 2021 Neuville, Petrucci, Wilkins, Anderson, Hoffman, Parker, Velisar and Bronte-Stewart. This is an open-access article distributed under the terms of the Creative Commons Attribution License (CC BY). The use, distribution or reproduction in other forums is permitted, provided the original author(s) and the copyright owner(s) are credited and that the original publication in this journal is cited, in accordance with accepted academic practice. No use, distribution or reproduction is permitted which does not comply with these terms.



Controlling Clinical States Governed by Different Temporal Dynamics With Closed-Loop Deep Brain Stimulation: A Principled Framework

Gerd Tinkhauser^{1*†} and Eduardo Martin Moraud^{2,3†}

¹ Department of Neurology, Bern University Hospital and University of Bern, Bern, Switzerland, ² Department of Clinical Neurosciences, Lausanne University Hospital, Lausanne, Switzerland, ³ Defitech Center for Interventional Neurotherapies (.NeuroRestore), Ecole Polytechnique Fédérale de Lausanne and Lausanne University Hospital, Lausanne, Switzerland

OPEN ACCESS

Edited by:

Doris D. Wang,
University of California,
San Francisco, United States

Reviewed by:

Phillip Starr,
University of California,
San Francisco, United States
Matthew N. Petrucci,
Stanford University, United States

*Correspondence:

Gerd Tinkhauser
gerd.tinkhauser@insel.ch

[†] These authors have contributed
equally to this work

Specialty section:

This article was submitted to
Neural Technology,
a section of the journal
Frontiers in Neuroscience

Received: 30 June 2021

Accepted: 18 October 2021

Published: 11 November 2021

Citation:

Tinkhauser G and Moraud EM
(2021) Controlling Clinical States
Governed by Different Temporal
Dynamics With Closed-Loop Deep
Brain Stimulation: A Principled
Framework.
Front. Neurosci. 15:734186.
doi: 10.3389/fnins.2021.734186

Closed-loop strategies for deep brain stimulation (DBS) are paving the way for improving the efficacy of existing neuromodulation therapies across neurological disorders. Unlike continuous DBS, closed-loop DBS approaches (cl-DBS) optimize the delivery of stimulation in the temporal domain. However, clinical and neurophysiological manifestations exhibit highly diverse temporal properties and evolve over multiple time-constants. Moreover, throughout the day, patients are engaged in different activities such as walking, talking, or sleeping that may require specific therapeutic adjustments. This broad range of temporal properties, along with inter-dependencies affecting parallel manifestations, need to be integrated in the development of therapies to achieve a sustained, optimized control of multiple symptoms over time. This requires an extended view on future cl-DBS design. Here we propose a conceptual framework to guide the development of multi-objective therapies embedding parallel control loops. Its modular organization allows to optimize the personalization of cl-DBS therapies to heterogeneous patient profiles. We provide an overview of clinical states and symptoms, as well as putative electrophysiological biomarkers that may be integrated within this structure. This integrative framework may guide future developments and become an integral part of next-generation precision medicine instruments.

Keywords: closed-loop DBS, local field potentials (LFP), basal ganglia, Parkinson's disease, multi-objective control

CLOSED-LOOP DEEP BRAIN STIMULATION: TOWARD MULTI-OBJECTIVE CONTROL ALGORITHMS IN SPACE AND TIME

Deep brain stimulation is an established treatment option for patients with movement disorders [Parkinson's disease (PD), Essential Tremor, and Dystonia], as demonstrated in randomized controlled trials (Krack et al., 2019). Current therapies are based on a constant delivery of stimulation with fixed parameters. Amplitude and contact selection are manually adjusted by clinicians, and then usually remain unchanged until follow-up clinical visits. Albeit widely spread and highly efficacious to alleviate predominant symptomatic traits, the static nature of this “one

Abbreviations: DBS, deep brain stimulation; PD, Parkinson's disease; LFP, local field potentials; STN, subthalamic nucleus.

fits all the time” approach cannot account for all symptom fluctuations or manifestations that are episodic in nature (Lozano et al., 2019).

Closed-loop strategies offer the possibility to optimize DBS by automatically adjusting the timing and parameters of stimulation in real time based on biomarkers (Bronte-Stewart et al., 2020). The adaptability of these approaches helps ensure a maximal clinical benefit, sustained over time, while minimizing side-effects. In this loop, sensing (feedback) and stimulation (actuation) components need to be tuned to match the dynamical properties of the targeted manifestation. A broad variety of stimulation strategies and biomarkers have flourished over the past years to address the limitations of constant stimulation, for instance by specifically controlling ON-OFF fluctuations, reducing side-effects, and additionally to give answer to symptoms that are not optimally addressed by standard protocols, such as freezing of gait.

A putative limitation of current closed-loop strategies is their restricted scope, in which biomarkers, controller design and parameter choices are optimized to a unique symptom or neural manifestation in isolation. However, clinical states are dynamic, multi-faceted, and inter-connected. Some operate at the millisecond range while others evolve over many hours. They can occur independently or influence each other. Consequently, even though aforementioned closed-loop approaches showed improved efficacy over standard continuous DBS in well-controlled research conditions, the question of whether a satisfactory 24 h therapeutic coverage of multiple symptoms may be achieved with such strategies is far from clear.

A global framework is critically missing to guide the integration of all these developments into a clinically relevant therapeutic portfolio that exploits recent advances in implantable neurotechnologies (Cagnan et al., 2019; Gunduz et al., 2019; Parastarfeizabadi et al., 2020). This integrative framework needs to be modular, flexible, and easily adaptable by clinicians. It also needs to offer the possibility to address multiple symptoms while robustly dealing with dependencies that exist between clinical states, or interferences between parallel therapies.

We suggest that the structure of clinical and neurophysiological manifestations, segregated in time and space over multiple layers (see section below), may be mirrored by control strategies to steer the design of modular therapies embedding parallel control loops. This principled framework may guide future developments and become an integral part of next generation closed loop DBS systems.

MYRIAD TEMPORAL SCALES OF CLINICAL AND NEUROPHYSIOLOGICAL MANIFESTATIONS

Clinical Manifestations

Motor and non-motor symptoms exhibit highly diverse temporal properties. They emerge at different timepoints, progress at various speeds over the course of the disease, and diurnally fluctuate in intensity with according to their own

variable time-constants. These distinct temporal behaviors are further intertwined since clinical manifestations can occur simultaneously or influence each other, adding a layer of complexity in the management of symptoms. For instance, tremor oscillations (~5 Hz, 5 oscillations per second) stand in contrast to slow-changing states such as a dopaminergic wearing off episodes, which affect the condition of patients in the range of hours. Yet both states can be temporally related, as the likelihood of tremor episodes in PD may increase during wearing OFF dopaminergic states. Moreover, throughout the day, patients are engaged in different physiological states such as walking, talking, or sleeping, which may also continuously or intermittently be affected by disease-specific symptoms.

Neurophysiological Manifestations

Signals to control DBS may be derived from neural recordings in the brain, peripheral sensors, or a combination of sources. Neural signals may encode various slow- or fast-changing states. Even depending on the way they are analytically processed, a same biomarker may be used to regulate control loops operating at different time scales. For instance, the better explored closed-loop DBS approaches for PD have employed beta oscillations in subthalamic nucleus (STN), which correlate with bradykinesia and rigidity (Brown et al., 2001; Neumann et al., 2016). Closed-loop approaches targeted either fast transient states of excessive synchrony (in the range of milliseconds) (Little et al., 2013; Moraud et al., 2018; Velisar et al., 2019) or instead beta activity fluctuations in the range of minutes to hours. These examples highlight the capacity to exploit the same biological signal *via* different temporal dynamics to address the same or various clinical goals.

A comprehensive understanding of the temporal properties governing different clinical manifestations and neurophysiological signatures, along with their interdependencies, is thus critical for the design of therapies that can optimally address multiple states in parallel. We outline a selection of different clinical and neurophysiological layers relevant to closed-loop therapies.

TREMOR

Across disorders, tremor tends to appear episodically (lasting from less than minutes up to hours), favored for instance by insufficient pharmacological control or agitation (Louis and Machado, 2015). Tremor occurrence is also influenced by motor states, as for example in PD tremor occurs prominently during rest, while in ET tremor is more pronounced during actions (Thengnatt and Jankovic, 2016).

Biomarkers and closed-loop strategies: Approaches for closed-loop DBS explored multiple control sources and control paradigms. Some used peripheral sensors to measure the amplitude of movements in the tremor frequency range (Yamamoto et al., 2013; Malekmohammadi et al., 2016) or delivered burst of stimulation locked to specific tremor phases (Cagnan et al., 2013, 2014, 2017). Tremor could also be detected from brain signals, either indexed by the lower frequency

components (3–7 Hz) or more accurately by using machine-learning techniques allowing to combine multiple features from the whole-spectrum LFP (Hirschmann et al., 2017; Shah et al., 2018). Additionally, the action-induced occurrence of tremor in ET leveraged the development of closed-loop DBS algorithms with voluntary movement related modulations in LFPs as triggers for stimulation (Herron et al., 2017; Houston et al., 2017; Tan et al., 2018; He et al., 2020, 2021). All approaches ended up being tuned to operate in the range of milliseconds to multiple seconds.

GAIT AND GAIT DISTURBANCES

Gait and balance deficits are common in PD, and induce a broad range of impairments including reduced arm swing and step length, shuffling steps, festination, freezing of gait or lack of postural control (Fasano et al., 2015). This phenomenological and temporal diversity, which include both continuous and episodic manifestations that are often interconnected, are difficult to treat. The effect of DBS on gait deficits is variable and patient specific spanning, from improvement to even worsening of gait (Hausdorff et al., 2009; Pötter-Nerger and Volkmann, 2013; Barbe et al., 2020).

Biomarkers and closed-loop strategies: During gait execution, alternating right and left gait cycles (1–2 Hz) are accompanied by periodic, time-locked modulations in the beta and gamma band power in STN LFP (Fischer et al., 2018; Hell et al., 2018). Recent work showed that alternating right and left DBS patterns, delivered intermittently at similar frequencies, could entrain stepping movements and increase gait regularity (Fischer et al., 2020; Wang and Choi, 2020). Additionally, beta modulations exhibit a degree of spectral segregation, with a stronger modulation in the high-beta range during leg vs. arm movements, (Fischer et al., 2018; Tinkhauser et al., 2019), which helped discriminate walking vs. standing (Canessa et al., 2020).

In addition, how freezing of gait (FoG) episodes could be delineated and targeted remains unanswered. In contrast to the alternating neuronal activity patterns during locomotion, FoG has been linked to the occurrence of prolonged bursts of beta activity (Anidi et al., 2018) and first data show promising results for beta-triggered cl-DBS to prevent FoG (Petrucci et al., 2020). Interestingly, the increase in beta activity associated with freezing of gait is more evident in the lower beta frequency ranges (15–21 Hz) and is also accompanied by an increase in the theta (5–8 Hz) activity (Chen C.-C. et al., 2019). Moreover, the electrophysiological signatures for vulnerability of freezing may be maintained >5 s and shows some degree of spatial segregation, as the theta power increase is more evident in the ventral part of the STN and in the substantia nigra. In line with this observation, stimulation at lower frequencies, or through ventral electrodes, has been suggested as option to reduce the occurrence of FoG (Sidiropoulos et al., 2013; Valldeoriola, 2019).

Considering these multi-faceted manifestations, therapies may need to flexibly combine (i) continuous adaptations in DBS during gait execution, as well as (ii) actively switching settings to improve and stabilize locomotion and prevent FoG (Fischer et al., 2020; Wang and Choi, 2020).

SPEECH

Progressive speech impairments are common in various neurological disorders. Both in PD and ET, DBS often leads to further deterioration of speech performance which plays a limiting factor in the optimization of DBS (Hariz et al., 2008).

Biomarkers and closed-loop strategies: Closed-loop DBS may prevent speech deterioration, which is often encountered as a side-product during continuous DBS (Little et al., 2016b). It may do so by reducing the overall current spread to capsular structures, as an indirect effect of closed-loop DBS targeting other clinical manifestations (Little et al., 2016a,b). Speech could also actively be integrated in stimulation control loops, for instance by recognizing speech from brain signals or peripheral sensors. Recent data suggest that the STN is involved in speech processing, with articulator-specific information being spatially and temporally organized within the target structure (Chrabaszcz et al., 2019). In addition, and currently more easily, speech could be recognized from peripheral sensors, that might also allow to extract information of the clinical state and to help calibrate stimulation parameters (Rusz et al., 2015; Akçay and Oğuz, 2020).

SYMPTOM FLUCTUATIONS IN PARKINSON'S DISEASE

The later stages of PD are characterized by fluctuations of motor and non-motor symptoms that are difficult to control with standard therapies (Martínez-Fernández et al., 2016). ON/OFF fluctuations evolve in the range of minutes to hours, with transitions that become faster, more abrupt and less predictable as the disease progresses.

Biomarkers and closed-loop strategies: Currently, beta activity recorded from the basal ganglia (particularly the STN), represents the best-characterized biomarker to inform about drug-induced fluctuations, bradykinesia and rigidity (Brown et al., 2001; Kuhn et al., 2006; Hammond et al., 2007; Tinkhauser et al., 2017b). Different temporal scales may be considered to interact and influence beta activity.

Fast Beta Modulations

Physiologically beta activity appears as short bursts (100 and 200 ms) (Feingold et al., 2015). However, in untreated PD patients, beta bursts are prolonged (between 200 and 1,000 ms) with higher amplitudes, both of which correlate with the level of clinical impairment (bradykinesia and rigidity) (Tinkhauser et al., 2017a,b, 2018; Duchet et al., 2021a). The direct impact of such temporally refined bursting dynamics on motor performance has been confirmed (Torrecillos et al., 2018; Khawaldeh et al., 2020, 2021; Tinkhauser et al., 2020). Therapies need to operate with a temporal resolution that matches the millisecond range, in order to properly detect and react to such fast-changing dynamics. One clinically successful approach computes beta power over a moving average of 400 ms (Little et al., 2013) and triggers stimulation whenever the windowed beta activity would surpass a pre-defined threshold, which allows to selectively trim pathologically long bursts (Tinkhauser et al., 2017a;

Moraud et al., 2018). Another study processed the beta envelope using a larger timescale (800 ms) (Velisar et al., 2019), which might be at the limit to depict bursts. Importantly, during exposure to dopaminergic medication (Kuhn et al., 2006), beta bursts become shorter in duration and smaller in amplitude, hence they become more alike physiological bursts (Tinkhauser et al., 2017b). Closed-loop algorithms that track beta bursts would allow to take medication-induced changes into account to avoid cumulative (drug + stim) effects (Little et al., 2016a).

Slow Beta Modulations

The temporal dynamics of beta activity can also be processed at longer temporal scales, with time-constants in the range of minutes. This processing does not capture beta burst dynamics, but instead accounts for clinical OFF/ON fluctuations related to medication intake. Adaptive DBS trials using this temporal resolution have been successfully piloted with a smoothing time constant of 50 s and a slow proportional controller that adapted stimulation accordingly (Rosa et al., 2017; Arlotti et al., 2018). A direct comparative study has demonstrated superiority of this closed-loop DBS approach over continuous DBS in improving motor UPDRS and reducing dyskinesias (Bocci et al., 2021).

Finely Tuned Gamma

60–90 Hz frequency activity detected in the electrocorticogram, has been linked to the presence of dyskinesia in the ON medication state, and represents a promising electrophysiological biomarker to regulate DBS for such manifestations (Swann et al., 2016). This approach has been tested with a time constant of 30 s on narrow band gamma activity followed by a 600 ms decision window for stimulation control (Swann et al., 2018). However, the full electrophysiological and clinical picture of finely tuned gamma activity (FTG) still needs to be characterized, as stimulation-induced FTG measured in the STN and coherent to cortical activity, can also occur OFF medication and in the absence of dyskinesia (Wiest et al., 2021). Similarly the FTG frequency peak seems to differ in the OFF and ON medication state (Swann et al., 2018; Muthuraman et al., 2020; Wiest et al., 2021). Interestingly, the occurrence and duration of FTG can outlast stimulation delivery by (on average) 20 s, or even appear for the first time after stimulation (Wiest et al., 2021). The first chronic recordings during varying medication and stimulation states are now available and will help to refine the properties and value of FTG as well as other biomarkers (Gilron et al., 2021).

Current knowledge already delineates how control algorithms may need to follow and integrate different temporal dynamics of distinct biomarkers.

CIRCADIAN RHYTHMICITY

Standard DBS therapies assume that the patient is in the same clinical state throughout the whole 24-h cycle. However, PD can be associated with different sleep problems such as REM-sleep behavior disorders (RBD), which can range from seconds to minutes, and alterations of sleep architecture. Several studies reported that STN DBS has a deepening and consolidating impact

on nocturnal sleep (Baumann-Vogel et al., 2017; Zuzuárregui and Ostrem, 2020).

Biomarkers and closed-loop strategies: It is not yet clear how DBS should optimally act during sleep. Treatment goals and stimulation parametrization are likely to be different than those during daytime. Sleep therapies could potentially be optimized by considering sleep architecture and pathological sleep phenomena. An important prerequisite is the recognition of sleep stages, so that therapies may adapt to their specific requirements. NREM 1–3 and REM stages alternate cyclically, as defined by standard 30-s epochs classification systems (AASM, 2020). Recordings from the STN during sleep show similar sleep related oscillatory patterns as during polysomnography surface EEG (Urrestarazu et al., 2009; Thompson et al., 2018). Sleep stage information may be derived in real time with a high prediction accuracy of 91% (Christensen et al., 2019). In this latter work, the time-evolving spectra had a 15 s time constant and 0.5 Hz frequency resolution, which was sufficient to detect transitions. Shorter time-constants have also been proposed (Chen Y. et al., 2019). Multi-layered closed-loop control that differently reacts during wakefulness and sleep are becoming necessary, as supported by the observation that STN beta activity is high during REM sleep (similar as during wakefulness), but decreases with deeper sleep stages (N1->N3) (Urrestarazu et al., 2009). Hence, a closed-loop algorithm solely based on the daily beta profile, is likely to decrease stimulation toward NREM 3 and increase during REM sleep.

LEVERAGING TEMPORAL DYNAMICS TO ENABLE MULTI-OBJECTIVE CLOSED-LOOP DBS

Despite the heterogeneity of clinical manifestations and neurophysiological signatures, the time-constants that govern their individual behaviors may be categorized into discrete temporal layers (**Figure 1**). This layered organization makes it possible to simplify, cluster or distribute how multiple manifestations are jointly monitored and addressed. For instance, manifestations evolving in the millisecond range require sensing and control loops to operate at fast time scales, using algorithms that are computationally efficient and simple in complexity (e.g., PID or bang-bang control). Slower manifestations may instead use model-based control approaches that additionally include predictions in the control loops. Accounting for dependencies between manifestations as well as interfaces between controllers may be feasible.

Cross-layer interferences inevitably arise in multi-objective control. They happen when one control loop (for instance, regulating manifestation 1) induces (directly, or indirectly) a change in manifestation 2, which in turn triggers a response in a second control loop, and so on. If unaccounted for, interferences may lead controllers to diverge. Importantly, interferences are less likely to occur when controlled variables have different time constants. This “temporal decoupling” allows to pause one therapy, for instance a slow controller operating in the hour range, and to temporarily deliver another one (a fast controller

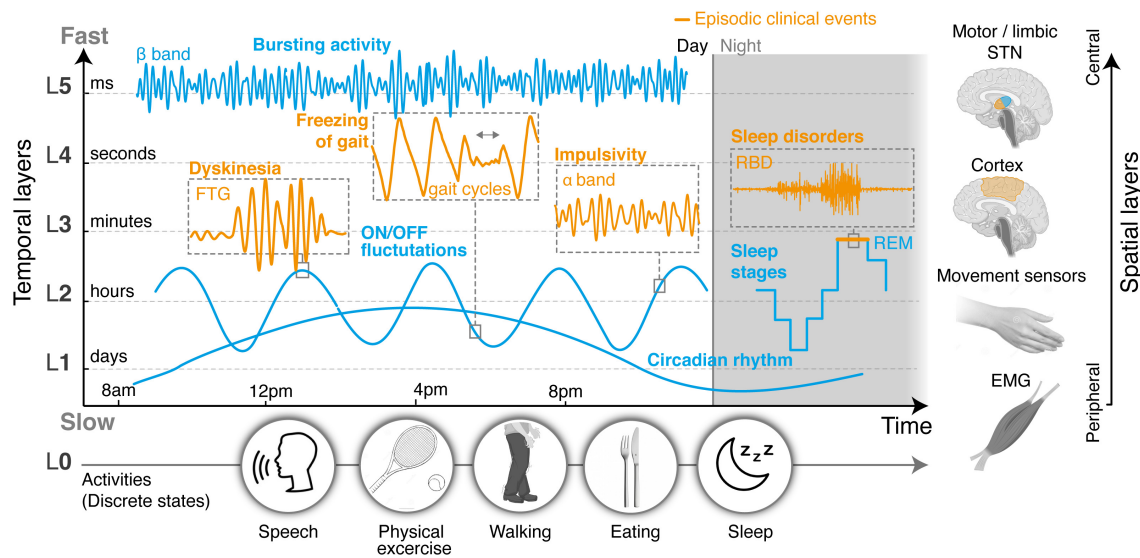


FIGURE 1 | Layered organization of control sources, segregated in time and space. Clinical and neural manifestations, both episodic and non-episodic, evolve according to distinct time-constants that can be categorized into a range of temporal layers, from milliseconds (fastest layer, L5) to days (slowest layer, L1). An additional layer (L0) could capture changes in manifestations related to discrete states, such as daily activities, and operate in parallel to the others. In this proposed modular structure, layers may not be independent, since manifestations at different timescales can affect each other. Thus cross-layer interactions must also be accounted for. On top of differences in their temporal properties, neural processes may also be spatially segregated, and picked up from different locations in the brain or the periphery. Hence temporal and spatial layers may be combined to simplify, cluster, or distribute how symptoms are optimally monitored, detected, and addressed. Overall, this representation establishes a conceptual framework by which the clinical state of a patient can be described as the modular superposition of parallel, yet inter-dependent manifestations segregated in time and space. Closed-loop control approaches may mirror this layered organization in the design of multi-objective therapies that can concurrently address multiple symptoms, while suitably dealing with dependencies. L, temporal layer; STN, subthalamic nucleus; ON/OFF, with/without medication; FTG, finely tuned gamma oscillations.

reacting to an episodic event in the range of seconds), without much impact on the earlier.

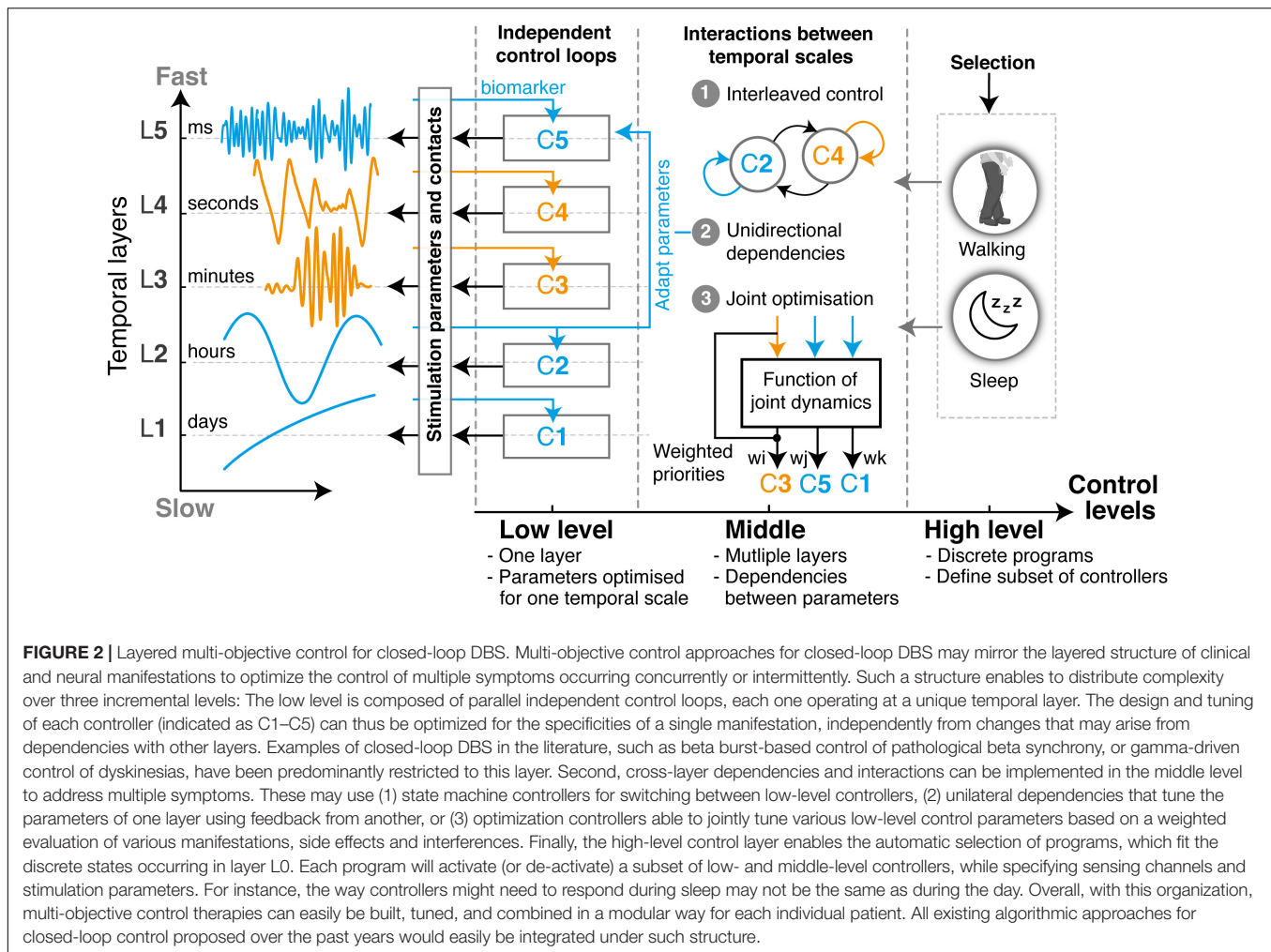
Overall, the complexity of developing therapies that can address multiple manifestations may be distributed over three hierarchical levels of operation (**Figure 2**): the lowest level embeds closed-loop control algorithms that are optimized for individual manifestations, each one operating at a single temporal layer, regardless of other parallel ones. For instance, one controller may monitor beta band modulations and trim pathological beta bursts in the millisecond range, while another may track gamma band activity and identify dyskinetic episodes in the second to minute range. Most existing closed-loop DBS strategies developed to date could be integrated within this level. Second, a middle level manages the combined outcomes of low level-controllers and accounts for cross-layer dependencies and interferences that arise when two or more therapies operate concurrently. This control level ensures that multiples objectives are being respected. Finally, a higher-level encodes discrete programs or activities, which activate (or de-activate) subsets of low- and middle-level control loops. This higher level may either be automatically or manually selected by patients or clinicians, for instance to switch between day or night modes, or for specific tasks.

We propose that this hierarchical organization may simplify the design of multi-objective control therapies, while allowing to easily integrate existing algorithmic strategies for closed-loop DBS. In this integrative framework, control loops targeting

different temporal layers are combined in a modular manner and operate in parallel (**Figure 2**). For a given patient, specific modules may easily be activated, and their joint operations managed to establish suitable therapeutic strategies that target all required manifestations.

Low-Level Controllers: Targeting Individual Manifestations

A variety of control strategies have been proposed for addressing individual manifestations through closed-loop DBS. They relied predominantly on fast control approaches, either bang-bang controllers triggered by one (Little et al., 2013; Pina-Fuentes et al., 2019) or two (Velisar et al., 2019) thresholds, or using PID controllers (Rosa et al., 2017). These strategies relied predominantly on neural feedback from local field potentials (beta power from the STN (Little et al., 2013), gamma or theta power from cortical signals (Swann et al., 2018; Johnson et al., 2021) or movement measures (Cagnan et al., 2017). Few feedforward components that use predictive models have been included in real-life applications, even though biophysical or data-driven black-box models may greatly improve accuracy (Gorzelic et al., 2013; Su et al., 2019), especially for slowly changing biomarkers. To date, modeling has predominantly been used to better understand the dynamics of manifestations (Holgado et al., 2010; Fleming et al., 2020a), the impact that DBS may have on the circuits (Hahn and McIntyre, 2010;



Weerasinghe et al., 2019; Fleming et al., 2020b) and to suggest possible control strategies for closed-loop DBS (Holt et al., 2016; Duchet et al., 2021b).

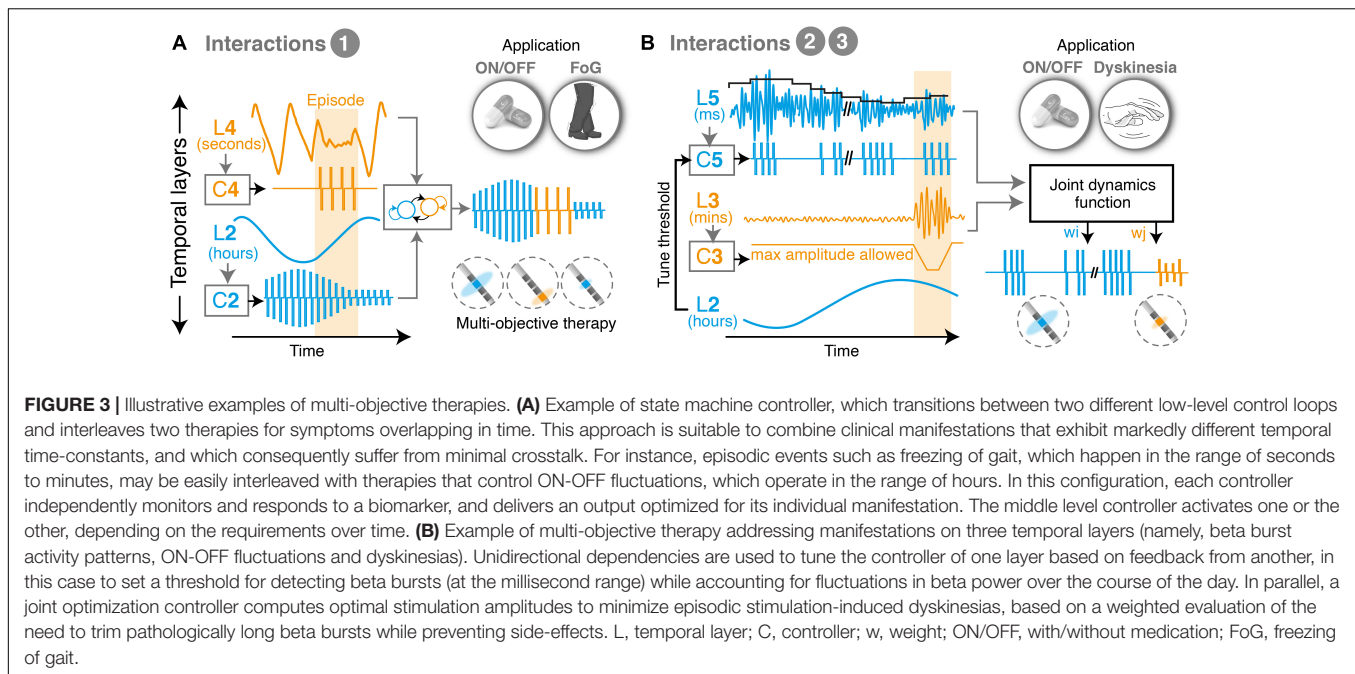
Examples from other neural engineering applications highlight the benefits of data-driven predictive models in closed-loop therapies. These used either movement sensor data or neural signals (commonly intra-cortical signals, with >100 channels) to control prostheses or robotic systems (Ethier et al., 2012; Hochberg et al., 2012), spinal cord stimulation for restoring movement (Wenger et al., 2014; Moraud et al., 2016; Bonizzato et al., 2018) and hemodynamic instability (Squair et al., 2021), or peripheral nerve stimulation for sensory feedback (Raspopovic et al., 2014). Many of these approaches may be easily integrated as low-level control loops within the proposed framework.

Middle Control Level: Managing Multiple Objectives

The variety of clinical and neurophysiological manifestations also shapes the choice of middle-level control strategies to manage the joint outcome of multiple objectives, and critically affects the

robustness and stability when addressing them concurrently. We outline various approaches that may be used:

1. State machine controllers allow to switch between independent states and make it possible to deliver various therapies in an interleaved manner. This approach is simple and easy to tune, as it only requires a few parameters (transitions). However, state machines do not directly manage interferences. They are thus most useful for processes that operate at clearly distinct layers (Toth et al., 2020). Examples in the literature using such approaches have been proposed for addressing beta bursts and episodic events such as FoG (Bronte-Stewart et al., 2020; **Figure 3**).
2. Unidirectional adaptations allow to tune the parameters of one controller using feedback of another temporal layer. This cross-layer interaction makes it possible to link two (or more) temporal layers, regardless of how far apart layers are. Examples include tuning the threshold for detecting beta-bursts based on feedback of ON-OFF fluctuations (**Figure 3**).
3. Optimization controllers employ a function of joint dynamics and are thus able to intrinsically account for



interactions between manifestations. They provide the best way to deal with dependencies and are appropriate for layers that have similar time-constants (i.e., manifestations operating at similar dynamics and overlapping). However, these strategies are complex and require building models of the underlying processes and their responses to stimulation. Models may use biophysical, population-based or data-driven black box (machine learning) approaches, and allow to include feedforward and feedback control loops to more accurately control multiple objectives (Neumann and Rodriguez-Oroz, 2021).

Overall for a specific patient, the implementation of a suitable therapy capable of addressing multiple symptomatic traits would involve (i) establishing the patient profile, his/her specific therapeutic requirements and their time constants (similar to a “system identification” step), (ii) establishing what low-level controllers (modules) need to be activated to address each one of these manifestations, (iii) defining the neuro-physiological signatures or feedback signals that will drive each low-level controller, along with the objective to be achieved by each one of them, (iv) calibrating the individual parameters of each controller, e.g., threshold values, control coefficients, adaptation rates (optimized for each module in isolation), (v) defining possible inter-dependencies and interferences, and the best way to address them (choice of middle-level control type) based on the number of low-level controllers, their expected crosstalk and the relative importance of the manifestations that they monitor (defining priorities), (vi) evaluate the stability of the combined control strategy and establishing boundaries and safety measures to prevent divergence. This process may be repeated separately for each discrete program (high level control layer) e.g., one for the day and one for the night.

Steps (i–vi) may need to be done iteratively, over multiple sessions. Modularity would allow to incrementally refine therapies, adding one low-level controller at a time and tuning middle-layer control strategies accordingly to cope with added modules.

To increase stability and robustness over time, each low-level controller may include a self-adaptation term that tracks changes occurring over time and slowly adapts (Zaknich, 2005). Its implementation will strongly depend on the control type and the temporal layer on which it operates: Controllers with slow time-constants may exploit daily periodicity to track changes occurring from day to day, and use a forgetting factor that iteratively updates control parameters (e.g., daily update based on an average biomarker value over the previous day). Controllers that regulate episodic events such as freezing of dyskinesia may iteratively update control parameters after every few episodes.

TECHNOLOGICAL IMPLICATIONS

Beside the conceptual framework of multi layered control, the technological requirements (hardware and software) to implement such comprehensive closed-loop strategies should not be left unmentioned. There are crucial technical capability demands for neurostimulators in the future. For instance, devices need to be able to monitor and differentially process multiple electrophysiological brain biomarkers and integrate them in the decision-making process (as outlined above). Such co-processing capabilities to flexible handle multiple inputs have been piloted (Stanslaski et al., 2018), and need to be refined in the future. As aforementioned, brain biomarkers can come from multiple sources (cortex, basal ganglia) including their

corresponding somatotopic subdivisions, thus neurostimulators must be capable to handle multiple independent signal sources. Optimally, neurostimulator platforms need to process and synchronized bio signals other than brain activity, derived from sensors embedded in the neurostimulator itself (e.g., gyroscope) or from peripheral sensors. In addition, the patient should be part of the loop, as important feedback on treatment satisfaction could be provided by interactive and patients suitable apps. Finally, the multidimensionality of multi-objective control requires simple and intuitive integrative platforms that can be efficiently handled and adjusted by the medical personnel.

MULTI-LAYER CLOSED-LOOP DEEP BRAIN STIMULATION: A PRECISION MEDICINE APPROACH

For over 30 years, DBS therapies have been restricted to continuous paradigms. Advances in implantable technology now offer the possibility to monitor and control neural signatures in chronically implanted patients, providing the technical substrate to deploy truly personalized therapies. More than ever, it is important to draw awareness on the multifaceted and dynamic nature of clinical and neurophysiological manifestations. A conceptual framework is critical to steer the development of therapies that can manage multiple dynamical objectives in parallel and integrate existing closed-loop strategies into a clinically relevant therapeutic portfolio. Modularity will play a key role in rendering these approaches manageable,

allowing to easily select and tune therapies that operate on multiple temporal layers, and linking them to patient-specific electro-clinical profiles. While several technological and neurophysiological advances are still needed to enable nested multilayer control capabilities, hardware, software and therapeutic developments will need to go hand in hand. The proposed conceptual framework may thus represent an integral part next generation precision medicine instruments.

DATA AVAILABILITY STATEMENT

The original contributions presented in the study are included in the article/supplementary material, further inquiries can be directed to the corresponding author/s.

AUTHOR CONTRIBUTIONS

GT and EMM contributed to the conceptual design, writing, editing, and generation of figures for the manuscript. All authors contributed to the article and approved the submitted version.

FUNDING

GT received grant support from the Swiss Parkinson Association and Baasch-Medicus Foundation. EMM was funded by the Swiss National Science Foundation (fellowship number PZ00P3_180018).

REFERENCES

- AASM (2020). *AASM Manual for the Scoring of Sleep and Associated Events: Rules, Terminology and Technical Specifications; Scoring Manual Version 2.6*. Darien, IL: AASM.
- Akçay, M. B., and Oğuz, K. (2020). Speech emotion recognition: emotional models, databases, features, preprocessing methods, supporting modalities, and classifiers. *Speech Commun.* 116, 56–76. doi: 10.1016/j.specom.2019.12.001
- Anidi, C., O'Day, J. J., Anderson, R. W., Afzal, M. F., Syrkin-Nikolau, J., Velisar, A., et al. (2018). Neuromodulation targets pathological not physiological beta bursts during gait in Parkinson's disease. *Neurobiol. Dis.* 120, 107–117. doi: 10.1016/j.nbd.2018.09.004
- Arlotti, M., Marceglia, S., Foffani, G., Volkmann, J., Lozano, A. M., Moro, E., et al. (2018). Eight-hours adaptive deep brain stimulation in patients with Parkinson disease. *Neurology* 90, e971–e976. doi: 10.1212/WNL.0000000000005121
- Barbe, M. T., Tonder, L., Krack, P., Debû, B., Schüpbach, M., Paschen, S., et al. (2020). Deep brain stimulation for freezing of gait in Parkinson's disease with early motor complications. *Mov. Disord.* 35, 82–90. doi: 10.1002/mds.27892
- Baumann-Vogel, H., Imbach, L. L., Sürücü, O., Stieglitz, L., Waldvogel, D., Baumann, C. R., et al. (2017). The impact of subthalamic deep brain stimulation on sleep-wake behavior: a prospective electrophysiological study in 50 parkinson patients. *Sleep*. 40:zsx033. doi: 10.1093/sleep/zsx033
- Bocci, T., Prenassi, M., Arlotti, M., Cogiamanian, F. M., Borrellini, L., Moro, E., et al. (2021). Eight-hours conventional versus adaptive deep brain stimulation of the subthalamic nucleus in Parkinson's disease. *NPJ Parkinsons Dis.* 7:88. doi: 10.1038/s41531-021-00229-z
- Bonizzato, M., Pidpruzhnykova, G., DiGiovanna, J., Shkorbatova, P., Pavlova, N., Micera, S., et al. (2018). Brain-controlled modulation of spinal circuits improves recovery from spinal cord injury. *Nat. Commun.* 9:3015. doi: 10.1038/s41467-018-05282-6
- Bronte-Stewart, H. M., Petrucci, M. N., O'Day, J. J., Afzal, M. F., Parker, J. E., Kehnemouyi, Y. M., et al. (2020). Perspective: evolution of control variables and policies for closed-loop deep brain stimulation for Parkinson's disease using bidirectional deep-brain-computer interfaces. *Front. Hum. Neurosci.* 14:353. doi: 10.3389/fnhum.2020.00353
- Brown, P., Oliviero, A., Mazzone, P., Insola, A., Tonali, P., and Di Lazzaro, V. (2001). Dopamine dependency of oscillations between subthalamic nucleus and pallidum in Parkinson's disease. *J. Neurosci.* 21, 1033–1038. doi: 10.1523/JNEUROSCI.21-03-01033.2001
- Cagnan, H., Brittain, J. S., Little, S., Foltynie, T., Limousin, P., Zrinzo, L., et al. (2013). Phase dependent modulation of tremor amplitude in essential tremor through thalamic stimulation. *Brain* 136(Pt. 10), 3062–3075. doi: 10.1093/brain/awt239
- Cagnan, H., Denison, T., McIntyre, C., and Brown, P. (2019). Emerging technologies for improved deep brain stimulation. *Nat. Biotechnol.* 37, 1024–1033. doi: 10.1038/s41587-019-0244-6
- Cagnan, H., Little, S., Foltynie, T., Limousin, P., Zrinzo, L., Hariz, M., et al. (2014). The nature of tremor circuits in parkinsonian and essential tremor. *Brain* 137(Pt. 12), 3223–3234. doi: 10.1093/brain/awu250
- Cagnan, H., Pedrosa, D., Little, S., Pogossyan, A., Cheeran, B., Aziz, T., et al. (2017). Stimulating at the right time: phase-specific deep brain stimulation. *Brain* 140, 132–145. doi: 10.1093/brain/aww286
- Canessa, A., Palmisano, C., Isaías, I. U., and Mazzoni, A. (2020). Gait-related frequency modulation of beta oscillatory activity in the subthalamic nucleus of parkinsonian patients. *Brain Stimul.* 13, 1743–1752. doi: 10.1016/j.brs.2020.09.006
- Chen, C.-C., Yeh, C.-H., Chan, H.-L., Chang, Y.-J., Tu, P.-H., Yeh, C.-H., et al. (2019). Subthalamic nucleus oscillations correlate with vulnerability to freezing of gait in patients with Parkinson's disease. *Neurobiol. Dis.* 132:104605. doi: 10.1016/j.nbd.2019.104605

- Chen, Y., Gong, C., Hao, H., Guo, Y., Xu, S., Zhang, Y., et al. (2019). Automatic sleep stage classification based on subthalamic local field potentials. *IEEE Trans. Neural Syst. Rehabil. Eng.* 27, 118–128. doi: 10.1109/TNSRE.2018.2890272
- Chrabaszcz, A., Neumann, W. J., Stretcu, O., Lipski, W. J., Bush, A., Dastolfo-Hromack, C. A., et al. (2019). Subthalamic nucleus and sensorimotor cortex activity during speech production. *J. Neurosci.* 39, 2698–2708. doi: 10.1523/JNEUROSCI.2842-18.2019
- Christensen, E., Abosch, A., Thompson, J. A., and Zylberberg, J. (2019). Inferring sleep stage from local field potentials recorded in the subthalamic nucleus of Parkinson's patients. *J. Sleep Res.* 28:e12806. doi: 10.1111/jsr.12806
- Duchet, B., Ghezzi, F., Weerasinghe, G., Tinkhauser, G., Kühn, A. A., Brown, P., et al. (2021a). Average beta burst duration profiles provide a signature of dynamical changes between the ON and OFF medication states in Parkinson's disease. *PLoS Comput. Biol.* 17:e1009116. doi: 10.1371/journal.pcbi.1009116
- Duchet, B., Weerasinghe, G., Bick, C., and Bogacz, R. (2021b). Optimizing deep brain stimulation based on isostable amplitude in essential tremor patient models. *J. Neural Eng.* 18:046023. doi: 10.1088/1741-2552/abd90d
- Ethier, C., Oby, E. R., Bauman, M. J., and Miller, L. E. (2012). Restoration of grasp following paralysis through brain-controlled stimulation of muscles. *Nature* 485, 368–371. doi: 10.1038/nature10987
- Fasano, A., Aquino, C. C., Krauss, J. K., Honey, C. R., and Bloem, B. R. (2015). Axial disability and deep brain stimulation in patients with Parkinson disease. *Nat. Rev. Neurol.* 11, 98–110. doi: 10.1038/nrneurol.2014.252
- Feingold, J., Gibson, D. J., DePasquale, B., and Graybiel, A. M. (2015). Bursts of beta oscillation differentiate postperformance activity in the striatum and motor cortex of monkeys performing movement tasks. *Proc. Natl. Acad. Sci. U.S.A.* 112, 13687–13692. doi: 10.1073/pnas.1517629112
- Fischer, P., Chen, C. C., Chang, Y. J., Yeh, C.-H., Pogossyan, A., Herz, D. M., et al. (2018). Alternating modulation of subthalamic nucleus beta oscillations during stepping. *J. Neurosci.* 38, 5111–5121. doi: 10.1523/JNEUROSCI.3596-17.2018
- Fischer, P., He, S., de Roquemaurel, A., Akram, H., Foltynie, T., Limousin, P., et al. (2020). Entraining stepping movements of Parkinson's patients to alternating subthalamic nucleus deep brain stimulation. *The J. Neurosci.* 40, 8964–8972. doi: 10.1523/JNEUROSCI.1767-20.2020
- Fleming, J. E., Dunn, E., and Lowery, M. M. (2020a). Simulation of closed-loop deep brain stimulation control schemes for suppression of pathological beta oscillations in Parkinson's Disease. *Front. Neurosci.* 14:166. doi: 10.3389/fnins.2020.00166
- Fleming, J. E., Orlowski, J., Lowery, M. M., and Chaillet, A. (2020b). Self-tuning deep brain stimulation controller for suppression of beta oscillations: analytical derivation and numerical validation. *Front. Neurosci.* 14:639. doi: 10.3389/fnins.2020.00639
- Gilron, R., Little, S., Perrone, R., Wilt, R., de Hemptinne, C., Yaroshinsky, M. S., et al. (2021). Long-term wireless streaming of neural recordings for circuit discovery and adaptive stimulation in individuals with Parkinson's disease. *Nat. Biotechnol.* 39, 1078–1085. doi: 10.1038/s41587-021-00897-5
- Gozelec, P., Schiff, S. J., and Sinha, A. (2013). Model-based rational feedback controller design for closed-loop deep brain stimulation of Parkinson's disease. *J. Neural Eng.* 10:026016. doi: 10.1088/1741-2560/10/2/026016
- Gunduz, A., Opri, E., Gilron, R., Kremen, V., Worrell, G., Starr, P., et al. (2019). Adding wisdom to 'smart' bioelectronic systems: a design framework for physiologic control including practical examples. *Bioelectron. Med.* 2, 29–41. doi: 10.2217/bem-2019-0008
- Hahn, P. J., and McIntyre, C. C. (2010). Modeling shifts in the rate and pattern of subthalamic nucleus network activity during deep brain stimulation. *J. Comput. Neurosci.* 28, 425–441. doi: 10.1007/s10827-010-0225-8
- Hammond, C., Bergman, H., and Brown, P. (2007). Pathological synchronization in Parkinson's disease: networks, models and treatments. *Trends Neurosci.* 30, 357–364. doi: 10.1016/j.tins.2007.05.004
- Hariz, M. I., Rehncrona, S., Quinn, N. P., Speelman, J. D., and Wensing, C. (2008). Multicenter study on deep brain stimulation in Parkinson's disease: an independent assessment of reported adverse events at 4 years. *Mov. Disord.* 23, 416–421. doi: 10.1002/mds.21888
- Hausdorff, J. M., Gruendlinger, L., Scollins, L., O'Herron, S., and Tarsy, D. (2009). Deep brain stimulation effects on gait variability in Parkinson's disease. *Mov. Disord.* 24, 1688–1692. doi: 10.1002/mds.22554
- He, S., Baig, F., Mostofi, A., Pogossyan, A., Debarros, J., Green, A. L., et al. (2021). Closed-Loop deep brain stimulation for essential tremor based on thalamic local field potentials. *Mov. Disord.* 36, 863–873. doi: 10.1002/mds.28513
- He, S., Debarros, J., Khawaldeh, S., Pogossyan, A., Mostofi, A., Baig, F., et al. (eds) (2020). "Closed-loop DBS triggered by real-time movement and tremor decoding based on thalamic LFPs for essential tremor," in *Proceedings of the 2020 42nd Annual International Conference of the IEEE Engineering in Medicine & Biology Society (EMBC); 20-24 July 2020*, (Montreal, QC). doi: 10.1109/EMBC44109.2020.9175433
- Hell, F., Plate, A., Mehrkens, J. H., and Bötzel, K. (2018). Subthalamic oscillatory activity and connectivity during gait in Parkinson's disease. *NeuroImage Clin.* 19, 396–405. doi: 10.1016/j.nicl.2018.05.001
- Herron, J. A., Thompson, M. C., Brown, T., Chizeck, H. J., Ojemann, J. G., and Ko, A. L. (2017). Chronic electrocorticography for sensing movement intention and closed-loop deep brain stimulation with wearable sensors in an essential tremor patient. *J. Neurosurg.* 127, 580–587. doi: 10.3171/2016.8.JNS16536
- Hirschmann, J., Schoffelen, J. M., Schnitzler, A., and van Gerven, M. A. J. (2017). Parkinsonian rest tremor can be detected accurately based on neuronal oscillations recorded from the subthalamic nucleus. *Clin. Neurophysiol.* 128, 2029–2036. doi: 10.1016/j.clinph.2017.07.419
- Hochberg, L. R., Bacher, D., Jarosiewicz, B., Masse, N. Y., Simeral, J. D., Vogel, J., et al. (2012). Reach and grasp by people with tetraplegia using a neurally controlled robotic arm. *Nature* 485, 372–375. doi: 10.1038/nature11076
- Holgado, A. J., Terry, J. R., and Bogacz, R. (2010). Conditions for the generation of beta oscillations in the subthalamic nucleus-globus pallidus network. *J. Neurosci.* 30, 12340–12352. doi: 10.1523/JNEUROSCI.0817-10.2010
- Holt, A. B., Wilson, D., Shinn, M., Moehlis, J., and Netoff, T. I. (2016). Phasic burst stimulation: a closed-loop approach to tuning deep brain stimulation parameters for Parkinson's disease. *PLoS Comput. Biol.* 12:e1005011. doi: 10.1371/journal.pcbi.1005011
- Houston, B. C., Thompson, M. C., Ojemann, J. G., Ko, A. L., and Chizeck, H. J. (eds) (2017). "Classifier-based closed-loop deep brain stimulation for essential tremor," in *Proceedings of the 2017 8th International IEEE/EMBS Conference on Neural Engineering (NER); 25-28 May 2017*, (Shanghai). doi: 10.1109/NER.2017.8008354
- Johnson, V., Wilt, R., Gilron, R., Anso, J., Perrone, R., Beudel, M., et al. (2021). Embedded adaptive deep brain stimulation for cervical dystonia controlled by motor cortex theta oscillations. *Exp. Neurol.* 345:113825. doi: 10.1016/j.expneurol.2021.113825
- Khawaldeh, S., Tinkhauser, G., Shah, S. A., Peterman, K., Debove, I., Nguyen, T. A. K., et al. (2020). Subthalamic nucleus activity dynamics and limb movement prediction in Parkinson's disease. *Brain* 143, 582–596. doi: 10.1093/brain/awz417
- Khawaldeh, S., Tinkhauser, G., Torrecillos, F., He, S., Foltynie, T., Limousin, P., et al. (2021). Balance between competing spectral states in subthalamic nucleus is linked to motor impairment in Parkinson's disease. *Brain* Online ahead of print. doi: 10.1093/brain/awab264
- Krack, P., Volkmann, J., Tinkhauser, G., and Deuschl, G. (2019). Deep brain stimulation in movement disorders: from experimental surgery to evidence-based therapy. *Mov. Disord.* 34, 1795–1810. doi: 10.1002/mds.27860
- Kuhn, A. A., Kupsch, A., Schneider, G. H., and Brown, P. (2006). Reduction in subthalamic 8–35 Hz oscillatory activity correlates with clinical improvement in Parkinson's disease. *Eur. J. Neurosci.* 23, 1956–1960. doi: 10.1111/j.1460-9568.2006.04717.x
- Little, S., Beudel, M., Zrinzo, L., Foltynie, T., Limousin, P., Hariz, M., et al. (2016a). Bilateral adaptive deep brain stimulation is effective in Parkinson's disease. *J. Neurol. Neurosurg. Psychiatry* 87, 717–721. doi: 10.1136/jnnp-2015-310972
- Little, S., Tripoliti, E., Beudel, M., Pogossyan, A., Cagnan, H., Herz, D., et al. (2016b). Adaptive deep brain stimulation for Parkinson's disease demonstrates reduced speech side effects compared to conventional stimulation in the acute setting. *J. Neurol. Neurosurg. Psychiatry* 87, 1388–1389. doi: 10.1136/jnnp-2016-313518
- Little, S., Pogossyan, A., Neal, S., Zavala, B., Zrinzo, L., Hariz, M., et al. (2013). Adaptive deep brain stimulation in advanced Parkinson disease. *Ann. Neurol.* 74, 449–457. doi: 10.1002/ana.23951
- Louis, E. D., and Machado, D. G. (2015). Tremor-related quality of life: a comparison of essential tremor vs. Parkinson's disease patients. *Parkinsonism Relat. Disord.* 21, 729–735. doi: 10.1016/j.parkreldis.2015.04.019

- Lozano, A. M., Lipsman, N., Bergman, H., Brown, P., Chabardes, S., Chang, J. W., et al. (2019). Deep brain stimulation: current challenges and future directions. *Nat. Rev. Neurol.* 15, 148–160. doi: 10.1038/s41582-018-0128-2
- Malekmohammadi, M., Herron, J., Velisar, A., Blumenfeld, Z., Trager, M. H., Chizeck, H. J., et al. (2016). Kinematic adaptive deep brain stimulation for resting tremor in Parkinson's disease. *Mov. Disord.* 31, 426–428. doi: 10.1002/mds.26482
- Martínez-Fernández, R., Schmitt, E., Martínez-Martin, P., and Krack, P. (2016). The hidden sister of motor fluctuations in Parkinson's disease: a review on nonmotor fluctuations. *Mov. Disord.* 31, 1080–1094. doi: 10.1002/mds.26731
- Moraud, E. M., Capogrosso, M., Formento, E., Wenger, N., DiGiovanna, J., Courtine, G., et al. (2016). Mechanisms underlying the neuromodulation of spinal circuits for correcting gait and balance deficits after spinal cord injury. *Neuron* 89, 814–828. doi: 10.1016/j.neuron.2016.01.009
- Moraud, E. M., Tinkhauser, G., Agrawal, M., Brown, P., and Bogacz, R. (2018). Predicting beta bursts from local field potentials to improve closed-loop DBS paradigms in Parkinson's patients. *Annu. Int. Conf. IEEE Eng. Med. Biol. Soc.* 2018, 3766–3796. doi: 10.1109/EMBC.2018.8513348
- Muthuraman, M., Bange, M., Koirala, N., Ciolac, D., Pintea, B., Glaser, M., et al. (2020). Cross-frequency coupling between gamma oscillations and deep brain stimulation frequency in Parkinson's disease. *Brain* 143, 3393–3407. doi: 10.1093/brain/awaa297
- Neumann, W. J., and Rodríguez-Oroz, M. C. (2021). Machine learning will extend the clinical utility of adaptive deep brain stimulation. *Mov. Disord.* 36, 796–799. doi: 10.1002/mds.28567
- Neumann, W. J., Degen, K., Schneider, G. H., Brucke, C., Huebl, J., Brown, P., et al. (2016). Subthalamic synchronized oscillatory activity correlates with motor impairment in patients with Parkinson's disease. *Mov. Disord.* 31, 1748–1751. doi: 10.1002/mds.26759
- Parastarfeizabadi, M., Sillitoe, R. V., and Kouzani, A. Z. (2020). Multi-disease deep brain stimulation. *IEEE Access* 8, 216933–216947. doi: 10.1109/ACCESS.2020.3041942
- Petrucchi, M. N., Neuville, R. S., Afzal, M. F., Velisar, A., Anidi, C. M., Anderson, R. W., et al. (2020). Neural closed-loop deep brain stimulation for freezing of gait. *Brain Stimul.* 13, 1320–1322. doi: 10.1016/j.brs.2020.06.018
- Pina-Fuentes, D., van Zijl, J. C., van Dijk, J. M. C., Little, S., Tinkhauser, G., Oterdoom, D. L. M., et al. (2019). The characteristics of pallidal low-frequency and beta bursts could help implementing adaptive brain stimulation in the parkinsonian and dystonic internal globus pallidus. *Neurobiol. Dis.* 121, 47–57. doi: 10.1016/j.nbd.2018.09.014
- Pötter-Nerger, M., and Volkmann, J. (2013). Deep brain stimulation for gait and postural symptoms in Parkinson's disease. *Mov. Disord.* 28, 1609–1615. doi: 10.1002/mds.25677
- Raspopovic, S., Capogrosso, M., Petrini, F. M., Bonizzato, M., Rigosa, J., Di Pino, G., et al. (2014). Restoring natural sensory feedback in real-time bidirectional hand prostheses. *Sci. Transl. Med.* 6:222ra19. doi: 10.1126/scitranslmed.3006820
- Rosa, M., Arlotti, M., Marceglia, S., Cogiamanian, F., Ardolino, G., Fonzo, A. D., et al. (2017). Adaptive deep brain stimulation controls levodopa-induced side effects in Parkinsonian patients. *Mov. Disord.* 32, 628–629. doi: 10.1002/mds.26953
- Rusz, J., Hlavnička, J., Čmejla, R., and Růžicka, E. (2015). Automatic evaluation of speech rhythm instability and acceleration in dysarthrias associated with basal ganglia dysfunction. *Front. Bioeng. Biotechnol.* 3:104. doi: 10.3389/fbioe.2015.00104
- Shah, S. A., Tinkhauser, G., Chen, C. C., Little, S., and Brown, P. (2018). Parkinsonian tremor detection from subthalamic nucleus local field potentials for closed-loop deep brain stimulation. *Annu. Int. Conf. IEEE Eng. Med. Biol. Soc.* 2018, 2320–2324. doi: 10.1109/EMBC.2018.8512741
- Sidiropoulos, C., Walsh, R., Meaney, C., Poon, Y. Y., Fallis, M., and Moro, E. (2013). Low-frequency subthalamic nucleus deep brain stimulation for axial symptoms in advanced Parkinson's disease. *J. Neurol.* 260, 2306–2311. doi: 10.1007/s00415-013-6983-2
- Squair, J. W., Gautier, M., Mahe, L., Soriano, J. E., Rowald, A., Bichat, A., et al. (2021). Neuroprosthetic baroreflex controls haemodynamics after spinal cord injury. *Nature* 590, 308–314. doi: 10.1038/s41586-020-03180-w
- Stanslaski, S., Herron, J., Chouinard, T., Bourget, D., Isaacson, B., Kremen, V., et al. (2018). A chronically implantable neural coprocessor for investigating the treatment of neurological disorders. *IEEE Trans. Biomed. Circuits Syst.* 12, 1230–1245. doi: 10.1109/TBCAS.2018.2880148
- Su, F., Kumaravelu, K., Wang, J., and Grill, W. M. (2019). Model-based evaluation of closed-loop deep brain stimulation controller to adapt to dynamic changes in reference signal. *Front. Neurosci.* 13:956. doi: 10.3389/fnins.2019.00956
- Swann, N. C., de Hemptinne, C., Miocinovic, S., Qasim, S., Wang, S. S., Ziman, N., et al. (2016). Gamma oscillations in the hyperkinetic state detected with chronic human brain recordings in Parkinson's Disease. *J. Neurosci.* 36, 6445–6458. doi: 10.1523/JNEUROSCI.1128-16.2016
- Swann, N. C., de Hemptinne, C., Thompson, M. C., Miocinovic, S., Miller, A. M., Gilron, R., et al. (2018). Adaptive deep brain stimulation for Parkinson's disease using motor cortex sensing. *J. Neural Eng.* 15:046006. doi: 10.1088/1741-2552/aabc9b
- Tan, H., Debarros, J., Pogossyan, A., Aziz, T. Z., Huang, Y., Wang, S., et al. (2018). Decoding voluntary movements and postural tremor based on thalamic LFPs for closed-loop stimulation for essential tremor. *Biorxiv [Preprint]*. doi: 10.1101/436709
- Thenganatt, M. A., and Jankovic, J. (2016). The relationship between essential tremor and Parkinson's disease. *Parkinsonism Relat. Disord.* 22(Suppl. 1), S162–S165. doi: 10.1016/j.parkreldis.2015.09.032
- Thompson, J. A., Tekriwal, A., Felsen, G., Ozturk, M., Telkes, I., Wu, J., et al. (2018). Sleep patterns in Parkinson's disease: direct recordings from the subthalamic nucleus. *J. Neurol. Neurosurg. Psychiatry* 89, 95–104. doi: 10.1136/jnnp-2017-316115
- Tinkhauser, G., Pogossyan, A., Little, S., Beudel, M., Herz, D. M., Tan, H., et al. (2017a). The modulatory effect of adaptive deep brain stimulation on beta bursts in Parkinson's disease. *Brain* 140, 1053–1067. doi: 10.1093/brain/awx010
- Tinkhauser, G., Pogossyan, A., Tan, H., Herz, D. M., Kuhn, A. A., and Brown, P. (2017b). Beta burst dynamics in Parkinson's disease OFF and ON dopaminergic medication. *Brain* 140, 2968–2981. doi: 10.1093/brain/awx252
- Tinkhauser, G., Shah, S. A., Fischer, P., Peterman, K., Debove, I., Nygyuen, K., et al. (2019). Electrophysiological differences between upper and lower limb movements in the human subthalamic nucleus. *Clin. Neurophysiol.* 130, 727–738. doi: 10.1016/j.clinph.2019.02.011
- Tinkhauser, G., Torrecillos, F., Duclos, Y., Tan, H., Pogossyan, A., Fischer, P., et al. (2018). Beta burst coupling across the motor circuit in Parkinson's disease. *Neurobiol. Dis.* 117, 217–225. doi: 10.1016/j.nbd.2018.06.007
- Tinkhauser, G., Torrecillos, F., Pogossyan, A., Mostofi, A., Bange, M., Fischer, P., et al. (2020). The cumulative effect of transient synchrony states on motor performance in Parkinson's disease. *J. Neurosci.* 40, 1571–1580. doi: 10.1523/JNEUROSCI.1975-19.2019
- Torrecillos, F., Tinkhauser, G., Fischer, P., Green, A. L., Aziz, T. Z., Foltynie, T., et al. (2018). Modulation of beta bursts in the subthalamic nucleus predicts motor performance. *J. Neurosci.* 38, 8905–8917. doi: 10.1523/JNEUROSCI.1314-18.2018
- Toth, R., Zamora, M., Ottaway, J., Gillbe, T., Martin, S., Benjaber, M., et al. (2020). DyNeuMo Mk-2: an investigational circadian-locked neuromodulator with responsive stimulation for applied chronobiology. *Conf. Proc. IEEE Int. Conf. Syst. Man Cybern.* 2020, 3433–3440. doi: 10.1109/SMC42975.2020.9283187
- Urrestarazu, E., Iriarte, J., Alegre, M., Clavero, P., Rodríguez-Oroz, M. C., Guridi, J., et al. (2009). Beta activity in the subthalamic nucleus during sleep in patients with Parkinson's disease. *Mov. Disord.* 24, 254–260. doi: 10.1002/mds.22351
- Valdeorola, F. (2019). Simultaneous low-frequency deep brain stimulation of the substantia nigra pars reticulata and high-frequency stimulation of the subthalamic nucleus to treat levodopa unresponsive freezing of gait in Parkinson's disease: a pilot study. *Parkinsonism Relat. Disord.* 63:231. doi: 10.1016/j.parkreldis.2018.12.009
- Velisar, A., Syrkin-Nikolau, J., Blumenfeld, Z., Trager, M. H., Afzal, M. F., Prabhakar, V., et al. (2019). Dual threshold neural closed loop deep brain stimulation in Parkinson disease patients. *Brain Stimul.* 12, 868–876. doi: 10.1016/j.brs.2019.02.020

- Wang, D. D., and Choi, J. T. (2020). Brain network oscillations during gait in Parkinson's disease. *Front. Hum. Neurosci.* 14:568703. doi: 10.3389/fnhum.2020.568703
- Weerasinghe, G., Duchet, B., Cagnan, H., Brown, P., Bick, C., and Bogacz, R. (2019). Predicting the effects of deep brain stimulation using a reduced coupled oscillator model. *PLoS Comput. Biol.* 15:e1006575. doi: 10.1371/journal.pcbi.1006575
- Wenger, N., Moraud, E. M., Raspopovic, S., Bonizzato, M., DiGiovanna, J., Musienko, P., et al. (2014). Closed-loop neuromodulation of spinal sensorimotor circuits controls refined locomotion after complete spinal cord injury. *Sci. Transl. Med.* 6:255ra133. doi: 10.1126/scitranslmed.3008325
- Wiest, C., Tinkhauser, G., Pogossyan, A., He, S., Baig, F., Morgante, F., et al. (2021). Subthalamic deep brain stimulation induces finely-tuned gamma oscillations in the absence of levodopa. *Neurobiol. Dis.* 152:105287. doi: 10.1016/j.nbd.2021.105287
- Yamamoto, T., Katayama, Y., Ushiba, J., Yoshino, H., Obuchi, T., Kobayashi, K., et al. (2013). On-demand control system for deep brain stimulation for treatment of intention tremor. *Neuromodulation* 16, 230–235. doi: 10.1111/j.1525-1403.2012.00521.x
- Zaknich, A. (2005). *Principles of Adaptive Filters and Self-learning Systems*. Berlin: Springer Science & Business Media.
- Zuñuáregui, J. R. P., and Ostrem, J. L. (2020). The impact of deep brain stimulation on sleep in Parkinson's disease: an update. *J. Parkinsons Dis.* 10, 393–404. doi: 10.3233/JPD-191862
- Conflict of Interest:** The authors declare that the research was conducted in the absence of any commercial or financial relationships that could be construed as a potential conflict of interest.
- Publisher's Note:** All claims expressed in this article are solely those of the authors and do not necessarily represent those of their affiliated organizations, or those of the publisher, the editors and the reviewers. Any product that may be evaluated in this article, or claim that may be made by its manufacturer, is not guaranteed or endorsed by the publisher.

Copyright © 2021 Tinkhauser and Moraud. This is an open-access article distributed under the terms of the Creative Commons Attribution License (CC BY). The use, distribution or reproduction in other forums is permitted, provided the original author(s) and the copyright owner(s) are credited and that the original publication in this journal is cited, in accordance with accepted academic practice. No use, distribution or reproduction is permitted which does not comply with these terms.



Dopaminergic Modulation of Spectral and Spatial Characteristics of Parkinsonian Subthalamic Nucleus Beta Bursts

Matthias Sure^{1*}, Jan Vesper², Alfons Schnitzler^{1,3} and Esther Florin^{1*}

¹ Institute of Clinical Neuroscience and Medical Psychology, Medical Faculty, Heinrich-Heine University Düsseldorf, Düsseldorf, Germany, ² Department of Functional Neurosurgery and Stereotaxy, Medical Faculty, University Hospital Düsseldorf, Düsseldorf, Germany, ³ Department of Neurology, Center for Movement Disorders and Neuromodulation, Medical Faculty, Heinrich Heine University Düsseldorf, Düsseldorf, Germany

OPEN ACCESS

Edited by:

Doris D. Wang,
University of California,
San Francisco, United States

Reviewed by:

Ignacio Delgado Martinez,
Hospital del Mar Medical Research
Institute (IMIM), Spain
Gerd Tinkhauser,
Bern University Hospital, Switzerland
Simon J. Little,
University College London,
United Kingdom

*Correspondence:

Matthias Sure
Sure.Matthias@hhu.de
Esther Florin
Esther.Florin@hhu.de

Specialty section:

This article was submitted to
Neural Technology,
a section of the journal
Frontiers in Neuroscience

Received: 12 June 2021

Accepted: 08 October 2021

Published: 11 November 2021

Citation:

Sure M, Vesper J, Schnitzler A
and Florin E (2021) Dopaminergic
Modulation of Spectral and Spatial
Characteristics of Parkinsonian
Subthalamic Nucleus Beta Bursts.
Front. Neurosci. 15:724334.
doi: 10.3389/fnins.2021.724334

In Parkinson's disease (PD), subthalamic nucleus (STN) beta burst activity is pathologically elevated. These bursts are reduced by dopamine and deep brain stimulation (DBS). Therefore, these bursts have been tested as a trigger for closed-loop DBS. To provide better targeted parameters for closed-loop stimulation, we investigate the spatial distribution of beta bursts within the STN and if they are specific to a beta sub-band. Local field potentials (LFP) were acquired in the STN of 27 PD patients while resting. Based on the orientation of segmented DBS electrodes, the LFPs were classified as anterior, postero-medial, and postero-lateral. Each recording lasted 30 min with (ON) and without (OFF) dopamine. Bursts were detected in three frequency bands: ± 3 Hz around the individual beta peak frequency, low beta band (IBB), and high beta band (hBB). Medication reduced the duration and the number of bursts per minute but not the amplitude of the beta bursts. The burst amplitude was spatially modulated, while the burst duration and rate were frequency dependent. Furthermore, the hBB burst duration was positively correlated with the akinetic-rigid UPDRS III subscore. Overall, these findings on differential dopaminergic modulation of beta burst parameters suggest that hBB burst duration is a promising target for closed-loop stimulation and that burst parameters could guide DBS programming.

Keywords: beta bursts, directional leads, local field potentials, closed-loop DBS, Parkinson's disease

INTRODUCTION

Increased beta band activity in the subthalamic nucleus (STN) is considered to be a hallmark of Parkinson's disease (PD): It correlates with motor symptoms and is reduced by dopaminergic medication or deep brain stimulation (DBS) in the STN (Ray et al., 2008; Kühn et al., 2009). Recent evidence points to beta activity occurring in phasic bursts in the cortex (Lobb, 2014;

Abbreviations: STN, subthalamic nucleus; PD, Parkinson's disease; DBS, deep brain stimulation; UPDRS III, motor Unified Parkinson's Disease Rating Scale; IBB, low beta band; hBB, high beta band; iBP, individual beta peak frequency.

Feingold et al., 2015) and within the STN (Tinkhauser et al., 2017a,b). These transient bursts have been suggested to indicate episodes of long-range synchronization in the basal ganglia-cortical circuit (Tinkhauser et al., 2018; Cagnan et al., 2019). Moreover, beta bursts can be used as a feedback signal for closed-loop DBS to improve the stimulation outcome, highlighting their clinical relevance (Arlotti et al., 2018; Velisar et al., 2019). As closed-loop stimulation is still under investigation, different approaches for the feedback signal have been proposed (Swann et al., 2011; Abosch et al., 2012; Lettieri et al., 2012; Little et al., 2013; Priori et al., 2013; Neumann et al., 2014; Qasim et al., 2016; Arlotti et al., 2018; Velisar et al., 2019). In the case of beta bursts, it is not known which burst properties lead to the best clinical outcome if they are used as feedback signal for closed-loop DBS.

Using directional DBS leads as opposed to the spatially unspecific omnidirectional leads we investigate the spatial distribution of STN bursts and analyze whether their characteristics differ within the functional subsystems of the STN. Spatially and functionally, the STN itself can be subdivided into three parts corresponding to the motor, limbic, and associative system (Haynes and Haber, 2013). We also aim for a more precise characterization of STN beta bursts along the frequency dimension. Previously it was demonstrated that PD severity as measured by the motor Unified Parkinson's Disease Rating Scale (UPDRS III) score, on the one hand, correlates positively with the spectral power in the low beta band (IBB) (Neumann et al., 2016). On the other hand, it correlates positively with the temporal stability of the amplitude in the high beta band (hBB) (Little et al., 2012). At the same time, most PD patients have one spectral power peak in the beta band at an individual frequency (iBP).

Finally, we investigate the effect of dopaminergic medication on STN beta bursts and the relation between burst characteristics and the UPDRS III score. As dopamine alleviates the motor symptoms, a change in burst characteristics due to dopamine would highlight their pathological nature. Such pathological burst parameters would be a good target signal for closed-loop DBS and instrumental to optimize closed-loop STN-DBS.

MATERIALS AND METHODS

Subjects and Surgery

In total 27 (8 female) PD patients (age: 59.0 ± 8.7 years) undergoing surgery for therapeutic STN-DBS in both hemispheres were recruited for this study. Patients had been selected for DBS treatment according to the guidelines of the German Society for Neurology. The Edinburgh Handedness score (81.1 ± 27.0) showed a clear preference for the right side, whereas the side of the main PD impairment was not lateralized (left = 12, right = 12, equal = 3), which was determined by a laterality score based on the UPDRS part III score (Goetz et al., 2008; Heinrichs-Graham et al., 2017). The UPDRS score was assessed 2 days before surgery OFF and ON dopaminergic medication (in the following: OFF and ON).

Written informed consent was obtained from all participants. The study was approved by the local ethics committee

(study no. 5608R) and conducted in accordance with the Declaration of Helsinki. DBS electrodes with directional leads were implanted within the dorsal part of each STN at the Department of Functional Neurosurgery and Stereotaxy in Düsseldorf. The implanted DBS electrodes used were the St. Jude Medical Directional lead 6172 (Abbott Laboratories, Lake Bluff, United States) and in one case the Boston Scientific Vercise segmented lead (Boston Scientific Corporation, Marlborough, United States). To enable LFP measurements, the implanted DBS electrodes were externalized using the St. Jude Medical Directional extension 6373 (Abbott Laboratories, Lake Bluff, United States).

The entry point of the STN was identified based on intraoperative microelectrode recordings (Sterio et al., 2002; Moran et al., 2006; Hartmann et al., 2018). Only the height of directional contacts that matched the STN entry point was selected for further analysis. We thus selected only three out of six possible directional contacts, but ensured that the selected contacts were in a comparable anatomic position. Due to a radiopaque marker on the electrode, we identified the segmented contacts facing the anterior, postero-medial, and postero-lateral orientation based on two orthogonal x-ray images. We compared the contacts selected based on the STN entry with the contacts that showed the best clinical outcome. The contact of the best clinical outcome was determined 3–6 months after stimulator implantation and characterized by the best clinical effect due to DBS without any side effects as ascertained by a clinician. In 38% of the cases, the selected contacts were at the height of the clinically chosen contact for therapeutic DBS.

Subthalamic nucleus recordings of four hemispheres were excluded from further analysis because intraoperative microelectrode measurements showed no typical STN activity or the electrode orientation was not visible on the available x-ray images. Additionally, the LFPs of one patient could not be included due to excessive artifacts of unknown origin. In the end, we included LFP recordings from 44 STNs of 24 patients in our analysis.

Experimental Setup and Recordings

The measurement took place 1–3 (1.3 ± 0.8) days after surgery. The externalized DBS electrodes were connected to an EEG amplifier. All patients were asked to sit relaxed and still. The data were recorded with a sampling rate of 2,400 Hz and a low-pass filter of 800 Hz was applied. The LFP signals were measured against a reference electrode placed at the mastoid. To ensure that patients did not fall asleep, we used an eye tracker, tracking the pupil diameter.

We recorded resting-state activity in three consecutive blocks of 10 min in two conditions for a total of 60 min: once OFF and once ON medication. OFF medication PD oral medication was withdrawn overnight for at least 12 h. In case a patient had an apomorphine pump, this pump was stopped at least 1 h before the measurement. After the three OFF measurement blocks, patients received 1.5 times their levodopa morning dose in the form of rapidly acting dispersible levodopa (173.0 ± 48.9 mg). To ensure a stable ON, we waited for at least 30 min and tested the clinical symptoms before the second half

of the measurement. One patient could only be measured ON medication and one only OFF.

Signal Processing

All data processing and analyses were performed using MATLAB (version R 2016b; MathWorks, Natick, United States). Custom-written MATLAB scripts and the toolbox Brainstorm¹ (Tadel et al., 2011) were used. To ensure artifact-free data, two persons independently inspected the data visually, cleaned artifacts, and compared the cleaned output. In case of differences, the questioned time segment was rejected. The line noise was removed from all channels with a notch filter with a 3-dB bandwidth of 1 Hz at 50, 100, 150, ..., 550, and 600 Hz. The LFP recordings from the DBS electrode were re-referenced against the mean of all LFP channels. Noisy or flat LFP channels were excluded from further analysis. Time segments containing artifacts were removed from the time series, but if artifacts just occurred frequently in one channel, only this whole channel was removed. All data were high-pass filtered with 1 Hz to remove movement-related artifacts. Furthermore, the data were down-sampled to 1,000 Hz. To avoid the influence of different impedance values between patients and recording sessions, we finally calculated the z-transformation of the preprocessed time series separately for each recording session.

Detection of Bursts in the Beta-Frequency Range

Within the beta band, different activity patterns have been described for the lower and higher beta-frequency range (Priori et al., 2004; Kühn et al., 2006). As the definition and segmentation of the beta band differ among research groups, we decided to divide the beta band into a lower and a higher sub-band of equal size (12–24 Hz and 24–35 Hz). Moreover, we considered a ± 3 -Hz band around the iBP (mean \pm SD: 22.1 \pm 5.8 Hz) of each patient. The iBP was determined OFF medication based on the beta peak in the individual power spectrum. For this purpose, the power spectrum in the beta band was examined for local maxima. In case the maximum was at the corner frequencies of 12 Hz or 35 Hz, the amplitude at 11 or 36 Hz needed to be lower for the iBP to be considered at 12/35 Hz. The maximum with the highest amplitude in all contacts of one patient was considered as iBP frequency. ON medication, the beta peak was generally reduced or vanished completely for some patients. In case a peak was still visible ON medication, it was always within 1 Hz of the OFF peak, i.e., covered by our ± 3 -Hz interval. The power spectra were determined based on the z-score normalized time series with 1-Hz resolution using the Welch method with a window length of 1 s and an overlap of 50% (Welch, 1967). To compare different spectra, we corrected for the 1/f characteristic of the LFP signal and normalized to the total power of 5–45 Hz and 55–95 Hz analog to Neumann et al. (2016).

The preprocessed LFP data were used to detect bursts within the two beta sub-bands and the iBP. Our approach follows Tinkhauser et al. (2017a, 2017b), but we determined the bursts based on the z-value normalized data rather than the raw

data. Afterward, following the burst detection approach by Tinkhauser et al. (2017a, 2017b), Morlet wavelets (Tallon-Baudry et al., 1997) as implemented in Brainstorm were calculated for the IBB, the hBB, and around the iBP. The time-evolving amplitude was smoothed by a 200-ms moving average, followed by a DC-offset correction with a time constant of 20 s to correct for a potential baseline offset. For each patient, channel, and frequency, we calculated the 75th percentile of the OFF and ON time series and took the average of both of them. The separate z-score normalization of the LFP data OFF and ON medication could potentially mask the differences in the burst amplitudes between OFF and ON. Despite the z-value normalization, there were significant differences in beta power. Moreover, the bursts were detected based on a common threshold from the combined ON and OFF recording, which ensures that differences in burst amplitude between OFF and ON can be detected.

For a time point to be part of a burst in the respective frequency band, the amplitude needed to be higher than the 75th percentile. All consecutive time points with an amplitude exceeding the threshold were assigned to the same burst. The minimal burst duration was set to 80 ms, which is equivalent to two oscillatory cycles at 24 Hz. For every burst, the time point of the amplitude crossing the threshold and again dropping below were stored. The value of the maximum burst amplitude and its time of occurrence were also stored. Due to the applied burst detection scheme, we are referring to the power based on the z-score transformed time series and not to the power of the raw time series when we are considering the burst amplitude.

Statistical Analysis

For the number of bursts per minute which is calculated by the total number of bursts detected for one channel divided by the total recording time in minutes (in the following: burst rate), burst duration, and amplitude, we compared the recording orientation of the LFP contacts, frequency band, and the medication state. Therefore, we performed a three-way ANOVA (Yates, 1934) in MATLAB. The dependent variables were burst rate, duration, and amplitude, respectively, and the independent variables were directions (anterior, postero-medial, and postero-lateral), frequency bands (iBP, IBB, and hBB), and medication states (OFF and ON). Because the correlation of the burst parameters between the hemispheres was partially significant, but a paired *t*-test showed no significant differences between hemispheres, the evidence on hemisphere dependence is inconclusive. Following the previous literature (Zavala et al., 2017), we opted to pool both hemispheres. Therefore, the incoming sample size for ANOVA was the total number of good LFP data by orientation (anterior: OFF and ON each of the 31 LFPs; postero-medial: OFF and ON each of the 37 LFPs; postero-lateral: OFF 31 LFPs and ON 32 LFPs). For the *post hoc* test, a *t*-test was used, which was corrected for multiple comparisons using the Bonferroni method, again using the MATLAB implementation. We corrected for two medication states, three frequency bands, and three contact directions for a total of 18 comparisons.

¹<http://neuroimage.usc.edu/brainstorm/Introduction>

Finally, the Pearson correlation between the akinetic/rigid (AR) UPDRS III subscore (sum of the 13 items 3.3 a–c, 3.4 ab, 3.5 ab, 3.6 ab, 3.7 ab, and 3.8 ab) and the beta burst characteristics, as well as the power values from the power spectra, were calculated OFF medication. All reported correlation p -values are Bonferroni corrected for the three contact orientations and the three frequency bands.

RESULTS

Beta Power

Figure 1 displays the average power spectra OFF and ON medication across patients for the three different LFPs at the STN entry from 5 to 35 Hz. The power spectra are $1/f$ corrected and normalized to the total power of 5–45 Hz and 55–95 Hz. There were no significant differences between power of the different recording orientations in each medication condition but between the power OFF and ON medication. The difference was significant in the anterior direction from 32 to 34 Hz, the postero-medial one from 24 to 28 Hz, and the postero-lateral one from 31 to 34 Hz. Beta peaks OFF medication occurred mainly around 24 Hz at the anterior and postero-medial contact (**Figure 1**). As the beta peak frequency differed between the recording directions, we investigate in the following to what extent the recording orientation and frequency band influence beta bursts.

Burst Characteristics

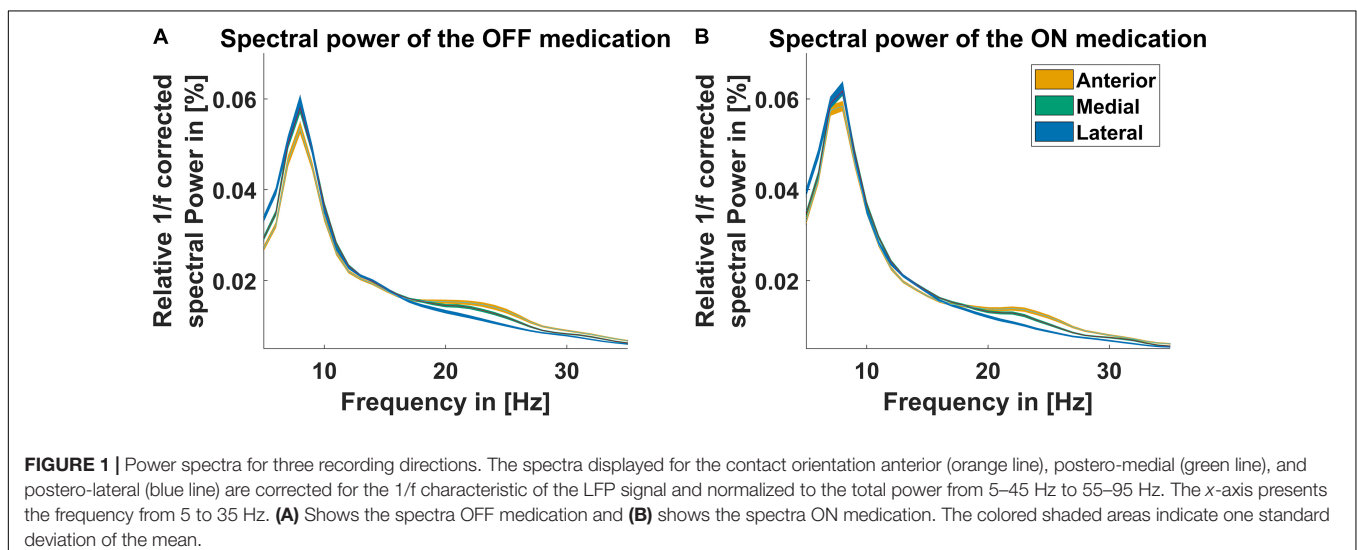
Figure 2 illustrates characteristics of STN beta bursts depending on medication state, pre-defined frequency band, and electrode contact orientation. Panel A displays the burst rate for the two medication states, the three contact orientations, and frequency bands. Medication had a significant main effect indicating that dopaminergic medication decreased the burst rate for all orientations and frequency bands [$F(1,579) = 97.1$, $p = 2.8E-21$, $\eta^2p = 0.144$]. This was also evident in the *post hoc* test for

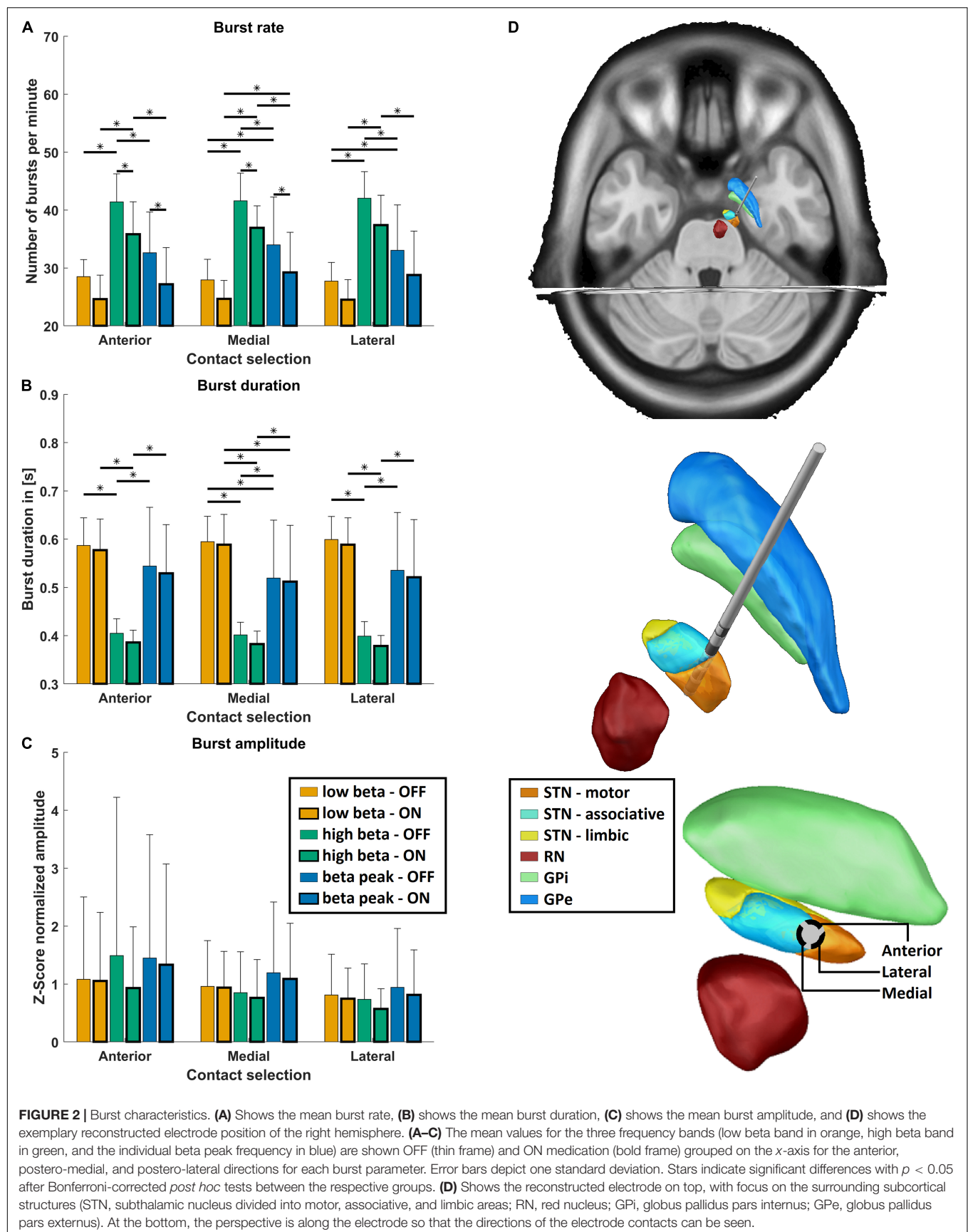
the hBB and iBP in anterior and postero-medial orientation ($p < 0.05$). Thus, a high burst rate seems to be a characteristic of PD pathology. In addition, there was a significant main effect of frequency for the burst rate [$F(2,579) = 283.9$, $p = 1.2E-86$, $\eta^2p = 0.495$] but no significant main effect of the contact orientation. Based on *post hoc* tests, the hBB burst rate was higher compared to the lBB and the iBP for all contact orientations and both medication states ($p < 1.0E-6$; **Figures 2A,B**). The rate at the iBP was only significantly higher compared to the lBB OFF medication for the postero-medial and postero-lateral direction and ON medication only for the postero-medial direction ($p < 0.05$; **Figure 2A**).

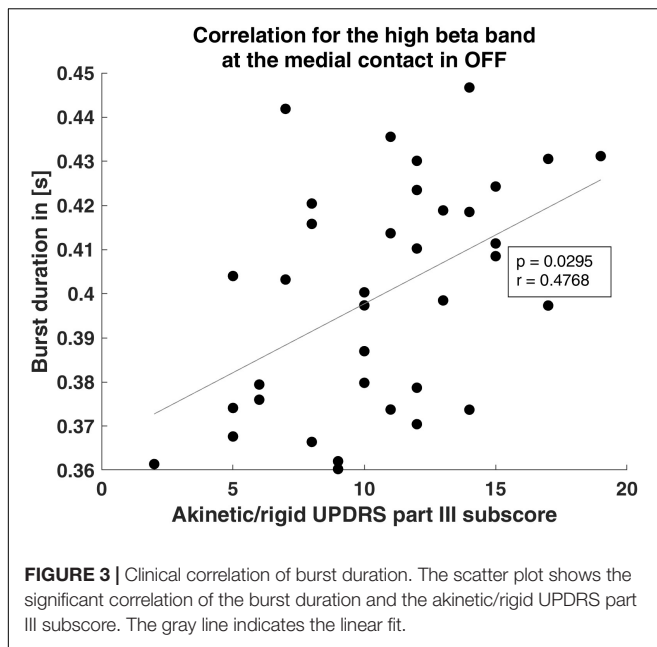
Medication had also a significant main effect for burst duration, which was reduced due to dopaminergic medication [$F(1,579) = 4.6$, $p = 0.03$, $\eta^2p = 0.144$], which can be seen in **Figure 2B**. Moreover, the burst duration was influenced by the frequency band but not by the contact orientation [$F(2,579) = 341.6$, $p = 1.0E-98$, $\eta^2p = 0.495$]. *Post hoc* analysis revealed that the burst duration was significantly shorter for the hBB compared to the lBB as well as the iBP in both medication states ($p < 1.0E-7$; **Figures 2C,D**). The burst duration was also significantly shorter at the iBP compared to the lBB ($p < 0.01$; **Figures 2C,D**) but only for the postero-medial direction both OFF and ON medication. Interestingly for the burst amplitude, the contact orientation had a significant main effect across medication states and frequency bands [$F(2,579) = 6.7$, $p = 0.001$, $\eta^2p = 0.003$] but not for the medication and frequency itself.

Clinical Relevance of Burst Characteristics

Because a positive correlation between bradykinesia and overall beta oscillations has previously been reported (Ray et al., 2008), we tested whether beta burst characteristics correlate with the AR UPDRS subscore. We focused on the AR UPDRS subscore, because, based on the UPDRS score, 70.4% of our patients were of the akinetic-rigid subtype. The OFF hBB burst duration of







the postero-medial contact was significantly positively correlated with the OFF AR subscore ($p = 0.03$, $r = 0.48$; **Figure 3**). For the other contact orientations and frequency bands, there was no significant correlation.

DISCUSSION

To our knowledge, this is the first work to investigate the spatial characteristics of STN beta bursts recorded with directional electrodes. Spatially, we found a non-homogeneous distribution of the burst amplitude. However, we could not identify any outstanding direction with respect to the amplitude or the rate and duration of the bursts. However, the burst rate and duration in particular are frequency-dependent, which makes frequency selection very important for applications such as closed-loop DBS.

Slight Directionality of the Beta Burst Amplitude

It has been shown that for each patient, a preferential contact exists in terms of best clinical outcome and many patients benefit from directional stimulation (Gordon et al., 2017; Hartmann et al., 2019). Therefore, we wanted to identify whether beta burst properties differ between the three recording orientations and thus could serve as an indicator for stimulation selection. There was a main effect of recording orientation for burst amplitude. However, *post hoc* tests did not reveal one prominent direction for amplitude or any other measure. Therefore, based on our analysis, no particular anatomic direction can be recommended for directional DBS. The reason for this could be that all contacts used were placed in the dorsal end of the STN, which is functionally attributed to the motor system (Parent and Hazrati, 1995). Therefore, a comparable neurophysiological signal at all

contact orientations is plausible and suggests a homogeneous structure of this area. In line with this reasoning, the connectivity between STN and cortex is functionally organized based on the functional subareas of the STN (Lambert et al., 2012). Nevertheless, there is a significant main effect of direction for the burst amplitude. One possibility is that the anatomical dependence of the bursts will only reveal itself with a larger number of cases.

Beta Burst Activity Is Frequency Specific

We considered three different frequency bands within the beta band: the IBB, the hBB, and the frequency range around the individual beta peak frequency. The reason for this choice was that previous publications reported results specifically for sub-bands of the beta band (Priori et al., 2004; Little et al., 2012; Tinkhauser et al., 2017a,b). We found that burst characteristics differ depending on the chosen frequency band. The burst rate increases for higher frequencies, while the duration decreases. In line with this finding, the AR score correlated with the burst duration in the hBB but no other frequency band. In addition, duration was significantly reduced by dopaminergic medication only for the hBB and iBP. This suggests that bursts in the hBB are likely linked to the pathophysiology of PD, which is consistent with the results of Little et al. (2012). However, it contrasts with the results of Priori et al. (2004) and Neumann et al. (2016), but these studies considered beta power, not beta bursts. A pairwise test of power values compared to Priori et al. (2004) showed significant influence of dopaminergic medication on power in the hBB but not in the IBB.

To further investigate the importance of the frequency band definition, we performed our analysis with a modified frequency band definition, assigning the IBB to 12–20 Hz and the hBB to 21–35 Hz. When comparing the results for the two frequency band definitions, there were no differences with respect to significant findings for the medication dependence or the direction dependence of the burst parameters. However, while for the frequency band separation at 24 Hz there were no significant differences for the burst amplitude between the frequency bands, for the separation at 20 Hz, there were significant differences in the burst amplitude between the IBB and iBP and between hBB and iBP for both medication states and all three directions. In addition, significant differences for burst rate and duration were found between the IBB and iBP. This change in findings based on the beta band separation is most likely due to beta peaks formerly assigned to the IBB now being assigned to the hBB with the separation at 20 Hz. This difference in results suggests that if a beta peak occurs in the power spectra, the frequency band around this peak should be favored for closed-loop stimulation for example; if no peak is present, our results indicate that the hBB could be a good alternative.

Burst Duration Best Suited as Stimulation Trigger in Closed-Loop Deep Brain Stimulation

Burst characteristics OFF medication are linked to the pathology of PD, while those ON medication approximate physiological

activity. As expected based on previous publications, we could find an effect of dopaminergic medication on beta bursts (Ray et al., 2008; Kühn et al., 2009; Tinkhauser et al., 2017a,b). Since we could detect a main effect only with respect to the duration and the rate of the bursts, this suggests that these are more pathologically altered by PD than the amplitude of the individual bursts. The burst amplitude is a necessary quantity for the burst detection method employed in the present study. However, according to our results it is less suitable for distinguishing between pathological and physiological bursts.

In contrast, it has previously been described that a long burst duration is being positively correlated and a short burst duration is being negatively correlated with clinical motor impairment (Tinkhauser et al., 2017a). In our study, only the duration significantly correlated with the AR score and the duration was reduced under medication. Therefore, burst duration seems to be more tightly linked to PD motor symptoms than the burst amplitude and rate. This suggests that the burst duration is the best candidate for a stimulation trigger in closed-loop DBS. This conjecture is in line with previous results that reduced burst duration is associated with improved movement velocity due to DBS (Kehnemouyi et al., 2020). However, since amplitude is the key parameter in burst detection, further studies are needed to understand the interplay of amplitude and burst duration for detecting pathological bursts and their usefulness as stimulation triggers in closed-loop DBS.

To use electrophysiological signals as control parameters for closed-loop DBS, they should remain stable over months and years. We recorded the LFP signals a few days after electrode implantation, when the tissue is still subject to transient processes such as inflammation, which may affect recording properties and neuronal activity. However, previous studies indicate that STN beta band LFP patterns and response profiles stay almost unchanged for years after DBS electrode implantation (Abosch et al., 2012; Giannicola et al., 2012). Moreover, beta activity continues to correlate with severity of PD motor symptoms 8 months after implantation (Neumann et al., 2017). Therefore, it is likely that the duration of beta bursts remains stable over a long period of time and thus provides a valid control parameter for closed-loop DBS. Still, the stability of beta burst duration over longer time periods needs to be investigated in future studies.

Limitations

Because we at the latest recorded the LFP data 3 days after the DBS surgery, our recordings might be affected by the stun effect (Chen et al., 2006). Due to the magnitude of the stun effect being unknown and immeasurable, it is impossible to correct the electrophysiological data for it. In line with other studies, the UPDRS values were collected before the DBS surgery and thus do not capture the stun effect on the clinical symptoms. This timing difference likely also influences the calculated correlation between the UPDRS and the beta burst parameters. A further limitation is our assumption that beta bursts in one STN arise independently from the other STN. Based on our data, the evidence on the STN activity being independent of the hemisphere was inconclusive. Our decision to pool the data

follows previous literature treating the LFPs of both STNs as independent (e.g., Zavala et al., 2017).

Conclusion

Using directional contacts, we intended to identify the spatial distribution of beta bursts at the entry point of the STN. However, based on the electrode's recording orientation, we could not identify one orientation with significantly different burst parameters than the other orientations, even though there was an overall effect of orientation for the burst amplitude.

Still, we could identify a strong frequency dependence of beta bursts. Correlation with the akinesia and rigidity scores indicates in particular that hBB burst duration is pathologically increased. In addition, dopaminergic medication influences burst rate and duration. These two findings speak in favor of the hBB bursts as feedback signal for stimulation in closed-loop DBS.

DATA AVAILABILITY STATEMENT

The raw data supporting the conclusions of this article will be made available by the authors, without undue reservation.

ETHICS STATEMENT

The studies involving human participants were reviewed and approved by the Ethics Committee, Medical Faculty, Heinrich Heine University Düsseldorf. The patients/participants provided their written informed consent to participate in this study.

AUTHOR CONTRIBUTIONS

MS: software, validation, formal analysis, investigation, data curation, writing—original draft, and visualization. JV: resources and writing—review and editing. AS: methodology, resources, and writing—review and editing. EF: conceptualization, methodology, validation, formal analysis, investigation, data curation, writing—review and editing, supervision, project administration, and funding acquisition. All authors contributed to the article and approved the submitted version.

FUNDING

EF gratefully acknowledges support by the Volkswagen Foundation (Lichtenberg program 89387). Computational support and infrastructure were provided by the “Centre for Information and Media Technology” (ZIM) at the University of Düsseldorf (Germany).

ACKNOWLEDGMENTS

The authors would like to thank Johannes Pfeifer for his critical review of the manuscript and fruitful discussions.

REFERENCES

- Abosch, A., Lanctin, D., Onaran, I., Eberly, L., Spaniol, M., and Ince, N. F. (2012). Long-term recordings of local field potentials from implanted deep brain stimulation electrodes. *Neurosurgery* 71, 804–814. doi: 10.1227/NEU.0b013e3182676b91
- Arlotti, M., Marceglia, S., Foffani, G., Volkmann, J., Lozano, A. M., Moro, E., et al. (2018). Eight-hours adaptive deep brain stimulation in patients with Parkinson disease. *Neurology* 90, e971–e976. doi: 10.1212/WNL.0000000000005121
- Cagnan, H., Mallet, N., Moll, C. K. E., Gulberti, A., Holt, A. B., Westphal, M., et al. (2019). Temporal evolution of beta bursts in the parkinsonian cortical and basal ganglia network. *Proc. Natl. Acad. Sci. U. S. A.* 116, 16095–16104. doi: 10.1073/pnas.1819975116
- Chen, C. C., Pogossyan, A., Zrinzo, L. U., Tisch, S., Limousin, P., Ashkan, K., et al. (2006). Intra-operative recordings of local field potentials can help localize the subthalamic nucleus in Parkinson's disease surgery. *Exp. Neurol.* 198, 214–221. doi: 10.1016/j.expneurol.2005.11.019
- Feingold, J., Gibson, D. J., Depasquale, B., and Graybiel, A. M. (2015). Bursts of beta oscillation differentiate postperformance activity in the striatum and motor cortex of monkeys performing movement tasks. *Proc. Natl. Acad. Sci. U. S. A.* 112, 13687–13692. doi: 10.1073/pnas.1517629112
- Giannicola, G., Rosa, M., Servello, D., Menghetti, C., Carrabba, G., Pacchetti, C., et al. (2012). Subthalamic local field potentials after seven-year deep brain stimulation in Parkinson's disease. *Exp. Neurol.* 237, 312–317. doi: 10.1016/j.expneurol.2012.06.012
- Goetz, C. G., Tilley, B. C., Shaftman, S. R., Stebbins, G. T., Fahn, S., Martinez-Martin, P., et al. (2008). Movement disorder society-sponsored revision of the unified Parkinson's disease rating scale (MDS-UPDRS): scale presentation and clinimetric testing results. *Mov. Disord.* 23, 2129–2170. doi: 10.1002/mds.22340
- Gordon, E. M., Laumann, T. O., Gilmore, A. W., Newbold, D. J., Greene, D. J., Berg, J. J., et al. (2017). Precision functional mapping of individual human brains. *Neuron* 95, 791–807.e7.
- Hartmann, C. J., Fliegen, S., Groiss, S. J., Wojtecki, L., and Schnitzler, A. (2019). An update on best practice of deep brain stimulation in Parkinson's disease. *Ther. Adv. Neurol. Disord.* 12:1756286419838096. doi: 10.1177/1756286419838096
- Hartmann, C. J., Hirschmann, J., Vesper, J., Wojtecki, L., Butz, M., and Schnitzler, A. (2018). Distinct cortical responses evoked by electrical stimulation of the thalamic ventral intermediate nucleus and of the subthalamic nucleus. *Neuroimage Clin.* 20, 1246–1254. doi: 10.1016/j.nicl.2018.11.001
- Haynes, W. I. A., and Haber, S. N. (2013). The organization of prefrontal-subthalamic inputs in primates provides an anatomical substrate for both functional specificity and integration: implications for basal ganglia models and deep brain stimulation. *J. Neurosci.* 33, 4804–4814. doi: 10.1523/JNEUROSCI.4674-12.2013
- Heinrichs-Graham, E., Santamaria, P. M., Gendelman, H. E., and Wilson, T. W. (2017). The cortical signature of symptom laterality in Parkinson's disease. *Neuroimage Clin.* 14, 433–440. doi: 10.1016/j.nicl.2017.02.010
- Kehnemouy, Y. M., Wilkins, K. B., Anidi, C. M., Anderson, R. W., Afzal, M. F., and Bronte-Stewart, H. M. (2020). Modulation of beta bursts in subthalamic sensorimotor circuits predicts improvement in bradykinesia. *Brain* 144, 473–486. doi: 10.1093/brain/awaa394
- Kühn, A. A., Doyle, L., Pogossyan, A., Yarrow, K., Kupsch, A., Schneider, G. H., et al. (2006). Modulation of beta oscillations in the subthalamic area during motor imagery in Parkinson's disease. *Brain* 129, 695–706. doi: 10.1093/brain/awh715
- Kühn, A. A., Tsui, A., Aziz, T., Ray, N., Brücke, C., Kupsch, A., et al. (2009). Pathological synchronisation in the subthalamic nucleus of patients with Parkinson's disease relates to both bradykinesia and rigidity. *Exp. Neurol.* 215, 380–387. doi: 10.1016/j.expneurol.2008.11.008
- Lambert, C., Zrinzo, L., Nagy, Z., Lutti, A., Hariz, M., Foltynie, T., et al. (2012). Confirmation of functional zones within the human subthalamic nucleus: patterns of connectivity and sub-parcellation using diffusion weighted imaging. *Neuroimage* 60, 83–94. doi: 10.1016/j.NEUROIMAGE.2011.11.082
- Lettieri, C., Rinaldo, S., Devigili, G., Pualetto, G., Verriello, L., Budai, R., et al. (2012). Deep brain stimulation: subthalamic nucleus electrophysiological activity in awake and anesthetized patients. *Clin. Neurophysiol.* 123, 2406–2413. doi: 10.1016/j.clinph.2012.04.027
- Little, S., Pogossyan, A., Kühn, A. A., and Brown, P. (2012). Beta band stability over time correlates with Parkinsonian rigidity and bradykinesia. *Exp. Neurol.* 236, 383–388. doi: 10.1016/j.expneurol.2012.04.024
- Little, S., Pogossyan, A., Neal, S., Zavala, B., Zrinzo, L., Hariz, M., et al. (2013). Adaptive deep brain stimulation in advanced Parkinson disease. *Ann. Neurol.* 74, 449–457. doi: 10.1002/ana.23951
- Lobb, C. J. (2014). Abnormal bursting as a pathophysiological mechanism in Parkinson's disease. *Basal Ganglia* 3, 187–195. doi: 10.1016/j.baga.2013.11.002
- Moran, A., Bar-Gad, I., Bergman, H., and Israel, Z. (2006). Real-time refinement of subthalamic nucleus targeting using Bayesian decision-making on the root mean square measure. *Mov. Disord.* 21, 1425–1431. doi: 10.1002/mds.20995
- Neumann, W.-J., Degen, K., Schneider, G.-H., Brücke, C., Huebl, J., Brown, P., et al. (2016). Subthalamic synchronized oscillatory activity correlates with motor impairment in patients with Parkinson's disease. *Mov. Disord.* 31, 1748–1751. doi: 10.1002/mds.26759
- Neumann, W. J., Huebl, J., Brücke, C., Gabriëls, L., Bajbouj, M., Merkl, A., et al. (2014). Different patterns of local field potentials from limbic DBS targets in patients with major depressive and obsessive compulsive disorder. *Mol. Psychiatry* 19, 1186–1192. doi: 10.1038/mp.2014.2
- Neumann, W.-J., Staub-Bartelt, F., Horn, A., Schanda, J., Schneider, G.-H., Brown, P., et al. (2017). Long term correlation of subthalamic beta band activity with motor impairment in patients with Parkinson's disease. *Clin. Neurophysiol.* 128:2286. doi: 10.1016/J.CLINPH.2017.08.028
- Parent, A., and Hazrati, L. N. (1995). Functional anatomy of the basal ganglia. II. The place of subthalamic nucleus and external pallidum in basal ganglia circuitry. *Brain Res. Rev.* 20, 128–154. doi: 10.1016/0165-0173(94)00008-D
- Priori, A., Foffani, G., Pesenti, A., Tamma, F., Bianchi, A. M., Pellegrini, M., et al. (2004). Rhythm-specific pharmacological modulation of subthalamic activity in Parkinson's disease. *Exp. Neurol.* 189, 369–379. doi: 10.1016/j.expneurol.2004.06.001
- Priori, A., Foffani, G., Rossi, L., and Marceglia, S. (2013). Adaptive deep brain stimulation (aDBS) controlled by local field potential oscillations. *Exp. Neurol.* 245, 77–86. doi: 10.1016/j.expneurol.2012.09.013
- Qasim, S. E., de Hemptinne, C., Swann, N. C., Miocinovic, S., Ostrem, J. L., and Starr, P. A. (2016). Electrocorticography reveals beta desynchronization in the basal ganglia-cortical loop during rest tremor in Parkinson's disease. *Neurobiol. Dis.* 86, 177–186. doi: 10.1016/j.nbd.2015.11.023
- Ray, N. J., Jenkinson, N., Wang, S., Holland, P., Brittain, J. S., Joint, C., et al. (2008). Local field potential beta activity in the subthalamic nucleus of patients with Parkinson's disease is associated with improvements in bradykinesia after dopamine and deep brain stimulation. *Exp. Neurol.* 213, 108–113. doi: 10.1016/j.expneurol.2008.05.008
- Sterio, D., Zonenshayn, M., Mogilner, A. Y., Rezaei, A. R., Kiprovski, K., Kelly, P. J., et al. (2002). Neurophysiological refinement of subthalamic nucleus targeting. *Neurosurgery* 50, 58–67. doi: 10.1097/00006123-200201000-00012
- Swann, N., Poizner, H., Houser, M., Gould, S., Greenhouse, I., Cai, W., et al. (2011). Deep brain stimulation of the subthalamic nucleus alters the cortical profile of response inhibition in the beta frequency band: a scalp EEG study in parkinson's disease. *J. Neurosci.* 31, 5721–5729. doi: 10.1523/JNEUROSCI.6135-10.2011
- Tadel, F., Baillet, S., Mosher, J. C., Pantazis, D., and Leahy, R. M. (2011). Brainstorm: a user-friendly application for MEG/EEG analysis. *Comput. Intell. Neurosci.* 2011:879716. doi: 10.1155/2011/879716
- Tallon-Baudry, C., Bertrand, O., Delpuech, C., and Pernier, J. (1997). Oscillatory γ -band (30–70 Hz) activity induced by a visual search task in humans. *J. Neurosci.* 17, 722–734. doi: 10.1523/JNEUROSCI.17-02-00722.1997
- Tinkhauser, G., Pogossyan, A., Little, S., Beudel, M., Herz, D. M., Tan, H., et al. (2017a). The modulatory effect of adaptive deep brain stimulation on beta bursts in Parkinson's disease. *Brain* 140, 1053–1067. doi: 10.1093/brain/awx010

- Tinkhauser, G., Pogosyan, A., Tan, H., Herz, D. M., Kühn, A. A., and Brown, P. (2017b). Beta burst dynamics in Parkinson's disease off and on dopaminergic medication. *Brain* 140, 2968–2981. doi: 10.1093/brain/awx252
- Tinkhauser, G., Torrecillos, F., Duclos, Y., Tan, H., Pogosyan, A., Fischer, P., et al. (2018). Beta burst coupling across the motor circuit in Parkinson's disease. *Neurobiol. Dis.* 117, 217–225. doi: 10.1016/j.nbd.2018.06.007
- Velisar, A., Syrkin-Nikolau, J., Blumenfeld, Z., Trager, M. H., Afzal, M. F., Prabhakar, V., et al. (2019). Dual threshold neural closed loop deep brain stimulation in Parkinson disease patients. *Brain Stimul.* 12, 868–876. doi: 10.1016/j.brs.2019.02.020
- Welch, P. D. (1967). The use of fast fourier transform for the estimation of power spectra: a method based on time averaging over short, modified periodograms. *IEEE Trans. Audio Electroacoust.* 15, 70–73. doi: 10.1109/TAU.1967.1161901
- Yates, F. (1934). The analysis of multiple classifications with unequal numbers in the different classes. *J. Am. Stat. Assoc.* 29, 51–66. doi: 10.1080/01621459.1934.10502686
- Zavala, B. A., Jang, A. I., and Zaghloul, K. A. (2017). Human subthalamic nucleus activity during non-motor decision making. *Elife* 6:e31007. doi: 10.7554/eLife.31007

Conflict of Interest: AS has been serving as a consultant for Medtronic Inc., Boston Scientific, St. Jude Medical, and Grünenthal, and received lecture fees from AbbVie, Boston Scientific, St. Jude Medical, Medtronic Inc., and UCB.

The remaining authors declare that the research was conducted in the absence of any commercial or financial relationships that could be construed as a potential conflict of interest.

Publisher's Note: All claims expressed in this article are solely those of the authors and do not necessarily represent those of their affiliated organizations, or those of the publisher, the editors and the reviewers. Any product that may be evaluated in this article, or claim that may be made by its manufacturer, is not guaranteed or endorsed by the publisher.

Copyright © 2021 Sure, Vesper, Schnitzler and Florin. This is an open-access article distributed under the terms of the Creative Commons Attribution License (CC BY). The use, distribution or reproduction in other forums is permitted, provided the original author(s) and the copyright owner(s) are credited and that the original publication in this journal is cited, in accordance with accepted academic practice. No use, distribution or reproduction is permitted which does not comply with these terms.



A New Implantable Closed-Loop Clinical Neural Interface: First Application in Parkinson's Disease

Mattia Arlotti¹, Matteo Colombo¹, Andrea Bonfanti^{1,2}, Tomasz Mandat³, Michele Maria Lanotte^{4,5}, Elena Pirola⁶, Linda Borellini⁶, Paolo Rampini⁶, Roberto Eleopra⁷, Sara Rinaldo⁷, Luigi Romito⁷, Marcus L. F. Janssen^{8,9}, Alberto Priori¹⁰ and Sara Marceglia^{11*}

¹ Newronika SpA, Milan, Italy, ² Dipartimento di Elettronica, Informazione e Bioingegneria, Politecnico di Milano, Milan, Italy, ³ Narodowy Instytut Onkologii im. Marii Skłodowskiej-Curie, Warsaw, Poland, ⁴ Department of Neuroscience, University of Torino, Torino, Italy, ⁵ AOU Città della Salute e della Scienza, Molinette Hospital, Turin, Italy, ⁶ Fondazione IRCCS Ca' Granda Ospedale Maggiore Policlinico, Milan, Italy, ⁷ Movement Disorders Unit, Department of Clinical Neurosciences, Fondazione IRCCS Istituto Neurologico C. Besta, Milan, Italy, ⁸ Department of Neurology and Clinical Neurophysiology, Maastricht University Medical Center, Maastricht, Netherlands, ⁹ Faculty of Health, Medicine and Life Sciences, School for Mental Health and Neuroscience, Maastricht University, Maastricht, Netherlands, ¹⁰ Department of Health Sciences, Aldo Ravelli Research Center for Neurotechnology and Experimental Neurotherapeutics, University of Milan, Milan, Italy, ¹¹ Dipartimento di Ingegneria e Architettura, Università degli Studi di Trieste, Trieste, Italy

OPEN ACCESS

Edited by:

Coralie De Hemptinne,
University of Florida, United States

Reviewed by:

Ignacio Delgado Martinez,
Hospital Del Mar Medical Research
Institute (IMIM), Spain
Stefano Vassanelli,
University of Padua, Italy

*Correspondence:

Sara Marceglia
s.marceglia@units.it

Specialty section:

This article was submitted to
Neural Technology,
a section of the journal
Frontiers in Neuroscience

Received: 23 August 2021

Accepted: 04 November 2021

Published: 07 December 2021

Citation:

Arlotti M, Colombo M, Bonfanti A, Mandat T, Lanotte MM, Pirola E, Borellini L, Rampini P, Eleopra R, Rinaldo S, Romito L, Janssen MLF, Priori A and Marceglia S (2021) A New Implantable Closed-Loop Clinical Neural Interface: First Application in Parkinson's Disease. *Front. Neurosci.* 15:763235. doi: 10.3389/fnins.2021.763235

Deep brain stimulation (DBS) is used for the treatment of movement disorders, including Parkinson's disease, dystonia, and essential tremor, and has shown clinical benefits in other brain disorders. A natural path for the improvement of this technique is to continuously observe the stimulation effects on patient symptoms and neurophysiological markers. This requires the evolution of conventional deep brain stimulators to bidirectional interfaces, able to record, process, store, and wirelessly communicate neural signals in a robust and reliable fashion. Here, we present the architecture, design, and first use of an implantable stimulation and sensing interface (AlphaDBS^R System) characterized by artifact-free recording and distributed data management protocols. Its application in three patients with Parkinson's disease (clinical trial n. NCT04681534) is shown as a proof of functioning of a clinically viable implanted brain-computer interface (BCI) for adaptive DBS. Reliable artifact free-recordings, and chronic long-term data and neural signal management are in place.

Keywords: deep brain stimulation, neuromodulation, closed-loop, local field potential (LFP), Parkinson's disease, neural interface, implantable device

INTRODUCTION

Deep brain stimulation (DBS) device and implant design was developed on the learnings and advancements owned by cardiac pacemakers. After the first commercially DBS device approved by Food and Drug Administration for Parkinson's disease (PD) in 1997 (Paff et al., 2020), DBS technology did not witness significant advances, until recently, when new companies introduced technology innovations while entering the DBS market (Guidetti et al., 2021; Krauss et al., 2021). They include novel electrode designs and materials, stimulation waveforms, neural sensing capabilities, stimulation directionality, and battery size reduction with life extension (Krauss et al., 2021).

In particular, neural sensing is of critical importance to explore the pathophysiology of diseases targeted by DBS and, in turn, to develop new closed-loop devices (Starr, 2018; Gilron et al., 2021). In addition, a fully implantable device capable of bidirectional communication with the brain can be considered as a real brain-computer interface (BCI) implementation (Starr, 2018).

Signals recorded from DBS electrodes were used to gain insights into basal ganglia functioning both during intra-operative recording sessions and during peri-operative experimental settings [after the implant of the DBS electrode and before the connection of the implantable pulse generator (IPG)]. More specifically, local field potentials (LFPs), representing the compound activity of neuronal ensembles around DBS macroelectrode, are explored as a valuable feedback variable for closed-loop or adaptive DBS (aDBS) (Priori et al., 2013; Habets et al., 2018; Starr, 2018; Guidetti et al., 2021; Krauss et al., 2021).

In PD, oscillatory activity obtained by LFP recordings correlates with a range of symptomatic states (Brown, 2003; Priori et al., 2013; Arlotti et al., 2016a; Meidahl et al., 2017). These LFPs can be chronically recorded (Giannicola et al., 2012) and are modulated by DBS (Rossi et al., 2008; Giannicola et al., 2010; Eusebio et al., 2012). aDBS is coming closer to the clinical practice by increasing amount of proof of concept studies (Little et al., 2013, 2016a,b; Rosa et al., 2015, 2017; Piña-Fuentes et al., 2017; Arlotti et al., 2018; Swann et al., 2018; Velisar et al., 2019). LFPs have been proposed as a control variable for other pathologies including dystonia (Piña-Fuentes et al., 2020; Johnson et al., 2021), essential tremor (He et al., 2020; Opri et al., 2020), depressive and obsessive compulsive disorders (Neumann et al., 2014), and Tourette syndrome (Marceglia et al., 2017; Molina et al., 2017).

The first commercially available implantable neurostimulators with sensing capabilities was introduced for the treatment of epilepsy (Morrell and On behalf of the RNS System in Epilepsy Study Group, 2011). This device, which was then used for aDBS in Tourette syndrome (Molina et al., 2017), is able to record and analyze brain activity to provide a closed-loop stimulation. The aDBS strategy implemented follows the concept of “responsive neuromodulation” where stimulation is triggered on a determined event/episodes rather than being continuously administered. Although the paradigm of responsiveness is suitable for epilepsy or other disorders characterized by symptomatic episodes (i.e., Tourette), clinical applications as PD require continuous stimulation and simultaneous monitoring of the pathophysiological clinical state. The implementation of this type of devices, allowing continuous recording while stimulation is ON, faces a major challenge: recording signals having < 1 μ V amplitude in occurrence of > 1 V stimulation artifact (Arlotti et al., 2016b; Zhou et al., 2019). Embedding concurrent sensing and stimulation circuitry in an implantable device is further complicated by the power and size constraints.

Here, we present an implantable neurostimulator for LFPs-based aDBS (AlphaDBS^R System), where the sensing problem is fully addressed. We discuss preliminary results with regard to the

stimulation and sensing performances as tested in three patients with PD during a pilot study (clinical trial n. NCT04681534).

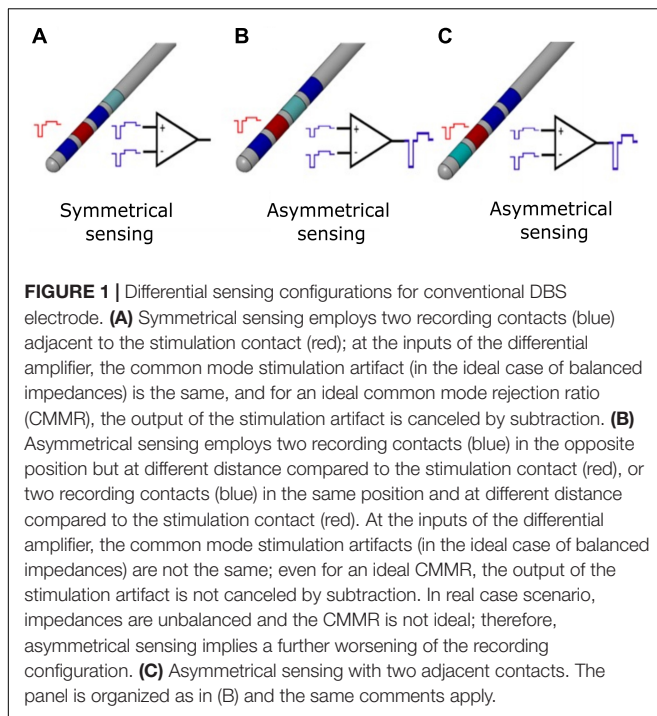
STATE OF THE ART AND INNOVATIVE REQUIREMENTS

Stimulation Design Inputs

In commercial systems for DBS treatment, stimulation parameters range from 0 to 25 mA of amplitude, from 10 to 450 μ s of pulse-width, and 2 to 500 Hz of frequency, provided both in monopolar and bipolar fashion (Paff et al., 2020). Empirical observations showed that, in PD, clinical benefits can be fully achieved with a narrower parameters space. For instance, when considering patients with PD, tremor, bradykinesia, and rigidity progressively improved between 2 and 3 V and did not continue to improve beyond 3 V (Moro et al., 2002) that, for an average monopolar impedance of 1,000 Ω , is equal to 3 mA. In the absence of lead damages, for platinum-iridium electrode with area of 0.06 cm², impedances may vary between 500 and 2 K Ω (Kuncel and Grill, 2004). In clinical practice, the amplitude threshold for inducing a clinical response or side effect for each electrode contact is determined by using monopolar stimulation and a stepwise increase in amplitude of 0.2–0.5 V (0.2–0.5 mA) (Volkman et al., 2002), thus requiring a minimum amplitude resolution of 0.2 mA. For STN stimulation, a 60- μ s pulse width is generally used because of its neurons' chronaxie, and it was empirically observed as being effective on rigidity and bradykinesia (Moro et al., 2002). Lowering the pulse width helps in augmenting the therapeutic window based on the intensity-pulse duration chronaxie relationship (Reich et al., 2015). Frequency stimulation above 200 Hz (Moro et al., 2002) did not show any notable improvements, whereas frequencies below 50 Hz generally worsen Parkinsonian symptoms (Wojtecki et al., 2006).

Despite specific parameters choice, because the electrical safety of the stimulation has to be guaranteed, intrinsic constraints depend on the material and geometries of the electrodes. Stimulation waveforms shall be charge balanced, in active/or passive manner for preventing electrode and tissue interface damage (Cogan et al., 2004). Moreover, intensity and pulse width combination shall be controlled, on the basis of electrode surface, to avoid excessive charge density injection per phase (Merrill et al., 2005). In particular, for conventional platinum-iridium electrodes (i.e., Model 3389, Medtronic), the limit for charge density is 30 μ C/cm²/phase.

In AlphaDBS System, the narrower parameter space (frequency of 50–200 Hz, pulse width of 40–250 μ s, and amplitude of 0–5 mA), with charge balanced waveforms and with specific controls allowing to reliably guarantee electrical safety, is considered as stimulation requirement for AlphaDBS, without introducing any specific innovation in the stimulation module, which is an established technology. The parameters space, however, could be suitable also for other potential DBS applications (e.g., dystonia or tremor). The sensing and data management modules are the places where innovation for bidirectional neural interfaces is needed.



Sensing Design Inputs

To implement aDBS, clinical IPGs need to record artifact-free neural activity during stimulation delivery.

Although external systems were able to solve the artifact rejection problem (Rossi et al., 2007; Arlotti et al., 2016b; Petkos et al., 2019), the size and power constraints of implantable operations make the rejection of stimulation artifact a technical implementation challenge. The stimulation artifact consists of direct components (stimulus time-locked voltage transients) and indirect components (voltage decay in the inter-pulse period) (Zhou et al., 2019). Direct artifacts at the adjacent recording electrodes are in the order of volts (common mode artifact) or hundreds of millivolts (differential mode artifact). In DBS applications, the differential artifact amplitude imposes a minimum input range of 100 mVpp, but real-world impedances mismatch may lead to greater values. The sensing module should avoid saturation for differential artifact greater than 100 mVpp while resolving 1- μ V signals. In fact, as reported in the literature, implantable DBS devices with sensing capabilities (i.e., Medtronic Activa PC + S) are not able to provide artifact-free meaningful recordings (Cummins et al., 2021). Symmetric electrode configuration (**Figure 1A**) with input blanking has been applied as means to mitigate the differential and common mode artifacts (Stanslaski et al., 2018), providing better artifact management (Cummins et al., 2021) but introducing a limitation in choosing the best stimulation configuration for the patient.

Any combinations of electrode contacts should be selectable for recording with respect to the stimulation one (**Figure 1**). In the absence of this requirement, given a conventional quadripolar linear DBS lead, the selection of the extreme contacts would deny recording possibilities, because of the unavailability of

recording contacts symmetrical to the stimulation one. Even worse, for directional leads (Eleopra et al., 2019), the electrode position together with the different area of directional contacts vs. cylindric contacts would lead both to unbalanced impedances and spatially asymmetrical recording contacts, thus deteriorating artifact rejection.

In case of clinical closed-loop DBS, a stimulation agnostic sensing module, able to reject the stimulation artifact independently from the stimulation shape and configuration (monopolar and bipolar), is preferable to freely set the most effective stimulation. The possibility to be stimulation agnostic depends on the artifact rejection strategy. For instance, employing input blanking techniques, as described in Stanslaski et al. (2018), limits the choice of the stimulus shape. Ideally, the pulse waveform should be actively charge balanced and symmetrical to minimize the time duration of the stimulus artifact and maximize the benefit of blanking. Conversely, in monophasic passively charge-balanced stimulation, the voltage decay of a single pulse may last for hundreds of microseconds, thus requiring to increase the duration of blanking and data loss.

An optimal sensing module should be also software needless, not requiring for additional software for artifact mitigation or removal. Back-end software solutions have been proposed and implemented in other devices ranging from interpolation (Zhou et al., 2019), support vector machines (Stanslaski et al., 2018), and template matching (Qian et al., 2017). Real-time processing on implantable devices requires computational power, which, as a rule of thumb, should be minimized, but as long as back-end solutions prove to be compatible with low-power real-time processing constraints, they can still be employed.

Therefore, the requirements of the AlphaDBS sensing module to implement a bidirectional deep brain neurostimulator are (1) resolving 1 μ V LFPs signals, (2) eliminating differential stimulus artifact (>100 mVpp) and common mode stimulus artifact (>1V), (3) being stimulation agnostic, (4) being electrode configuration independent, and (5) being needless for back-end processing. Requirements (3), (4), and (5) are innovative with respect to other available options of implantable DBS devices with sensing capabilities, altogether providing a reliable and robust system for artifact-free recordings.

Data Management Design Inputs

Having the object of accelerating neurophysiological research, a core requirement for a bidirectional IPG acting as a clinical BCI is to store and transmit neural signals. Although chronic data streaming represents a heuristic goal, its practical implementation still needs to overcome important limitations such as high-power demand, consequent fast battery drain, and maintenance of a permanent external receiver link; all these features ultimately add unnecessary burdens for patients. For instance, continuous data streaming with an implantable rechargeable device (Gilron et al., 2021) require the use of a transmitter that has to be continuously worn by the patient. Many bidirectional neuromodulation platforms are targeting chronic wireless communication (Zhou et al., 2019) at the preclinical or investigational stage.

A less power-consuming solution for chronic neural activity monitoring is to collect data in an embedded memory located inside the IPG. Its implementation requires to compress the neural data in their spectral features or any features being relevant under a clinical and neurophysiological perspective. The correct trade-off between the tracking needs and the size of the embedded memory is application specific. For instance, in PD, the beta power time course is linked to daily motor fluctuations of the patients (Arlotti et al., 2018; Gilron et al., 2021), thus suggesting that extracting the beta power band and continuously storing it could provide an efficient clinical monitoring. However, available devices have limited memories that are overwritten if data are not downloaded and therefore have time-limited monitoring capabilities (Jimenez-Shahed, 2021).

Embedding compressed data (i.e., spectral power) requires to have an *a priori* knowledge of what signal features are significant for the specific disease, but because of the exploratory application of clinical BCI, time domain data are necessary to the discovery of new biomarkers and physiological mechanisms of action. Moving from the concept of chronic monitoring to exploratory recording, the requirement of data wireless streaming can be relaxed by limiting it to on-demand and time-constrained streaming sessions that allow for controlled experimental investigations without burdening the patient.

The AlphaDBS System will therefore implement two innovative features: (1) the continuous real-time streaming and visualization of data to be used in experimental settings and (2) a long-term continuous recording of embedded data, with an innovative download strategy guaranteeing no data loss.

Processing Design Inputs

Adapting stimulation in real time requires to process a physiological variable and to calculate a new set of parameters based on a given relationship (proportional/adaptive mode) or a lookup table (digital mode or state machine). In the AlphaDBS System, the chosen requirement is to implement embedded data processing that ensures lower power consumption, better data privacy, and shorter time delays in stimulation changes, compared with external processing that, however, increases flexibility and research applicability (Pulliam et al., 2020).

Therefore, the AlphaDBS System is a fully closed-loop system, with an embedded algorithm that uses recorded LFPs as biomarker and adapts the stimulation amplitude accordingly, without the need of any external processing.

MATERIALS AND METHODS

AlphaDBS System Architecture

According to the requirement defined above, the AlphaDBS system (Figure 2) consists of four main components: an IPG (AlphaDBSipg), a patient controller (AlphaDBSPat), a physician controller (NWKStation), and an external device for data recording and streaming from externalized leads (AlphaDBSext). These components together implement a distributed data management platform for data recording, processing, streaming, and storing.

The AlphaDBSipg sensing is implemented in two modes: the “embedded” mode and the “streaming” mode. In the embedded mode, the IPG records and stores neural data during chronic treatment delivery (conventional DBS, cDBS, or aDBS) in an embedded not volatile memory. During stimulation (either cDBS or aDBS), the system extracts the power value of a selected frequency band and stores one value for each side every minute, two full spectra (from 5 to 35 Hz, one per side) every 10 min, and two values of the stimulation amplitude every 10 min. The patient controller downloads the data stored in the embedded memory of the IPG at every recharging cycle and stores them in a second not volatile memory having higher capacity. These data can be downloaded to a smartphone or laptop through a Bluetooth connection using dedicated custom application programming interfaces (APIs). At present, embedded data downloaded through the AlphaDBSpat are transferred to an app that implements a fast healthcare interoperability resource (FHIR)-based standard data management (ready for future interoperability) and allows historical data visualization and power spectral analysis (Figure 2B). In the streaming mode, the IPG, on demand, streams data to the physician programmer (NWKStation) that acts as a receiver and, in turn, transmits data via UART-to-USB connection to a smartphone or a laptop, which can be used for data storing and visualization thanks to custom APIs. Figure 2C shows the present implementation of a Python-based graphic user interface (GUI) that receives, visualizes, and saves real-time data.

The AlphaDBSipg has a total volume of 20.96 cc and weight of 32.70 g, with a medical grade rechargeable battery of 200 mA/h, retaining the 90% of the capacity at 2,000 cycles. The size is in line with other rechargeable DBS IPGs, such as Boston Scientific Vercise (volume of 20.7 cc and weight of 33 g) and Medtronic Activa RC (volume of 22 cc and weight of 40 g). The header is compatible with Medtronic DBS lead extensions model 37086, and it can allocate two extensions for a total of 16 independent contacts. The AlphaDBSipg electronic board has circuitry for driving 16 stimulation channels, each of them can be configured independently. The output current for each channel ranges from 0 to 5 mA. Multisite stimulation is possible by keeping the duration and the frequency of the pulses fixed. The stimulation waveform is firmware selectable, with both active and passive charge balancing available. In case of active return, the ratio between the cathode and the anode current amplitude is 5, leading to a balancing anodic pulse lasting five times the cathodic one. The AlphaDBSipg has been configured for providing capacitive coupled active charge balanced asymmetric pulses, with frequency ranging between 40 and 200 Hz and pulse width ranging between 40 and 250 μ s, despite that frequency can be extended to 2.5 KHz and pulse width to 1 ms. At 5 mA and 250 μ s, the charge density injected per phase is 20 μ V/cm²/phase, when considering a platinum-iridium electrode having a surface of 0.06 cm² (i.e., Model 3389, Medtronic, Inc.) and the maximum charge density injection accepted is 30 μ C/cm²/phase.

The AlphaDBSipg can deliver DBS both in the conventional mode (cDBS), in which stimulation parameters are set using the physician controller and remain fixed, and the adaptive

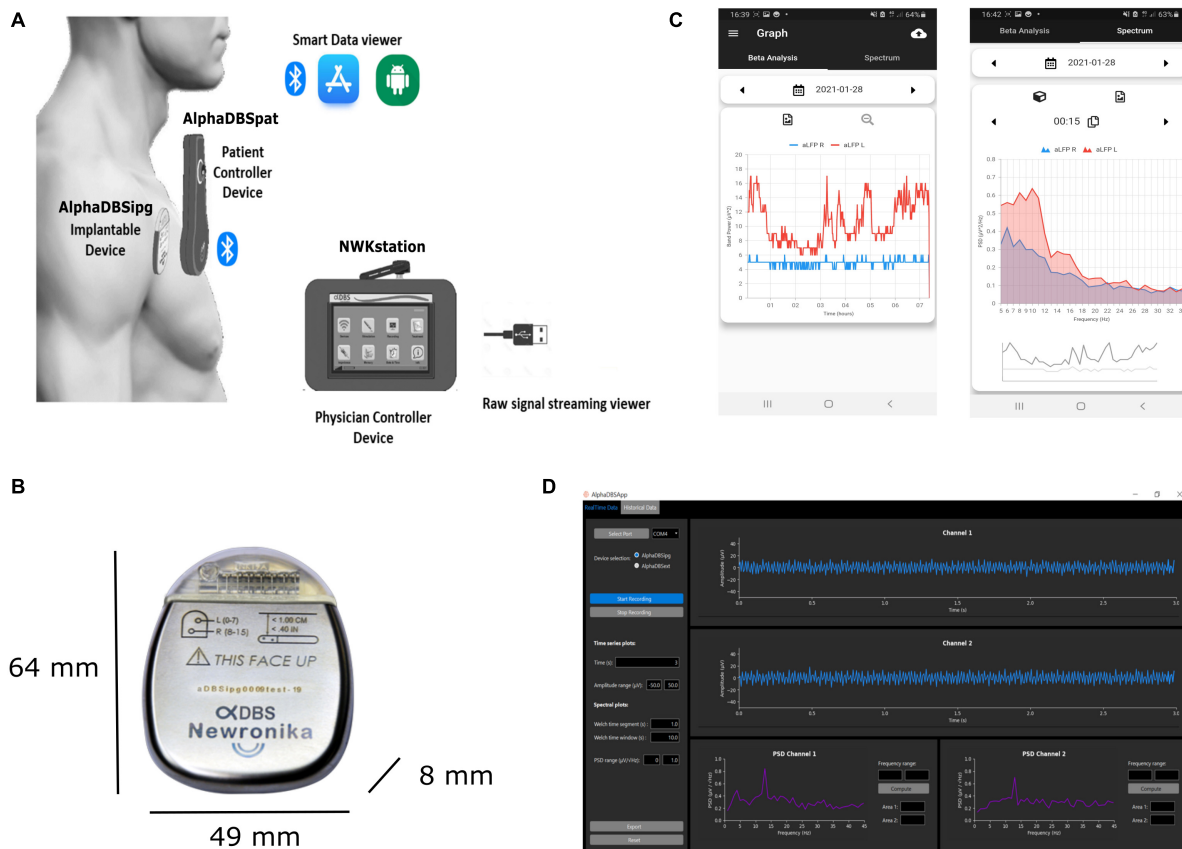


FIGURE 2 | AlphaDBS System architecture. **(A)** AlphaDBS System components: the AlphaDBSipg implantable device is recharged using a patient controller (AlphaDBSpat) that also allows downloading data and signals recorded using the embedded mode. A mobile app allows data visualization. The physician controller device (NWKstation) is used to program the AlphaDBSipg and to visualize LFPs recorded in the streaming mode. **(B)** AlphaDBSipg dimensions. **(C)** Screenshot of the mobile app showing beta band amplitude time changes (on the left) and power spectrum at a given time point (on the right). **(D)** Python-based GUI for real-time LFPs processing, visualization, and storing.

mode (aDBS). In this last case, stimulation amplitude, pulse width, and frequency are dynamically changed on the basis of the embedded closed-loop logic or pre-set *via* physician programmer and radio frequency (RF) communication. The closed-loop logic implementation now tested is based on the linear proportional feedback mode that uses the LFP beta band (10–35 Hz) as neurophysiological biomarker (Arlotti et al., 2018; Guidetti et al., 2021). In summary, the specific personalized beta band of the patient is chosen by inspecting recorded LFPs using the streaming mode. Then, both the personalized beta band and the therapeutic window are set in the physician controller. When aDBS is ON, the recorded beta band is analyzed and the DBS amplitude is modulated linearly between the maximum and minimum amplitudes set as therapeutic window (Arlotti et al., 2018; Prenassi et al., 2021). The closed-loop logic is fully embedded and implemented at the microcontroller firmware level and does not need for external units.

The inputs of two differential sensing channels can be multiplexed, respectively, on any of the eight contacts of each lead, and no blanking technique is used for artifact mitigation.

The neural signals, analogically filtered for artifact suppression, are digitally converted by the analogue to digital converter (ADC) at a frequency of 512 Hz. Residual harmonic artifacts, when not completely suppressed, require for a sample frequency being greater than the double of the stimulation frequency to avoid aliasing. No additional digital signal processing for artifact removal is needed. The firmware is fully employed for feature extraction and closed-loop logic implementation. This patented sensing technology was (Priori et al., 2005) already implemented and illustrated in external devices (Rossi et al., 2007; Arlotti et al., 2016b) that were used to collect preliminary data on aDBS in more than 40 patients (Rosa et al., 2015, 2017; Arlotti et al., 2018, 2019; Bocci et al., 2021; Prenassi et al., 2021).

A 2.4-GHz ISM/SRD chip allows data streaming of two sensed signals for a distance up to 10 m, firmware upgrade, and bidirectional communication with the patient and the physician controller. The firmware is upgradable through an on-air boot loading functionality.

The AlphaDBSipg has two different microcontrollers: one dedicated to the sensing module, and one to manage the stimulation module, the battery functions, and the RF streaming.

The AlphaDBS System received european (CE) mark for conventional DBS and sensing in January 2021.

System Use

Study Protocol and Surgery

The AlphaDBS system is undergoing clinical testing in a pilot multicenter randomized cross-over study on adaptive versus conventional DBS (aDBS vs. cDBS). All the details of the protocol are available on clinicaltrials.gov (study ID: NCT04681534). The study was approved by all regulatory authorities involved, and all the patients gave their informed consent to the study.

In summary, the study protocol is organized in two phases: the “short-term follow-up” (3 days in the hospital setting, 1 day for the system calibration + 1 day per each mode) and the “long-term follow-up” (1 month at home, 2 weeks per each mode). Patients with PD are screened from a population in need for IPG replacement for battery depletion if bilaterally treated using a Medtronic Activa PC or Activa RC IPG (mono-channel or dual channel) with DBS leads implanted in the STN (Model 3389) and extensions (Model 37806) compatible with the IPG of the AlphaDBS System (called AlphaDBSipg). The aDBS algorithm tested in this pilot study is the one reported in previous studies with external systems (Rosa et al., 2017; Arlotti et al., 2018).

During surgery for IPG replacement, after removal of the previously implanted device, *via* subclavicular incision, the DBS lead extensions were connected with a sterilized trial cable and an adapter to the external wireless recording device (AlphaDBSext) to test leads impedances and the presence of electrocardiographic artifact. After this check, the AlphaDBSipg was connected to Medtronic extensions with the patient under local anesthesia. In case of bilateral stimulation with two devices, the left DBS lead extension was replaced and transferred to the right side under general anesthesia to allow the replacement with a single IPG.

After IPG replacement, the impedances of each contact were measured again to ensure the absence of short/open circuits and also to confirm the consistency with the measurements done with the previous implant. Then, the new IPG was switched ON in continuous DBS (cDBS) with stimulation parameters selected in accordance with previous settings. In case of a previous voltage-controlled IPG, a simple translation to current on the basis of measured impedances parameter was performed following the Ohm's law. The response of the patient was clinically assessed (Unified Parkinson's Disease Rating Scale – part III in MedOFF/StimOFF and MedOFF/StimON) to further adjust stimulation parameters if needed.

Then, on days 2 and 3, patients entered the study protocol and underwent 2 days of stimulation, one in aDBS and one in cDBS (randomized), before being sent home for one additional month (2 weeks in aDBS and 2 weeks in cDBS, in the same order as during the short-term follow up).

Because the pilot study is still ongoing, here, we report only the results of neurophysiological recordings obtained from the first three patients enrolled. Clinical data cannot be reported until the end of the study.

In-Clinic Local Field Potential Data Collection

During hospitalization (short-term follow up), LFPs were recorded both in the streaming and in the embedded mode.

LFP streaming, as indicated in the design input, was limited to a short time window, whereas LFP recording using internal memory was always ON.

LFP streaming was used to choose the best contact pair to be used in chronic recording (calibration session on day 1). More specifically, LFPs were recorded and streamed out from all the possible contacts pairs (excluding the one used for stimulation) that, considering bilateral monopolar configuration, it includes six differential traces, three per side. The patients were in the MedOFF/StimOFF condition and were asked to stay in rest position during the data streaming. Each recording lasted 10 s, to minimize the time in which the patients experienced the return of motor symptoms (MedOFF/StimOFF condition). The power spectra were directly visualized for each trace, and the contact pair showing higher beta (10–35 Hz) activity was selected for chronic recording during DBS treatment. The recorded beta band is defined as ± 5 Hz from the peak frequency in the beta band (personalized beta band).

At the end of the experimental session with LFP data streaming, LFP chronic recording (embedded mode) was activated and consisted in storing physiological data inside the IPG on a not-volatile memory for chronic recording and offline downloading and processing. Embedded mode was switched ON continuously (except during LFP real-time streaming) and provided data for all days starting from day 1.

Signal Processing

LFPs recorded *via* RF streaming were imported and post-processed in MATLAB. The power spectral density (PSD) with a confidence interval of 95% of each 10-s time series was computed with the “pwelch” function using a rectangular window of 250 ms with 50% overlapping. The background neural activity was fitted between 4 and 40 Hz, as 1/f shaped noise, with the MATLAB function “robustfit.” Significant oscillatory activity was defined as the oscillatory activity whose power is above the neural background noise with a 95% confidence interval. A similar approach was used elsewhere, considering as true oscillations those being above 1/f noise of 0 or 0.5 standard deviation (Watrous et al., 2018; Goyal et al., 2021).

PSDs extracted from the embedded data were calculated as the average PSD in the ± 10 min interval around a clinical evaluation (Arlotti et al., 2018).

RESULTS

Local Field Potential Recordings

Here, we report the results of LFP recordings in the first three patients implanted with the AlphaDBS System and involved in the pilot study NCT04681534. All patients were previously implanted with Medtronic 3389 electrodes, having four cylindrical contacts per side (left side: contacts 0-1-2-3, where contact 0 represents the most ventral and contact 3

TABLE 1 | Details of data streaming in all patients.

Patient	% of samples lost during streaming	SNR Ch1 (log)	SNR Ch2 (log)	EKG artifact observed
01	1.93%	4.22	4.13	0 of 6 tracks
02	1.92%	4.03	4.06	0 of 6 tracks
03	2.35%	3.83	4.17	0 of 6 tracks

SNR, signal-to-noise ratio (log); EKG, electrocardiographic.

represents the most dorsal; right side: contacts 8-9-10-11, where contact 8 represents the most ventral and contact 11 represents the most dorsal).

Data streamed showed limited data loss (average 2%) and no cardiac artifact in any recordings (**Table 1**). The signal-to-noise ratio (SNR) calculated on the beta peak was always greater than three logs, suggesting an optimal recording performance (**Table 1**). Representative raw LFPs and the correspondent PSDs obtained during data streaming are reported in **Figure 3**. As shown in **Figure 3**, significant (see METHODS – Signal Processing for explanation of “significant”) beta peak was found in at least one side per each patient. More specifically, the highest beta band activity was found in patients 01, 02, and 03 in contact pair 0–2 (left side), 0–3 (left side), and 10–11 (right side), respectively.

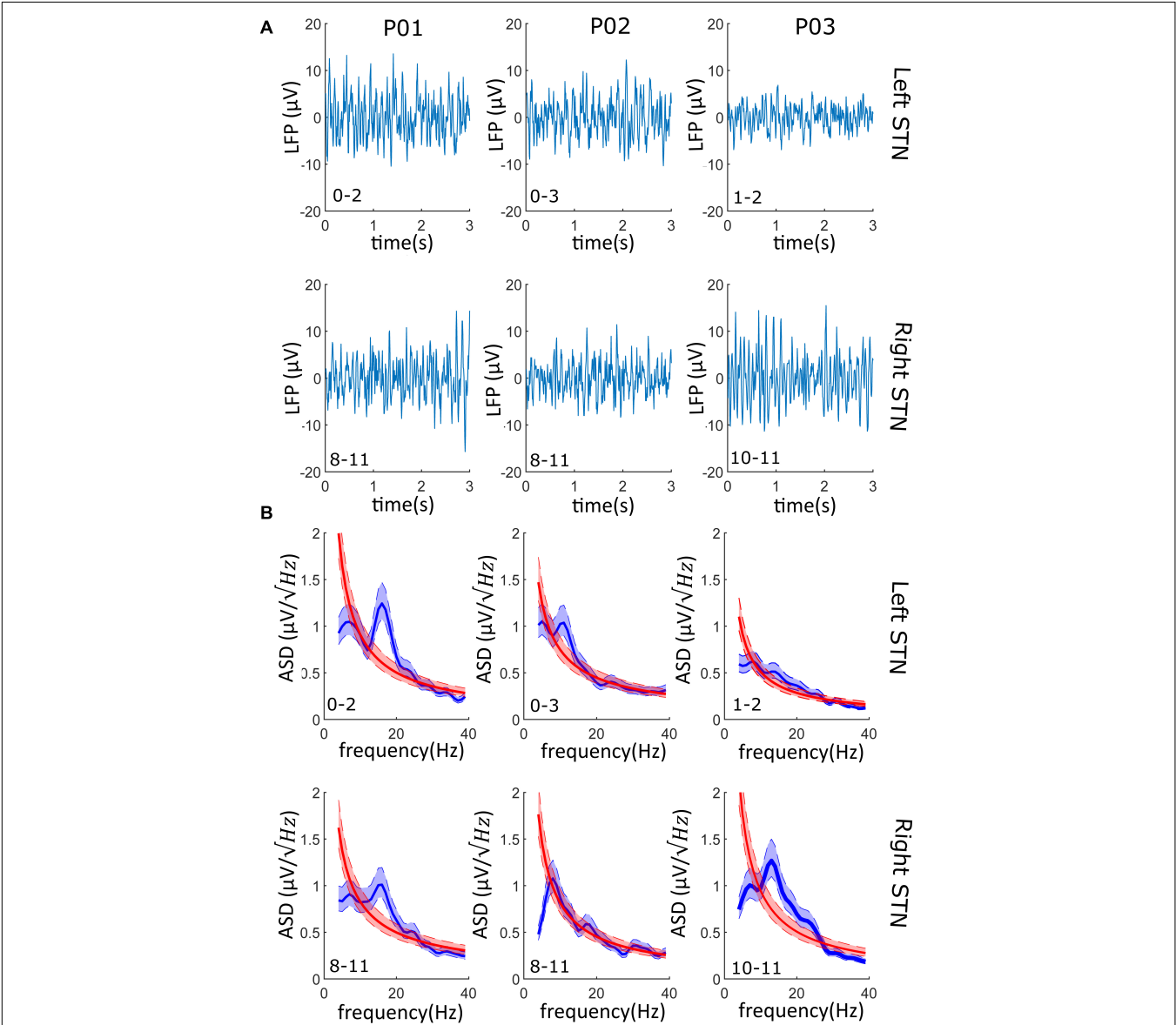


FIGURE 3 | LFPs from the streaming mode: **(A)** Left and right LFPs time series. 3-s LFPs recordings are shown for both the left and right STN of each patient; on the bottom left corner, the contact pair used for recording is reported (i.e., “0–2” and “8–11”). **(B)** The PSD of the LFPs recordings of panel (a) is shown (blue line) and superimposed to the PSD of the 1/f background noise (red line). 95% confidence interval is shadowed around the PSD average (lighter blue and lighter red overlapped band). In at least one side per patient (four of the six recordings), the beta oscillations have a significative higher power than the background neural noise.

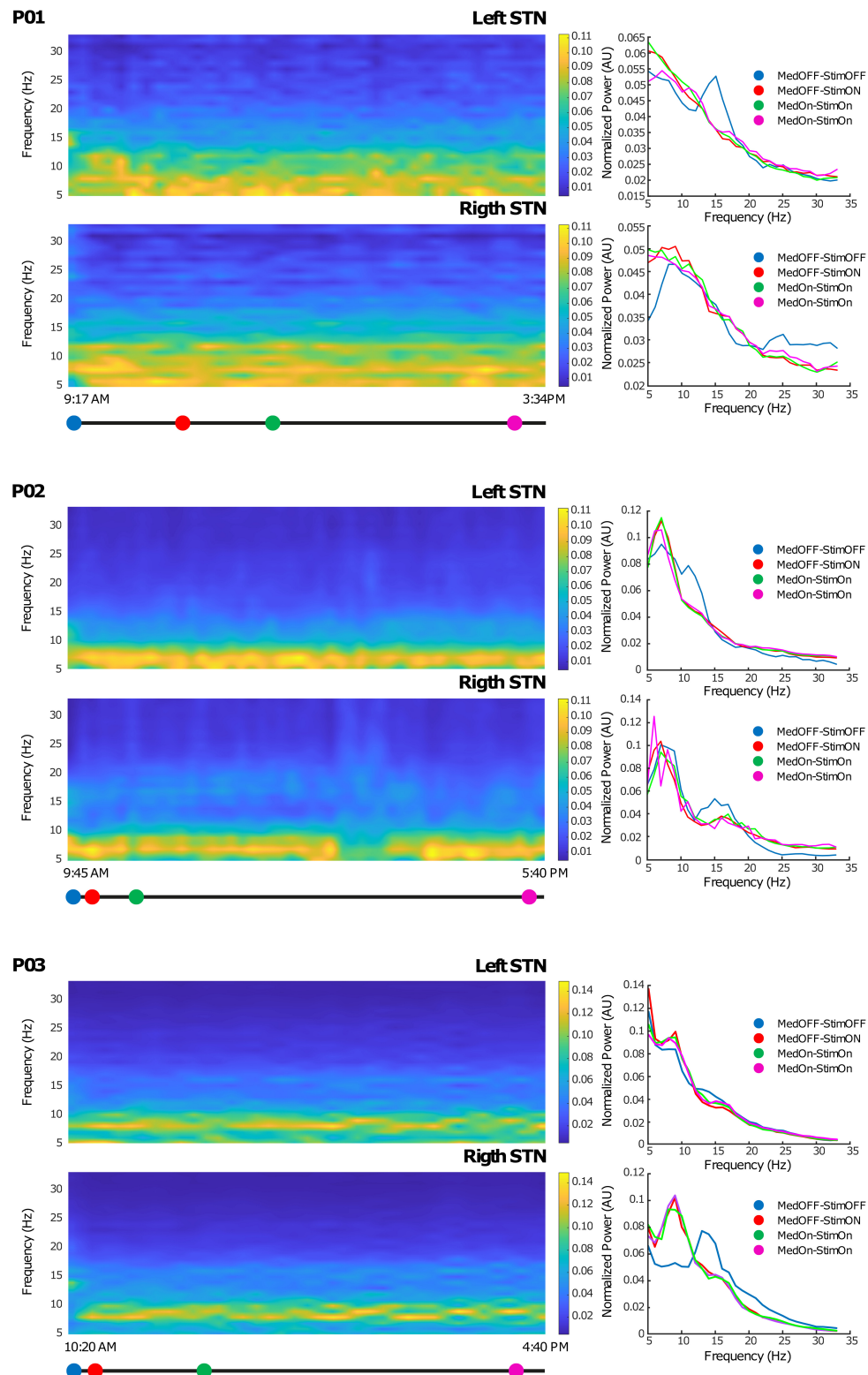


FIGURE 4 | Chronic LFP recordings in the embedded mode: Left side: Time-frequency plots of six representative hours. The x-axis represents time and the y-axis frequency (from 5 to 35 Hz). The colored dots (blue, red, green, and magenta) correspond to clinical evaluations at MedOFF/StimOFF, MedOFF/StimON, MedON/StimON, and MedON/StimON, respectively. Right side: Amplitude spectrum of the LFPs of both the left and right STN extracted as the mean of the ± 10 -min interval around the evaluation point (MedOFF/StimOFF, MedOFF/StimON, MedON/StimON, and MedON/StimON) obtained at the time indicated in the left side panels. Please note that, in MedOFF-StimOFF, a clear beta peak is present in the left STN of patients 01 and 02 and the right STN of patient 03. This beta peak was disappeared by the stimulation.

TABLE 2 | Parameter setting details.

Patient	Stim Config	Imp (k Ω)	Previous IPG (cDBS mode)				AlphaDBSipg (cDBS mode)			
			Amp (mA)	Freq (Hz)	PW (μ s)	TEED** (μ W)	Amp (mA)	Freq (Hz)	PW (μ s)	TEED** (μ W)
01	Left: C + 1–	0.84	4*	130	90	187	4	130	60	124
	Right: C + 9–	0.94	3.4*	130	90	143	3.5	130	60	90
02	Left: C + 1–	0.81	3.2*	130	60	80	2.4	130	60	45
	Right: C + 9–	0.86	2.4*	130	60	45	1.8	130	60	25
03	Left: C + 3–	1.47	2.5	130	60	49	3.0	130	60	70
	Right: C + 11–	0.96	2.3	130	60	41	2.5	130	60	49

*Previous implant voltage controlled. Current values were calculated using a simple translation to current on the basis of measured impedances parameter following Ohm's law.

**TEED calculated using nominal 1 k Ω impedance.

From the internal memory of the IPG, we downloaded the PSD of the contact pair selected from streamed LFPs, thus allowing a full monitoring of LFP fluctuation over time. The AlphaDBSipg stored the power spectrum every 10 min and downloaded it (together with the beta power value every minute and the stimulation value every 10 min) on the AlphaDBSpat at each recharging. **Figure 4** shows the time-frequency spectra during 6 h of chronic recordings in the short-term follow-up conducted in clinic for each of the three patients. As shown, the embedded mode provided high-quality data that were successfully used for closed-loop stimulation. Note that, for patients 01 and 02, the recording configuration was symmetric (stimulation contact between recording contacts), whereas for patient 03, it was asymmetric (stimulation contact outside recording contacts). Iterative storing and downloading allowed for chronic data collection, providing highlights on the system functioning in terms of beta power tracking, closed-loop implementation, and neurophysiological monitoring.

Stimulation Parameters

DBS parameter settings for all patients in cDBS mode are reported in **Table 2**. Despite the small number of patients, which prevents from running a statistical comparison, stimulation parameters were similar, for cDBS, using the AlphaDBSipg and the previously implanted IPG. The total electrical energy delivered per second (TEED) by AlphaDBSipg in cDBS was lower than the previous IPG in patient 01 (-116μ W), in patient 02 (-55μ W), and higher in patient 03 ($+29 \mu$ W) (see **Table 2**).

DISCUSSION

Here, the AlphaDBS system presented and tested in patients implements a distributed architecture, allowing data collection and management for interfacing with the deep neural system and presents several innovative features that, combined altogether, create a reliable platform for aDBS and closed-loop neuromodulation applications.

First, the system provides fully artifact-free recordings, but, unlike other devices, it is stimulation agnostic, electrode configuration independent, and needless for back-end processing. In fact, we found that the system was

capable to work both with different types of stimulation (different pulse widths in patient 01) and with asymmetric electrode configuration (as for patient 03). The stimulation artifact rejection has been achieved at the chip level (no blanking, no symmetrical sensing, and no back-end software) and not at the system level (Stanslaski et al., 2018). A further advantage of these features is that the IPG software is employed only for implementing the closed-loop strategy and not to mitigate the artifact, thus increasing the flexibility of the device for potential new closed-loop strategies that would not have to take care of artifact management.

The reliability of the sensing module is also demonstrated by the ability to provide a fully closed-loop aDBS in all patients: the performance of the sensing technology in rejecting the stimulation artifact allowed the implementation of the embedded linear proportional feedback aDBS, which is based on continuous sensing of beta band power, with consequent continuous adjustment of the stimulation amplitude in a proportional fashion (Arlotti et al., 2018; Guidetti et al., 2021), all done without any need of external processing. In addition, consistency between LFP features recorded through the AlphaDBS System and LFP features recorded in classical experimental settings was proved by the observation of a significant beta oscillatory activity detected in at least one contact pair for each patient and of a suppression of beta activity with concurrent reduction of the symptomatology during stimulation.

Second, data management has two major innovative features: (1) the capability to provide on-demand raw LFP streaming and (2) continuous embedded recording of a subset of data that are stored in the IPG and then downloaded to the patient controller at each recharging, without data loss or memory overwrite. These two, when combined, allows the system both to be used in experimental settings with high-fidelity real-time data, both when stimulation is OFF and ON, and also in clinical applications, collecting a significant amount of ecologic data with a download strategy that does not introduce additional burdens for the patient. In fact, because embedded data are downloaded while the patient is recharging and because the memory capacity was designed to fit the maximum time lapse allowed between two recharging sessions, data are never overwritten and are collected without the need of additional devices or intervention of the

clinician. Therefore, data collection is also continuous when the patient is at home without any time constraint.

Finally, as expected, although the stimulation module requirements were designed on PD therapy, the DBS parameter space in dystonia is similar to that in PD (Magown et al., 2018): average stimulation voltage is around $3.3 \text{ V} \pm 0.6 \text{ V}$, average frequency is $131 \text{ Hz} \pm 5 \text{ Hz}$, and average pulse width ranges from 80 to 450 μs . Similarly, in essential tremor, DBS of the ventralis intermedium nucleus (Vim-DBS) can be successfully applied using the same ranges of parameters (Rodríguez Cruz et al., 2016). Therefore, the AlphaDBS System could be suitable also for dystonia and essential tremor. In all cases, the choice of specific parameters depends on the neurobiological electrical properties of the target neural populations (i.e., STN, GPi, and Vim), on the relative position between electrode and neurons' ensembles, and on the expected mechanism of afferent/efferent neural structures inhibition/excitation.

The system has, however, some limitations. The AlphaDBSipg has two sensing channels, cutting information at 40 Hz, thus introducing a limitation in the implementation of closed-loop algorithms based on gamma activity. However, the system architecture is modular and the sensing problem has been resolved at the chip level not at the design level (Stanslaski et al., 2018; Goyal et al., 2021), thus allowing sensing channel replacing by others with higher bandwidth including gamma (100 Hz cutoff frequency). Cutting information at 40 Hz is a selective and conservative choice for targeting beta power in PD applications while saving memory space and reducing the streaming load.

Similarly, the closed-loop algorithm implemented was conservatively chosen as a simple one, on the basis of previous experiences with external devices. It has several limitations largely debated in the scientific community (Beudel and Brown, 2016; Cagnan et al., 2019a,b; Krauss et al., 2021), especially related to the lack of relationship between beta activity and complex symptoms (e.g., gait/speech disturbances), and the limited time resolution of spectral features (Cagnan et al., 2019b). The effectiveness of the closed-loop algorithm, not only from a technical standpoint but also from a clinical endpoint, is the objective of the ongoing study. However, the AlphaDBS system closed-loop technology is firmware-controlled, and, because the sensing module does not require additional digital signal processing, all the capabilities of the microprocessor firmware can be used for closed-loop implementation.

In conclusion, the system here presented and tested can be considered as a proof of functioning of a clinically

viable deep BCI for closed-loop stimulation delivery, reliable artifact-free recording, and chronic long-term data and neural signal management.

DATA AVAILABILITY STATEMENT

The raw data supporting the conclusions of this article will be made available by the authors, without undue reservation.

ETHICS STATEMENT

The studies involving human participants were reviewed and approved by Comitato Etico Milano Area 2 (Milano) Comitato Etico Fondazione IRCCS Istituto Neurologico C. Besta (Milano) Comitato Etico Interaziendale A.O.U. Città della Salute e della Scienza di Torino—A.O. Ordine Mauriziano—A.S.L. Città di Torino (Torino) Comitato Etico per la Sperimentazione Clinica della Provincia di Padova (Padova) Bioethics Committee at the National Institute of Oncology of Maria Skłodowska-Curie (Warsaw) De Medisch Ethisch Toetsingscommissie van Maastricht UMC. The patients/participants provided their written informed consent to participate in this study.

AUTHOR CONTRIBUTIONS

MA, SM, and AP: system design and conceptualization. MA, MC, and AB: technology development. MA and SM: data analysis, clinical study design, and manuscript drafting. TM, EP, LB, PR, ML, RE, LR, SR, and MJ: study conduct. All authors: manuscript reviewing and approval.

FUNDING

The study was sponsored by Newronika SpA.

ACKNOWLEDGMENTS

We wish to thank all the patients that agreed to be enrolled in the study.

REFERENCES

- Arlotti, M., Marceglia, S., Foffani, G., Volkmann, J., Lozano, A. M., Moro, E., et al. (2018). Eight-hours adaptive deep brain stimulation in patients with Parkinson disease. *Neurology* 90, e971–e976. doi: 10.1212/WNL.0000000000005121
- Arlotti, M., Palmisano, C., Minafra, B., Todisco, M., Pacchetti, C., Canessa, A., et al. (2019). Monitoring subthalamic oscillations for 24 hours in a freely moving Parkinson's disease patient. *Mov. Disord.* 34, 757–759. doi: 10.1002/mds.27657
- Arlotti, M., Rosa, M., Marceglia, S., Barbieri, S., and Priori, A. (2016a). The adaptive deep brain stimulation challenge. *Parkinsonism Relat. Disord.* 28, 12–17. doi: 10.1016/j.parkreldis.2016.03.020
- Arlotti, M., Rossi, L., Rosa, M., Marceglia, S., and Priori, A. (2016b). An external portable device for adaptive deep brain stimulation (aDBS) clinical research in advanced Parkinson's Disease. *Med. Eng. Phys.* 38, 498–505. doi: 10.1016/j.medengphy.2016.02.007
- Beudel, M., and Brown, P. (2016). Adaptive deep brain stimulation in Parkinson's disease. *Parkinsonism Relat. Disord.* 22, S123–S126. doi: 10.1016/j.parkreldis.2015.09.028
- Bocci, T., Prenassi, M., Arlotti, M., Cogiamanian, F. M., Borrellini, L., Moro, E., et al. (2021). Eight-hours conventional versus adaptive deep brain stimulation of the subthalamic nucleus in Parkinson's disease. *NPJ Parkinsons Dis.* 7:88. doi: 10.1038/s41531-021-00229-z

- Brown, P. (2003). Oscillatory nature of human basal ganglia activity: relationship to the pathophysiology of Parkinson's disease. *Mov. Disord.* 18, 357–363. doi: 10.1002/mds.10358
- Cagnan, H., Denison, T., McIntyre, C., and Brown, P. (2019a). Emerging technologies for improved deep brain stimulation. *Nat. Biotechnol.* 37, 1024–1033. doi: 10.1038/s41587-019-0244-6
- Cagnan, H., Mallet, N., Moll, C. K. E., Gulberti, A., Holt, A. B., Westphal, M., et al. (2019b). Temporal evolution of beta bursts in the Parkinsonian cortical and basal ganglia network. *Proc. Natl. Acad. Sci. U.S.A.* 116, 16095–16104. doi: 10.1073/pnas.1819975116
- Cogan, S. F., Guzelian, A. A., Agnew, W. F., Yuen, T. G. H., and McCreery, D. B. (2004). Over-pulsing degrades activated iridium oxide films used for intracortical neural stimulation. *J. Neurosci. Methods* 137, 141–150. doi: 10.1016/j.jneumeth.2004.02.019
- Cummins, D. D., Kochanski, R. B., Gilron, R., Swann, N. C., Little, S., Hammer, L. H., et al. (2021). Chronic sensing of subthalamic local field potentials: comparison of first and second generation implantable bidirectional systems within a single subject. *Front. Neurosci.* 15:725797. doi: 10.3389/fnins.2021.725797
- Eleopra, R., Rinaldo, S., Devigili, G., Lettieri, C., Mondani, M., D'Auria, S., et al. (2019). Brain impedance variation of directional leads implanted in subthalamic nuclei of Parkinsonian patients. *Clin. Neurophysiol.* 130, 1562–1569. doi: 10.1016/j.clinph.2019.06.001
- Eusebio, A., Cagnan, H., and Brown, P. (2012). Does suppression of oscillatory synchronisation mediate some of the therapeutic effects of DBS in patients with Parkinson's disease? *Front. Integr. Neurosci.* 6:47. doi: 10.3389/fnint.2012.00047
- Giannicola, G., Marceglia, S., Rossi, L., Mrakic-Sposta, S., Rampini, P., Tamma, F., et al. (2010). The effects of levodopa and ongoing deep brain stimulation on subthalamic beta oscillations in Parkinson's disease. *Exp. Neurol.* 226, 120–127. doi: 10.1016/j.expneurol.2010.08.011
- Giannicola, G., Rosa, M., Servello, D., Menghetti, C., Carrabba, G., Pacchetti, C., et al. (2012). Subthalamic local field potentials after seven-year deep brain stimulation in Parkinson's disease. *Exp. Neurol.* 237, 312–317. doi: 10.1016/j.expneurol.2012.06.012
- Gilron, R., Little, S., Perrone, R., Wilt, R., de Hemptinne, C., Yaroshinsky, M. S., et al. (2021). Long-term wireless streaming of neural recordings for circuit discovery and adaptive stimulation in individuals with Parkinson's disease. *Nat. Biotechnol.* 39, 1078–1085. doi: 10.1038/s41587-021-00897-5
- Goyal, A., Goetz, S., Stanslaski, S., Oh, Y., Rusheen, A. E., Klassen, B., et al. (2021). The development of an implantable deep brain stimulation device with simultaneous chronic electrophysiological recording and stimulation in humans. *Biosens. Bioelectron.* 176:112888. doi: 10.1016/j.bios.2020.112888
- Guidetti, M., Marceglia, S., Loh, A., Harmsen, I. E., Meoni, S., Foffani, G., et al. (2021). Clinical perspectives of adaptive deep brain stimulation. *Brain Stimul.* 14, 1238–1247. doi: 10.1016/j.brs.2021.07.063
- Habets, J. G. V., Heijmans, M., Kuijff, M. L., Janssen, M. L. F., Temel, Y., and Kubben, P. L. (2018). An update on adaptive deep brain stimulation in Parkinson's disease: update on adaptive DBS in Parkinson's disease. *Mov. Disord.* 33, 1834–1843. doi: 10.1002/mds.115
- He, S., Debarros, J., Khawaldeh, S., Pogossyan, A., Mostofi, A., Baig, F., et al. (2020). "Closed-loop DBS triggered by real-time movement and tremor decoding based on thalamic LFPs for essential tremor, in *Proceedings of the 2020 42nd Annual International Conference of the IEEE Engineering in Medicine & Biology Society (EMBC)*, Montreal, QC, 3602–3605. doi: 10.1109/EMBC44109.2020.9175433
- Jimenez-Shahed, J. (2021). Device profile of the percept PC deep brain stimulation system for the treatment of Parkinson's disease and related disorders. *Exp. Rev. Med. Devices* 18, 319–332. doi: 10.1080/17434440.2021.1909471
- Johnson, V., Wilt, R., Gilron, R., Anso, J., Perrone, R., Beudel, M., et al. (2021). Embedded adaptive deep brain stimulation for cervical dystonia controlled by motor cortex theta oscillations. *Exp. Neurol.* 345:113825. doi: 10.1016/j.expneurol.2021.113825
- Krauss, J. K., Lipsman, N., Aziz, T., Boutet, A., Brown, P., Chang, J. W., et al. (2021). Technology of deep brain stimulation: current status and future directions. *Nat. Rev. Neurol.* 17, 75–87. doi: 10.1038/s41582-020-00426-z
- Kuncel, A. M., and Grill, W. M. (2004). Selection of stimulus parameters for deep brain stimulation. *Clin. Neurophysiol.* 115, 2431–2441. doi: 10.1016/j.clinph.2004.05.031
- Little, S., Beudel, M., Zrinzo, L., Foltynie, T., Limousin, P., Hariz, M., et al. (2016a). Bilateral adaptive deep brain stimulation is effective in Parkinson's disease. *J. Neurol. Neurosurg. Psychiatr.* 87, 717–721. doi: 10.1136/jnnp-2015-310972
- Little, S., Tripoliti, E., Beudel, M., Pogossyan, A., Cagnan, H., Herz, D., et al. (2016b). Adaptive deep brain stimulation for Parkinson's disease demonstrates reduced speech side effects compared to conventional stimulation in the acute setting. *J. Neurol. Neurosurg. Psychiatry* 87, 1388–1389. doi: 10.1136/jnnp-2016-313518
- Little, S., Pogossyan, A., Neal, S., Zavala, B., Zrinzo, L., Hariz, M., et al. (2013). Adaptive deep brain stimulation in advanced Parkinson disease. *Ann. Neurol.* 74, 449–457. doi: 10.1002/ana.23951
- Magown, P., Andrade, R. A., Soroceanu, A., and Kiss, Z. H. T. (2018). Deep brain stimulation parameters for dystonia: a systematic review. *Parkinsonism Relat. Disord.* 54, 9–16. doi: 10.1016/j.parkreldis.2018.04.017
- Marceglia, S., Rosa, M., Servello, D., Porta, M., Barbieri, S., Moro, E., et al. (2017). Adaptive deep brain stimulation (aDBS) for Tourette syndrome. *Brain Sci.* 8:4. doi: 10.3390/brainsci8010004
- Meidahl, A. C., Tinkhauser, G., Herz, D. M., Cagnan, H., Debarros, J., and Brown, P. (2017). Adaptive deep brain stimulation for movement disorders: the long road to clinical therapy. *Mov. Disord.* 32, 810–819. doi: 10.1002/mds.27022
- Merrill, D. R., Bikson, M., and Jefferys, J. G. R. (2005). Electrical stimulation of excitable tissue: design of efficacious and safe protocols. *J. Neurosci. Methods* 141, 171–198. doi: 10.1016/j.jneumeth.2004.10.020
- Molina, R., Okun, M. S., Shute, J. B., Opri, E., Rossi, P. J., Martinez-Ramirez, D., et al. (2017). Report of a patient undergoing chronic responsive deep brain stimulation for Tourette syndrome: proof of concept. *J. Neurosurg.* 129, 308–314. doi: 10.3171/2017.6.JNS17626
- Moro, E., Esselink, R. J. A., Xie, J., Hommel, M., Benabid, A. L., and Pollak, P. (2002). The impact on Parkinson's disease of electrical parameter settings in STN stimulation. *Neurology* 59, 706–713. doi: 10.1212/WNL.59.5.706
- Morrell, M. J., and On behalf of the RNS System in Epilepsy Study Group (2011). Responsive cortical stimulation for the treatment of medically intractable partial epilepsy. *Neurology* 77, 1295–1304. doi: 10.1212/WNL.0b013e3182302056
- Neumann, W.-J., Huebl, J., Brücke, C., Gabriëls, L., Bajbouj, M., Merkl, A., et al. (2014). Different patterns of local field potentials from limbic DBS targets in patients with major depressive and obsessive compulsive disorder. *Mol. Psychiatry* 19, 1186–1192. doi: 10.1038/mp.2014.2
- Opri, E., Cernera, S., Molina, R., Eisinger, R. S., Cagle, J. N., Almeida, L., et al. (2020). Chronic embedded cortico-thalamic closed-loop deep brain stimulation for the treatment of essential tremor. *Sci. Transl. Med.* 12:eay7680. doi: 10.1126/scitranslmed.aay7680
- Paff, M., Loh, A., Sarica, C., Lozano, A. M., and Fasano, A. (2020). Update on current technologies for deep brain stimulation in Parkinson's disease. *J. Mov. Disord.* 13, 185–198. doi: 10.14802/jmd.20052
- Petkos, K., Guiho, T., Degenar, P., Jackson, A., Brown, P., Denison, T., et al. (2019). A high-performance 4 nV (vHz)⁻¹ analog front-end architecture for artefact suppression in local field potential recordings during deep brain stimulation. *J. Neural Eng.* 16:066003. doi: 10.1088/1741-2552/ab2610
- Piña-Fuentes, D., Beudel, M., Van Zijl, J. C., Van Egmond, M. E., Oterdoom, D. L. M., Van Dijk, J. M. C., et al. (2020). Low-frequency oscillation suppression in dystonia: implications for adaptive deep brain stimulation. *Parkinsonism Relat. Disord.* 79, 105–109. doi: 10.1016/j.parkreldis.2020.08.030
- Piña-Fuentes, D., Little, S., Oterdoom, M., Neal, S., Pogossyan, A., Tijssen, M. A. J., et al. (2017). Adaptive DBS in a Parkinson's patient with chronically implanted DBS: a proof of principle. *Mov. Disord.* 32, 1253–1254. doi: 10.1002/mds.26959
- Prenassi, M., Arlotti, M., Borellini, L., Bocci, T., Cogiamanian, F., Locatelli, M., et al. (2021). The relationship between electrical energy delivered by deep brain stimulation and levodopa-induced dyskinesias in Parkinson's disease: a retrospective preliminary analysis. *Front. Neurol.* 12:643841. doi: 10.3389/fneur.2021.643841
- Priori, A., Foffani, G., and Rossi, L. (2005). Apparatus for Treating Neurological Disorders by Means of Adaptive Electro-Stimulation Retroacted by Biopotentials. European Patent no. EP1940508, US Patent no. 8,078,281, Israel Patent no 191068.
- Priori, A., Foffani, G., Rossi, L., and Marceglia, S. (2013). Adaptive deep brain stimulation (aDBS) controlled by local field potential oscillations. *Exp. Neurol.* 245, 77–86. doi: 10.1016/j.expneurol.2012.09.013

- Pulliam, C. L., Stanslaski, S. R., and Denison, T. J. (2020). "Industrial perspectives on brain-computer interface technology," in *[Handbook of Clinical Neurology] Brain-Computer Interfaces*, Vol. 168, eds N. F. Ramsey and J. R. Millán (Amsterdam: Elsevier), 341–352. doi: 10.1016/B978-0-444-63934-9.00025-1
- Qian, X., Chen, Y., Feng, Y., Ma, B., Hao, H., and Li, L. (2017). A method for removal of deep brain stimulation artifact from local field potentials. *IEEE Trans. Neural Syst. Rehabil. Eng.* 25, 2217–2226. doi: 10.1109/TNSRE.2016.2613412
- Reich, M. M., Steigerwald, F., Sawalhe, A. D., Reese, R., Gunalan, K., Johannes, S., et al. (2015). Short pulse width widens the therapeutic window of subthalamic neurostimulation. *Ann. Clin. Transl. Neurol.* 2, 427–432. doi: 10.1002/acn3.168
- Rodríguez Cruz, P. M., Vargas, A., Fernández-Carballal, C., Garbizu, J., De La Casa-Fages, B., and Grandas, F. (2016). Long-term thalamic deep brain stimulation for essential tremor: clinical outcome and stimulation parameters. *Mov. Disord. Clin. Pract.* 3, 567–572. doi: 10.1002/mdc3.12337
- Rosa, M., Arlotti, M., Ardolino, G., Cogiamanian, F., Marceglia, S., Di Fonzo, A., et al. (2015). Adaptive deep brain stimulation in a freely moving Parkinsonian patient. *Mov. Disord.* 30, 1003–1005. doi: 10.1002/mds.26241
- Rosa, M., Arlotti, M., Marceglia, S., Cogiamanian, F., Ardolino, G., Fonzo, A. D., et al. (2017). Adaptive deep brain stimulation controls levodopa-induced side effects in Parkinsonian patients. *Mov. Disord.* 32, 628–629. doi: 10.1002/mds.26953
- Rossi, L., Foffani, G., Marceglia, S., Bracchi, F., Barbieri, S., and Priori, A. (2007). An electronic device for artefact suppression in human local field potential recordings during deep brain stimulation. *J. Neural Eng.* 4, 96–106. doi: 10.1088/1741-2560/4/2/010
- Rossi, L., Marceglia, S., Foffani, G., Cogiamanian, F., Tamma, F., Rampini, P., et al. (2008). Subthalamic local field potential oscillations during ongoing deep brain stimulation in Parkinson's disease. *Brain Res. Bull.* 76, 512–521. doi: 10.1016/j.brainresbull.2008.01.023
- Stanslaski, S., Herron, J., Chouinard, T., Bourget, D., Isaacson, B., Kremen, V., et al. (2018). A chronically implantable neural coprocessor for investigating the treatment of neurological disorders. *IEEE Trans. Biomed. Circuits Syst.* 12, 1230–1245. doi: 10.1109/TBCAS.2018.2880148
- Starr, P. A. (2018). Totally implantable bidirectional neural prostheses: a flexible platform for innovation in neuromodulation. *Front. Neurosci.* 12:619. doi: 10.3389/fnins.2018.00619
- Swann, N. C., de Hemptinne, C., Thompson, M. C., Miocinovic, S., Miller, A. M., Giron, R., et al. (2018). Adaptive deep brain stimulation for Parkinson's disease using motor cortex sensing. *J. Neural Eng.* 15:046006. doi: 10.1088/1741-2552/aabc9b
- Velisar, A., Syrkin-Nikolau, J., Blumenfeld, Z., Trager, M. H., Afzal, M. F., Prabhakar, V., et al. (2019). Dual threshold neural closed loop deep brain stimulation in Parkinson disease patients. *Brain Stimul.* 12, 868–876. doi: 10.1016/j.brs.2019.02.020
- Volkman, J., Herzog, J., Kopfer, F., and Deuschl, G. (2002). Introduction to the programming of deep brain stimulators. *Mov. Disord.* 17, S181–S187. doi: 10.1002/mds.10162
- Watrous, A. J., Miller, J., Qasim, S. E., Fried, I., and Jacobs, J. (2018). Phase-tuned neuronal firing encodes human contextual representations for navigational goals. *eLife* 7:e32554. doi: 10.7554/eLife.32554
- Wojtecki, L., Timmermann, L., Jörgens, S., Südmeyer, M., Maarouf, M., Treuer, H., et al. (2006). Frequency-dependent reciprocal modulation of verbal fluency and motor functions in subthalamic deep brain stimulation. *Arch. Neurol.* 63, 1273–1276. doi: 10.1001/archneur.63.9.1273
- Zhou, A., Santacruz, S. R., Johnson, B. C., Alexandrov, G., Moin, A., Burghardt, F. L., et al. (2019). A wireless and artefact-free 128-channel neuromodulation device for closed-loop stimulation and recording in non-human primates. *Nat. Biomed. Eng.* 3, 15–26. doi: 10.1038/s41551-018-0323-x

Conflict of Interest: MA and MC were employed by Newronika and held stock options. AB is a consultant for Newronika. AP, SM, and PR are founders and shareholders of Newronika.

The study was funded by Newronika SpA. The funder had the following involvement with the study: study design of NCT04681534, signal collection and analysis (clinical data collection is performed by a CRO), the writing of this article, and the decision to submit it for publication.

The remaining authors declare that the research was conducted in the absence of any commercial or financial relationships that could be construed as a potential conflict of interest.

Publisher's Note: All claims expressed in this article are solely those of the authors and do not necessarily represent those of their affiliated organizations, or those of the publisher, the editors and the reviewers. Any product that may be evaluated in this article, or claim that may be made by its manufacturer, is not guaranteed or endorsed by the publisher.

Copyright © 2021 Arlotti, Colombo, Bonfanti, Mandat, Lanotte, Pirola, Borellini, Rampini, Eleopra, Rinaldo, Romito, Janssen, Priori and Marceglia. This is an open-access article distributed under the terms of the Creative Commons Attribution License (CC BY). The use, distribution or reproduction in other forums is permitted, provided the original author(s) and the copyright owner(s) are credited and that the original publication in this journal is cited, in accordance with accepted academic practice. No use, distribution or reproduction is permitted which does not comply with these terms.



Closing the Loop With Cortical Sensing: The Development of Adaptive Deep Brain Stimulation for Essential Tremor Using the Activa PC+S

Tomasz M. Frączek¹, Benjamin I. Ferleger², Timothy E. Brown³, Margaret C. Thompson², Andrew J. Haddock², Brady C. Houston¹, Jeffrey G. Ojemann⁴, Andrew L. Ko⁴, Jeffrey A. Herron^{4*} and Howard J. Chizeck²

¹ Neuroscience Program, University of Washington, Seattle, WA, United States, ² Department of Electrical and Computer Engineering, University of Washington, Seattle, WA, United States, ³ Department of Philosophy, University of Washington, Seattle, WA, United States, ⁴ Department of Neurological Surgery, University of Washington, Seattle, WA, United States

OPEN ACCESS

Edited by:

Coralie de Hemptinne,
University of Florida, United States

Reviewed by:

J. Luis Lujan,
Mayo Clinic College of Medicine and
Science, United States
Kara A. Johnson,
University of Florida, United States

*Correspondence:

Jeffrey A. Herron
jeffherr@uw.edu

Specialty section:

This article was submitted to
Neural Technology,
a section of the journal
Frontiers in Neuroscience

Received: 29 July 2021

Accepted: 04 November 2021

Published: 08 December 2021

Citation:

Frączek TM, Ferleger BI, Brown TE, Thompson MC, Haddock AJ, Houston BC, Ojemann JG, Ko AL, Herron JA and Chizeck HJ (2021) Closing the Loop With Cortical Sensing: The Development of Adaptive Deep Brain Stimulation for Essential Tremor Using the Activa PC+S. *Front. Neurosci.* 15:749705. doi: 10.3389/fnins.2021.749705

Deep Brain Stimulation (DBS) is an important tool in the treatment of pharmacologically resistant neurological movement disorders such as essential tremor (ET) and Parkinson's disease (PD). However, the open-loop design of current systems may be holding back the true potential of invasive neuromodulation. In the last decade we have seen an explosion of activity in the use of feedback to "close the loop" on neuromodulation in the form of adaptive DBS (aDBS) systems that can respond to the patient's therapeutic needs. In this paper we summarize the accomplishments of a 5-year study at the University of Washington in the use of neural feedback from an electrocorticography strip placed over the sensorimotor cortex. We document our progress from an initial proof of hardware all the way to a fully implanted adaptive stimulation system that leverages machine-learning approaches to simplify the programming process. In certain cases, our systems out-performed current open-loop approaches in both power consumption and symptom suppression. Throughout this effort, we collaborated with neuroethicists to capture patient experiences and take them into account whilst developing ethical aDBS approaches. Based on our results we identify several key areas for future work. "Graded" aDBS will allow the system to smoothly tune the stimulation level to symptom severity, and frequent automatic calibration of the algorithm will allow aDBS to adapt to the time-varying dynamics of the disease without additional input from a clinician. Additionally, robust computational models of the pathophysiology of ET will allow stimulation to be optimized to the nuances of an individual patient's symptoms. We also outline the unique advantages of using cortical electrodes for control and the remaining hardware limitations that need to be overcome to facilitate further development in this field. Over the course of this study we have verified the potential of fully-implanted, cortically driven aDBS as a feasibly translatable treatment for pharmacologically resistant ET.

Keywords: essential tremor, deep brain stimulation, machine learning, motor cortex, adaptive deep brain stimulation, fully implantable

1. INTRODUCTION

Essential Tremor (ET) is one of the most common neurological movement disorders. By some estimates, it affects as much as 1% of the world's adult population and up to 4.5% of the senior population to some extent (Louis and Ferreira, 2010). ET manifests itself primarily as a 2–8 Hz tremor during active motion or holding of posture. Classically, the strongest tremor is apparent in the extremities, especially the hands, but will often also be accompanied by trunk tremor (Haubenberger and Hallett, 2018). Despite its prevalence, the non-lethal nature of the disorder means that it has been understudied for many years and the pathophysiology is still poorly understood (Soto and Fasano, 2020). Once patients are diagnosed, initial treatment is usually pharmacological, but for severe, pharmacologically refractive cases DBS is a promising option (Lyons and Pahwa, 2004).

Deep brain stimulation (DBS) is a common therapy used to treat neurological disorders. It has been approved by the FDA to treat ET, Parkinson's disease (PD), dystonia, and epilepsy; and is under investigation for treatment of depression, addiction, Tourette syndrome, and many others (Lozano et al., 2019). In current clinical practice, conventional or continuous DBS (cDBS) is used in an open-loop fashion. Stimulation is configured manually by a clinician and the applied stimulation pattern is fixed (Lyons and Pahwa, 2004). Parameter tuning is a lengthy process that, even with the expertise of a neurologist, may require several visits before a satisfactory setting is found. Optimal stimulation settings are those that significantly suppress tremor, without causing intolerable side effects. The patient is provided a “patient programmer” that they can use to turn the stimulator on or off, but this control is rather coarse at best and used primarily to conserve battery at night while patients sleep. As a result, stimulation is often delivered even when it is not necessary, which may unnecessarily increase exposure to side effects (Meidahl et al., 2017).

Adaptive DBS (aDBS) offers to solve many of the limitations of cDBS systems (Arlotti et al., 2016; Meidahl et al., 2017). In this approach, stimulation is delivered in a closed-loop format that allows the system to adapt to the patient's state. Stimulation can be applied only when necessary, thereby reducing side effects while maintaining clinical efficacy. Since the stimulation could adapt to the severity of symptoms, stimulation would always be delivered at the optimal level. Moreover, recent evidence suggests that intermittent stimulation may be more effective at suppressing symptoms than cDBS (Little et al., 2014; Ferleger et al., 2020). ET is a particularly attractive application for this approach since the primary symptom, tremor, manifests itself almost exclusively during movement. This clearly defines the periods when stimulation would be the most beneficial, greatly reducing the complexity of the control problem to be solved. It is worth noting that naming several conventions exist, with adaptive, closed-loop, and responsive DBS having overlapping definitions. In this work we use adaptive DBS as an umbrella term to describe the various ways in which we have automatically adjusted stimulation based on biomarkers of the patient's state

At the start of our study, aDBS had been demonstrated successfully in patients with PD. Several studies have even shown that in some cases aDBS could be more effective than traditional cDBS or randomly applied intermittent stimulation in ameliorating certain symptoms of PD (Little et al., 2013, 2014). However, at the start of our study, there was only one known attempt at developing aDBS for ET. In that study, the authors used motion detected through an EMG system on the patient's arm as a control variable for turning DBS on and off (Yamamoto et al., 2013). This study and the encouraging results in the PD space guided much of our early work.

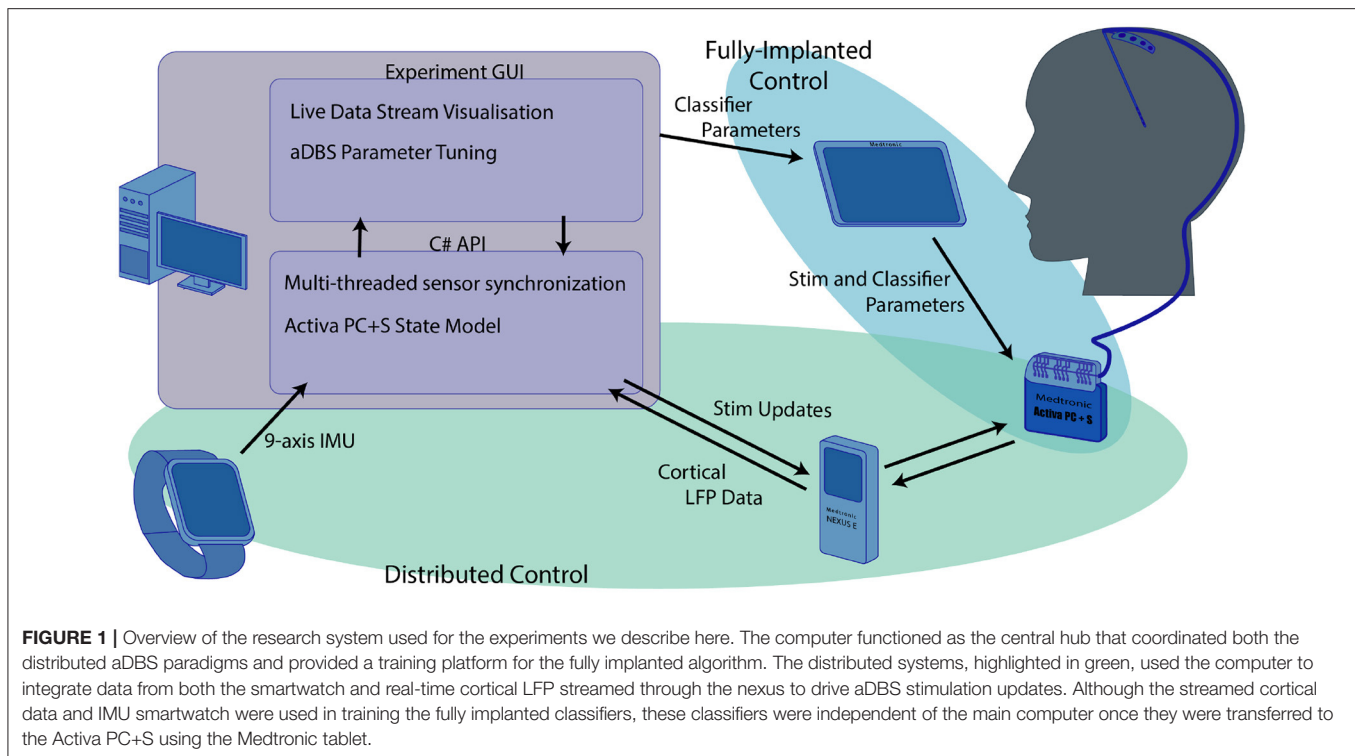
In this paper we review the development process of aDBS in ET patients carried out at the University of Washington. We begin with an overview of both the hardware and software in the research platform we developed around the Medtronic Activa PC+S. We then outline how we reproduced earlier results and developed a proof-of-concept aDBS system using cortical LFPs as a control signal. We then improved this system by leveraging machine learning and investigating volitional BCI-style control of aDBS. By the end of the study, we had arrived at a clinically translatable, fully implantable aDBS paradigm, accompanied by a largely automated programming process. Consequently, aDBS seems to have now reached the threshold where it could be evaluated as a clinical therapy to improve patients' lives. This however brings with it a plethora of neuro-ethical and practical consideration which we discuss. This review paper is intended to provide a an overview of the development process and preliminary clinical results from start to finish. We hope it will provide a unique viewpoint and present practical context for the ongoing development of aDBS for ET.

2. SYSTEM INTEGRATION OF THE ACTIVA PC+S AND NEXUS-D SYSTEMS

The research system we developed was an integration of multiple independent components. As a result, the system required a significant amount of software development. A full schematic of the system is shown in **Figure 1**. All research was carried out with the approval of the UW IRB and the FDA. Patients provided informed consent before participating in the study.

2.1. The Medtronic Activa PC+S and Nexus-D

The central component of the research system was the investigational-use Medtronic Activa PC+S, used with FDA permission under an investigational device exemption (IDE, clinical trial number NCT02443181) (Stanslaski et al., 2012). This device consists of a pulse generator implanted (IPG) in the chest which controls both stimulation and sensing capability. The IPG is connected via a subcutaneous clinical lead extension to the stimulation and sensing electrodes. For this protocol, stimulation was delivered using a clinical standard four-electrode DBS stimulation lead, the Medtronic Model 3387, implanted into the ventral intermediate nucleus of the thalamus (VIM). Sensing was performed utilizing a Medtronic Resume-II four-contact strip electrode placed on the surface of the cortex,

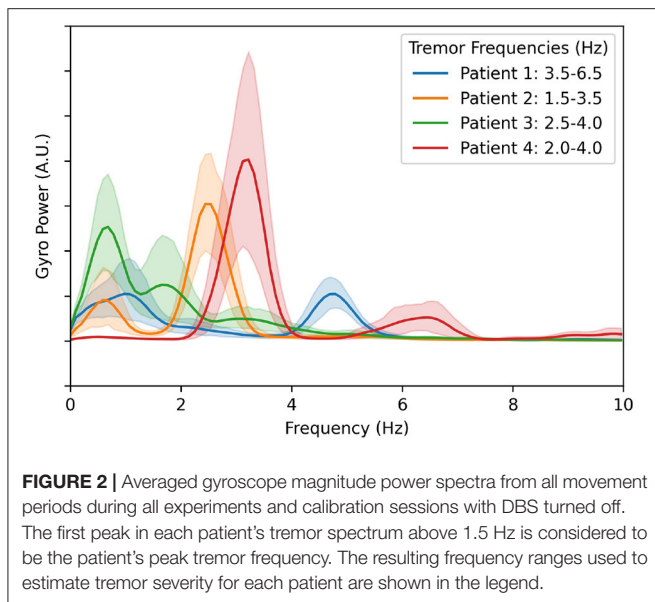


spanning the central sulcus, roughly over the hand motor area. This configuration allowed for standard tremor-mitigating stimulation to be delivered to the VIM while also allowing the sensing of cortical local field potentials (LFPs) related to hand motor activity. The IPG supports both cDBS and aDBS. cDBS can be configured using the Medtronic 8,840 clinical programmer. aDBS can be performed either in a distributed fashion with control decisions made outside the device, or in a fully implanted fashion with stimulation decisions made on-board after configuration using the Activa PC+S Sensing Tablet. For distributed control of stimulation, the IPG can be paired via a short-range inductive connection with the Medtronic Nexus-D or Nexus-E telemetry bridges. The choice of sampling frequency for the neural data was largely driven by the hardware specifications. This setup can stream raw LFP data to a desktop computer via a USB connection with a sampling rate of up to 422Hz if streaming from one electrode, or 200 Hz if streaming from two simultaneously. In the work presented here, we used the 422 Hz LFP data streams. We found that the benefit to aDBS control of the addition of VIM data was not worth the loss in sampling rate, since LFP data from the VIM was heavily contaminated by stimulation artifacts. However, data is transmitted in discreet packets every 400ms. In practice, the half-duplex inductive link's bandwidth limitations resulted in a small window for stimulation updates to be transmitted to the PC+S without resulting in streamed neural data loss, so stimulation updates in a distributed algorithm needed to be performed with 400 ms resolution. All neural recordings consist of differential voltage recordings between pairs of electrodes. In this use-case we selected our cortical recordings to utilize pairs of electrodes

that lay on opposite sides of the central sulcus. These were identified as the pair with the highest beta-band power while the patient was at rest, determined through a standardized montage-sweep provided by the Activa PC+S instruments. The Activa PC+S can also stream analog estimates of power bands at a sampling frequency of 5Hz, with frequency ranges configured on the proprietary Medtronic Sensing Tablet. When not streaming, the sampling rate of the IPG can be increased up to 800 Hz for raw LFP data, and the resulting LFP or power band data can be downloaded to a USB drive via the Medtronic tablet. In the fully implanted aDBS configuration the IPG uses the analog power band estimates from the attached electrodes in combination with a simple linear classifier to control stimulation. Both the power bands and the weights of the classifier are also configured via the Medtronic Sensing Tablet.

2.2. Tremor Sensing and Measurement

To better evaluate the severity of the patient's symptoms and the efficacy of the aDBS paradigm, several modalities of data were collected in parallel to those described above. An Android smartwatch worn on the patient's wrist capable of streaming 9 axis inertial measurement unit (IMU) data (3-axis accelerometer, 3-axis gyroscope, and 3-axis compass) at 100 Hz, was connected to the PC via a Bluetooth connection. This IMU data served as the basis of quantitative and automatic evaluation of tremor. In addition, we asked the patients to perform the tasks from the Fahn-Telosa-Marin tremor rating scale (FTM) (Fahn et al., 1988). Spiral and line drawings were recorded either on paper or through a custom application on a Microsoft Surface tablet (Sonnet et al., 2020). These, along with videos of the patients,



were then rated by a panel of three blinded neurologists to obtain an objective, clinically translatable metric to evaluate the efficacy of DBS. For some experiments, we also used the gTec Mobilab to collect EMG from the study participant's tremoring limb using wet gel electrodes as both a trigger for stimulation and as a method of evaluating the effect of aDBS.

2.3. Software Development and C# API

The distributed elements of the research platform described above were integrated through the PC using an application development framework written in C# (Herron et al., 2017). This framework utilized a custom developed C# API for generic Nexus-D/Activa PC+S control which enabled simultaneous communication with all sensors and asynchronous dispatch of commands to the Activa PC+S. This C# API was used to develop protocol-specific applications responsible for the collecting and processing data from additional sensors. Multi-threaded coding techniques were used to ensure that sensing, processing, and device communication would not impact the responsiveness of the closed-loop algorithms being investigated. This was further complicated by the fact that the Nexus D and E could not concurrently send data and receive a command, leading to a very narrow timeout window. The API therefore independently maintained an internal model of the Nexus and IPG system states to ensure that all command timings remained in sync. This had additional battery power-saving benefits as the Activa IPG did not need to be queried for its system state. Even with this precise timing capability, the half-duplex nature of the communication hardware and the narrow window for stimulation adjustments to be made before the next data packet needed to be transmitted resulted in a potential delay of 800 ms between the time a biomarker appeared in the patients' brain signals and the time the system could respond by adjusting DBS.

Using this framework, we constructed an experiment control application that enabled rapid development and testing of novel

aDBS paradigms. This application, also written in C#, allowed data from any subset of the potential signal sources (neural or wearable) to be streamed simultaneously. Each sensor's data could be visualized in real time and used to control stimulation. Under the hood, each new aDBS paradigm was implemented by editing a single class within the application. This class managed the buffers for all data streams and made the required most recent data available. Once the decision about how to adjust stimulation amplitude was made, the change was passed through another buffer to the Nexus-D API which handled the changing of stimulation. To minimize side effects, stimulation was slowly ramped up, step wise to and from its maximum value. A maximum ramp rate was set for each patient and the software was configured to send individual simulation change commands at the appropriate clock times to manage ramping. This setup allowed development of each new aDBS approach to focus on the meaningful interpretation of biomarkers and stimulation patterns rather than control of individual sensors and timing of stimulation updates.

2.4. Post-hoc Framework

To accurately compare the effectiveness of each of the aDBS algorithms discussed here, we use an evaluation of tremor based on the IMU gyroscope data. For this, we calculate the total power in the frequency band that corresponds to each patient's maximum tremor amplitude. The power spectral density along each of the three axes was calculated independently, and then the magnitude was taken for each frequency using the Euclidean distance. The results are plotted in **Figure 2**. The components below 1.5 Hz are considered normal characteristics of movement, power in this band indicates that the patient is actively moving. The largest peak in the spectrum in the 1.5–8.0 Hz band was determined to be the patient's peak tremor frequency. Power in this band quantifies the amount of tremor the patient is experiencing.

Tremor algorithms were also evaluated based on total power delivered. Since the onboard circuitry of the Activa PC+S uses relatively little power, stimulation is the largest drain on battery power. Since the Activa PC+S was not rechargeable, ensuring that algorithms delivered stimulation effectively with respect to power consumption was important. To calculate total electrical energy delivered (TEED) we used the following metric:

$$TEED = \frac{V^2 \cdot f \cdot p}{z \cdot \tau} \cdot t \quad (1)$$

where V is the voltage, f is the stimulation frequency, p is the pulse width, z is the impedance, τ is the duration of the experiment, and t is the duration that stimulation is applied at this voltage (Moro et al., 2002; Koss et al., 2005). To make this metric easier to understand, we give values for TEED as the ratio between the TEED by aDBS, and TEED as if cDBS was applied with the same stimulation parameters. For comparison between algorithms, we use both *TEED per second during movement*, and *TEED per second during rest*. Lower TEED during movement with minimal tremor indicates that the stimulation paradigm used was efficient in suppressing tremor. TEED during

rest indicates that the algorithm delivered stimulation even when it might not have been necessary. Since suppressing tremor is the prime purpose of aDBS, minor over-stimulation is not considered to be the primary concern. However, if over-stimulation leads to excessive side-effects, or rapidly drains the battery, then it quickly become unacceptable.

At the end of this multi-year study, we had amassed a large collection of longitudinal data. Due to the iterative nature of the development process, the data was not stored in consistent formats and did not always have complete metadata. We therefore developed a python analysis framework to standardize the data formats and enable large-scale longitudinal analysis of all the experiments and data modalities collected. This framework, built around a flexible experiment object, can search a directory tree to discover any sources of potential data and attempt to interpret missing metadata. This resulting dataset can easily be filtered by experiment type or data modalities available. Additionally, any missing or corrupted data resulting from a loss of connectivity or sensor saturation, respectively, was detected and filtered out. This framework has been used to examine the stability of biomarkers over the duration of the study period, as presented in Frączek et al. (2021), and discussed in Section 4.3. In the context of this work, we used the framework to re-illustrate previously published data.

3. DEVELOPMENT OF ADBS FOR TREMOR

Our effort to develop aDBS for ET proceeded from a technology demonstration study in one patient to a clinically translatable, fully implanted system. Here, we will outline the process by which we developed each of these systems and the most important outcomes that informed the next generation of the work.

3.1. Initial Demonstrator

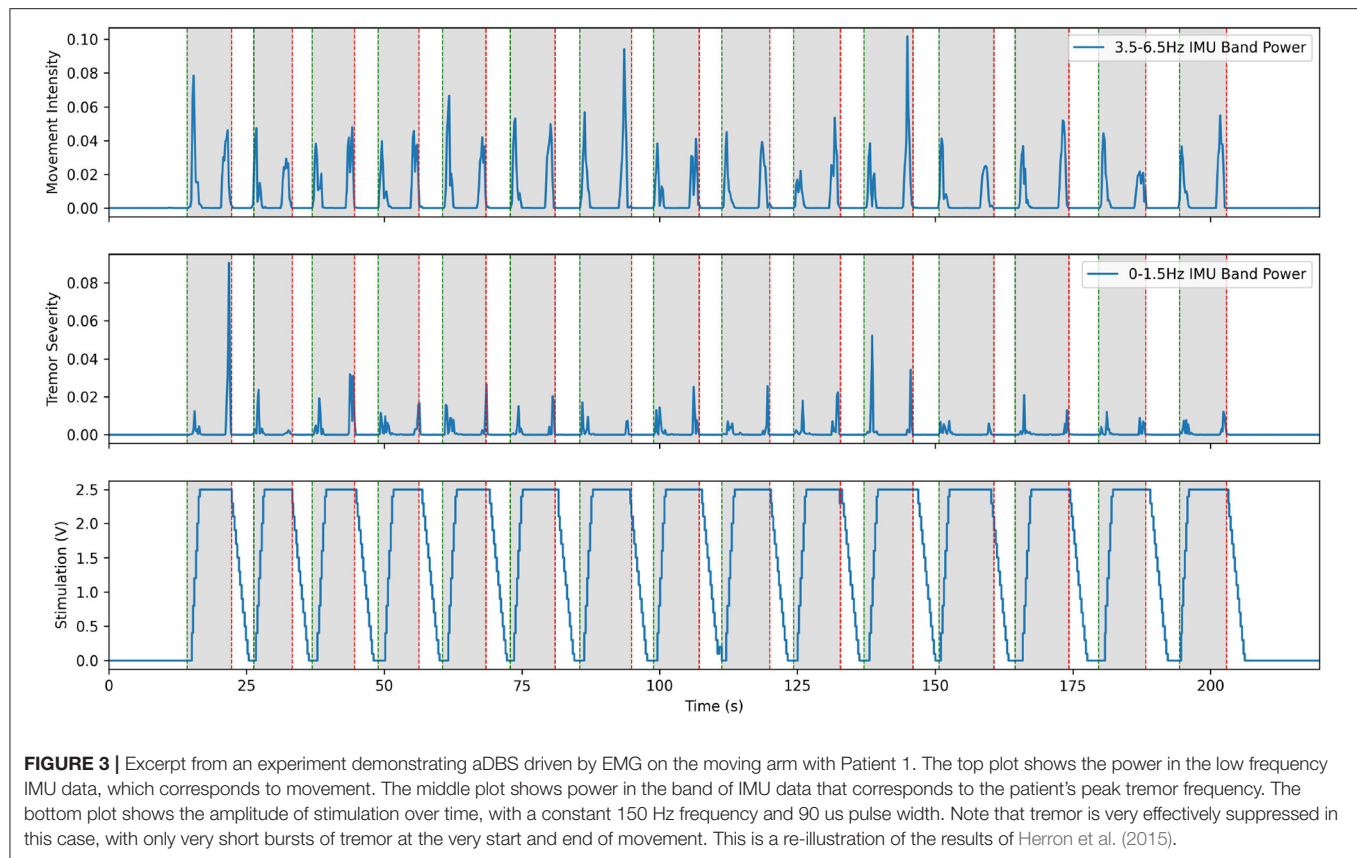
Initial feasibility studies began with the implantation of our first patient in 2015. The goal of this initial work was to demonstrate that system integration was successful and could be used to prototype aDBS paradigms, which had never been done before (Herron et al., 2015, 2016). These initial experiments would validate the system and allow us to correlate the various modalities of data to the patient's state. Using this data, we began the development and verification of neural biomarkers of movement and tremor to enable neural-driven aDBS (Herron, 2016; Herron et al., 2017). To objectively evaluate the effectiveness of any aDBS paradigm, we needed to develop an IMU-based measurement of tremor that could track fast changes in tremor severity. This would then be a test bed that would enable the identification of biomarkers that would not only reliably distinguish times when stimulation was needed but also be robust to changes in stimulation.

Hardware validation experiments with our first patient began before the post-operative lesion effect wore off, about 2 weeks after the implantation surgery. During this time, we calibrated the Activa PC+S recording capabilities and fine-tuned the research setup. The lesion effect had disappeared by the third visit, and the difference in tremor between the stim on and stim off states was fully visible in spiral drawing tasks. Taking inspiration from

prior literature described in Yamamoto et al. (2013) where EMG was used to drive a DBS system using a re-engineered patient programmer, we first implemented prototype aDBS paradigms driven by EMG and IMU signals. Each of these devices was used to monitor the patient and detect whether they were actively moving. When movement was detected, stimulation was rapidly ramped up to the therapeutic threshold and maintained until the patient returned to rest. A representative trial for the EMG system is shown in **Figure 3**. These trials consisted of a comparison of the relevant data during repeated rest, movement, and imagined movement trials. During rest, the patient was asked to simply sit in the chair, while all sensors recorded data to use as a baseline. During movement, they were prompted to raise their hand (at the time of the green vertical lines) and hold it out in front of themselves, until prompted to return to rest (at the time of the red vertical lines). This movement was found to reliably elicit tremor for this patient. Prompt intervals of various lengths, were interleaved so that multiple comparisons could be collected quickly. A similar approach was used for imagined movements, but instead of moving, the patient was asked to instead imagine performing the same movement. This prompt paradigm was used as a template for many of the later experiments through the study. Data collected during these trials allowed us to verify that data was correctly streaming to the central control desktop. Analysis of the IMU data allowed us to develop a metric for tremor severity, described below and shown in the second plot below, which could be computed in near real time. We found this metric correlated to the tremor observed in the patient, based on the FTM scale, while reducing the movement onset and offset artifacts (Herron et al., 2017). By comparing the neural data obtained during these trials we tested whether our system was able to detect beta band desynchronization both during overt and imagined movement. Moreover, these changes were apparent even during stimulation, despite the dramatic changes in the frequency spectrum observed during DBS. Throughout this initial process, we conducted interviews with the patients to assess their level of comfort and gain a greater understanding of the patient experience.

$$\text{Tremor Severity} = \frac{(\text{IMU Tremor Band Power})^2}{\text{IMU Total Power}} \quad (2)$$

This system fulfilled its primary goal as a technology demonstrator. aDBS triggered by movement, particularly in the case of EMG, was successful in suppressing tremor while delivering less total stimulation. With an average delay to max level stimulation of 2.40 ± 0.33 s, this resulted in stimulation delivered 76.6% of the time the patient was moving and 15.3% of the time the patient was at rest. This resulted in tremor severity (per Equation 2) during movement of 0.277 compared to 1.296 during no stimulation and 0.6473 during cDBS trials conducted with the same patient during the same session. aDBS driven directly by tremor severity interpreted from IMU data was less successful, due to feedback causing the stimulation to fluctuate wildly. Beta band desynchronization was shown to be reliably identifiable with the hardware available, and therefore a potential control variable for future aDBS systems triggering



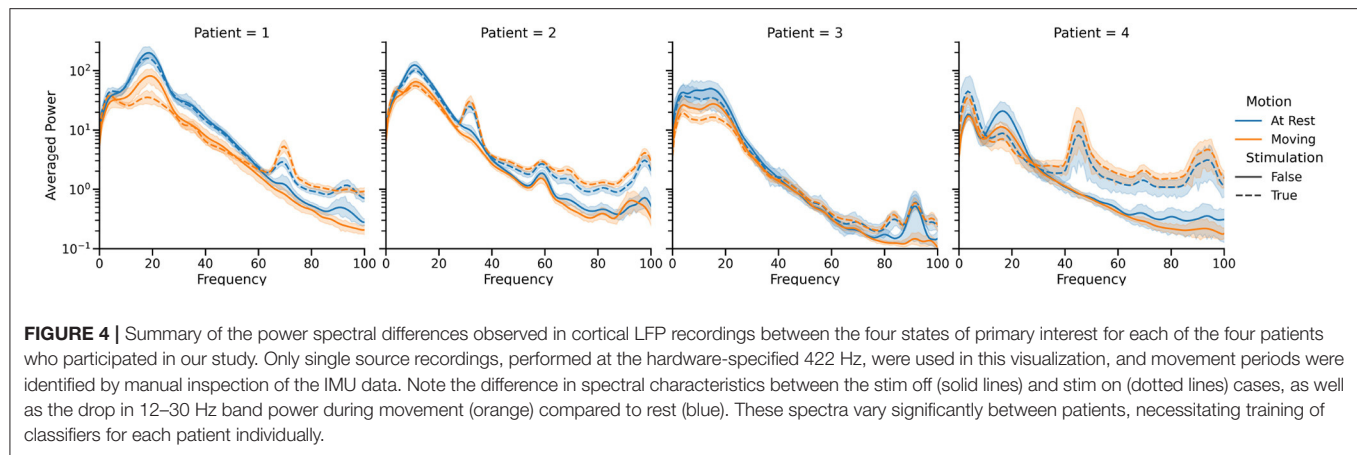
off of movement-related biomarkers. Although this initial work showed the potential of our system as an investigational device and the promise of aDBS for ET, it also highlighted many of the challenges that would need to be resolved over the rest of the study. Conversations with the patients exposed their reticence to undergo battery replacement surgery, thereby highlighting the importance of conserving battery power. Since streaming neural data used approximately 10 times as much battery as normal operation, experimental sessions were kept succinct and avoided unnecessarily draining the patient's battery. Moreover, using aDBS to minimize the energy usage of stimulation would be an important consideration throughout the rest of the project. The delays inherent in the distributed Activa PC+S system made the control scheme for distributed aDBS difficult to implement. We often observed transient periods of significant tremor at the onset of movement, before the aDBS control caught up and turned-on stimulation. Solving this issue would be one of the main targets we would pursue.

3.2. Distributed BCI Control

Informed by these initial results, we endeavored to build a neural driven, BCI aDBS system (Herron et al., 2015, 2017; Houston et al., 2017; Castaño-Candamil et al., 2020). A system like this, driven by the well-documented beta band desynchronization phenomenon, would allow stimulation to only be delivered when necessary during movement (Pfurtscheller and Aranibar, 1977; Toro et al., 1994; Unterwieser et al., 2020). Since the

Activa PC+S is capable of using cortical LFP power bands to control stimulation, validating beta desynchronization driven aDBS in a distributed fashion, would pave the way for fully implanted aDBS systems. As a further extension to this cortically driven aDBS, we also endeavored to build a volitional aDBS system. This approach offered to make aDBS more flexible and applicable to more diseases by handing control of the stimulation directly back to the patient. The idea was that although controlling stimulation would take conscious effort initially, repeated training and daily use would allow the patient to develop automatic, almost subconscious control of the stimulation. As indicated by our conversations with the patients, this also had the potential to greatly improve the patient experience by increasing the sensation of agency and strengthening the identification of the device as a part of themselves (Figure 4) (Brown et al., 2016; Herron et al., 2017).

The method we chose to detect movement was the well documented phenomenon of event-related-desynchronization in the beta band (12–30 Hz). This approach consisted of training linear discriminant classifiers to detect significant drops in power in the beta band that corresponded to movement for each patient. Since the application of high-frequency DBS significantly altered the power spectra visible on cortical recordings, two classifiers were trained in parallel, one with DBS off and one with DBS on. Classifier training used the prompted movement task described above. Average power spectra were computed in each of the four states for that patient on that day. A weight was assigned



to each frequency bin, based on how much the power in that bin changed between the rest and prompted movement states for each stimulation state. Once the classifiers were trained, the adaptive DBS algorithm proceeded as follows. Starting in the stim off state, the off classifier listened to the neural data stream, calculated power spectra using Welch's method with a Hann window and normalized by the average and standard deviation of the classifier training data. We then took the dot product of this power spectrum with the classifier weights and fed it into a logistic regression function. When this result crossed a pre-set threshold, indicating the onset of volitional movement, stimulation was ramped up to its maximum clinically permitted value over the course of a few seconds, and the system switched to using the stim-on classifier. Since the ramping of stimulation is known to lead to the greatest number of side effects, the ramp rate was carefully tuned to be the fastest pre-set possible ramp rate that was tolerable for the patient. When the stim-on classifier detected that the beta band power had risen back up to levels indicating rest, stim was ramped back down and the system switched back to the stim-off classifier. The progression of cortical beta is shown in the third row of **Figure 5**. The thresholds were tuned for stimulation sensitivity, as reliably delivering stimulation during movement was considered more important than reliably turning stimulation off when at rest.

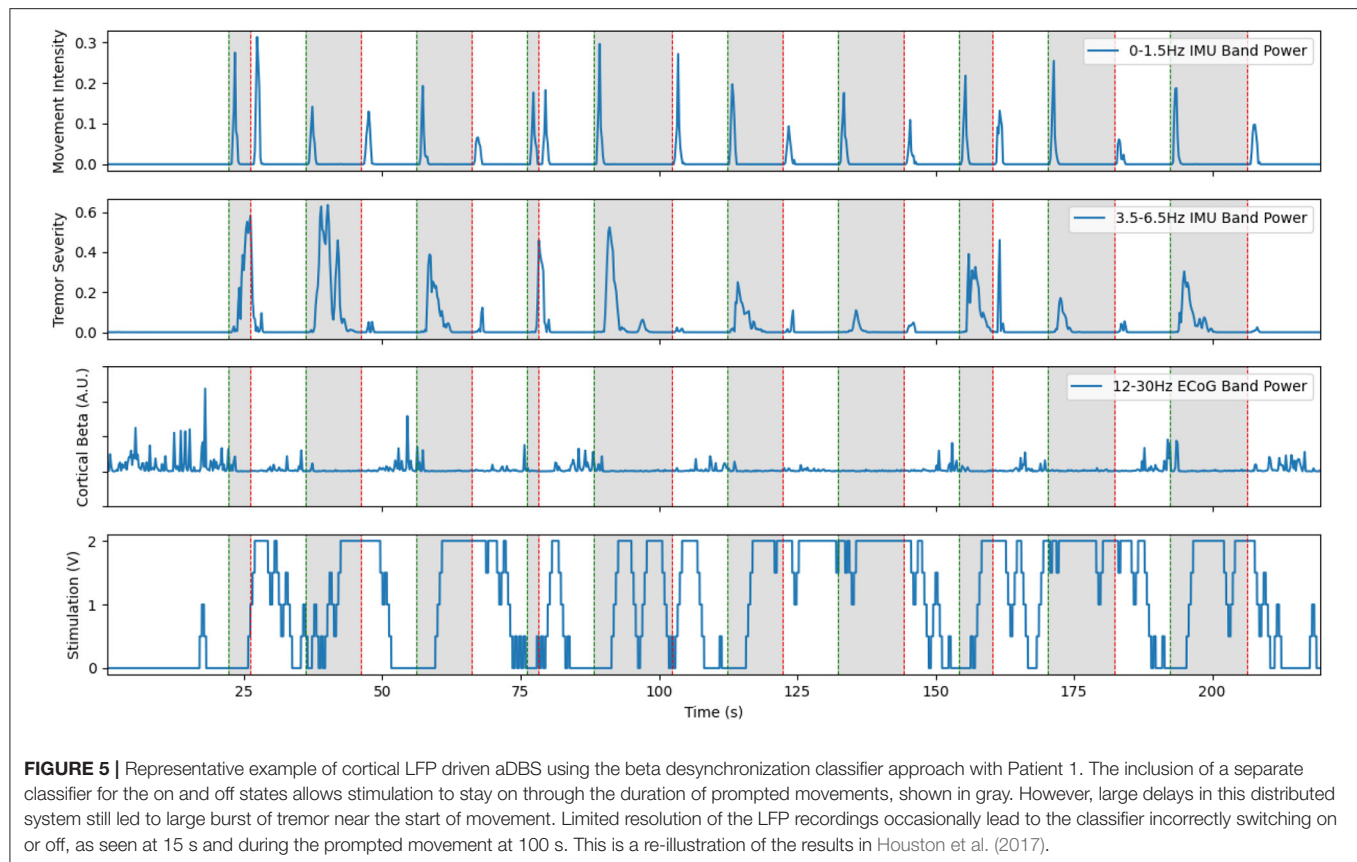
The neural BCI approach resulted in a system that could control the delivery of stimulation with a sensitivity of 90 and 100% for the prompted movement and FTM drawing tasks, respectively (Houston et al., 2018). For this trial, stimulation was delivered 64.8% of the time the patient was moving and 29.0% of the time the patient was at rest. Tremor severity (per Equation 2) during movement was 3.750 compared to 0.4338 during no stimulation and 8.271 during cDBS trials conducted with the same patient during the same session. However, over all patients and all sessions, we found a 46.0% average improvement in clinical FTM scores over the no stimulation condition, compared to a 42% average improvement during cDBS. Although the difference between each of these and the stimulation off state was statistically significant, the difference between the two stimulation paradigms was not. A representative trial of this aDBS paradigm is shown in **Figure 5**. Although the system was

always able to identify movement periods in this excerpt, the identification was often delayed and noisy. This was in large part due to the comparatively low spatial and temporal resolution of the cortical strips. Only four electrodes were available, and only a single pair could be used at a time to provide the differential recordings required for the system. The strip was placed during the implantation surgery and could not be adjusted afterwards. This meant that any imperfections in the initial placement and shifts over time left the electrode not in position to optimally observe beta band desynchronization. Moreover, the delay between the onset of movement and the onset of stimulation was 1.5 s on average. For the trial shown above, we observed an average delay to the clinically effective level of stimulation of 3.35 ± 1.50 s. In certain cases, this delay time could reach up to 5 s. This was due to the transmission delays inherent in the system architecture, the extra time required to compute power spectra, and the limitations of the ramp rate. These confounding effects can be clearly seen in **Figure 5** as stimulation starts well into the gray prompted movement periods (bottom row), leading to a large burst of tremor before stimulation becomes effective (second row). However, once stimulation did ramp up to clinical levels, the tremor was effectively suppressed.

In a similar vein, we conducted a study in collaboration with the University of Freiburg to investigate distributed aDBS in a way that could more smoothly adapt stimulation and better adapt to the patient state (Castaño-Candamil et al., 2020). This approach used bollinger bands to perform local estimates of high and low tremor states to dynamically drive stimulation, which allowed the system to more robustly respond to movement and non-movement states in a variety of tasks without the need for re-training. Although this work provided a more robust method of driving aDBS that led to greater power savings than the simpler method presented above, the more advanced calculations required meant it could not be implemented in a fully implantable state. However, it remains a promising avenue to explore as the hardware available improves.

3.3. Fully Implanted Adaptive DBS

The fully implanted system was the culmination of all the work performed and the first potentially clinically translatable system

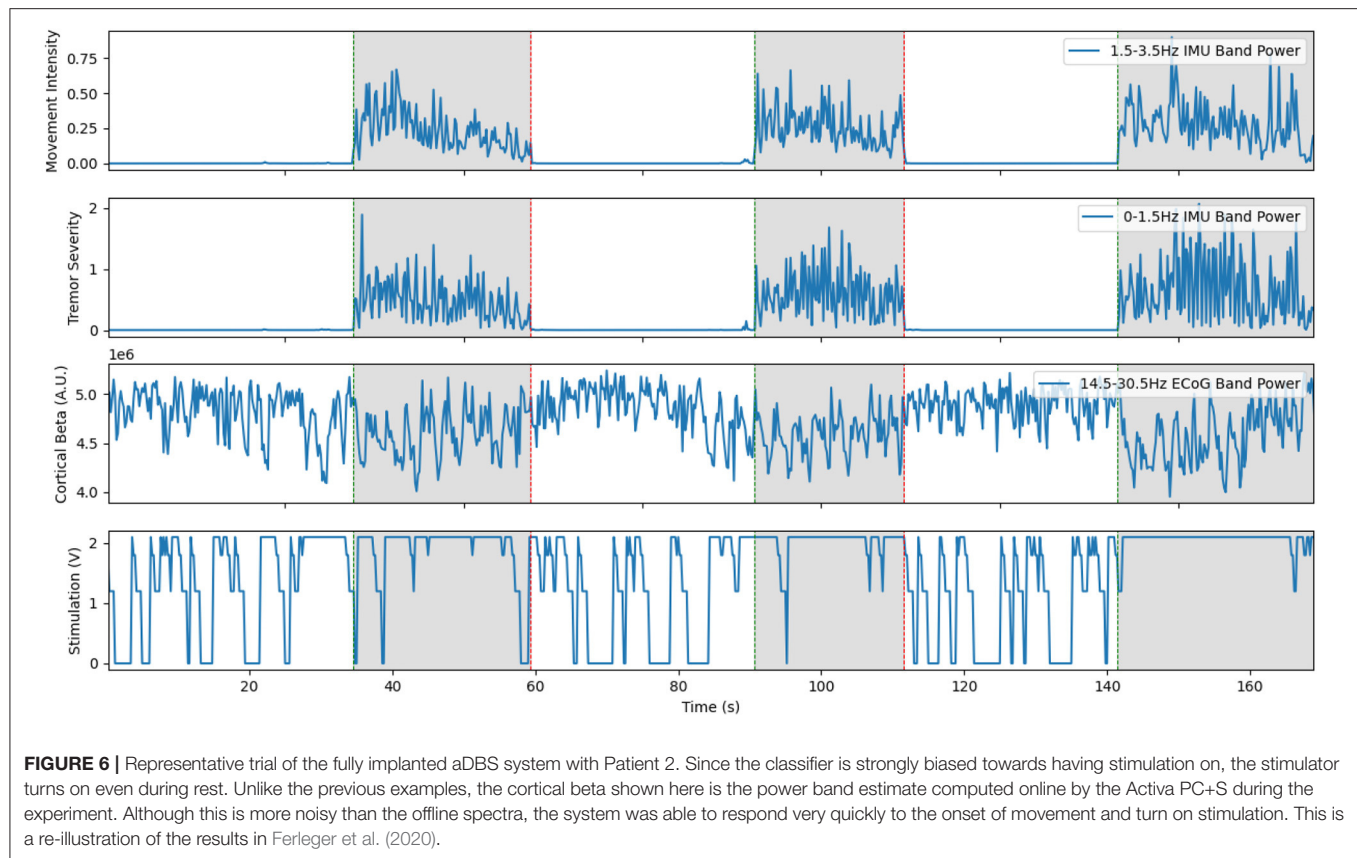


(Ferleger et al., 2020). As identified in previous work, the time delays inherent in the distributed architecture were a major source of aDBS paradigm design difficulties. Since the aDBS algorithm implemented in this case would function entirely within the IPG, these communication delays would be massively reduced. Additionally, there would be no constraints placed on the patient in terms of additional wearable hardware. As a result, IMU data from the android smartwatch and the computational power of a desktop PC could only be used in the training process. The real time updating of stimulation would have to rely entirely on the capabilities of the IPG. Moreover, the resultant system should be easily adaptable to new patients to reduce the large time commitment from both patient and clinician required to tune stimulation parameters. By automating the programming methods used to develop the initial aDBS system, patients could benefit from aDBS without requiring the prolonged manual tuning of the classifier necessary in previous versions (Figure 6).

Classifier training proceeded in a semi-automated fashion leveraging the convenience of a desktop PC to determine a classifier that could be used entirely within the capabilities of the implanted device. Due to hardware limitations, there was no explicit way to pass stimulation state as a parameter to the onboard mechanism. To overcome this, classifiers were trained for each of the four possible states the patient and stimulation system could find themselves in: Stim off, rest; stim on, rest; stim off, movement; and stim on, movement. Thirty seconds

of data were collected for each state, with optional repetition of selected tasks. For each of the patients, data from these individual classifiers was combined, which resulted in a classifier that used the power in the band near the stimulation frequency to determine the stimulation state, and the power in the beta band (usually 12.0–28) to distinguish whether the patient was moving or not. Again, since unnecessary stimulation was considered less of an issue that missed stimulation, the classifier was strongly biased towards favoring the stimulated state. This classifier was then uploaded to the IPG and used to switch stimulation on and off. Total time to train this system was under 20 min for each patient. Evaluation of this system was performed in a manner similar to previous experiments, using both tremor suppression calculated from IMU data and total electrical energy delivered.

This system demonstrated the advantages of a fully embedded aDBS system. Although classification had to be performed on simpler hardware, it maintained high levels of effectiveness. The system had a sensitivity of 91.8%, and a false positive rate of 28.7% (Ferleger et al., 2020). Due to classifier bias, and the limited resolution available in this implanted configuration, the classifier often interpreted temporary drops in beta power as movement. Tremor was suppressed as well or even better than cDBS. Overall, the dramatic reduction in control delays seem to outweigh limitation on the complexity of the classifier. Additionally, the ability of this system to be deployed to patients without the need for a tether to external hardware cannot be overstated. This



is the first reported, full-translatable, aDBS system for ET. In related work published by our the group at the University of Florida, the value of embedded closed-loop for the treatment of ET has been further demonstrated upon in an expanded group of patients over a time period of several months (Opri et al., 2020). This study used similar cortical biomarkers, but achieved much higher specificity, potentially due to a more sophisticated paradigm for training their neural classifiers. Our approach for the classifier was based on a large block structure. We collected data during movement and rest, with stimulation both on and off. The classifier was then trained by comparing the power spectra between these four conditions. Conversely, the UF team used data from a prompted movement task to train their classifiers. It seems that these repeated small samples were better able to generalize to the tested behavior, potentially by capturing the transitions between states. Additionally, motivated by clinical considerations, we biased our classifiers towards avoiding false negatives. This resulted in our system having a higher sensitivity than it would otherwise by compromising specificity, although the prioritization of therapy over power savings resulted in stimulation turning on when not needed. There is still much that future studies could do to improve performance with newer hardware. However, this system showed better performance in TEED and greater tremor suppression than cDBS. Although more study is necessary to understand the source of this improved performance, it is an encouraging sign

that aDBS systems could improve the lives of patients even more than cDBS systems when deployed in clinical practice.

4. DISCUSSION

Over the course of this study, we made several important advancements. We demonstrated the feasibility of aDBS for ET using cortical LFPs as a control signal. We then developed preliminary machine-learning driven BCI and volitional control systems. These elements were then put together to create a fully implantable, clinically translatable aDBS system for ET. Over the course of this process, we came to many conclusions that we hope will be helpful to future generations of aDBS for ET. Here we outline some of the most important conclusions that we came to over the course of this study, both practical and theoretical. We also provide our outlook on what the key hardware and ethical challenges that need to be solved in aDBS for ET.

4.1. Remaining Work

One of the most prevalent issues that we ran into was the control delay inherent in the distributed system. A large part of this delay can be attributed to the hardware limitations of the Activa PC+S. However, any distributed system will necessarily have larger delays due to the increased communication distance over a fully implanted one. Conversely, a distributed system will have much higher computational power and flexibility than

a fully implanted one. As we demonstrated in our embedded aDBS experiments, the tradeoffs between these two types of systems can be minimized by utilizing a hybrid approach. By training the system in a distributed fashion, we can utilize the full computational power that larger hardware offers to adapt stimulation in a high dimensional parameter space. By using this system to set the parameters on a simpler, fully-embedded classifier, we can retain the fast response times of a fully embedded system. Future studies will endeavor to further tighten and automate this two-stage control loop. It is likely that the classifier used in the implanted system will not remain effective for long periods of time as the patient's state and medications change. Multi-modal monitoring of the patient's symptoms, with simultaneous streaming of neural, IMU, and even video data, would detect when these changes occur. The system would then either prompt the patient to re-train the classifier or substitute in a previously trained classifier that would better suit the patient's current state.

As has been well documented; side effects of stimulation, especially paresthesia, are often exacerbated while stimulation is being ramped up. To ensure the comfort of our patients, we always set a maximum ramp rate for each patient that did not induce intolerable side effects. Several studies have noted the nuances of stimulation ramp rates but to our knowledge no conclusive best practices have been established (Petrucci et al., 2021). In our patients, we noticed that the maximum tolerable ramp rate differed drastically. Further studies will be required to better understand this phenomenon. With a better understanding of the nuances of ramp rates, stimulation could be applied in a way to circumvent paresthesia while still allowing for fast control of DBS.

Due to the communication delays discussed above, we often observed large bursts of transient tremor at the onset of movement. Limitations on the ramp rate necessary for patient comfort mean that the delay between the need for stimulation and when stimulation reached clinically effective levels was even longer. Future studies should therefore investigate aDBS systems with different levels of minimal and maximal stimulation. Instead of switching stimulation between the on and off states, we would instead switch between high and low amplitude stimulation states. The low voltage state would be set low enough to not be noticeable for the patient, and the high level would be at the clinically effective threshold. Since the difference in voltage between states would be smaller, this would enable the system to respond faster without inducing ramping side effects.

All our work has focused on changing the amplitude of the delivered stimulation. There is evidence showing that stimulation amplitude offers the most control of any single parameter adjustment (Cooper et al., 2008). However, DBS efficacy is highly dependent on the other two tunable parameters: pulse width and stimulation frequency. Stimulation frequency is of particular importance according to theories that tremor may be caused by excessive coupling between oscillatory activity in different regions of the brain (Raethjen and Deuschl, 2012; Helmich et al., 2013; Filip et al., 2016). If this is the case, adjusting stimulation frequency could reveal stimulation frequencies that both improve and worsen tremor. The existence of multiple

harmonic stimulation frequencies that have similar therapeutic effects would be a strong confirmation of this phenomenon. As a result, the effect of stimulation frequency on DBS should be investigated both for the sake of improving clinical effectiveness and for the potential of a greater understanding of the pathology of ET.

Another aspect of aDBS that has been shown to be important is the exact methodology of training the neural data classifier. This is highlighted by the comparison between our results and those recently published from the University of Florida (Opri et al., 2020). It is clear that the training data and paradigm must be designed with the ability to translate into a more naturalistic context in mind. Their study achieved higher sensitivity, specificity, and overall accuracy. When classifiers such as these are designed, we believe it is important to take the patient experience and clinical practice into account. False negatives, lack of stimulation when it is needed, are more detrimental to the patient than false positives, stimulation even when it is not needed. For this reason, it is important that classifiers are optimized primarily for sensitivity instead of just overall accuracy. These considerations will help ensure that aDBS is best optimized for the needs of the patient.

4.2. Alternative Approaches

A potential direction of research that we did not fully explore in our study is the potential to smoothly adapt the levels of stimulation to the severity of symptoms. Systems like this could follow a similar approach to the beta thermostat approach demonstrated in the PD literature (Qasim et al., 2016; Swann et al., 2018), adjusting stimulation to even out therapy when provided in conjunction with medication. We performed proof-of-concept distributed studies using bollinger bands to drive 'graded-DBS' (Castaño-Candamil et al., 2020). This work showed promise in handling the non-stationary dynamics and adapting the stimulation algorithms in a patient-specific way. However, hardware limitations prevented us from implementing this approach in a fully implanted context. This approach would allow the aDBS system to adapt stimulation levels more precisely to the changes in patient.

One of the great remaining hurdles in the development of aDBS for ET and treatments for ET in general is the limited understanding of the pathology of the disease. Although progress has been made recently suggesting the involvement of multiple network components and the central role of the cerebellum many unanswered questions remain (Raethjen and Deuschl, 2012; Filip et al., 2016; Ibrahim et al., 2020; Pan et al., 2020). With this growing evidence for the role of the cerebellum, it will be important to identify whether the cerebellum is the sole generator of pathological oscillations, or do further changes need to happen for resonant frequencies to arise. Moreover, it is unclear whether pathological changes occur in other brain region that facilitate the propagation of tremor oscillations. An improved understanding of the pathology of ET could lead to new stimulation targets and stimulation paradigms that better counteract the symptoms of ET, or even pharmacological treatments that directly target the underlying pathological changes. Due to the acute control

possible in aDBS systems, this research will be able to help answer many of these important questions.

aDBS for ET lacks the sort of robust neural biomarkers that are directly correlated to symptoms. In PD, for example, abnormally long bursts of STN beta activity has been shown to be directly correlated to symptoms, while a sharp peak in the gamma band has been shown to be directly correlated to stimulation-induced dyskinesia, resulting in a perfect control signal for ramping DBS amplitude up and down (Whitmer et al., 2012; Little et al., 2013; Swann et al., 2018). The ET DBS systems described here must rely on proxy biomarkers such as beta band desynchronization as a measure of movement, which is correlated with symptoms. Since this biomarker imperfectly follows symptoms, there is a hard cap on how close to optimal performance our systems can come. Thankfully future aDBS research is well positioned to begin unraveling these questions. Recent work has shown evidence that there may be alternative biomarkers of movement visible in VIM LFPs (Opri et al., 2016). The potential of this VIM approach was further demonstrated by the researchers at Oxford, who developed a VIM based aDBS paradigm using extremely detailed neural recordings (He et al., 2021). We look forward to seeing how this work develops the field, as VIM aDBS would remove the need to implant the additional cortical strip required for our approach. If a direct biomarker of tremor severity, identifiable both during and off stimulation, could be found, the aDBS could be driven exactly as needed. Further verification and development of both these and cortical biomarkers of tremor is essential for robust aDBS systems for ET. The presence of multiple simultaneously computable biomarkers would allow for cross-validation and increased robustness.

Future studies of aDBS with larger numbers of patients will also be capable of investigating the variations observed between patients. Recent work is increasingly suggesting that ET is not a single disorder, but rather a family of related disorders that need to be treated slightly differently (Soto and Fasano, 2020). This is also supported by the wide variation in effective stimulation settings observed even in our relatively small cohort of patients. For most ET patients, the recommended stimulation frequency is close to 140 Hz, but for one of our patients we found the most effective stimulation occurred near frequencies of about 90 Hz. A survey of optimal stimulation parameters determined in an automated way, matched with neural recordings on and off stimulation would be a promising avenue to investigate these differences. In this context, aDBS is firmly in the regime of personalized medicine. Future aDBS applications should retain the focus on tuning stimulation individually to the needs of each specific patient. Broad generalization is useful only in so far as it simplifies the training process of each patients individualized aDBS paradigm and highlights the nuances of each patient's needs.

One of the developments that could most dramatically push aDBS for ET forward is a well-verified, explanatory model of ET. Specifically, such a model should explain at a high level the interactions between brain areas that give rise to pathological ET tremor oscillations. Though one such promising model has recently been proposed, more work is needed to verify this model and determine how it can be fit to patient data (Yousif

et al., 2017; Duchet et al., 2020). This modeling effort should proceed in conjunction with the imaging-based modeling efforts (Dembek et al., 2017; Al-Fatly et al., 2019; Middlebrooks et al., 2021b). As these models move towards more predictive power, they will allow for more insight during the process of selecting the implant site and tuning aDBS parameters for new patients (Middlebrooks et al., 2021a). Neural and biophysical recordings of patient state could be used to cluster the patient with other patients that display similar symptoms, with the expectation that similar stimulation would be similarly effective for patients within a cluster. This could dramatically reduce the number of parameters sets that need to be tested to find an effective stimulation paradigm. When repeated with multiple patients this would result in a map of ET disease states and related diseases. Even once DBS parameters are set, it is likely that over the course of the patient's daily life, optimal stimulation parameters will change. As the patient takes medicine, for example, the stimulation amplitude and frequency change. A reliable model could then be used to help inform automatic switching of stimulation parameters as the patient's state changes. Fundamentally, a good enough model could provide insight into the pathology of the disease and aid the search for ET treatments that target the underlying cause rather than just treat symptoms.

4.3. Challenges of Clinical Translatability

As has been noted in several reviews in this field, there is a large gap between the experimental demonstration of aDBS and a clinically translatable treatment (Arlotti et al., 2016; Meidahl et al., 2017). We took part in collaborations to address some of these challenges with our development of automated tools for optimization of DBS and aDBS paradigms (Haddock et al., 2018). However, several challenges remain.

One of the largest challenges to the clinical translatability of the neural-driven aDBS systems we developed over the course of this study is the availability of on-label cortical strips. These are a required component for the implementation of aDBS systems with that use movement intention sensed from cortex as a control parameter. As implied by our BCI control work, these could also be used in a volitional fashion to seamlessly offer the patient a greater degree of control over stimulation. Recent work along with our own analysis have shown that cortical electrodes such as these retain a high signal to noise ratio for years after implantation (Nurse et al., 2017; Frączek et al., 2021). This has been further confirmed by the group at UF, who have shown that aDBS driven by cortical strips is robust over several months (Opri et al., 2020). Moreover, in the context of our study we observed no adverse effects as a result of the implantation of the cortical strips, which may motivate work pursuing their clinical validation as a safe extension to existing DBS systems.

In the fully implanted aDBS system we describe above, training of the implanted algorithm proceeds in a distributed fashion. In our experiments, we train and test the classifiers within a reasonably short time scale of less than a few hours. However, this begs the question of how often these sorts of classifiers will need to be updated. If training need only be repeated once every few months, then a system like this could be tuned during routine clinical visits. Thanks to the automated

nature of the system, this could be carried out by a trained technician instead of a neurologist. However, if the algorithm requires updating on a near daily basis, then any clinically translatable approach would need to be deployable to the patient's home. Both the algorithm update itself and detection of the ineffectiveness of the current algorithm would have to be fully automated. It is also not clear how well the control variables used in our experiments would translate to daily activities. In either case, more work will be required to evaluate the robustness of aDBS paradigms developed in this way.

Finally, there are a number of ethical considerations that arise as aDBS systems are translated into common clinical practice. We have discussed a number of these elsewhere, but we provide a short review here (Brown et al., 2016). Concerns have been raised about the potential for stimulation to cause shifts in the user's perception of selfhood and agency e.g., in cases where stimulation causes behavioral changes as a side effect (Klein et al., 2015). aDBS might 1 day mitigate and manage these side effects. Questions remain, however, about how users will interact with more robust aDBS systems; how those interactions impact clinical outcomes and quality of life (Brown, 2020). It is not clear, for example, how much control users will want over stimulation parameters, or how involved they want to be in aDBS algorithm training, or how different algorithms will impact user experience. To investigate these questions, a neuroethicist on our team (TB) lead a series of longitudinal, semi-structured phenomenological interviews with each patient the goal of which were to give patients the opportunity to describe using the experimental aDBS platform (Brown et al., 2016). A final analysis of these interviews is underway.

4.4. Hardware and Future Systems Outlook

Next generation systems which have been developed and are on the horizon offer significant improvements over the Activa PC+S system.

The Medtronic Summit RC+S offers many of the same capabilities as the Activa PC+S but with greatly improved specifications (Stanslaski et al., 2018). The Summit system can record at 1 kHz, which enables use of gamma band activity (50–100 Hz) to inform aDBS decisions without excessive contamination from Nyquist noise. This is coupled with more advanced, onboard digital spectral power estimation hardware that will provide better accuracy and resolution than the analog system available in the Activa system. The Summit also supports a much more intricate state table for switching stimulation parameters in a fully embedded fashion. This device is already being used to perform aDBS research at several locations (Petrucci et al., 2020; Johnson et al., 2021). The increased capabilities of the Summit RC+S will allow the embedded system to detect biomarkers more reliably and respond with stimulation changes faster and more precisely. Since the device is also re-chargeable the worry about battery conservation is greatly reduced. Battery intensive experiments and streaming of neural data can now be done in the patient's home without excessively accelerating the need for a battery replacement surgery. Such day-to-day monitoring will allow for a more nuanced understanding of both DBS and the disease being treated.

Another upcoming system is the Medtronic Percept (Goyal et al., 2021). This system does not include cortical electrodes, but still offers the ability to record from the implantation target. Raw LFP data can be streamed out to a programming tablet in a manner similar to the Activa PC+S. Alternatively, chronic average band powers on pre-set power bands can be recorded to the on-board memory of the device, and then later downloaded for analysis. Although this device offers lower resolution data than the Summit, it is labeled for clinical treatment. This means that chronic sensing during stimulation could soon enter more regular clinical practice as a diagnostic tool that can aid clinicians in adjusting stimulation parameters. As a side effect, future studies could leverage this chronic data to better understand the pathology of ET and as a jumping-off point for next generation aDBS paradigms. When combined with wearable sensors to monitor the patient's activity, this could prove an invaluable tool for adapting aDBS into daily life.

5. CONCLUSIONS

aDBS for ET remains a growing area of investigation. Since the start of this study, the field has developed from a single demonstrative case study to a clinically translatable approach. We have developed aDBS for ET from its initial state to a fully implantable system that could be adapted to clinical practice. This fully implantable system is able to suppress tremor more effectively than cDBS while delivering less total stimulation. Despite this, numerous avenues for advancement remain. The longitudinal efficacy of fully-implanted aDBS algorithms have not been tested in a chronic, at-home environment. All work to date has trained and tested the classifiers within the space of a day, so it is likely that transitioning to a chronic setup will require the development of automated tools that would allow the patient to re-train the aDBS algorithm on a regular basis with minimal input from a clinician. Any clinical translation of this work will depend on the availability of safe, reliable, on-label cortical electrodes. We look forward to the life-changing work that will be done in this space as new hardware, techniques, and understanding becomes available.

AUTHOR CONTRIBUTIONS

TF prepared the figures and wrote the manuscript. BF helped with figure preparation. TB provided input on neuro-ethical considerations and drafting the relevant sections of the manuscript. BF, MT, AH, BH, and JH performed the experiments reviewed here. JO, AK, JH, and HC provided oversight of the research. All authors reviewed the final manuscript.

FUNDING

This work was supported by a donation of devices and funds from Medtronic. Reviewed work also includes funding from the following sources: the Department of Defense through the National Defense and Engineering Graduate Fellowship (DoD NDSEG), the National Science Foundation

Graduate Research Fellowship Program (NSF GRFP), the National Institutes of Health (NIH) award R01-NS065186, BrainLinks-BrainTools Cluster of Excellence funded by the German Research Foundation (DFG, grant no. EXC1086), the Federal Ministry

of Education and Research (BMBF, grant no. 16SV8012), and by Award Number EEC-1028725 from the National Science Foundation for the Center for Sensorimotor Neural Engineering, now known as the Center for Neurotechnology.

REFERENCES

- Al-Fatly, B., Ewert, S., Kübler, D., Kroneberg, D., Horn, A., and Kühn, A. A. (2019). Connectivity profile of thalamic deep brain stimulation to effectively treat essential tremor. *Brain* 142, 3086–3098. doi: 10.1093/brain/awz236
- Arlotti, M., Rosa, M., Marceglia, S., Barbieri, S., and Priori, A. (2016). The adaptive deep brain stimulation challenge. *Parkinsonism Relat. Disord.* 28, 12–17. doi: 10.1016/j.parkreldis.2016.03.020
- Brown, T. (2020). Building intricate partnerships with neurotechnology: deep brain stimulation and relational agency. *Int. J. Fem. Approaches Bioeth.* 13, 134–154. doi: 10.3138/ijfab.13.1.09
- Brown, T., Thompson, M. C., Herron, J., Ko, A., Chizeck, H., and Goering, S. (2016). Controlling our brains—a case study on the implications of brain-computer interface-triggered deep brain stimulation for essential tremor. *Brain Comput. Interfaces* 3, 165–170. doi: 10.1080/2326263X.2016.1207494
- Castaño-Candamil, S., Ferleger, B. I., Haddock, A., Cooper, S. S., Herron, J., Ko, A., et al. (2020). A pilot study on data-driven adaptive deep brain stimulation in chronically implanted essential tremor patients. *Front. Hum. Neurosci.* 14:421. doi: 10.3389/fnhum.2020.541625
- Cooper, S. E., Kuncel, A. M., Wolgamuth, B. R., Rezai, A., and Grill, W. M. (2008). A model predicting optimal parameters for deep brain stimulation in essential tremor. *J. Clin. Neurophysiol.* 25, 265. doi: 10.1097/WNP.0b013e318182ed44
- Dembek, T. A., Barbe, M. T., Åström, M., Hoevels, M., Visser-Vandewalle, V., Fink, G. R., et al. (2017). Probabilistic mapping of deep brain stimulation effects in essential tremor. *Neuroimage Clin.* 13:164–173. doi: 10.1016/j.nicl.2016.11.019
- Duchet, B., Weerasinghe, G., Cagnan, H., Brown, P., Bick, C., and Bogacz, R. (2020). Phase-dependence of response curves to deep brain stimulation and their relationship: from essential tremor patient data to a wilson-cowan model. *J. Math. Neurosci.* 10, 1–39. doi: 10.1186/s13408-020-00081-0
- Fahn, S., Tolosa, E., Marin, C., et al. (1988). Clinical rating scale for tremor. *Parkinsons Dis. Mov. Disord.* 2, 271–280.
- Ferleger, B. I., Houston, B., Thompson, M. C., Cooper, S. S., Sonnet, K. S., Ko, A. L., et al. (2020). Fully implanted adaptive deep brain stimulation in freely moving essential tremor patients. *J. Neural Eng.* 17, 056026. doi: 10.1088/1741-2552/abb416
- Filip, P., Lungu, O. V., Manto, M.-U., and Bareš, M. (2016). Linking essential tremor to the cerebellum: physiological evidence. *Cerebellum* 15, 774–780. doi: 10.1007/s12311-015-0740-2
- Frączek, T. M., Ko, A. L., Chizeck, H. J., and Herron, J. A. (2021). “Robustness of beta desynchronization from chronically implanted cortical electrodes on multiple time scales,” in *Submitted to: 43rd Annual International Conference of the IEEE Engineering in Medicine and Biology Society (EMBC)* (IEEE), 6041–6044.
- Goyal, A., Goetz, S., Stanslaski, S., Oh, Y., Rusheen, A. E., Klassen, B., et al. (2021). The development of an implantable deep brain stimulation device with simultaneous chronic electrophysiological recording and stimulation in humans. *Biosens. Bioelectron.* 176:112888. doi: 10.1016/j.bios.2020.112888
- Haddock, A., Mitchell, K. T., Miller, A., Ostrem, J. L., Chizeck, H. J., and Miciocinovic, S. (2018). Automated deep brain stimulation programming for tremor. *IEEE Trans. Neural Syst. Rehabil. Eng.* 26, 1618–1625. doi: 10.1109/TNSRE.2018.2852222
- Haubenberger, D., and Hallett, M. (2018). Essential tremor. *N. Engl. J. Med.* 378, 1802–1810. doi: 10.1056/NEJMcip1707928
- He, S., Baig, F., Mostofi, A., Pogossyan, A., Debarros, J., Green, A. L., et al. (2021). Closed-loop deep brain stimulation for essential tremor based on thalamic local field potentials. *Mov. Disord.* 36, 863–873. doi: 10.1002/mds.28513
- Helmich, R. C., Toni, I., Deuschl, G., and Bloem, B. R. (2013). The pathophysiology of essential tremor and parkinson's tremor. *Curr. Neurol. Neurosci. Rep.* 13, 1–10. doi: 10.1007/s11910-013-0378-8
- Herron, J., Denison, T., and Chizeck, H. J. (2015). “Closed-loop dbs with movement intention,” in *2015 7th International IEEE/EMBS Conference on Neural Engineering (NER)* (IEEE), 844–847.
- Herron, J. A. (2016). *Closed-Loop Deep Brain Stimulation: Bidirectional Neuroprosthetics for Tremor and BCI* (Ph.D. thesis).
- Herron, J. A., Thompson, M. C., Brown, T., Chizeck, H. J., Ojemann, J. G., and Ko, A. L. (2016). Chronic electrocorticography for sensing movement intention and closed-loop deep brain stimulation with wearable sensors in an essential tremor patient. *J. Neurosurg.* 127, 580–587. doi: 10.3171/2016.8.JNS16536
- Herron, J. A., Thompson, M. C., Brown, T., Chizeck, H. J., Ojemann, J. G., and Ko, A. L. (2017). Cortical brain-computer interface for closed-loop deep brain stimulation. *IEEE Trans. Neural Syst. Rehabil. Eng.* 25, 2180–2187. doi: 10.1109/TNSRE.2017.2705661
- Houston, B., Thompson, M., Ko, A., and Chizeck, H. (2018). A machine-learning approach to volitional control of a closed-loop deep brain stimulation system. *J. Neural Eng.* 16, 016004. doi: 10.1088/1741-2552/aae67f
- Houston, B. C., Thompson, M. C., Ojemann, J. G., Ko, A. L., and Chizeck, H. J. (2017). “Classifier-based closed-loop deep brain stimulation for essential tremor,” in *2017 8th International IEEE/EMBS Conference on Neural Engineering (NER)* (IEEE), 316–320.
- Ibrahim, M. F., Beevis, J. C., and Empson, R. M. (2020). Essential tremor—a cerebellar driven disorder? *Neuroscience* 462, 262–273. doi: 10.1016/j.neuroscience.2020.11.002
- Johnson, V., Wilt, R., Gilron, R., Anso, J., Perrone, R., Beudel, M., et al. (2021). Embedded adaptive deep brain stimulation for cervical dystonia controlled by motor cortex theta oscillations. *Exp. Neurol.* 345:113825. doi: 10.1016/j.expneurol.2021.113825
- Klein, E., Brown, T., Sample, M., Truitt, A. R., and Goering, S. (2015). Engineering the brain: ethical issues and the introduction of neural devices. *Hast. Center Rep.* 45, 26–35. doi: 10.1002/hast.515
- Koss, A. M., Alterman, R. L., Tagliati, M., and Shils, J. L. (2005). Calculating total electrical energy delivered by deep brain stimulation systems. *Ann. Neurol.* 58, 168. doi: 10.1002/ana.20525
- Little, S., Pogossyan, A., Neal, S., Zavala, B., Zrinzo, L., Hariz, M., et al. (2013). Adaptive deep brain stimulation in advanced parkinson disease. *Ann. Neurol.* 74, 449–457. doi: 10.1002/ana.23951
- Little, S., Pogossyan, A., Neal, S., Zrinzo, L., Hariz, M., Foltynie, T., et al. (2014). Controlling parkinson's disease with adaptive deep brain stimulation. *J. Vis. Exp.* 89:51403. doi: 10.3791/51403
- Louis, E. D., and Ferreira, J. J. (2010). How common is the most common adult movement disorder? update on the worldwide prevalence of essential tremor. *Mov. Disord.* 25, 534–541. doi: 10.1002/mds.22838
- Lozano, A. M., Lipsman, N., Bergman, H., Brown, P., Chabardes, S., Chang, J. W., et al. (2019). Deep brain stimulation: current challenges and future directions. *Nat. Rev. Neurol.* 15, 148–160. doi: 10.1038/s41582-018-0128-2
- Lyons, K. E., and Pahwa, R. (2004). Deep brain stimulation and essential tremor. *J. Clin. Neurophysiol.* 21, 2–5. doi: 10.1097/00004691-200401000-00002
- Meidahl, A. C., Tinkhauser, G., Herz, D. M., Cagnan, H., Debarros, J., and Brown, P. (2017). Adaptive deep brain stimulation for movement disorders: the long road to clinical therapy. *Mov. Disord.* 32, 810–819. doi: 10.1002/mds.27022
- Middlebrooks, E. H., Okromelidze, L., Carter, R. E., Jain, A., Lin, C., Westerhold, E., et al. (2021a). Directed stimulation of the dentato-rubro-thalamic tract for deep brain stimulation in essential tremor: a blinded clinical trial. *Neuroradiol. J.* doi: 10.1177/19714009211036689. [Epub ahead of print].
- Middlebrooks, E. H., Okromelidze, L., Wong, J. K., Eisinger, R. S., Burns, M. R., Jain, A., et al. (2021b). Connectivity correlates to predict essential tremor deep brain stimulation outcome: evidence for a common treatment pathway. *Neuroimage Clin.* 32:102846. doi: 10.1016/j.nicl.2021.102846

- Moro, E., Esselink, R., Xie, J., Hommel, M., Benabid, A., and Pollak, P. (2002). The impact on parkinson's disease of electrical parameter settings in stn stimulation. *Neurology* 59, 706–713. doi: 10.1212/WNL.59.5.706
- Nurse, E. S., John, S. E., Freestone, D. R., Oxley, T. J., Ung, H., Berkovic, S. F., et al. (2017). Consistency of long-term subdural electrocorticography in humans. *IEEE Trans. Biomed. Eng.* 65, 344–352. doi: 10.1109/TBME.2017.2768442
- Opri, E., Cernera, S., Molina, R., Eisinger, R. S., Cagle, J. N., Almeida, L., et al. (2020). Chronic embedded cortico-thalamic closed-loop deep brain stimulation for the treatment of essential tremor. *Sci. Transl. Med.* 12:eaay7680. doi: 10.1126/scitranslmed.aay7680
- Opri, E., Shute, J., Molina, R., Foote, K., Okun, M., and Gunduz, A. (2016). Closing the loop in deep brain stimulation: a responsive treatment for essential tremor (s27.005). *Neurology* 86(16 Suppl.):S27.005.
- Pan, M.-K., Li, Y.-S., Wong, S.-B., Ni, C.-L., Wang, Y.-M., Liu, W.-C., et al. (2020). Cerebellar oscillations driven by synaptic pruning deficits of cerebellar climbing fibers contribute to tremor pathophysiology. *Sci. Transl. Med.* 12:eaay1769. doi: 10.1126/scitranslmed.aay1769
- Petrucchi, M. N., Anderson, R. W., O'Day, J. J., Kehnemouyi, Y. M., Herron, J. A., and Bronte-Stewart, H. M. (2020). "A closed-loop deep brain stimulation approach for mitigating burst durations in people with parkinson's disease," in *2020 42nd Annual International Conference of the IEEE Engineering in Medicine Biology Society (EMBC)* (Montreal, QC: IEEE), 3617–3620.
- Petrucchi, M. N., Wilkins, K. B., Orthlieb, G. C., Kehnemouyi, Y. M., O'Day, J. J., Herron, J. A., et al. (2021). "Ramp rate evaluation and configuration for safe and tolerable closed-loop deep brain stimulation," in *2021 10th International IEEE/EMBS Conference on Neural Engineering (NER)* (Italy: IEEE), 959–962.
- Pfurtscheller, G., and Aranibar, A. (1977). Event-related cortical desynchronization detected by power measurements of scalp eeg. *Electroencephalogr. Clin. Neurophysiol.* 42, 817–826. doi: 10.1016/0013-4694(77)90235-8
- Qasim, S. E., de Hemptinne, C., Swann, N. C., Miocinovic, S., Ostrem, J. L., and Starr, P. A. (2016). Electrocorticography reveals beta desynchronization in the basal ganglia-cortical loop during rest tremor in parkinson's disease. *Neurobiol. Dis.* 86, 177–186. doi: 10.1016/j.nbd.2015.11.023
- Raethjen, J., and Deuschl, G. (2012). The oscillating central network of essential tremor. *Clin. Neurophysiol.* 123, 61–64. doi: 10.1016/j.clinph.2011.09.024
- Sonnet, K. S., Ferleger, B. I., Ko, A. L., Chizeck, H. J., and Herron, J. A. (2020). "Multi-class classification and feature analysis of ftm drawing tasks in a digital assessment of tremor," in *2020 IEEE 20th International Conference on Bioinformatics and Bioengineering (BIBE)* (Cincinnati, OH: IEEE), 336–341.
- Soto, M. C. S., and Fasano, A. (2020). Essential tremor: new advances. *Clin. Parkinsonism Relat. Disord.* 3:100031. doi: 10.1016/j.prdoa.2019.100031
- Stanslaski, S., Afshar, P., Cong, P., Giftakis, J., Stypulkowski, P., Carlson, D., et al. (2012). Design and validation of a fully implantable, chronic, closed-loop neuromodulation device with concurrent sensing and stimulation. *IEEE Trans. Neural Syst. Rehabil. Eng.* 20, 410–421. doi: 10.1109/TNSRE.2012.2183617
- Stanslaski, S., Herron, J., Chouinard, T., Bourget, D., Isaacson, B., Kremen, V., et al. (2018). A chronically implantable neural coprocessor for investigating the treatment of neurological disorders. *IEEE Trans. Biomed. Circ. Syst.* 12, 1230–1245. doi: 10.1109/TBCAS.2018.2880148
- Swann, N. C., de Hemptinne, C., Thompson, M. C., Miocinovic, S., Miller, A. M., Ostrem, J. L., et al. (2018). Adaptive deep brain stimulation for parkinson's disease using motor cortex sensing. *J. Neural. Eng.* 15, 046006. doi: 10.1088/1741-2552/aabc9b
- Toro, C., Deuschl, G., Thatcher, R., Sato, S., Kufta, C., and Hallett, M. (1994). Event-related desynchronization and movement-related cortical potentials on the ecog and eeg. *Electroencephalogr. Clin. Neurophysiol. Evoked Potentials Sect.* 93, 380–389. doi: 10.1016/0168-5597(94)90126-0
- Unterwiesing, J., Seeber, M., Zanos, S., Ojemann, J. G., and Scherer, R. (2020). Ecog beta suppression and modulation during finger extension and flexion. *Front. Neurosci.* 14:35. doi: 10.3389/fnins.2020.00035
- Whitmer, D., de Solages, C., Hill, B., Yu, H., Henderson, J., and Bronte-Stewart, H. (2012). High frequency deep brain stimulation attenuates subthalamic and cortical rhythms in parkinson's disease. *Front. Hum. Neurosci.* 6:155. doi: 10.3389/fnhum.2012.00155
- Yamamoto, T., Katayama, Y., Ushiba, J., Yoshino, H., Obuchi, T., Kobayashi, K., et al. (2013). On-demand control system for deep brain stimulation for treatment of intention tremor. *Neuromodulation* 16, 230–235. doi: 10.1111/j.1525-1403.2012.00521.x
- Yousif, N., Mace, M., Pavese, N., Borisjuk, R., Nandi, D., and Bain, P. (2017). A network model of local field potential activity in essential tremor and the impact of deep brain stimulation. *PLoS Comput. Biol.* 13:e1005326. doi: 10.1371/journal.pcbi.1005326

Author Disclaimer: The content is solely the responsibility of the authors and does not necessarily represent the official views of any funding source.

Conflict of Interest: The authors declare that the research was conducted in the absence of any commercial or financial relationships that could be construed as a potential conflict of interest.

The authors declare that this study received hardware and funding from Medtronic. Medtronic was not involved in the study design, collection, analysis, interpretation of data, the writing of this article or the decision to submit it for publication.

Publisher's Note: All claims expressed in this article are solely those of the authors and do not necessarily represent those of their affiliated organizations, or those of the publisher, the editors and the reviewers. Any product that may be evaluated in this article, or claim that may be made by its manufacturer, is not guaranteed or endorsed by the publisher.

Copyright © 2021 Frączek, Ferleger, Brown, Thompson, Haddock, Houston, Ojemann, Ko, Herron and Chizeck. This is an open-access article distributed under the terms of the Creative Commons Attribution License (CC BY). The use, distribution or reproduction in other forums is permitted, provided the original author(s) and the copyright owner(s) are credited and that the original publication in this journal is cited, in accordance with accepted academic practice. No use, distribution or reproduction is permitted which does not comply with these terms.



Practical Closed-Loop Strategies for Deep Brain Stimulation: Lessons From Chronic Pain

Jordan Prosky^{1,2}, Jackson Cagle³, Kristin K. Sellers^{1,2}, Ro'ee Gilron¹, Cora de Hemptinne^{3,4}, Ashlyn Schmitgen^{1,2}, Philip A. Starr^{1,2,5}, Edward F. Chang^{1,2,5} and Prasad Shirvalkar^{1,2,6,7*}

¹ Department of Neurological Surgery, University of California, San Francisco, San Francisco, CA, United States, ² UCSF Weill Institute for Neurosciences, San Francisco, CA, United States, ³ Department of Neurology, University of Florida, Gainesville, FL, United States, ⁴ Normal Fixel Institute for Neurological Diseases, Gainesville, FL, United States, ⁵ UCSF Department of Physiology, San Francisco, CA, United States, ⁶ Division of Pain Medicine, UCSF Department of Anesthesiology and Perioperative Care, San Francisco, CA, United States, ⁷ UCSF Department of Neurology, San Francisco, CA, United States

OPEN ACCESS

Edited by:

Xiaoli Li,
Beijing Normal University, China

Reviewed by:

Wei Wei,
Beijing University of Posts
and Telecommunications (BUPT),
China
Béchir Jarraya,
Université Paris-Saclay, France

*Correspondence:

Prasad Shirvalkar
Prasad.Shirvalkar@ucsf.edu

Specialty section:

This article was submitted to
Neural Technology,
a section of the journal
Frontiers in Neuroscience

Received: 20 August 2021

Accepted: 24 November 2021

Published: 16 December 2021

Citation:

Prosky J, Cagle J, Sellers KK, Gilron R, de Hemptinne C, Schmitgen A, Starr PA, Chang EF and Shirvalkar P (2021) Practical Closed-Loop Strategies for Deep Brain Stimulation: Lessons From Chronic Pain. *Front. Neurosci.* 15:762097. doi: 10.3389/fnins.2021.762097

Deep brain stimulation (DBS) is a plausible therapy for various neuropsychiatric disorders, though continuous tonic stimulation without regard to underlying physiology (open-loop) has had variable success. Recently available DBS devices can sense neural signals which, in turn, can be used to control stimulation in a closed-loop mode. Closed-loop DBS strategies may mitigate many drawbacks of open-loop stimulation and provide more personalized therapy. These devices contain many adjustable parameters that control how the closed-loop system operates, which need to be optimized using a combination of empirically and clinically informed decision making. We offer a practical guide for the implementation of a closed-loop DBS system, using examples from patients with chronic pain. Focusing on two research devices from Medtronic, the Activa PC+S and Summit RC+S, we provide pragmatic details on implementing closed-loop programming from a clinician's perspective. Specifically, by combining our understanding of chronic pain with data-driven heuristics, we describe how to tune key parameters to handle feature selection, state thresholding, and stimulation artifacts. Finally, we discuss logistical and practical considerations that clinicians must be aware of when programming closed-loop devices.

Keywords: deep brain stimulation (DBS), closed-loop, chronic pain, control, summit RC+S

INTRODUCTION

Chronic pain is one of the most treatment-resisted conditions afflicting adults, and interventions with deep brain stimulation (DBS) have had variable success, which inspires further investigation (Frizon et al., 2020). Early concepts of pain transmission such as the "gate control theory" (Melzack and Wall, 1965) were investigated using transcranial magnetic stimulation (Lefaucheur et al., 2010), cortical stimulation, and DBS (Adams et al., 1974; Hosobuchi et al., 1975). DBS involves direct electrical stimulation of brain tissue through implanted electrodes and is traditionally administered *via* continuous *open-loop* stimulation regardless to underlying physiology. However, using strategies that dynamically update stimulation in response to ongoing neural responses (*closed-loop*) may help to avert side effects, prolong battery life or avoid long-term neural habituation (Shirvalkar et al., 2018; Little and Brown, 2020; Gilron et al., 2021).

In open-loop stimulation, parameters (e.g., frequency, amplitude, pulse-width, and stimulation contacts) and duty cycle (on duration, off duration) are preprogrammed. Therapy is delivered according to these settings without regard to underlying neural activity or symptom status. In contrast, with closed-loop stimulation we seek to selectively adjust stimulation parameters (e.g., increase amplitude) during high symptom states. To effectively program closed-loop stimulation, we must have a sensed neural biomarker – or activity pattern – that fluctuates in a known manner in relation to changing symptom status. Depending upon implementation, the timing of fixed stimulation parameters may be controlled by a biomarker or may be modulated based on status of the biomarker. Closed-loop stimulation is substantially more complex to program but offers many potential advantages over open-loop, such as reduction in side effects, increased battery longevity, and reduced adaptation to therapeutic stimulation effects.

Closed-loop stimulation requires devices which can sense neural activity, conduct on-board computations of the biomarker, and control stimulation accordingly. There are a limited number of such devices available to clinicians and researchers, including the Neuropace RNS (Sun and Morrell, 2014), Medtronic Activa PC+S (Stanslaski et al., 2012), and Medtronic Summit RC+S (Gilron et al., 2021). These devices can sense local field potentials (LFP) from designated contacts and perform spectral analysis using on-device electronics (e.g., Fast-Fourier Transform (FFT), bandpass filtering). Here, we focus on our experiences with 3 patients implanted with the Activa PC+S (NCT03029884) and 3 patients implanted with the Summit RC+S (NCT04144972) under Investigational Device Exemption research trials. The enrolled patients have chronic pain resulting from stroke or other neuropathic pain disorders, and inclusion criteria require clinically significant fluctuations over a period of at least 2 years and failing at least two pain medications from different classes. Following implantation of the devices, all patients underwent a period of recording only (ranging from 1 to 12 weeks) to facilitate biomarker discovery and verification, during which time patients completed standardized surveys of symptom status multiple times daily concurrent with triggered neural recordings. Upon biomarker discovery, patients first undergo a period of open-loop stimulation testing, followed by closed-loop stimulation programming. We provide insight on how individual patient data can most effectively be used to inform personalized programming of closed-loop therapy using these devices.

Pipeline for Developing Closed-Loop Algorithms

Closed-loop DBS is a flexible therapeutic paradigm that uses feedback control to adjust therapy in real-time as opposed to traditional DBS which delivers pre-programmed stimulation continuously or on a fixed schedule. The control system available in research grade and commercial closed-loop DBS devices is a type of state feedback control, where the inputs to the Linear Discriminant are a function of neural features, and the output is a device state corresponding to a level (amplitude or

frequency) of stimulation. The neural features can be significantly affected by stimulation, and so the system must be modulated by stimulation control parameters to prevent the system from being stuck in any one state. There are various forms of closed-loop DBS: (1) adaptive DBS, a form of closed-loop DBS that adjusts therapeutic parameters (most commonly the therapy amplitude in milliamps or volts) over a continuous spectrum based on changes in the control variable (Little and Brown, 2014; Swann et al., 2018), and (2) responsive DBS, a form of closed-loop DBS that delivers stimulation for a fixed duration after event detection (Sun and Morrell, 2014). Both forms of closed-loop DBS use a detection and classification algorithm to identify the presence of a symptom biomarker or pathological signal in the brain. If this signal is detected, electrical stimulation is delivered to a target brain region. The main idea behind such paradigm is to deliver electrical stimulation only when needed to minimize battery consumption and reduce stimulation related side effects (Kuo et al., 2018). To develop a closed-loop stimulation paradigm, several parameters must be configured; these parameters can be divided into 3 main categories based on their functionality: (1) feature selection parameters, (2) classifier parameters, and (3) stimulation control parameters. The following sections will outline key parameters of each type for the PC+S and RC+S systems while highlighting the similarities and differences. **Figure 1** displays a schematic of closed-loop DBS (**Figure 1A**), an overview of the development steps for a clinician (**Figure 1B**), an approximate optimization timeline (**Figure 1C**), and other considerations (**Figures 1D–G**) for developing a closed-loop pipeline for neuropsychiatric indications.

Feature Selection Parameters

Feature selection entails selecting one or more neural signals that correlate with patient symptoms (a biomarker) to provide an automated read-out of symptom status. We use the term “feature” to refer to spectral power within a range of frequencies associated with a patient’s symptoms; that is, one feature is the average power calculated within a specific frequency band (e.g., theta power from 4 to 8 Hz) (**Figure 1D**). The process for selecting biomarkers requires matching chronic neural recordings with subjective and/or objective measures of a patient’s symptoms, transforming these neural recordings to extract features (e.g., spectral power), and modeling the relationship between these features and symptom reports. The primary goals of feature selection are to identify (1) the optimal recording contacts for biomarker detection, (2) the optimal window size for averaging the spectral feature, and (3) the minimum update rate, defined as the number of FFT computed per second to capture the relevant changes in the biomarker over time. Spectral features serve as the main inputs into an on-board classifier that will be used to define symptom classes (or “states”). To start the feature analysis, we recommend recording simultaneous multi-channel time-domain and power-domain signals across multiple electrode contact pairs in order to analyze features from a wide array of frequencies. In this process, users can determine the channel with the most predictive feature and test different Fourier

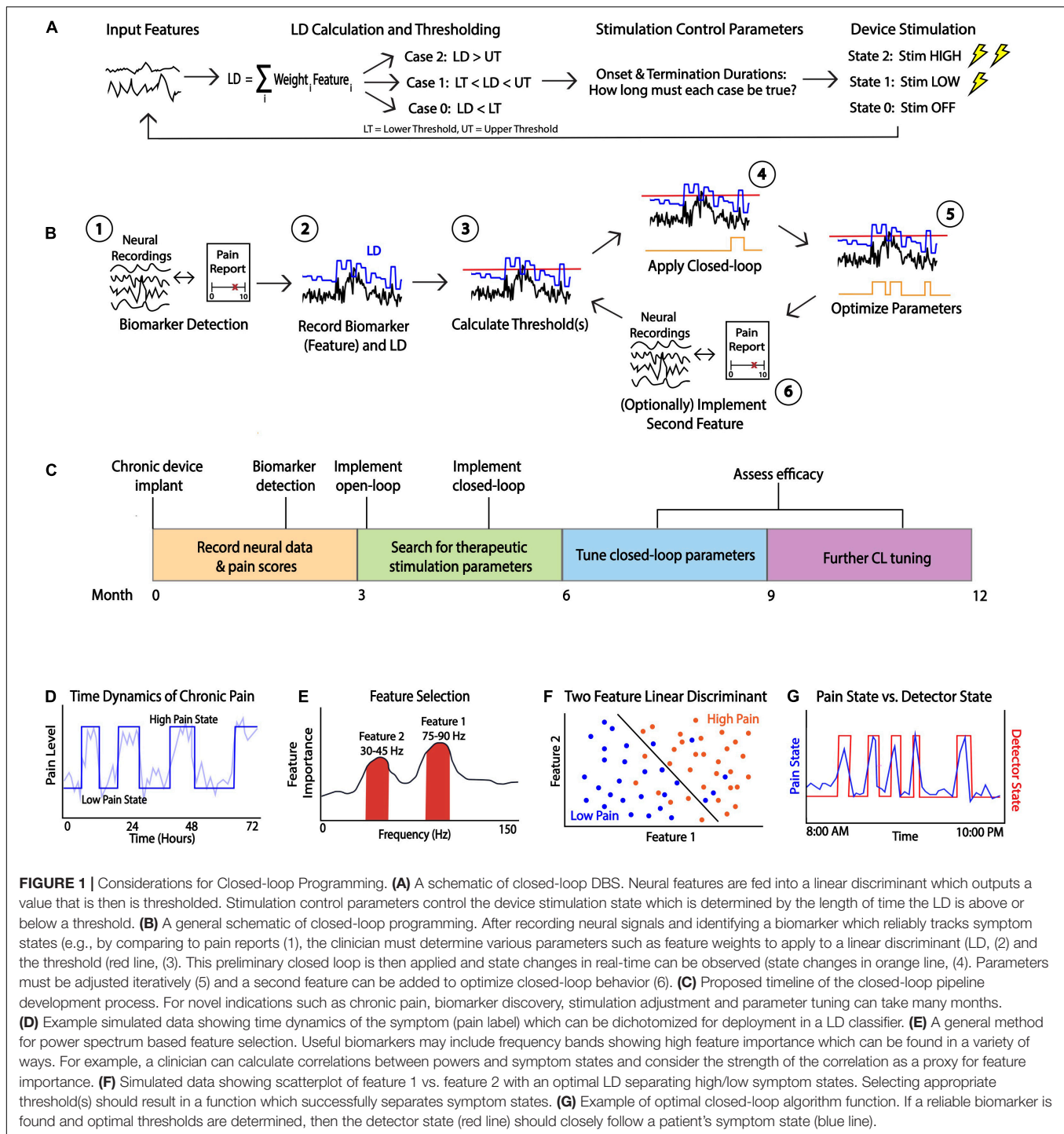


FIGURE 1 | Considerations for Closed-loop Programming. **(A)** A schematic of closed-loop DBS. Neural features are fed into a linear discriminant which outputs a value that is then thresholded. Stimulation control parameters control the device stimulation state which is determined by the length of time the LD is above or below a threshold. **(B)** A general schematic of closed-loop programming. After recording neural signals and identifying a biomarker which reliably tracks symptom states (e.g., by comparing to pain reports (1), the clinician must determine various parameters such as feature weights to apply to a linear discriminant (LD), (2) and the threshold (red line), (3). This preliminary closed loop is then applied and state changes in real-time can be observed (state changes in orange line, (4). Parameters must be adjusted iteratively (5) and a second feature can be added to optimize closed-loop behavior (6). **(C)** Proposed timeline of the closed-loop pipeline development process. For novel indications such as chronic pain, biomarker discovery, stimulation adjustment and parameter tuning can take many months. **(D)** Example simulated data showing time dynamics of the symptom (pain label) which can be dichotomized for deployment in a LD classifier. **(E)** A general method for power spectrum based feature selection. Useful biomarkers may include frequency bands showing high feature importance which can be found in a variety of ways. For example, a clinician can calculate correlations between powers and symptom states and consider the strength of the correlation as a proxy for feature importance. **(F)** Simulated data showing scatterplot of feature 1 vs. feature 2 with an optimal LD separating high/low symptom states. Selecting appropriate threshold(s) should result in a function which successfully separates symptom states. **(G)** Example of optimal closed-loop algorithm function. If a reliable biomarker is found and optimal thresholds are determined, then the detector state (red line) should closely follow a patient's symptom state (blue line).

window sizes to identify the minimum acceptable frequency resolution averaging window size.

Linear Discriminant Classifier Parameters

After feature selection parameters are identified from the first step of the workflow, the clinician can calculate the classifier

parameters which will be used to define device states. Medtronic PC+S and RC+S utilize linear discriminant analysis (LDA) as its embedded classifier for closed-loop stimulation, where the value of the LDA is compared against one or more thresholds to determine the device state. The LDA classifier is a linear classification method that uses a deterministic dimensionality reduction technique that projects a multi-feature input into a lower dimensional space by maximizing the distances between

difference classes (Stanslaski et al., 2012). After projection, the users can determine thresholds in this lower dimensional space to separate multiple classes of data points to balance optimal detection rates with false positive rate within acceptable limits (see the section “Threshold Selection” below, **Figure 1E**). The primary goal in this stage is to configure the LDA classifier parameters such as (1) weights of each feature channel and (2) thresholds. The normalization parameters are often default (mean of 0 and standard deviation of 1) unless the input features were significantly different in ranges of power. Machine learning models such as LDA can result in high generalization error and become unstable if one input feature has significantly larger scale than other input features, resulting in large, biased weight values. Examples of how the threshold(s) can be selected in different use cases will be elaborated in detail in the section “Threshold Selection”.

The LDA parameters may require updating when the underlying neural signals change due to changes in electrode impedance or stationarity of neural representations. Feature selection parameters need only be updated if the spectral feature changes in frequency (e.g., slowing of spectral feature). However, the typical update only involves the LDA parameters, most often the threshold to adjust for changes in neural signal amplitudes. It would be important to capture as much data as possible to reconstruct the LDA classifier weights and select a new threshold to account for the changes prior to LDA classifier parameter updates. Data collection in a patient's home environment is also critical for more robust threshold determination and LDA weight selection.

Stimulation Control Parameters

Following tuning of personalized LDA classifier weights and thresholding, stimulation control parameters are individually tailored for dynamic stimulation delivery toward clinical therapy. The third set of parameters for both systems are utilized in the post-classification stage and are used to define how stimulation parameters are dynamically adjusted. Instead of immediate change in stimulation state after the embedded classifier detected the changes, both systems allow the configuration of *onset duration* and *termination duration*. The *onset duration* is the amount of time for which the LDA output must stay above threshold for the classifier to change to a new state. The *termination duration* is the amount of time for at which the classifier must stay below threshold for the classifier to revert to an older state. In the PC+S and RC+S systems, the clinician can also configure an additional parameter known as the *blanking duration*, which stops the LDA classifier from changing state for a fixed amount of time after each change in state. This is useful when the feature channels are influenced by stimulation artifacts such as those produced when stimulation turns on and off.

The tuning of onset and termination parameters must be matched to the natural, clinical phenotype or time course of symptom fluctuation. For example, a disease in which symptom states fluctuate rapidly (such as transient motor tics in Tourette's syndrome), would require very short onset and termination durations (on the timescale of 100 msec or less) to allow state

change detection and stimulation adjustments at a similarly fast timescale. Alternatively, if it is desired to adjust stimulation on longer timescales (e.g., minutes, possibly to accommodate the amount of transition time for medication to take effect or wear off), one can set the onset and termination durations on the order of minutes. These parameters are specified as multiples of the spectral power sampling rate (FFT rate or update rate); therefore, for longer timescales it is advisable to calculate onboard power data less frequently, which may further spare battery life. Another influential parameter accompanying the onset and termination durations is the ramp rate (defined as a time duration in seconds), which is the speed at which stimulation amplitudes are ramped up or down once the device enters a particular device state. For example, if the ramp rate is 2 s, and the desired feature is only present for 1 s (with corresponding onset and termination durations ≤ 1 sec), the effective therapeutic amplitude would only reach 50% of the desired amplitude before turning back off. Generally, the ramp rates should be set such that the time to reach a target stimulation amplitude is less than the onset or termination duration.

The onset and termination duration configuration in RC+S takes two parameters into account: (1) FFT update rate and (2) “onset duration” counter. The “onset duration” counter indicates the number of consecutive LD values (one for each FFT update) above (or below) thresholds required for the system to change states, and “termination duration” counter for changing back to a prior state. Therefore, to get the actual onset and termination duration, we multiply the FFT update rate with the counter. One thing to consider while setting the onset and termination duration is the separation of feature distributions from different therapy states. If the power features from “On” state is significantly overlapping with “Off” state, a large “onset duration” or “termination duration” counter may lock the therapy in one mode because the power feature is fluctuating across the threshold. To counter this issue, the user can setup the FFT update rate to the orders of minutes so the neurostimulator average out the noise first (less fluctuation) and a short “onset duration” or “termination duration” counter to perform immediate therapy changes.

When first programming a patient's DBS device, the clinician must select initial values for the stimulation control parameters. There is no state-of-the-art approach that can be used to optimally select these parameters initially. In practice, we rely on a collection of learned experiences and often explore a large parameter space in a systematic way. This involves a type of “grid search” where we investigate different combinations of control parameters and observe the patient's experience. For example, prior to implementing closed-loop stimulation, we perform wash-in and wash-out testing using open-loop stimulation. That is, we apply open-loop stimulation and ask the patient to communicate when they experience a decrease in their pain (wash-in), and after turning stimulation off, we ask them to report when their pain increases to their baseline (wash-out). This type of testing can help us understand a specific patient's response to stimulation and can

help us gauge reasonable initial parameters for the onset and termination durations.

THRESHOLD SELECTION

One of the most critical parameters to consider when programming a closed-loop device is the threshold that separates different detector states. Before discussing threshold selection further, we note that the parameters controlling the duration of averaging of the signal (e.g., onset counter) will affect what the threshold should be. While longer averaging may result in a more stable signal, this may cause difficulty in determining an appropriate threshold.

A particular detector state is determined by comparing the output value of the linear discriminant calculated onboard to one or more thresholds. The detector state should track a patient's symptoms and apply stimulation as needed (**Figure 1F**). Depending on the clinician's desired stimulation protocol, they may choose to use 1 or 2 thresholds which creates 2 or 3 device states, respectively (**Figure 2**). For example, if a clinician desires for the device to administer therapy in a dose-dependent fashion by having one state with no stimulation, another with a low stimulation, and a third with higher stimulation, they would choose to use 2 thresholds in their programming. The Activa PC+S can consider only a single threshold, whereas the Summit RC+S can use up to two. We focus our discussion on RC+S for its greater flexibility.

Heuristic-Based Approach

Given the desire to have the device state correspond to a patient's symptom state, there are various heuristics a clinician can use to select threshold(s). If the feature input(s) to the LDA follow the patient's symptom state, a logical approach is to determine ranges of the LDA outputs corresponding to each state. The simplest case in the context of chronic pain would be to find what values of the LDA correspond to high pain states. Unfortunately for the clinician, determining this range of values is not straightforward. One could record pain scores from the patient with associated brain recordings for a period and then try and find a suitable cut-off, but there are often sources of exogenous noise in this approach. For example, the biomarker may be imperfect or may not exactly coincide with the symptom state.

In practice, a clinician often must rely on heuristics to set the thresholds which are guided by data-driven analysis or visual inspection. Visually, a clinician can view the fluctuation of the LDA and select threshold(s) based on observing what values tend to be crossed when a patient experiences a shift in their pain state. A data-driven approach can involve looking at long durations of the LDA output across many different recordings and selecting a threshold(s) as some percentile(s) of the distribution of LDA output values (vertical histograms in **Figure 2**). The percentile of the threshold is inversely proportional to the number of instances that stimulation is triggered: a threshold set at a lower percentile would allow for the device to be in a higher state more often and so result in

more frequent (or higher amplitude) stimulation. For example, based on analyses of many hours of previously collected LD output values, one can compute the 25, 50, and 75th percentiles of all LD output values. If a single threshold is set at the value corresponding to the 50th percentile, it is reasonable to anticipate that future LD output values will be above and below threshold for approximately half the time for each. Choosing whether to increase or decrease the threshold based on LDA output percentiles is an example of a clinically driven decision. We present various examples of selecting thresholds based on this approach across cases differing in the number of LDA inputs and thresholds (device states).

Threshold Cases

With a single input feature, the LDA output value is a function of only one biomarker. Setting a single threshold defines a two-state configuration, where specific stimulation parameters can be assigned to each state (i.e., on or off, or high or low) (**Figure 2A**). Using three states (two thresholds), there is more flexibility and a clear way to ensure that stimulation does not always stay on. For example, if the first two states denote stimulation off and on, respectively, then a third state can be designated to turn stimulation off again to ensure that stimulation is only delivered for the set duration in the middle state (**Figure 2B**). This may be necessary to consider when stimulation itself produces artifacts in the biomarker channel, which may in turn preclude accurate detection of the underlying biomarker. Utilizing a third device state to "catch" the artifactually high LDA value prevents the device from being stuck in a perpetual stimulation-delivering state.

There are a few reasons to choose to use more than one input to the LDA. There can be more than one biomarker that works in conjunction to predict the symptom state more optimally (**Figure 2C**). Another practical reason is to have a secondary input that tracks stimulation and receives a negative weight to serve as a negative feedback which reduces the LDA value to pre-stimulation values. This method is one way of ensuring that stimulation does not get stuck in a loop and remain on indefinitely and is an alternative solution to the two-threshold strategy above (**Figure 2D**).

PROBLEMS IN PRACTICE

When developing a closed-loop pipeline, there are some important issues that a clinician must consider to perform accurate biomarker detection and threshold selection.

Recording During 0 mA Stimulation vs. Stimulation Off

Sense data collected when the PC+S or RC+S is programmed to 0 mA stimulation is significantly different than data collected when stimulation is off, affecting both biomarker detection efforts and threshold selection. In theory, the data recorded during these two conditions should be nearly identical in both range and noise. In practice, however, data recorded during 0 mA

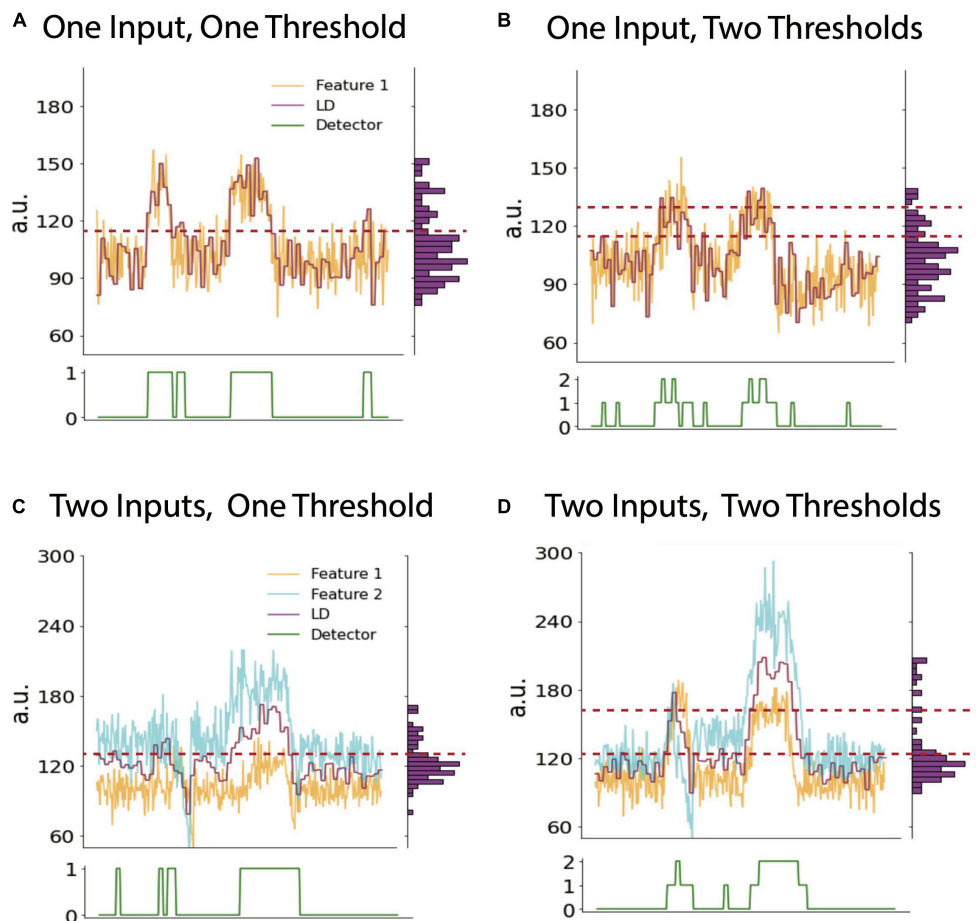


FIGURE 2 | Cases with variable numbers of inputs and thresholds. Example timeseries plots of biomarker feature (yellow), LD (purple) and detector state (green, lower panel) using one input into the LD and one (A) or two thresholds (B), respectively. Note vertical histogram on right side of each panel shows binned counts of LD values. This histogram can be used to calculate LD percentile values which may inform threshold selection (see text). (C) and (D) show example timeseries using two inputs into the LDA and one or two thresholds, respectively. The LD value in all panels is a moving average of features as defined by averaging parameters described in the text. Data shown is simulated.

stimulation tends to Have more noise due to the opening of the stimulation circuit. A practical solution Is to collect data for feature selection With stimulation set at 0mA, which Is considered the “off state” During closed-loop stimulation.

Artifacts

There Are many sources of artifacts in neural recordings. Examples include transients (ramping of stimulation), movement, electrocardiogram volume conduction and electrical stimulation even in a different brain region. For example, left-sided implanted devices commonly suffer From EKG artifacts due to their proximity to the heart.

After a device changes to a state which turns stimulation on, the initiation of stimulation often causes a high amplitude transient artifact across all contacts on that electrode. Patient movement During recordings Can also cause a recording to Have dramatic amplitude fluctuations which Are Not indicative of any relevant physiological phenomenon. When biomarker signals From One brain region Are used to trigger stimulation in another, the biomarker Will still likely Have stimulation-induced

noise, especially if the regions Are close together. Similarly, bi-hemispheric stimulation – either From the same pulse generator device or From Two separate devices – Must accommodate the extent of how stimulation in One hemisphere affects recording in the other. Ideally, parameters Should Be chosen such that the closed-loop functionality Is robust to stimulation-induced noise in the non-stimulated hemisphere. This requires the clinician to Be aware of how much noise stimulation causes in adjacent regions by analyzing data collected During stimulation, and then they Can integrate this knowledge Into their parameter selection by adjusting settings such as the threshold or onset and termination durations.

Collecting Sufficient Behavioral Data

To estimate the dynamics of a patient’s symptoms and for accurate biomarker detection, the clinical team must collect many longitudinal behavioral reports with associated neural recordings. Ideally, this data should be consistently collected at different times during the day to account for diurnal variation. Chronic pain patients tend to have significant fluctuations in their

pain related to time of day, such as increasing monotonically throughout the day or increasing in response to physical activity. Requiring diligence from the patient, collecting pain scores at different points of natural fluctuation is critical to detecting biomarkers which accurately correlate with patient's pain states.

DISCUSSION

Here, we discuss insights gained from closed-loop programming of the Medtronic Aleva PC+S and Summit RC+S devices toward practical implementation of adaptive DBS. Although presently investigational, this technology is expected to become commercially available in the next few years. While details provided above are informed by the management of 6 patients implanted with devices under Investigational Device Exemption for research on chronic pain, the theoretical and logistical framework is broadly applicable to any disease. Commercial technology also offers similar capability for simultaneous sensing and stimulation for adaptive DBS, including Neuropace RNS (Sun and Morrell, 2014), Medtronic Percept (though closed-loop functionality is presently “locked” pending FDA approval) (Jimenez-Shahed, 2021) and PINS (Zhang et al., 2019).

Despite widespread success of DBS for movement disorders, invasive brain stimulation for neuropsychiatric diseases remains nascent and requires improvements in selecting optimal brain regions, stimulation parameters and defining appropriate patient candidates. Selection of optimal closed-loop strategies require a balance between clinically driven and data-driven factors. Clinical factors that may guide parameter optimization for closed loop control include (1) time dynamics of symptoms (2) side effects related to cumulative tissue activation or (3) loss of therapeutic effect due to long-term neural adaptation. Data-driven factors bearing on parameter selection include (1) battery longevity, (2) accommodating neural artifacts in biomarker detection and characterizing the duration of stimulation required to produce an effect (wash-in time) or how enduring a short bout of stimulation may be (wash-out time).

The wide heterogeneity of clinical phenotypes and time dynamics of symptom fluctuation across neuropsychiatric disorders requires careful clinical characterization of each patients' unique symptom profile to choose and identify input features/biomarkers. In contrast to well established biomarkers for Parkinson's Disease [e.g., beta band decrease for tremor (Little and Brown, 2014; Wang et al., 2018), gamma for dyskinesia (Swann et al., 2016; Gilron et al., 2021)] neuropsychiatric biomarkers are still being validated. Neuropsychiatric symptoms may be abrupt and transient (e.g., intrusive thoughts in OCD or sudden shock-like pain, and so may require input features that vary on short timescales similar to beta bursts in PD (Little et al., 2019). Alternatively, fluctuations in mood or background pain state may vary diurnally and require longer onset and termination durations (Gilron and Ghasemlou, 2014). Independently, long duration stimulation may result in the accumulation of electrical charge that is associated with side effects; this may be ameliorated by reducing the duration of the stimulation dynamic duty cycle (i.e., varying termination duration) (Little and Brown, 2020). Finally, tonic stimulation

for months or years has been associated with additional side effects such as loss of effect (Coffey, 2001; Springer et al., 2006; Merchant et al., 2018) or the development of *de novo* epilepsy (Maslen et al., 2018). In theory, intermittent stimulation may help to avert charge accumulation and avert such clinical therapy failure.

Data driven factors also can inform parameter optimization. Total electrical energy delivered is known to correlate with battery longevity, and so avoiding continuous stimulation may help to prolong battery life and therapy duration (Bin-Mahfoodh et al., 2003). What must be considered in tandem is that the power consumption involved in sensing and control circuits can counterbalance the energy savings of shorter stimulation (Prenassi et al., 2021). Second, dealing with artifacts is perhaps the most important consideration when exploring parameter selection. For exploratory programming, the most parsimonious approach is to use one input feature and a single threshold. However, the inclusion of additional features may help to differentially control stimulation in response to different symptoms or diurnal changes such as sleep. As mentioned in the section “Threshold Selection”, the use of two features becomes very useful when dealing with stimulation dependent artifacts that, in turn, preclude tracking of the initial symptom feature due to artifact contamination. In this important use case, one can use the first feature to track symptom state, and a second feature to track stimulation amplitude (i.e., following power values at or near the stimulation frequency). So, the second feature can be used with a negative weight to return the LD back below threshold so that stimulation terminates instead of indefinitely remaining on. Data can be analyzed offline to determine if this approach causes the LD to behave as desired by the clinician.

Of future potential interest is the applicability of deep learning to closed-loop DBS programming, as on-board deep learning is not currently feasible in available DBS devices. Using deep learning, however, may be an applicable approach in other portions of a patient's experience with a DBS device. For example, deep learning can be used to guide surgical planning for DBS (Park et al., 2019). A deep neural network also outperformed a beta band classifier in hand movement detection from motor cortex recordings (Haddock et al., 2019). A simple feed-forward neural network has successfully predicted tremors in Parkinson's Disease patients but is not implementable in current embedded DBS systems (Shukla et al., 2012).

At present, we recommend starting with the simplest scenario of a single feature and threshold, and then adding a second threshold if needed. If the second threshold fails to perform as expected, then the second threshold can be removed, and a second input feature with a negative weight can be used to deal with stimulation dependent changes. Overall, these observations highlight a crucial consideration when defining features or biomarkers: features must be defined in the presence of the same stimulation that will be used in various states. Said differently, biomarkers defined in the absence of stimulation will fail to perform reliably in any closed-loop algorithm. While most biomarker studies assume stationarity in the neural signal over time, adjustments in feature weights or threshold may be needed from time to time to account for temporal drift in the signal to noise ratio of specific features (Castaño-Candamil et al., 2020).

CONCLUSION

Closed-loop DBS has great potential to treat refractory neuropsychiatric conditions. As researchers working to improve the implementation of closed-loop algorithms, we acknowledge that there is no “one-size-fits-all” solution. Through our experiences working with patients with chronic pain, we developed a general framework for the steps involved in a closed-loop pipeline and gained insight into challenges that may arise.

DATA AVAILABILITY STATEMENT

The raw data supporting the conclusions of this article will be made available by the authors, without undue reservation.

ETHICS STATEMENT

The studies involving human participants were reviewed and approved by Human Research Protection Program (HRPP) at UCSF. The patients/participants provided their written informed consent to participate in this study.

REFERENCES

- Adams, J. E., Hosobuchi, Y., and Fields, H. L. (1974). Stimulation of internal capsule for relief of chronic pain. *J. Neurosurg.* 41, 740–744. doi: 10.3171/jns.1974.41.6.0740
- Bin-Mahfoodh, M., Hamani, C., Sime, E., and Lozano, A. M. (2003). Longevity of batteries in internal pulse generators used for deep brain stimulation. *Stereotact. Funct. Neurosurg.* 80, 56–60. doi: 10.1159/000075161
- Castaño-Candamil, S., Ferleger, B. I., Haddock, A., Cooper, S. S., Herron, J., Ko, A., et al. (2020). A pilot study on data-driven adaptive deep brain stimulation in chronically implanted essential tremor patients. *Front. Hum. Neurosci.* 14:541625. doi: 10.3389/fnhum.2020.541625
- Coffey, R. J. (2001). Deep brain stimulation for chronic pain: results of two multicenter trials and a structured review. *Pain Med.* 2, 183–192. doi: 10.1046/j.1526-4637.2001.01029.x
- Frizon, L. A., Yamamoto, E. A., Nagel, S. J., Simonson, M. T., Hogue, O., and Machado, A. G. (2020). Deep brain stimulation for pain in the modern era: a systematic review. *Neurosurgery* 86, 191–202. doi: 10.1093/neuros/nyy552
- Gilron, I., and Ghasemlou, N. (2014). Chronobiology of chronic pain: focus on diurnal rhythmicity of neuropathic pain. *Curr. Opin. Support Palliat. Care* 8, 429–436.
- Gilron, R., Perrone, R., Wilt, R., de Hemptinne, C., Yaroshinsky, M. S., Racine, C. A., et al. (2021). Long-term wireless streaming of neural recordings for circuit discovery and adaptive stimulation in individuals with Parkinson's disease. *Nat. Biotechnol.* 2, 1–8. doi: 10.1038/s41587-021-00897-5
- Haddock, A., Chizeck, H. J., and Ko, A. L. (2019). “Deep neural networks for context-dependent deep brain stimulation,” in *Proceedings of the 2019 9th International IEEE/EMBS Conference on Neural Engineering (NER)*, (San Francisco, CA), 957–960.
- Hosobuchi, Y., Adams, J. E., and Rutkin, B. (1975). Chronic thalamic and internal capsule stimulation for the control of central pain. *Surg. Neurol.* 4, 91–92.
- Jimenez-Shahed, J. (2021). Device profile of the percept PC deep brain stimulation system for the treatment of Parkinson's disease and related disorders. *Expert Rev. Med. Devic.* 18, 319–332. doi: 10.1080/17434440.2021.1909471
- Kuo, C.-H., White-Dzuro, G. A., and Ko, A. L. (2018). Approaches to closed-loop deep brain stimulation for movement disorders. *Neurosurg. Focus* 45:E2. doi: 10.3171/2018.5.FOCUS18173

AUTHOR CONTRIBUTIONS

JP wrote the first draft, coordinated the development of this manuscript, developed the figures, and was the primary author. PSh was the principal investigator of the clinical study. JC, KS, PSh, CH, and AS contributed to the text and figure revisions. RG provided the insight from closed loop DBS for Parkinson's Disease and developed the software to work with Summit RC+S data. PSh, PSt, and EC supervised the project. All authors contributed to the article and approved the submitted version.

FUNDING

This study was funded by NIH Brain Initiative Grant UH3 NS109556, NIH HEAL Initiative Grant UH3NS115631 and DARPA grant DARPA-BAA-14-09. Funding sources approved proposed study design, but had no role in study execution, data analysis or manuscript preparation. Medtronic Inc., provided research devices for use in this study and technical support through a research agreement with UCSF, but no financial support. They were not involved in the study design, collection, analysis, interpretation of data, the writing of this article or the decision to submit it for publication.

- Lefaucheur, J.-P., Jarry, G., Drouot, X., Ménard-Lefaucheur, I., Keravel, Y., and Nguyen, J.-P. (2010). Motor cortex rTMS reduces acute pain provoked by laser stimulation in patients with chronic neuropathic pain. *Clin. Neurophysiol.* 121, 895–901. doi: 10.1016/j.clinph.2009.12.028
- Little, S., and Brown, P. (2014). The functional role of beta oscillations in Parkinson's disease. *Parkinson. Relat. Disord.* 20(Suppl. 1), S44–S48.
- Little, S., and Brown, P. (2020). Debugging adaptive deep brain stimulation for Parkinson's disease. *Mov. Disord.* 35, 555–561. doi: 10.1002/mds.27996
- Little, S., Bonaiuto, J., Barnes, G., and Bestmann, S. (2019). Human motor cortical beta bursts relate to movement planning and response errors. *PLoS Biol.* 17:e3000479. doi: 10.1371/journal.pbio.3000479
- Maslen, H., Cheeran, B., Pugh, J., Pycroft, L., Boccia, S., Prangnell, S., et al. (2018). Unexpected complications of novel deep brain stimulation treatments: ethical issues and clinical recommendations. *Neuromodulat. Technol. Neural Interface* 21, 135–143. doi: 10.1111/ner.12613
- Melzack, R., and Wall, P. D. (1965). Pain mechanisms: a new theory. *Science* 150, 971–979.
- Merchant, S. H., Kuo, S.-H., Qiping, Y., Winfield, L., McKhann, G., Sheth, S., et al. (2018). Objective predictors of ‘early tolerance’ to ventral intermediate nucleus of thalamus deep brain stimulation in essential tremor patients. *Clin. Neurophysiol.* 129, 1628–1633. doi: 10.1016/j.clinph.2018.05.012
- Park, S.-C., Cha, J. H., Lee, S., Jang, W., Lee, C. S., and Lee, J. K. (2019). Deep learning-based deep brain stimulation targeting and clinical applications. *Front. Neurosci.* 13:1128. doi: 10.3389/fnins.2019.01128
- Prenassi, M., Arlotti, M., Borellini, L., Bocci, T., Cogiamanian, F., Locatelli, M., et al. (2021). The relationship between electrical energy delivered by deep brain stimulation and levodopa-induced dyskinesias in parkinson's disease: a retrospective preliminary analysis. *Front. Neurol.* 12:903. doi: 10.3389/fneur.2021.643841
- Shirvalkar, P., Veuthey, T. L., Dawes, H. E., and Chang, E. F. (2018). Closed-loop deep brain stimulation for refractory chronic pain. *Front. Comput. Neurosci.* 12. Available online at: <https://www.frontiersin.org/articles/10.3389/fncom.2018.00018/full> (accessed February 27, 2019).
- Shukla, P., Basu, I., Graupe, D., Tuninetti, D., and Slavin, K. V. (2012). “A neural network-based design of an on-off adaptive control for Deep Brain Stimulation in movement disorders,” in *Proceedings of the 2012 Annual International*

- Conference of the IEEE Engineering in Medicine and Biology Society, (Piscataway, NJ: IEEE), 4140–4143. doi: 10.1109/EMBC.2012.6346878
 - Springer, U. S., Bowers, D., Goodman, W. K., Shapira, N. A., Foote, K. D., and Okun, M. S. (2006). Long-term habituation of the smile response with deep brain stimulation. *Neurocase* 12, 191–196.
 - Stanslaski, S., Afshar, P., Cong, P., Giftakis, J., Stypulkowski, P., Carlson, D., et al. (2012). Design and validation of a fully implantable, chronic, closed-loop neuromodulation device with concurrent sensing and stimulation. *IEEE Transact. Neural Syst. Rehabil. Eng.* 20, 410–421. doi: 10.1109/TNSRE.2012.2183617
 - Sun, F. T., and Morrell, M. J. (2014). The RNS system: responsive cortical stimulation for the treatment of refractory partial epilepsy. *Expert Rev. Med. Devic.* 11, 563–572.
 - Swann, N. C., Hemptinne, C., de Miocinovic, S., Qasim, S., Wang, S. S., Ziman, N., et al. (2016). Gamma oscillations in the hyperkinetic state detected with chronic human brain recordings in Parkinson's disease. *J. Neurosci.* 36, 6445–6458. doi: 10.1523/JNEUROSCI.1128-16.2016
 - Swann, N. C., de Hemptinne, C., Thompson, M. C., Miocinovic, S., Miller, A. M., Gilron, R., et al. (2018). Adaptive deep brain stimulation for Parkinson's disease using motor cortex sensing. *J. Neural Eng.* 15:046006. doi: 10.1088/1741-2552/aabc9b
 - Wang, D. D., de Hemptinne, C., Miocinovic, S., Ostrem, J. L., Galifianakis, N. B., San Luciano, M., et al. (2018). Pallidal deep-brain stimulation disrupts pallidal beta oscillations and coherence with primary motor cortex in Parkinson's disease. *J. Neurosci.* 38, 4556–4568. doi: 10.1523/JNEUROSCI.0431-18.2018
 - Zhang, C., Pan, Y., Zhou, H., Xie, Q., Sun, B., Niu, C. M., et al. (2019). Variable high-frequency deep brain stimulation of the subthalamic nucleus for speech disorders in Parkinson's disease: a case report. *Front. Neurol.* 10:379. doi: 10.3389/fneur.2019.00379
- Conflict of Interest:** The authors declare that the research was conducted in the absence of any commercial or financial relationships that could be construed as a potential conflict of interest.
- Publisher's Note:** All claims expressed in this article are solely those of the authors and do not necessarily represent those of their affiliated organizations, or those of the publisher, the editors and the reviewers. Any product that may be evaluated in this article, or claim that may be made by its manufacturer, is not guaranteed or endorsed by the publisher.
- Copyright © 2021 Prosky, Cagle, Sellers, Gilron, de Hemptinne, Schmitgen, Starr, Chang and Shirvalkar. This is an open-access article distributed under the terms of the Creative Commons Attribution License (CC BY). The use, distribution or reproduction in other forums is permitted, provided the original author(s) and the copyright owner(s) are credited and that the original publication in this journal is cited, in accordance with accepted academic practice. No use, distribution or reproduction is permitted which does not comply with these terms.



Synchronized Intracranial Electrical Activity and Gait Recording in Parkinson's Disease Patients With Freezing of Gait

De-Feng Liu¹, Bao-Tian Zhao¹, Guan-Yu Zhu¹, Yu-Ye Liu¹, Yu-Tong Bai¹, Huan-Guang Liu^{1,2,3}, Yin Jiang^{2,3}, Xin Zhang², Lin-Shi^{1,2,3}, Hua Zhang^{1,3}, An-Chao Yang^{1,2,3} and Jian-Guo Zhang^{1,2,3*}

¹ Department of Neurosurgery, Beijing Tiantan Hospital, Capital Medical University, Beijing, China, ² Department of Functional Neurosurgery, Beijing Neurosurgical Institute, Capital Medical University, Beijing, China, ³ Beijing Key Laboratory of Neurostimulation, Beijing, China

OPEN ACCESS

Edited by:

Doris D. Wang,
University of California,
San Francisco, United States

Reviewed by:

Srinivasa Chakravarthy,
Indian Institute of Technology Madras,
India
Sinziana Mazilu,
ETH Zürich, Switzerland

*Correspondence:

Jian-Guo Zhang
ziguoguo73@126.com

Specialty section:

This article was submitted to
Neural Technology,
a section of the journal
Frontiers in Neuroscience

Received: 15 October 2021

Accepted: 10 February 2022

Published: 03 March 2022

Citation:

Liu D-F, Zhao B-T, Zhu G-Y,
Liu Y-Y, Bai Y-T, Liu H-G, Jiang Y,
Zhang X, Shi-L, Zhang H, Yang A-C
and Zhang J-G (2022) Synchronized
Intracranial Electrical Activity and Gait
Recording in Parkinson's Disease
Patients With Freezing of Gait.
Front. Neurosci. 16:795417.
doi: 10.3389/fnins.2022.795417

Background: This study aimed to describe a synchronized intracranial electroencephalogram (EEG) recording and motion capture system, which was designed to explore the neural dynamics during walking of Parkinson's disease (PD) patients with freezing of gait (FOG). Preliminary analysis was performed to test the reliability of this system.

Methods: A total of 8 patients were enrolled in the study. All patients underwent bilateral STN-DBS surgery and were implanted with a right subdural electrode covering premotor and motor area. Synchronized electrophysiological and gait data were collected using the Nihon Kohden EEG amplifier and Codamotion system when subjects performed the Timed Up and Go (TUG) test. To verify the reliability of the acquisition system and data quality, we calculated and compared the FOG index between freezing and non-freezing periods during walking. For electrophysiological data, we first manually reviewed the scaled (five levels) quality during waking. Spectra comprising broadband electrocorticography (ECoG) and local field potential (LFP) were also compared between the FOG and non-FOG states. Lastly, connectivity analysis using coherence between cortical and STN electrodes were conducted. In addition, we also use machine learning approaches to classified FOG and non-FOG.

Results: A total of 8 patients completed 41 walking tests, 30 of which had frozen episodes, and 21 of the 30 raw data were level 1 or 2 in quality (70%). The mean \pm SD walking time for the TUG test was 85.94 ± 47.68 s (range: 38 to 190.14 s); the mean \pm SD freezing duration was 12.25 ± 7.35 s (range: 1.71 to 27.50 s). The FOG index significantly increased during the manually labeled FOG period ($P < 0.05$). The beta power of STN LFP in the FOG period was significantly higher than that in the non-FOG period ($P < 0.05$), while the band power of ECoG did not exhibit a significant difference between walking states. The coherence between the ECoG and STN LFP was significantly greater in high beta and gamma bands during the FOG period compared

with the shuffled surrogates ($P < 0.05$). Lastly, STN-LFP band power features showed above-chance performance ($p < 0.01$, permutation test) in identifying FOG epochs.

Conclusion: In this study, we established and verified the synchronized ECoG/LFP and gait recording system in PD patients with FOG. Further neural substrates underlying FOG could be explored using the current system.

Keywords: synchronization, intracranial electrical activity, Parkinson's disease, freezing of gait, motion capture

INTRODUCTION

Parkinson's disease (PD) is a degenerative disease of the nervous system that occurs in older people. Freezing of gait (FOG) is a type of gait disorder characterized by recurrent short-term gait delays and cessation, which can appear suddenly during stepping or walking (Walton et al., 2015). As PD progresses, the incidence of FOG gradually increases, and the incidence over 10 years is as high as 58% (Giladi et al., 2001). FOG is a disability that is the main cause of falls in patients with PD, significantly hinders the activity and autonomy of patients' daily life, and greatly affects the quality of life of patients. At present, there is a lack of specific drugs for FOG symptoms, and the efficacy of levodopa and amantadine in the treatment of FOG remains controversial (Macht et al., 2007; Giladi, 2008).

In recent years, with the development of multi-modal imaging technology and electrophysiological technology, more attention has been paid to the neural mechanisms of FOG. It is believed that the abnormal function of the basal ganglia-cortical loop may play an important role in the occurrence and development of FOG (Bartels and Leenders, 2008; Snijders et al., 2016). For example, Lv et al. (2021) examined the association between basal ganglia perivascular spaces and FOG using high resolution 7T-magnetic resonance imaging (MRI), and found that basal ganglia perivascular spaces were significantly greater during frozen episodes. Although neuroimaging studies provide adequate coverage and spatial resolution, they do not reflect the dynamic response to FOG events.

Electroencephalogram (EEG) studies are advantageous in depicting the neural dynamics underlying FOG. In previous studies on electrophysiology of FOG, many scholars recorded scalp EEG of PD-FOG patients during walking, and some scholars also used gait analysis (Handojoseno et al., 2015; Günther et al., 2019; Brugger et al., 2020; Asher et al., 2021; Cao et al., 2021; Stuart et al., 2021). The results reported the characteristics of EEG dynamics and the coupling of different cortical locations of PD-FOG. However, these studies have some limitations. First, they did not obtain information on subcortical structures, and second, they did not use synchronized gait analysis to accurately distinguish whether FOG durations. Other scholars have recorded the LFP of the subcortical STN in DBS patients during walking, and combined gait analysis simultaneously, reporting the relationship between the features of STN and the occurrence of FOG (Fischer et al., 2018; Chen et al., 2019). At present, there are few researches on the combination of multi-target electrophysiological signal recording and gait analysis. Pozzi et al. (2019) added scalp EEG on

above basis and reported the derangement of locomotor network dynamics in PD-FOG. However, scalp EEG cannot eliminate the attenuation effect of the scalp, skull, dura, and other structures on electrical activity, limiting its efficacy on spatial resolution and discernibility of some frequency components. In our study, the electrodes were placed under the dura to ameliorate this shortcoming. Our method platform still achieved synchronous record of ECoG, STN-LFP and gait data, which means that gait data characteristics can be used to accurately distinguish the onset of freezing and study the pathogenesis of FOG from the perspective of locomotor network dynamics. The described platform features high temporal and spatial resolution, and provides a set of effective data analysis methodologies to facilitate exploration of the dynamic electrophysiological patterns underlying FOG.

METHODS

Patients and Surgical Procedure

Eight patients were enrolled in the study from January 2019 to June 2020. All patients underwent subthalamic nucleus-deep brain stimulation (STN-DBS) surgery in the Department of Neurosurgery of Beijing Tiantan Hospital (Table 1). All patients provided informed consent and signed the operation informed consent form. This study was approved by the Ethics Committee of Beijing Tiantan Hospital (No. KY 2018-008-02).

As a routine clinical procedure, a Leksell stereotactic head frame was mounted onto the patient's skull on the day of surgery under local anesthesia and was then aligned as closely as possible parallel to the anterior commissure-posterior commissure line. Then, an axial volumetric computed tomography (CT; slice thickness 0.625 mm, interslice gap 0 mm, 120 kVp) scan was taken. A General Electric 3.0 T magnetic resonance (MR) imaging scanner was used as a positioning scan (axial and coronal T1- and T2-weighted images with 1.0 mm slice thickness and no spacing). CT and MRI data were superimposed and fused in the surgical planning system (ELEKTA, Stockholm, Sweden). The surgeon confirmed the coordinates of the surgical target and the angle of trajectory based on MR images. Under local anesthesia, the surgical incision was made according to the calculated target coordinates, and a hole was drilled into the skull. After drilling, 8-contact cortical electrodes (Sinovation Medical Technology Co., Ltd., Beijing, China) were placed on the right sides parallel to the direction of the superior sagittal sinus. The electrode contacts covered the premotor area (PM), then the cortical electrode was fixed. The target position

of the STN was confirmed by intraoperative microelectrode recording and electrode stimulation (L301; PINS Medical, Ltd., Beijing, China). Further details of this surgical procedure have been described previously (Meng et al., 2013). The position of the electrodes was examined again in a postoperative review, and any necessary adjustments were made after intracranial edema subsided. Through the open source software package, combined with preoperative MRI and postoperative CT images, the positions of the deep electrode contacts in the STN and the cortical electrode contacts could be determined (Hamilton et al., 2017; Horn et al., 2019).

Recording Equipment

The EEG recording system (Nihon Kohden, Tokyo, Japan): the EEG recording system comprised a 64-channel electrode input box that can receive input signals from an external transducer. Cortical electrodes can be directly connected to the box, and through a customized connection cable, the STN electrode test cable of PD patients can also be connected to the box. The digital video system was used to record and view the patient's video and the synchronized EEG waveform. NeuroWorkbench software was used to review, clip and export EEG data.

The Codamotion 3-D Movement Capture System (CODAMotion, Charnwood Dynamics Ltd., Rothley, Leicester): The codamotion system is an advanced three-dimensional motion capture system. Four cameras fixed on the bilateral roof capture the movements of nodes through active infrared wearable markers. If conditions permit, the system should be worn bilaterally according to the human bone model. The markers include the posterior superior iliac spine, thigh, shank, heel and fifth metatarsal. Codamotion provides convenient, efficient and accurate three-dimensional movement acquisition.

Deep brain stimulation electrode (L301; PINS Medical, Ltd., Beijing, China): the deep brain stimulation electrode comprises a 1.3-mm-diameter electrode with four stimulating contacts and four connecting contacts. The contact shape is cylindrical. The stimulating contact length is 1.5 mm and the stimulating contact spacing is 0.5 mm.

Subdural electrode (PSE-8A; Sinovation Medical Technology Co., Ltd., Beijing, China): the subdural electrode comprises eight stimulating contacts and an array of 1×8 electrode contacts. The silica gel sheet size is 8×80 mm, and contact spacing is 10 mm. The coverage of the subdural electrode includes the premotor, primary motor and sensory cortex.

Synchronized Electrophysiology and Gait Data Acquisition

The electrophysiology acquisition parameters were a 0.08–660 Hz hardware filter and a sampling rate of 2000 Hz. A system reference averaging the electrical potentials of the fifth and sixth subdural electrodes was used during EEG acquisition. Electrical signal acquisition began 1–2 days after surgery. The trials were generally conducted during the OFF phase of the drug cycle (i.e., more than 12 h after the last anti-Parkinson's drug was administered) (Bächlin et al., 2010). Electrical signals were collected when walking with or without cognitive load. The single

TABLE 1 | Preoperative characteristics of the eight patients.

No. of patients	8
Sex	3M/5F
Age at time of surgery (Years)	
Range/Mean \pm SD	52–73/62.63 \pm 7.60
Age at disease onset (Years)	
Range/Mean \pm SD	37–65/52.25 \pm 9.15
Disease duration (Years)	
Range/Mean \pm SD	7–15/10.38 \pm 2.45
Dose of levodopa equivalent medication (mg/d)	
Range/Mean \pm SD	488–1439.25/924.03 \pm 356.49
Hoehn-Yahr Stage	
Range/Mean \pm SD	2–3/2.56 \pm 0.42
UPDRS III Score	
Range/Mean \pm SD	32–79/52.88 \pm 13.52
FOGQ Score	
Range/Mean \pm SD	15–23/18.88 \pm 2.75

record consisted of multiple repeated tasks, and the patient was prompted to start or stop the task by a random signal (**Figure 1**).

After the markers had been worn and the patient had adapted to a period of free activity, the gait data were collected. PD patients with FOG were asked to walk 5 m in an experimental area to collect gait features. The data were collected by the Codamotion 3-D Movement Analysis System with a sampling rate of 200 Hz.

To perform gait analysis, a number of steps need to be carried out in sequence. (1) Marker set: markers are required to complete a full lower body gait analysis. The different positions for clusters/marker drive boxes and markers are described in **Figure 1**. The markers can be classifying in two categories. Real markers are markers for which the 3D position is directly obtained from the position of a Codamotion active marker, and their spatial position data are used in current gait analysis. Virtual markers are markers for which their positions are obtained through computation. (2) Digitizing the pointer landmarks: a prompt window displays the name of the pointer that the experimenter needs to digitize. Once that pointer is digitized, the name of the following pointer is automatically displayed and the system waits for it to be digitized. (3) Visualizing the data: once calculation of the statistical data has been performed the user is able to see all of the results by selecting different layouts. (4) The raw data are exported in c3d format.

When the clinician presses the codamotion recording switch, a 5 V direct current signal is output, and the input signal is directly displayed on the interface of the EEG recording signal through the transducer. Similarly, when the clinician ends the gait signal recording, a 5 V TTL pulse is output and recorded by the EEG amplifier (**Figure 1**). Therefore, the collection of LFP and ECoG signals is synchronized with the collection of gait data.

Gait Evaluation and Freezing of Gait Labeling

For the time up and go (TUG) test (Podsiadlo and Richardson, 1991; Herman et al., 2011), subjects wear flat shoes and sit on a

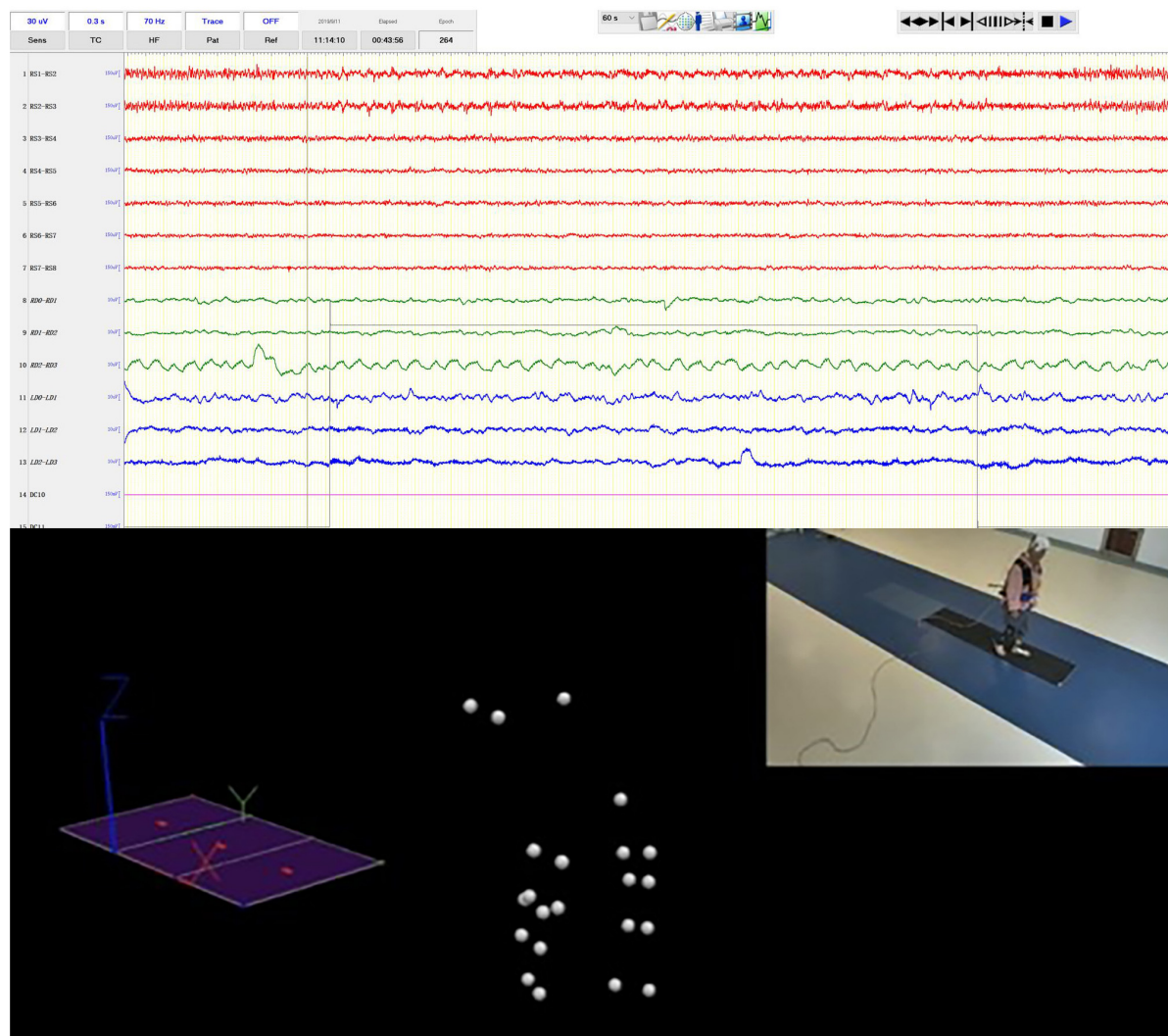


FIGURE 1 | Synchronized iEEG recording and motion capture. The video clip in the upper right was simultaneously recorded by the video-EEG and real-time spatial positions of the optical sensitive nodes worn by the patients were captured by multiple surrounding cameras.

chair (~46 cm high) with their hands naturally resting on their legs. The ground is marked 5 m away from the seat and a sign is placed at this position. When the subject hears "start," they are asked to stand up straight, walk at normal pace, turn around the sign, return to the seat and sit down, and then the timer is ended. No physical assistance can be given during the process. The time is recorded, and the subject can rest for 1 min between each test. Dual tasking (Fritz et al., 2015) that distracts patients' attention allows FOG to be analyzed if the patient does not exhibit frozen gait during walking. Dual tasking usually consists of two tasks: primary motor or balance tasks (such as walking, standing) and secondary tasks required for distraction, such as simple computation tasks and language fluency tasks.

A PD expert manually labeled the freezing period by reviewing the synchronized high resolution video footage according to its definition, namely "brief, episodic absence or marked reduction of forward progression of the feet despite the intention to walk"

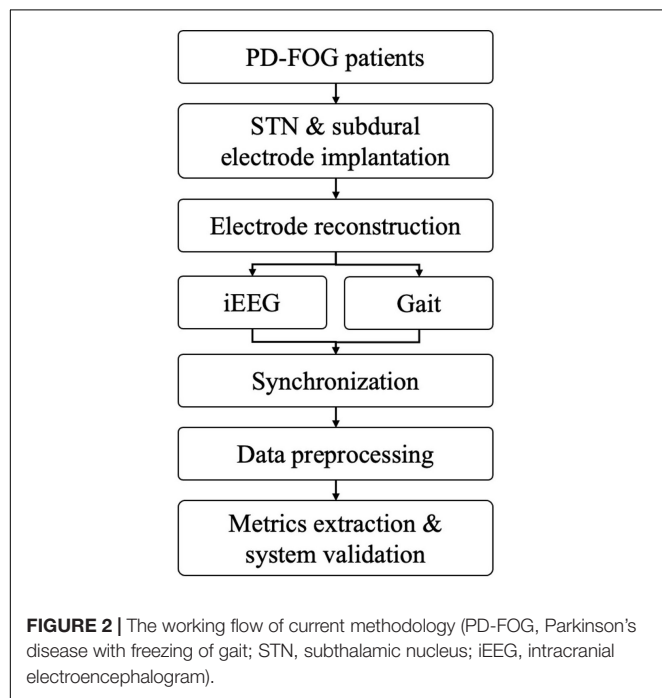
(Heremans et al., 2013). The onset and ending of the FOG period were labeled.

Machine Learning Approaches to Classified Freezing of Gait and Non-freezing of Gait

We used machine learning approaches to classified between FOG-epochs and non-FOG-epochs. From each of the 21 trials, we extracted 2 FOG epochs each lasted 2s and 4 same-length nFOG epochs, resulting in a total of 126 epochs (42 FOG epochs and 84 nFOG epochs). We extracted band power features (delta: 1–3 Hz, theta: 3–8 Hz, alpha: 8–13Hz, beta: 13–30 Hz, gamma: 30–60 Hz, and high-frequency oscillation: 60–300 Hz) from each epoch using a fast Fourier transform of 512 points. We employed a previously reported "mixed-effects random forest" (MERF) (Hajjem et al., 2014) to build classification models, which

TABLE 2 | Classification of data quality.

Classification	Description
Level 1	The data quality is excellent in all time ranges, and there are almost no artifacts
Level 2	The data quality in most of the time range is excellent, with some artifacts, but the basic EEG waveforms are still reserved
Level 3	The data quality is acceptable in most of the time range, and the artifact interference is more obvious
Level 4	Most of the data is of poor quality and artifacts are obvious
Level 5	The entire signal is heavily contaminated by noise, and no normal EEG signal components can be seen



combines the linear mixed effects model and the random forest model, and is especially suitable for repeated measurement data. In building the model, we divided 70% of data into the training set and 30% of data into the testing set. Ten-fold cross validation was employed to cross-validate the classifier in the training set. Permutation test with 1,000 permutations was used to assess model robustness.

Data Quality Manual Inspection

Collecting electrophysiological signals while the patient is walking is likely disturbed by motion artifacts. Therefore, before selecting each segment of electrical signal for analysis, we manually reviewed and scaled the signal quality, and selected level 1 or level 2 for subsequent analysis (Table 2).

Data Analysis and System Validation

After data inspection, interception and filtering, subsequent data analysis was performed, including FI calculation, band power analysis and coherence between cortical electrodes and STN (Figure 2).

Freeze index (FI) calculation: after quality control, we firstly calculated the FI with the hypothesis that FI would be significantly higher during the manually labeled FOG period. The FI was initially proposed by Moore et al. (2008) as the power ratio of the locomotor band (0.5–3.0 Hz) to the freeze band (3–8 Hz) derived from the frequency spectrum (Moore et al., 2008). A high FI is indicative of FOG. Originally the authors used vertical linear acceleration of the lower limb; however, in this study, we used spatial data on the vertical direction of the right heel. The reasons are as follows: the original version of the FI was based on acceleration data, however, in our system, the raw 3D trace was tracked by the high-speed camera. To generate the expected input of the FI algorithm, we calculated the second derivatives of the raw trace, representing instantaneous acceleration of the marker, from here on, we follow the original methods and parameters to calculate the FI. We used the erosion algorithm to correct the baseline, then, acceleration data was generated using the second derivative of the raw trace. Time frequency transformation was performed using the short-time fast Fourier method, then the FI was calculated. The FI values were compared between normal walking and FOG periods.

Band power analysis: firstly preprocessing of the electrophysiological data was performed, which included down-sampling to 1000 Hz (if the raw frequency rate was 2000 Hz), notch filtering of the 50 Hz line noise and its harmonics and re-referencing to bipolar montage before time frequency transformation. Any trials with an apparent artifact or drift were discarded. Time-frequency decomposition was carried out using a Morlet wavelet transform with frequencies of interest log-spaced between 1 and 170 Hz (38 total values). Subsequently, we performed averaging of power amplitude estimates within seven frequency bands: δ (1–3 Hz), θ (4–7 Hz), α (8–12 Hz), β_1 (13–20 Hz), β_2 (21–35 Hz), γ (36–69 Hz), and high γ (70–170 Hz). We then compared the power of the different frequency bands between two freezing and non-freezing conditions for each channel.

Coherence between cortical electrodes and STN: Pairwise coherence was calculated between bilateral STN depth electrodes and all cortical electrodes. The coherence was defined as below and the frequencies of interest were 1 to 200 Hz with a 1 Hz step length:

$$Coherence = \frac{|E[S_{xy}]|}{\sqrt{E[S_{xx}] * E[S_{yy}]}}$$

where, S_{xy} and S_{xx} , S_{yy} are estimates of the cross- and power-spectral densities (CSD/PSD). $E[\cdot]$ denotes the average of the data segments. We firstly performed a statistical comparison between the raw electrophysiological data and shuffled surrogates to identify the significantly synchronized frequency band of interest. Then, based on the significant frequency band, coherence between FOG and non-FOG periods were further compared. To test the hemisphere difference, the coherence between ipsilateral STN/cortical pairs and contralateral STN/cortical pairs was also compared.

The codes used in this study can be found at: https://github.com/THIENC/DBS_FOG_Project_Analysis_Pipeline-master.

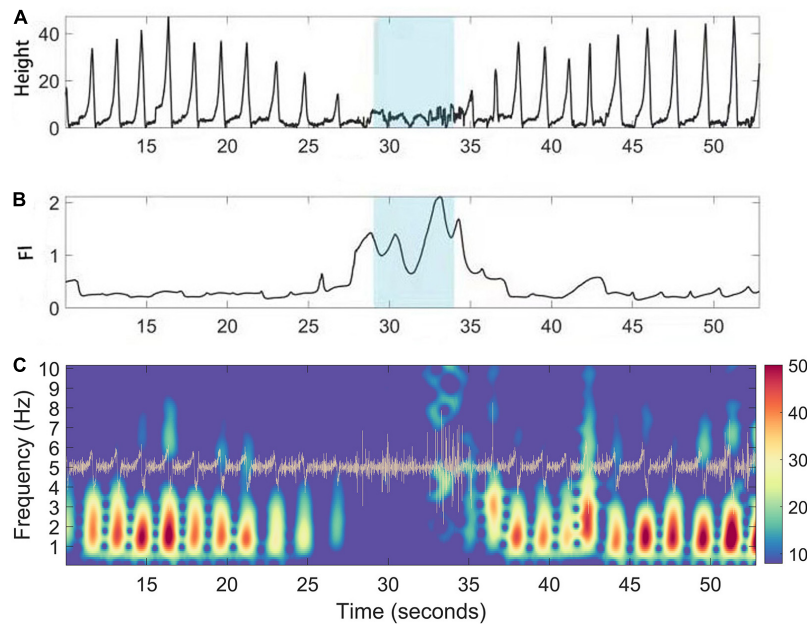


FIGURE 3 | A case illustration of FI (Freeze index) increase during manually labeling freezing phase. **(A)** Gait positioning data (vertical Z axis) captured by the CODA system of PD patients during walking. **(B)** The corresponding dynamic fluctuation of FI; Blue area indicates the occurrence time of FOG determined manually. **(C)** Time frequency representation of the acceleration (trace in yellow) of the raw trace during walking of PD patients. During freezing, the power of the “locomotion band” (0–3 Hz) decreased.

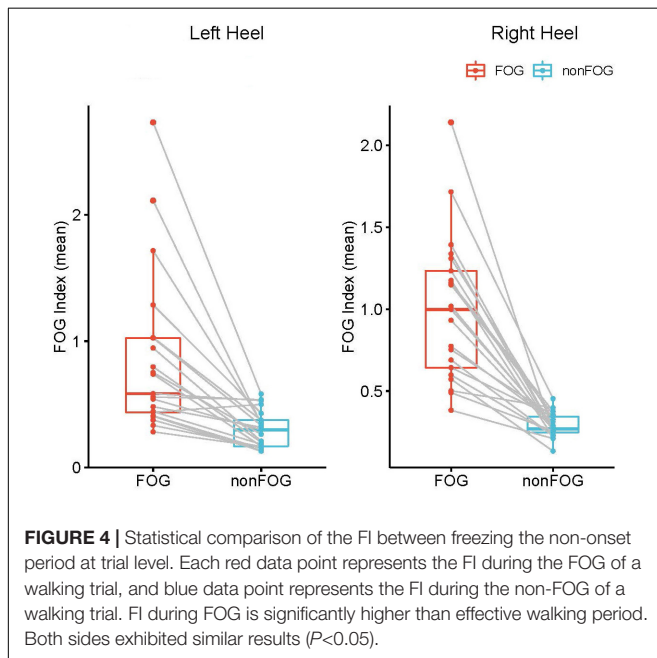


FIGURE 4 | Statistical comparison of the FI between freezing the non-onset period at trial level. Each red data point represents the FI during the FOG of a walking trial, and blue data point represents the FI during the non-FOG of a walking trial. FI during FOG is significantly higher than effective walking period. Both sides exhibited similar results ($P < 0.05$).

Statistical Analysis

SPSS 23.0 software (IBM SPSS Statistics Inc., Chicago, IL, United States) was used for statistical analysis. Patient characteristics data are expressed as the mean \pm standard deviation ($\bar{x} \pm s$). The paired t -test was used to calculate FI and Band Power between FOG and non-FOG periods ($P < 0.05$ was considered statistically significant).

RESULTS

Patient Characteristics

All enrolled patients were clinically diagnosed as having primary PD and fit the following criteria: Hoehn–Yahr stage (Hoehn and Yahr, 1967) ≥ 2.0 in the drug-off period; the third item in the FOG questionnaire score (Giladi et al., 2000) ≥ 2.0 ; regarding the UPDRS-II score (Goetz et al., 2008), item 14 ≥ 2.0 and item 15 ≥ 2.0 ; displayed no major cognitive decline (Mini-Mental State Examination score (Folstein et al., 1983) ≥ 24 points). Recordings were made during walking for the eight patients (three males, five females; average age: 62.63 years, SD: 7.60 years). Clinical details are summarized in **Table 1**.

Data Quality and Freezing of Gait Index

The eight patients completed a total of 41 walking tests, 30 of which had frozen episodes, and 21 of the 30 raw data were level 1 or 2 in quality (70%). The mean \pm SD walking time for the TUG test was 85.94 ± 47.68 s (range: 38 to 190.14 s), the median was 67.32s; the mean \pm SD freezing duration was 12.25 ± 7.35 s (range: 1.71 to 27.50 s), the median was 10.18s (**Supplementary Table 1**).

Validation of CODA Data and the Freezing of Gait Index

During walking, the CODA system captured the position track of multiple active markers, and we chose the position track of the heel for demonstration and FI analysis. The illustrative case example (**Figure 3A**) showed the change in the Z-axis of the heel

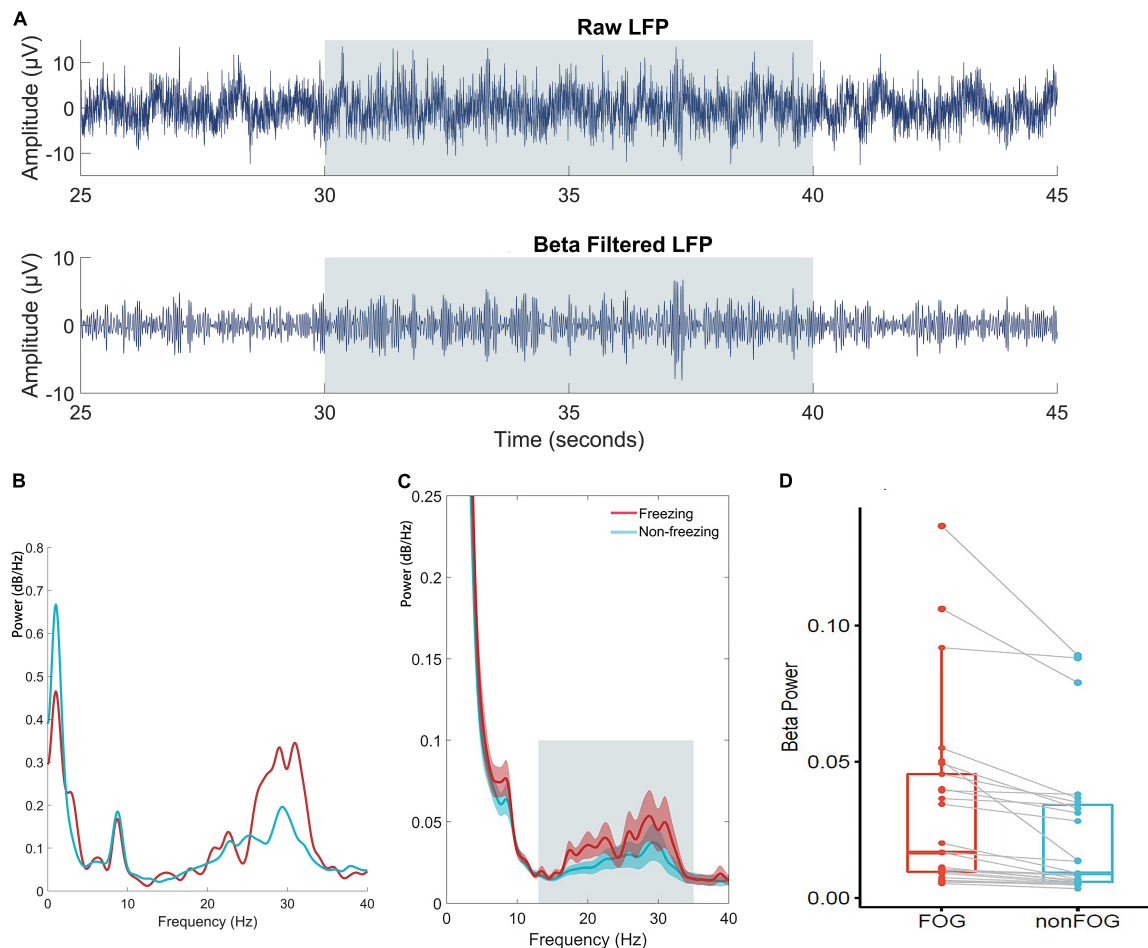


FIGURE 5 | (A) Time series of raw and beta band filtered LFP. **(B)** An individual case illustration of power spectrum density of LFP in the STN between freezing and non-freezing period; The red line represents the power spectrum of LFP during FOG, and the blue line represents the power spectrum of LFP during non-FOG. **(C)** The group analysis of power spectrum density averaged by all included walking epochs. The shaded error bar indicates SEM and the gray square indicates beta range. **(D)** Statistical comparison of averaged beta band power of LFP between conditions at trial level indicated significantly increased beta power during freezing ($P < 0.05$).

marker during the walking test. The height of steps decreased around 29–34 seconds, suggesting that FOG had occurred. As expected, the FI increased during the same period (**Figure 3B**). The acceleration data was generated by taking the derivatives of the raw trace (**Figure 3C**).

Between the different walking states (freezing or non-freezing), the paired t -test was conducted for the FI, and the statistical results showed that the FI values in the FOG period were statistically higher, as expected ($P < 0.05$), and this was replicable between each side of the data (**Figure 4**).

Band Power Analysis of Electrocorticography/ Local Field Potential

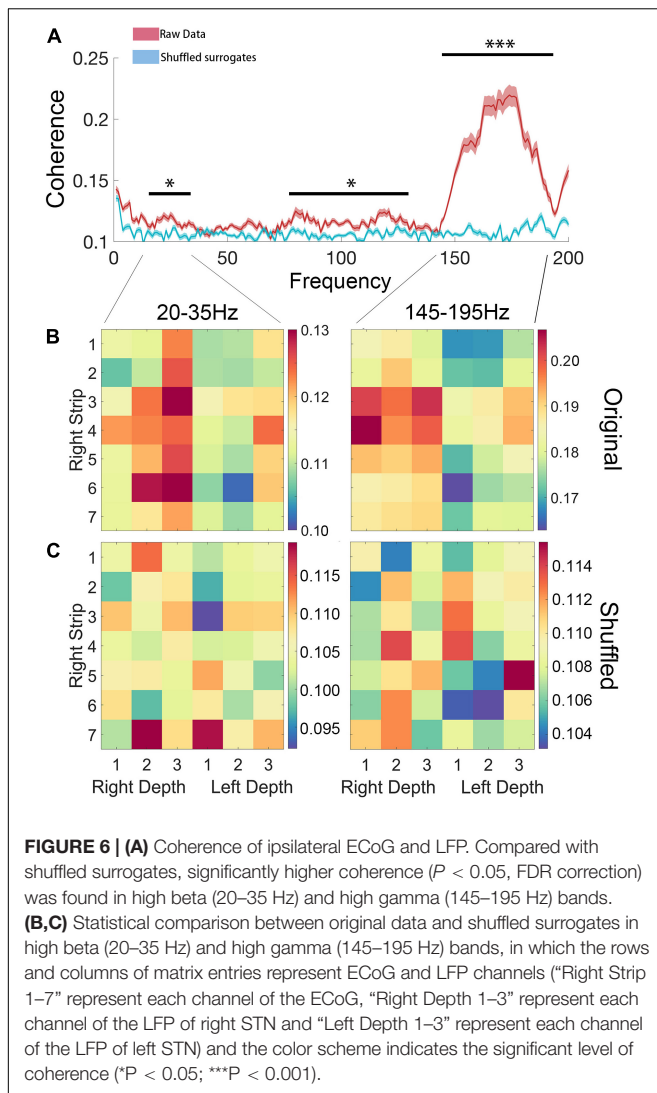
In the band power analysis, we compared the power of different frequency bands as described in the methods for each subdural and depth electrode between effective walking and FOG. The data from ECoG were all negative, indicating no significant band

power difference between the freezing and non-freezing states. However, for the LFP from the depth electrodes, beta band power was significantly increased ($P < 0.05$) during freezing, and this was clear even at the individual level (**Figure 5**).

Connectivity Between Cortical Regions and Subthalamic Nucleus

Pairwise coherence was calculated between bilateral STN depth electrodes and all cortical electrodes. Compared with shuffled surrogates, significantly higher coherence (cluster-based permutation test, $P < 0.05$, FDR correction) was found in high beta (20–35 Hz) and high gamma (145–195 Hz) bands (**Figure 6**). However, no coherence difference was found between walking states, which might be attributed to the short freezing period in each epoch.

We further tested whether there was a side preference of the connectivity between the STN and cortical areas for each significant band. To test the hemisphere difference, the coherence



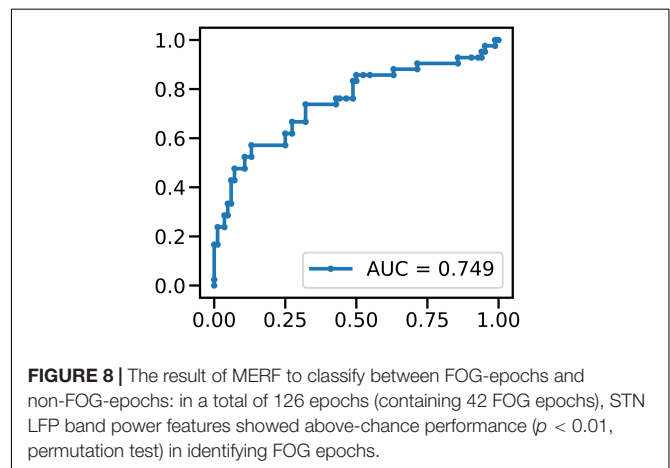
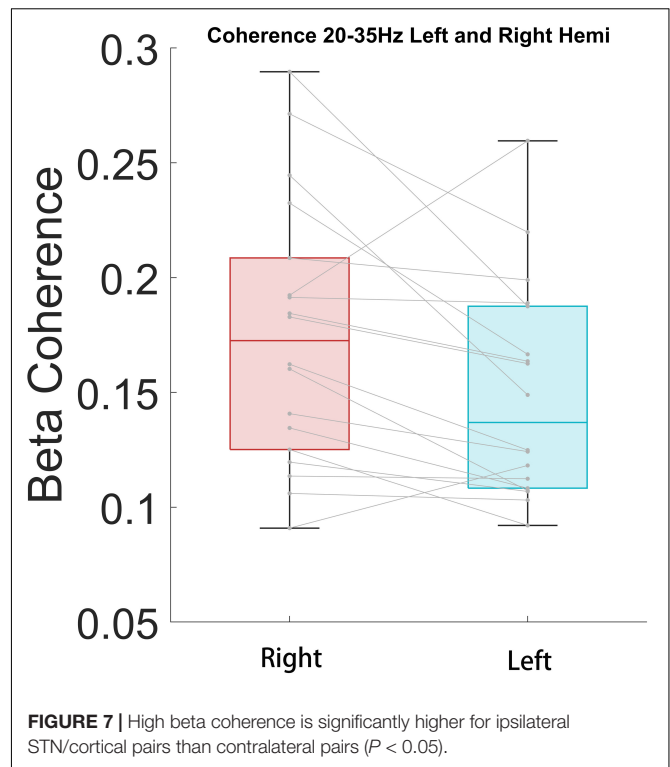
between bilateral STN and the right hemisphere ECoG of high beta and high gamma bands was compared. The high beta coherence of ipsilateral STN-cortical pairs was stronger than the contralateral equivalent ($P < 0.05$), but the high gamma coherence showed no difference ($P = 0.42$) (Figure 7).

Machine Learning Classification

We used MERF to classify between FOG-epochs and nFOG-epochs. In a total of 126 epochs (containing 42 FOG epochs), STN LFP band power features showed above-chance performance ($p < 0.01$, permutation test) in identifying FOG epochs, rendering an accuracy of 77% and an area under the receiver operating characteristic curve (AUC) of 0.75 (Figure 8).

DISCUSSION

Freezing of gait (FOG) is a common pathological gait in PD patients. It is widely believed that dysfunction of the basal ganglia circuit and related locomotor system is key in the occurrence of



FOG in PD (Snijders et al., 2016). The study of the abnormal neural signature in patients with PD-FOG is valuable in revealing the mechanism of FOG in patients with PD, and thereby for seeking a new treatment model and guiding clinical DBS surgery.

Imaging studies have shown that there are structural and metabolic abnormalities in several brain regions in the basal ganglia–cortical circuit in PD-FOG patients. Pietracupa et al. (2018) compared PD-FOG patients and non-FOG PD patients (PD-nFOG) by MRI and found that the thickness of the gray matter of the frontal lobe, motor cortex and cingulate gyrus was decreased in PD-FOG patients. Canu et al. (2015) applied diffusion tensor imaging (DTI) combined with functional magnetic resonance imaging (fMRI) and observed that the

functional connectivity of multiple brain areas, including the primary motor cortex, supplementary motor area and premotor area, is weakened in PD-FOG patients. Imaging studies have innate limitations because of the low time resolution; however, electrophysiological studies on the mechanisms in FOG patients, are still lacking at this stage. Storzer et al. (2017) pointed out that the occurrence of FOG has an electrophysiological basis in the basal ganglia region. The LFP in the STN region of PD-FOG patients shows a significant energy difference between the low β frequency band and the high β frequency band. Neurons in the STN area of PD-FOG patients showed different firing patterns in the two different states of riding and walking, suggesting functional differences depending on sensory feedback. Chen et al. (2019) recorded the LFP from the STN while PD patients performed single-task gait or walked while dual-tasking, which demonstrated that low beta and theta band oscillations within the STN area occur during gait susceptible to freezing in PD. However, there is still a lack of evidence at the circuit level. We implanted the STN deep electrode and the cortical electrode covering the primary motor and other areas in PD-FOG patients, and analyzed the LFP, ECoG, and gait data recorded simultaneously in the patient's walking and freezing gait states.

In addition, Brain-Computer Interface (BCI) is a hot topic in neuroscience. Closed loop BCI is one of the main research directions at present. Through the feedback of biological signals, BCI can apply stimulus signals to the research object, so as to improve its external behavior, namely adaptive DBS. In this experimental platform, electrodes were directly implanted into the motor cortex and the STN, aiming to collect feedback signals through multiple targets. Subsequently, the feedback of biological signals could be further combined with DBS treatment, so that the startup and parameter setting of DBS could be regulated according to the onset of FOG. In other words, the patient's movement performance is fed back to BCI as a biological signal, and then adaptive DBS is realized.

In this study, we first verified the reliability of the CODA system to assist in determining the period of FOG. The gait data collected by the CODA system in all channels can be directly decomposed into spatial three-dimensional coordinates. FOG is a type of gait disorder characterized by periodic and sudden gait delays and stops, lasting from a few seconds to a few minutes, which is manifested as a sudden decrease in the Z-axis on the time domain diagram (Figure 3A). This is also consistent with our manual labeling of the period of occurrence of FOG by reviewing the synchronized high resolution video footage. Previously, the FI was proposed to reflect the severity of FOG Moore et al. (2008). We also calculated the FI during the selected freezing period for system validating purposes. As expected, the FI during the freezing period was significantly higher than during the non-freezing period, indicating that the CODA system is reliable in assisting judgment of the freezing period (Figure 4).

After verifying the stability and reliability of the CODA system to determine the occurrence of FOG, we focused on the ECoG and LFP of the FOG period and the non-FOG period during walking. We selected each segment of electrical signal reaching

level 1 or 2 for analysis, and of all the data collected in this study, more than 70% have limited motion artifacts, which also confirms the stability of our data collection platform.

We next performed band power analysis (Figure 5). The results suggested that the beta power of STN LFP during the FOG period was significantly higher than that of the non-FOG period, which was consistent with previous literature (Storzer et al., 2017; Chen et al., 2019). However, the ECoG spectrum did not exhibit a statistical difference between walking states, which may be attributed to insensitivity for fast dynamics of spectrum metrics. Previous literature confirmed structural and functional connectivity between the cortex and the basal ganglia in the resting state of PD patients (Tard et al., 2015; Mi et al., 2017; Bharti et al., 2019, 2020). Our study preliminarily confirmed that the coupling between the bilateral STN and the right cortical motor area, represented by the beta and high gamma band coherence, increased during walking (Figure 6), and high beta coherence is significantly higher for ipsilateral STN/cortical pairs than contralateral pairs (Figure 7). However, there was no significant difference between the FOG and non-FOG periods. The reason for this may be that FOG is a transient process, and the calculation of coherence required repeatedly measured trials to form stable results, thus lacking trial level dynamic sensitivity.

To improve the analysis the difference between the coherence during FOG/No-FOG periods, we used machine learning approaches to classified between FOG-epochs and non-FOG-epochs. After signal preprocessing, feature extraction and machine learning algorithm modeling, we used MERF algorithm for training and found all band power of LFP features showed above-chance performance ($p < 0.01$, permutation test) in identifying FOG epochs. This preliminary result suggests that the subsequent real-time monitoring of FOG episodes in patients' daily life can provide quantitative and reliable reference for doctors' diagnosis and treatment. In addition, the number of patients included was small, which may bias the results of machine learning classification even when MERF model was employed. But since this is a preliminary report stressing mainly the methodological platform of synchronized intracranial electrical activity and gait recording, further large cohort study adopting this approach reporting detailed clinical and electrophysiological outcomes will be conducted in the future.

This study has some limitations. First, the number of patients was small, and the sample size needs to be expanded in the future; Second, only the medicine-off state was evaluated; Third, the influence of motion on the electrophysiological signal is inevitable, but we tried to fix the collection line on the patient as much as possible to reduce external interference.

CONCLUSION

This study aimed to describe a feasible synchronized recording system including intracranial EEG and gait data during walking. We verified the stability and reliability of the current system. In addition, preliminary results confirmed the stronger LFP beta power of STN during FOG and the functional connection

between the cortex and STN in FOG patients. In the future, further exploration of the electrophysiological biomarker and neural substrate underlying FOG could be performed based on the current platform, which may provide a theoretical basis for optimizing and perfecting the development of DBS in the treatment of PD and the development of new neuromodulation technologies.

DATA AVAILABILITY STATEMENT

The original contributions presented in the study are included in the article/**Supplementary Material**, further inquiries can be directed to the corresponding author.

ETHICS STATEMENT

The studies involving human participants were reviewed and approved by the Ethics Committee of Beijing Tiantan Hospital. The patients/participants provided their written informed consent to participate in this study.

REFERENCES

- Asher, E. E., Plotnik, M., Günther, M., Moshel, S., Levy, O., Havlin, S., et al. (2021). Connectivity of EEG synchronization networks increases for Parkinson's disease patients with freezing of gait. *Commun. Biol.* 4:1017. doi: 10.1038/s42003-021-02544-w
- Bächlin, M., Plotnik, M., Roggen, D., Maidan, I., Hausdorff, J. M., Giladi, N., et al. (2010). Wearable assistant for Parkinson's disease patients with the freezing of gait symptom. *IEEE Trans. Inf. Technol. Biomed.* 14, 436–446. doi: 10.1109/TTTB.2009.2036165
- Bartels, A. L., and Leenders, K. L. (2008). Brain imaging in patients with freezing of gait. *Mov. Disord.* 23, S461–S467. doi: 10.1002/mds.21912
- Bharti, K., Suppa, A., Pietracupa, S., Upadhyay, N., Gianni, C., Leodori, G., et al. (2019). Abnormal Cerebellar Connectivity Patterns in Patients with Parkinson's Disease and Freezing of Gait. *Cerebellum* 18, 298–308. doi: 10.1007/s12311-018-0988-4
- Bharti, K., Suppa, A., Pietracupa, S., Upadhyay, N., Gianni, C., Leodori, G., et al. (2020). Aberrant functional connectivity in patients with Parkinson's disease and freezing of gait: a within- and between-network analysis. *Brain Imag. Behav.* 14, 1543–1554. doi: 10.1007/s11682-019-00085-9
- Brugger, F., Wegener, R., Walch, J., Galovic, M., Hägele-Link, S., Bohlhalter, S., et al. (2020). Altered activation and connectivity of the supplementary motor cortex at motor initiation in Parkinson's disease patients with freezing. *Clin. Neurophysiol.* 131, 2171–2180. doi: 10.1016/j.clinph.2020.05.023
- Canu, E., Agosta, F., Sarasso, E., Volontè, M. A., Basaia, S., Stojkovic, T., et al. (2015). Brain structural and functional connectivity in Parkinson's disease with freezing of gait. *Hum. Brain Mapp.* 36, 5064–5078. doi: 10.1002/hbm.22994
- Cao, Z., Ma, B., Cui, C., Zhao, J., Liu, S., Qiu, Y., et al. (2021). Identification of EEG Dynamics During Freezing of Gait and Voluntary Stopping in Patients With Parkinson's Disease. *IEEE Trans. Neural Syst. Rehabil. Eng.* 29, 1774–1783. doi: 10.1109/TNSRE.2021.3107106
- Chen, C. C., Yeh, C. H., Chan, H. L., Chang, Y. J., Tu, P. H., Yeh, C. H., et al. (2019). Subthalamic nucleus oscillations correlate with vulnerability to freezing of gait in patients with Parkinson's disease. *Neurobiol. Dis.* 132:104605. doi: 10.1016/j.nbd.2019.104605
- Fischer, P., Chen, C. C., Chang, Y. J., Yeh, C. H., Pogossyan, A., Herz, D. M., et al. (2018). Alternating Modulation of Subthalamic Nucleus Beta Oscillations during Stepping. *J. Neurosci.* 38, 5111–5121. doi: 10.1523/JNEUROSCI.3596-17.2018

AUTHOR CONTRIBUTIONS

D-FL and H-GL performed the surgery. D-FL and B-TZ analyzed the data and wrote the manuscript. D-FL, Y-YL, Y-TB, YJ, and XZ participated in the data collection. J-GZ, D-FL, B-TZ, H-GL, G-YZ, L-S, HZ, and A-CY designed the topic. J-GZ supervised the research process and modified the manuscript. All authors contributed to the article and approved the submitted version.

FUNDING

This work was supported by the National Natural Science Foundation of China [Grant Number 81830033].

SUPPLEMENTARY MATERIAL

The Supplementary Material for this article can be found online at: <https://www.frontiersin.org/articles/10.3389/fnins.2022.795417/full#supplementary-material>

- Folstein, M. F., Robins, L. N., and Helzer, J. E. (1983). The Mini-Mental State Examination. *Arch. Gen. Psychiatry* 40:812. doi: 10.1001/archpsyc.1983.01790060110016
- Fritz, N. E., Cheek, F. M., and Nichols-Larsen, D. S. (2015). Motor-Cognitive Dual-Task Training in Persons With Neurologic Disorders: a Systematic Review. *J. Neurol. Phys. Ther.* 39, 142–153. doi: 10.1097/NPT.0000000000000090
- Giladi, N. (2008). Medical treatment of freezing of gait. *Mov. Disord.* 23, S482–S488. doi: 10.1002/mds.21914
- Giladi, N., McDermott, M. P., Fahn, S., Przedborski, S., Jankovic, J., Stern, M., et al. (2001). Freezing of gait in PD: prospective assessment in the DATATOP cohort. *Neurology* 56, 1712–1721. doi: 10.1212/wnl.56.12.1712
- Giladi, N., Shabtai, H., Simon, E. S., Biran, S., Tal, J., and Korczyn, A. D. (2000). Construction of freezing of gait questionnaire for patients with Parkinsonism. *Park. Relat. Disord.* 6, 165–170. doi: 10.1016/s1353-8020(99)00062-0
- Goetz, C. G., Tilley, B. C., Shaftman, S. R., Stebbins, G. T., Fahn, S., Martinez-Martin, P., et al. (2008). Movement Disorder Society-sponsored revision of the Unified Parkinson's Disease Rating Scale (MDS-UPDRS): scale presentation and clinimetric testing results. *Mov. Disord.* 23, 2129–2170. doi: 10.1002/mds.22340
- Günther, M., Karygianni, L., Argyropoulou, A., Anderson, A. C., Hellwig, E., Skaltsounis, A. L., et al. (2019). Coupling Between Leg Muscle Activation and EEG During Normal Walking, Intentional Stops, and Freezing of Gait in Parkinson's Disease. *Front. Physiol.* 10:870. doi: 10.3389/fphys.2019.00870
- Hajjem, A., Bellavance, F., and Larocque, D. (2014). Mixed-effects random forest for clustered data. *J. Stat. Comput. Sim.* 84, 1313–1328. doi: 10.1080/00949655.2012.741599
- Hamilton, L. S., Chang, D. L., Lee, M. B., and Chang, E. F. (2017). Semi-automated Anatomical Labeling and Inter-subject Warping of High-Density Intracranial Recording Electrodes in Electroencephalography. *Front. Neuroinform.* 11:62. doi: 10.3389/fninf.2017.00062
- Handojoseno, A. M., Shine, J. M., Nguyen, T. N., Tran, Y., Lewis, S. J., and Nguyen, H. T. (2015). Analysis and Prediction of the Freezing of Gait Using EEG Brain Dynamics. *IEEE Trans. Neural Syst. Rehabil. Eng.* 23, 887–896. doi: 10.1109/TNSRE.2014.2381254
- Heremans, E., Nieuwboer, A., and Vercruyse, S. (2013). Freezing of gait in Parkinson's disease: where are we now? *Curr. Neurol. Neurosci. Rep.* 13:350. doi: 10.1007/s11910-013-0350-7

- Herman, T., Giladi, N., and Hausdorff, J. M. (2011). Properties of the 'timed up and go' test: more than meets the eye. *Gerontology* 57, 203–210. doi: 10.1159/000314963
- Hoehn, M. M., and Yahr, M. D. (1967). Parkinsonism: onset, progression and mortality. *Neurology* 17, 427–442. doi: 10.1212/wnl.17.5.427
- Horn, A., Li, N., Dembek, T. A., Kappel, A., Boulay, C., Ewert, S., et al. (2019). Lead-DBS v2: towards a comprehensive pipeline for deep brain stimulation imaging. *Neuroimage* 184, 293–316. doi: 10.1016/j.neuroimage.2018.08.068
- Lv, W., Jia, Y., Wang, J., Duan, Y., Wang, X., Liu, T., et al. (2021). Normal-sized basal ganglia perivascular space related to motor phenotype in Parkinson freezers. *Aging* 13, 18912–18923. doi: 10.18632/aging.203343
- Macht, M., Kausser, Y., Möller, J. C., Stiasny-Kolster, K., Eggert, K. M., Krüger, H. P., et al. (2007). Predictors of freezing in Parkinson's disease: a survey of 6,620 patients. *Mov. Disord.* 22, 953–956. doi: 10.1002/mds.21458
- Meng, F. G., Hu, W., Ge, Y., Ma, Y., Ge, M., Zhang, K., et al. (2013). Essential tremor: treatment with deep brain stimulation of the ventral intermediate nucleus of the thalamus. *Chin. Med. J.* 126, 1192–1193.
- Mi, T. M., Mei, S. S., Liang, P. P., Gao, L. L., Li, K. C., Wu, T., et al. (2017). Altered resting-state brain activity in Parkinson's disease patients with freezing of gait. *Sci. Rep.* 7:16711. doi: 10.1038/s41598-017-16922-0
- Moore, S. T., MacDougall, H. G., and Ondo, W. G. (2008). Ambulatory monitoring of freezing of gait in Parkinson's disease. *J. Neurosci. Meth.* 167, 340–348. doi: 10.1016/j.jneumeth.2007.08.023
- Pietracupa, S., Suppa, A., Upadhyay, N., Gianni, C., Grillea, G., Leodori, G., et al. (2018). Freezing of gait in Parkinson's disease: gray and white matter abnormalities. *J. Neurol.* 265, 52–62. doi: 10.1007/s00415-017-8654-1
- Podsiadlo, D., and Richardson, S. (1991). The timed "Up & Go": a test of basic functional mobility for frail elderly persons. *J. Am. Geriatr. Soc.* 39, 142–148. doi: 10.1111/j.1532-5415.1991.tb01616.x
- Pozzi, N. G., Canessa, A., Palmisano, C., Brumberg, J., Steigerwald, F., Reich, M. M., et al. (2019). Freezing of gait in Parkinson's disease reflects a sudden derangement of locomotor network dynamics. *Brain* 142, 2037–2050. doi: 10.1093/brain/awz141
- Snijders, A. H., Takakusaki, K., Debu, B., Lozano, A. M., Krishna, V., Fasano, A., et al. (2016). Physiology of freezing of gait. *Ann. Neurol.* 80, 644–659. doi: 10.1002/ana.24778
- Storzer, L., Butz, M., Hirschmann, J., Abbasi, O., Gratkowski, M., Saupe, D., et al. (2017). Bicycling suppresses abnormal beta synchrony in the Parkinsonian basal ganglia. *Ann. Neurol.* 82, 592–601. doi: 10.1002/ana.25047
- Stuart, S., Wagner, J., Makeig, S., and Mancini, M. (2021). Brain Activity Response to Visual Cues for Gait Impairment in Parkinson's Disease: an EEG Study. *Neurorehabil. Neural Repair* 35, 996–1009. doi: 10.1177/15459683211041317
- Tard, C., Delval, A., Devos, D., Lopes, R., Lenfant, P., Dujardin, K., et al. (2015). Brain metabolic abnormalities during gait with freezing in Parkinson's disease. *Neuroscience* 307, 281–301. doi: 10.1016/j.neuroscience.2015.08.063
- Walton, C. C., Shine, J. M., Hall, J. M., O'Callaghan, C., Mowszowski, L., Gilat, M., et al. (2015). The major impact of freezing of gait on quality of life in Parkinson's disease. *J. Neurol.* 262, 108–115. doi: 10.1007/s00415-014-7524-3

Conflict of Interest: The authors declare that the research was conducted in the absence of any commercial or financial relationships that could be construed as a potential conflict of interest.

Publisher's Note: All claims expressed in this article are solely those of the authors and do not necessarily represent those of their affiliated organizations, or those of the publisher, the editors and the reviewers. Any product that may be evaluated in this article, or claim that may be made by its manufacturer, is not guaranteed or endorsed by the publisher.

Copyright © 2022 Liu, Zhao, Zhu, Liu, Bai, Liu, Jiang, Zhang, Shi, Zhang, Yang and Zhang. This is an open-access article distributed under the terms of the Creative Commons Attribution License (CC BY). The use, distribution or reproduction in other forums is permitted, provided the original author(s) and the copyright owner(s) are credited and that the original publication in this journal is cited, in accordance with accepted academic practice. No use, distribution or reproduction is permitted which does not comply with these terms.

Advantages of publishing in Frontiers



OPEN ACCESS

Articles are free to read
for greatest visibility
and readership



FAST PUBLICATION

Around 90 days
from submission
to decision



HIGH QUALITY PEER-REVIEW

Rigorous, collaborative,
and constructive
peer-review



TRANSPARENT PEER-REVIEW

Editors and reviewers
acknowledged by name
on published articles

Frontiers

Avenue du Tribunal-Fédéral 34
1005 Lausanne | Switzerland

Visit us: www.frontiersin.org

Contact us: frontiersin.org/about/contact



REPRODUCIBILITY OF RESEARCH

Support open data
and methods to enhance
research reproducibility



DIGITAL PUBLISHING

Articles designed
for optimal readership
across devices



FOLLOW US

@frontiersin



IMPACT METRICS

Advanced article metrics
track visibility across
digital media



EXTENSIVE PROMOTION

Marketing
and promotion
of impactful research



LOOP RESEARCH NETWORK

Our network
increases your
article's readership